GHENT UNIVERSITY

FACULTY OF SCIENCES

Elucidation of the protein-protein interaction network at play during strigolactone and karrikin signaling

Sylwia Struk

Academic year 2017-2018
Promoters: Prof. Dr. Sofie Goormachtig and Prof. Dr. Dirk Inzé

Thesis submitted as partial fulfillment of the requirements for obtaining the degree of
Doctor of Philosophy in Science: Biochemistry and Biotechnology

VIB

VIB-UGENT CENTER FOR PLANT SYSTEMS BIOLOGY

Examination Board

Chair

Prof. Dr. Moritz Nowack

Ghent University – Faculty of Sciences, Department of Biotechnology and Bioinformatics

VIB – Center for Plant Systems Biology

Secretary

Dr. Jelle Van Leene

Ghent University – Faculty of Sciences, Department of Biotechnology and Bioinformatics

VIB – Center for Plant Systems Biology

Promoters

Prof. Dr. Sofie Goormachtig

Ghent University – Faculty of Sciences, Department of Biotechnology and Bioinformatics

VIB – Center for Plant Systems Biology

Prof. Dr. Dirk Inzé

Ghent University – Faculty of Sciences, Department of Biotechnology and Bioinformatics

VIB – Center for Plant Systems Biology

Other members

Prof. Dr. Geert De Jaeger

Ghent University – Faculty of Sciences, Department of Biotechnology and Bioinformatics

VIB – Center for Plant Systems Biology

Prof. Dr. Ive De Smet

Ghent University – Faculty of Sciences, Department of Biotechnology and Bioinformatics

VIB – Center for Plant Systems Biology

Prof. Dr. Els Van Damme

Ghent University – Faculty of Bioscience Engineering, Department of Biotechnology

Dr.Sandrine Bonhomme

Institut Jean-Pierre Bourgin, INRA AgroParisTech – CNRS - Université Paris-Saclay

Acknowledgments

After more than five years of working at PSB, the time has come to thank many people who supported me throughout this journey. First of all, I would like to thank my promoter Sofie, for giving me a chance to join (at that time) the Strigolactone group. Already from our first conversation I was convinced that it would be a good choice, and I was not disappointed. Thank you for creating a really enjoyable atmosphere in the lab, which makes everyone happy at work. I am enormously grateful for all the guidance, time and input you have given to my project, including all the drawings of the strigolactone mode of action. Also, for being so enthusiastic about my results and always, in contradiction to me, seeing the glass half full. Besides all the nice time at work, I will keep lots of great memories from Christmas dinners, summer BBQs and our team buildings (although without paintball). Thank you for the confidence you have in me and the chance to enjoy the lab atmosphere for a bit longer.

Next, of course a big thanks to all the lab members! I will start with THE queen of cloning (and every other experiment in the lab), Annick. Thank you so much for all your help! Every time you were happy to help so at the end I did not dare to ask you anymore. Next, to my desk colleague Lukas, who was with me in the lab from the very beginning. It was always fun to discuss science with you and listen to your crazy ideas, but also outside the lab for all the squash sessions, drinks and game nights. Only the sea sponge will be never forgiven! To the youngest member of the strigo team, Anse, for not letting strigolactone research end. You can still show the rhizo's which project is more interesting! Well, I think I have to thank Stien as well… for making me the second meanest person in the lab (yes, just after you!) but also for trying really hard to understand strigolactone research. It was fun to do baking course with you and hopefully more yet to come! Thanks to Sarah, Emily, Dexian, Ho, Antoine and Amber for making the rhizosphere THE best lab in PSB, where the team-work is combined with a friendly and relaxed atmosphere!

Next, to former group members, Justine, Cedrick, Belen and Alan for making the first years of my PhD unforgettable! For all the activities, dinners, game nights, weekends out, holidays together. Next holiday destination -> Poland! To Carolien and Nathan, thanks for being my desk colleagues for a little while, all

the insight that you gave to my project and the help to get going in the beginning. To Tibby and Tom for all the very competitive squash games and hopefully more in the future!

Thanks to Geert, Dominique, Nancy and Eveline for all the help with teaching me but also performing and analyzing all the TAP experiments. To Nancy, for your patience when I was trying to solve the problem with my continuously dying cell cultures. To Nancy, Kristof, Peter, Wilson, Carina, Nico, Miguel, Thomas, Tim, Stefaan and Olivier for all the technical support without which I would not be able to progress so fast. A big thank to Martine for correcting and submitting my manuscripts and also reading and giving your suggestion for this thesis.

To all the polish girls I have met in PSB, Aga, Asia and Ola for not letting me forget my mother tongue at work but also being my friends outside the lab. And to some more polish girls, Karolina and Zuza for our nice evenings filled with gossips and science of course! To all other friends, Dagmara, Jaime, Andres, Damian, Magda, Mateusz and Sebastien who made my stay in Belgium so enjoyable!

Finally, but most importantly thank to my family for supporting me throughout the whole of my studies. To my parents for allowing me to go for the Erasmus exchange to Belgium and that is how it all started. Lastly, to Milek for leaving me alone when I needed to write my thesis ;). Thanks for helping me get through all of it and for making Ghent my home!

Summary

Over the past years, the strigolactone and karrikin signalling pathways have been extensively studied. Nevertheless, many gaps still exist in our understanding of the downstream targets but also of how the signalling mechanism is controlled. In this PhD, we aimed at expanding our knowledge of the protein-protein interaction network involved in both strigolactone and karrikin pathways, that might be linked to the observed phenotypes. We focused on the identification of interaction partners of the core signaling components in *Arabidopsis thaliana* by means of tandem affinity purification (TAP).

To analyze the TAP experiments of SMXL7, two different approaches have been used. In the first one, TAP was combined with label-free quantification to allow quantitative analysis of the changes in the protein complexes formed around the bait in the presence and absence of *rac*-GR24. In this way we confirmed previously described dynamic interaction between SMXL7 and D14, but also proposed a new model of the SL mode of action. The second, qualitative TAP analysis resulted in the identification of five novel interacting partners of SMXL7. Although the validation studies between SMXL7 and SINT1, SINT2 and SINT3 proteins confirmed these interactions, no plant phenotypic link has been observed yet that could biologically explain these associations. Two other preys copurified with SMXL7, FyPP1/3 and SAL4 have been previously described to form a PP6-type phosphatase complex. Both the validation studies and the mutant analysis suggested the role of this complex as a negative regulator of lateral root density and possibly also shoot branching. It remains to be resolved whether the observed phenotypes are due to a direct regulation of SMXL7 by the PP6 complex or an indirect effect of disturbed auxin transport. Then, the evidence has been provided for the SMAX1-KAI2 interaction and degradation of SMAX1 proteins in response to *rac*-GR24. The combination of the qualitative and quantitative TAP was used to further expand our knowledge of the SMAX1 interactome, which resulted in new candidate proteins for future studies. Lastly, from all the proteins copurified with MAX2 in *Arabidopsis* cell cultures and seedling two preys were selected for further investigation. The protein phosphatase PAPP5 and katanin-related CCP1 seem to be exclusively linked to the karrikin pathway influencing seed germination and, in case of CCP1, also hypocotyl elongation. On the contrary, ACD32.1 protein identified as a prey of KAI2, has been shown to directly interact with all known components of strigolactone and karrikin pathways, however its exact role in both signalling cascades remains to be determined.

Taken together, by the discovery of new players in the strigolactone and karrikin signalling networks, we deliver an important contribution to the understanding of the molecular mechanism of both pathways resulting in the execution of downstream physiological responses.

Samenvatting

In de afgelopen jaren zijn de strigolacton en karrikine signaaltransductie pathways uitgebreid bestudeerd. Desondanks begrijpen we nog weinig van de downstream targets en hoe de signalisatie wordt gecontroleerd. In dit doctoraat werd gefocust op de verdere ontrafeling van het eiwit-eiwit interactienetwerk, betrokken bij zowel de strigolacton- als karrikine- pathways, dat gekoppeld zou kunnen worden aan de geobserveerde fenotypes. We hebben ons gericht op de identificatie van interactiepartners van de centrale signalisatiecomponenten in *Arabidopsis thaliana* door middel van tandem-affiniteitszuivering (TAP).

Voor het analyseren van de TAP-experimenten van SMXL7 zijn twee verschillende benaderingen gebruikt. Eerst werd TAP gecombineerd met labelvrije kwantificatie om een kwantitatieve analyse van de veranderingen in de eiwitcomplexen gevormd rond SMXL7 in aan- en afwezigheid van rac-GR24 mogelijk te maken. Op deze manier bevestigden we de reeds beschreven dynamische interactie tussen SMXL7 en D14 maar stelden we ook een nieuw model voor over de werking van SL. Een tweede, een kwalitatieve TAP analyse, resulteerde in de identificatie van vijf nieuwe interactiepartners van SMXL7. Hoewel validerende studies de eiwit-eiwit interacties tussen SMXL7 en SINT1, SINT2 en SINT3 bevestigden, werd geen fenotypische link waargenomen die deze connectie kan verklaren op een biologische manier. Twee andere eiwitten die opgezuiverd werden met SMXL7, FyPP1/3 en SAL4, werden eerder beschreven om een PP6-type phosphatase complex te vormen. Zowel de validerende interactiestudie als de geobserveerde fenotypes bevestigden de rol van dit complex als een negatieve regulator van de laterale worteldensiteit en mogelijks ook de vorming van scheutvertakkingen. Het moet nog onderzocht worden of het geobserveerde fenotype te wijten is aan een directe regulatie van SMXL7 door het PP6 complex of door een indirect effect veroorzaakt door een verstoord auxine transport. Ten slotte werd bewijs geleverd voor de SMAX1-KAI2 interactie en de degradatie van SMAX1 eiwitten als respons op rac-GR24. De combinatie van de kwalitatieve en kwantitatieve TAP werd gebruikt om onze kennis te vergroten over het SMAX1 interactoom, wat resulteerde in nieuwe kandidaateiwitten voor verdere studies. Van alle eiwitten die samen met MAX2 werden opgezuiverd werden twee kandidaten geselecteerd voor verder onderzoek: PAPP5 en CCP1. Het eiwitfosfatase PAPP5 en katanine-gerelateerde CCP1 lijken uitsluitend gelinkt te zijn aan de karrikin-pathway die de zaadkieming beïnvloedt en, in het geval van CCP1, ook de verlenging van het hypocotyl. Daarentegen

is aangetoond dat het eiwit ACD32.1, geïdentificeerd als een interactiepartner van KAI2, rechtstreeks interageert met alle bekende componenten van zowel de strigolacton- als de karrikine- signalisatie maar de exacte rol ervan in beide cascades moet nog worden bepaald.

In conclusie, door de ontdekking van nieuwe spelers in de strigolacton en karrikine signaaltransductie netwerken leveren we een belangrijke bijdrage tot het begrijpen van het moleculair mechanisme van beide pathways die resulteren in de uitvoering van de downstream fysiologische responsen.

Table of Contents

Abbreviations

A.	Arabidopsis
ABC	ATP BINDING CASSETTE
ABI	ABSCISIC ACID INSENSITIVE
ACD	ALPHACRYSTALLIN DOMAIN
ACT	ACTIN
AD	activation domain
ADE	phosphoribosylaminoimidazole carboxylase
AE	affinity enrichment
AGI	Arabidopsis Genome Identifier
AM	arbuscular mycorrhiza
AN	ANGUSTIFOLIA
ANL	ANTHOCYANINLESS
ANOVA	Analysis of variance
ACR	ARABIDOPSIS CRINKLY
ARF	AUXIN RESPONSE FACTOR
ASK	ARABIDOPSIS SKP1 HOMOLOGUE
Asp	Asparagine
ATJ	DNAJ HOMOLOGUE
Aux	AUXIN
BAK	BRI1-ASSOCIATED KINASE
BD	binding domain
BES	BRASSINOLIDE-INSENSITIVE1-EMS-SUPPRESSOR
bHLH	basic helix–loop–helix
BiFC	Bimolecular Fluorescent Complementation
BioID	proximity-dependent biotin identification
BRC	BRANCHED
BRET	Bioluminescence Resonance Energy Transfer
BRI	BRASSINOSTEROID INSENSITIVE
BY	Bright Yellow
BZR	BRASSINAZOLE RESISTANT
C	carboxy
CCCH	Cysteine3Histidine
CCD	CAROTENOID CLEAVAGE DIOXYGENASE
CCP	ONSERVED IN CILIATED SPECIES AND IN THE LAND PLANTS

CCR	Carbon catabolite repressed
cDNA	complementary DNA
CHS	chalcone synthase
CLIM	covalently linked intermediate molecule
CLV	CLAVATA
COI	CORONATINE-INSENSITIVE
co-IP	co-immunoprecipitation
Col-0	Columbia-0
COP	CONSTITUTIVE PHOTOMORPHOGENIC
CSN	COP SIGNALOSOME
CTLH	C-Terminal Lissencephaly Homology
CUL	CULLIN
D	DWARF
DAD	DECREASED APICAL DOMINANCE
DLK	D14-LIKE
DNA	Deoxyribonucleic acid
EAR	ETHYLENE RESPONSE FACTOR
EMS	EPITHIOSPECIFIER MODIFIER
ent	enantiomer
ER	endoplasmic reticulum
FCCS	fluorescence cross-correlation spectroscopy
FCS	fluorescence correlation spectroscopy
FDR	false discovery rate
flg	flagellin
FLIM	fluorescence lifetime imaging microscopy
FLuc	firefly luciferase
FLuCI	floated-leaf luciferase complementation imaging
FRET	Förster/Fluorescence resonance energy transfer
FyPP	PHYTOCHROME-ASSOCIATED PROTEIN PHOSPHATASE
GA	gibberellic acid
GFP	GREEN FLUORESCENT PROTEIN
GID	GIBBERELLIN INSENSITIVE DWARF
GR	Gerald Roseberry
GRF	GROWTH-REGULATING FACTOR
GUS	β-glucuronidase
GS	G/streptavidin-binding peptide
HDA	HISTONE DEACETYLASE
HDC	HISTONE DEACETYLATION COMPLEX
HEPES	4-(2-hydroxyethyl)-1-piperazineethanesulfonic acid
His	Histidine
HIS	imidazoleglycerolphosphate dehydratase

HSP	Heat shock protein
HTL	HYPOSENSITIVE TO LIGHT
HY	ELONGATED HYPOCOTYL
IAA	indole-3-acetic acid
JAL	JACALIN-RELATED LECTIN
JAZ	JASMONATE ZIM-DOMAIN
JKD	JACKDAW
KAI	KARRIKIN INSENSITIVE
KAR	karrikin
KL	KAI2-ligand
KTN	KATANIN
LBO	LATERAL BRANCHING OXIDOREDUCTASE
LC	liquid chromatography
LFQ	label-free quantification
Lj	*Lotus japonicus*
LR	Lateral root
LRD	Lateral root density
LT	Leucine-Tryptophan
LTH	Leucine-Tryptophan-Histidine
MAX	MORE AXILLARY GROWTH
MFIS	multiparameter fluorescence image spectroscopy
MOT	Modulator Of Transcription
MS	Murashige and Skoog
MS	Mass spectrometry
Mt	*Medicago truncatula*
N	amino
NINJA	Novel Interactor of JAZ
nM	nanomolar
NOT	negative on TATA-less
OD	optical density
ONPG	O-nitrophenyl β-D-galactopyranoside
ORF	open reading frame
PAMP	pathogen-associated molecular pattern
PAP	peroxidase-antiperoxidase
PAPP	PHYTOCHROME-ASSOCIATED PROTEIN PHOSPHATASE
PCA	protein fragment complementation assay
PCR	polymerase chain reaction
PEG	polyethylene glycol
PDR	PLEIOTROPIC DRUG RESISTANCE
PHY	phytochrome
PIN	PIN-FORMED

PMSF	phenylmethylsulfonyl fluoride
POI	protein of interest
PP	PROTEIN PHOSPHATASE
PPI	protein–protein interaction
PPP	phosphoprotein phosphatase
PRR	pattern recognition receptor
PTAC	PLASTID TRANSCRIPTIONALLY ACTIVE
PTI	PRR- triggered immunity
PTM	posttranslational modification
PVDF	polyvinylidene fluoride
q	quantitative
qRT-PCR	quantitative reverse-transcription polymerase chain reaction
rac	racemic
rLUC	Renilla luciferase
RBX	RING-BOX
RCN	ROOTS CURL IN NAPHTHYLPHTHALAMIC
RFP	red fluorescent protein
rms	ramosus
RNA	ribonucleic acid
ROS	reactive oxygen species
SAL	SIT4 phosphatase-associated
SAP	SIN3 ASSOCIATED POLYPEPTIDE
SAP	SIT4-associated protein
SCF	Skp1-Cullin-F-box
SD	Synthetic Defined
SDS	sodium dodecyl sulfate
SDS-PAGE	sodium dodecyl sulphate-polyacrylamide gel electrophoresis
SE	standard error
SEC	exocyst complex component
Ser	Serine
Sh	*Striga hermonthica*
SHR	SHORT-ROOT
SILAC	stable isotope labelling with amino acids in cell culture
SINT	SMXL7 INTERACTING PROTEIN
SIS	*Strigolactone-induced putative secreted protein*
SKP	S-PHASE-KINASE-ASSOCIATED-PROTEIN
SL	strigolactone
Sm	*Selaginella moellendorfii*
SMAX	SUPPRESSOR OF MAX2
SMXL	SUPPRESSOR OF MAX2 1 LIKE
SOE	Spliced Overlap Extension

SRET	sequential BRET-FRET
TAP	tandem affinity purification
TCA	trichloroacetic acid
T-DNA	transfer DNA
TEV	Tobacco Etch Virus
TIR	TRANSPORT INHIBITOR RESPONSE
TPL	TOPLESS
TRM	TRNA METHYLTRANSFERASE
TPR	TOPLESS-RELATED
TPR	tetratricopeptide repeat
UBC	Ubiquitin-conjugating enzyme
UBP	Ubiquitin-specific protease
WT	Wild type
X-gal	5-bromo-4-chloro-3-indolyl-β-D-galactopyranoside
Y2H	yeast 2-hybrid
Y3H	yeast 3-hybrid
YFP	yellow fluorescent protein
Zm	*Zea mays*

Scope of research

Strigolactones are a unique class of plant hormones that act as endogenous compounds but also as signaling molecules in the rhizosphere. As hormones, strigolactones regulate many physiological processes including shoot branching, root architecture or leaf shape and senescence. While, after exudation into the soil, they promote symbiosis with arbuscular mycorrhizal fungi and detrimental interactions with parasitic plants. On the contrary, karrikins are smoke-derived compounds that stimulate seed germination of fire-following plant species. Although these molecules are not synthesized inside plants, there are hints of yet unidentified endogenous compound referred to as KARRIKIN INSENSITIVE 2 (KAI2) ligand. A strong connection between strigolactones and karrikins is observed through comparison of their chemical structures as well as their signaling pathways, which include common and related protein components. In the recent years fundamental breakthroughs have been made by identifying the likely receptors and their downstream targets, yet key pieces are missing in our understanding of these signaling cascades. During this PhD project, we aimed at further expanding our knowledge on the strigolactone and karrikin signaling network, by investigating the protein complexes that are formed with the known components of these pathways by means of tandem affinity purification (TAP). Newly identified players are further characterized using biochemical and genetic approach and are positioned in the available strigolactone and karrikin regulatory network map to understand their role in plant development and/or rhizosphere interactions.

The first part of my thesis is an introductory overview of the most recent findings in strigolactone and karrikin research and of the techniques used to identify the key protein players and their interaction networks in plants. In **Chapter 1** the current model of strigolactone and karrikin signaling is presented with a critical overview of the different biological processes they regulate as well as their overlapping functions in plant development. This is followed by **Chapter 2,** in which we describe in detail commonly used techniques for the discovery and validation of protein-protein interactions and discuss the unique features of each of them, that might help plant scientists to choose the most appropriate method to answer their research question.

The second part contains the research chapters that describe in detail the main findings of this thesis. In each chapter TAP is used to identify protein complexes involved in strigolactone and/or karrikin signaling. The first three research chapters are focused on getting deeper inside into SUPPRESSOR OF

MAX2 1 (SMAX1)-LIKE (SMXL) 7 interaction network in *Arabidopsis* cell cultures. In **Chapter 3,** TAP is combined with label-free quantification (LFQ) allowing quantitative analysis of changes in the protein complexes formed around the bait in the presence and absence of *rac*-GR24. Novel interactors of SMXL7 detected by the standard, qualitative TAP analyses are further characterized in **Chapter 4** and **Chapter 5.** In **Chapter 6** we focus on SMAX1, provide evidence for its degradation and validate interactions with the known core components of karrikin pathway. We further expand our knowledge of the SMAX1 interactome using the qualitative and quantitative TAP analysis and propose some candidate proteins to study in the future. In **Chapter 7** and **Chapter 8** the F-box protein MORE AXILLARY GROWTH 2 (MAX2), a central player in both pathways and the receptors DWARF 14 (D14) and KAI2 are selected as the bait proteins to co-purify complexes in *Arabidopsis* cell cultures and seedlings, respectively. Newly identified interactors are studied in depth by biochemical and phenotypic analysis in order to understand their role in both signaling pathways.

In the final part of my thesis, the obtained results are discussed and placed in a broader context. We also present the main conclusions and future perspectives on how the research on our new players can be continued.

I

INTRODUCTION

Chapter 1

Strigolactones, karrikins and beyond

Modified from De Cuyper et al. 2017

Carolien De Cuyper[1,2], Sylwia Struk[1,2], Lukas Braem[1,2,3,4], Kris Gevaert[3,4], Geert De Jaeger[1,2] & Sofie Goormachtig[1,2]

[1] Ghent University, Department of Plant Biotechnology and Bioinformatics, 9052 Ghent, Belgium,
[2]VIB, Center for Plant Systems Biology, 9052 Ghent, Belgium,
[3]Ghent University, Department of Biochemistry, 9000 Ghent, Belgium,
[4]VIB, Center for Medical Biotechnology, 9000 Ghent, Belgium

Author contributions: C.D.C. was the main author of the manuscript. S.S. and L.B. performed the literature search and contributed to the writing. S.G. supervised the project and contributed to writing of the manuscript.

ABSTRACT

The plant hormones strigolactones are synthesized from carotenoids and signal via the α/β hydrolase DWARF 14 (D14) and the F-box protein MORE AXILLARY GROWTH 2 (MAX2). Karrikins, molecules produced upon fire, share MAX2 for signaling, but depend on the D14 paralog KARRIKIN INSENSITIVE 2 (KAI2) for perception with strong evidence that the MAX2-KAI2 protein complex might also recognize so far unknown plant-made molecules referred to as KAI2 ligand. Thus, the phenotypes of the *max2* mutants are the complex consequence of a loss of both D14- and KAI2-dependent signaling, hence the reason why some biological roles, attributed to strigolactones based on *max2* phenotypes, could never be observed in *d14* or in the strigolactone-deficient *max3* and *max4* mutants. Moreover, the broadly used synthetic strigolactone analog *rac*-GR24 has been shown to mimic strigolactone as well as karrikins/KAI2 ligand, providing an extra level of complexity in the distinction of the unique and common roles of both molecules in plant biology. Here, a critical overview is provided of the diverse biological processes regulated by strigolactones and/or karrikins. These two growth regulators are considered beyond their boundaries and the importance of the yet unknown KAI2 ligand is discussed as well.

STRIGOLACTONES AND KARRIKINS, THE MAKING OF

Strigolactones are plant-made signaling compounds consisting of a tricyclic lactone, the ABC scaffold that is connected by means of an enol ether unit to a butenolide ring, referred to as the D-ring (Zwanenburg & Pospíšil 2013) (Figure 1). The first strigolactone compound was isolated from root exudates of cotton (*Gossypium hirsutum*) and was designated strigol, based on its ability to stimulate seed germination of the parasitic plant *Striga lutea* (Cook et al. 1966). Striga plants are known as witchweeds, referring to the mythical witch Striga, who sucked blood of infants at night (Spallek et al. 2013). As more strigol-related compounds were discovered, these parasitic seed germination-inducing molecules were generally called strigolactones based on their functional similarity with strigol and their lactone ring-containing chemical structure (Butler 1995). To date, the structure of at least 20 different naturally occurring strigolactones has been characterized (Tokunaga et al. 2015). Due to their low concentration and chemical instability, the isolation of strigolactones is challenging, making only limited amounts available for scientific purposes. However, in compensation, different strigolactone analogs, abbreviated as GR, after their inventor Gerald Rosebery (Johnson et al. 1981), have been synthesized (Zwanenburg & Pospíšil 2013), of which GR24 is the most active and widely used in strigolactone research (Besserer et al. 2008) (Figure 2).

Strigolactones are synthesized from carotenoids through the consecutive action of a β-carotene isomerase and two carotenoid cleavage dioxygenases, CCD7 and CCD8, known as *At*D27, MORE AXILLARY GROWTH 3 (MAX3), and MAX4 in *Arabidopsis thaliana*, respectively (Matusova et al. 2005; Gomez-Roldan et al. 2008; Umehara et al. 2008; Lin et al. 2009; Waters et al. 2012a) (Figure 1). Together, they give rise to the strigolactone intermediate carlactone, a bioactive molecule that can rescue several strigolactone mutant phenotypes (Alder et al. 2012). Downstream, the cytochrome P450-encoding MAX1 protein oxidizes carlactone to produce carlactonoic acid that is further converted by an unknown enzyme to methyl carlactonoate (Booker et al. 2005; Kohlen et al. 2011; Alder et al. 2012; Seto et al. 2014; Zhang et al. 2014). Furthermore, the recently reported LATERAL BRANCHING OXIDOREDUCTASE (LBO) facilitates the conversion of methyl carlactonoate to an unknown strigolactone-like compound, which is required for the suppression of shoot branching (Brewer et al. 2016). Although many insights into strigolactone biosynthesis are now available, it remains unclear whether *Arabidopsis* synthesizes canonical strigolactones or only carlactone-derived molecules (Kohlen et al. 2011; Abe et al. 2014).

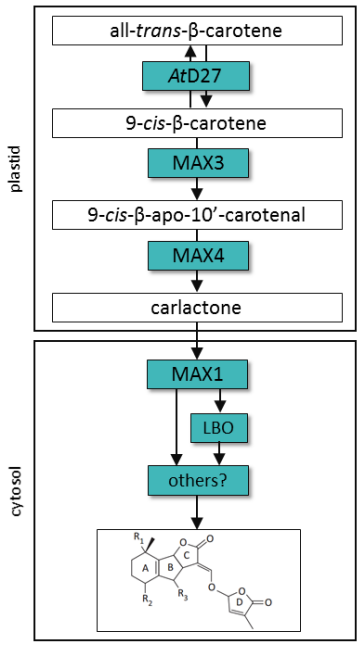

Figure 1. Strigolactone biosynthesis in *Arabidopsis.* Initial steps in strigolactone biosynthesis in the plastids involve the conversion of carotenoids to the mobile strigolactone precursor carlactone via the consecutive action of the β-carotene isomerase D27 and the carotenoid cleavage dioxygenases (CCDs) MAX3 and MAX4. In the cytosol, carlactone is converted into strigolactones through the cytochrome P450 MAX1, LBO, and other unknown enzymes. For orthologous genes regulating strigolactone biosynthesis in other species, see Table 1. Abbreviations: MAX, MORE AXILLARY GROWTH.

Karrikins relate to strigolactones because they share a substituted butenolide moiety (Flematti et al. 2004). In contrast, karrikin molecules are not produced by the plant itself, but are formed by heating or combustion of carbohydrates, such as cellulose (Flematti et al. 2011). As a result, karrikins are found in smoke from burning vegetation and play a main role in activating germination of dormant seeds. Indeed, smoke derived from burning plant material has been shown to positively affect seed germination of more than 1,200 plant species from 80 different genera, including *Arabidopsis* (Chiwocha et al. 2009). The main bioactive compound responsible for smoke-induced germination has been characterized as the chemical 3-methyl-2*H*-furo[2,3-*c*] pyran-2- one (Flematti et al. 2004; van Staden et al. 2004). To induce seed germination, the pyran moiety of karrikins is important, although slight modifications can be tolerated (Flematti et al. 2007, 2010). Later on, other compounds with similar structures and bioactivities were identified and were collectively designated as karrikins, based on the word 'karrik', the aboriginal term for smoke used by Australian Noongar people (Chiwocha et al. 2009). Until now, six karrikin or KAR molecules, annotated as KAR_1 to KAR_6, have been identified in plant-derived smoke, differing in their methyl substitutions (Flematti et al. 2009). The first karrikin discovered, KAR_1, is the main seed germination stimulant and is known as karrikinolide, in which the 'olide' suffix refers to the lactone group in the chemical structure (Dixon et al. 2009) (Figure 2). In addition, almost 50 karrikin analogs have been synthesized, all with different substitutions (Flematti et al. 2007; Goddard-Borger et al. 2007; Sun et al. 2008).

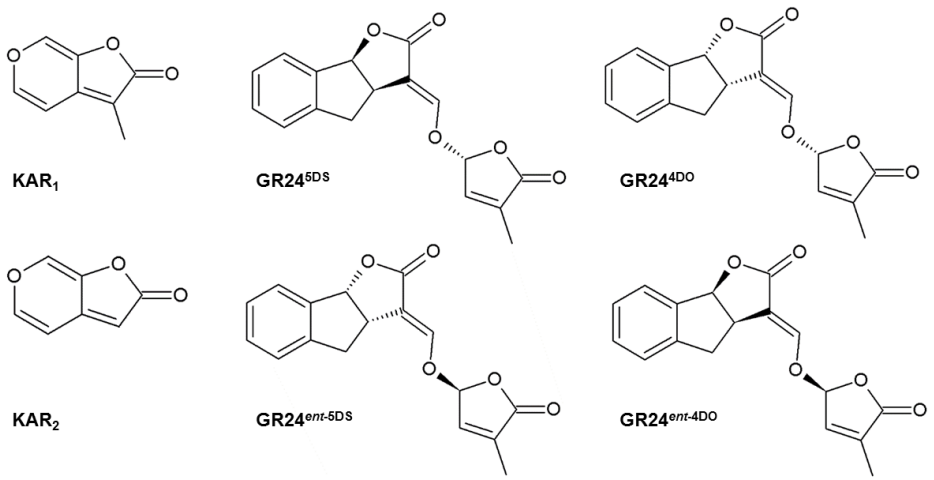

Figure 2. Chemical structures of karrikins and four GR24 stereoisomers. Structures of two karrikin representatives (KAR_1 and KAR_2) are shown. Commonly used in research is the synthetic strigolacone analog *rac*-GR24, which is a mixture of $GR24^{5DS}$ and its enantiomer $GR24^{ent\text{-}5DS}$. The enantiomers $GR24^{4DO}$ and $GR24^{ent\text{-}4DO}$ are also generated during the chemical synthesis of GR24, but these compounds are typically discarded and not used for biological assays.

IT'S ALL ABOUT MAX2

Although strigolactones and karrikins have different origins, they share highly similar perception and signaling components, including MAX2 (Stirnberg et al. 2007; Gomez-Roldan et al. 2008; Umehara et al. 2008; Nelson et al. 2011) (Figure 4). As an F-box protein, MAX2 confers substrate specificity to the Skp1-Cullin-F-box (SCF) class of E3 ligase complexes that ubiquitinate specific target proteins to mark them for proteolysis by the 26S proteasome (Stirnberg et al. 2007; Vierstra 2009). MAX2 belongs to the leucine-rich-repeat subfamily of F-box proteins, which also includes the well-known auxin receptor TRANSPORT INHIBITOR RESPONSE 1 (TIR1) and the jasmonate receptor CORONATINE-INSENSITIVE 1 (COI1) (Xie et al. 1998; Stirnberg et al. 2002; Dharmasiri et al. 2005; Kepinski & Leyser 2005; Sheard et al. 2010). Upon auxin binding, TIR1 directly interacts with AUXIN/INDOLE-3-ACETIC ACID (Aux/IAA) repressor proteins, thereby marking them for proteasomal degradation. As a result, the repression of the AUXIN RESPONSE FACTOR transcription factors is relieved and auxin-responsive genes are activated (Peer 2013). Similarly, jasmonate perception by COI1 promotes the interaction and degradation of JASMONATE ZIM DOMAIN (JAZ) repressor proteins, thereby releasing the repression of transcription factors, such as MYC2, that further activate jasmonate response genes (Gfeller et al. 2010). In the absence of auxin or jasmonate, transcription is repressed by TOPLESS or TOPLESS-RELATED corepressor proteins that interact with the Aux/IAA repressors or Novel Interactor of JAZ

(NINJA) adaptor proteins via an ETHYLENE RESPONSE FACTOR-associated amphiphilic repression (EAR) motif (Szemenyei et al. 2008; Pauwels et al. 2010).

Table 1. Strigolactone biosynthesis and signaling genes in different species

Function	*Arabidopsis thaliana* (thale cress)	*Oryza sativa* (rice)	*Pisum sativum* (pea)	*Petunia hybrida* (petunia)	*Medicago truncatula* (barrel medic)	*Lotus japonicus* (lotus)
Biosynthesis						
9-cis/all-*trans*-β-carotene isomerase	*AtD27*	*D27*			*MtD27*	
Carotenoid cleavage dioxygenase 7 (CCD7)	*MAX3*	*D17/HTD1*	*RMS5*	*DAD3*	*MtCCD7*	*LjCCD7*
Carotenoid cleavage dioxygenase 8 (CCD8)	*MAX4*	*D10*	*RMS1*	*DAD1*	*MtCCD8*	
Cytochrome P450	*MAX1*	*OsMAX1*		*PhMAX1*		
Lateral branching oxidoreductase	*LBO*					
Perception and signaling						
α/β Hydrolase	*AtD14*	*D14/D88/HTD2*	*RMS3*	*DAD2*	*MtD14*	
F-box protein	*MAX2*	*D3*	*RMS4*	*PhMAX2*		
				PhMAX2B		
Class I Clp ATPase protein	*SMXL6*					
	SMXL7	*D53, D53-LIKE*				
	SMXL8					
TCP transcription factor	*BRC1*	*OsTB1*	*PsBRC1*			
	BRC2					

Genetic and biochemical studies revealed a similar mode of action for MAX2-dependent signaling. Target of MAX2, SUPPRESSOR OF MAX2 1 (SMAX1) has been identified in *Arabidopsis* by the ethyl methanesulfonate (EMS) mutagenesis screen for the genetic suppressor of the enhanced seed dormancy phenotype of *max2* mutant (Stanga et al. 2013). Simultaneously, a naturally occurring rice (*Oryza sativa*) mutant *e9* was characterized as a dominant SL-insensitive mutant *dwarf 53* (*d53*) (Jiang et al. 2013; Zhou et al. 2013). These proteins have been shown to function as signaling repressors that are degraded upon treatment with the synthetic strigolactone analog *rac*-GR24 (Jiang et al. 2013; Stanga et al. 2013; Zhou et al. 2013). The SMAX1-LIKE (SMXL) family consists of eight members (Stanga et al. 2013), for which different specificities and activities have been proposed with a functional separation into strigolactone and karrikin signaling factors. Members of the subclade 1, SMAX1 and SMXL2, are involved in karrikin signaling, whereas the subclade 4, containing the SMXL6, SMXL7, and SMXL8 proteins, mediate strigolactone signaling (Soundappan et al. 2015). Members of subclade 2, SMXL3, and subclade 3, SMXL4 and SMXL5, play a role in phloem development independent of strigolactone and karrikin (Wallner et al., 2017). In rice, D53 assembles with the SMXL6, SMXL7, and SMXL8 phylogenetic clade (Figure 3) (Zhou et al. 2013; Soundappan et al. 2015).

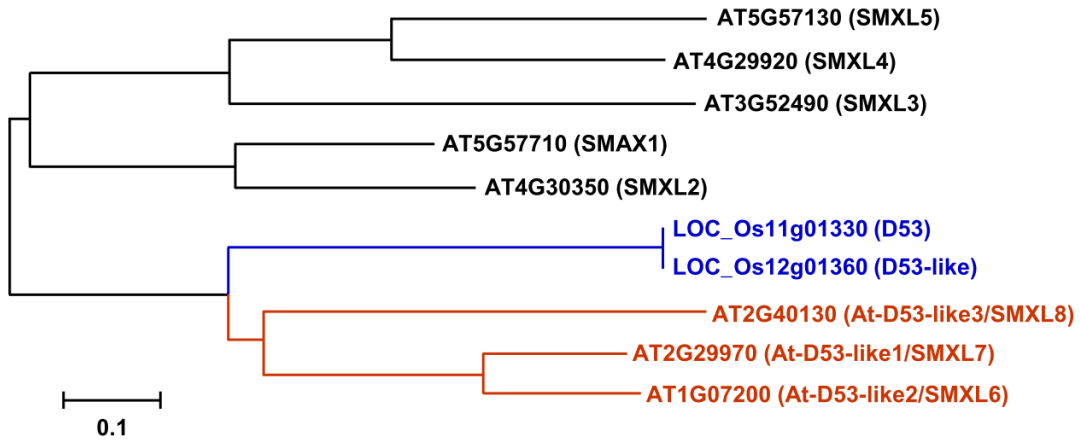

Figure 3. Phylogenetic tree of D53 (-like), and SMXL family proteins. The *Arabidopsis* D53-like1/SMXL7, D53-like2/SMXL6, and D53-like3/SMXL8 proteins (shown in orange) are here classified as D53-like SMXLs. The rice orthologs are shown in blue. Figure modified from Wang et al. 2015.

The molecular role of the SMXL proteins is still obscure, but, based on their size (approximately 1,000 amino acids), a broad network of interacting proteins is assumed. SMXL/D53 proteins are characterized by a conserved C-terminal EAR motif and can, therefore, function as transcriptional repressors, analogously to the Aux/IAA and JAZ-NINJA proteins (Jiang et al. 2013; Soundappan et al. 2015; Wang et al. 2015). However, SMXL7 was found to regulate some aspects of shoot development in a partially EAR motif-independent manner, suggesting that distinct mechanisms, besides transcriptional regulation, are at play downstream of the SMXL proteins (Liang et al. 2016). Alternatively, because SMXL proteins are most closely related to the molecular chaperones Heat shock protein 100/Caseinolytic peptidase B (Hsp100/ClpB), known to unravel protein aggregates in an ATP-dependent manner, they might play a role in unfolding or remodeling protein complexes (Jiang et al. 2013; Stanga et al. 2013; Zhou et al. 2013).

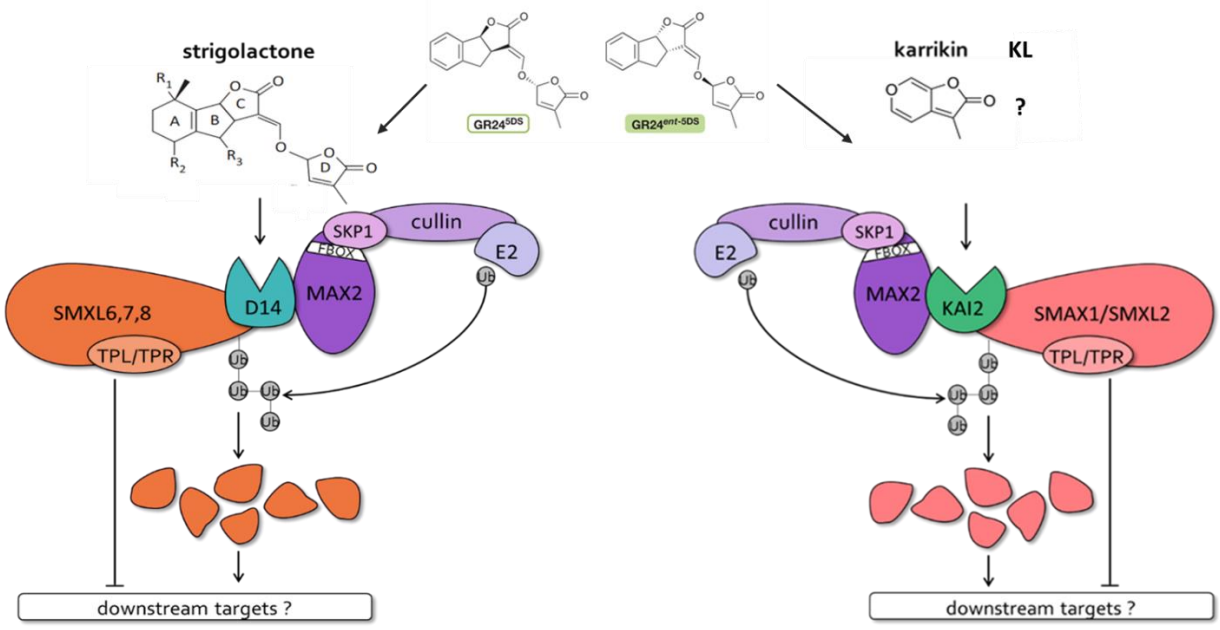

Figure 4. Protein interaction network in strigolactone signaling and presumed interactions in karrikins/KAI2 ligand signaling. Signaling components specific for strigolactones and karrikins/KAI2 ligand (KL) molecules are represented on the left and right, respectively. Strigolactones are perceived via D14 after which SMXL6,7,8 are ubiquitinated and degraded to activate unknown downstream targets. In analogy but not demonstrated yet, recognition of karrikins/KAI2 ligand is expected to induce ubiquitination and degradation of SMAX1/SMXL2 to activate downstream responses. The commonly used in research strigolactone analog *rac*-GR24 is a mixture of two enantiomers from which GR24^{5DS} activates D14 signaling, while GR24$^{ent\text{-}5DS}$ acts via KAI2 pathway.

WHAT YOU PERCEIVE IS WHAT YOU RECEIVE

Besides the F-box protein MAX2, a crucial role for α/β hydrolases has been described in strigolactone as well as karrikin signaling (Figure 4). Indeed, the α/β hydrolase D14 and its paralog KARRIKIN INSENSITIVE 2 (KAI2) are characterized as the strigolactone and karrikin receptors in *Arabidopsis*, respectively, whereas orthologs have been found in other species as well (Arite et al. 2009; Hamiaux et al. 2012; Waters et al. 2012b; Guo et al. 2013; Nakamura et al. 2013; Zhao et al. 2015; Marzec et al. 2016; de Saint Germain et al. 2016; Zheng et al. 2016). KAI2 is also designated as D14-LIKE, because of its structure similar to that of D14 and, additionally, can be referred to as HYPOSENSITIVE TO LIGHT (HTL) (Sun & Ni, 2011; Waters et al. 2012b). In *Arabidopsis*, besides KAI2, a second protein with high similarity to D14 has been identified as D14-LIKE 2 (DLK2) (Waters et al. 2012b). Despite the structural similarity to D14, DLK2 is not able to bind and hydrolyze natural 5DS but weakly hydrolyzes its non-

natural enantiomer ent-5DS. Moreover, DLK2 does not influense strigolactone responses, but it was proposed to act independently of MAX2 to regulate seedling photomorphogenesis (Vegh et al., 2017).

Chemical and structural biology provided in-depth insight into the mode of action of the strigolactone signaling complex. Binding or hydrolysis of strigolactones by D14 has already been reported in *Arabidopsis*, petunia (*Petunia hybrida*), and rice (Hamiaux et al. 2012; Kagiyama et al. 2013; Zhao et al. 2013). Recently it was shown that while D14 is binding and hydrolyzing a strigolactone molecule, a conformational change is induced in the protein (Yao et al. 2016). This D14 enzymatic activity requires the conserved Ser-His-Asp catalytic triad in a hydrophobic active site and causes the D-ring to dissociate from the ABC scaffold though a nucleophilic attack, whereafter the D-ring is transiently connected to the Ser96 residue (Scaffidi et al. 2012; Zhao et al. 2013). Subsequently, a covalent bond is formed between the His247 residue and the D-ring, resulting in a covalently linked intermediate molecule (CLIM). This irreversible binding between ligand and receptor has not been described before in plant hormone signaling, thus making D14 a non-canonical plant hormone receptor (Yao et al. 2016; de Saint Germain et al. 2016). In petunia, none of the strigolactone hydrolysis products are able to rescue the shoot branching phenotype of the *d14*/*dad2* mutant, hinting at a lack of biological activity (Hamiaux et al. 2012). Binding of the D-ring provokes a thermal protein destabilization of the D14 homologs of several plant species, as revealed by differential scanning fluorimetry assays (Hamiaux et al. 2012; Nakamura et al. 2013; Zhao et al. 2015; de Saint Germain et al. 2016). Recently, X-ray crystallography analysis of D14 in complex with D3 and ARABIDOPSIS SKP1 HOMOLOGUE 1 (ASK1) showed that the D14 conformational change into the closed state occurs because the D-ring becomes trapped inside the binding pocket. This conformational shift allows the binding of the D3/MAX2 protein to the receptor and may also facilitate an interaction between the D14 and SMXL proteins (Yao et al. 2016). This finding is further supported by yeast 2-hybrid (Y2H) and pull-down experiments in *Arabidopsis*, rice, and petunia confirming that the nuclear interactions of D14 with MAX2/D3 or with SMXL6,SMXL7,SMXL8/D53 are improved after treatment with *rac*-GR24 (Hamiaux et al. 2012; Zhou et al. 2013; Jia et al. 2014; Zhao et al. 2014, 2015; Umehara et al. 2015; Wang et al. 2015). Study of the *d14-5* mutant allele revealed that the enzymatic activity of D14 is not sufficient for the activation of the downstream signal transduction. This mutated receptor had an increased hydrolytic activity *in vitro*, but was unable to undergo conformational changes, ultimately leading to a strigolactone-insensitive phenotype. This Gly158→Glu substitution in the D14 protein impaired the *rac*-GR24-dependent interaction with MAX2, but not with SMXL6, suggesting that different conformational changes are needed for the interaction with the signaling repressor (Yao et al. 2016). Similarly, in *d14-2*/*seto5 Arabidopsis* mutants, the strigolactone-insensitive phenotype is caused by the mutation

located on the surface of the protein, probably involved in protein-protein interactions rather than in strigolactone hydrolysis (Chevalier et al. 2014).

In summary, the biological activity of the receptor has currently been proposed to require the formation of the D14-MAX2 complex that is triggered by strigolactone hydrolysis (Yao et al. 2016). However, the direct interaction between MAX2/D3 and SMXL6,SMXL7,SMXL8/D53 remains unclear. In pull-down and co-immunoprecipitation assays, MAX2/D3 and SMXL6,SMXL7,SMXL8/D53 interacted independently of the *rac*-GR24 treatment or of D14 (Jiang et al. 2013; Wang et al. 2015), whereas no direct physical interaction between MAX2 and SMXL7 was observed *in planta* by means of Förster resonance energy transfer (FRET) with fluorescence lifetime imaging microscopy (FLIM) (Liang et al. 2016). Hence, the D14 protein might evenly act as a bridge to bring SMXL6,SMXL7,SMXL8/D53 in close proximity to SCF^{MAX2} to allow ubiquitination.

Compared to the D14 signaling, the mode of action of KAI2 is less clear. The hydrophobic pocket in which the catalytic triad is located is smaller than that of D14, suggesting binding of smaller molecules (Bythell-Douglas et al. 2013; Guo et al. 2013; Kagiyama et al. 2013). However, although binding of KAR_1 to KAI2 has been demonstrated (Guo et al. 2013; Nakamura et al. 2013), KAR hydrolysis is not expected because of its chemical properties (Zhao et al. 2013, 2015). Nevertheless, just like for D14, the catalytic triad is also required for the KAI2 functionality and thermal destabilization can be induced upon treatment with the unnatural 2'S strigolactone stereoisomer, but not with karrikins (Waters et al. 2015b). Moreover, crystal structure studies of KAI2 with KAR_1 attached to the binding pocket in *Arabidopsis* and *Striga hermonthica* show different orientations of the molecule and a conformational change of the receptor, similar to what was described for D14, has not been described (Guo et al. 2013; Xu et al. 2016). Although in *Arabidopsis* the interaction between KAI2 and MAX2 has been detected by Y2H (Toh et al. 2014), whether KAI2 interacts with SMAX1/SMXL2 and whether this interaction can be enhanced by KAR or *rac*-GR24 still need to be determined. Following perception of *rac*-GR24 and KAR, D14 and KAI2 themselves are degraded as well, in a MAX2-dependent and MAX2-independent manner, respectively, suggesting that a feedback regulation mechanism is at play to dampen further signaling (Chevalier et al. 2014; Waters et al. 2015a). Recent study in rice revealed that strigolactone-induced D14 degradation occurs following D53 degradation and is strongly correlated with level of D53 protein. Moreover, a point mutation at Lys280 of the D14 amino acid sequence was proven to be important for its degradation but had only slight effect on the signal transduction (Hu et al., 2017a).

THE MORE THE MERRIER: A KAI2 LIGAND

Many species, including *Arabidopsis* and several crop species, that do not occur in fire-prone regions, are able to respond to karrikins, although they are not under selective pressure to retain this capacity (Flematti et al. 2004; Stevens et al. 2007; Long et al. 2011). Hence, KAI2 potentially perceives still unknown plant-made molecules, KAI2 ligand (Waters et al. 2012b; Conn & Nelson 2016). Indeed, in addition to the lack of response to karrikins, *kai2* mutants also display developmental defects that support a role for KAI2 in the perception of a yet unidentified signal. Accordingly, KAI2 is not only expressed in seeds, but also in seedlings and adult plants (Sun & Ni 2011). Phylogenetic analysis backs up the idea of the existence of a KAI2 ligand. In fact, KAI2, but not D14 orthologs, were identified in basal land plants, indicating that the *KAI2* gene is ancestral and that the functional specialization of the *D14* gene has evolved subsequently from an ancient *KAI2* duplication (Delaux et al. 2012; Waters et al. 2012b). Moreover, cross-species complementation studies revealed that the KAI2 ortholog *Sm*KAI2a from the lycophyte *Selaginella moellendorfii* could partially rescue the phenotypes of *Arabidopsis kai2* mutants, but the transgenic lines did not confer responses to KAR or *rac*-GR24. Consequently, KAI2 has been hypothesized to serve in basal plants as a receptor for an unknown endogenous KAI2 ligand and karrikin and strigolactone perception have been proposed to have evolved later on (Conn & Nelson 2016).

Determination of the specific roles of strigolactone and karrikin/KAI2 ligand signals during plant development has been challenging and is still ongoing. Indeed, *max2* phenotypes are the sum of *d14* and *kai2* phenotypes, resulting from the loss of signaling depending on both D14 and KAI2 (Waters et al. 2012b; Soundappan et al. 2015; Conn & Nelson 2016). In agreement, several early transcriptional response markers have revealed that *Arabidopsis max2* mutants are completely insensitive to both KAR_1 and *rac*-GR24 treatments (Nelson et al. 2011; Waters et al. 2012b). Hence, before karrikins had been shown to use a signaling pathway similar to that of strigolactones with MAX2 as a key component, some phenotypes of *max2* were falsely attributed to strigolactone signaling and could, therefore not be observed in *d14* or strigolactone-deficient mutants (Nelson et al. 2011; Shen et al. 2012). Another level of complexity hampering the discrimination of the biological roles of strigolactones and karrikin/KAI2 ligand has been added by the synthetic and broadly used strigolactone analog *rac*-GR24 that mimics both strigolactone and karrikin/KAI2 ligand responses. Indeed, *rac*-GR24 is an equimolar racemic mixture of a natural strigol-like molecule $GR24^{5DS}$ that activates the D14-dependent signal transduction and its unnatural enantiomer $GR24^{ent\text{-}5DS}$ that initiates KAI2-specific signaling (Scaffidi et al. 2014) (Figure 5). Chemical studies indicated that $GR24^{ent\text{-}5DS}$ can bind D14 as well, but without

support of physiological experiments until now (Nakamura et al. 2013; Scaffidi et al. 2014; Waters et al. 2015a; Flematti et al. 2016).

STRIGOLACTONES VERSUS KARRIKIN/KAI2 LIGAND, LET THE GAME BEGIN

Strigolactones and karrikins/KAI2 ligand molecules mainly regulate different biological processes, but overlapping functions have been reported as well, in which both molecules can have either similar or opposite effects (Figure 5).

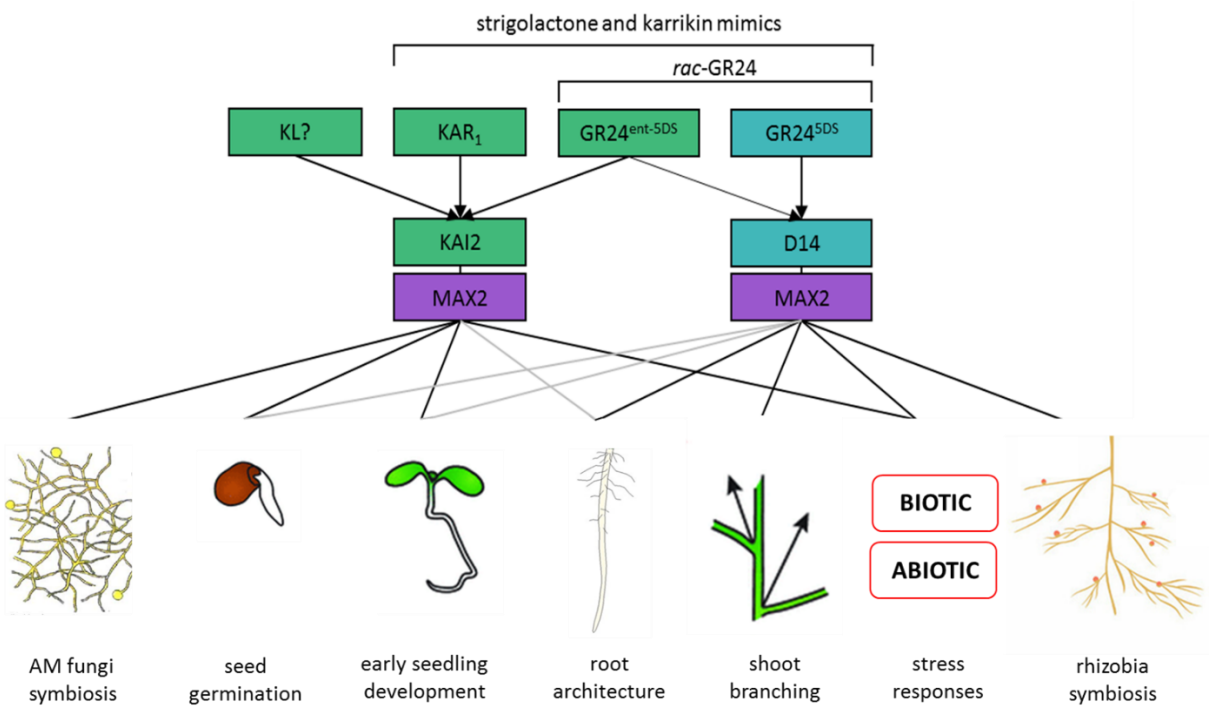

Figure 5. Different biological processes regulated by strigolactone and karrikin mimics. Signaling components specific for strigolactones and karrikins/KL are presented in cyan and green, respectively, whereas the shared F-box protein MAX2 is indicated in purple. Grey lines indicate uncertainties.

Seed germination

Strigolactones are well described as seed germination stimulants of parasitic plants. After the discovery of strigol, a molecule that induces the germination of *Striga lutea*, other natural strigolactones as well as *rac*-GR24 were found to activate the germination of a wide range of parasites belonging to the Orobanchaceae family (Cook et al. 1966; Yoneyama et al. 2010). An expression analysis carried out on the parasitic plant *Phelipanche ramosa* (broomrape) revealed that the abscisic acid catabolic gene

CYP707A1 was rapidly induced upon *rac*-GR24 treatment, indicating that strigolactones stimulate parasitic seed germination by abscisic acid degradation (Lechat et al. 2012; Boyer et al. 2014). However, the molecular mechanisms of strigolactone perception and signaling in the parasite are still not fully understood. Whereas in *Arabidopsis* D14 and its paralog KAI2 have been characterized as the strigolactone and karrikin receptors, respectively (Waters et al. 2012b), strigolactone perception by the parasite is most probably mediated through a divergent KAI2 receptor complex that has undergone selective pressure to induce seed germination in response to strigolactones instead of karrikins (Conn & Nelson 2016). Indeed, the KAI2 receptor in parasitic plants underwent multiple duplication events, resulting in a copy number between 5 to 12, depending on the species (Conn et al. 2015; Toh et al. 2015; Tsuchiya et al. 2015). Based on their similarity on the protein level, these different *KAI2* genes can be grouped into different clades, with one group retaining the highest identity to the KAI2 protein of *Arabidopsis*. This conserved group, referred to as KAI2c, can complement all *kai2* phenotypes in *Arabidopsis*, but because the transgenic lines are still unresponsive to *rac*-GR24 or KAR_1, KAI2c has been proposed to be specific for the perception of unknown KAI2 ligand only (Conn & Nelson 2016). In contrast, the divergent clade, referred to as KAI2d, could complement the *kai2* mutant and make it highly sensitive again to *rac*-GR24-mediated germination, but not to KAR_1 (Toh et al. 2015; Conn & Nelson 2016). In addition, the MAX2 signaling pathway was largely conserved between parasitic plants and *Arabidopsis*. Indeed, the MAX2 ortholog of *Striga hermonthica* could complement the root and shoot phenotypes, but not the germination phenotype, whereas the MAX2 ortholog of *Phelipanche aegyptiaca* was able to complement all phenotypes of the *max2* mutants in *Arabidopsis* (Liu et al. 2014; Li et al. 2016a). Recently, just like D14, the KAI2 ortholog, ShHTL7 in *Striga hermonthica* has been demonstrated to hydrolyze strigolactones to the intermediate CLIM, promoting conformational changes of the receptor that allow it to interact with MAX2/ShMAX2 and, hence, to possibly regulate *Striga* seed germination. Moreover, pull-down assays revealed the interaction between SMAX1 and ShHTL7, which can be strongly enhanced by addition of *rac*-GR24 (Yao et al. 2017).

Parasitic plants already germinate in the presence of nanomolar concentrations of *rac*-GR24, but the role of endogenous strigolactone molecules in *Arabidopsis* seed germination is less clear. Under specific light and temperature conditions, a reduced germination has been described for both *max2* and *max1* mutants (Nelson et al. 2009, 2010; Tsuchiya et al. 2010; Toh et al. 2012a), whereas under normal conditions, an enhanced seed dormancy was observed only for *max2* mutants while the strigolactone-deficient mutants *max1*, *max3,* and *max4* had a normal seed germination phenotype (Nelson et al. 2011; Shen et al. 2012). These results rather point to a role for karrikin signaling only in seed germination. In agreement, KAR_1 and *rac*-GR24 could both promote the germination of *Arabidopsis* seeds, but karrikins were much more effective (Stevens et al. 2007; Nelson et al. 2009,

2010; Flematti et al. 2010). In other nonparasitic plants, besides *Arabidopsis*, strigolactones seem only to play a minor role in promoting seed germination. Although *rac-GR24* had been reported as a germination stimulant of lettuce (*Lactuca sativa*), the natural strigol molecule was unable to do so (Bradow et al. 1988). On the contrary, karrikins strongly enhance the germination of primary dormant *Arabidopsis* seeds, independently of abscisic acid, but depending on both light and GA synthesis (Nelson et al. 2009). Accordingly, *kai2* mutants were not responsive to *rac*-GR24 (Waters et al, 2015b). During seed germination, SMAX1 is expected to be a downstream target of MAX2 for degradation. Indeed, *smax1,* but not *smxl6,smxl7,smxl8*, could suppress the dormancy phenotype of *Arabidopsis max2* mutants (Stanga et al. 2013; Soundappan et al. 2015).

Although karrikins induce seed germination of many species, they do not trigger germination of parasitic weeds (Nelson et al. 2009; Flematti et al. 2010; Conn et al. 2015). Yet, karrikins have a butenolide moiety in common with the D-ring of strigolactones that, in addition to the enol ether bound, was also shown to be necessary, but not sufficient, for germination induction of parasitic weeds (Mangnus & Zwanenburg 1992). Correspondingly, whereas $GR24^{5DS}$ induces germination of *Orobanche crenata* and *S. hermonthica,* $GR24^{ent\text{-}5DS}$ did not (Thuring et al. 1997). However, the discrimination between strigolactones and karrikins as germination signals for parasitic and nonparasitic plants, respectively, might not be 100%. Indeed, the broad-host parasite *Orobanche minor* germinates in response to both *rac*-GR24 enantiomers, whereas it is totally insensitive to karrikins (Scaffidi et al. 2014). Additionally, KAR_1 purified from smoke-water has been reported to stimulate seed germination of numerous parasitic weeds (Daws et al. 2007). As parasitic plants are known to contain large KAI2 gene families and because studies on the binding specificity of the parasitic KAI2 receptors suggest that the binding pockets of KAI2 proteins are probably adapted to different ligands, these observations might be explained by the presence of KAI2 receptors with different affinities for a variety of molecules, hence accounting for the wide range of parasitic host specificities (Morffy et al. 2016; Stanga et al. 2016).

Taken together, both strigolactones and karrikins can induce germination, albeit for different plant species, with a role for strigolactones as germination-inducing signals mainly for parasitic plants and for karrikins and endogenous KAI2 ligand as germination stimulants of nonparasitic plants. This difference might be relevant because both signals have a dissimilar ecological context. Indeed, karrikins signal that competitive plants have been burned and are thus absent, whereas strigolactones denote to parasitic seeds that host plants are present.

Early seedling development

Application of *rac*-GR24 as well as of KAR_1 or KAR_2 inhibited hypocotyl elongation in *Arabidopsis*, with *rac*-GR24 as the most effective compound (Nelson et al. 2010; Tsuchiya et al. 2010; Waters et al. 2012b). In agreement, the hypocotyl of *max2* mutants was longer than that of wild-type plants (Stirnberg et al. 2002). Although these observations hint at a role for both strigolactones and karrikins in hypocotyl growth, some reports indicate that strigolactones are probably not involved in this process. As the strigolactone biosynthesis mutants *max1*, *max3,* and *max4* and the strigolactone signaling mutant *Atd14,* all display a normal seedling phenotype without abnormalities in hypocotyl length, the unknown endogenous karrikin-like molecules and not strigolactones seem to control hypocotyl elongation (Nelson et al. 2011; Waters et al. 2012b). In fact, the hypocotyl elongation in *Arabidopsis* was only very weakly inhibited upon treatment with carlactone, the biosynthetic precursor of strigolactones (Scaffidi et al. 2013). Furthermore, similar to the *max2* seedlings, the *kai2* seedlings had a longer hypocotyl (Waters et al. 2012b).

Nevertheless, the picture looks different when the effect of exogenous *rac*-GR24 is taken into account. *d14* mutants are sensitive to *rac*-GR24 treatment, although to a lesser extent than wild-type plants, whereas their response to KAR_1 does not differ. On the contrary, the hypocotyl elongation inhibition in *kai2* seedlings was insensitive to KAR_1, but was still visible upon *rac*-GR24 treatment, indicating that the activated D14 signaling can reduce hypocotyl length in response to *rac*-GR24 (Waters et al. 2012b). These observations point to a partially functional redundancy of KAI2 and D14 in the response to exogenous *rac*-GR24 during seedling development and, accordingly, only the *kai2d14* double mutants were completely insensitive to both KAR_1 and *rac*-GR24 (Scaffidi et al. 2014; Stanga et al. 2016). Nevertheless, because mutants affected solely in the strigolactone signaling pathway lacked a hypocotyl phenotype, it is unclear whether signaling via D14 is physiologically relevant during early seedling growth (Stanga et al. 2016). In fact, the analysis of the *smax1* mutants does not support a role for D14 in hypocotyl growth, because *smax1* could suppress the *max2* hypocotyl phenotype and the *smxl6,smxl7* and *smxl6,smxl7,smxl8* double and triple mutants could not, hinting at a role for KAI2-mediated signaling only in the control of hypocotyl growth (Soundappan et al. 2015).

The hypocotyl of the *smax1smxl2* double mutants was insensitive to both KAR_1 and *rac*-GR24, indicating that SMAX1 and SMXL2 are the only targets of MAX2 during early seedling development. Additionally, hypocotyl elongation inhibition in the *smax1smxl2* mutants was also insensitive to $GR24^{5DS}$, implying that the redundant role of D14 together with KAI2 in hypocotyl growth regulation upon exogenous treatments might involve only SMAX1/SMXL2-dependent signaling (Stanga et al. 2016).

In addition to an effect on the hypocotyl length, rac-GR24 and KAR_1 treatments could also regulate cotyledon growth, albeit in an opposite manner. Indeed, whereas *rac*-GR24 inhibits cotyledon expansion, karrikins enhance their growth (Nelson et al. 2011; Waters et al. 2012b; Baldrianová et al. 2015). However, analysis of the strigolactone biosynthesis mutants did not clearly indicate whether the impact of *rac*-GR24 mimics a strigolactone action. Only *max1* and *max2* in *Arabidopsis* and *ramosus* 3 (*rms3)* and *rms4* in pea (*Pisum sativum)*, defective in the *D14* and *MAX2* orthologs of *Arabidopsis*, respectively (Table 1), displayed rounded instead of elongated leaves observed in wild-type plants (Beveridge et al. 1996; Stirnberg et al. 2002), hinting at a rather unlikely role for strigolactones. Whatever the signal is that acts opposite to karrikins, the reduced cotyledon expansion phenotype of *max2* mutants was suppressed by *smax1*, resulting in cotyledons significantly larger than those of the wild type (Shen et al. 2007; Stanga et al. 2013). In contrast, two *smxl6,smxl7* alleles enhanced the *max2* phenotype, demonstrating that SMAX1 and SMXL6,SMXL7 have opposite and antagonistic effects on cotyledon expansion (Soundappan et al. 2015). To complete the picture, the phenotypes of *d14* as well as of *kai2* mutants should be checked to help to determine unequivocally that the D14 and KAI2 signaling pathways exert opposite effects on leaf growth.

Although several reports indicate a strong interplay between light and karrikins in cotyledon expansion and hypocotyl growth, such an interaction is far from clear. In a screen for light-signaling mutants, KAI2 was independently identified as HTL and *htl* mutants were characterized by diverse photomorphogenesis phenotypes (Sun & Ni 2011), similar to those described for the *max2* mutants (Shen et al. 2007). In addition, KAI2 and ELONGATED HYPOCOTYL 5 (HY5), a key transcription factor in light signaling, were shown to influence each other's expression. The direct regulation of *KAI2* expression by HY5 was speculated based on the HY5-binding G-box domain identified in its promoter (Sun & Ni 2011). However, later studies revealed that *rac*-GR24 induced *HY5* transcript levels and stabilized the HY5 protein in a MAX2-dependent manner. Accordingly, *max2* mutants display a reduced *HY5* expression (Toh et al. 2012b), but, because HY5 and MAX2 mutations have an additive effect on hypocotyl length and seed germination, the relevance of this interplay is unclear and both might act largely independently from each other (Waters & Smith 2013). Many, but not all, karrikin-related markers were still activated upon treatment of the *hy5* mutant with KAR_1 (Toh et al. 2012b; Waters & Smith 2013). High concentrations of *rac*-GR24 promoted the migration of CONSTITUTIVE PHOTOMORPHOGENIC 1 (COP1) outside the nucleus, thereby stabilizing HY5 in a MAX2-independent manner, hence, clarifying the additive effect on hypocotyl length in *max2hy5* double mutants (Tsuchiya et al. 2010; Waters & Smith 2013; Toh et al. 2014). In conclusion, early seedling development is mainly regulated via KAI2, whereas D14 signaling is suggested to play only a minor role upon exogenous treatment.

Root development

Although an important role for *rac*-GR24 in shaping root architecture has been reported (Kapulnik et al. 2011; Koltai 2011; Ruyter-Spira et al. 2011; Rasmussen et al. 2012), it still remains to be clarified how D14 and KAI2 signaling complexes are exactly involved in this process. Treatment with *rac*-GR24 inhibits adventitious root formation, whereas the strigolactone signaling mutants display an increased number of adventitious roots (Rasmussen et al. 2012). In addition, *rac*-GR24 slightly enhances the primary root length by affecting the cortical cell number and the primary root is shorter for *max1*, *max4,* and *max2* mutants than that for wild-type plants (Ruyter-Spira et al. 2011). Hence, these results support a role for strigolactones in adventitious rooting and primary root growth.

In contrast, the involvement of D14 and KAI2 signaling in root hair growth and lateral root development remains more enigmatic. Indeed, the positive effect of *rac*-GR24 on root hair elongation depends on MAX2 but could not be backed with aberrant phenotypes in strigolactone biosynthesis mutants (Kapulnik et al. 2011). Concerning lateral roots, under phosphate-sufficient conditions, *rac*-GR24 negatively affects both lateral root outgrowth and priming in a MAX2-dependent manner (Jiang et al. 2016), whereas under phosphate-limiting conditions, it has a positive effect on lateral root development (Ruyter-Spira et al. 2011). Accordingly, *max2* mutants are characterized by an enhanced lateral root density, although the lateral root phenotypes of the strigolactone-deficient mutants *max3* and *max4* are currently unclear (Kapulnik et al. 2011; Koltai 2011; Ruyter-Spira et al. 2011). When compared to wild-type plants, both phenotypes were reported a similar as well as a slightly higher lateral root density (Kapulnik et al. 2011; Ruyter-Spira et al. 2011). These observations might result from residual strigolactone metabolites that are still present in the biosynthesis mutants or might indicate that unknown KAI2 ligand is at play (Matthys et al. 2016). Nevertheless, because the lateral root density in *smax1max2* seedlings did not significantly differ from that in *max2* and the *max2,smxl6,smxl7,smxl8* quadruple mutant could rescue the increased lateral root density phenotype of *max2* mutants, D14 rather than KAI2 signaling is considered to play the most important role in the control of lateral root development (Soundappan et al. 2015). With the exception of the reported enhanced lateral root length by KAR_1 treatment (Baldrianová et al. 2015), the role of karrikins in shaping root architecture is poorly studied and a detailed analysis of the root phenotype of *d14* and *kai2* mutants is still missing. Considering that both KAI2 and D14 might be involved in young seedling development, one could speculate that they might also share a function in root architecture shaping, affecting both lateral root formation and root hair elongation. Indeed, analysis of *HTL/KAI2::GUS* lines revealed a strong *KAI2* expression in the hypocotyl and the root of young *Arabidopsis* seedlings (Sun & Ni 2011). Furthermore, flavonol production in *Arabidopsis* root was induced mutually by both *rac*-GR24 enantiomers and both through D14 and/or KAI2 signaling (Walton et al. 2016). These results suggest

that in roots, a crosstalk between both receptors exists and further supports the hypothesis that root development can be controlled mutually by strigolactone and karrikin/KAI2 ligand. A detailed analysis of the root architecture upon treatment with *rac*-GR24 and its individual enantiomers in *d14* and *kai2* mutants will undoubtedly clarify how signaling mediated by D14 and KAI2 can regulate root development in a coordinated manner.

Shoot branching

An array of strigolactone biosynthesis and signaling mutants in different species, e.g. *Arabidopsis*, pea, rice, petunia, and chrysanthemum (*Dendranthema grandiflorum*), is characterized by a bushy phenotype, whereas for *kai2* mutants the shoot branching is normal (Sorefan et al. 2003; Snowden et al. 2005; Arite et al. 2007; Gomez-Roldan et al. 2008; Umehara et al. 2008; Liang et al. 2010; Braun et al. 2012). When compared to *rac*-GR24, KAR_1 could not restore the increased branching of the strigolactone-deficient mutants *max3* and *max4* in *Arabidopsis* or *rms5* and *rms1* in pea (Nelson et al. 2011). Likewise, the loss of SMXL6,SMXL7,SMXL8 proteins was sufficient to suppress the bushy phenotype of both *max2* and *max3* mutants, implying a specific role for strigolactones in axillary bud outgrowth (Soundappan et al. 2015; Wang et al. 2015). In contrast to other processes, the signaling events for the strigolactone action downstream of the SMXL proteins have been identified in the shoot. Two nonexclusive mechanisms have been proposed. On the one hand, strigolactones repress outgrowth of axillary buds by inducing the gene expression of specific TCP transcription factors in the buds, such as *BRANCHED 1* (*BRC1*) (Braun et al. 2012; Dun et al. 2012) and, on the other hand, they can inhibit branching by triggering the removal of the PIN-FORMED 1 (PIN1) auxin efflux proteins from the plasma membrane (Bennett et al. 2006; Crawford et al. 2010; Shinohara et al. 2013). Both pathways probably act in parallel, because *tir3-1* mutant plants with a deficient PIN1 accumulation have no increased *BRC1* expression levels and *brc1-2brc2-1* double mutants have no altered PIN1 distribution or auxin flow (Bennett et al. 2016). In addition to branching inhibition, an even more general role for strigolactones has been suggested in the shoot, such as branch angle influence, leaf margin serrations, internode elongation, leaf senescence, and secondary growth processes (Gomez-Roldan et al. 2008; Umehara et al. 2008; Agusti et al. 2011; de Saint Germain et al. 2013; Lauressergues et al. 2014; Sang et al. 2014; Yamada et al. 2014; Ueda & Kusaba 2015). Strigolactone signaling during shoot development has been shown to be regulated by both MAX2 and D14 and to depend on the degradation of SMXL6,SMXL7,SMXL8 proteins, but without requirement of other previously proposed MAX2 targets, such as BRASSINOSTEROID INSENSITIVE 1-ETHYL METHANESULFONATE-SUPPRESSOR1 (BES1) and DELLA (Bennett et al. 2016). In rice another transcription factor Ideal Plant Architecture 1

(IPA1) was reported to be a downstream target of D53 to regulate tiller number (Song et al., 2017) however its homologs in *Arabidopsis* SPL9 and SPL15 possibly regulate branching through a separate mechanism not related to strigolactones (Bennett et al. 2016).

Recent studies in pea and rice demonstrated that D14 is a mobile signal for fine-tuning axillary bud outgrowth. The RMS3/D14 protein is transported through the phloem to axillary buds independently of the presence of strigolactones and thereby partially suppresses shoot branching and tillering (Kameoka et al. 2016). In contrast, in *Arabidopsis* and petunia, the branching phenotype was not restored by grafting on a wild-type rootstock, although the presence of AtD14 in the phloem sap and its transport over short distances have been evidenced (Simons et al. 2007; Chevalier et al. 2014). These controversial observations could be explained by the limitation of the grafting method or by the fact that the D14 protein transport is species dependent (Kameoka et al. 2016).

Interaction with arbuscular mycorrhizal fungi

Natural strigolactones as well as *rac*-GR24 have been shown to be extremely effective in inducing hyphal branching of arbuscular mycorrhizal fungi, thereby facilitating direct contact between the fungus and the host (Akiyama et al. 2005, 2010). In addition to hyphal branching, *rac*-GR24 stimulated spore germination and also boosted fungal metabolism (Besserer et al. 2006, 2008). The enantiomer $GR24^{5DS}$ was the most active in hyphal branching and, accordingly, KAR_1 did not affect fungal growth (Akiyama et al. 2010).

As arbuscular mycorrhizal fungi respond to *rac*-GR24, they must be able to perceive them, but the perception and signaling mechanisms in the fungus are still unclear. Although the protein sequences of both MAX2 and D14 match with sequences in the translated fungal genome, the matching has a low identity, indicating that the ability to respond to strigolactones might have evolved separately in plants and fungi (Koltai, 2014). Indeed, thus far, no real MAX2, D14, or KAI2 ortholog has been identified. Fungal responses upon *rac*-GR24 treatment have been proposed to rely on reactive oxygen species (ROS) and mitochondria (Belmondo et al. 2016). In the fungus *Rhizophagus irregularis*, the protein encoded by *Strigolactone-induced putative secreted protein 1* (*SIS1*) gene is predicted to be secreted and to play a positive role in the regulation of host colonization, because this protein was upregulated upon *rac*-GR24 treatment as well as during symbiosis (Besserer et al. 2008; Tsuzuki et al. 2016). Inside rice roots, the KAI2 ortholog, D14 LIKE, was found to be required for the initiation of symbiosis with arbuscular mycorrhizal fungi, hinting at a role for karrikins or KAI2 ligand (Gutjahr et al. 2015). However, it is still unknown whether these molecules are derived from the plant or from the fungus,

an interesting issue to be investigated in the future. This finding undoubtedly implied an unexpected plant recognition strategy for arbuscular mycorrhiza and an unspecified link between symbiosis and plant development. In conclusion, thus far, shoot branching inhibition and hyphal branching induction are reported to be unique strigolactone responses.

Abiotic stress responses

Different studies have revealed that MAX2 plays an important role in the plant's adaptation to nutrient, drought, chilling and salt stress (Marzec et al. 2013; Bu et al. 2014; Ha et al. 2014; Cooper et al., 2018; Luo et al., 2018). Indeed, under phosphorous and nitrogen deficiency, both the strigolactone biosynthesis and exudation increased (Marzec et al. 2013). Also, the strigolactone-deficient carotenoid cleavage dioxygenase 7 mutant of *Lotus japonicus* (*Ljccd7*), affected in the MAX3 ortholog of *Arabidopsis* (Table 1), coped less well with osmotic stress than wild-type plants (Liu et al. 2015). Furthermore, in *Arabidopsis*, a comparative microarray analysis of *max2* mutant and wild-type leaves under dehydration uncovered a number of dehydration- and/or abscisic acid-inducible genes that were downregulated in a *max2* background (Ha et al. 2014). Moreover, *max2* mutants were hypersensitive to drought stress and evaporated more water than the wild-type plants (Bu et al. 2014; Ha et al. 2014). It might be related to a novel role of strigolactones in regulation of stomatal aperture independently of abscisic acid as this process was impaired in *max2* and *d14* mutants (Lv et al., 2018; Zhang, Lv, & Wang, 2018). In tomato (*Solanum lycopersicum)* roots, the strigolactone biosynthesis was repressed upon drought and the low hormone levels in the root were suggested to act as a systemic drought stress signal, triggering the stomatal sensitivity to abscisic acid, probably via a locally enhanced strigolactone synthesis in the shoots (Visentin et al. 2016). However, the ABA, osmotic stress, drought-sensitive phenotypes in *Arabidopsis* have been found to be restricted to *max2* and the strigolactone-biosynthetic pathway mutants *max1*, *max3*, and *max4* not to display any defects in these responses (Bu et al. 2014). Based on these observations, a potential role for karrikins in the plant's adaptation to abiotic stresses has been proposed. Recent study demonstrated a positive role of KAI2 signaling in the control of drought resistance in *Arabidopsis* by both drought avoidance and drought tolerance mechanisms, including enhanced cuticle formation, stomatal closure, cell membrane integrity and anthocyanin biosynthesis (Li et al., 2017a). Indeed, smoke-water and butenolide alleviate seed germination and seedling growth under high temperature, high salinity, and low osmotic potential (Ghebrehiwot et al. 2008; Jamil et al. 2014). Moreover, a transcriptome analysis of maize (*Zea mays*) kernels treated with smoke-water revealed a number of smoke-responsive genes among which stress and abscisic acid-related genes were overrepresented (Soós et al. 2009). To conclude, both

strigolactone and karrikin pathways provide potential for manipulation for improvement of drought resistance.

BETTER TOGETHER?

In summary, the use of *rac*-GR24 attributed falsely some *max2* phenotypes to strigolactone signaling that were later shown to be rather related to karrikin and KAI2 ligand. In fact, because a complex network is hiding behind the signaling mediated by KAI2 and D14, unraveling responses specific to strigolactones and karrikin/KAI2 ligand can be challenging. Based on the current knowledge, we can conclude that to study D14-regulated responses in wild-type plants the $GR24^{5DS}$ enantiomer has to be used, whereas KAI2-regulated responses can be studied by means of the KAR_1 molecule. In addition, a detailed study of both biosynthesis and signaling mutants is essential to get a clear view on how strigolactones and karrikins/KAI2 ligand can regulate different responses.

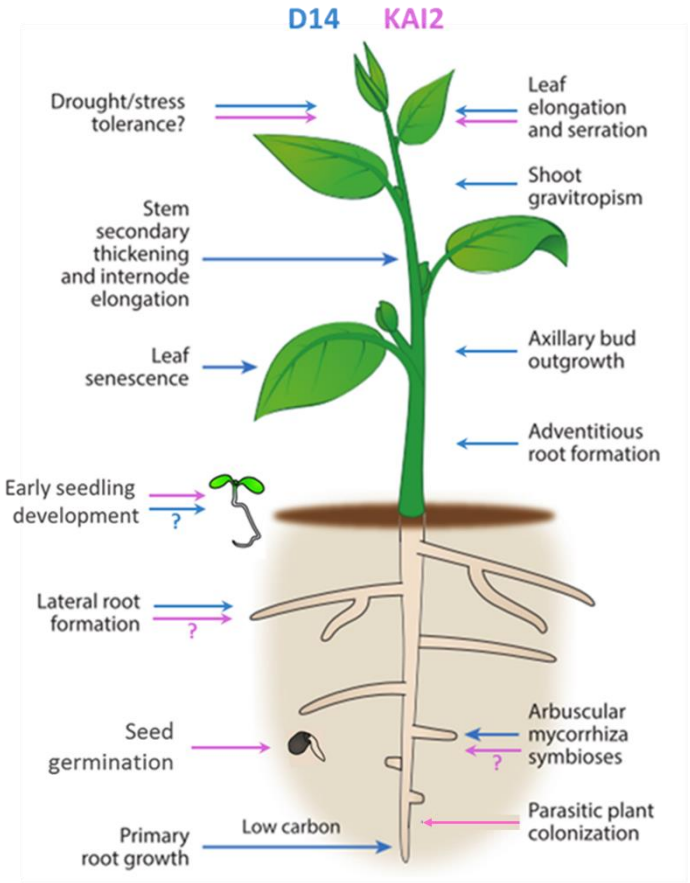

Figure 6. The effects of the D14 and KAI2 pathways on plant development.

During their various developmental stages plants need to distinguish between strigolactones and endogenous KAI2 ligand to trigger the appropriate environmental and developmental responses (Figure 6). The relative expression patterns and levels of *D14* and *KAI2* are consistent with the plant's capacity to respond to strigolactones and karrikins. Indeed, *KAI2* is preferentially expressed in seeds and seedlings. In the seeds, the *KAI2* transcript levels are up to 100-fold more abundant than those of *D14* transcripts, allowing KAI2 to play a dominant role. In contrast, in seedlings, the *D14* expression is slightly higher than that of *KAI2*, suggesting a further domination at later stages of development, such as during flowering and secondary bud outgrowth (Waters et al. 2012b). Although a major progress has been made in understanding the role of strigolactone and karrikins/KAI2 ligand in plant development, an in-depth knowledge of their signaling mechanisms will be crucial to explain how strigolactones, karrikins, and KAI2 ligand can regulate plant development together. New tools, such as the biosensor StrigoQuant, can be very useful to unravel the strigolactone network (Samodelov et al. 2016). A better comprehension is necessary on how different MAX2 signaling complexes can discriminate between the various members of the SMXL family and how their degradation induces specific responses by affecting the gene expression and/or PIN1 localization. Another serious challenge for the near future is the discovery of the KAI2 ligand that not only will resolve many unanswered questions in strigolactone and karrikin biology, but also might provide new insights for the improvement of agriculture.

Chapter 2

Exploring the protein-protein interaction landscape in plants

Submitted to Plant, Cell & Environment

Sylwia Struk[1,2], Anse Jacobs[1,2,3,4], Elena Sanchez Martín-Fontecha[5], Kris Gevaert[3,4], Pilar Cubas[5] & Sofie Goormachtig[1,2]

[1] Ghent University, Department of Plant Biotechnology and Bioinformatics, 9052 Ghent, Belgium
[2] VIB, Center for Plant Systems Biology, 9052 Ghent, Belgium
[3] Ghent University, Department of Biochemistry, 9000 Ghent, Belgium
[4] VIB, Center for Medical Biotechnology, 9000 Ghent, Belgium
[5]Plant Molecular Genetics Department, Centro Nacional de Biotecnología (CSIC), Campus Universidad Autónoma de Madrid, 28049 Madrid, Spain

Author contributions: S.S. was the main author of the manuscript and performed the literature search. A.J. and E.S.M.F. contributed to the writing. S.G., K.G. and P.C. supervised the project and contributed to writing of the manuscript.

ABSTRACT

Protein-protein interactions (PPIs) represent an essential aspect of plant systems biology. Identification of key protein players and their interaction networks provide crucial insights into the regulation of plant developmental processes as well as into interactions of plants with their biotic and abiotic environments. Despite the great advance in the methods for the discovery and validation of PPIs, several challenges still remain. First, the PPI networks are usually highly dynamic and the *in vivo* interactions are often transient and difficult to detect. Thus, the properties of the PPIs under study need to be considered to select the most suitable technique, because each method has its own advantages and limitations. Secondly, besides knowledge on the interacting partners of a protein of interest, characteristics of this interaction, such as the spatial or temporal dynamics, are of high importance. Hence, a combination of multiple approaches is required to obtain a comprehensive view on the PPI network present in a cell. Here, we summarize recent progress in commonly used methods to detect and validate PPIs in plants with a special emphasis on the PPI features that are assessed in each approach.

INTRODUCTION

Most physiological processes in plants are regulated by complex signal transduction pathways required for plant development, differentiation, and adaptation to a constantly changing environment (Vanstraelen & Benková, 2012). For such signalling networks, the cooperation of thousands of molecules is needed, including proteins, nucleic acids, lipids, chromatin, and low-molecular weight compounds (Uhrig, 2006). Thus far, among them all, protein–protein interactions (PPIs) are the most thoroughly studied (Dedecker et al., 2015). A plant's proteome is estimated to consist of an average 36 795 proteins, from which 75 000-150 000 interaction pairs are predicted (Morsy et al., 2008; Ramírez-Sánchez et al., 2016). Hence, in the post-genomic era, the research focus is moving towards the analysis of functions and properties of encoded proteins and characterisation of their interaction networks.

Proteins seldom act on their own, but rather fulfil most of their biological tasks in complexes with other proteins (Alberts, 1998; Charbonnier et al., 2008). Therefore, to fully understand a protein's function, information about its biochemical activity, cellular localization, and abundance has to be complemented with the knowledge on its interacting partners. According to the 'guilty by association' principle, identification of a protein interactors can help to predict its function (Lalonde et al., 2008). In general, two types of PPIs can be distinguished, constitutive and regulative ones (Fujikawa et al., 2014). Constitutive PPIs are very stable and mostly form subunits of permanent complexes that carry out structural functions in the cell. Such complexes are usually macromolecular machines, such as replisomes, ribosomes, proteasomes, and signalosomes (Morsy et al., 2008). Constitutive interactions are generally easily detected by both *in vivo* and *in vitro* methods. On the contrary, regulative PPIs occur only in certain cellular or developmental contexts or in response to specific environmental cues. These PPIs are part of biochemical cascades and are often highly sensitive to regulatory stimuli and signalling events. In terms of binding affinity, these dynamic protein interactions are classified as weak or strong (Syafrizayanti et al., 2014). Mostly, regulative PPIs are transient, because proteins continuously associate with and dissociate from each other (Nooren & Thornton, 2003). For instance, protein-modifying enzymes, such as phosphatases, acetyl transferases, and proteases, engage for very short periods in interactions with their substrates (Ferro & Trabalzini, 2013). Thanks to these dynamic PPI changes, cells can rapidly respond to intra- and extracellular stimuli; thus, such interactions are essential for many biological processes, including signal transduction, homeostasis control, stress responses, plant defence, and organ formation (Wang et al., 2014; Zhang et al., 2010). Typically, the study of these interactions is more challenging, because of their quick occurrence and easy destabilization. Additionally, PPIs can also be influenced by posttranslational modifications (PTMs) or protein re-localization to specific cellular structures (Scott & Pawson, 2009).

Diverse methods have been developed to dissect the PPI landscape in plants. Currently, the most frequently used techniques are yeast two-hybrid (Y2H), affinity-purification coupled to mass spectrometry (AP-MS), and assays based on protein-fragment complementation (Dedecker et al., 2015). These assays conveniently deliver qualitative data, often on a large scale, but they do not necessarily reflect native cellular situations or provide spatial and temporal information on PPIs. The interaction characteristics are important when PPIs are analysed. To date, not one single method assesses all the specific aspects of PPIs (e.g. localization, interaction mode, lifetime, and affinity). Often, a combination of different approaches is required to obtain a more complete view of the physiologically relevant protein complexes in a cell. In this review, we focus on the most commonly used technologies to discover and validate PPIs with a particular emphasis on the specific interaction characteristics assessed by these methods (Table 1).

EXPLORING THE PLANT INTERACTOME IN SEARCH FOR NOVEL INTERACTORS

Identification of novel PPIs in plants is mostly achieved by two types of techniques, namely yeast two-hybrid (Y2H) screenings of plant cDNA libraries and purification assays starting from plant material (Figure 1) (Van Leene et al., 2007; Zhang et al., 2010). Both methods are complementary regarding the type of detected interactors and, if possible, they should be used in parallel. Whereas Y2H screens detect direct, binary interactions, purification assays determine all the components of a large complex, that do not necessarily interact directly with each other.

Direct interactions revealed by yeast two-hybrid screens

Yeast two-hybrid (Y2H) is one of the earliest PPI assays that had been developed and is widely applied in plant research. In this binary system, interactions between two proteins are assessed based on the transcriptional activation of a reporter gene that allows growth on selective media or can be detected by an enzymatic, colour reaction. In the classical Y2H, two proteins of interest (POIs) are tagged with either the DNA-binding domain (BD) or the trans-activation domain (AD) of the GAL4 transcription factor and their interaction is detected based on the reconstruction of GAL4 followed by the induction of a reporter gene (Fields and Song, 1989). Although Y2H is limited to the analysis of protein pairs, it can be easily automated for cDNA library screening to identify novel interactors of a POI. In this setup, the POI fused to the BD, called “bait”, is used to search the library with putative ‘‘preys’’ fused to the AD domain (Bruckner et al., 2009). In addition, cDNA libraries can be created from specific tissues or organs, thereby facilitating the detection of physiologically or developmentally relevant interactions (Xing et al., 2016).

Since the implementation of the original Y2H system (Fields & Song, 1989), many variations and improvements have been developed to overcome the limitations of the classical method. For instance, for *in vivo* analysis of interactions with membrane proteins that was problematic with the classical approach due to the requirement to translocate interacting proteins into the nucleus, the split-ubiquitin system has been adapted. In this approach, the reconstituted ubiquitin upon interaction between bait and prey leads to the activation of a ubiquitin-specific protease and the subsequent release of a tethered transcription factor (Stagljar et al., 1998). Also, the *Arabidopsis thaliana* protoplast two-hybrid has been introduced as a potentially more sensitive system than the heterologous one, overcoming the problem of the lack of plant-related PTMs in yeast (Ehlert et al., 2006). This method has been successfully applied for large-scale screening of interacting partners of transcription factors (Wehner et al., 2011).

In general, Y2H is advantageous when elucidation of weak and transient PPIs is wanted. Once the interaction takes place, transcriptional activation of the reporter gene amplifies the signal, thus increasing the sensitivity of the method. As a result, various weak or transient interactions have been identified through Y2H, such as those occurring during plant hormone signalling (Cheng et al., 2017; Lumba et al., 2014), cell cycle progression (Boruc et al., 2010; Van Leene et al., 2011), immune signalling (Couto et al., 2016), light-controlled development (Tang et al., 2017), or stress responses (Liu et al., 2017). Nevertheless, Y2H does not deliver information about the conditions in which the interaction takes place and provides only a very limited knowledge on the PPI dynamics. Y2H cannot be used to detect fast changes in interaction affinity caused, for instance, by external factors, because of the length of an experiment (2-3 days), required for activation of the reporter gene. Furthermore, context-dependent PPIs are difficult to study in this heterologous system, because the cellular environment is distinct from the native one and, thus, certain signalling molecules might be absent (Xing et al., 2016). Despite all these disadvantages and the fact that Y2H is prone to yield relatively high false-positive and false-negative rates (Bruckner et al., 2009), over the years, this system has proved to be efficient to discover many new PPIs. Y2H has been successfully used to create large interaction networks in many plant species, such as *Arabidopsis thaliana* (de Folter et al., 2005; Vernoux et al., 2011; Mukhtar et al., 2011; Trigg et al., 2017) barley (*Hordeum vulgare* L.) (Schoonheim et al., 2007), wheat (*Triticum aestivum*) (Tardif et al., 2007), and rice (*Oryza sativa*) (Ding et al., 2009). The classical Y2H system and all its variations have been extensively reviewed (Morsy et al., 2008, Ferro and Trabalzini, 2013), including detailed technical descriptions, pitfalls, and benefits. Recently, a multiplexed Cre-reporter-mediated Y2H coupled with next-generation sequencing (CrY2H-seq) has been developed to accelerate high-throughput and large-scale interactome mapping. In CrY2H-seq, in addition to well-characterized auxotrophic rescue reporters, such as imidazoleglycerol-phosphate

dehydratase 3 (HIS3) or phosphoribosylaminoimidazole carboxylase 2 (ADE2), a Cre recombinase is used as a second PPI reporter that covalently fuses the coding sequences of two interacting proteins. After a massively multiplexed screening of pools of baits against pools of preys, the fused protein-coding sequences are further identified by next-generation DNA sequencing. Application of CrY2H-seq to investigate the *Arabidopsis* transcription factors and regulators in 'all-by-all' screens revealed a network of approximately 8 500 binary interactions. Thus, CrY2H-seq offers a cost-effective and time-efficient alternative for the classical Y2H screening methods with improved screening capacity, efficiency, and sensitivity. CrY2H-seq is a promising approach that can be further optimized, for instance, for different variants of the Y2H assay, such as yeast one-hybrid that allows screening of genome-wide protein–DNA interactions, or of the cDNA library against another cDNA library to compare large-scale interactomes under different conditions or tissues (Trigg et al., 2017).

Mass spectrometry-based discovery of protein complexes

Affinity purification coupled to mass spectrometry (AP-MS) is a fast, selective, and sensitive tool for the identification of PPIs under near-physiological conditions (Van Leene et al., 2015). Protein complexes can be isolated from cell or tissue lysates with antibodies raised against the POI or an epitope-tagged POI. Theoretically, application of protein-specific antibodies has the great advantage of capturing the physiological state of the POI, its abundance, and its interactions without the need for cloning or overexpression. Nevertheless, the limited availability of antibodies against plant proteins and the risk that antibodies might shield off interaction sites on the bait protein with incomplete or aberrant protein complexes as a consequence drove the research focus towards the use of tagged versions of the POI (Yang et al., 2015). In the general workflow, the POI (bait) is fused to an affinity tag, which allows purification of the bait together with the interacting partners (prey). After several washing steps, non-specific interactions are removed, whereas the isolated protein complex is eluted and analysed by liquid chromatography tandem-mass spectrometry (LC-MS/MS) (Fukao, 2012; Lee et al., 2017). Nonetheless, introduction of an epitope tag might result in steric hindrance of interactions or non-native folding of the tagged proteins and usually involves overexpression of the bait protein, possibly influencing the physiological properties of the bait or the complex stoichiometry. For these reasons, it is necessary to confirm by means of complementation studies that the tag does not interfere with the endogenous function, localization, or properties of the POI. Furthermore, the current development of the CRISPR technology enables the direct insertion of affinity tags into endogenous loci, thereby maintaining the genomic context of the gene (Lackner et al., 2015).

In recent years, the affinity-based methods have been significantly ameliorated, mostly thanks to the increased mass spectrometry sensitivity for detecting peptides and the application of novel bioinformatics approaches for accurate data analysis (Armean et al., 2013; Walton et al., 2015; Qu et al., 2017). Single-tag AP-MS is widely used in large-scale studies. The development of a tandem affinity purification (TAP) technology platform (see below) for *Arabidopsis* cell suspension cultures has allowed the high-throughput identification of protein complexes involved in the control of diverse cellular processes (Van Leene et al., 2015). Moreover, associated protein groups could be studied in their relevant biological contexts, such as specific plant organs, e.g., flowers (Chang et al., 2009), leaves (Batelli et al., 2007), and roots (Tamura et al., 2010), providing an enhanced view on the complex composition during plant growth and development. In addition, AP-MS can give some insight into PTMs that might regulate the ability of proteins to establish spatially or temporally dependent interactions (Miteva et al., 2013). Directly from the MS/MS, the modified peptides can be detected, but only when their abundance is high enough and the modification remains stable during MS and MS/MS analyses (Parker et al., 2010).

Among the tags used for single-step purifications, the most common are the fluorescent tags (green fluorescent protein [GFP], yellow fluorescent protein [YFP] and cyan fluorescent protein [CFP]), which provide an additional handle for protein localization studies (Cristea et al., 2005). One of the shortcomings of the single-step purification methods is the detection of large amounts of non-specifically bound proteins that interact, with either the solid-phase support, the affinity reagent, or the epitope tag and are difficult to distinguish from true interactors. Generally, protein extracts from mock wild type, mutant lines, or from plants expressing the tag only are used as negative controls to determine these non-specific background proteins. Proteins present in these control samples can be simply subtracted from the list of interactors identified with a bait or various algorithms can be applied; for example, the reliability of the interactors can be evaluated based on the ratio of spectral counts in the AP-MS experiment of the bait versus controls (Nesvizhskii et al., 2012).

Moreover, to reduce the amount of non-specifically binding proteins, a second purification step has been introduced by means of a double affinity tag (Li, 2011). One of the most frequently applied TAP tags in plant research is the GS tag with its derivatives (Bürckstummer et al., 2006; Van Leene et al., 2008). The GS tag consists of two immunoglobulin G (IgG) domains of protein G and a streptavidin-binding peptide (SBP) separated by a cleavage site for the tobacco etch virus (TEV) protease. After a first purification step with IgG agarose beads, the protein complexes are incubated with the TEV protease to separate both parts of the tag. In the second purification round, streptavidin-conjugated beads trap the bait complex. After several washing steps, the sample is eluted and analysed by LS-MS/MS (Van Leene et al., 2007). Recently, a multifunctional TAP tag GS^{yellow} has been developed, that

combines properties of the fluorescent protein Citrine YFP and SBP tag, to broaden the use of double affinity tag, for instance, for protein localization in living cells (Besbrugge et al., 2018).

In TAP, the second purification step helps to obtain cleaner samples with an increased signal-to-noise ratio, i.e. true interactors vs background proteins. The *bona fide* interactors can be distinguished from non-specifically binding proteins, again with mock wild-type protein extracts or protein extracts derived from plants expressing tagged bait proteins, such as GFP or β-glucuronidase, as a negative control (Van Leene et al., 2015). In addition, based on their occurrence in more than 500 TAP experiments with different baits, a list of non-specific proteins has been created (Van Leene et al., 2015). The list includes highly expressed proteins, such as ribosomal proteins, actins, and heat shock proteins, as well as sticky proteins detected at reduced concentrations in multiple experiments. Whereas single-step AP-MS protocols are more effective for the detection of low-abundant and weak PPIs, TAP is better fitted for the characterisation of stable interactions (Miteva et al., 2013). Nevertheless, the GS tag has also been successfully applied for the identification of new players in plant hormone signalling, such as NOVEL INTERACTOR OF JAZ (NINJA) (Pauwels et al., 2010) and the RING E3 ligase KEEP ON GOING (Pauwels et al., 2015), components of the jasmonate pathway, proteins associated with the transcription factor BRASSINAZOLE-RESISTANT 1 (BZR1) involved in brassinosteroid signalling (Tang et al., 2011; Wang et al., 2013a), and phosphatase 2A-associated protein ROTUNDA3 regulating auxin transport (Karampelias et al., 2016). Transient or weak PPIs that are often lost during purification procedure can be stabilized by chemical crosslinking (Rohila et al. 2004). *In vivo* crosslinking using formaldehyde has been reported as particularly useful for the detection of membrane protein interactions (Bellati et al. 2016). Further on, the addition of reversible DSP crosslinker *in vitro* during protein extraction can also increase sensitivity of the interactome analysis (Glatter et al., 2011).

A promising breakthrough in the characterisation of PPIs has been the introduction of a quantitative dimension to AP-MS experiments. Quantitative information can help to overcome the problem of non-specifically binding proteins and also allows the study of regulative PPIs under changing conditions (Meyer & Selbach, 2015). In general, AP-MS alone gives a static view on the interacting partners in a multi-subunit complex and it cannot address the question of how cell perturbations alter the complex composition (Uhrig, 2006). However, to measure dynamic changes in protein complex composition, two analytical strategies can be applied: stable isotopic labelling and label-free quantification (LFQ). Beyond plant research, AP-MS combined with stable isotope labelling with amino acids in cell culture (SILAC) has been successfully implemented to study protein complexes influenced by different cellular perturbation types (Mosbech et al., 2012; Satpathy et al., 2015) or to follow the temporal dynamics of PPIs throughout the cell cycle (Pagliuca et al., 2011). In *Arabidopsis*, stable isotope labelling has been

linked with AP-MS to quantitatively distinguish the B-box protein complex, involved in integrating light and hormone signalling pathways during photomorphogenesis, from non-specific background proteins (Wei et al., 2016). Although isotope labelling methods are very sensitive and more accurate than LFQ, their use in plants is restricted, mostly due to the very high cost as in the case of SILAC (Lewandowska et al., 2013).

In comparison, label-free techniques are cost effective, easy to perform, and suitable for comparative analyses of large sample numbers (Ramisetty & Washburn, 2011). LFQ-based methods use statistical algorithms to quantify relative LC-MS peptide peak abundances in multiple replicates based on intensity or counting strategies (Cox et al., 2014), allowing the comparison of the samples analysed in separate LC-MS runs. One of the best-known LFQ algorithms has been integrated into the MaxQuant software (Cox & Mann, 2008). The algorithm assumes that the abundance of most proteins (including the non-specific background proteins) remains unchanged by the experimental setup, thus facilitating detection of proteins that are differentially enriched under the tested conditions (Smaczniak et al., 2012b). The combination of LFQ and AP-MS has been proposed to be renamed to affinity enrichment (AE) (Keilhauer et al., 2015). It has become a common approach to distinguish between true interactors and the background. Here, the increased amounts of unspecific binding proteins can also be advantageous, because they are used in the post-processing pipeline for a more exact normalization and as a kind of quality control. Proteins that physically interact with a bait are expected to be enriched in the tested sample in comparison to the negative control, whereas very similar amounts of contaminants are anticipated under both conditions (Keilhauer et al., 2015; Meyer & Selbach, 2015). Usually, AE requires at least three replicates and is better suited for large-scale studies to ensure a sufficient amount of data for statistical analyses (Smaczniak et al., 2012b; Wendrich et al., 2017). AE using the GFP tag has been successfully implemented in plant research and allowed the characterisation of MADS-domain transcription factor complexes during *Arabidopsis* flower development (Smaczniak et al., 2012a), dynamin-related proteins interacting with the PIN-FORMED (PIN) auxin efflux carriers (Mravec et al., 2011), and basic helix–loop–helix (bHLH) transcription factor dimers regulating vascular development (De Rybel et al., 2013).

The LFQ combined with AP-MS can also be used to assess the dynamics of PPIs during cellular signalling or after cellular perturbations, because protein complexes copurified with the same bait under two different conditions can be compared in a quantitative manner. Through quantitative TAP, distinct GROWTH-REGULATING FACTORs (GRFs) were copurified with the maize (*Zea mays*) ANGUSTIFOLIA3 (ZmAN3) in the division zone compared to those found in the expansion zone of the growing leaf, demonstrating a spatio-temporal specificity of the interactions between ZmAN3 and GRFs (Nelissen et al., 2015).

Lysis-free methods as a novel approach

In all AP-MS methods, PPIs are captured after cell lysis that can lead to increased amounts of both false positives and false negatives. Weak interactions might be disrupted due to the lysis process, whereas other proteins can be brought close enough to the bait or true prey proteins, causing interactions that would never occur under physiological conditions (Roux et al., 2012; Miteva et al., 2013). Therefore, proximity-labelling methods have been developed to overcome this problem and preserve the spatial information about the interactions. For instance, in the proximity-dependent biotin identification (BioID) assay, a bait protein is genetically fused with a promiscuous, non-specific version of the biotin ligase, BirA. This enzyme can covalently biotinylate proteins that potentially interact with the bait in a radius of less than 10 nm. As the reaction occurs in living cells only, physiologically irrelevant interactions that might take place after cell lysis are avoided. Subsequently, the biotinylated proteins are captured by streptavidin beads and identified by immunoblot analysis or MS (Roux et al., 2012). BioID and other proximity-labelling methods can detect transient and low-affinity interactions or insoluble proteins that are commonly lost during the affinity purification procedure (Roux et al., 2012). Usually, MS data from BioID experiments contain a long list of potential complex components, including non-specifically biotinylated proteins or highly abundant background proteins; hence, as for AP-MS, appropriate controls need to be included (Lin et al., 2017).

BioID has been effectively used to screen principally PPIs in mammalian cells and in unicellular eukaryotes (reviewed in Kim & Roux, 2016), but recently the protocol has also been established in plants (Lin et al., 2017). BioID in rice protoplasts has been used to select interacting and neighbouring proteins of the transcription factor OsFD2, involved in plant vegetative growth. However, although new interacting partners had been detected and further validated by Bimolecular Fluorescence Complementation (BiFC) and Y2H, previously described OsFD2 interactors, 14-3-3 and Heading date 3a (Hd3a), could not be identified, possibly due to the very low expression level or due to lack of direct interaction (Tsuji et al., 2013; Lin et al., 2017). Rice protoplasts provide a good system for the BioID assay because they can be transformed efficiently and manipulated in a manner similar to that of mammalian cells. Even though plant cells are able to synthesize biotin, its abundance might not be sufficient for promiscuous protein biotinylation. Therefore, several parameters need to be optimised for each assay, such as the biotin ligase protein expression levels, the concentration of exogenous biotin, and the duration of the protoplast incubation (Lin et al., 2017). The major challenge in adapting proximity-labelling protocols to plant research is the optimal temperature for enzymatic activity. Most of the enzymes used in proximity-labelling techniques work best at 37˚C that is not ideal for growth of many plant species, such as the model organism Arabidopsis (Kim and Roux, 2016).

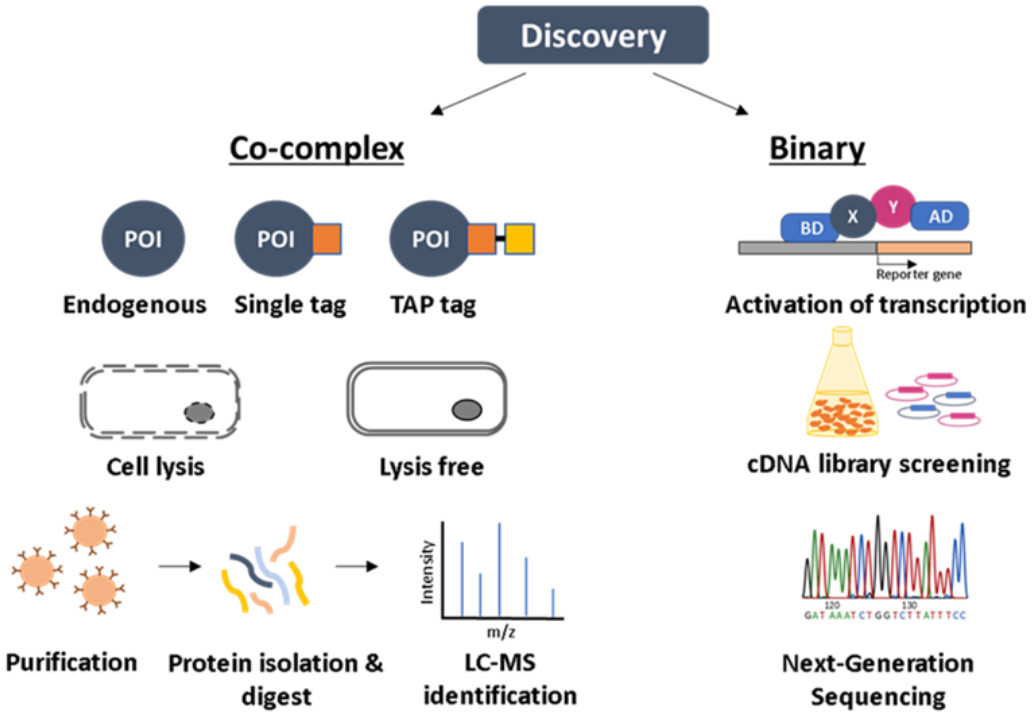

Figure 1. Techniques commonly used for PPI discovery. Detection methods can be divided into co-complex and binary. In co-complex approaches, a tagged POI is purified together with its interacting partners and proteins are identified by means of MS. In binary systems (such as Y2H), a PPI is identified upon activation of transcriptional reporters. Prey cDNAs that interact with the bait are analysed by means of next-generation sequencing.

In addition to the commonly used approaches for the discovery of PPIs reviewed here, other methods have been established that have still not been implemented in plants. Indeed, PPI studies in plants are still remarkably lagging behind most other model species (Buntru et al., 2016). Novel techniques, such as variants of proximity-labelling techniques (Roux et al., 2012), are being developed to overcome the problems related to cell lysis. For instance, proximity labelling with ascorbate peroxidase that can biotinylate neighbouring proteins within minutes provides the additional advantage of temporal resolution (Martell et al., 2012; Rhee et al., 2013). In another proximity-based labelling approach, limitations related to protein fusion can be overcome. Biotinylation by antibody recognition (BAR) uses a specific antibody to deposit the biotin onto proteins in close proximity of the target antigen in fixed cells and primary tissues (Bar et al., 2018). Moreover, in the “lysis-free” MS-based method Virotrap the POI is fused to HIV-1 Gag, a protein able to trap interacting partners into virus-like particles, which are subsequently purified from the medium (Eyckerman et al., 2016; Titeca et al., 2017). Elimination of the need for homogenization or lysis and of the utilization of harsh washing steps, allows easy identification of physiologically relevant interactions and reduction of the rate of false positives and negatives. Other methods focus on co-elution instead of specific purification, such as high-throughput

complex fractionation in combination with MS that has been used to profile human soluble protein complexes (Havugimana et al., 2012).

CHOOSING THE RIGHT VALIDATION TECHNIQUE

Once PPIs are identified, they must be validated. It is advisable to use more than one technique (Figure 2), which preferentially complements the discovery method. For instance, a binary approach, such as Y2H, can detect direct interactions from co-complex data obtained by AP-MS, helping to unravel the molecular architecture of the complex. Validation of the interactions can also be carried out by reciprocal isolations, whereby a newly identified interactor is used as a bait and copurification of the initial POI is expected. Accordingly, screening of the initially identified interacting partners in reciprocal AP-MS experiments allowed the elucidation of the multi-subunit TPLATE complex, essential for clathrin-mediated endocytosis in plants (Gadeyne et al., 2014).

IDENTIFICATION OF LOW-AFFINITY INTERACTIONS

The biological features of the interactions should be considered when a validation technique is selected for the identified PPIs. Certainly, a crucial factor is the binding affinity between interacting proteins. Strong, constitutive PPIs are generally the easiest to validate, because they are stable and permanently present in the cell (Fujikawa et al., 2014). In contrast, weak interactions with low affinity, which are often important in the signalling cascades, are more difficult to detect (Xing et al., 2016). Therefore, for the identification of weak interactions, technologies are being developed that can accumulate or amplify the signal after occurrence of the interaction with an increased sensitivity as a consequence. Examples are the protein fragment complementation assays (PCAs), in which the complemented protein has a much higher stability than the tested PPI. In PCAs, a bait-prey interaction brings together the fragments of a split reporter protein close enough to allow non-covalent, specific protein reassembly, thus restoring its structure and activity (Morell et al., 2009). Nevertheless, the high stability of the reconstituted reporter might hinder the interaction dynamics and increase the rate of false positives due to accumulation of random protein associations (Kerppola, 2008).

Bimolecular fluorescence complementation

One of the most commonly used PCAs in plants is the bimolecular fluorescence complementation (BiFC) that is based on the reconstitution of a fluorescent protein. In this technique, two POIs are fused each to the N- and C-terminal parts of a fluorescent protein and the fluorescence is restored when the tested candidates interact (Bracha-Drori et al., 2004; Walter et al., 2004). BiFC might result in a positive

signal even when POIs fused to the florescent protein fragments do not directly bind, but are part of the complex. An additional advantage is the direct visualization of PPIs in living plant cells, thus, providing information about the subcellular localization of the interaction. BiFC assays have been successfully applied in a variety of plant species, including *Arabidopsis, Nicotiana* spp. (Wang et al., 2016), *Allium* spp. (Yoshida et al., 2015), and rice (Chen et al., 2006). One of its major limitations is the intrinsic affinity of both parts of the fluorescent protein towards each other, possibly leading to protein reconstitution without an interaction between the POIs and, hence, in false positive results. Therefore, it is essential to use appropriate controls in BiFC experiments. Many reports have been published in which one of the tested proteins fused to a YFP fragment or the co-expression with one of the YFP fragments was used as a negative control (Horstman et al., 2014). A more adequate control would be the coexpression with a protein version with a mutated interaction interface. When this mutated protein version is not available, a closely related or an unrelated, but structurally similar, protein can also be used as a negative control (Kudla & Bock, 2016). All the aspects regarding appropriate controls for BiFC have been extensively reviewed elsewhere (Horstman et al., 2014; Kudla &d Bock, 2016).

As the reconstitution of the fluorophore is irreversible, this technique is ideal to detect low-affinity interactions, but unsuitable to study interaction dynamics and to obtain temporal information (Horstman et al., 2014). In yeast and mammalian cells, this problem has been solved by the introduction of a reversible BiFC system, based on a reconstituted infrared fluorescent protein (IFP1.4), i.e., an engineered chromophore-binding domain of a bacteriophytochrome from *Deinococcus radiodurans.* The IFP PCA has been used to study the spatio-temporal dynamics of protein complexes in hormone-induced signalling pathways. Nevertheless, this method needs to be improved to overcome drawbacks, such as low quantum yield or low brightness, and to be tested for the study of PPIs in plant systems (Tchekanda et al., 2014).

Split-luciferase assay

Enzyme complementation assays with luciferase are alternatives for BiFC, overcoming the problem of high auto-fluorescence in plant cells and resulting in a readout with a high signal-to-noise ratio, because no exogenous light is required for excitation (Morsy et al., 2008). In the split-luciferase assay, the candidate protein interactions can complement the luciferase activity that emits light through substrate oxidation (Luker et al., 2004). To date, six types of luciferases have been used to detect PPIs, each with a unique enzymatic character, different emission peaks, and brightness. Of all of them, the firefly luciferase (FLuc) is the most extensively applied in plants (Dale & Kato, 2016). Addition of the substrate can be easily achieved *in planta* with high efficiency by protoplast incubation or dissolved substrate spraying of the plants (Chen et al., 2008). Unlike BiFC, the split-luciferase assay does not

suffer from the spontaneous reformation of the enzyme. Additionally, the short half-life of the luciferases, the reversibility of the split protein assembly, and the high turn-over of the reconstituted protein make this technique useful to study both the association and dissociation of a protein pair (Luker et al., 2004; Xing et al., 2016). Therefore, the split-luciferase assay is suitable to study regulative PPIs, as nicely demonstrated in *Arabidopsis* and rice protoplasts by the elucidation of light-dependent and hormone-dependent interactions (Kato et al., 2010; Fujikawa et al., 2014). Although temporal information on PPIs can be obtained, the split-luciferase assay is less sensitive to low-affinity interactions than BiFC. Furthermore, floated-leaf luciferase complementation imaging (FLuCI) enabled the visualization of real-time complex assembly and disassembly and allowed quantitative analyses of protein interaction intensities, an indication of the interaction strengths (Gehl et al., 2011). Nonetheless, in the plant research, despite its advantages, the split-luciferase assay is not as popular as BiFC and other PPI validation methods, mostly because it is unable to point to the subcellular localization of the interaction (Xing et al., 2016). Optimization of assays that use novel luciferases more suitable for plant systems would make this approach more attractive for plant researchers. For instance, the recently engineered NanoBiT, characterised by the small size and the bright luminescence of the product should provide quantitative data and might be adapted for use in plants (Dixon et al., 2016). The size of the split luciferase is an important feature to consider; the large sizes of the protein fragments might mask interaction sites and in that manner disturb the detection of PPIs. Another ongoing challenge that can be tackled with NanoBiT is the increase of the light output to obtain an enhanced sensitivity.

Yeast two-hybrid

As mentioned above, Y2H is a widely used technique to identify PPIs in the discovery phase, but it can also be used as a validation method to confirm pairwise interactions. The main advantages of Y2H assays are simplicity, time-efficiency, and low cost. In addition, Y2H can be used to compare the relative interaction strength between tested proteins in a (semi-)quantitative manner. To this end, the enzymatic β-galactosidase-encoding reporter LacZ has been introduced that labels yeast cells with a colorimetric substrate, such as O-nitrophenyl β-D-galactopyranoside (ONPG) (Möckli & Auerbach, 2004). This approach has been already successfully applied in plant hormone signalling, e.g. jasmonate Goossens et al., 2015), abscisic acid (Lynch et al., 2017), auxin (Blakeslee et al., 2007), and strigolactones (Hamiaux et al., 2012), as well as for PPIs involved in photomorphogenesis (Luo et al., 2014) and stress responses (Mahfouz et al., 2006). However, it should be kept in mind that the rather non-physiological yeast environment, the forced protein coexpression, and the re-direction of tested proteins to the nucleus might limit the application of this method to (semi)quantification of binding affinities (Estojak et al., 1995). In the classic Y2H assay, interactions between the components of a

multi-subunit complex cannot be detected. Therefore, yeast three-hybrid (Y3H) has been developed, in which the third protein can serve as a ‘‘bridge’’ to connect two not directly interacting proteins or to stabilize a weak interaction (Maruta et al., 2016; Holtkotte et al., 2017). Alternatively, Y3H can be used to identify PPI inhibitors, i.e., proteins that modify or compete with one of the POIs (Li et al., 2011; Ling et al., 2017; Pesch et al., 2015).

CHARTING SPATIAL AND TEMPORAL DYNAMICS OF PPIS

PPI assays in which the sensitivity is enhanced by amplification of the signal might disturb other important PPI features, such as spatial and temporal resolution. Regulatory molecular complexes constantly assemble and disassemble in response to environmental stimuli or cellular status, possibly accompanied by subcellular re-localization of some proteins (Day & Schaufele, 2005). If the tested interaction is irreversible or its stability has been artificially increased by the use of PCA, the physiological dynamics of the interaction might be hampered. Therefore, several methods have been developed to assess this issue and provide additional information about localization and interaction lifespan.

Förster resonance energy transfer

Förster resonance energy transfer (FRET) is one of the techniques with the best spatial and temporal resolutions for the analysis of directly interacting proteins (Förster, 2012; Piston & Kremers, 2007). In FRET, the energy of a donor can be transferred to an acceptor fluorophore, when the former has an emission spectrum that overlaps with the absorption spectrum of the latter. Hence, FRET can lead to a decrease in the fluorescence emission intensity and lifetime of the donor, concomitantly with an increase in fluorescence emission intensity of the acceptor (Clegg, 1995; Stryer, 1978). However, FRET can only occur when the donor and acceptor molecules are in close proximity (< 10 µm) and in a permissive orientation; hence, FRET is useful only to analyse bimolecular, direct PPIs (Sun et al., 2013). Of the numerous methods available to detect FRET, the most commonly used are acceptor sensitized emission, acceptor photobleaching, and fluorescence lifetime imaging (FLIM) (Xing et al., 2016). FRET has emerged as a powerful approach to study PPIs, because it can be applied *in vivo*, thus allowing real-time quantitative analysis in living cells or whole plants (Russinova et al., 2004; Bücherl et al., 2013; Stahl et al., 2013). POIs are expressed in physiological or close-to-native environments in which essential cofactors are present and protein PTMs can occur. Additionally, confocal microscopy allows the spatial resolution of the studied PPI and it can even provide insights into the cell types within a tissue, or the subcellular compartment in which the interaction takes place. For instance, FRET-FLIM in combination with multiparameter fluorescence image spectroscopy (MFIS), showed that CLAVATA1 (CLV1) and ARABIDOPSIS CRINKLY4 (ACR4), involved in root stemness control, can form homo- and

heteromeric complexes that differ in their composition, according to the subcellular localizations at the plasma membrane and plasmodesmata (Stahl et al., 2013). In another study, *in vivo* FRET–FLIM was used to resolve cell-type-specific complex formation between the transcription factors SHORT-ROOT (SHR), SCARECROW (SCR), and JACKDAW (JKD), stably expressed under control of their endogenous promoters in the *Arabidopsis* root. FRET-FLIM revealed the spatial separation of protein interactions depending on the cell fate specification (Long et al., 2017). In addition, FRET has a good time resolution; hence it can be used to study transient interactions in real time, in the relevant physiological contexts. As an example, FRET-FLIM has been used to monitor receptor-complex formation dynamics over time between FLAGELLIN-SENSITIVE2 (FLS2) and BRI1-ASSOCIATED KINASE1 (BAK1) in the presence of the bacterial elicitor flagellin22 (flg22) at the plasma membrane (Somssich et al., 2015). Nevertheless, FRET has not been used extensively in PPI studies, because its sensitivity is lower than that of other validation techniques, it is highly labour intensive, and it requires advanced equipment. Indeed, the measurement of FRET signals usually needs careful interpretation and multiple control experiments. Moreover, the technology is often subjected to problems with background auto-fluorescence and it is only feasible on small scales (Bhat et al., 2006).

Bioluminescence resonance energy transfer

To overcome the problem of background fluorescence in FRET, Bioluminescence Resonance Energy Transfer (BRET) was developed. In this method, the fluorescent donor protein is replaced by a bioluminescent molecule (usually *Renilla* luciferase), whereas the acceptor remains a fluorophore (for instance, YFP) (Xu et al., 1999; Subramanian et al., 2006). The oxidative reaction catalysed by the bioluminescent donor, in the presence of an appropriate substrate, generates light emission that excites the acceptor fluorophore when both molecules are closer than 10 nm (Pfleger & Eidne, 2006). A key difference of BRET is the lack of an external light source for the donor excitation, so the problems associated with FRET are avoided, such as photobleaching, auto-fluorescence of plant tissues, or acceptor bleed-through, with an increased sensitivity as a consequence. Hence, BRET is an interesting technique for real-time monitoring of PPIs in living plant cells. It is also more suitable for high-throughput screening than FRET (Boute et al., 2002; Xu et al., 2007; Maloney et al., 2015). Nevertheless, because light emission generated by bioluminescent molecules is typically low, thus requiring long exposure times, even with very responsive charge-coupled device cameras, BRET makes it impossible to analyse dynamic interactions (Xu et al., 1999). Constant progress in the development of novel luciferases that deliver enhanced signals can significantly increase the sensitivity of BRET assays. Several examples of enzyme-substrate pairs have been described with up to 15-fold increased sensitivity (Kimura et al., 2010; Kim et al., 2011). Interestingly, BRET and FRET can be combined in

sequential BRET-FRET (SRET), a technique that allows PPI analysis of three different proteins (Carriba et al., 2008). In SRET, the light emission by a luciferase-tagged protein triggers excitation of a first fluorophore-fused protein and subsequent FRET with the second fluorescent fusion protein. SRET is especially suitable for the study of the formation of higher-order protein complexes of plasma membrane-associated proteins that is rather problematic with other PPI assays. SRET has been shown to work well in the mammalian field for the detection of heterodimers between CD4, CXCR4, and CCR5 proteins involved in HIV-1 cell infection (Martínez-Muñoz et al., 2014) or complexes formed between dopamine receptors (Navarro et al., 2013). Thus far, although SRET has not been applied in plant research, it could be an attractive approach to study protein heterodimerization under physiological conditions. To this end, the right combination needs to optimised of donors and acceptors for BRET and FRET and of the adequate luciferase substrates.

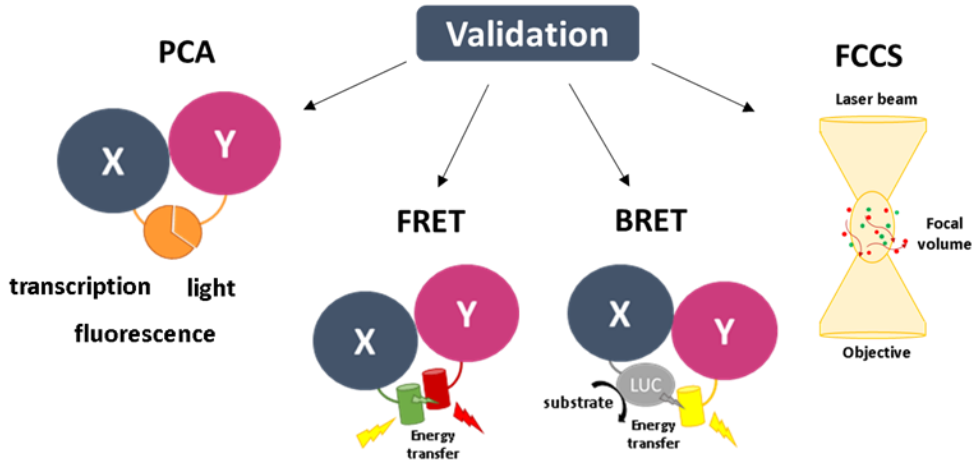

Figure 2. Schematic representation of PPI validation assays. In PCA, a physical interaction between bait and prey reconstitutes a functional protein (transcription factor, fluorescent protein, or luciferase) that activates the reporter gene, fluorescence, or light. In FRET and BRET, the close proximity between a FRET/BRET donor and an acceptor is mediated by a physical interaction between bait and prey. As a result, resonance energy transfer can be detected. FCCS quantifies co-migration of two fluorescently labelled proteins under a confocal laser scanning microscope diffusing through a minute focal volume.

Fluorescence correlation spectroscopy

Another approach to monitor protein complex formation in vivo that also allows to study spatial and temporal PPI dynamics is fluorescence correlation spectroscopy (FCS) and its dual-colour version, fluorescence cross-correlation spectroscopy (FCCS). The main principle of FCS is the measurement of fluorescence intensity fluctuations generated by diffusion of fluorescently labelled proteins after their excitation by a confocal laser scanning microscope in a very small detection volume (Wehry, 1984). Binding of an interacting partner to the fluorescently-labelled molecule limits its mobility, thereby

affecting the fluctuation rate (Langowski, 2008). FCS in combination with fluorescence recovery after photobleaching (FRAP) has been successfully applied to investigate the mobility of a receptor kinase in plant protoplasts and in living ovules of *Arabidopsis* (Kwaaitaal et al., 2011). More recently, a protocol has been developed for scanning FCS in *Arabidopsis* roots to assess the rate and direction of protein movement (Clark and Sozzani, 2017). However, this method is not suitable for studying particular PPIs, because the decreased protein diffusion coefficient indicates a complex formation but does not allow the direct identification of the binding partner (Macháň & Wohland, 2014). To determine the POI interactors, the dual-colour FCCS has been designed, in which the tested proteins are labelled with different fluorophores and their intensity fluctuations are cross-correlated to follow whether they diffuse as one complex. In this technique, it is essential to use two fluorophores with non-overlapping spectra to avoid energy transfer and bleed-through fluorescence (Schwille et al., 1997; Langowski, 2008; Wachsmuth et al., 2015). If the tested proteins interact with each other, they might probably fluctuate in a synchronized manner, causing an increase in the amplitude of the cross-correlation function. Application of FCCS determined the oligomeric state of SHR and SCR with subcellular resolution in root cells, confirmed the interaction between the two proteins, and resolved their stoichiometric binding ratio (Clark et al., 2016). In another study, FCCS was used to assess the mobility of SERK1, SERK3, and BRASSINOSTEROID INSENSITIVE 1 (BRI1) receptors and to settle the complex protein composition (Hink et al., 2008). Nevertheless, it is worth mentioning that FCCS calculates the probability that two tested proteins occur simultaneously in the same small volume rather than detect their direct interaction. Therefore, the use of additional, more stringent PPI validation techniques is advisable to demonstrate direct interactions (Lalonde et al., 2008). Although the F(C)CS field is improving continuously, there is still a need for progress in various aspects, including novel detection and data analysis schemes and the development of brighter and more photostable fluorescent proteins in various colours (Li et al., 2016b).

CONCLUSIONS

The interactions between proteins are crucial for the correct coordination of signalling processes as well as of metabolic and structural functions in every cell. As shown in this review, numerous techniques are available to detect PPIs, both *in vivo* and *in vitro,* all with their unique characteristics and detection profiles that provide insight into the dynamics, the localization and timing of PPIs during cellular events (Table 1). Only combinations of several complementing methods can provide a reliable and comprehensive view on PPIs in living cells. In the future, new technologies should be developed to facilitate large-scale PPI studies with a view on the dynamics and on the spatial and temporal resolution of interactions in selected cell types and even whole plants.

Table 1. Comparison of PPI techniques used thus far in plants that are discussed in this chapter

Method	Application	Properties					PPI nature		
		Read-out	Signal enhancement	*In vitro/in vivo*	Sensitiviy	Throughput	Interaction mode	Localization	Low-affinity	Dynamics
Y2H	D, V	Transcriptional activation of reporter gene	Yes	*In vivo* (h)	***	***	Binary	No	Yes	No
AP-MS	D	MS	No	*In vitro*	**	**	Co-complex	No	No	Yes
Bio-ID	D	MS	No	*In vitro*	**	**	Co-complex	No	Yes	No
BiFC	V	Fluorescence	No	*In vitro*	***	*	Binary	Yes	Yes	No
Split-LUC	V	Luminescence	Yes	*In vivo*	**	**	Binary	No	Yes	Yes
FRET	V	FI variations	No	*In vivo*	*	*	Binary	Yes	No	Yes
BRET	V	Fluorescence	No	*In vivo*	*	*	Binary	Yes	No	Yes
FCCS	V	FI fluctuations	No	*In vivo*	*	*	Binary	Yes	No	Yes

D, detection; V, validation; MS, mass spectrometry; FI, fluorescence intensity; (h), heterologous; *, low; **, medium: ***, high.

II

RESULTS

Overview of the results

In each result chapter tandem affinity purification (TAP) was used to identify novel protein complexes formed around the core components of the strigolactone and karrikin pathways (Table 1). In the first three chapters SUPPRESSOR OF MAX2 1 (SMAX1)-LIKE (SMXL) 7 and its resistant to degradation version, ΔSMXL7 were used as baits to perform TAP in *Arabidopsis* cell cultures. The obtained data was analyzed in the quantitative manner, using the label free quantification algorithm of MaxQuant software or the normalization on the bait level (**Chapter 3**), and in a qualitative manner, by subtracting the background proteins from the list of all copurified preys (**Chapter 4 and Chapter 5**) (Van Leene et al., 2015). In **Chapter 6,** the SMAX1 and ΔSMAX1 TAP experiments in *Arabidopsis* cell cultures were analyzed using both the quantitative and qualitative approach. In **Chapter 7** and **Chapter 8**, MORE AXILLARY GROWTH 2 (MAX2), DWARF 14 (D14) and KARRIKIN INSENSITIVE 2 (KAI2) were selected as the bait proteins to co-purify complexes in *Arabidopsis* cell cultures and seedlings, respectively and the qualitative approach was used for the data analysis.

Table 1. The overview of all TAP experiments described in the results chapters

BAIT	ENVIRONMENT	ANALYSIS	INTERACTORS	CHAPTER
SMXL7 ΔSMXL7	*Arabidopsis* cell cultures	Quantitative	D14 TPL/TPR	Chapter 3
		Qualitative	SINT1 SINT2 SINT3	Chapter 4
			FyPP1/3 SAL4	Chapter 5
SMAX1 ΔSMAX1	*Arabidopsis* cell cultures	Quantitative Qualitative	___	Chapter 6
MAX2 D14 KAI2	*Arabidopsis* cell cultures	Qualitative	PAPP5	Chapter 7
	Arabidopsis seedlings	Qualitative	CCP1 ACD32.1	Chapter 8

Chapter 3

Quantitative tandem affinity purification, an effective tool to investigate protein complex composition in plant hormone signaling: strigolactones in the spotlight

Adapted from Frontiers in Plant Science

Sylwia Struk[1,2], Lukas Braem[1,2,3,4], Alan Walton[1,2,3,4] , Annick De Keyser[1,2], François-Didier Boyer[5], Geert Persiau[1,2], Geert De Jaeger[1,2], Kris Gevaert[3,4] & Sofie Goormachtig[1,2]

[1] Ghent University, Department of Plant Biotechnology and Bioinformatics, 9052 Ghent, Belgium
[2]VIB, Center for Plant Systems Biology, 9052 Ghent, Belgium
[3] Ghent University, Department of Biochemistry, 9000 Ghent, Belgium
[4] VIB, Center for Medical Biotechnology, 9000 Ghent, Belgium
[5]Institut National de la Recherche Agronomique, Institut Jean-Pierre Bourgin, Versailles, France

S.S. was the main author of the manuscript and performed all experiments, except the molecular cloning that was done by A.D.K. and the acquisition of the TAP data prepared by G.P. and G.D.J. L.B and A.W. were involved in MS/MS data analysis. F.D.B. kindly provided the synthetic strigolactone analog rac-GR24. K.G. and S.G. supervised the project and contributed to the writing of the manuscript.

Abstract

Phytohormones tightly regulate plant growth by integrating changing environmental and developmental cues. Although the key players have been identified in many plant hormonal pathways, the molecular mechanisms and mode of action of perception and signaling remain incompletely resolved. Characterization of protein partners of known signaling components provides insight into the formed protein complexes, but, unless quantification is involved, does not deliver much, if any, information about the dynamics of the induced or disrupted protein complexes. Therefore, in proteomics research, the discovery of what actually triggers, regulates or interrupts the composition of protein complexes is gaining importance. Here, tandem affinity purification coupled to mass spectrometry (TAP-MS) is combined with label-free quantification (LFQ) to a highly valuable tool to detect physiologically relevant, dynamic protein-protein interactions in *Arabidopsis thaliana* cell cultures. To demonstrate its potential, we focus on the signaling pathway of one of the most recently discovered phytohormones, strigolactones.

INTRODUCTION

Plants produce a broad range of phytohormones, which are small molecules that regulate their growth and development and control their responses to biotic and abiotic stresses, locally as well as throughout the entire plant. Although phytohormones have been intensively studied, a lot remains to be resolved about the mechanisms underlying their mode of action (Černý et al., 2016). Proteins that are crucial for the perception and the transduction of molecular signals, such as phytohormones, often form complexes to fulfill their biological function. Most of the protein–protein interactions (PPIs) are not static, but rather dynamic, because they are constantly subjected to changes in the crowded cellular environment. Knowledge of the interaction partners of a given protein may provide insight into its function at the molecular level or into the process in which it is involved. Although quite some methods exist to detect PPIs, for a better understanding of cellular mechanisms, the identification of functionally relevant PPIs and, in particular, the characterization of how they are influenced by varying physiological conditions are required (Buntru et al., 2016).

Affinity purification techniques coupled to mass spectrometry (AP-MS) are established tools to investigate the spectrum of possible interaction partners of a protein of interest. The proteome-wide insight they offer provides information on both direct as well as indirect interactors. In the plant field, tandem affinity purification (TAP) is probably one of the most successful AP-MS approaches (Dedecker et al., 2015) and has been efficiently used to purify protein complexes from different tissues and from several plant species (Rohila et al., 2006; Van Leene et al., 2007, 2015; Nelissen et al., 2015; Goossens et al., 2016). To execute TAP, a bait protein is fused translationally with a double affinity tag, most commonly the GS-tag, consisting of two immunoglobulin G-binding domains of protein G, combined with a streptavidin-binding peptide, separated by a specific tobacco etch virus (TEV) protease cleavage site (Bürckstümmer et al., 2006; Van Leene et al., 2007) or by a rhinovirus 3C protease cleavage site in the improved version (Van Leene et al., 2015). The protein complex, in which the tagged bait is engaged, is retrieved in two consecutive purification steps under near physiological conditions, whereafter the proteins are digested and identified by means of MS (Van Leene et al., 2015). Two-step purifications generally lead to less complex samples that are relatively free from the unspecific binding proteins in comparison with single-step purifications, thereby allowing a higher resolution view of the members of a complex (Li, 2011). However, TAP-MS typically identifies only stable interactors and is faced with difficulties in the case of proteins interacting with weak affinity (Gavin et al., 2011).

It is becoming increasingly clear that not only knowledge of the interaction partners of a bait protein is important, but also the conditions under which such interactions occur (Buntru et al., 2016). Proteins involved in plant hormone signaling provide a good example. During auxin signaling, the simple spectrum of all possible interaction partners of the AUXIN/INDOLE-3-ACETIC ACID (AUX/IAA) proteins includes the AUXIN RESPONSE FACTOR (ARF) activators, TOPLESS (TPL), TOPLESS RELATED (TPR) proteins, the generic members of the SCF complex ARABIDOPSIS SKP1-LIKE (ASK1) and CULLIN1 (CUL1), the auxin-related F-BOX protein TRANSPORT INHIBITOR RESPONSE 1 (TIR1), E2 proteins, and ubiquitin. However, this list does not reveal the underlying dynamics, such as the fact that the AUX/IAA proteins interact with the SCF^{TIR1} complex only in the presence of auxin, while otherwise being linked to ARF activators to repress their transcriptional activity through the action of TPL/TPR proteins (reviewed in Leyser, 2018). Obviously, information on the dynamics of the AUX/IAA complexes and on the effect of auxin is required to gain full insight into the signaling cascade of this hormone. Similar signal-dependent interactions have been identified for jasmonates, brassinosteroids, and ethylene, as well as for other, non-hormone-related dynamic interactions that modulate responses to environmental cues or developmental stages (Larrieu and Vernoux, 2015).

Hence, it is important to study how protein complexes act in response to (different) stimuli. To this end, a technique is required that fulfills three criteria: (i) comprehensive coverage of proteins engaged in a complex; (ii) compatibility with a biological system in which a trigger (stimulus) can be applied; and (iii) a quantitative readout. Therefore, we have developed a quantitative method based on TAP in cell cultures to study protein complex dynamics in *Arabidopsis thaliana*. Label-free quantification (LFQ) is applied to determine shifts in the levels of protein complex members in a trigger-dependent manner, thus mapping the dynamics of the protein complexes. We used the MaxLFQ algorithm integrated into the MaxQuant software (Cox et al., 2014). This comparison of proteome samples avoids stable isotope labeling, of which the metabolic version is somewhat restricted in plants due to very high costs or labeling efficiency issues (Gruhler et al., 2005). LFQ relies on the replicates analyses to quantify differences in peptide ion intensities between different samples by means of statistical algorithms. For AP-MS studies, LFQ is based on the observation that most experimental conditions do not influence the abundance of nonspecifically interacting proteins, thereby allowing accurate identification of the proteins that interact differentially, for instance, because of a treatment. Thus, in general, LFQ techniques are promising alternatives, because they are cost effective, easy to perform, and suitable for comparative analysis of large numbers of samples (Ramisetty and Washburn, 2011).

We focused on the protein complex involved in strigolactone signaling. This hormone was discovered a decade ago and its essential role in modulating various aspects of above- and below-ground plant architecture has been demonstrated (Smith and Waters, 2012). However, full knowledge of the signaling components is missing. In *Arabidopsis,* the synthetic strigolactone analog *rac*-GR24 is perceived and hydrolyzed by the α/β hydrolase DWARF14 (D14). As a result, D14 undergoes a conformational change (Yao et al., 2016) that allows its interaction with the F-box protein MORE AXILLARY BRANCHES 2 (MAX2), that is part of an SCF E3 ubiquitin ligase complex (Stirnberg et al., 2007; Hamiaux et al., 2012), and with proteins from the SMAX1-like (SMXL) family, which are the most recently described components of the strigolactone pathway (Jiang et al., 2013; Stanga et al., 2013; Zhou et al., 2013). Forward genetics in rice (*Oryza sativa*) revealed that a SMXL homolog, DWARF 53 (D53) is a repressor of the strigolactone signaling involved in tiller number regulation (Jiang et al., 2013; Zhou et al., 2013). Indeed, a gain-of-function *d53* mutant had a high tillering, dwarf phenotype, and was insensitive to the addition of strigolactones (Zhou et al., 2013). The gain-of-function phenotype was caused by the mutation of an amino acid region, resulting in resistance against strigolactone-induced protein degradation (Jiang et al., 2013; Zhou et al., 2013). In *Arabidopsis*, the SMXL family consists of eight members divided into four subclades, from which SMXL6, SMXL7, SMXL8 together with D53 form one phylogenic clade (Stanga et al., 2013). These *Arabidopsis* SMXL proteins were also rapidly degraded by the 26S proteasome upon treatment with *rac*-GR24 in a D14- and MAX2-dependent manner, thereby influencing the shoot and root architecture. Mutation of the amino acid residues of SMXL6 or SMXL7, corresponding to those mutated in *d53* allele, conferred resistance to *rac*-GR24–dependent degradation. The role of this region and its involvement in the observed resistance to strigolactone-induced degradation remains unclear (Soundappan et al., 2015; Wang et al., 2015).

Here, we aimed at investigating whether the reported changes in the protein complexes formed around SMXL7 could be discovered by means of quantitative TAP (qTAP) in *Arabidopsis* cell cultures in the presence and absence of *rac*-GR24. As baits, both SMXL7 and its modified version that is resistant to strigolactone-induced degradation were used. We show that the study of protein complexes involving a proteasome target as the bait protein is challenging, because of the bait degradation. Nevertheless, we demonstrate that the TAP technology combined with LFQ provides a sensitive platform with sufficient resolution to detect *rac*-GR24–dependent SMXL7 interactions in *Arabidopsis*.

RESULTS

Arabidopsis cell suspension cultures respond to *rac*-GR24 treatment

Cell cultures provide a good system to study PPIs involved in basic cellular pathways, because they offer a high protein yield and the possibility to perform hormone-induced studies (Van Leene et al., 2015). Indeed, they have already allowed the characterization of signaling complexes in different hormonal pathways, including, auxin, abscisic acid, and jasmonate (Pauwels et al., 2010; Fernandez-Calvo et al., 2011; Irigoyen et al., 2014; Karampelias et al., 2016). However, this environment has never been used to study strigolactone signaling. To test whether the strigolactone pathway is active, the response of the cell cultures to *rac*-GR24 was tested. To this end, SMXL7 was N- and C-terminally fused with a GS^{rhino} tag and expressed in *Arabidopsis* cell cultures (see Materials and Methods). Only the N-terminal fusion (*35S::GSrhino-SMXL7*) yielded high protein levels, whereas no protein was detected for the C-terminal construct (Supplemental Figure 1). Therefore, only *35S::GSrhino-SMXL7* was utilized. The response to treatments with 1 µM *rac*-GR24 or with acetone (mock) was checked at different time points by Western blot analysis (Figure 1).

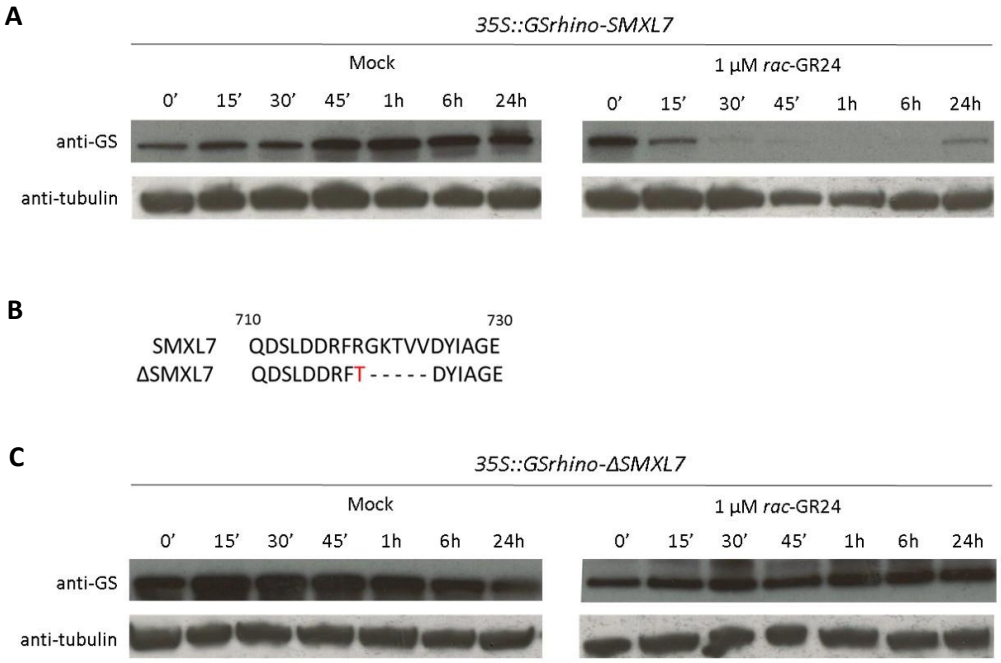

Figure 1. Response of *Arabidopsis* cell suspension cultures to *rac*-GR24. SMXL7 protein levels in cell cultures transformed with *35S::GSrhino-SMXL7* (A) or *35S::GSrhino-ΔSMXL7* (C) at different time points after treatment with either 0.01% acetone (mock) or 1 µM *rac*-GR24 (' minutes, h, hours after treatment). Detection was done with anti-GS (top) and anti-tubulin (bottom) antibodies, the latter as loading control. (B) Protein sequence alignment of the amino acid region of SMXL7 and ΔSMXL7. The ΔSMXL7 protein carries an Arg-to-Thr mutation followed by a deletion of residues 719-723 (Gly-Lys-Thr-Val-Val).

The SMXL7 protein level decreased starting from 15 min after treatment and was partially recovered after 24 h (Figure 1A). Additionally, we tested a ΔSMXL7 allele that carries a mutation similar to that described in the *d53* allele in rice (Figure 1B) to render the protein resistant to *rac*-GR24–induced degradation (Jiang et al., 2013). Protein expression was detected in cell cultures for both N- and C-terminal fusions of GS^{rhino}-tagged ΔSMXL7, although the levels were higher for the N-terminally tagged protein (Supplemental Figure 1). The ΔSMXL7 sensitivity to *rac*-GR24 was tested in cell cultures expressing *35S::GSrhino-ΔSMXL7* similarly as for *35S::GSrhino-SMXL7* and the *ΔSMXL7* protein level did not decrease upon treatment with *rac*-GR24, in agreement with previously published data (Jiang et al., 2013; Soundappan et al., 2015) (Figure 1C).

Taken together, these data demonstrate that *Arabidopsis* cell cultures respond to *rac*-GR24 and that all signaling components that are required for strigolactone-induced SMXL7 degradation are present in the cell cultures. Additionally, the change in the amino acid sequence of *ΔSMXL7* stabilized the protein after *rac*-GR24 treatment, confirming the importance of this region for protein degradation in both rice and *Arabidopsis* (Jiang et al., 2013; Soundappan et al., 2015).

Quantitative TAP reveals changes in the SMXL7 protein complex compositions

To examine the dynamics of the protein complexes formed around SMXL7 and their role in strigolactone signaling, we carried out TAPs in *Arabidopsis* cell cultures expressing GS^{rhino}-tagged *SMXL7* or *ΔSMXL7* (see Material and Methods). After the LC-MS/MS analysis of the TAP samples, spectra were searched with the MaxQuant software and resulted in the identification of 299 proteins for SMXL7 and 347 for ΔSMXL7. MaxLFQ was then used to quantify the identified proteins between the tested conditions over the four replicates. Further analysis was performed with the Perseus software as described in Smaczniak et al., 2012b. Changes in protein abundances were expressed after log2 transformation of protein LFQ intensity values. Proteins that were not assigned LFQ values in the MaxQuant search, because their abundance was below the detection limit under that specific condition or replicate, were assigned a value based on a normal distribution centered around the lowest detection limit of the measured intensities as previously described (Smaczniak et al., 2012b) (Supplemental Dataset 1). To evaluate the reproducibility of the analysis, scatter plots were made to calculate the correlations of LFQ values between replicates. Noteworthy, the consistency between replicates is crucial for downstream statistical analysis. In our experiment, the Pearson correlation coefficients for all replicate pairs ranged from 0.765 to 0.959 for

SMXL7 and from 0.891 to 0.976 for ΔSMXL7, indicating a good to very good reproducibility (Supplemental Figure 2).

Given the fast degradation of the SMXL7 protein (Figure 1A), TAP analysis was performed after 10 min of *rac*-GR24 treatment. To test the influence of this treatment, bait protein levels were compared between the conditions. The intensity of the SMXL7 protein was significantly lower in the hormone-treated samples than that in the mock samples (Figure 2). In agreement with the Western blot analysis, the protein intensity levels of ΔSMXL7 were not influenced by the treatment with the strigolactone analog (Figure 2).

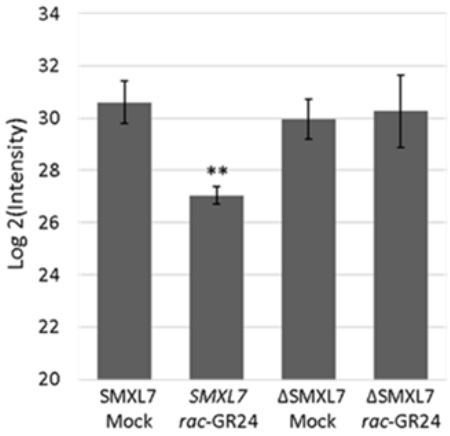

Figure 2. Response of the bait SMXL7 and ΔSMXL7 proteins to the treatment with *rac*-GR24 in TAP samples. Average intensity values between all mock and treated replicates with standard deviation indicated. Asterisks indicate statistical significant differences ($P < 0.01$, Student's *t* test).

Statistical analysis was used to identify SMXL7-interacting proteins enriched in one of the tested conditions. In short, samples were assembled into either 'mock' or 'treatment' groups, with each group containing four biological repeats. In the first assessment, a *t* test was done on the LFQ intensity values, allowing us to detect D14 as the only significant outlier. D14 was identified at significantly higher levels in *rac*-GR24–treated samples, indicating that the strigolactone receptor was recruited to the SMXL7 complex only in the presence of *rac*-GR24 (Figure 3C).

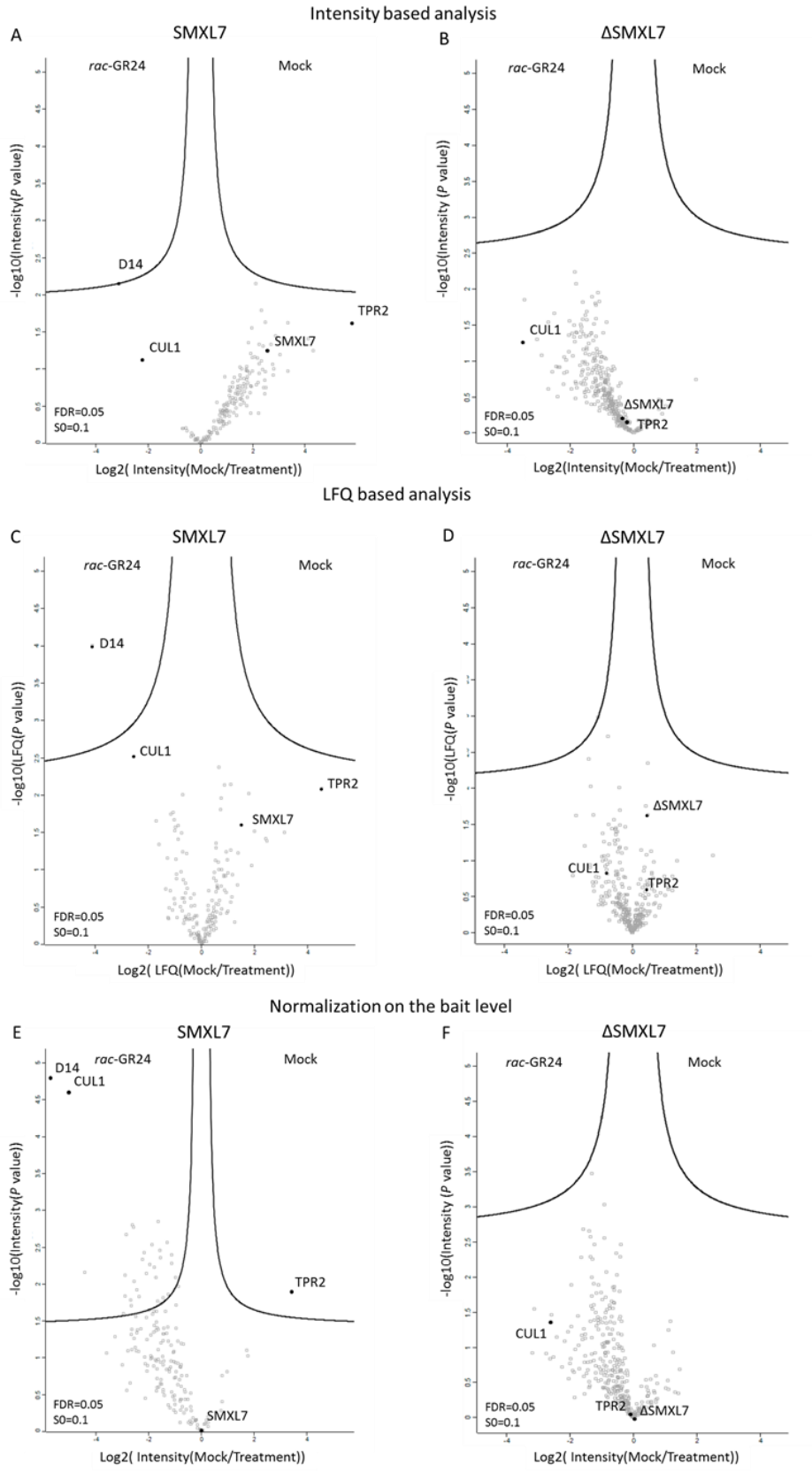
Intensity based analysis
A
SMXL7
rac-GR24
Mock
-log10(Intensity(P value))
D14
TPR2
CUL1
SMXL7
FDR=0.05
S0=0.1
Log2(Intensity(Mock/Treatment))
B
ΔSMXL7
rac-GR24
Mock
-log10(Intensity (P value))
CUL1
ΔSMXL7
TPR2
FDR=0.05
S0=0.1
Log2(Intensity(Mock/Treatment))
LFQ based analysis
C
SMXL7
rac-GR24
Mock
-log10(LFQ(P value))
D14
CUL1
TPR2
SMXL7
FDR=0.05
S0=0.1
Log2(LFQ(Mock/Treatment))
D
ΔSMXL7
rac-GR24
Mock
-log10(LFQ(P value))
ΔSMXL7
CUL1
TPR2
FDR=0.05
S0=0.1
Log2(LFQ(Mock/Treatment))
Normalization on the bait level
E
SMXL7
rac-GR24
Mock
-log10(Intensity(P value))
D14
CUL1
TPR2
FDR=0.05
S0=0.1
SMXL7
Log2(Intensity(Mock/Treatment))
F
ΔSMXL7
rac-GR24
Mock
-log10(Intensity (P value))
CUL1
FDR=0.05
S0=0.1
TPR2
ΔSMXL7
Log2(Intensity(Mock/Treatment))

Figure 3. Dynamics of SMXL7 and ΔSMXL7 protein complexes. Volcano plots showing the distribution of all quantified proteins after filtering and statistical analysis, with their corresponding protein abundance ratios between two samples (Mock/Treatment) over the *t* test *P* value (FDR=0.05, S0=0.1). The cutoff curve indicates which proteins are significantly more associated with SMXL7/ΔSMXL7 in mock (right) and after addition of *rac*-G24 (left). Analysis was based on intensity values (A, B, E, F) or on LFQ values (C, D). Protein distribution after normalization of the bait level (E, F).

The LFQ values are normalized based on the overall protein abundance in the replicates. When non-normalized protein intensity values were used, the SMXL7 levels were clearly higher under mock conditions than those after treatment (Figure 3A), and this difference was also visible after LFQ application (Figure 3C). We then implemented another normalization step, in which we normalized on the bait level by subtracting the intensity values of the bait from those of the interacting proteins (Figures 3E). This drastically increased the number of preys identified as significantly associated with SMXL7 in the presence of *rac*-GR24; the total list of candidate interactors now contained 33 proteins (Supplemental Table 2). Many of the proteins associated with SMXL7 upon *rac*-GR24 treatment were related to the 26S proteasome (Figure 4), hinting at a very active degradation process after hormone addition. Besides D14, CUL1 was also a protein that was significantly more associated with SMXL7 upon *rac*-GR24 treatment. The reason might be that in the current model of strigolactone signaling D14 recruits the SCF^{MAX2} complex of which CUL1 is one of its members (Stirnberg et al., 2007). Additionally, under the same condition, ubiquitin was significantly enriched, in line with the model of the ubiquitin-mediated degradation of SMXL7 upon strigolactone treatment.

Interestingly, TPR2 was the only protein significantly more associated with SMXL7 under mock than in treatment conditions. It is thus likely that in response to *rac*-GR24, TPR2 might disassociate from the SMXL7 complex prior to the SMXL7 degradation. In the volcano plot based on the LFQ analysis, the distribution of both CUL1 and TPR2 is clearly separated from all the other quantified proteins, although not crossing the significance line (Figure 3C).

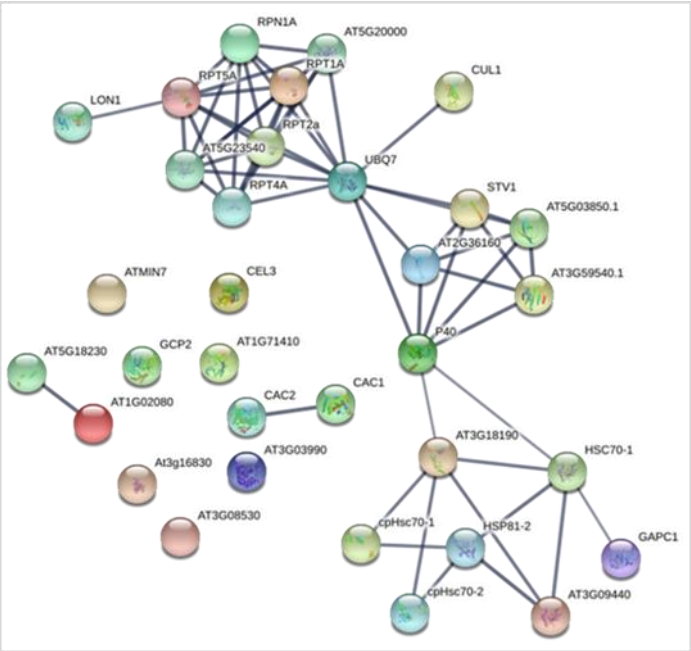

Figure 4. STRING network revealing connections between the proteins associated with SMXL7. All the proteins that were significantly more associated with SMXL7 in *rac*-GR24-treated condition after normalization on the bait level were analyzed. Only high confidence interactions (score > 0.900) are shown. The three main complexes are involved in degradation mediated by 26S proteasome and 26S regulatory modules (top cluster), ribosome-related proteins (middle cluster), and chaperones involved in protein folding (bottom cluster).

To assess whether the mutation of the amino acid region in ΔSMXL7 might influence the dynamics of protein complexes formed with SMXL7, we repeated the experiment with the ΔSMXL7 TAP constructs and applied the same statistical analysis. First, in the volcano plot based on non-normalized protein intensity values, the ΔSMXL7 levels were stable under both conditions (Figure 3B). Further, no proteins were detected as significantly more associated with the bait in one of the tested conditions (Figure 3B, D, E), demonstrating the importance of the mutated amino acid region for *rac*-GR24–induced interactions. D14 did not only no longer interact with ΔSMXL7 in a *rac*-GR24–dependent manner, but also it was not identified in any of the tested conditions (Figure 5). Additionally, TPR2 was detected at the similar intensity level both in mock and after treatment with the strigolactone analog (Figure 5).

	SMXL7 Mock				SMXL7 *rac*-GR24				ΔSMXL7 Mock				ΔSMXL7 *rac*-GR24			
replicate	1	2	3	4	1	2	3	4	1	2	3	4	1	2	3	4
CUL1	0.0	0.0	0.0	14.3	15.9	19.5	17.1	15.6	15.2	11.5	13.3	16.4	15.3	15.6	18.4	18.8
TPR2	21.2	23.4	18.9	20.0	0.0	20.0	0.0	0.0	18.2	19.0	20.6	19.0	19.4	17.7	20.5	20.6
D14	0.0	0.0	0.0	0.0	17.5	19.7	17.3	17.1	0.0	0.0	0.0	0.0	0.0	0.0	0.0	0.0

Figure 5. Identification of CUL1, TPR2, and D14 in SMXL7 and ΔSMXL7 TAP experiments. The heat map displays the log2 intensity values of CUL1, TPR2 and D14 found in SMXL7 and ΔSMXL7 TAP experiments in mock and after *rac*-GR24 treatment in four repeats. Red 0.0 values indicate that the protein was not found in the repeat.

To validate the interaction of SMXL7 and ΔSMXL7 with D14 and TPR2, we used the Y2H LexA system, based on the detection of interactions through blue coloring of the yeast colony when spotted on selective SD-Ura-Trp-His medium supplemented with X-gal. In agreement with the qTAP analysis, SMXL7 interacted with D14 in a *rac*-GR24–dependent manner (Figure 6). The same was observed for ΔSMXL7 which is in contradiction with the results of the ΔSMXL7 qTAP analysis. To test the interaction with TPR2, we used the N-terminal fragment of TPL (TPL-N), consisting of the first 189 amino acids which is highly conserved between TPL and TPR2 proteins. TPL-N contains the LisH, CTLH and TOP domains, that had previously been described as crucial for binding to the EAR motif and mediating protein-protein interactions (Szemenyei et al., 2008; Nagels Durand et al., 2012; Cuéllar Pérez et al., 2014; Gonzalez et al., 2015). Y2H analysis confirmed the direct interaction of TPL-N with SMXL7 and ΔSMXL7 under both conditions. The SMXL7-TPL-N interaction was not disturbed after addition of *rac*-GR24, as would have been expected from the qTAP analysis. Taken together, although we can confirm the interaction between SMXL7, D14 and between SMXL7 and TPL, we cannot catch the entire *rac*-GR24–induced dynamics of the SMXL7-D14–TPR2 complex in the binary assay.

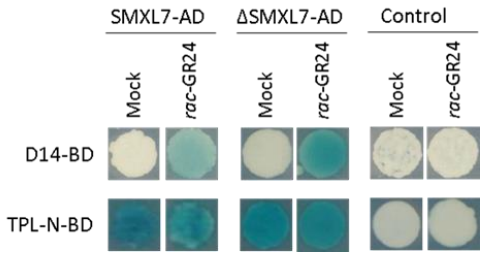

Figure 6. Interactions between SMXL7/ΔSMXL7 and D14 or TPL-N. The EGY48 (p8opLacZ) yeast (*Saccharomyces cerevisiae*) strain was cotransformed with D14 or TPL-N in pGILDA (BD) and SMXL7/ΔSMXL7 in pB42AD (AD) or pB42AD alone (control). Transformed yeasts were spotted on inducing medium containing Gal and Raf supplemented with 5-bromo-4-chloro-3-indolyl-β-D-galactopyranoside acid (X-Gal).

DISCUSSION

Here, we describe the use of LFQ MS-based analysis of samples generated by TAP to assess changes in protein–protein interactions in response to plant hormones. We used *Arabidopsis* cell cultures to set up the method, because this system had already been shown to be highly useful to study plant hormone signaling (Pauwels et al., 2010; Fernandez-Calvo et al., 2011; Irigoyen et al., 2014; Karampelias et al., 2016).

Previously, the LFQ method has been proven to be efficient for the characterization of novel protein complexes in single-step AP-MS. Two independent protocols have been developed for plant research in which LFQ is used to distinguish between unspecific binding proteins and true interactors (Smaczniak et al., 2012b; Wendrich et al., 2017). Implementation of LFQ in AP-MS successfully allowed the identification of a critical regulator of the vascular development, the basic helix-loop-helix (bHLH) transcription factor dimer (De Rybel et al., 2013), the detection of the interaction network between five major floral homeotic MADS domain proteins (Smaczniak et al., 2012a), and the discovery of an association between PIN-FORMED (PIN) auxin efflux carriers and dynamin-related proteins (Mravec et al., 2011). Nevertheless, these protocols did not take into consideration the changes in the formed protein complexes upon perturbations but show a stable view on all possible interactors.

In our approach, the basic idea is that TAP is performed on the cell cultures expressing a bait protein after they have been triggered with a particular plant hormone for a specific time. For data analysis, an LFQ algorithm, in this case MaxLFQ, was used in combination with statistical tests to identify the relevant interacting proteins. MaxLFQ requires sufficient numbers of stable background proteins to allow sample normalization (Pardo and Choudhary, 2012), thus many data points are needed to discriminate true interactors that associate differentially with a bait due to the treatment only. Although TAP provides relatively clean samples with rather low numbers of such background proteins, it has been already successfully used for the quantitative analysis of the changes in protein complexes formed around ANGUSTIFOLIA3 (ZmAN3) in maize (*Zea mays*); ZmAN3 was shown to engage in an interaction with distinct GROWTH-REGULATING FACTORs (GRFs) in the division zone when compared to the expansion zone of the growing leaf (Nelissen et al., 2015).

As a proof of concept, we focused on the protein complexes involved in strigolactone signaling. We demonstrated that *Arabidopsis* cell suspension cultures are suitable for studying the strigolactone pathway, because all the components required for the *rac*-GR24–dependent degradation of SMXL7 are present. Indeed, through Western blot and qTAP analysis, we detected a decrease in SMXL7 protein levels

upon treatment with the strigolactone analog, indicative of *rac*-GR24–induced protein degradation, in agreement with former *in planta* studies (Soundappan et al., 2015; Wang et al., 2015; Liang et al., 2016). Additionally, consistent with previous reports, ΔSMXL7 that contains an amino acid change/deletion resembling that present in the *d53* allele in rice (Jiang et al., 2013) caused the protein to be resistant to *rac*-GR24–dependent degradation. As a result, the ΔSMXL7 protein levels under mock conditions and after hormonal treatment were the same.

SMXL7 as a direct target of SCF^{MAX2} is degraded upon *rac*-GR24 treatment in a D14-dependent manner (Soundappan et al., 2015; Wang et al., 2015). By means of the LFQ-based analysis, we identified an association of D14 with SMXL7 only in the presence of the hormone. Previously, the strigolactone-dependent interaction between SMXL7 (or D53 in rice) and D14 has been validated by different methods, including *in vitro* pull-down (Jiang et al., 2013), Förster resonance energy transfer (FRET) with fluorescence lifetime imaging microscopy (FLIM) (Liang et al., 2016), Y2H (Zhou et al., 2013; Wang et al., 2015), co-immunoprecipitation (Co-IP) (Wang et al., 2015), and bimolecular fluorescence complementation (BiFC) (Zhou et al., 2013). Here, we present the first MS-based view on this dynamic D14–SMXL7 interaction.

When proteins copurified with SMXL7 are compared in the presence and the absence of the strigolactone analog, a skewing of the protein intensity values occurs in the volcano plots toward an increased abundance under mock conditions. The reason might be that the *rac*-GR24–induced degradation of the bait causes a decrease in the intensity levels of all the proteins interacting with it and, consequently, they are less abundant after hormone treatment. As a result, the difference in bait protein levels between the tested conditions might hamper the detection of differentially interacting preys that follow the same trend as the bait protein levels. Therefore, we applied a normalization step on the intensity level of the bait protein itself rather than use a normalization based on background proteins (LFQ). Consequently, an increased number of proteins was identified that significantly associated with SMXL7 after treatment with the strigolactone analog. Although the list of candidate interactors might contain false positives, it might hint at processes that occur around the bait. Indeed, the STRING analysis revealed that some of these proteins are related to the 26S proteasome, indicating that the proteasomal degradation pathway is activated in response to *rac*-GR24. This observation is in agreement with the model in which the strigolactone action involves SCF^{MAX2}-dependent ubiquitination of SMXL7 and its subsequent degradation by the 26S proteasome (Jiang et al., 2013; Zhou et al., 2013; Soundappan et al., 2015). The two most differentially accumulating proteins after normalization based on the bait levels, were indeed D14 and CUL1, implying the presence of the SCF^{MAX2} complex in close proximity of SMXL7 after addition of the

strigolactone analog. Although these observations suggest that the normalization based on the bait level leads to a list of candidate interactors, from which at least a part is relevant and most likely bona fide interactors, further validation is required. When the same analysis was done with ΔSMXL7, no proteins belonging to the 26S proteasome-dependent protein turnover pathway were associated with the bait upon *rac*-GR24 treatment. Indeed, no proteins related to the 26S proteasome are expected to be recruited to the complex as ΔSMXL7 is resistant to *rac*-GR24–induced degradation, thereby blocking the strigolactone signaling (Soundappan et al., 2015; Wang et al., 2015).

In none of the tested conditions, MAX2 had been identified as an interactor of SMXL7. Independently of the *rac*-GR24 addition, an association between MAX2 and SMXL7 (or D53) had been reported by *in vitro* pull-down (Jiang et al., 2013) and Co-IP in *Arabidopsis* protoplasts (Wang et al., 2015), although a FRET-FLIM study indicated that the two proteins did not directly interact (Liang et al., 2016). The reason for the absence of MAX2 in our analysis might be due to a too transient interaction between SMXL7 and MAX2 to survive the multi-step TAP protocol. Nevertheless, after normalization based on bait levels, CUL1 was significantly more associated with SMXL7 after treatment with *rac*-GR24. Although direct interaction with CUL1 is not expected because of its position in the SCF complex, it might hint at the presence of MAX2 near SMXL7 after the strigolactone analog addition.

Thus far, we gained insights into the composition of the SMXL7 protein complex that had previously often been shown by binary methods, confirming the power of the qTAP method. Interestingly, our analysis also revealed some results that do not fit with the current strigolactone signaling model. First, D14 was not found within the list of proteins copurified with ΔSMXL7 under any of the tested conditions, indicating the lack of interaction between these proteins in the cell cultures. This observation does not concur with our own Y2H data and with previous reports that used various binary PPI validation methods, such as Y2H, BiFC, pull-down, and FRET-FLIM (Zhou et al., 2013; Jiang et al., 2013; Liang et al., 2016). Second, according to the qTAP, the interaction between SMXL7 and TPR2 depends on *rac*-GR24, in contradiction with our own Y2H results and the mammalian two-hybrid assay used previously (Jiang et al., 2013). In the qTAP analysis of SMXL7, TPR2 was more associated with the bait under mock conditions than under the hormone treatment, particularly when normalization of the bait levels was applied. On the contrary, treatment with *rac*-GR24 had no influence on the interaction between ΔSMXL7 and TPR2, because the TPR2 level was similar under both conditions.

These discrepancies could be explained in different manners, of which one would be deviations on the stoichiometric balances between the proteins of the complex. Indeed, in most of the PPI methods, such as

Y2H, BiFC, Co-IP, and FRET-FLIM, both tested proteins are overexpressed, whereas other potential complex components are absent (Y2H) or available at basal levels (BiFC, Co-IP, and FRET-FLIM). In this sense, qTAP is a unique approach, because it involves the overexpression of only one protein (bait) that retains stoichiometric relations with other members of the complex. This might be a possible reason for the inconsistency of the results obtained using qTAP compared to the other methods.

Thus, the qTAP data might shed new light on the dynamics of protein complexes formed around SMXL7 in response to strigolactones. We hypothesize that after perception of *rac*-GR24, the TPL/TPR proteins might dissociate from the SMXL7 complex, potentially because an interaction with (an)other protein(s) interrupts or weakens the SMXL7-TPL/TPR association. Our analysis suggest that D14 could play this role, because its interaction profile is opposite that of TPR2. Thus, the conformational change of D14 triggered upon perception of strigolactones might enable binding to SMXL7 with such a high affinity that the TPL/TPR-SMXL7 interaction is disrupted. Subsequently, the ubiquitination and 26S proteasome-mediated degradation of SMXL7 would occur and downstream responses are activated (Figure 7) (Soundappan et al., 2015; Wang et al., 2015; Liang et al., 2016). Hence, the TPL/TPR-mediated repression is potentially released, not only because of the degradation of the repressors, but also because of the disruption of the interaction between SMXL7 and TPL/TPR proteins by the D14-to-SMXL7 binding. ΔSMXL7 might then act as a dominant-negative protein due to its stronger affinity to TPL/TPR proteins than the wild-type protein. As a result, the strigolactone-bound D14 cannot disrupt the ΔSMXL7-TPL/TPR interaction and, consequently, activate the downstream signaling (Figure 7). This hypothesis would explain the discrepancies observed between the qTAP data and the results obtained by binary methods, because such dynamic interactions can only be seen when more than two proteins are present in the assay. In the future, this hypothesis can be tested in various manners. Co-crystallization studies of SMXL7 together with TPL/TPR or D14 could indicate whether these proteins bind SMXL7 in the same domain, in which case sterical hindrance could dislocate TPL/TPR proteins upon strigolactone perception by D14. Additionally, binding studies with purified proteins in various combinations and conditions might shed light on their affinities.

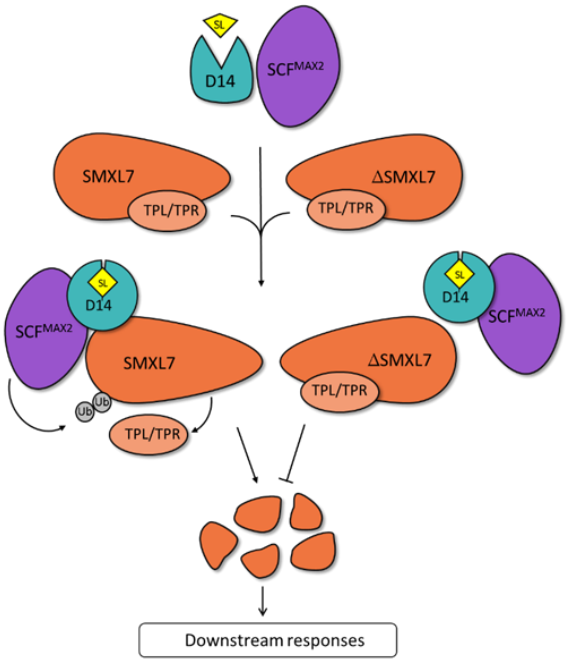

Figure 7. Proposed model for the strigolactone-induced dynamics of the SMXL7/ΔSMXL7 protein complex. In the presence of strigolactone, D14 and SCF^{MAX2} are recruited to SMXL7, whereas the TPL/TPR proteins dissociate from the complex. Subsequent ubiquitination of SMXL7 and its degradation by the 26S proteasome releases the repression of downstream responses. On the contrary, ΔSMXL7-TPL/TPR interaction does not allow binding of *rac*-GR24-bound D14 to ΔSMXL7, preventing the protein from degradation and activation of downstream responses.

To conclude, given the progress in the MS field, mainly on increased sensitivities, combining TAP-MS with LFQ can become a powerful tool to study PPI dynamics. Tracking changes in the protein complex composition, as well as their assembly and disassembly during plant development can help to understand the role played by PPIs in several important plant growth processes. It would be interesting to use qTAP to resolve the complex dynamics in the signaling pathways of other plant hormones, because this approach has not been used yet. In the future, quantitative MS-based analysis of the interactions should be implemented in parallel with binary methods, because it provides novel insights into PPIs, accurately reflecting the cellular situation of their dynamic nature.

MATERIALS AND METHODS

Molecular cloning

For all TAP constructs, cloning was performed by means of Gateway® recombination (Thermo Fisher Scientific). The open reading frame (ORF) of SMXL7 was amplified from *Arabidopsis* cDNA with iProof™ High-Fidelity DNA Polymerase (Bio-Rad) and Gateway®-specific primers. The PCR product flanked with attB sites was cloned in pDONR207 with the BP Clonase® II enzyme mix (Invitrogen). The resulting entry vector was used to clone the bait into the destination vector pKNGSrhino and pKCTAP for N- and C-terminal fusions, respectively, under the control of the 35S promoter (Van Leene et al., 2015) with the LR Clonase® II Plus enzyme mix (Invitrogen). For the construction of the modified version of SMX7 (hereafter designated ΔSMXL7), the Arg (R) at amino acid position 719 of the pDONR207-SMXL7 was mutated into a Thr (T), and the next five amino acids were deleted with the Spliced Overlap Extension PCR (SOE-PCR) (Higuchi et al., 1988). After sequence confirmation, the cloning steps were done in the same manner as for SMXL7. All primers used for cloning are listed in Supplemental Table 1.

Cell culture transformation

The wild-type *Arabidopsis thaliana* (ecotype Landsberg erecta) cell suspension cultures can be ordered at the Arabidopsis Biological Resource Center (ABRC). The cell cultures PSB-D (ABRC clone no. CCL84840) were transformed through cocultivation with *Agrobacterium tumefaciens* containing the N- terminal or both N- and C-terminal GSrhino fusions to SMXL7 and ΔSMXL7, respectively (Van Leene et al., 2007). After transformation, transgenic cell cultures were selected with a mixture of three antibiotics (25 µg/ml kanamycin, 500 µg/ml carbenicillin, and 500 µg/ml vancomycin) supplemented to the MSMO medium (4.43 g/L Murashige and Skoog basal salts with minimal organics [Sigma-Aldrich], 30 g/L sucrose, 0.5 mg/L α-naphtaleneacetic acid, 0.05 mg/L kinetin, pH 5.7). Cultures were subcultured in fresh MSMO medium at 21°C in a continuous dark with gentle agitation (130 rpm). Subsequently they were transferred to light/dark (16 h/8 h) regime and three weeks after the protein level was analyzed. Cultures expressing the bait were upscaled for TAP analysis.

Western blot analysis

Arabidopsis cell cultures expressing *35S::GSrhino-SMXL7* and *35S::GSrhino-ΔSMXL7* were subcultured in 20 mL of fresh MSMO medium and grown at 25°C in the dark by gentle agitation (130 rpm). The synthetic strigolactone analog *rac*-GR24 was dissolved in acetone to a 10-mM concentration. Three days after subculturing, cell cultures were treated with 1 µM *rac*-GR24 or the equal volume of acetone (mock). Cell

material was harvested before and at six time points after treatment (15 min, 30 min, 45 min, 1 h, 6 h, and 24 h). Total protein extract was prepared by adding the extraction buffer (see below for the buffer composition) to homogenized samples. Concentrations were determined by the Bradford assay (Bio-Rad). Of the total protein extract, 60 µg was separated by sodium dodecyl sulfate-polyacrylamide gel electrophoresis (SDS-PAGE) (12% Mini-PROTEAN®TGX™ precast gels, Bio-Rad) and blotted on a polyvinylidene fluoride (PVDF) membrane (Trans-Blot® TurboTM Mini PVDF Transfer, Bio-Rad) according to the manufacturer's instructions. Blotted PVDF membranes were incubated in blocking buffer (3% [w/v] Difco™ skimmed milk in TBS-T buffer [50 mM Tris-HCl, 150 mM NaCl, pH 8.0, 0.1% Triton X-100]) for 1 h at room temperature on an orbital shaker. Afterward, the membranes were incubated with peroxidase-anti-peroxidase (PAP) antibody against the GS-rhino tag (Sigma-Aldrich) or anti-tubulin antibody (Sigma-Aldrich) to determine equal loading. The signal was captured by means of chemiluminescent substrates from the Western Lightning® Plus Enhanced Chemiluminescence kit (Perkin-Elmer) and X-ray films (Amersham Hyperfilm ECL; GE Healthcare). The Precision Plus Protein™ Dual Color Standards (Bio-Rad) was used as protein size marker.

TAP purification

TAP was carried out as described (Van Leene et al., 2015), with some modifications. Cell culture material was harvested after 10 min of treatment with 1 µM *rac*-GR24 or the equal volume of acetone. Total protein extract was prepared with extraction buffer (25 mM Tris-HCl pH 7.6, 15 mM $MgCl_2$, 150 mM NaCl, 15 mM *p*-nitrophenyl phosphate, 60 mM β-glycerophosphate, 0.1% NP-40, 0.1 mM Na_3VO_4, 1 mM NaF, 1 mM phenylmethylsulfonyl fluoride [PMSF], 1 µM E64, EDTA-free Ultra complete tablet [1/10 mL; Roche Diagnostics], 0.1% benzonase, and 5% ethylene glycol). Total protein extract (25 mg) was incubated for 1 h at 4°C with 25 µL IgG-Sepharose 6 Fast Flow beads (GE Healthcare), pre-equilibrated in extraction buffer. After careful removal of the unbound fraction, the beads were washed on the Mobicol column with wash buffer (10 mM Tris-HCl pH 7.6, 150 mM NaCl, 0.1% NP-40, 0.5 mM EDTA, 1 µM E64, 1 mM PMSF, and 5% ethylene glycol). The beads were incubated with 10 units of Rhinovirus 3C protease (GE Healthcare) for 1 h at 4°C. The IgG-eluted fraction was incubated with Streptavidin beads (GE Gealthcare), equilibrated in wash buffer for 1 h at 4°C on a tube rotator. Bound complexes were eluted by streptavidin elution buffer (20 mM desthiobiotin in wash buffer) and proteins were concentrated by trichloroacetic acid (TCA) precipitation at 4°C overnight. In total, for each condition, four replicates were done for the cell cultures expressing *35S::GSrhino-SMXL7*, two for *35S::GSrhino-ΔSMXL7*, and two for *35S::ΔSMXL7-GSrhino.* The latter two were combined for the quantitative analysis.

In-gel protein digestion

Purified protein samples were migrated on 4–12% gradient NuPAGE Bis-Tris gels (Life Technologies) for 7 min at 200 V and visualized with colloidal Coomassie Brilliant Blue G- 250 (Sigma-Aldrich). The NuPAGE gel was de-stained twice for 1 h in high-performance liquid chromatography (HPLC)-grade water (Thermo Fisher Scientific) and incubated in 6.48 mM dithiothreitol and 50 mM NH_4HCO_3 in HPLC-grade water for 40 min to reduce disulfide bridges, and subsequently for 30 min in 54 mM iodoacetamide and 50 mM NH_4HCO_3 in HPLC-grade water in the dark for alkylation of the reduced thiol groups. After the gel had been washed for 30 min in 25 mL of HPLC-grade water, it was placed on a glass plate. The section containing all eluted proteins was cut out and sliced into 18 gel plugs. These plugs were dehydrated in 600 µL 95% (v/v) acetonitrile for 10 min, rehydrated with HPLC-grade water, and dehydrated again. Then, the gel plugs were rehydrated in trypsin digest buffer (1.125 mg trypsin [MS Gold; Promega], 50 mM NH_4HCO_3, 10% [v/v] acetonitrile in HPLC-grade water) for 30 min at 4°C. Subsequently, proteins were digested for 3.5 h at 37°C. The resulting peptide samples in the trypsin solution were sonicated for 5 min. The remaining gel plugs were dehydrated with 95% (v/v) acetonitrile for 10 min and added to the peptide solution. The overall resulting trypsin digest was vacuum-dried.

LC–MS/MS analysis

The obtained peptide mixture was analyzed by liquid chromatography-tandem MS (LC-MS/MS) with a tandem UltiMate 3000 RSLCnano system (Thermo Fisher Scientific) in-line connected to an LTQ Orbitrap Velos mass spectrometer (Thermo Fisher Scientific) through a Pneu-Nimbus dual-column source (Phoenix S&T). Peptides were first loaded on a trapping column (made in-house, 100 µm internal diameter [I.D.] × 20 mm length, 5 µm beads C18 Reprosil-HD [Dr. Maisch]) and then eluted and bound onto a reverse-phase analytical column (made in-house, 75 µm I.D. × 150 mm length, 5 µm beads C18 Reprosil-HD [Dr. Maisch]). The peptides were solubilized in 20 µL loading solvent (0.1% [v/v] trifluoroacetic acid in 98/2 water/acetonitrile [v/v]), of which 10 µL was loaded and separated with a linear gradient from 98% of solvent A (0.1% [v/v] formic acid in water) to 40% of solvent B (0.1% [v/v] formic acid in 20/80 [v/v] water/acetonitrile) in 30 min at a flow rate of 300 nL/min, and followed by a 5-min wash reaching 99% of solvent B. The mass spectrometer was operated in data-dependent, positive ionization mode, automatically switching between MS and MS/MS acquisition for the 10 most abundant peaks in a given MS spectrum. In the LTQ-Orbitrap Velos, full-scan MS spectra were acquired in the Orbitrap at a target value of 1E6 with a resolution of 60,000. The 10 most intense ions were then isolated for fragmentation in the linear ion trap, with a dynamic exclusion of 20 s. Peptides were fragmented after filling the ion trap at

a target value of 1E4 ion counts. The background ion Asn3 at 445.120025 Da was used for internal calibration (lock mass).

MS/MS data processing

All raw files were processed with the MaxQuant software (version 1.4.1.2) (Cox and Mann, 2008). The derived data were searched with the built-in Andromeda search engine against the *Arabidopsis thaliana* forward/reversed version of the TAIR10_pep_20101214 database containing also sequences of frequently observed contaminants, including human keratins, bovine serum proteins, or proteases. Carbamidomethylation of cysteines was selected as the fixed modification, whereas variable modifications were set to oxidation and acetylation (protein N-term). Trypsin\P was selected as enzyme setting. Cleavage was allowed when arginine or lysine was followed by proline with two missed cleavages permitted. Matching between runs was enabled with a matching window time of 30 s. Relative, label-free quantification of proteins was selected by means of the MaxLFQ algorithm integrated into MaxQuant. With the minimum ratio count set to 1, the FastLFQ option was enabled, LFQ minimum number of neighbors was set to 3, and the LFQ average number of neighbors to 6, as per default. Proteins identified with at least one unique peptide were retained. The false discovery rate (FDR) for peptide and protein identifications was set to 1%, and the minimum peptide length was set to 7 amino acids. Detailed MaxQuant search parameters can be found in Supplemental Table 2. The mass spectrometry proteomics data have been deposited to the ProteomeXchange Consortium via the PRIDE (Vizcaino et al., 2016) partner repository with the dataset identifier PXD009083.

Data analysis

After MS data processing, LFQ values from the “proteinGroups.txt” output file of MaxQuant were further analyzed in the Perseus software (version 1.5.3.2). First, the reverse database hits, contaminants, and proteins identified only by modified peptides were filtered out. Then, log2 values were taken from the LFQ intensities, whereafter samples were grouped in ‘mock’ and ‘treatment’. Proteins that did not contain at least four valid values in at least one group were filtered out and missing LFQ values were imputed/replaced by values from a normal distribution that were slightly lower than the lowest (Log) value measured, as described (Smaczniak et al., 2012b; Wendrich et al., 2017). All the imputed missing values can be found in the Supplemental Dataset 1. For normalization on the bait level, the intensity values from the “proteinGroups.txt” of the MaxQuant output file were analyzed in the same manner as the LFQ values. Before the imputation step, the SMXL7 intensity was subtracted from the intensity value of each protein. A Student’s *t* test was applied to determine statistical outliers between ‘mock’ and ‘treatment’ groups.

The resulting differences between the means of the two groups ("log2(mock/treatment") and the negative log10 *P* values were plotted against each other in volcano plots. The multiple hypothesis testing problem was corrected with a permutation based FDR (0.05). The threshold value S0 was set at 0.1 by default.

Yeast two-hybrid analysis

Yeast two-hybrid (Y2H) analysis was done as described (Cuéllar Pérez et al., 2013) in two independent repeats. SMXL7 and ΔSMXL7 were cloned into the pB42AD Gateway vector (bait), whereas D14 and the N-terminal fragment of the TPL protein (TPL-N, Cuéllar Pérez et al., 2014) were cloned in the prey vector pGILDA. The polyethylene glycol (PEG)/lithium acetate method was used to co-transform *Saccharomyces cerevisiae* EGY48 strain (Estojak et al., 1995) with the bait and prey. Transformants were selected on Synthetic Defined media containing galactose and raffinose (SD Gal/Raf) and lacking Ura, Trp, and His (Clontech). Three individual colonies were grown overnight in liquid cultures at 30°C and 10- and 100-fold dilutions were dropped on control media (SD Gal/Raf-Ura-Trp-His) and selective media containing X-Gal (Duchefa). To test the influence of the strigolactone analog on the interactions, 10 µM *rac*-GR24 or acetone (control) was added to the medium.

SUPPLEMENTARY DATA

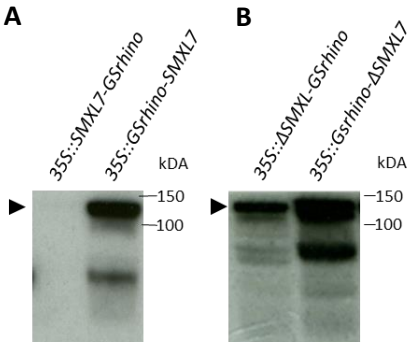

Supplemental Figure 1. Protein expression analysis of GSrhino-tagged constructs. SMXL7 and ΔSMXL7 were N- and C-terminally tagged with the GSrhino tag and overexpressed in *Arabidopsis* cell suspension cultures. Protein expression analysis was done before the up-scaling. Proteins were detected with the peroxidase anti-peroxidase (PAP) anti-GS tag antibodies during immunoblotting. The correct band is marked with an arrow.

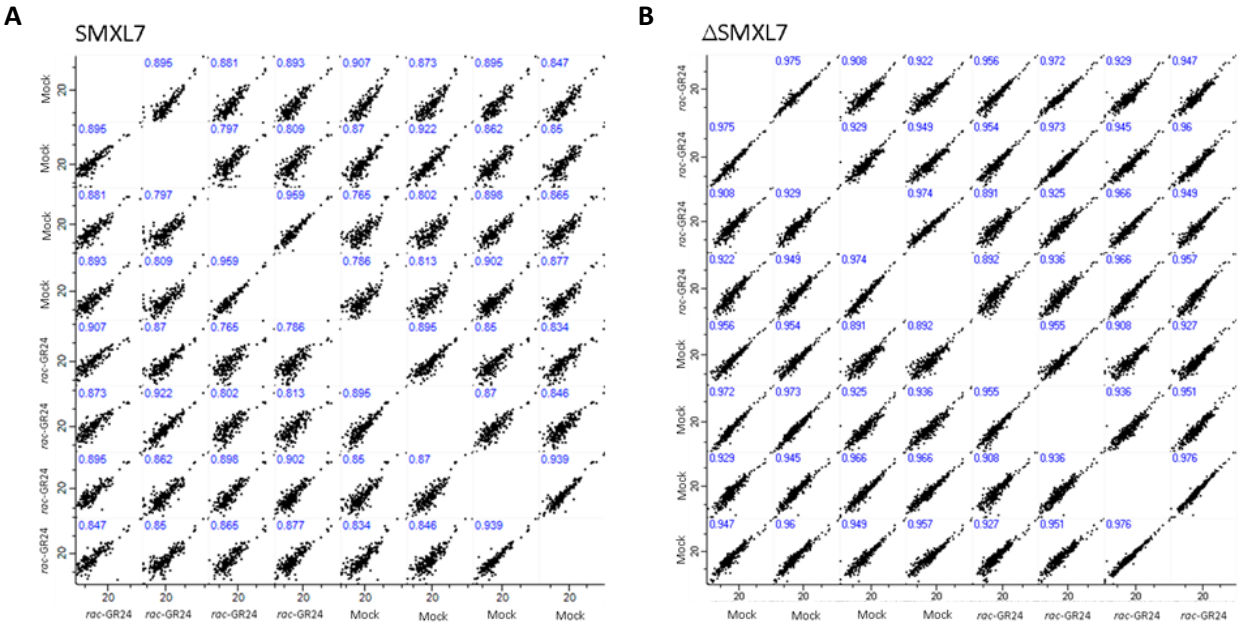

Supplemental Figure 2. Pearson correlation coefficients for *35S::SMXL7-GSrhino* and *35S::ΔSMXL7-GSrhino* combined with *35S::GSrhino-ΔSMXL7* samples mock or treated with *rac*-GR24. The matrix of 56 correlation plots reveals high correlations between LFQ intensities within replicates.

Supplemental Table 1. Primers used in this study

ID		Sequence	Use
SMXL7	Fw	GGGGACAAGTTTGTACAAAAAAGCAGGCTCAATGCCGACACCAGTAACCACG	Cloning
SMXL7	Rev	GGGGACCACTTTGTACAAGAAAGCTGGGTATCAGATCACTTCGACTCTCG	Cloning
SMXL7	Rev	GGGGACCACTTTGTACAAGAAAGCTGGGTAGATCACTTCGACTCTCG	Cloning
ΔSMXL7	Fw	CACAAGACAGTCTTGACGATAGATTCACAGATTACATTGCTGGCGAAGTGGCGAG	Mutagenesis
ΔSMXL7	Rev	CGCCACTTCGCCAGCAATGTAATCTGTGAATCTATCGTCAAGACTGTCTTGTGAC	Mutagenesis
D14	Fw	GGGGACAAGTTTGTACAAAAAAGCAGGCTCAATGAGTCAACACAACATCTTAG	Cloning
D14	Rev	GGGGACCACTTTGTACAAGAAAGCTGGGTATCACCGAGGAAGAGCTCGCCG	Cloning

Supplemental Table 2. Proteins found significantly different between mock and treatment in SMXL7 TAP.

AGI	Name	*P* value	Fold change
AT3G03990.1	α/β-Hydrolases superfamily protein	1.62E-05	5.73
AT4G02570.4	Cullin 1	2.55E-05	5.05
AT1G53750.1	Regulatory particle triple-A 1A	0.0014	1.64
AT5G35360.1	Acetyl Co-enzyme a carboxylase biotin carboxylase subunit	0.0016	2.63
AT5G16390.2	Chloroplastic acetylcoenzyme A carboxylase 1	0.0017	2.58
AT2G35635.1	Ubiquitin 7	0.0021	2.85
AT5G26860.1	Ion protease 1	0.0027	1.30
AT5G03850.1	Nucleic acid-binding, OB-fold-like protein	0.0029	1.87
AT5G23540.2	Mov34/MPN/PAD-1 family protein	0.0035	1.59
AT5G56030.1	Heat shock protein 81-2	0.0037	2.18
AT4G29040.1	Regulatory particle AAA-ATPase 2A	0.0040	1.14
AT5G20000.1	AAA-type ATPase family protein	0.0044	1.56
AT5G49910.1	Chloroplast heat shock protein 70-2	0.0046	2.24
AT3G05530.1	Regulatory particle triple-A ATPase 5A	0.0052	1.13
AT3G04120.1	Glyceraldehyde-3-phosphate dehydrogenase C subunit 1	0.0054	1.95
AT4G24280.1	Chloroplast heat shock protein 70-1	0.0059	1.79
AT5G43010.1	Regulatory particle triple-A ATPase 4A	0.0069	4.43
AT5G18230.1	Transcription regulator NOT2/NOT3/NOT5 family protein	0.0072	2.10
AT3G59540.1	Ribosomal L38e protein family	0.0075	2.90
AT5G02500.1	Heat shock cognate protein 70-1	0.0081	0.98
AT1G72370.2	40s Ribosomal protein SA	0.0081	1.72
AT1G71410.1	ARM repeat superfamily protein	0.0091	2.57
AT5G05620.1	γ-Tubulin complex protein 2	0.0120	2.46
AT3G16830.1	TOPLESS-related 2	0.0125	3.41
AT2G20580.1	26S Proteasome regulatory subunit S2 1A	0.0139	1.27
AT3G43300.2	HOPM interactor 7	0.0146	2.90
AT1G02080.2	Transcription regulators	0.0147	2.38
AT3G18190.1	TCP-1/cpn60 chaperonin family protein	0.0152	1.46
AT3G08530.1	Clathrin, heavy chain	0.0164	2.70
AT2G36160.1	Ribosomal protein S11 family protein	0.0172	1.66
AT3G09440.2	Heat shock protein 70 (Hsp 70) family protein	0.0182	1.53
AT1G71380.1	Cellulase 3	0.0195	2.66
AT3G53020.1	Ribosomal protein L24e family protein	0.0251	2.96

Student's *t* test analysis results from the Perseus software on a set of four independent TAP experiments on both mock and *rac*-GR24 treatment after intensity-based normalization for bait (FDR=0.05, S0=0.1).

Supplemental Table 3. MaxQuant search parameters

Parameter	Value
Version	1.4.1.2
Fixed modifications	Carbamidomethyl (C)
Decoy mode	revert
Special Aas	KR
Include contaminants	TRUE
MS/MS tol. (FTMS)	20 ppm
Top MS/MS peaks per 100 Da. (FTMS)	12
MS/MS deisotoping (FTMS)	TRUE
MS/MS tol. (ITMS)	0.5 Da
Top MS/MS peaks per 100 Da. (ITMS)	8
MS/MS deisotoping (ITMS)	FALSE
MS/MS tol. (TOF)	0.1 Da
Top MS/MS peaks per 100 Da. (TOF)	10
MS/MS deisotoping (TOF)	FALSE
MS/MS tol. (Unknown)	0.5 Da
Top MS/MS peaks per 100 Da. (Unknown)	10
MS/MS deisotoping (Unknown)	FALSE
PSM FDR	0.01
Protein FDR	0.01
Site FDR	0.01
Use Normalized Ratios For Occupancy	TRUE
Min. peptide Length	7
Min. score for unmodified peptides	0
Min. score for modified peptides	40
Min. delta score for unmodified peptides	0
Min. delta score for modified peptides	17
Min. unique peptides	1
Min. razor peptides	1
Min. peptides	1
Use only unmodified peptides and	TRUE
Modifications included in protein quantification	Acetyl (Protein N-term);Oxidation (M)
Peptides used for protein quantification	Unique
Discard unmodified counterpart peptides	TRUE
Min. ratio count	1
Site quantification	Use least modified peptide
Re-quantify	TRUE
Use delta score	FALSE
iBAQ	FALSE
iBAQ log fit	FALSE
MS/MS recalibration	FALSE

Match between runs	TRUE
Matching time window [min]	0.5
Alignment time window [min]	20
Find dependent peptides	FALSE
Fasta file	TAIR10_pep_20101214
Labeled amino acid filtering	TRUE
Site tables	Oxidation (M)Sites.txt
Cut peaks	TRUE
Decoy mode	revert
Special AAs	KR
Include contaminants	TRUE
RT shift	FALSE
Advanced ratios	FALSE
AIF correlation	0.47
First pass AIF correlation	0.8
AIF topx	20
AIF min mass	0
AIF SIL weight	4
AIF ISO weight	2
AIF iterative	TRUE
AIF threshold FDR	0.01

Supplemental dataset 1. The list of all proteins copurified with SMXL7 and ΔSMXL7 with their corresponding LFQ and intensity values before and after imputation of missing values. Available via https://www.dropbox.com/sh/8urjdds5r7r8ceu/AAC1ogPcP3TaB7psi_qR0t1Za?dl=0

Chapter 4

Towards a better understanding of the SMXL7 signaling complexes in *Arabidopsis thaliana*

Sylwia Struk[1,2], Fabrizio Ticchiarelli[3], Annick De Keyser[1,2], Robin Vanden Bossche[1,2], Sally Ward[3], François-Didier Boyer[4], Geert Persiau[1,2], Dominique Eeckhout[1,2], Alain Goossens[1,2], Geert De Jaeger[1,2] Ottoline Leyser[3] and Sofie Goormachtig[1,2]

[1]Ghent University, Department of Plant Biotechnology and Bioinformatics, 9052 Ghent, Belgium;
[2] VIB, Center for Plant Systems Biology, 9052 Ghent, Belgium;
[3]The Sainsbury Laboratory, University of Cambridge, Cambridge, United Kingdom,
[4]Institut National de la Recherche Agronomique, Institut Jean-Pierre Bourgin, Versailles, France

S.S. was the main author of the manuscript and performed all experiments, except FRET-FLIM that was carried out by F.T. and O.L., the molecular cloning partially performed by A.D.K., the acquisition of the TAP data prepared by G.P., D.E. and G.D.J., shoot branching assay done by S.W. and O.L. and transcriptional repression activity performed by R.V.B and A.G. F.D.B. kindly provided the synthetic strigolactone analog rac-GR24. S.G. supervised the project and contributed to the writing of the manuscript.

ABSTRACT

Strigolactones (SLs) are plant hormones, synthesized in response to environmental and endogenous clues, that modulate many aspects of plant architecture, of which the most pronounced is the control of shoot branching. The SUPPRESSOR OF MORE AXILLARY GROWTH 1 (SMAX1)-like (SMXL) 6, SMXL7, and SMXL8 (SMXL6/7/8) proteins are essential components of the SL signaling pathway and are possibly required for the repression of still unknown SL target genes. The SMXL6/7/8 protein level is tightly regulated by the SL-induced signaling complex, consisting of the receptor DWARF14 (D14) and the F-box protein MORE AXILLARY GROWTH2 (MAX2), component of the Skp–Cullin–F-box (SCF) E3 ubiquitin ligase complex that ubiquitinates SMXL6/7/8 to target them for proteasomal degradation. Here, we show that the SL-dependent interaction between SMXL7 and the receptor protein requires the conserved catalytic triad of D14, which is crucial for hormone hydrolysis. We further expand the knowledge about the SMXL7 interaction network by using tandem affinity purification (TAP) in *Arabidopsis thaliana* cell cultures. Our TAP analysis revealed three novel interacting partners of SMXL7 and their putative role in SL signaling is discussed.

INTRODUCTION

Strigolactones (SLs) are a novel class of terpenoid phytohormones that modulate plant growth (Woo et al., 2001; Gomez-Roldan et al., 2008; Umehara et al., 2008; Ruyter-Spira et al., 2011; Ha et al., 2013), but also function as a communication signal in the rhizosphere (Cook et al., 1966; Akiyama et al., 2010). Recent studies have shown that the perception mechanism of SLs differs from that of other plant hormones. DWARF 14 (D14) is a noncanonical SL receptor, because it acts as both an enzyme and a receptor (de Saint Germain et al., 2016; Yao et al., 2016). D14 is a member of the α/β hydrolase superfamily of proteins with a conserved Serine (Ser/S)-Histidine (His/H)-Aspartate (Asp/D) catalytic triad (Hamiaux et al., 2012; Nakamura et al., 2013). Although additional research is required to determine the details and the exact order of the signaling events, in the current model D14 in its open state is proposed to act as an enzyme and to hydrolyze the SL molecule, resulting in the formation of the D-ring–derived covalently-linked intermediate molecule (CLIM) that is bound to His in the catalytic triad (Hamiaux et al., 2012; Kagiyama et al., 2013; Zhao et al., 2013, 2015; Yao et al., 2016). This leads to conformational changes in the receptor to a closed state forming a new surface for the interaction with other signaling components, the Skp1-Cullin-F-box (SCF) MORE AXILLARY GROWTH2 (MAX2) complex and trapping inside either a D-ring or its intermediate (Yao et al., 2016).

The direct targets of the SCF^{MAX2} complex for ubiquitination and degradation have been identified simultaneously in *Arabidopsis thaliana* and rice (*Oryza sativa*) as members of the SUPPRESSOR OF MAX2 1 (SMAX1)-like or DWARF53 (D53) protein families, respectively (Jiang et al., 2013; Stanga et al., 2013; Zhou et al., 2013). The D53/SMXL6/7/8 proteins are quickly degraded in response to the synthetic SL analog *rac*-GR24 in a D14- and D3/MAX2-dependent manner (Jiang et al., 2013; Zhou et al., 2013; Soundappan et al., 2015; Wang et al., 2015). Although a direct interaction with MAX2 has been reported, current evidence supports the model in which D14 serves as a bridge between MAX2 and the SMXL6/7/8 proteins (Chapter 3; Wang et al., 2015; Liang et al., 2016). Furthermore, a *smxl678* loss-of-function mutant has been demonstrated to suppress all SL-related phenotypes of the *max2* plants, including shoot branching, leaf morphology, and root architecture (Soundappan et al., 2015; Wang et al., 2015), implying that the D53/SMXL6/7/8 proteins are the primary and probably only targets of SCF^{MAX2} in response to SLs. Other members of the SMXL protein family play a role in MAX2- and KARRIKIN INSENSITIVE2 (KAI2)-mediated karrikin (KAR) signaling (SMAX1 and SMXL2) (Stanga et al., 2013, 2016) or in phloem development independently of SLs and KARs (SMXL3/4/5) (Wallner et al., 2017).

The molecular role of D53/SMXL6/7/8 proteins is still unknown. Based on the presence of a well-conserved ETHYLENE-RESPONSE FACTOR Amphiphilic Repression (EAR) motif, they are predicted to

function as transcriptional repressors during SL signaling (Jiang et al., 2013; Soundappan et al., 2015; Wang et al., 2015). EAR motifs are known to mediate the interaction with TOPLESS (TPL) and its paralogs (TPR), but also with other proteins containing the C-Terminal to Lissencephaly Homology (CTLH) domains (Szemenyei et al., 2008; Causier et al., 2012). Interaction studies have suggested that a D53/SMXL6/7/8–TPL complex may repress the activities of downstream transcription factors involved in SL signaling (Smith & Li, 2014; Soundappan et al., 2015; Wang et al., 2015). Although still controversial, the BRANCHED1 (BRC1) transcription factor has been proposed as a plausible downstream target in *Arabidopsis* (Aguilar-Martinez et al., 2007; Braun et al., 2012; Seale et al., 2017). Another transcription factor, Ideal Plant Architecture 1 (IPA1), was shown to act downstream of D53 to regulate the tiller number in rice (Song et al., 2017), but its closest homologs in *Arabidopsis*, SQUAMOSA PROMOTER BINDING PROTEIN-LIKE 9 (SPL9) and SPL15, do not seem to be SL signaling targets (Bennett et al., 2016). In the second model, the SL responses are supposedly triggered in a transcription-independent manner by the depletion of the PIN-FORMED 1 (PIN1) protein from the plasma membrane, resulting in an altered auxin transport (Prusinkiewicz et al., 2009; Crawford et al., 2010; Shinohara et al., 2013). This hypothesis is supported by the fact that the EAR motif-lacking SMXL7 is still able to control some plant developmental aspects (Liang et al., 2016). Thus, SLs might regulate shoot branching by both mechanisms, transcription dependent via influence on *BRC1* expression and transcription independent through regulation of the PIN1 trafficking (Aguilar-Martinez et al., 2007; Chevalier et al., 2014; Seale et al., 2017).

Although in the past years, rapid progress has been made in understanding the SL pathway, many questions remain to be answered regarding downstream signaling. Members of the SMXL family are the most recently identified signaling components, but still not much is known about their function and signal transduction mechanism. Here, we focus on the closest ortholog of rice D53, SMXL7 (Chapter 1). We reveal details about the interaction between D14 and SMXL7 and further broaden the SMXL7 interaction network by means of tandem affinity purification (TAP).

RESULTS

Resolving the *rac*-GR24–induced D14-SMXL7 interaction

The interaction between the SL receptor D14 and its downstream target, SMXL7, has been reported to occur only in the presence of *rac*-GR24 (Wang et al., 2015; Liang et al., 2016). Indeed, upon binding and hydrolysis of *rac*-GR24, D14 changes its conformation, consequently allowing the interaction with other SL-signaling components (Figure 1A; de Saint Germain et al., 2016; Yao et al., 2016). The enzymatic activity of D14 requires the conserved Ser-His-Asp catalytic triad and the substitution of one of the key amino acids to alanine (A) (S97A, H247A, and D218A) impairs the *rac*-GR24 hydrolysis. A more conservative substitution of serine to cysteine (S97C) retains a limited hydrolytic activity (Hamiaux et al., 2012; Nakamura et al., 2013; de Saint Germain et al., 2016). We wondered whether these mutations can also affect the *rac*-GR24–dependent interaction between D14 and SMXL7.

To test this hypothesis, we carried out a yeast two-hybrid (Y2H) LexA assay with the mutated D14 versions (S97A, H247A, D218A, and S97C) as well as the wild-type D14 fused with the GAL4-binding domain (BD) and SMXL7 fused to the GAL4 activation domain (AD). As previously described, SMXL7 was able to interact with D14 only in the presence of the SL analog (Figure 1B), whereas no interaction was detected between SMXL7 and any of the catalytic triad mutant versions of D14 (Figure 1B). Although slightly blue-colored yeast colonies were detected for the SMXL7-D14 D218A protein pair, a similar observation was made for yeast cotransformed with the BD-fused D14 D218A and pB42AD (Figure 1B), hinting at autoactivation of this allele. No interaction was detected when yeasts were cotransformed with SMXL7-BD and mutated AD-fused D14 proteins (data not shown). In conclusion, the catalytic triad of D14 is crucial, not only for SL hydrolysis, but also for *rac*-GR24–dependent interaction with SMXL7.

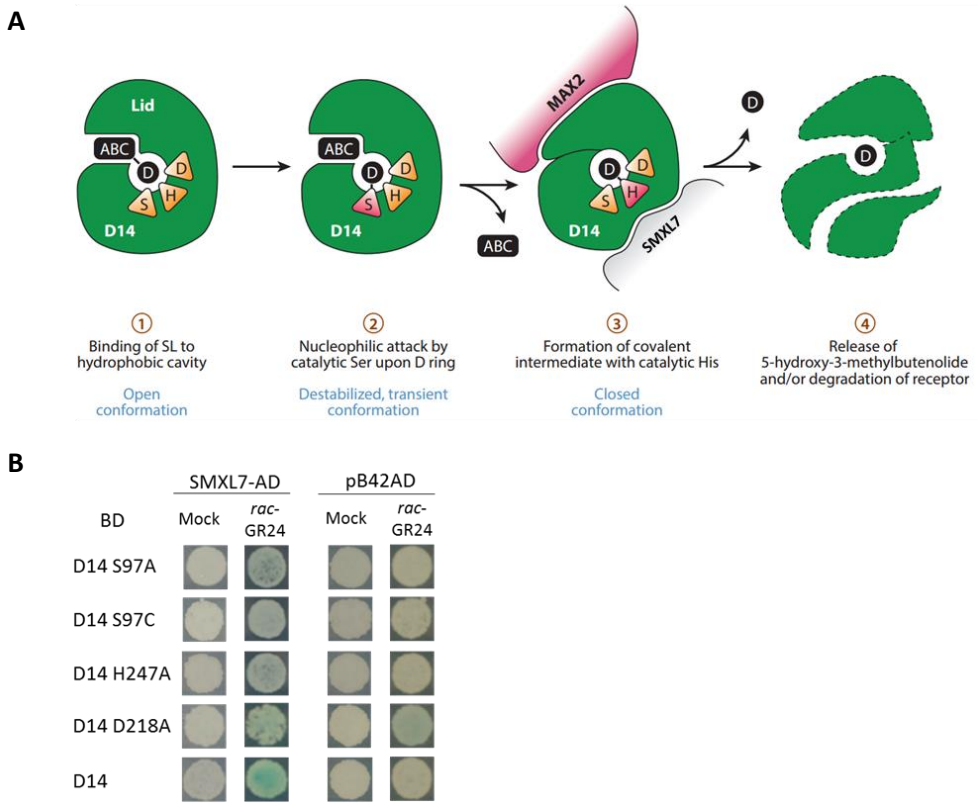

Figure 1. Analysis of the *rac*-GR24–induced interactions between SMXL7 and D14 catalytic triad mutants. Figure modified from Waters et al. (2017). (A) Binding of the *rac*-GR24 molecule in the hydrophobically active site of D14, with the D ring in the direction of the catalytic triad (1). The nucleophilic attack of the Ser residue initiates the hydrolysis process, separating the D ring from the ABC rings. As a result, the D ring is transiently attached to the Ser residue (2). The D ring is next covalently bound to the His residue initiating the conformational change of D14, allowing the binding of MAX2 and SMXL7 (3). Degradation of the D14 protein takes place after signaling (4). (B) The EGY48 (p8opLacZ) yeast (*S. cerevisiae*) strain cotransformed with D14 S97A, D14 S97C, D14 H247A, D14 D218A, or D14 fused with GAL4 BD and SMXL7-AD or pB42AD alone (control). Transformed yeasts were selected on Synthetic Defined (SD) Raf/GAL-Ura-Trp-His+X-gal medium. The experiment was repeated twice and from three independent yeast colonies one representative is shown.

Isolation of SMXL7 protein complexes by means of tandem affinity purification

Novel interactors of SMXL7 were discovered by TAP followed by mass spectrometry analysis (TAP-MS). To this end, we generated *Arabidopsis* cell cultures expressing SMXL7 tagged on its N and C terminus with the protein G/streptavidin-binding peptide (GS^{rhino}) tag under control of the cauliflower mosaic virus (CaMV) *35S* promoter. We selected the cell cultures expressing *35S::GSrhino-SMXL7,* because immunoblotting revealed high recombinant protein levels, whereas no protein expression was detected with the C-terminal fusion (Supplementary Figure 1A). Furthermore, we constructed a ΔSMXL7 allele that has been shown to render the protein resistant to *rac*-GR24-

induced degradation (Chapter 3, Jiang et al., 2013). Both the N- and the C-terminal ΔSMXL7 GSrhino fusions revealed high level of the bait protein (Supplementary Figure 1B). In addition, to verify the effect of SL on the complex formation, cell cultures expressing both baits were treated for 10 min with 1 µM *rac*-GR24 or mock (0.01% acetone).

The TAP experiment was carried out as described (Van Leene et al., 2015). To identify *bona fide* interactors, the retrieved MS spectra were analyzed according to a well-established, qualitative procedure, in which proteins that were present in a list of non-specific and sticky binders (Van Leene et al., 2015) were filtered out from our dataset. In this manner, 11 putative SMXL7 prey proteins were identified from which ten were found only in mock (Table 1; Supplemental dataset 1). Interestingly, all members of the TPL/TPR family were retrieved, in agreement with previous reports (Soundappan et al., 2015; Wang et al., 2015). Other identified preys have diverse functions. PHYTOCHROME-ASSOCIATED PROTEIN PHOSPHATASE 1 (FyPP1, AT1G50370) and SIT4 phosphatase-associated family protein (SAL4, AT3G45190) have been described to be part of the Ser/Thr protein phosphatase 6 (PP6)-type complex that is involved in the regulation of auxin and abscisic acid signaling (Dai et al., 2012, 2013). The RNA-binding family protein (SMXL7 INTERACTING PROTEIN 3 [SINT3], AT3G45630) is a presumed homolog of the yeast Carbon catabolite repressed 4 (CCR4)–negative on TATA-less (NOT) 4 (NOT4). The CCR4-NOT complex is a general regulator of eukaryotic gene expression at many different levels (Collart, 2016). Finally, a tRNA methyltransferase homolog (SINT1, AT2G28450), a nucleoporin (NUP133, AT2G05120) and a protein of unknown function (SINT2, encoded by AT2G35900) were retrieved.

TAP experiments with N-terminally tagged ΔSMXL7 yielded in 15 putative prays (Supplemental Table 1), while for the C-terminal fusion only the bait protein was retrieved and no interactors were detected using the qualitative analysis. The lists of SMXL7 and ΔSMXL7 interacting proteins contain five common candidates, which are TPL, TPR2, SINT1, SAL4 and NUP133.

Table 1. Overview of the SMXL7 prey proteins purified by TAP

AGI	Protein	*35S::GSrhino-SMXL7*	
		Mock	*rac*-GR24
AT2G29970	SMXL7, SMAX1-LIKE 7	4	4
AT1G15750	TPL, TOPLESS	4	-
AT1G50370	FyPP1, PHYTOCHROME-ASSOCIATED PROTEIN PHOSPHATASE 1	3	1
AT3G16830	TPR2, TOPLESS-related 2	3	-
AT5G27030	TPR3, TOPLESS-related 3	2	-
AT3G15880	TPR4, TOPLESS-related 4	2	-
AT2G28450	SINT1, SMXL7 INTERACTING PROTEIN 1	2	-
AT2G35900	SINT2, SMXL7 INTERACTING PROTEIN 2	1	-
AT3G45630	SINT3, SMXL7 INTERACTING PROTEIN 3	1	-
AT3G45190	SAL4, SIT4 phosphatase-associated family protein	1	-
AT2G05120	NUP133, Nucleoporin	1	-
AT1G80490	TPR1, TOPLESS-related 1	1	-

TAP experiments were performed in *Arabidopsis* cell cultures expressing *35S::GSrhino-SMXL7* treated for 10 min mock or with 1µM *rac*-GR24. Prey proteins were identified with peptide-based homology analysis of MS data. Background proteins were withdrawn based on the occurrence frequency of copurified proteins in a large GS TAP data set (Van Leene et al., 2015). The number indicates the times the prey was identified in four experiments. AGI, Arabidopsis Genome Identifier; -, pray was not identified.

Validation of *bona fide* SMXL7 interactors

TAP allows the identification of both direct interactors of a bait as well as of proteins that are part of the complex. For this reason, we wanted first to verify whether the copurified preys directly interacted with SMXL7 by means of the Y2H LexA assay. The interaction with the TPL/TRP proteins has been investigated (see Chapter 3), whereas FyPP1 and SAL4 are the subject of Chapter 5. As shown in Figure 2A, among the remaining preys, the interaction could be detected between SMXL7 fused to the GAL4-BD and SINT1, SINT2, and SINT3 fused to the GAL4-AD, but not for NUP133. Furthermore, the addition of *rac*-GR24 to the selective medium did not affect the interactions. Next, we tested whether the three validated SMXL7 preys also interacted with each other and indeed, interaction between SINT2 and SINT3 could be observed (Figure 2B). SMXL7 belongs to a large multigene family, with SMXL6/7/8 acting downstream in the SL signaling pathway and SMAX1/SMXL2 being involved in the KAR pathway. To test whether the observed interactions were specific for the SMXL7-mediated responses or rather general for both SL and KAR signaling, we examined the association of SINT1, SINT2, and SINT3 with SMAX1. As shown in Figure 2C, the interaction was detected between SMAX1 and SINT3, but not other candidate proteins.

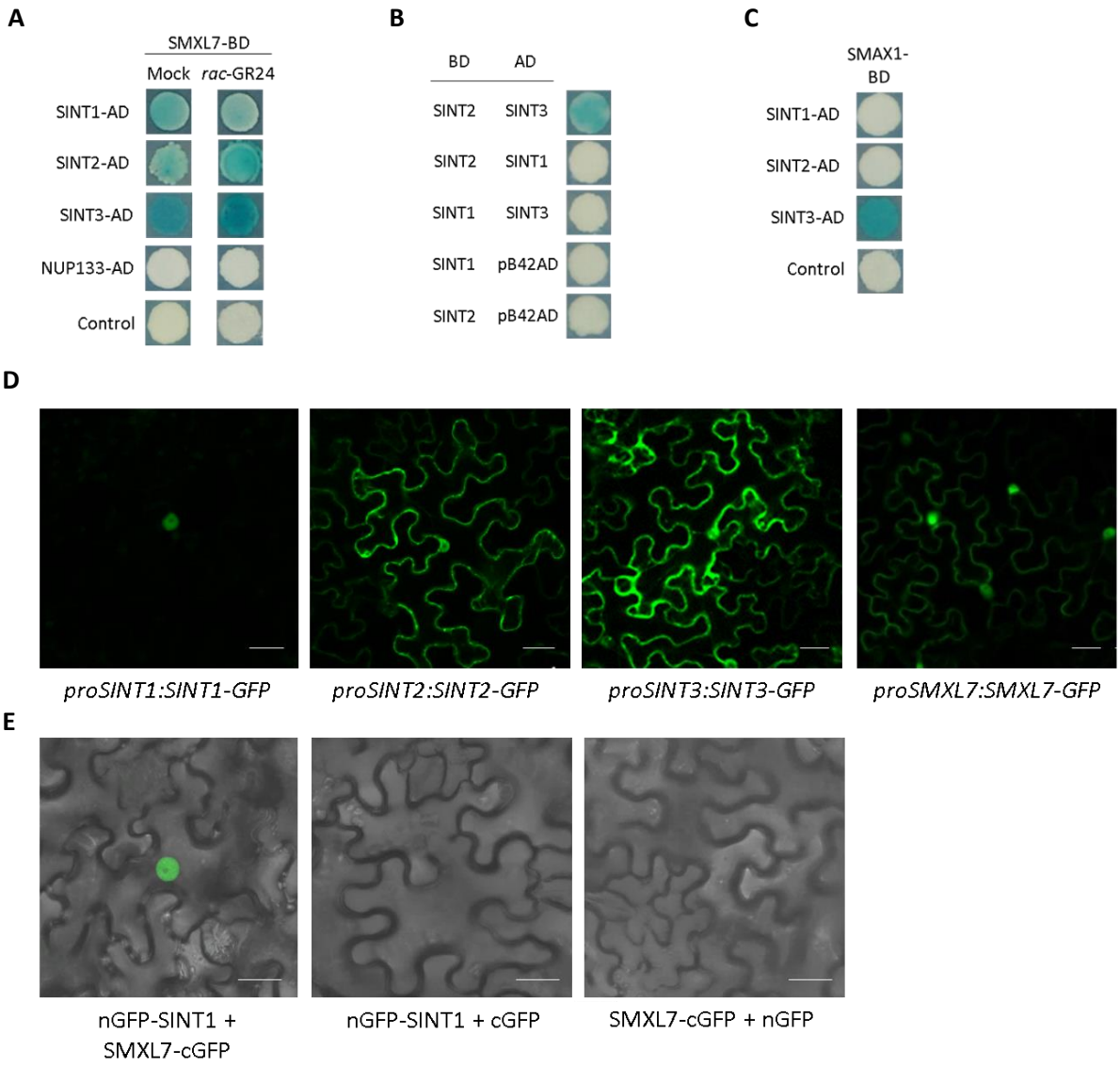

Figure 2. Validation of the newly identified SMXL7-interacting proteins. Y2H screen for interactions between SMXL7 and its preys identified by TAP (A), SINT proteins (B), SMAX1 and SINT proteins (C). The EGY48 yeast strain was cotransformed with bait and prey or B42AD alone (control). Transformed yeasts were selected on SD Raf/GAL-Ura-Trp-His+X-Gal medium. (D) Subcellular localization of SINT1, SINT2, SINT3, and SMXL7 with the C-terminal GFP fusion under control of their native promoters transiently expressed in *Nicotiana benthamina* epidermal leaf cells. (E) Interaction between SMXL7 and SINT1 revealed by BiFC. *N. benthamiana* leaves were transiently transformed with *35S::nGFP-SINT1* and *35S::SMXL7-cGFP*. For the negative control every construct was combined with the corresponding *35S::nGFP* or *35S::cGFP*. Scale bars represent 20 µm.

Based on the Y2H data, we continued our study with the three SMXL7 preys, SINT1, SINT2, and SINT3. In a next step, their localization pattern was investigated and compared with the SMXL7 expression. The C-terminal fusions of the green fluorescent protein (GFP) to SINT1, SINT2, SINT3, and SMXL7 driven by their native promoters were transiently expressed in *Nicotiana benthamiana* (tobacco) leaf epidermal cells. SINT1 exclusively localized to the nucleus, whereas SINT2 and SINT3

mostly to the cytoplasm and, in some cells, also to the nucleus (Figure 2D). Previously, only the nuclear localization of SMXL7 had been reported (Soundappan et al., 2015; Wang et al., 2015; Liang et al., 2016). However, in our experiment, we detected a SMXL7-GFP fusion protein both in the nucleus and cytoplasm (Figure 2D). Thus, the transient expression analysis confirms the overlapping subcellular localization of SMXL7 and SINT proteins.

Next, we used bimolecular fluorescence complementation (BiFC) to validate the interactions *in vivo* and to determine place of their occurrence in the cell. To this end, SMXL7 and the SINT proteins were fused with the N-terminal or C-terminal fragments of GFP (nGFP and cGFP, respectively) and coexpressed transiently in tobacco leaf epidermal cells. A strong fluorescence signal was visible only in the SMXL7-SINT1 protein pair in the nucleus (Figure 2E), but not for the SINT2-SMXL7 and SINT3-SMXL7 combinations (data not shown). As negative control, nGFP-SINT1 and SMXL7-cGFP were coexpressed together with the complementary GFP part (*35S::cGFP* and *35S::nGFP*, respectively). No fluorescence could be observed in any of the negative control combinations (Figure 2E), indicating that the GFP could not be reconstituted without interaction between the tested proteins.

To further assess the interactions between SMXL7 and SINT proteins *in vivo*, we used Förster resonance energy transfer (FRET) with fluorescence lifetime imaging microscopy (FLIM). The 405nm laser was used to excite the cyan fluorescent protein (CFP)-fused donor in the presence of yellow fluorescent protein (YFP)-fused acceptor or nuclear localized YFP alone as a control. The mean CFP lifetimes were calculated and the decreased value in the presence of the acceptor indicated the occurrence of FRET. As expected based on the previous BiFC assay, the average fluorescence lifetime of SINT1-CFP was shorter in the presence of SMXL7-YFP (green on the color scheme) is than YFP alone (orange) indicating the occurrence of FRET (Figure 3). In contrast to our BiFC results, FRET was also detected between the SINT2-CFP and SMXL7-YFP protein pair (Figure 3), confirming this interaction *in vivo*. In all cases, a nuclear YFP without SMXL7 (*35S::YFP-NS*) was used as a negative control and the average donor lifetime was measured in the nucleus. FRET between SINT3 and SMXL7 is under investigation.

To conclude, this study revealed three SMXL7-interacting proteins. Both SINT1 and SINT2 are possibly specific SMXL7 interactors, whereas SINT3 might also associate with SMAX1, indicative of its possible role in both SL and KAR signaling.

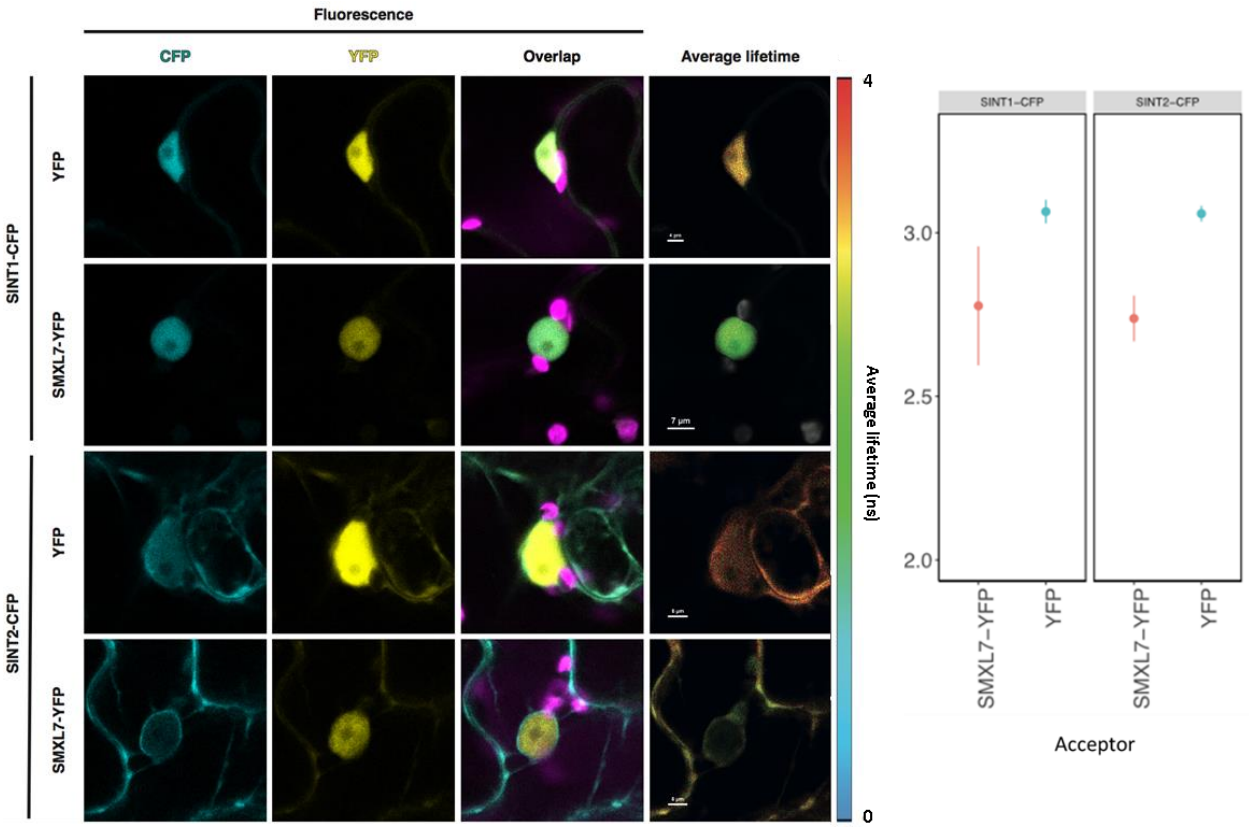

Figure 3. Physical interaction between SMXL7 and SINT1 or SINT2 analyzed by FRET. *N. benthamiana* leaf epidermal cells were cotransformed with *35S::SMXL7-YFP* and *35S::SINT1-CFP* or *35S::SINT2-CFP*. The *35S::YFP-NS* construct was cotransformed with SINT1-CFP or SINT2-CFP for a negative control. Representative images in each row show the localization of single-fusion proteins in the first and second panel, colocalization of the donor and acceptor in the third panel and average CFP donor lifetime (indicating FRET) in the last panel. Color scheme for FLIM analysis indicates the CFP donor fluorescence lifetimes between 4 and 0 ns. The graphs represent the quantification of average CFP donor lifetime between 2 and 3.5ns. For each protein pair, data were acquired from 6-10 cells.

Transcriptional repression activity of SINT proteins

TPL and TPR proteins play a crucial role as corepressors in various developmental processes and plant hormonal pathways (Szemenyei et al., 2008; Pauwels et al., 2010). Also, during SL signaling, they were reported to interact with SMXL6/7/8 to regulate transcription of still unknown genes (Wang et al., 2015). We then wondered whether the interactors of SMXL7 might also associate with TPL/TPR corepressors. Proteins interacting with TPL/TPR are in general characterized by an EAR motif in their sequence. EAR motifs are typically defined as LxLxL, DLNxxP, or the hybrid L/FDLNL/FxP (Ohta, 2001; Kagale et al., 2010). We scanned the amino acid sequence of SINT proteins in search for a putative EAR motif that would hint at an interaction with TPL/TPR. Indeed, one (LxLxL) motif could be

detected in the RNA recognition motif (RRM) of SINT3 (Figure 4B), but not in the SINT1 and SINT2 sequences. To prove that this motif is responsible for the TPL/TPR binding to SINT3, we carried out a Y2H LexA assay with the N-terminal fragment of TPL (TPL-N), previously reported to bind to the EAR motif and to mediate protein-protein interactions (Szemenyei et al., 2008; Pérez Cuéllar et al., 2013). As expected, the BD-fused TPL-N interacted with the SINT3-AD (Figure 4C). This interaction was abolished when yeasts were cotransformed with TPL-N and ΔEAR-SINT3, in which the putative EAR motif had been deleted (Figure 4B, C), indicating the importance of this amino acid sequence for the TPL binding.

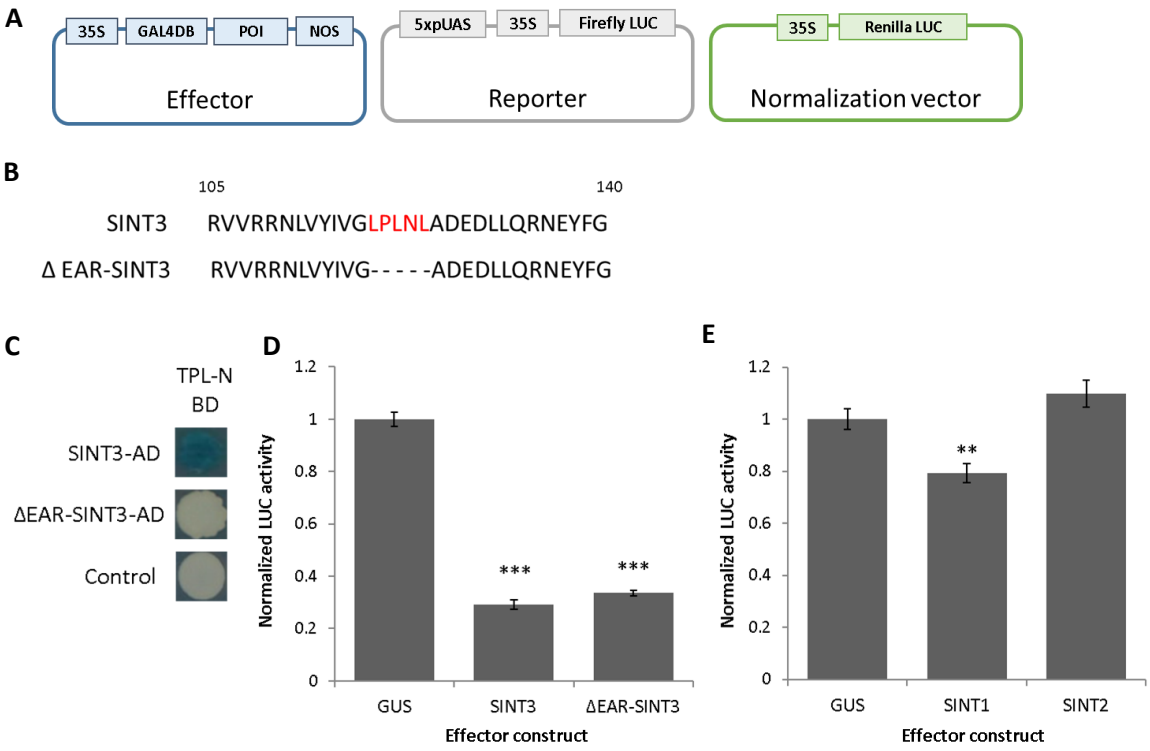

Figure 4. Transcriptional repression activities of SINT proteins. (A) Graphic repression of the reporter gene activity assay. Three plasmids are transfected into tobacco protoplasts. The protein of interest (POI) fused with GAL4BD (Effector) will bind to the pUAS of the reporter plasmid expressing firefly luciferase under the control of 35S promoter. If POI has repressing activity, the decreased fLUC activity is detected. Normalization vector is used to correct for the transfection efficiency. (B) Sequence comparison between SINT3 and ΔEAR-SINT3, in which the EAR motif (indicated in red) was deleted. (C) SINT3 interaction with TPL-N in a Y2H assay in an EAR motif-dependent manner. The EGY48 yeast strain was cotransformed with TPL-N fused with BD and SINT3/ΔEAR-SINT3 fused with AD or with pB42AD alone (control). Transformed yeasts were spotted on the inducing medium SD Raf/GAL -Ura-Trp-His supplemented with X-Gal. (D-E) Transient expression assay in tobacco protoplasts transfected with a pUAS–fLUC reporter construct, effector constructs, SINT3, ΔEAR-SINT3 and GUS (control) (D) or SINT1, SINT2 and GUS (control) (E) fused to GAL4-BD, and a 35S:rLUC normalization construct. Error bars represent ±SE of eight biological replicates. Asterisks represent significant differences (***, $P<0.001$, **, $P<0.01$, Student's *t* test).

The association with the TPL/TPR proteins suggests a possible involvement of SINT3 in transcriptional regulation. To investigate whether SINT3 carries a repressor activity, we used a transient expression assay in tobacco Bright Yellow-2 (BY-2) protoplasts (Figure 4A) (De Sutter et al., 2005; Vanden Bossche et al., 2013). SINT3 was fused to the GAL4-BD and coexpressed with the reporter plasmid containing the firefly luciferase (fLUC) reporter gene and renilla luciferase (rLUC) for normalization of the transfection efficiency. The relative luciferase activity was dramatically reduced when GAL4 was fused SINT3 when compared to the control p2GW7-GUS (Figure 4D). Deletion of the EAR motif in the SINT3 sequence did not affect its repressor activity, suggesting that SINT3 can act as a transcriptional repressor independently from the TPL proteins. Although no clear indication for the EAR motif was found in the sequences of other SINT proteins, we also controlled whether they carry a repressor activity. As shown in Figure 4E, SINT1 was able to repress the transcriptional activity, albeit to a lesser extent than SINT3, whereas the p2GW7-GUS control and SINT2 did not differ significantly.

Characterization of the SINT1 protein

SINT1, referred also as tRNA METHYLTRANSFERASE 2B (TRM2B) together with TRM2A (AT3G21300), had been described as putative homologs of tRNA (uracil(54)-C(5))-methyltransferase (TRM2) from *S. cerevisiae* (Wang et al., 2017b), which might be involved in tRNA stabilization or maturation in yeast (Johansson and Byström, 2002). The role of TRM2A and SINT1 in *Arabidopsis* remains unknown, although methylated nucleoside 5-methyluridine (m5U) might be implicated in plant development (Wang et al., 2017b).

SINT1 and TRM2A share 31% amino acid sequence similarity (21% identity) and they are both characterized by the presence of *S*-adenosyl-L-methionine (SAM)-dependent methyltransferase RNA m5U-type domain. SINT1, however, lacks the TRAM (from TRM2 and MiaB) domain, which has been found in *Arabidopsis* TRM2A and yeast TRM2 (Figure 5A). This TRAM domain is predicted to bind tRNA and bring the RNA-modifying enzymatic domains to their targets (Anantharaman et al., 2001). In addition, SINT1 has a cysteine3histidine (CCCH)-type zinc finger domain consisting of three cysteines and one histidine coordinated by a zinc cation. Some evidence suggests that the CCCH zinc finger proteins bind RNA and function in RNA processing, such as mRNA metabolism (Wang et al., 2008; Lai et al., 2000; Bogamuwa and Jang, 2014). Based on the *Arabidopsis* eFP browser, the relative SINT1 expression is higher than the average expression of all tested genes in imbibed seeds, root, vegetative rosette, and the shoot apex (Supplemental Figure 2).

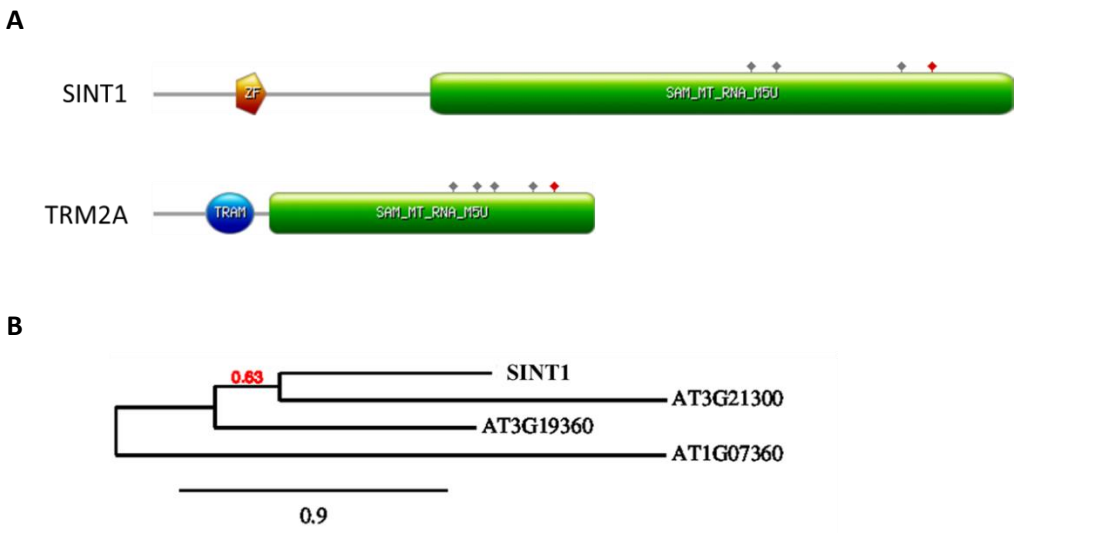

Figure 5. Structure and phylogenetic analysis of SINT1. (A) Graphical representations of SINT1 and TRM2A structures obtained from PROSITE (www.prosite.expasy.org). Protein domain abbreviations: ZF, Zinc finger CCCH domain; SAM_MT_RNA_M5U, SAM-dependent methyltransferase RNA m5U-type domain; TRAM, TRAM domain; red pin, nucleophile active site; grey pin, *S*-adenosyl-L-methionine binding site. (B) Maximum-likelihood tree obtained by PhyML, showing the relation of SINT1 with other proteins selected by a BLAST search with SINT1 against the *A. thaliana* genome. Values indicated at the branch nodes represent bootstrap support derived from 100 bootstrap replicates. The scale bar corresponds to the number of amino acid substitutions per site.

To better understand the potential role of SINT1 in the SMXL7-mediated signaling and to expand its interactome, we executed a reciprocal TAP with SINT1 as bait. For that, *Arabidopsis* cell cultures (PSB-D) were transformed with *35S::GSrhino-SINT1* and after examination of the bait expression levels (Supplemental Figure 3) TAP was carried out following the same protocol as for the SMXL7 TAP experiments with some modifications (see MATERIALS AND METHODS). Only proteins found in the two TAP experiments were retrieved, resulting in the characterization of six putative SINT1 preys (Table 2; Supplemental dataset 2) involved in many diverse processes. ABC transporter 1 (ABC1, AT4G01660) was discovered by functional complementation of a yeast *abc1* mutant. In yeast, the ABC1 protein is essential for ubiquinone biosynthesis and respiratory growth (Cardazzo et al., 1998). Later, *Arabidopsis* ABC1 has been reported to play a role in kin recognition which is the ability of plants to recognize other plants in their surroundings based on their genetic identity (Biedrzycki et al., 2011). The exocyst complex component SEC5 (SEC5B, AT1G21170) as part of a vesicle traffic complex was found that is important for pollen germination and pollen tube growth (Hala et al., 2008). Another identified prey, ANTHOCYANINLESS 2 (ANL2, AT4G00730) is a putative transcription factor implicated in the accumulation of anthocyanin, the regulation of cell wall mechanical properties, and in root development (Kubo, 1999; Kubo & Hayashi, 2011; Mabuchi et al., 2016).

Furthermore, protein phosphatase 2A regulatory B subunit (ATB' GAMMA, AT4G15415) was retrieved that had previously been found to control several processes, including defense responses under low light (Trotta et al., 2011a), endoplasmic reticulum stress (Trotta et al., 2011b), flowering (Heidari et al., 2013), and homeostasis of reactive oxygen species (Konert et al., 2015). Lastly, the protein kinase superfamily protein belonging to the mitogen-activated protein kinase MAP3K family (AT4G10730) (Champion et al., 2004) and an uncharacterized protein encoded by AT5G21080 were identified.

Table 2. Overview of the SINT1 prey proteins purified by TAP

AGI	Protein	*35S::GSrhino-SINT1*
AT2G28450	SINT1, SMAX7 INTERACTING PROTEIN 1	2
AT4G01660	ABC1, ABC transporter 1	2
AT1G21170	SEC5B, Exocyst complex component SEC5	2
AT4G00730	ANL2, ANTHOCYANINLESS 2	2
AT4G15415	ATB' GAMMA, Protein phosphatase 2A regulatory B subunit	2
AT4G10730	Protein kinase superfamily protein	2
AT5G21080	Uncharacterized protein	2

TAP experiments were performed in *Arabidopsis* cell cultures expressing *35S::GSrhino-SINT1*. Prey proteins were identified using peptide-based homology analysis of MS data. Background proteins were withdrawn based on the occurrence frequency of copurified proteins in a large GS TAP data set (Van Leene et al., 2015). The number indicates the times the prey was identified in two experiments. AGI, Arabidopsis Genome Identifier.

Next, our aim was to investigate the role of SINT1 in SL signaling. To this end, two mutant alleles were isolated in the Col-0 accession carrying a T-DNA insertion in the first (*sint1-2*) and seventh exon (*sint1-1*) (Figure 6A). The T-DNA insertion lines were genotyped and transcript levels were verified by reverse transcriptase (RT)-polymerease chain reaction (PCR). No transcript was detected for *sint1-1,* whereas in the *sint1-2* line the expression was only slightly reduced (Figure 6B); hence, only the *sint1-1* mutant was used for the phenotypic analysis. For additional confirmation that *sint1-1* is a knockout line, quantitative real-time PCR (qRT-PCR) was carried out, revealing that the SINT1 transcript level was significantly lower than that of Col-0 (Figure 6C). In addition, to avoid problems of gene redundancy, possibly resulting in lack of phenotype, we generated double mutants between the *sint1* and *trm2a* lines. We acquired a mutant carrying a T-DNA insertion in the first exon of the *TRM2A* gene and we crossed the homozygous knockout line (Figure 6D) with *sint1-1* plants. Furthermore, *sint1-1* was crossed into the *max2-1* mutant background to test whether it might act in the MAX2-mediated pathway.

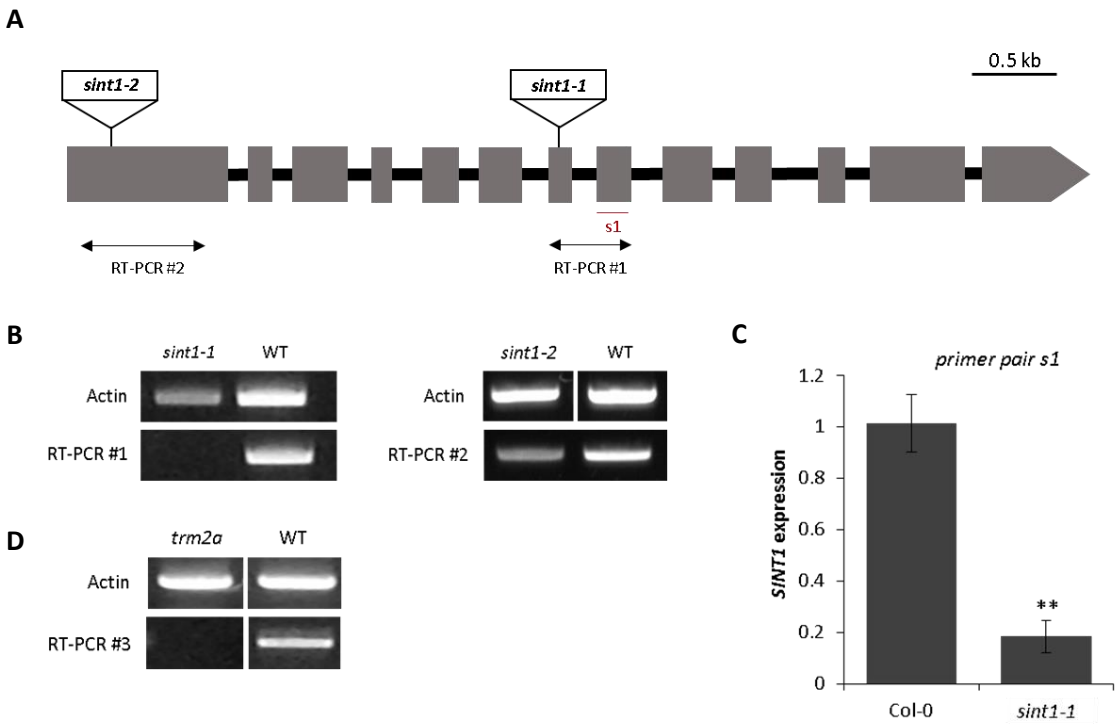

Figure 6. Characterization of *SINT1* T-DNA insertion mutants. Schematic visualization of the *SINT1* gene structure, T-DNA insertions, and primers used for RT-PCR and qRT-PCR (s1). Grey boxes represent exons. (B) Transcript level of *SINT1* in Col-0, *sint1-1,* and *sint1-2* mutants. *ACTIN2* (*ACT2*, AT3G18780) primers were used as a standard. (C) qRT-PCR analysis of *SINT1* expression in Col-0 and *sint1-1*. Error bars represent ±SE of three biological replicates (**, *P* <0.01; Student's *t* test). *ACT2* was used as internal control. (D) Transcript level of *TRM2A* in Col-0 and *trm2a* mutant with *ACT2* primers as a standard. All primer sequences can be found in Supplemental Table 2.

To study the involvement of SINT1 in the SMXL7 pathway, we decided to investigate the shoot branching and lateral root density (LRD) phenotypes of *sint1-1, sint1-1 trm2a,* and *sint1-1 max2-1* mutants. The most pronounced role of SLs as plant hormone is the control of the shoot architecture (Gomez-Roldan et al., 2008; Umehara et al., 2008). Both *max2-1* and *d14-1* mutants are characterized by a bushy phenotype (Stirnberg et al., 2007; Chevalier et al., 2014). The *smxl6/7/8* triple mutants display a phenotype similar to that of the wild type, but when crossed into the *max2-1* background, they can entirely suppress their increased shoot branching, indicating that SMXL6/7/8 act as negative regulators in SL signaling (Soundappan et al., 2015, Wang et al., 2015). To investigate the potential role of *SINT1* in the control of shoot branching, we counted the number of rosette branches in *sint1-1, sint1-1 trm2a,* and *sint1-1 max2-1* plants. No difference was noted in the branch number of the *sint1-1* single mutant when compared to Col-0 (Figure 7A). Then, we verified whether the mutation in the *SINT1* gene might affect the increased branching of *max2-1* plants. As shown in Figure 7A, the number of rosette branches was significantly higher in *max2-1* than WT, consistent

with previous data (Stirnberg et al., 2002, 2007), and remained unchanged in the *sint1-1 max2-1* double mutants (Figure 7A). Eventually, we tested the *sint1-1 trm2a* double mutants to exclude that the lack of phenotype was caused by gene redundancy. However, the number of shoot branches of both *trm2a* and *sint1-1 trm2a* plants was similar to that of the wild type (Figure 7B-C). Taken together, these data suggest that the SINT1 protein has no effect on shoot branching in *Arabidopsis*.

Besides a pronounced role in the control of shoot branching, SLs are important regulators of root development. In wild-type plants, treatment with *rac*-GR24 reduces both the total number of emerged lateral roots and LRD (Ruyter-Spira et al., 2011). In agreement, the SL signaling mutant *max2-1* has an higher LRD than wild-type plants that could be strongly suppressed in the *smxl6/7/8 max2-1* quadruple mutant (Kapulnik et al., 2011; Soundappan et al., 2015). To assess whether *SINT1* might be involved in this response, we grew Col-0, *sint1-1, sint1-1 trm2a,* and *sint1-1 max2-1* plants for 9 days on half strength Murashige & Skoog (½MS) medium supplemented either with 0.01% acetone (mock) or 1 µM *rac*-GR24. The LRD was calculated by dividing the number of counted lateral roots by the measured main root length. Both *sint1-1* and *sint1-1 trm2a* mutants showed a significant decrease in LRD in response to *rac*-GR24, similarly as Col-0 (*P* value <0.001), whereas the *sint1-1max2-1* seedlings were insensitive to the treatment (Figure 7D,F). Under mock conditions, the *sint1-1 max2-1* double mutant displayed a significantly higher LRD than the wild type (*P* value <0.001), consistent with previous reports for the *max2-1* seedlings (Kapulnik et al., 2011). Interestingly, a similar phenotype was observed for the *sint1-1 trm2a* (Figure 7F), but it might be caused by a mutation in *trm2a,* because a single mutation also displayed the same phenotype (Figure 7E).

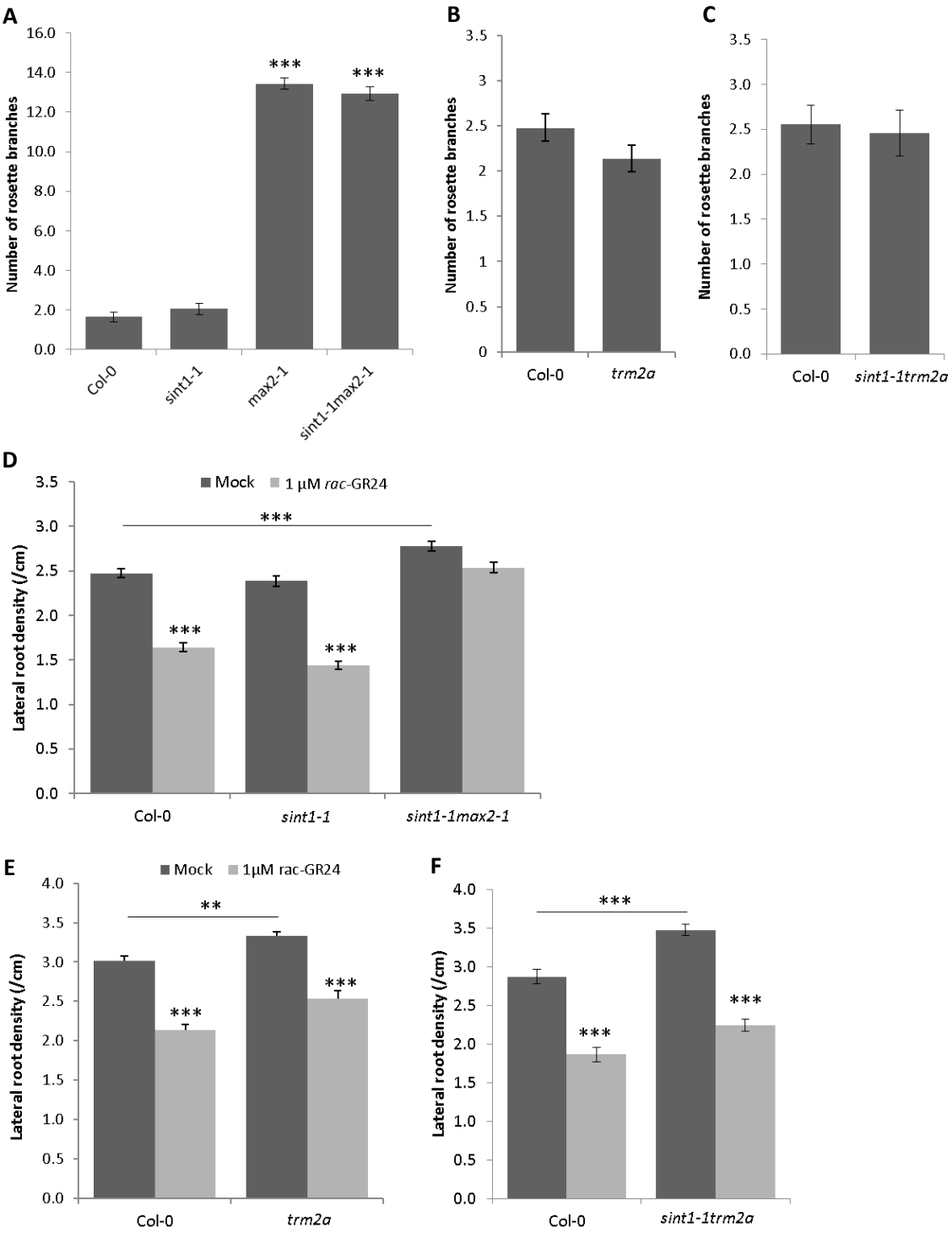

Figure 7. Shoot branching and lateral root density of *sint1* mutants. Number of primary rosette branches of Col-0, *sint1-1*, *max2-1*, *sint1-1 max2-1* (A), Col-0, *trm2a* (B) and Col-0, *sint1-1 trm2a* (C) measured at the proliferative arrest (A) or after 50 days of growth (B, C) (n=15). Lateral root density (LRD) assay of Col-0, *sint1-1*, *sint1-1 max2-1* (D), Col-0, *trm2a* (E) and Col-0, *sint1-1 trm2a* (F). LRD was analyzed in 9-day-old plants treated without (mock) or with 1 µM *rac*-GR24 (n>25). The experiments were repeated three times and the total mean of all biological repeats is presented ± SE. Asterisks indicate statistically significant differences between treatments and asterisks above the line- between genotypes [*** $P < 0.001$, Student's *t* test (A-C), Poisson regression model (D-F)].

Characterization of the SINT2 protein

SINT2 is a small protein consisting of 192 amino acids with a molecular mass of 21 kDa. No homologs of SINT2 have been identified in *Arabidopsis* and no characteristic motifs are present in the predicted secondary structure. The *Arabidopsis* eFP browser revealed rather low expression level of SINT2 during all stages of plant development, with the slightly higher relative expression in the embryo, dry and imbibed seeds (Supplemental Figure 4). SINT2 has been described as an ortholog of the XB24 protein from rice, although it has a deletion of the ATPase domain, which is crucial for the rice XB24 function (Holton et al., 2015). In rice, XB24 plays a role in pattern recognition receptor (PRR)-triggered immunity (PTI) by a negative regulation of the leucine-rich repeat receptor kinases XA21 (Chen et al., 2010). Before recognition of the pathogen-associated molecular patterns (PAMPs) from *Xanthomonas* and *Xylella*, XB24 is physically associated with XA21 and induces its autophosphorylation through the ATPase activity to keep it inactive. Upon ligand recognition, XB24 dissociates from the complex with XA21, causing its activation that further results in resistance (Chen et al., 2010; Holton et al., 2015). The *Arabidopsis* XB24 (SINT2) has been reported to interact with the EF-Tu receptor (EFR), belonging to the same subfamily as XA21, and this association was affected upon perception of the bacterial elongation factor Tu (elf18), similarly to the observation for XA21-XB24 interaction in rice. AtXB24, however, in contrast to the rice XB24, seems to be a positive regulator of the elf18-triggered reactive oxygen species burst in *Arabidopsis,* whereas other responses initiated by elf18 are unaffected (Holton et al., 2015).

First, to better understand the SINT2 function, we aimed at unravelling its interactome by a reciprocal TAP in *Arabidopsis* cell cultures (PSB-D) expressing *35S::GSrhino-SINT2* (Supplemental Figure 3). TAP was carried out according to the same protocol as described above for SINT1. The list of all copurified proteins can be found in Supplemental dataset 3. Here, we selected only those that were identified in both TAP experiments (Table 3). Among the putative preys, there are three proteasome core components (AT2G27020, AT5G35590, and AT4G14800) and two ATP-binding cassette (ABC) proteins (AT1G32500 and AT4G04770) with the last one involved in light responses (Hu et al., 2017b). The remaining preys are implicated in many diverse processes, including copper homeostasis (AT1G66240) (Li et al., 2017b), nuclear transport (AT2G41620), starch metabolism (AT3G10940) (Meekins et al., 2013), regulation of effector-triggered immunity (AT4G37460) (Kim et al., 2014), and vesicle transport (AT3G44340) (Belles-Boix et al., 2000).

Table 3. Overview of the prey proteins purified by TAP with SINT2

AGI	Protein	*35S::GSrhino-SINT2*
AT2G35900	SINT2, SMXL7 INTERACTING PROTEIN 2	2
AT2G41620	Nucleoporin interacting component (Nup93/Nic96-like) family protein	2
AT2G27200	P-loop containing nucleoside triphosphate hydrolases superfamily protein	2
AT5G60540	PDX2, pyridoxine biosynthesis 2	2
AT4G37460	SRFR1, Tetratricopeptide repeat (TPR)-like superfamily protein	2
AT4G04770	ABCI8, ATP binding cassette protein 1	2
AT5G35590	PAA1, proteasome alpha subunit A1	2
AT1G66240	ATX1, homolog of anti-oxidant 1	2
AT1G32500	NAP6, non-intrinsic ABC protein 6	2
AT4G14800	PBD2, 20S proteasome beta subunit D2	2
AT2G04740	Ankyrin repeat family protein	2
AT2G27020	PAG1, 20S proteasome alpha subunit G1	2
AT5G24020	ATMIND1, septum site-determining protein (MIND)	2
AT3G10940	Dual specificity protein phosphatase (DsPTP1) family protein	2
AT3G44340	CEF, clone eighty-four	2

TAP experiments were carried out in *Arabidopsis* cell cultures expressing *35S::GSrhino-SINT2*. Prey proteins were identified with peptide-based homology analysis of MS data. Background proteins were withdrawn based on the occurrence frequency of copurified proteins in a large GS TAP data set (Van Leene et al., 2015). The number indicates if the prey was identified in two experiments. Abbreviations: AGI, Arabidopsis Genome Identifier.

To investigate the contribution of *SINT2* to SL signaling, we acquired the *Arabidopsis* lines carrying T-DNA insertions in the intron (*sint2-1*) and in the promoter region (*sint2-2*) of *SINT2* (Figure 8A). After obtaining homozygous T-DNA insertion lines, the *SINT2* transcript levels were verified by RT-PCR (Figure 8B) and qRT-PCR (Figure 8C). As reduced transcript levels were detected in *sint2-1* and *sint2-2,* the phenotypes were analyzed for both lines to test the possible involvement in SMXL7-controlled phenotypes.

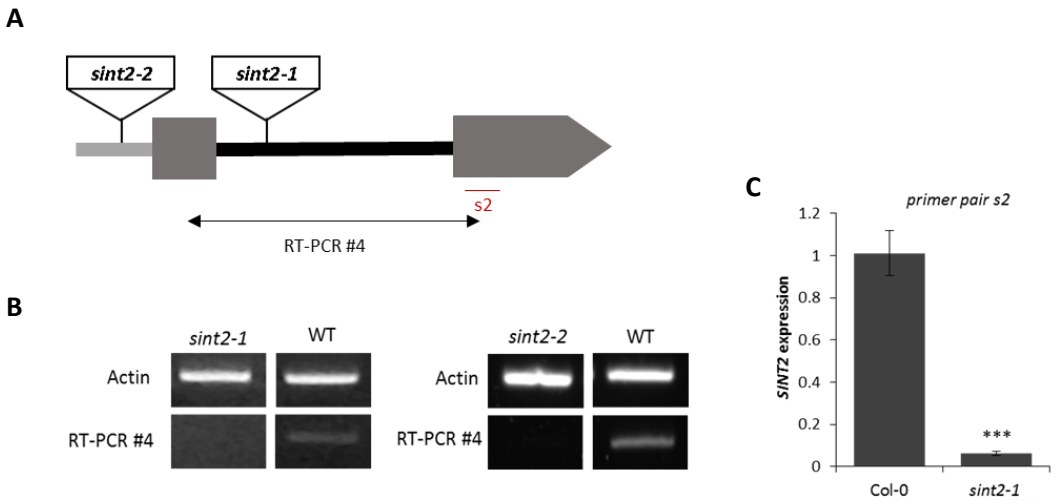

Figure 8. Characterization of *SINT2* T-DNA insertion mutants. Schematic visualization of the *SINT2* gene structure, T-DNA insertions, and primers used for RT-PCR and qRT-PCR (s2). Grey boxes represent exons. (B) Transcript level of *SINT2* in Col-0, *sint2-1,* and *sint2-2* mutants. *ACT2* primers were used as a standard. (C) qRT-PCR analysis of *SINT2* expression in Col-0 and *sint2-1.* Error bars represent ±SE of three biological replicates (***, *P* <0.001; Student's *t* test). *ACT2* was used as internal control.

In the first physiological assay, we investigated the number of rosette branches at the proliferative arrest. No difference was observed between Col-0 and the *sint2-1* mutant (Figure 9A). We then assessed the ability of *SINT2* to affect the increased shoot branching of the *max2-1* mutant, but both *sint2-1 max2-1* and *max2-1* plants had an equal number of rosette branches that was significantly higher than that of Col-0 (Figure 9A). Next, we validated whether the mutation in the *SINT2* gene might influence the LRD phenotype. As presented in Figure 9B, *sint2-1* and *sint2-2* mutants displayed a significant decrease in LRD upon treatment with *rac*-GR24, similar to that of Col-0 (30%, 22%, and 26%, respectively). Furthermore, the *sint2-1 max2-1* was characterized by an increased LRD under mock conditions and insensitivity to the *rac*-GR24 treatment (Figure 9B), consistently with the *max2-1* phenotype (Kapulnik et al., 2011). To conclude, these data suggest that *SINT2* is not involved in the regulation of either the shoot or root architecture.

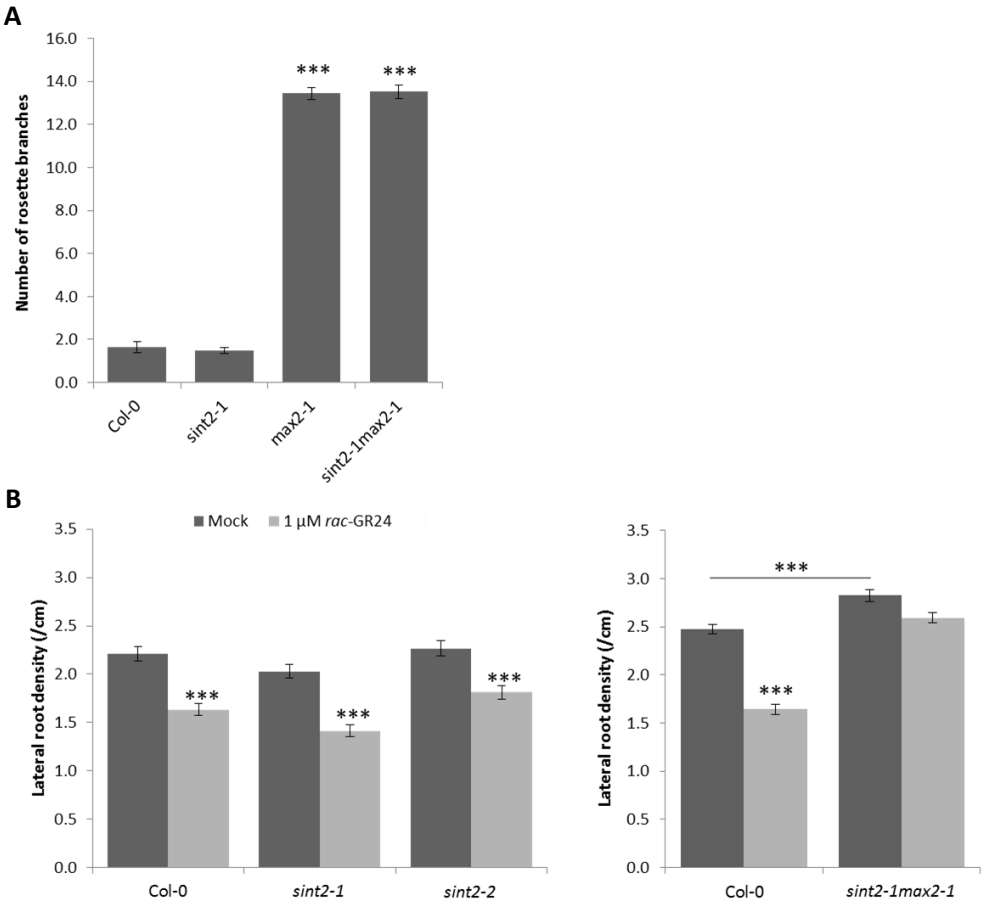

Figure 9. Shoot branching and lateral root density assay of *sint2* mutants. (A) Number of primary rosette branches of Col-0, *sint2-1*, *max2-1*, and *sint2-1 max2-1* measured at the proliferative arrest (n=15). (B) Lateral root density (LRD) assay of Col-0, *sint2-1*, *sint2-2* and Col-0, *sint2-1 max2-1*. LRD was analyzed in 9-day-old plants treated without (mock) or with 1 µM *rac*-GR24 (n>25). The experiments were repeated three times and the total mean of all biological repeats is presented ± SE. Asterisks indicate statistically significant differences between treatments and asterisks above the line- between genotypes [*** $P < 0.001$, Student's *t* test (A), Poisson regression model (B)].

Characterization of the SINT3 protein

SINT3, together with RNA-binding protein 1 (RBP1, AT5G60170) and RBP2 (AT2G28540) are putative homologs of NOT4/Modulator Of Transcription 2 (MOT2) from *S. cerevisiae*, which is a component of the CCR4-Not complex (Figure 10A). SINT3 shares 63% protein sequence identity with RBP1 and 40% with RBP2. All three proteins are characterized by the presence of a Zinc finger RING-type domain and RRM, which are also present in the NOT4/MOT2 protein sequence (Figure 10C).

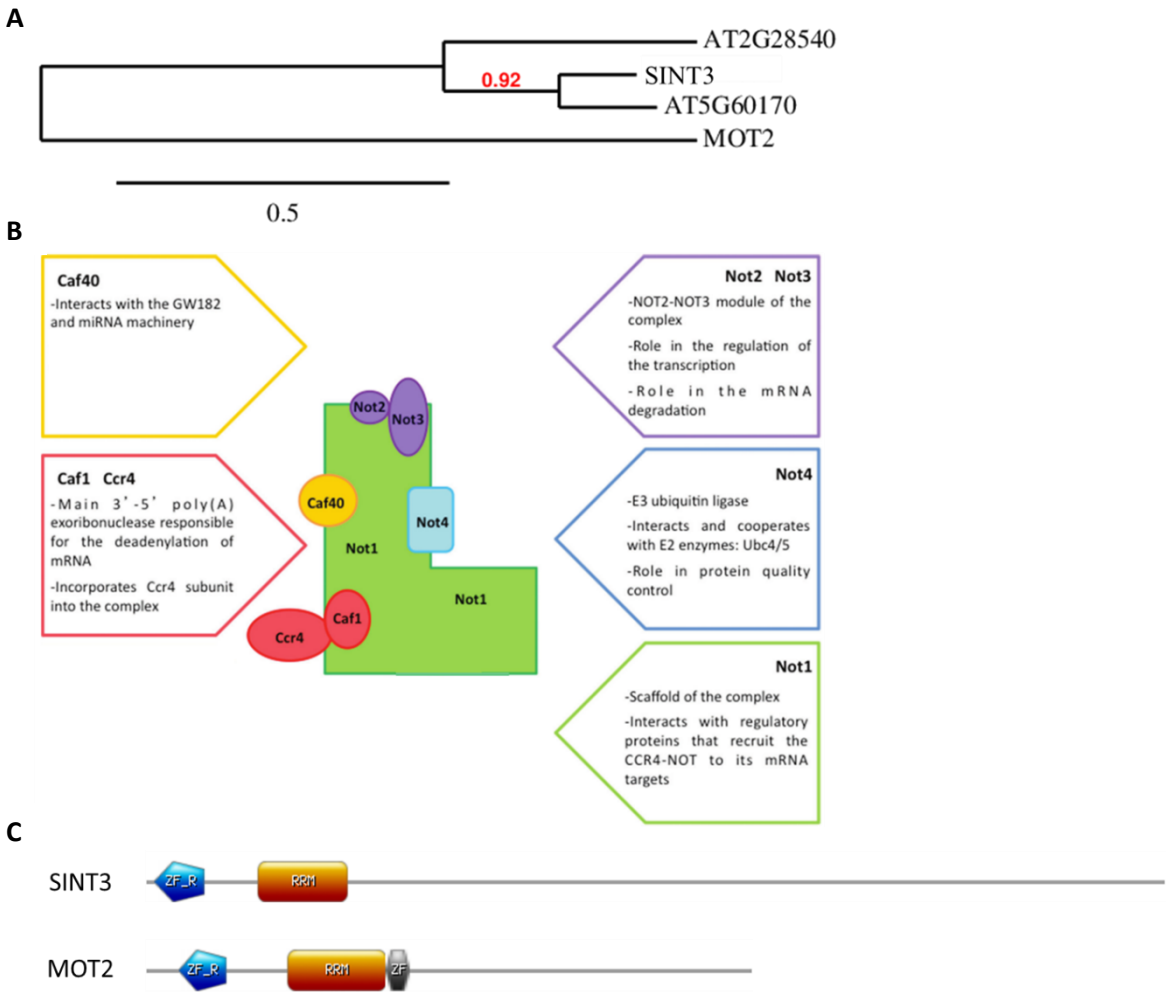

Figure 10. Phylogenetic analysis and structure of the SINT3 protein. (A) Maximum-likelihood tree by PhyML, showing the relation of MOT2 with *Arabidopsis* homologs. The sequences were analyzed with BLAST in combination with the reference protein database. Only homologs with a >40% sequence coverage compared to the *S. cerevisiae* MOT2 were selected. Values indicated at branch nodes represent bootstrap support derived from 100 bootstrap replicates. The scale bar corresponds to the number of amino acid substitutions per site. (B) Scheme of the CCR4-NOT complex in yeast showing its core subunits and their functions. Adapted from (Ukleja et al., 2016). (C) Graphical representations of SINT3 and its ortholog MOT2 from *S. cerevisiae* structures obtained from PROSITE (www.prosite.expasy.org). Protein domain abbreviations: ZF_R, Zinc finger RING-type domain; RRM, RNA Recognition Motif; ZF, Zinc finger C3H1-type domain.

The CCR4-NOT complex is implicated in the gene expression regulation at all the levels, starting from mRNA synthesis in the nucleus to its degradation in the cytoplasm (Figure 10B) (Collart, 2016). Both in yeast and human, the E3 ligase activity of CNOT4 was confirmed by an *in vitro* ubiquitination assay and by interaction with the E2 ligases, namely ubiquitin-conjugating enzyme (UBC)4/5p and the UBCH5B subfamily, respectively (Albert et al., 2002; Winkler et al., 2006; Mulder et al., 2007). Some of the substrates for this E3 ligase were shown to be polyubiquitinated and degraded by proteasome, whereas others were stably monoubiquitinated to regulate their function. The first substrates were

mostly involved in transcription and the latter were associated with ribosome (Panasenko & Collart, 2011; Gulshan et al., 2012).

To test whether SINT3 might also function as an E3 ubiquitin ligase, we used Y2H to screen for the interaction with different E2 ubiquitin conjugases of *Arabidopsis*. Out of 37 potential E2 ligases that carry thioester-linked ubiquitin encoded in the *Arabidopsis* genome (Kraft, 2005), 30 UBCs representing different groups (except for group XII) were fused with GAL4-BD and tested with SINT3-AD (based on Nagels Durand et al., 2016). Nevertheless, with these combinations, SINT3 did not interact with any of the tested E2 ligases (Figure 11).

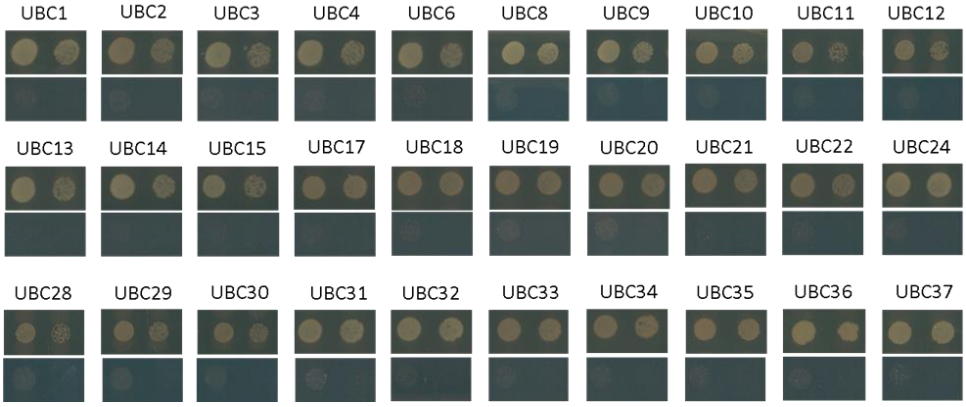

Figure 11. A yeast two-hybrid screen for E2 ligases interacting with SINT3. SINT3-AD was cotransformed with 30 *Arabidopsis* E2 ubiquitin-conjugating enzymes (UBCs) fused with BD. Transformed yeasts were spotted in 10-fold and 100-fold dilutions (on the left and right, respectively) on control medium (SD-Leu-Trp, upper panel) and selective medium (SD-Leu-Trp-His, lower panel).

The relative expression of *SINT3* is expected to be rather low during all stages of plant development. Only in dry seeds and senescent leaves the relative expression is slightly higher that the average expression of all genes tested in these tissues (Supplemental Figure 5). To examine the tissue-specific expression of *SINT3*, we constructed the *proSINT3::GUS* reporter line with approximately a 2-kb promoter region upstream of the ATG start codon and used this construct to transform *Arabidopsis* Col-0 plants. The *SINT3* expression was analyzed by the histochemical GUS assay in 10-day-old light-grown seedlings for two independent lines. GUS expression accumulated throughout the whole root, including vasculature, whereas low GUS staining was found in the shoot apex. No GUS expression was observed in the hypocotyl (Figure 12).

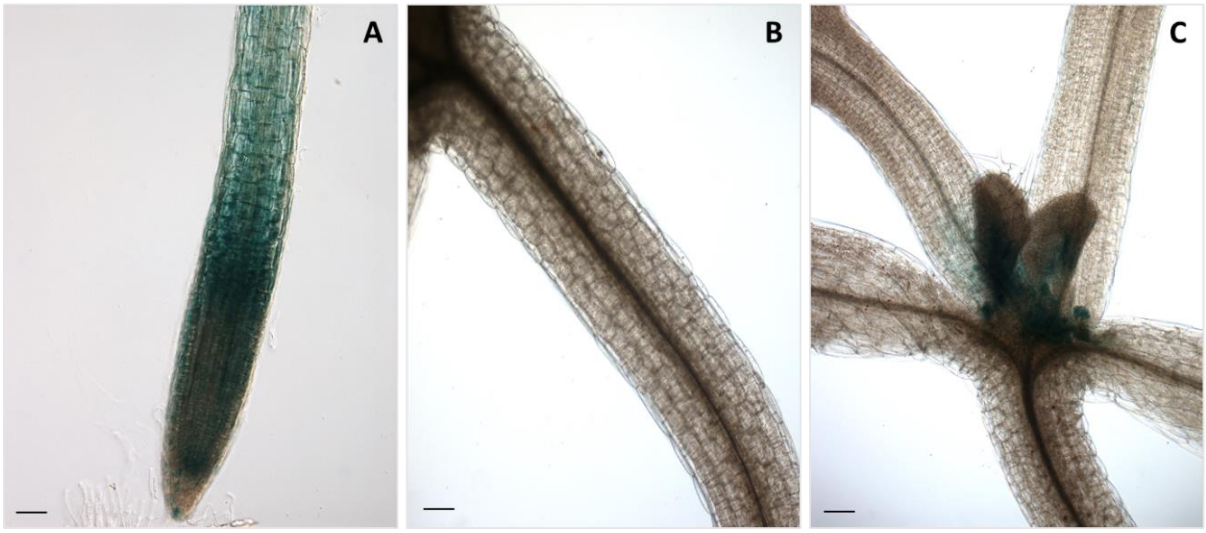

Figure 12. Expression pattern of *SINT3* in *Arabidopsis* seedlings. Expression of *proSINT3::GUS* fusions in 10-days-old light-grown seedlings. (A) primary root, (B) hypocotyl, and (C) shoot apex. Two independent lines were tested. Scale bars represent 0.1 mm.

Next, we carried out the reciprocal TAP in *Arabidopsis* cell cultures (PSB-D) expressing *35S::GSrhino-SINT3* (Supplemental Figure 3) according to the same protocol as described for SINT1 and SINT2 with some modifications. Before harvest, cell cultures were treated with 1 µM *rac*-GR24 or 0.01% acetone for 10 min and four repeats were carried out in each condition to allow the quantitative analysis. The list of putative preys found at least in two out of four repeats in the mock treatment after subtraction of background proteins (Van Leene et al., 2015) is presented in Table 4. All the copurified proteins can be found in the Supplemental dataset 4. Among 18 identified interactors of SINT3, seven are involved in proteasome-mediated protein degradation (AT3G14290, AT1G16470, AT3G53970, AT1G53850, AT2G27020, AT3G60820, and AT3G27430) (Figure 13). Some of the remaining proteins have been already reported to play a role in many different processes, such as regulation of peroxisome degradation (AT5G47040; Goto-Yamada et al., 2014), phosphate sensing in the root (AT5G23630; Ticconi et al., 2009), or mitotic cell cycle progression during female gametophyte development (AT5G19320; Rodrigo-Peiris et al., 2011). In addition, the ABC1 protein was identified that had previously been found also as a putative SINT1 interactor.

Table 4. Overview of the prey proteins copurified by TAP with SINT3

AGI	Protein	*35S::GSrhino -SINT3*
AT3G45630	SINT3, SMAX7 INTERACTING PROTEIN 3	4
AT3G14290	PAE2, 20S proteasome alpha subunit E2	4
AT1G16470	PAB1, proteasome subunit PAB1	4
AT3G53970	Proteasome inhibitor-related	4
AT1G53850	PAE1, 20S proteasome alpha subunit E1	4
AT4G36750	Quinone reductase family protein	4
AT5G47040	LON2, lon protease 2	4
AT2G06850	EXGT-A1, xyloglucan endotransglucosylase/hydrolase 4	4
AT2G44830	Protein kinase superfamily protein	4
AT5G23630	PDR2, phosphate deficiency response 2	4
AT2G34460	NAD(P)-binding Rossmann-fold superfamily protein	3
AT2G27020	PAG1, 20S proteasome alpha subunit G1	3
AT3G60820	PBF1, N-terminal nucleophile aminohydrolases superfamily protein	3
AT4G01660	ABC1, ABC transporter 1	2
AT3G17900	Unknown protein	2
AT3G27430	PBB1, N-terminal nucleophile aminohydrolases superfamily protein	2
AT5G42570	B-cell receptor-associated 31-like	2
AT1G01620	PIP1C, plasma membrane intrinsic protein 1C	2
AT5G19320	RANGAP2, RAN GTPase activating protein 2	2

TAP experiments were carried out in *Arabidopsis* cell cultures expressing *35S::GSrhino-SINT3*. Prey proteins were identified with peptide-based homology analysis of MS data. Background proteins were withdrawn based on the occurrence frequency of the copurified proteins in a large GS TAP data set (Van Leene et al., 2015). The number indicates how many times the prey was identified in four experiments. Abbreviations: AGI, Arabidopsis Genome Identifier.

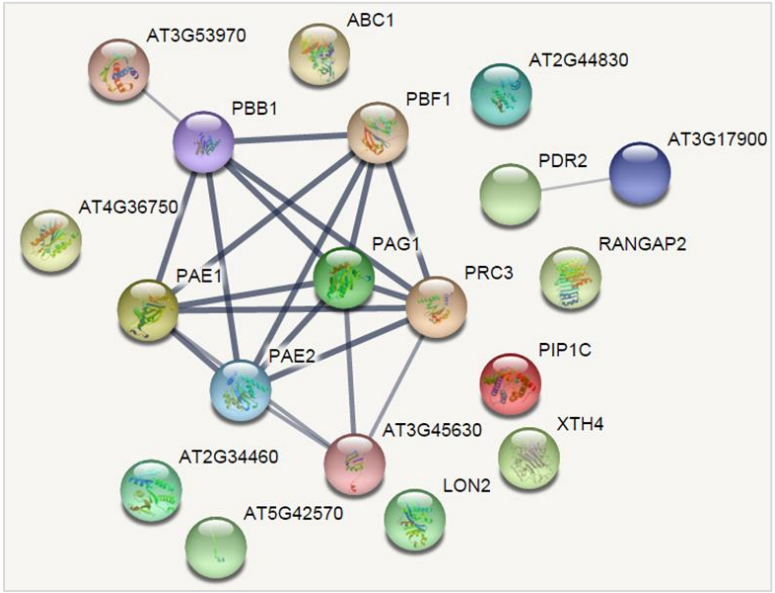

Figure 13. STRING network analysis of SINT3 putative preys. Only medium confidence interactions (score >0.400) are shown. The identified complex is involved in proteasome-mediated protein catabolic processes and it is connected with SINT3 (AT2G45630).

Then, the SINT3 TAP data were analyzed quantitatively to find prey proteins that specifically interacted with the bait only in one of the conditions, mock or treatment. LC-MS/MS spectra were searched with the MaxQuant software and label-free quantification (LFQ) was used to quantify the identified proteins between the tested conditions (Cox et al., 2014). Further, statistical analysis was performed with the Perseus software as described in detail in Chapter 3. In total, approximately 1600 proteins were identified, from which 33 were statistically more associated with SINT3 in the mock condition and 20 after treatment with *rac*-GR24 (FDR=0.05, S0=0.1; Supplemental Table 3; Supplemental dataset 5). Although this list might include background proteins, an interesting observation is detection of the auxin efflux carrier PIN1 as a putative prey associated with SINT3 only in the presence of the SL analog. No overlap was found between the qualitative (Table 4) and quantitative (Supplemental Table 3) analyses of SINT3 TAP data.

In addition, four TAP experiments were carried out on cell cultures expressing the *35S::GSrhino-ΔRING-SINT3* construct, in which the RING domain, that mediates the interaction with the E2 ligases, was deleted. As SINT3 is a predicted E3 ligase, we expected to find putative target proteins by quantitative comparison between TAP data of SINT3 and ΔRING-SINT3. ΔRING-SINT3 is anticipated to stop the interaction with the ubiquitin-charged E2 ligase, but probably to preserve the interaction with putative targets which can then no longer be ubiquitinated. The quantitative analysis was carried out as previously described for SINT3. As the number of differential interactors was very high (FDR=0.01, S0=0.1; 209 proteins; Supplemental dataset 5), we restricted the list by selecting preys that had not been identified in any of the four repeats for one of the tested conditions. As a result, 111 SINT3-specific preys were identified and only 18 proteins in the ΔRING-SINT3 TAP experiments (Supplemental Table 4). Although the list is still extensive and might contain unspecifically interacting proteins, some noteworthy observations could be made. First, UBC19 and UBC20 were detected only in the SINT3 TAPs, but the interaction was abolished when the RING domain was deleted, indicating that these two E2 ligases might work together with SINT3 as the ubiquitin donor. In addition, in the same conditions, the ubiquitin-specific protease 23 (UBP23) was found that is implicated in protein deubiquitination, suggesting again that SINT3 might be involved in the ubiquitination process. Interestingly, also previously identified putative interactors of SMXL7, the SIT4-associated protein (SAL) 4 and its homolog SAL1, were associated only with SINT3, but no longer when the RING domain was deleted. Among the proteins detected as specific for ΔRING-SINT3, we expect proteins that might be putative targets of the SINT3 E3 ligase activity. One of detected preys was the transcription factor, basic helix-loop-helix (bHLH) DNA-binding superfamily protein (AT1G05710). The STRING analysis revealed that among the remaining ΔRING-SINT3–specific interactors, three groups of proteins can be distinguished, involved in transcription/translation, chromatin assembly (core histones), and the citrate cycle (TCA cycle) (Figure 14).

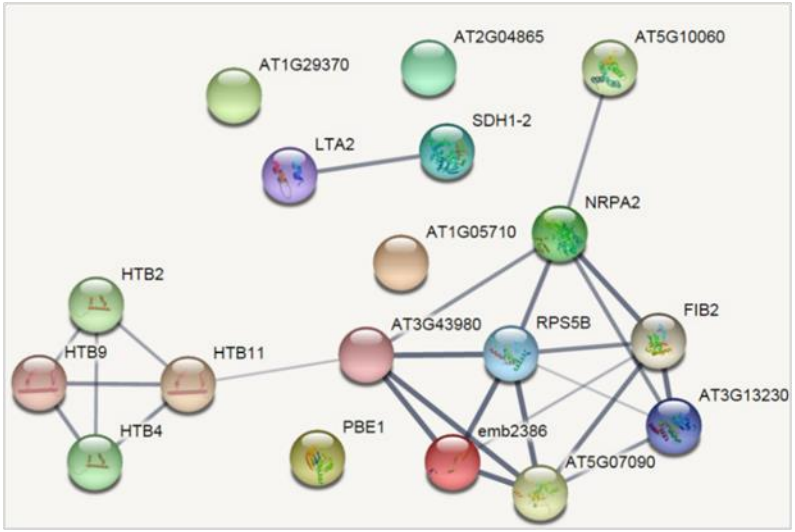

Figure 14. STRING network analysis of putative preys identified as ΔRING-SINT3 specific. Only medium confidence interactions (score > 0.400) are shown. The identified complexes are involved in transcription/translation (right), chromatin organization (left), and TCA cycle (top)

Further, we wanted to study a possible involvement of SINT3 in SMXL7- and SMAX1-mediated signaling. To this end, we first obtained two *Arabidopsis* lines carrying T-DNA insertions in the 12th (*sint3-1*) and in the fifth (*sint3-2*) exon of *SINT3* (Figure 15A). After the homozygous lines had been obtained, the *SINT3* transcript level was verified by RT-PCR (Figure 15B) and qRT-PCR (Figure 15C). No transcript was detected for the *sint3-2* mutant, whereas the residual transcript level was identified in *sint3-1* plants. In addition, the mutant with the T-DNA insertion in the exon of the *RBP1* gene was acquired and the transcript level was tested by RT-PCR (Figure 15D). Generation of the *rbp1 sint3* double mutant is in progress. Additionally, *sint3-1* was crossed into *max2-1*, *smxl6/7/8 max2-1* (*s678max2-1*), and *smax1* mutant backgrounds for further phenotypic analysis.

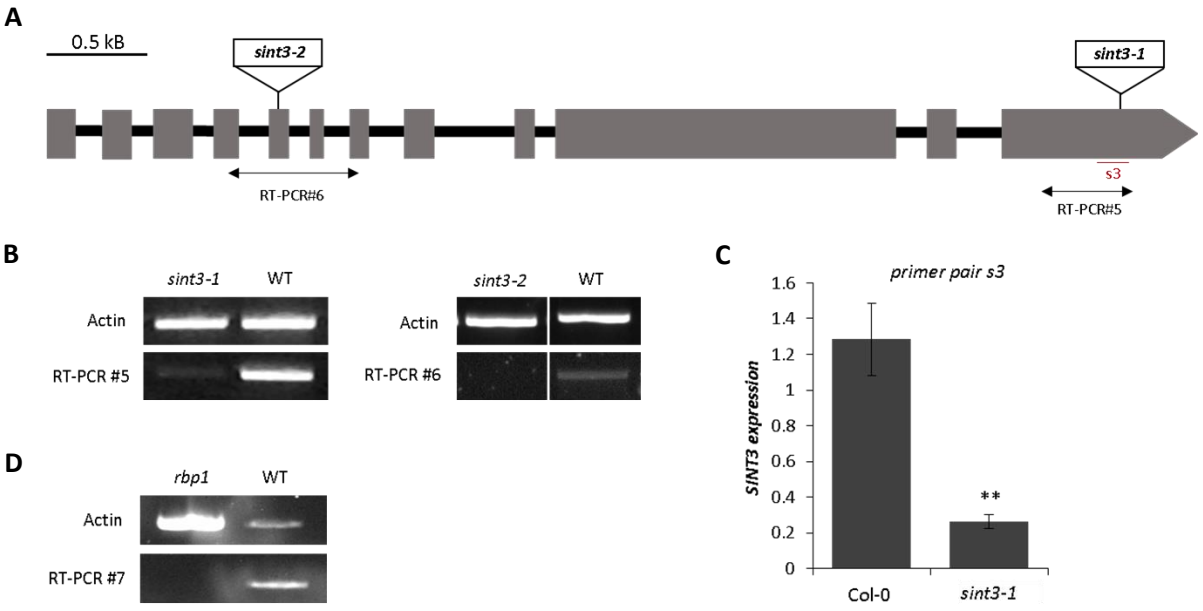

Figure 15. Characterization of the *SINT3* T-DNA insertion mutants. (A) Schematic visualization of the *SINT3* gene structure, T-DNA insertions, and primers used for RT-PCR and qRT-PCR (s3). Grey boxes represent exons. (B) Transcript level of *SINT3* in Col-0, *sint3-1,* and *sint3-2* mutants. *ACT2* primers were used as standard. (C) qRT-PCR analysis of *SINT3* expression in Col-0 and *sint3-1.* Error bars represent ±SE of three biological replicates (**, *P* <0.01; Student's *t* test). *ACT2* was used as internal control. (D) Transcript level of *RBP1* in Col-0 and *rbp1* mutant. *ACT2* primers were used as standard.

First, we investigated a potential role for *SINT3* in the control of shoot branching. The number of rosette branches was counted for *sint3-1* and *rbp1* mutants, but no differences were noted when compared to Col-0 (Figure 16A,B). Also, the *sint3-1 max2-1* double mutant had a significantly higher number of rosette branches than the wild type, consistent with the *max2-1* phenotype, suggesting that *SINT3* is not involved in shoot branching regulation (Figure 16A). Then, we tested whether *SINT3* might be implicated in the SL effect on the lateral root development. The *rac*-GR24–induced decrease in LRD did not differ in the *sint3-1, sint3-2,* and *rbp1* mutants from that in Col-0 plants (Figure 16C,D). Under mock conditions, the *rbp1* mutant was characterized by a slightly lower LRD than that in Col-0 plants (Figure 16D), which was not the case for *sint3-1*. On the contrary, under these conditions, the *max2-1* mutant had a slightly increased LRD, in agreement with previous data (Kapulnik et al., 2011) and this phenotype was suppressed in *s678m2-1* plants (Figure 16E) (Soundappan et al., 2015). The *sint3* mutation did not affect either the increased LRD of the *max2-1* plants or the *s678max2-1* mutant phenotype (Figure 16E), indicating that a mutation in *SINT3* had no impact on the SMXL7-regulated lateral root growth.

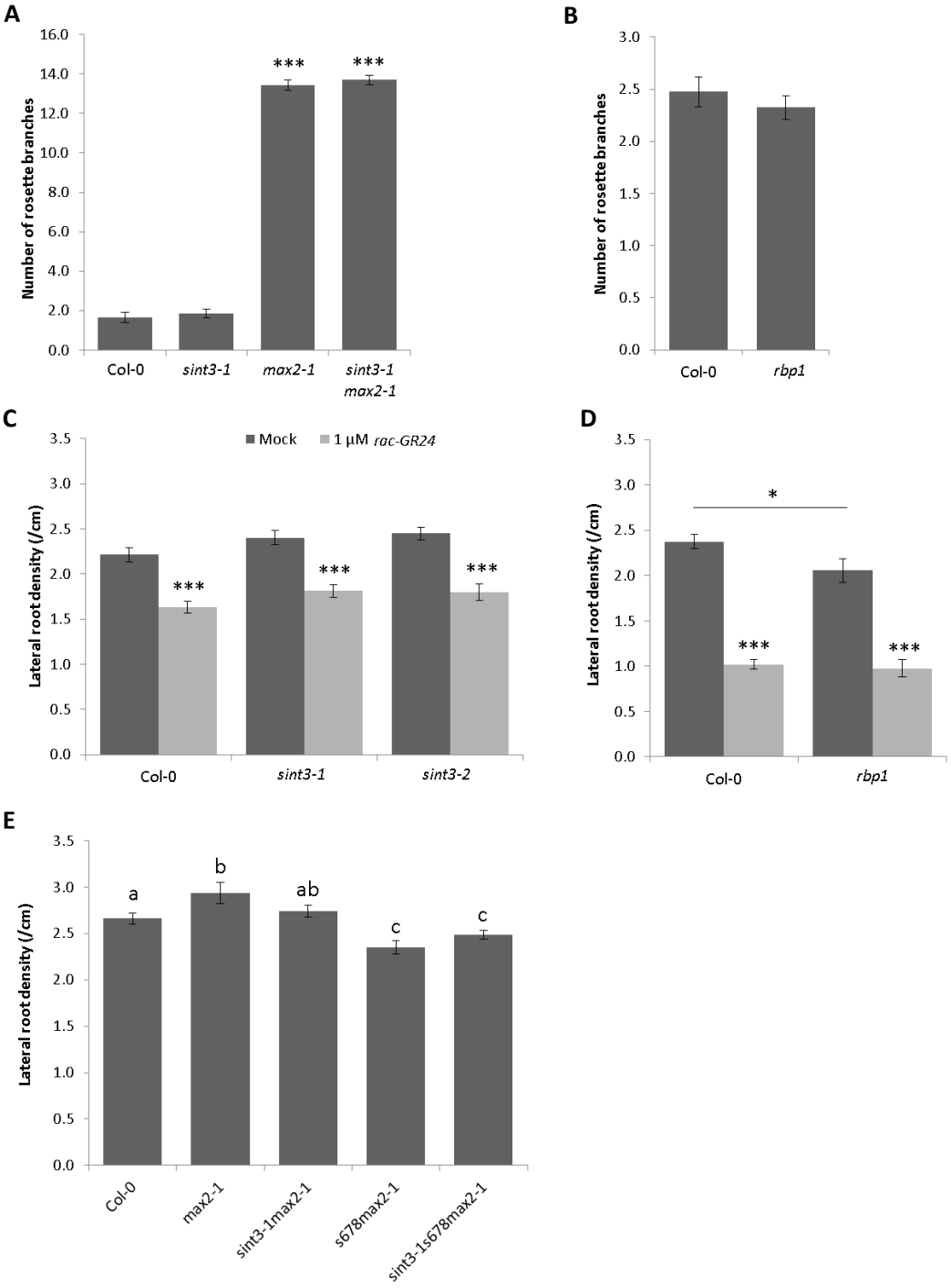

Figure 16. Shoot branching and LRD phenotypes of *sint3* mutants. Number of primary rosette branches of Col-0, *sint3-1*, *max2-1*, *sint3-1 max2-1* (A) and Col-0 and *rbp1* (B) measured at proliferative arrest (A) or after 50 days of growth (B) (n=15). Lateral root density assay of Col-0, *sint3-1*, and *sint3-2* (C) and Col-0 and *rbp1* (D), Col-0, *max2-1, sint3-1 max2-1*, *s678max2-1*, and *sint3-1s678max2-1* (E). LRD was analyzed in 9-day-old plants treated without (mock) or with 1 µM *rac*-GR24 (n>25) (C and D) or without treatment (E). The experiments were repeated three times and the total mean of all biological repeats is presented ± SE. Asterisks indicate statistically significant differences between treatments and asterisks above the line- between genotypes [*** $P < 0.001$, * $P < 0.05$, Student's *t* test (A-B), Poisson regression model (C-D), ANOVA with post- hoc Student's paired t test, $P < 0.05$ (E)].

As SINT3 had also been identified as a potential SMAX1 interactor, we tested whether it might be involved in SMAX1-controlled phenotypes, such as hypocotyl growth. Under continuous red light, *max2-1* had a longer hypocotyl than that of Col-0 plants (Waters et al., 2012). On the contrary, *smax1* exhibited a shorter hypocotyl and it was able to suppress the phenotype of the *max2-1* seedlings (Stanga et al., 2013, 2016). In our analysis, *sint3-1* (Figure 17A) as well as *rbp1* (Figure 17B) had a reduced hypocotyl length upon *rac*-GR24 treatment, just like Col-0 seedlings. In the mock treatment, the *max2-1* mutant had a longer hypocotyl and this phenotype was not affected in *sint3-1 max2-1* (Figure 17B-C). Also, *sint3-1 smax1* seedlings displayed a phenotype similar to that of the *smax1* single mutant (Figure 17D). Thus, we can conclude that *SINT3* is not involved in hypocotyl elongation and in response of young seedlings to *rac*-GR24.

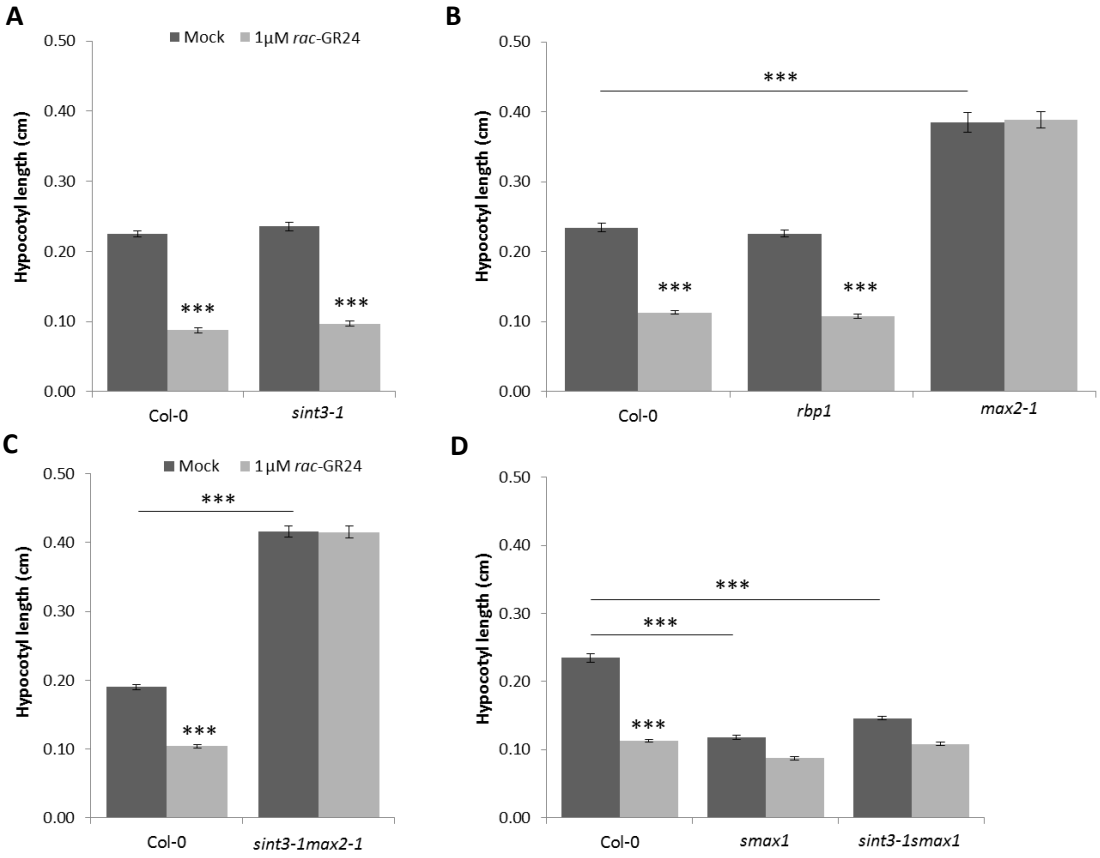

Figure 17. Hypocotyl elongation assay of *sint3* mutants. Seeds were sown on ½MS without sucrose, supplemented with 1 µM *rac*-GR24 or 0.01% acetone, incubated for 2 days at 4°C, exposed to light for 3 h, followed by dark incubation for 21 h before exposure to red light for 4 days. All the graphs represent means of three biological repeats ± SE. Asterisks indicate statistical significant differences between treatments and asterisks above the line- between genotypes (*** $P < 0{,}001$, linear mixed model).

DISCUSSION

The members of the SMXL family in *Arabidopsis,* SMXL6, SMXL7, and SMXL8, are the downstream components of the SL signaling pathway that control the shoot and root architecture, but also cotyledon expansion, leaf morphology, auxin transport, and PIN1 accumulation in the stem (Soundappan et al., 2015; Wang et al., 2015)**.** Although the SMXL protein family had been first described almost five years ago (Jiang et al., 2013; Stanga et al., 2013; Zhou et al., 2013), knowledge about their interacting partners remains limited. It is well established that SMXL7 interacts with the SL receptor in a *rac*-GR24–dependent manner and that D14 serves as a bridge to enable the SMXL7 association with MAX2 (Liang et al., 2016; Yao et al., 2016). Previously, a pull-down assay in rice has shown that mutation of one of the amino acids in the Ser-His-Asp catalytic triad of D14 weakens its *rac*-GR24–dependent interaction with D53 (Jiang et al., 2013). Here, we demonstrated by means of Y2H that the same mutation in the *Arabidopsis* D14 completely abolishes the interaction with SMXL7, indicative that SL hydrolysis is crucial for formation of this complex. In agreement, the mutated versions of D14 with a substitution in one of the amino acids of the catalytic triad to alanine is unable to complement the branching phenotype of *d14* (de Saint Germain et al., 2016). A possible reason might be the lack of interaction with SMXL7 that inhibits its degradation. Indeed, in rice, the mutation in the catalytic triad of D14 impairs the *rac*-GR24–induced degradation of D53 (Jiang et al., 2013). Although the D14-S97C protein version can perceive exogenous *rac*-GR24, but not endogenous SLs *in planta,* in our Y2H assay, no *rac*-GR24–dependent interaction between D14-S97C and SMXL7 occurred, suggesting that the full hydrolytic activity is required for detection of the interaction in the Y2H assay.

To characterize the downstream signaling partners, but also to identify proteins that might regulate the SMXL7 function, TAP-MS analysis was carried out in *Arabidopsis* cell cultures. In none of the TAP experiments with SMXL7 as bait, D14 or MAX2 proteins could be discovered using qualitative analysis, even after the addition of *rac*-GR24 (Soundappan et al., 2015; Wang et al., 2015; Liang et al., 2016), although both transcripts were present in the cell cultures (Supplemental Table 5). From all the identified putative preys of SMXL7, in this chapter we focused on three proteins, namely SINT1, SINT2, and SINT3. The validation studies, including Y2H, BiFC, and FRET-FLIM pointed toward SINT1 as the most convincing interaction partner of SMXL7, but the phenotypic analysis revealed that it does not play a role in the regulation of either the shoot or root architecture. TRM2A and TRM2B (SINT1) have been proposed to possibly be involved in various developmental processes in plants (Wang et al., 2017b). In our study, no difference was observed between wild-type plants and *sint1-1* mutant for the shoot branching, root architecture phenotype and the response to *rac*-GR24. Nevertheless, although the *sint1-1 trm2a* double mutant was equally responsive to SL analog to WT,

in mock it had a higher lateral root density than Col-0, consistent with the phenotype *trm2a* seedlings. This might suggest the role for TRM2A in the regulation of lateral root growth. Additionally, we could show that SINT1 has a transcriptional repression activity, albeit to a lesser extent than SINT3 or SMXL6/7/8 (Wang et al., 2015). As no putative EAR motif was found in the SINT1 sequence, no interaction with transcriptional corepressors, such as TPL/TPR proteins is expected, implying that another mechanism might be involved. In the reciprocal TAP of SINT1 (but also of SINT2 and SINT3), neither SMXL7 nor any other protein known to be involved in SL signaling was detected. This might be explained by the fact that SMXL proteins have been reported as rather instable and difficult to detect (Liang et al., 2016). In agreement, the RNAseq data of *Arabidopsis* cell cultures revealed that the transcript of *SMXL7* was present at the good level (Supplemental Table 5). Characterization of the interaction network of identified preys might give a hint about the processes in which this protein is implicated. Indeed, the reciprocal TAP revealed an interesting putative interactor of SINT1, ANL2, a probable transcription factor crucial for anthocyanin accumulation and cutin biosynthesis (Kubo, 1999; Nadakuduti et al., 2012). This protein might provide a link between SL/KAR and stress responses. In fact, MAX2 has been shown to be involved in plant resistance to drought and *max2* plants grown under drought stress conditions have a thinner cuticles and larger stomatal apertures (Bu et al., 2013). Recently, KAI2, the probable KAR receptor, has been found to control drought resistance in *Arabidopsis* by promoting cuticle development, stomatal closure, and anthocyanin biosynthesis but a contribution of D14 was proposed as well (Li et al., 2017a). In addition, the MAX2 pathway modulates the anthocyanin production in response to limited inorganic phosphate or nitrogen conditions (Ito et al., 2015). Thus far, it is still unknown whether the SMXL proteins are involved in the KAI2- and D14-mediated stress responses. Although SINT1 does not seem to be important for the regulation of the shoot and root architecture, it does not exclude a function in the SL- or even KAR-related phenotypes. In-depth phenotypic analysis of the *sint1* mutant needs to be continued. First, although the SMAX1-SINT1 interaction has not been validated with the Y2H assay, analysis of its role in germination would be worthwhile, because of a higher relative expression level of SINT1 in imbibed seeds. Second, considering a possible association of SINT1 with ALN2, it might be interesting to test stress-related phenotypes in the *sint1* mutant, such as drought tolerance, stomatal aperture, cuticle thickness, or anthocyanin content.

Another putative partner of SMXL7, SINT2, has been described as an ortholog of the rice XB24, which functions in PTI. Mutant analysis, however, demonstrated that the role of this protein is not conserved between rice and *Arabidopsis* (Holton et al., 2015). Curiously, the reciprocal TAP of SINT2 revealed a tetratricopeptide repeat (TPR)-like superfamily protein (SRFR1) as a putative prey that is involved in mediating effector-triggered immunity (Kim et al., 2014). Although this association still

needs to be validated, it can hint at a possible SINT2 role in the immune responses in *Arabidopsis.* Here, we further show that SINT2 has no transcriptional repression activity and seemingly does not function in SMXL7-controlled shoot branching and lateral root growth. Our Y2H analysis indicated a possible interaction between SINT2 and SINT3, suggesting that these proteins might act in one complex. Although the SINT2-SINT3 association was not detected in the reciprocal TAPs after subtraction of background proteins, when the SINT3 and ΔRING-SINT3 TAP data were searched with the MaxQuant software, SINT2 was discovered in every sample. Still, one has to keep in mind that the number of identified proteins was very high (1600; Supplemental dataset 6) and that nonspecific interactors were not removed. The hypothesis that SINT2 and SINT3 might be part of the same complex can also be supported by the fact that in the TAP experiments of SINT2 and SINT3, the proteasome core components were identified, implying that both proteins might play a role in processes related to proteasomal degradation.

SINT3 is one of the three *Arabidopsis* homologs of the yeast NOT4, which is part of the CCR4-NOT complex (Bai et al., 1999; Chen et al., 2001). CCR4-NOT is a large multisubunit structure conserved in all eukaryotes, referred to as the master regulator of gene expression. Although the complex composition might vary between different organisms, seven core components have been identified in all species that were analyzed until now. Not1 provides a scaffold and an anchoring platform for other constituents; Ccr4 and the CCR4-associated factor 1 (Caf1) perform the central enzymatic activity of the complex functioning in the mRNA deadenylation; Not2 and Not5 form a heterodimer; Caf40 participates in RNA degradation; and NOT4 functions as an E3 ligase (reviewed in Collart, 2016; Ukleja et al., 2016). Here, in all the TAP experiments in which SINT3 was used as bait, no other subunits of the CCR4-NOT complex could be identified. The reason might be that only in yeast is NOT4 a stable complex component, whereas in human and *Drosophila* it can perform some functions independently from the CCR4-NOT (Collart, 2016). Similarly, in the TAP data of Caf1 in *Medicago truncatula* hairy root cultures no ortholog of SINT3 (NOT4) was detected as prey (Goossens et al., 2016). Thus, also in *Arabidopsis,* the NOT4 homolog could plausibly be only transiently associated with CCR4-NOT.

In both yeast and human, NOT4 has been reported to interact with E2 ligases, the UBC4/5p and UBCH5B subfamily, respectively (Albert et al., 2002; Mulder et al., 2007). Here, we could not validate the interaction between SINT3 and any of the 30 UBCs from *Arabidopsis* by using the Y2H approach. Curiously, in the quantitative TAP analysis, UBC19 and UBC20 were significantly more associated with SINT3 than with ΔRING-SINT3. As the RING domain is responsible for the interaction with E2 ligases, these results might indicate that UBC19 and UBC20 form a complex with SINT3 that facilitates the transfer of ubiquitin to the target protein. UBC19 and UBC20 belong to XIII UBC group, together with

the human UBCH10 and the yeast UBC11 (Kraft, 2005) and function during the cell cycle (Criqui et al., 2002). Another indication that SINT3 might indeed be involved in ubiquitination leading to protein degradation is the identification of seven proteasome-related proteins in the list of putative SINT3 preys after subtraction of unspecific interactors. Also, the yeast NOT4 has been shown to genetically and biochemically interact with the proteasome and to be important for its activity and integrity (Laribee et al., 2007; Panasenko and Collart, 2011). Thus, this observation could be another explanation for the copurification of the proteasome subunits together with SINT3.

Several proteins involved in the transcriptional or translational regulation have been identified as substrates for NOT4 in yeast and human, including the histone H3 lysine 4 (H3K4) demethylase Jhd2/JARD1C (Mersman et al., 2009), CyclinC, a subunit of the conserved transcriptional regulator cyclin-Cdk8 complex (Cooper et al., 2012), Yap1 transcription factor (Gulshan et al., 2012), a small ribosomal protein (Rps7A) (Panasenko and Collart,2012), and a ribosome-associated chaperone, the nascent polypeptide-associated (NAC-EGD) complex (Panasenko et al., 2006, 2009). Thus, Not4 seems to ubiquitinate substrates that are present in both the cytoplasm and the nucleus. Transient expression of SINT3 in *N. benthamiana* leaf epidermal cells revealed that proteins localize into the cytoplasm and nucleus, indicating that SINT3 might also function in both compartments. In our study, we quantitatively compared the TAPs of SINT3 and ΔRING-SINT3 to identify the potential targets for ubiquitination. We presumed that by deletion of the RING domain, we could avoid ubiquitination and subsequent degradation of the target proteins which are then expected to be enriched in TAPs of ΔRING-SINT3. Quantitative TAP revealed 111 preys that were statistically more associated with SINT3 and 18 proteins identified only in ΔRING-SINT3. The STRING analysis showed that most of the ΔRING-SINT3–specific preys are involved in transcription, translation, and chromatin assembly. Thus, despite the necessary further validation of these preys as SINT3 targets of SINT3, the E3 ligase activity might indeed be important for the gene expression regulation.

Besides a probable function as an E3 ligase, SINT3 also displayed a repression activity in transient expression assays in tobacco protoplasts. The putative EAR motif present in the SINT3 sequence implicates association with the TPL/TPR corepressor proteins. Indeed, with the Y2H assay, we demonstrated an EAR motif–dependent interaction between SINT3 and the N-terminal fragment of TPL, but we could not identify the TPL/TPR proteins in the TAPs of SINT3. The EAR motif has also been shown to mediate the interaction with another corepressor, SIN3-ASSOCIATED POLYPEPTIDE P18 (SAP18). Accordingly, SAP18 was identified as a putative SINT3 prey in one out of four TAPs after subtraction of background proteins (Supplemental dataset 4) and as an interactor significantly more associated with SINT3 than ΔRING-SINT3 in the quantitative TAP analysis. The results of the quantitative TAP are intriguing, because the EAR motif is still present in the amino acid sequence of

ΔRING-SINT3. Thus, we can speculate that deletion of the RING domain might affect the SINT3 protein structure, altering, for instance, the EAR motif position. Interestingly, the removal of the EAR motif did not affect the repression activity of SINT3, indicating that the interaction with TPL/TPR or with SAP18 is not required for this function. On the contrary, the transcriptional repression activity of SMXL7 depends on the EAR motif (Wang et al., 2015). According to the current model, both TPL/TPR and SAP18 regulate the gene expression via the recruitment of chromatin-remodeling factors, such as HISTONE DEACETYLASE 19 (HDA19) (Kagale et al., 2010). Here, our quantitative TAP revealed that the HISTONE DEACETYLATION COMPLEX 1 (HDC1) was significantly more associated with SINT3 under mock conditions than after addition of *rac*-GR24. HDC1 is a component of the histone deacetylase complex that physically interacts with HDA6 and HDA19 and promotes histone deacetylation (Perrella et al., 2016). Thus, we can speculate that SINT3 can mediate the transcriptional repression, possibly via a direct interaction with HDC1. Whether TPL/TPR or SAP18 contribute to its repression activity needs to be further analyzed. Identification of HDC1 as less enriched in the presence of the SL analog would also suggest that under these conditions, histones are more acetylated, subsequently facilitating the transcription process. Several transcriptome data sets have been published, but they report relatively little on the impact of the SL addition on the transcriptome (Mashiguchi et al., 2009; Mayzlish-Gati et al., 2010; Ha et al., 2014; López-Ráez et al., 2017). Thus far, the best candidate for the SL-regulated transcriptional responses is BRC1 (Braun et al., 2012; Dun et al., 2012). Further on, because the interaction with HDC1 was abolished in ΔRING-SINT3, it would be interesting to test whether the repression activity is affected by the deletion of the RING domain in the SINT3 sequence. SMXL7 has been shown to regulate some aspects of the SL-related plant development, such as leaf morphology and branching angle, independently of the EAR motif (Liang et al., 2016). Therefore, SINT3 might possibly play a role in the control of these phenotypes, because the repression activity still occurs even after deletion of the EAR peptide. This hypothesis can be simply tested by analyzing the leaf morphology and branching angle in the *sint3* mutant plants crossed with the *proSMXL7-SMXL7$^{\Delta EAR}$-Venus(s678max2-1)* line (Liang et al., 2016).

Another observation that might draw attention is the detection of the PIN1 protein as significantly more associated with SINT3 in the presence of *rac*-GR24 than in that under mock conditions. Even although 20 putative preys have been identified as specific for this condition, PIN1 is of particular interest considering the SL mode-of-action. Two models for the control of the shoot branching by SLs have been put forward, one depends on transcription via the *BRC1* expression and the other is independent of transcription by influencing the PIN1 trafficking (Seale et al., 2017). SINT3 seems to be implicated in the general transcriptional regulation and, as this quantitative TAP results suggest, it might also play a role in transcription-independent responses by influencing PIN1, although this

association needs to be validated. PIN1 was found to be associated with SINT3 after *rac*-GR24 treatment, so under the conditions in which PIN1 levels at the plasma membrane are rapidly reduced (Bennett et al., 2006; Prusinkiewicz et al., 2009; Shinohara et al., 2013). This observation might hint at the involvement of SINT3 in the removal of the PIN1 protein from the membrane in response to the SL analog. Nonetheless, the lack of phenotype of the *sint3* mutant contradicts our hypothesis. Considering the fact that SINT3 has two close homologs in *Arabidopsis*, due to redundancy, also the *sint3 rbp1* double mutant and *sint3 rbp1 rb2* triple mutant need to be tested.

To summarize, here we provide biochemical evidence for the interactions between SMXL7 and SINT proteins. However, all three preys seem not to be involved in the most pronounced SL-related phenotypes, such as shoot branching and lateral root outgrowth. Nevertheless, the reciprocal TAP experiments of SINT1, SINT2, and SINT3 shed light on the processes, in which these proteins might be implicated, helping us in the future to choose the most adequate phenotype to discover their function.

MATERIALS AND METHODS

Molecular cloning

All cloning was carried out by means of Gateway® recombination (Thermo Fisher Scientific). Open reading frames for mutated D14 protein versions (S97A, H247A, D218A, and S97C) were kindly provided by A. de Saint Germain and C. Rameau (de Saint Germain et al., 2016). All primers used for cloning are listed in Supplemental Table 2.

TAP

Arabidopsis cell suspension cultures (PSB-D) were transformed through cocultivation with *Agrobacterium tumefaciens* as described previously (Van Leene et al., 2007). Cultures were subcultured in fresh MSMO medium at 21°C in continuous dark with gentle agitation (130 rpm) and a few weeks after they were transferred to a light/dark (16 h/8 h) regime. Three weeks later the protein level was analyzed and cultures expressing the bait were upscaled for TAP analysis. Immunoblotting was performed using peroxidase-anti-peroxidase (PAP) antibody against the GS-rhino tag (Sigma-Aldrich). For treatments, 1 µM *rac*-GR24 was added to the cell culture for 10 min before harvesting. Affinity purification and LC-MS/MS analysis were as described (Van Leene et al., 2014). For SMXL7 and ΔSMXL7, TAP samples were in-gel digested with trypsin while for SINT proteins on-bead digest was done. Quantitative TAP analysis was carried out with MaxQuant (version 1.4.1.2) and Perseus software (version 1.5.3.2) as described in detail in Chapter 3.

Y2H

Y2H analysis was carried out as described (Pérez Cuéllar et al., 2013). Bait (AD) and prey (BD) were cloned into pB42AD and pGILDA (LexA system) or pGAL424 and pGBT9 (GAL4 system). The *Saccharomyces cerevisiae* strains EGY48 (LexA system) or PJ69-4A (GAL4 system) were cotransformed with bait and prey by means of the polyethylene glycol (PEG)/lithium acetate method. For the LexA system, transformants were selected on SD media lacking Ura, Trp, and His (Clontech). Three individual colonies were grown overnight in liquid cultures at 30°C and 10- and 100-fold dilutions were dropped on control media (SD-Ura-Trp-His) and selective media (SD-Ura-Trp-His) containing X-Gal (Duchefa). To test the influence of SL on the interaction, 10 µM *rac*-GR24 or 0.1% acetone was added to the medium. For the GAL4 system, transformants were selected on SD media lacking Leu and Trp (Clontech). Three individual colonies were grown overnight in liquid cultures at 30°C and 10- and 100-fold dilutions were dropped on control media (SD-Leu-Trp) and selective media lacking Leu, Trp, and His (Clontech).

BiFC

The *35S::tag-ORF* and *35S:: ORF-tag* constructs with the N- and C-terminal parts of eGFP (nGFP and cGFP, respectively) were generated by double Gateway recombination with the pK7m24GW2 vector (Boruc et al., 2010). The constructs were coexpressed in *N. benthamiana* with the *Agrobacterium tumefaciens*-mediated transient transformation with a modified buffer (10 mM $MgCl_2$, 10 mM MES, and 100 µM acetosyringone). Interactions were scored 3 days after infiltration by screening the lower epidermal cells for fluorescence with the Zeiss LSM5 Exiter confocal microscope.

FRET-FLIM

FRET-FLIM analysis was done as described (Liang et al., 2016) with some modifications.

Transient expression assay

Transient expression assays were done as described (Vanden Bossche et al., 2013). Protoplasts prepared from a Bright Yellow-2 tobacco cell culture were cotransfected with a reporter plasmid containing the firefly luciferase (fLUC) reporter gene driven by the LOX3 promoter (Pauwels et al., 2008), a normalization construct expressing the Renilla luciferase (rLUC) under control of the 35S promoter (De Sutter et al., 2005), and effector constructs under the control of the 35S promoter. The p2GW7-GUS effector plasmid was used as a control. fLUC and rLUC activities were determined with the Dual-Luciferase reporter assay system (Promega). Variations in transfection efficiency and technical errors were corrected by normalization of fLUC by rLUC activities. All transactivation assays were carried out in an automated experimental set-up with eight biological replicates for each effector combination.

Histochemical analysis of the GUS activity

Approximately 2 kb of DNA 5' to the start codon of SINT3 was amplified by PCR from the Col-0 genomic DNA with the iProof polymerase (Bio-Rad), cloned by BP reaction into the Gateway entry vector pDONR221 (Invitrogen), and then subcloned by LR reaction into the pK7m24GW-FAST vector for GUS fusion. Constructs were transformed into Col-0 plants by the *Agrobacterium* floral dip method. GUS was analyzed in the T2 generation and two independent transgenic lines were compared. After 10 days of growth, whole seedlings were stained for GUS expression in multiwell plates as described (Jefferson et al., 1987). Samples were cleared as described (Malamy and Benfey, 1997) and analyzed by a differential interference contrast BX51 microscope (Olympus).

Plant material and growth conditions

Seeds of *Arabidopsis thaliana* (L.) Heynh. Columbia-0 (Col-0) accession plants were surface sterilized with consecutive treatments of 70% (v/v) ethanol with 0.05% (w/v) sodium dodecyl sulfate (SDS), washed with 95% (v/v) ethanol, sown on ½MS medium with 1% (w/v) sucrose (for root phenotyping) or without (for hypocotyl analysis), and stratified for 2 days at 4°C. All mutant lines used in this study are in the Col-0 accession background. The T-DNA insertion lines were ordered from the Salk Institute: *sint1-1* (SALK_106689), *sint1-2* (SALK_039998), *trm2a* (SALK_085796), *sint2-1* (SALK_126246), *sint2-2* (SALK_139882), *sint3-1* (SALK_061949), *sint3-2* (SAIL_274_D03), and *rbp1* (GABI_134E03). The *max2-1* (Stirnberg et al., 2002), *smax1* (Stanga et al., 2013), and *s678max2-1* (Soundappan et al., 2015) lines have been described previously. The homozygous mutant lines were selected with PCR genotyping. The RNA was extracted from 5-day-old seedlings and RT-PCR was used to assess transcripts with *ACTIN2* (*ACT2*, AT3G18780) as a control.

qRT-PCR

RNA was extracted with the RNeasy® Plant Mini Kit (Qiagen). RNA (1 µg) was used to make cDNA with the iScript™ cDNA Synthesis Kit and was diluted to a final volume of 500 µl. The primers were designed with the primer design tool of Roche Applied Science (http://www.roche-applied-science.com) (Supplemental Table 2). All primers were diluted with water to a concentration of 5 µM. All qRT-PCR experiments were done in three technical repeats with 384-multiwell plates and detection by SYBR® Green. Reaction mixes were composed by the Janus Robot with a final volume of 5 µl and a 10% cDNA fraction by means of the SYBR® Green Master Mix (PerkinElmer). The Roche Lightcycler® 480 system (Roche Diagnostics) was used to execute all qRT-PCR reactions with the following settings: 1x pre-incubation (at 95°C for 5 min), 45x amplification (at 95°C for 10 sec, at 60°C for 10 sec, at 72°C for 10 sec), 1x melting curve (at 95°C for 5 sec, from 65°C to 97°C for 1 min), and 1x cooling down (at 40°C for 10 sec). Ct values and efficiency values were determined by the Lightcycler® 480 software and analyzed by the 2-ΔΔCt method (Livak & Schmittgen, 2001). The obtained expression data were normalized to the expression levels of *ACTIN2* (*ACT2*, AT3G18780).

Physiological assays

For shoot branching assays, plants were grown in soil under a standard 16-h/8-h light/dark cycle (22°C/18°C) in controlled-environment rooms with light provided by white fluorescent tubes. Rosette branches (shoots >1 cm) were counted in 50-day-old plants or at the proliferative arrest. To analyze root phenotypes, seedlings were grown vertically for 9 days in growth chambers with a long-day (LD) photoperiod at 21˚C. The lateral root primordia were counted under a light microscope (S4E, Leica

Microsystems), whereafter the plates were scanned and the main root length was measured with the ImageJ software and a digitizer tablet (Wancom). LRD was calculated by dividing the number of lateral roots by the corresponding primary root length. For the hypocotyl elongation analysis, after the seeds had been stratified, they were exposed to white light for 3 h, transferred to darkness for 21 h, and then exposed to continuous red light for 4 days at 21°C. After scanning of the plates, the hypocotyls were measured with the ImageJ 1.41 software.

SUPPLEMENTARY DATA

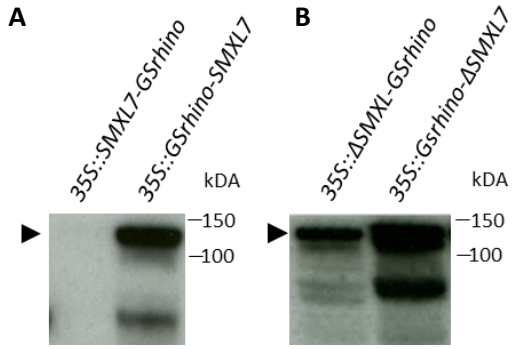

Supplemental Figure 1. Expression analysis of SMXL7 (A) and ΔSMXL7 (B) baits in *Arabidopsis* cell cultures. Protein levels were analyzed by immunoblotting. Total protein extract was loaded and detection was done with the peroxidase–antiperoxidase (PAP) antibody against the GS tag. The molecular mass of the tagged (Δ)SMXL7 protein (indicated by the arrow) is ~133 kDa.

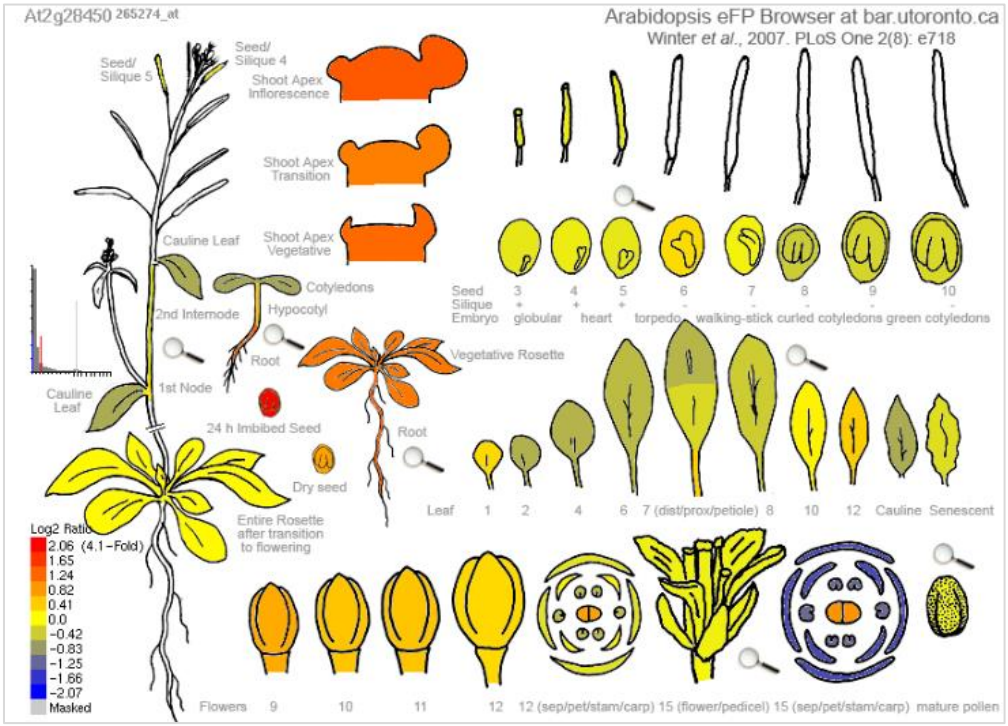

Supplemental Figure 2. The eFP visualization of the relative *SINT1* gene expression level during *Arabidopsis* development. The color scheme represents the ratio of a tissue's expression level of *SINT1* to the median expression value calculated across all displayed samples for each probe set.

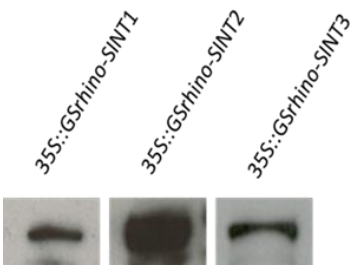

Supplemental Figure 3. Expression analysis of SINT1, SINT2, and SINT3 baits in *Arabidopsis* cell cultures. Protein levels were analyzed by immunoblotting. Total protein extract was loaded and detection was done with the peroxidase–antiperoxidase (PAP) antibody against the GS tag. Molecular masses: 89 kDa for SINT1, 21.3 kDa for SINT2, 108.4 kDa for SINT3, and 21.9 kDa for GSrhino tag.

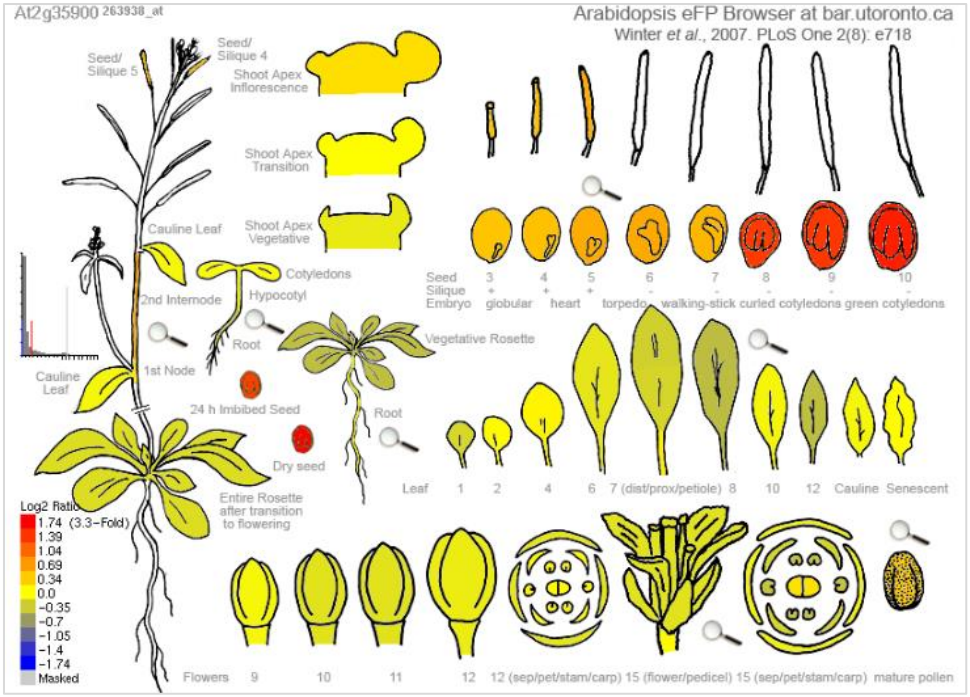

Supplemental Figure 4. The eFP visualization of the relative *SINT2* gene expression level during development in *Arabidopsis*. The color scheme represents the ratio of a tissue's expression level of *SINT2* to the median expression value calculated across all displayed samples for each probe set.

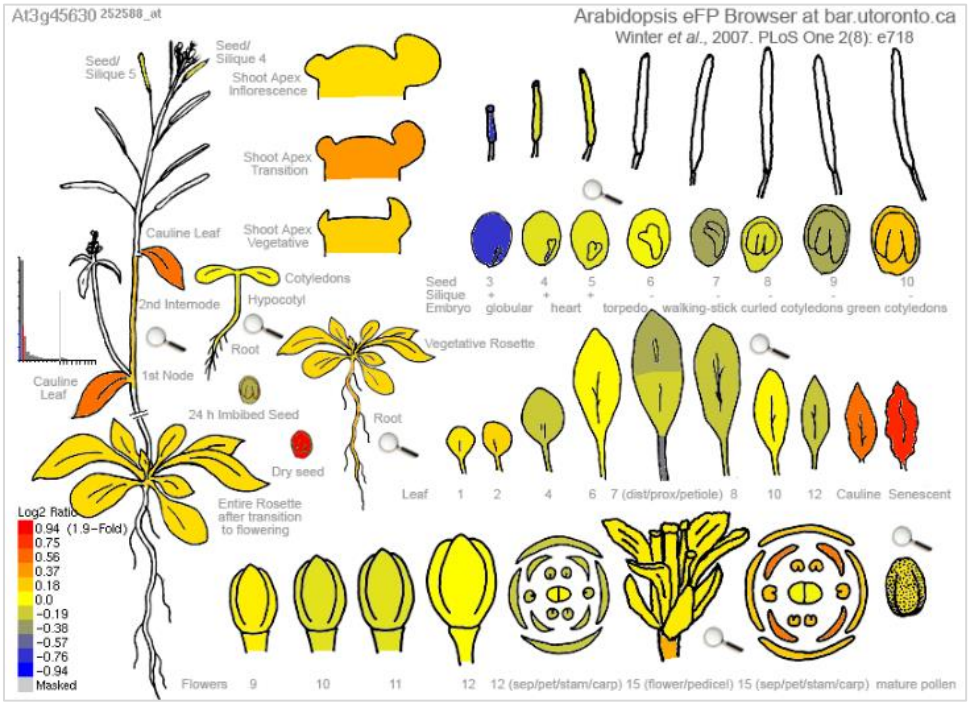

Supplemental Figure 5. The eFP visualization of the relative *SINT3* gene expression level during development in *Arabidopsis*. The color scheme represents the ratio of a tissue's expression level of *SINT3* to the median expression value calculated across all displayed samples for each probe set.

Supplemental Table 1. Overview of the ΔSMXL7 pray proteins purified by TAP

AGI	Protein	*35S::GSrhino-ΔSMXL7*	
		Mock	*rac*-GR24
AT2G29970	SMXL7, SMAX1-LIKE 7	2	2
AT3G16830	TPR2, TOPLESS-related 2	2	2
AT1G15750	TPL, TOPLESS	2	2
AT2G28450	SINT1, SMAX7 INTERACTING PROTEIN 1	2	2
AT5G20490	XIK, Myosin family protein with Dil domain	1	2
AT5G58410	HEAT/U-box domain-containing protein	-	1
AT5G41950	HLB1, HYPERSENSITIVE TO LATRUNCULIN B 1	-	-
AT5G11980	COG8, CONSERVED OLIGOMERIC GOLGI COMPLEX 8	-	-
AT3G45190	SAL4, SIT4 phosphatase-associated family protein	1	-
AT2G05120	NUP133, Nucleoporin	1	-
AT4G37460	SRFR1, SUPPRESSOR OF RPS4-RLD 1	-	1
AT4G01990	Tetratricopeptide repeat (TPR)-like superfamily protein	-	2
AT4G36750	Quinone reductase family protein	-	1
AT4G12420	SKU5, Cupredoxin superfamily protein	-	1
AT5G24020	ARC11, ACCUMULATION AND REPLICATION OF CHLOROPLASTS 11	-	1
AT2G26780	ARM repeat superfamily protein	-	-

TAP experiments were performed using *35S::GSrhino-ΔSMXL7* as bait, treated mock or with 1µM *rac*-GR24. Prey proteins were identified using peptide-based homology analysis of MS data. Background proteins identified in control experiments were withdrawn. The number indicates the times the prey was identified in 4 experiments with the bait protein. AGI, Arabidopsis Genome Identifier; -, pray was not identified.

Supplemental Table 2. All primers used in this study.

ID		Sequence	Use
SMXL7	Fw	GGGGACAAGTTTGTACAAAAAAGCAGGCTCAATGCCGACACCAGTAACCACG	Cloning
SMXL7	Rev	GGGGACCACTTTGTACAAGAAAGCTGGGTATCAGATCACTTCGACTCTCG	Cloning
D14	Fw	GGGGACAAGTTTGTACAAAAAAGCAGGCTCAATGAGTCAACACAACATCTTAG	Cloning
D14	Rev	GGGGACCACTTTGTACAAGAAAGCTGGGTATCACCGAGGAAGAGCTCGCCG	Cloning
SINT1	Fw	GGGGACAAGTTTGTACAAAAAAGCAGGCTCAATGGAAACATCATCAATCGAAATCAACG	Cloning
SINT1	Rev	GGGGACCACTTTGTACAAGAAAGCTGGGTATTACCTCTCAAGGAGCATTACC	Cloning
SINT2	Fw	GGGGACAAGTTTGTACAAAAAAGCAGGCTCAATGGGTTGGATCTGGATTGACG	Cloning
SINT2	Rev	GGGGACCACTTTGTACAAGAAAGCTGGGTATCAAACGTCCTTGGCCAAGCCC	Cloning
SINT3	Fw	GGGGACAAGTTTGTACAAAAAAGCAGGCTCAATGAGTGATTACGGTGAAAAG	Cloning
SINT3	Rev	GGGGACCACTTTGTACAAGAAAGCTGGGTATCAAATCCCGTATGTTCTG	Cloning
Nucleoporin	Fw	GGGGACAAGTTTGTACAAAAAAGCAGGCTCAATGTTCTCTCCATTGACGAAGAGAGCTAAGC	Cloning
Nucleoporin	Rev	GGGGACCACTTTGTACAAGAAAGCTGGGTATTACTCCATTGGAGATGAGAACTCTTCTGC	Cloning
ΔEAR SINT3	Fw	GAAATCTTGTTTACATTGTTGGAGCAGATGAAGATCTTCTCCAGCG	Mutagenesis
ΔEAR SINT3	Rev	CGCTGGAGAAGATCTTCATCTGCTCCAACAATGTAAACAAGATTTC	Mutagenesis
ΔRING SINT3	Fw	GGGGACAAGTTTGTACAAAAAAGCAGGCTCAATGAGTGATTACACTCCATATGACAAAG	Mutagenesis
sint1-1	Fw	CCGAACGGAATGCAACGATC	RT-PCR#1
sint1-1	Rev	ACCATTTCGCAGTGGTCAGT	RT-PCR#1

sint1-2	Fw	TTTTGAAACTCCTTCACTTCCAA	RT-PCR#2
sint1-2	Rev	TTCAATTCATCAGATTGCCATT	RT-PCR#2
sint1-1	Fw	CCGAACGGAATGCAACGATC	qRT-PCR s1
sint1-1	Rev	CAACGGCCATTGCTTTGACA	qRT-PCR s1
trm2a	Fw	TGGAAGGAATGTGGAGACTGG	RT-PCR#3
trm2a	Rev	GCAAGCTCTAACAAGCAGACAC	RT-PCR#3
sint2	Fw	TTGACGATTCATCCGCCTCT	RT-PCR#4
sint2	Rev	GCCAAGCCCGAGAGATCAAT	RT-PCR#4
sint2	Fw	TTTGGGAAGCCCTCTGAAGTC	qRT-PCR s2
sint2	Rev	CCGCTCAAGAAATGGCGTTC	qRT-PCR s2
sint3-1	Fw	ACAAGTGTCCGAGTGGTTCA	RT-PCR#5
sint3-1	Rev	TGGTGACATAATTATTGCAGGTC	RT-PCR#5
sint3-2	Fw	AGCTTGTCTAGGCAGCTGTG	RT-PCR#6
sint3-2	Rev	TATGCAATACCGTTCAGGGAG	RT-PCR#6
sint3-1	Fw	CTGTGGCGAGGACTCAAGTT	qRT-PCR s3
sint3-1	Rev	AGCTTGTCTAGGCAGCTGTG	qRT-PCR s3
rbp1	Fw	TGCATATCAAGTACCACCTCCA	RT-PCR#7
rbp1	Rev	TCCGGAATTTTGGTTCTTCA	RT-PCR#7

Supplemental Table 3. Proteins found significantly different between mock and treatment in SINT3 TAP experiments.

Significant	-Log (*P* value)	Fold change	AGI	Protein
Mock	4.401	2.502	AT2G45960	PIP1B, Plasma membrane intrinsic protein 1B
Mock	2.575	2.005	AT1G07410.1	RABA2b, RAB GTPase homolog A2B
Mock	2.245	2.995	AT1G61790.1	Oligosaccharyltransferase complex/magnesium transporter family protein
Mock	3.932	2.779	AT1G63070.1	Pentatricopeptide (PPR) repeat-containing protein
Mock	1.429	1.414	AT1G73110.1	P-loop containing nucleoside triphosphate hydrolases superfamily protein
Mock	1.796	1.947	AT2G02480.1	STI, AAA-type ATPase family protein
Mock	2.150	1.745	AT2G05940 AT1G06700 AT1G48210	Protein kinase superfamily protein
Mock	1.574	2.075	AT2G29190	PUM2, pumilio 2
Mock	2.107	0.931	AT2G34730	Myosin heavy chain-related
Mock	1.800	2.178	AT2G36360	Galactose oxidase/kelch repeat superfamily protein
Mock	1.724	1.998	AT2G36910.1	ABCB1, ATP binding cassette subfamily B1
Mock	3.298	3.530	AT2G42710.1	Ribosomal protein L1p/L10e family
Mock	3.656	1.145	AT3G22670.1	Pentatricopeptide repeat (PPR) superfamily protein
Mock	1.608	2.584	AT3G25680.1	SLH domain protein
Mock	1.918	1.381	AT3G26782.1	Tetratricopeptide repeat (TPR)-like superfamily protein
Mock	2.443	2.115	AT3G44330.1	M28 Zn-peptidase nicastrin
Mock	3.958	2.802	AT3G47470.1	LHCA4, light-harvesting chlorophyll-protein complex I subunit A4
Mock	1.525	1.962	AT3G48470.1	EMB2423, embryo defective 2423
Mock	2.148	1.223	AT3G53760.1	GCP4, GAMMA-TUBULIN COMPLEX PROTEIN 4
Mock	1.406	3.338	AT3G61070	PEX11E, peroxin 11E
Mock	1.628	2.114	AT3G62080	SNF7 family protein
Mock	2.484	0.991	AT4G07390.1	Mannose-P-dolichol utilization defect 1 protein

Mock	5.073	1.738	AT4G08320.1	TPR8, Tetratricopeptide repeat (TPR)-like superfamily protein
Mock	2.668	1.752	AT4G19640	ARA7, Ras-related small GTP-binding family protein
Mock	1.829	2.014	AT4G37330.1	CYP81D4, cytochrome P450, family 81, subfamily D, polypeptide 4
Mock	1.296	2.902	AT5G05670	Signal recognition particle binding
Mock	1.648	3.432	AT5G08450.3	HDC1, HISTONE DEACETYLATION COMPLEX 1
Mock	1.392	2.090	AT5G13260.1	Unknown protein
Mock	1.901	2.495	AT5G14790.1	ARM repeat superfamily protein
Mock	2.509	3.473	AT5G66910.1	Disease resistance protein (CC-NBS-LRR class) family
rac-GR24	4.457	5.174	AT1G21690.1	EMB1968, RFC4, ATPase family associated with various cellular activities (AAA)
rac-GR24	1.024	1.449	AT1G27752.1	Ubiquitin system component Cue protein
rac-GR24	2.188	1.514	AT1G31970.1	STRS1, DEA(D/H)-box RNA helicase family protein
rac-GR24	1.856	1.950	AT1G65440	GTB1, global transcription factor group B1
rac-GR24	1.334	2.349	AT1G73590	PIN1, Auxin efflux carrier family protein
rac-GR24	2.352	1.990	AT1G79890.1	RAD3-like DNA-binding helicase protein
rac-GR24	7.341	5.260	AT2G04865.1	Aminotransferase-like, plant mobile domain family protein
rac-GR24	3.313	1.332	AT2G31810	ACT domain-containing small subunit of acetolactate synthase protein
rac-GR24	3.692	3.644	AT2G32850	Protein kinase superfamily protein
rac-GR24	4.566	3.162	AT3G13230.1	RNA-binding KH domain-containing protein
rac-GR24	2.138	1.579	AT3G49240.1	Pentatricopeptide repeat (PPR) superfamily protein
rac-GR24	3.736	3.209	AT4G14420.1	HR-like lesion-inducing protein-related
rac-GR24	6.000	3.609	AT4G35850.1	Pentatricopeptide repeat (PPR) superfamily protein
rac-GR24	2.025	3.243	AT5G08560	Transducin family protein / WD-40 repeat family protein
rac-GR24	1.130	1.337	AT5G11670	NADP-ME2, NADP-malic enzyme 2
rac-GR24	1.854	1.933	AT5G20350.1	TIP1, Ankyrin repeat family protein with DHHC zinc finger domain
rac-GR24	4.133	3.223	AT5G23570.1	SGS3, XS domain-containing protein
rac-GR24	2.928	1.522	AT5G61450.1	P-loop containing nucleoside triphosphate hydrolases superfamily protein
rac-GR24	1.398	1.483	AT5G62560.1	RING/U-box superfamily protein with ARM repeat domain

Results of *t* test analysis (FDR=0.05, S0=0.1) based on LFQ values carried out using the Perseus software on a set of four independent SINT3 TAP experiments on both mock and *rac*-GR24 treatment.

Supplemental Table 4. **Proteins significantly different between SINT3 and ΔRING-SINT3 TAP experiments.**

Significant	-Log (*P* value)	Fold change	AGI	Protein
SINT3	4.597	2.786	AT2G45960.2	PIP1B, Plasma membrane intrinsic protein 1B
SINT3	3.216	2.350	AT1G06720.1	P-loop containing nucleoside triphosphate hydrolases superfamily protein
SINT3	2.323	0.800	AT1G07990.1	SAL1, SIT4 phosphatase-associated family protein
SINT3	2.154	1.934	AT1G10950.1	TMN1, Transmembrane nine 1
SINT3	5.040	5.092	AT1G11610.1	CYP71A18, cytochrome P450, family 71, subfamily A, polypeptide 18
SINT3	4.578	5.958	AT1G12310.1	Calcium-binding EF-hand family protein
SINT3	4.068	3.840	AT1G24240	Ribosomal protein L19 family protein
SINT3	2.631	3.716	AT2G34420	LHB1B2, photosystem II light harvesting complex gene B1B2
SINT3	6.201	5.349	AT1G32440.1	PKp3, Plastidial pyruvate kinase 3
SINT3	3.488	3.075	AT1G35620.1	ATPDIL5-2, PDI-like 5-2

SINT3	3.063	3.316	AT3G20060.2 AT1G50490.1	UBC19, ubiquitin-conjugating enzyme19 UBC20 ubiquitin-conjugating enzyme 20
SINT3	4.750	3.556	AT1G51160	SNARE-like superfamily protein
SINT3	1.404	1.279	AT3G14790	RHM3, Rhamnose biosynthesis 3
SINT3	3.112	3.662	AT1G61790.1	Oligosaccharyltransferase complex/magnesium transporter family protein
SINT3	2.573	2.293	AT1G62380.1	ACO2, ACC oxidase 2
SINT3	3.046	2.682	AT1G63070.1	Pentatricopeptide (PPR) repeat-containing protein
SINT3	4.044	3.499	AT1G66240	ATX1, Homolog of anti-oxidant 1
SINT3	1.199	1.119	AT1G72320	APUM23, Pumilio 23
SINT3	4.409	3.487	AT1G74470.1	Pyridine nucleotide-disulphide oxidoreductase family protein
SINT3	3.830	2.690	AT2G02480	STI, AAA-type ATPase family protein
SINT3	1.327	1.379	AT2G02800	APK2B, Protein kinase 2B
SINT3	3.699	2.622	AT2G20290.1	XIG, Myosin-like protein XIG
SINT3	6.052	5.522	AT2G27530	PGY1, Ribosomal protein L1p/L10e family
SINT3	3.888	3.976	AT2G30490.1	ATC4H, REF3 cinnamate-4-hydroxylase
SINT3	2.973	2.641	AT2G33610.1	ATSWI3B, Switch subunit 3
SINT3	4.812	3.720	AT2G37230.1	Tetratricopeptide repeat (TPR)-like superfamily protein
SINT3	1.744	1.197	AT2G38840.1	Guanylate-binding family protein
SINT3	4.007	3.614	AT2G39630	Nucleotide-diphospho-sugar transferases superfamily protein
SINT3	3.477	3.024	AT2G42710.1	Ribosomal protein L1p/L10e family
SINT3	2.257	2.201	AT2G45330.2	emb1067, RNA 2'-phosphotransferase, Tpt1 / KptA family
SINT3	7.088	3.169	AT2G45640	SAP18, SIN3 associated polypeptide P18
SINT3	2.046	1.652	AT2G47860	Phototropic-responsive NPH3 family protein
SINT3	4.298	4.109	AT3G02490.1	Pentatricopeptide repeat (PPR) superfamily protein
SINT3	1.680	2.640	AT3G06010.1	ATCHR12, Homeotic gene regulator
SINT3	5.409	5.367	AT3G12915.1	Ribosomal protein S5/Elongation factor G/III/V family protein
SINT3	5.027	3.979	AT3G15690	Single hybrid motif superfamily protein
SINT3	3.574	3.504	AT3G17465.1	RPL3P, ribosomal protein L3 plastid
SINT3	4.360	4.238	AT3G19820	DWF1, cell elongation protein / DWARF1 / DIMINUTO (DIM)
SINT3	3.748	3.285	AT3G19960	ATM1, Myosin 1
SINT3	1.379	1.033	AT3G26240.1	Cysteine/Histidine-rich C1 domain family protein
SINT3	2.365	2.316	AT3G44530.2	HIRA homolog of histone chaperone
SINT3	3.816	3.433	AT3G45190.1	SAL4, SIT4 phosphatase-associated family protein
SINT3	2.209	1.179	AT3G50380	Protein of unknown function (DUF1162)
SINT3	3.099	2.099	AT3G53700.1	MEE40, Pentatricopeptide repeat (PPR) superfamily protein
SINT3	6.287	3.208	AT4G30150.1	Nucleolar 27S pre-rRNA processing, Urb2/Npa2
SINT3	3.117	2.898	AT3G62080	SNF7 family protein
SINT3	3.776	3.244	AT3G25680	SLH domain protein
SINT3	1.799	0.618	AT3G46610.1	Pentatricopeptide repeat (PPR-like) superfamily protein
SINT3	3.557	2.746	AT3G47470.1	LHCA4, CAB4 light-harvesting chlorophyll-protein complex I subunit A4
SINT3	3.388	1.484	AT3G47730.1	ATATH1, ATP-binding cassette A2
SINT3	4.438	4.424	AT3G61130.1	GAUT1, Galacturonosyltransferase 1
SINT3	1.971	2.272	AT4G04790.1	Tetratricopeptide repeat (TPR)-like superfamily protein
SINT3	2.141	2.146	AT4G08350	GTA02, Global transcription factor group A2
SINT3	4.390	3.406	AT4G10955	alpha/beta-Hydrolases superfamily protein
SINT3	3.509	3.947	AT4G12420.2	SKU5, Cupredoxin superfamily protein

SINT3	5.816	2.254	AT4G14150.1	PAKRP1, KINESIN-12A phragmoplast-associated kinesin-related protein 1
SINT3	3.836	2.554	AT5G47540.1	Mo25 family protein
SINT3	4.324	4.519	AT4G21660.1	Proline-rich spliceosome-associated (PSP) family protein
SINT3	3.258	3.145	AT4G27080.1	ATPDIL5-4, PDI-like 5-4
SINT3	1.682	0.558	AT4G29900.1	ACA10, CIF1, ATACA10 autoinhibited Ca(2+)-ATPase 10
SINT3	4.3155	1.206	AT4G31210.1	DNA topoisomerase, type IA, core
SINT3	3.597	3.600	AT4G31390.2	Protein kinase superfamily protein
SINT3	4.601	4.554	AT4G33945.1	ARM repeat superfamily protein
SINT3	4.891	4.958	AT4G36750.1	Quinone reductase family protein
SINT3	2.482	1.921	AT4G37330.1	CYP81D4 cytochrome P450, family 81, subfamily D, polypeptide 4
SINT3	5.402	3.779	AT4G38470.1	ACT-like protein tyrosine kinase family protein
SINT3	4.497	4.528	AT5G04910.1	Unknown protein
SINT3	5.371	3.355	AT5G08450.3	Histone deacetylation protein Rxt3
SINT3	4.848	4.317	AT5G12350	Regulator of chromosome condensation (RCC1) family with FYVE zinc finger domain
SINT3	1.376	0.928	AT5G12480	CPK7 calmodulin-domain protein kinase 7
SINT3	6.430	4.658	AT5G14790.1	ARM repeat superfamily protein
SINT3	2.536	1.659	AT5G15680.1	ARM repeat superfamily protein
SINT3	1.748	1.453	AT5G16630	ATRAD4, RAD4 DNA repair protein Rad4 family
SINT3	2.602	1.928	AT5G17990.1	TRP1, pat1 tryptophan biosynthesis 1
SINT3	5.635	3.217	AT5G19320.1	RANGAP2, RAN GTPase activating protein 2
SINT3	5.252	3.836	AT5G23060.1	CaS, Calcium sensing receptor
SINT3	3.238	3.883	AT5G23140.1	CLPP2, NCLPP7 nuclear-encoded CLP protease P7
SINT3	5.290	2.932	AT5G27140.1	NOP56-like pre RNA processing ribonucleoprotein
SINT3	2.803	3.266	AT5G28040.1	DNA-binding storekeeper protein-related transcriptional regulator
SINT3	3.093	4.380	AT5G41790.1	CIP1, COP1-interactive protein 1
SINT3	3.812	2.958	AT5G48030	GFA2, Gametophytic factor 2
SINT3	1.309	1.161	AT5G50780.1	Histidine kinase-, DNA gyrase B-, and HSP90-like ATPase family protein
SINT3	2.752	0.872	AT5G55540.1	TRN1, LOP1 tornado 1
SINT3	3.770	2.923	AT5G57990.1	UBP23, ubiquitin-specific protease 23
SINT3	2.719	3.788	AT5G61730.1	ATATH11, ATH11 ABC2 homolog 11
SINT3	2.917	1.556	AT5G63220.1	Unknown protein
SINT3	2.804	2.729	AT5G66200.1	ARO2, Armadillo repeat only 2
SINT3	4.624	4.015	AT5G66910.1	Disease resistance protein (CC-NBS-LRR class) family
SINT3	3.899	5.036	ATCG00670.1	CLPP1, PCLPP plastid-encoded CLP P
SINT3	3.798	3.797	ATMG00090.1	Structural constituent of ribosome
SINT3	4.827	3.290	AT3G62600.1	ATERDJ3B, ERDJ3B DNAJ heat shock family protein
ΔRING	6.153	5.075	AT1G02780.1	emb2386, Ribosomal protein L19e family protein
ΔRING	1.784	0.988	AT1G05710	Basic helix-loop-helix (bHLH) DNA-binding superfamily protein
ΔRING	5.281	5.290	AT1G13060	PBE1, 20S proteasome beta subunit E1
ΔRING	2.363	2.079	AT1G29370.1	Kinase-related protein of unknown function (DUF1296)
ΔRING	3.694	1.834	AT1G29940.1	NRPA2, nuclear RNA polymerase A2
ΔRING	5.499	4.354	AT2G04865.1	Aminotransferase-like, plant mobile domain family protein
ΔRING	3.448	5.107	AT5G07090	Ribosomal protein S4 (RPS4A) family protein
ΔRING	5.041	2.590	AT2G18450	SDH1-2, Succinate dehydrogenase 1-2
ΔRING	4.328	5.496	AT2G37270	ATRPS5B, RPS5B ribosomal protein 5B
ΔRING	3.130	2.895	AT3G13230.1	RNA-binding KH domain-containing protein

ΔRING	1.725	1.152	AT3G25860.1	LTA2, PLE2 2-oxoacid dehydrogenases acyltransferase family protein
ΔRING	6.593	4.151	AT4G33865	Ribosomal protein S14p/S29e family protein
ΔRING	1.164	2.293	AT3G45980.1	H2B, HTB9 Histone superfamily protein
ΔRING	4.326	4.449	AT4G25630	FIB2, ATFIB2 fibrillarin 2
ΔRING	2.813	1.645	AT5G10060.1	ENTH/VHS family protein
ΔRING	2.095	0.951	AT5G59910.1	HTB4, Histone superfamily protein
			AT5G22880.1	HTB2, Histone B2
			AT3G46030.1	HTB11, Histone superfamily protein

Results of *t* test analysis (FDR=0.01, S0=0.1) based on LFQ values carried out using the Perseus software on a set of four independent SINT3 and ΔSINT3 TAP experiments

Supplemental Table 5. The RNA-seq counts for the core components of SL/KL pathways in *Arabidopsis* cell cultures and plant tissues

		FPKM RNA seq						
Locus	**Name**	**PSB-D**	**PSB-L**	**planta_all**	**root**	**seedling**	**shoot**	**rossette**
AT3G03990	D14	63.0	17.3	32.0	52.4	2.6	48.0	24.9
AT4G37470	KAI2	4.7	138.8	53.9	46.7	8.5	94.0	66.2
AT2G42620	MAX2	44.2	19.5	8.9	13.1	2.3	11.7	8.6
AT5G57710	SMAX1	10.0	8.1	34.1	12.9	14.2	65.5	43.8
AT4G30350	SMXL2	7.1	3.2	10.2	15.0	3.3	15.5	6.9
AT1G07200	SMXL6	8.5	2.0	10.0	22.1	1.8	12.4	3.7
AT2G29970	SMXL7	27.9	30.6	16.0	17.6	3.1	24.7	18.5
AT2G40130	SMXL8	2.2	5.1	8.4	7.5	0.4	21.0	4.8

Absent 0; > 0 very weak ≤ 0.8; > 0.8 weak ≤ 5; > 5 medium ≤ 20; > 20 good ≤ 80; > 80 high ≤ 400;> 400 very high; The FPKM values indicate Fragments Per Kilobase Million; unpublished data, Jelle Van Leene.

Supplemental dataset 1. All proteins identified in SMXL7 TAP experiments.

Supplemental dataset 2. All proteins identified in SINT1 TAP experiments.

Supplemental dataset 3. All proteins identified in SINT2 TAP experiments.

Supplemental dataset 4. All proteins identified in SINT3 TAP experiments.

Supplemental dataset 5. The list of proteins significantly different between SINT3 mock and *rac*-GR24 and between ΔRING-SINT3 and SINT3 TAP experiments.

Supplemental dataset 6. The list of all proteins copurified with SINT3 and ΔRING-SINT3 with their corresponding LFQ and intensity values before and after imputation of missing values.

All Supplemental datasets are available via

https://www.dropbox.com/sh/4856rigeg198y4y/AACNKCsIHLZ67lNR4gQLRivba?dl=0

Chapter 5

The role of PP6-type phosphatase complex in SMAX1- and SMXL7-mediated signaling

Sylwia Struk[1,2], Fabrizio Ticchiarelli[3], Annick De Keyser[1,2], François-Didier Boyer[4], Geert Persiau[1,2], Dominique Eeckhout[1,2], Geert De Jaeger[1,2] Ottoline Leyser[3] and Sofie Goormachtig[1,2]

[1]Department of Plant Biotechnology and Bioinformatics, Ghent University, 9052 Ghent, Belgium,
[2]VIB, Center for Plant Systems Biology, VIB, 9052 Ghent, Belgium,
[3]The Sainsbury Laboratory, University of Cambridge, Cambridge, United Kingdom,
[4]Institut National de la Recherche Agronomique, Institut Jean-Pierre Bourgin, Versailles, France

S.S. was the main author of the manuscript and performed all experiments, except FRET-FLIM that was carried out by F.T. and O.L., the molecular cloning partially performed by A.D.K., the acquisition of the TAP data prepared by G.P., D.E. and G.D.J.. F.D.B. kindly provided the synthetic strigolactone analog rac-GR24. S.G. supervised the project and contributed to the writing of the manuscript.

ABSTRACT

Strigolactones regulate multiple aspects of plant growth and development through ubiquitination and consequent degradation of the repressor proteins SUPPRESSOR OF MORE AXILLARY GROWTH 1 (SMAX1)-LIKE (SMXL) 6, SMXL7, and SMXL8. This process depends entirely on the action of the F-box protein MORE AXILLARY GROWTH2 (MAX2), which is part of the E3 ligase complex, and the strigolactone receptor DWARF 14 (D14). Reversible protein phosphorylation catalyzed by protein kinases and phosphatases is one of the major signaling mechanism in eukaryotic cells, described also to control plant hormonal pathways. Here, we report on the catalytic subunits of the serine/threonine-specific phosphoprotein phosphatase 6 (PP6), the phytochrome-associated serine/threonine protein phosphatase 1 (FyPP1), and its homolog FyPP3 as novel interacting partners of SMXL7. Our biochemical studies suggest that FyPP1/FyPP3 can also associate with SMAX1, a SMXL7 homolog that acts in the karrikin pathway. We further present physiological evidence for a possible involvement of FyPP1 and FyPP3 as well as of the regulatory subunits of the PP6-type holoenzyme, SAP domain-like protein 4 (SAL4) and ROOTS CURL IN NAPHTHYLPHTHALAMIC ACID1 (RCN1) in signaling mediated by SMXL7 and SMAX1.

INTRODUCTION

Strigolactones (SLs) and karrikins (KARs) are both butenolide compounds implicated in the regulation of plant growth and development, albeit provoking different responses (Morffy et al., 2016). SLs have been recognized as plant hormones controlling predominantly the shoot and root architecture (Gomez-Roldan et al., 2008; Umehara et al., 2008; Ruyter-Spira et al., 2011; Kapulnik & Koltai, 2014), whereas KARs, chemical signals found in smoke, promote seed germination and control seedling photomorphogenesis (Nelson et al., 2010, 2012). Remarkably, both SL and KAR pathways share similar signaling components with the central player the F-box protein MORE AXILLARY GROWTH2 (MAX2), which is part of a Skp-Cullin-F-box (SCF) complex involved in protein ubiquitination (Stirnberg et al., 2007; Nelson et al., 2011). In addition, the receptors are the closely related α/β-hydrolases DWARF14 (D14) and KARRIKIN INSENSITIVE2 (KAI2) for SLs and KARs, respectively. The downstream targets have been identified also to belong to the same protein family, designated as SUPPRESSOR OF MAX1 (SMAX1)-LIKE (SMXL) (Stanga et al., 2013; Soundappan et al., 2015; Wang et al., 2015). In response to the SL analog, *rac*-GR24, the SMXL6, SMXL7, and SMXL8 (SMXL6/7/8) proteins are ubiquitinated and degraded by the 26S proteasome, activating downstream responses (Soundappan et al., 2015; Wang et al., 2015; Liang et al., 2016). A similar mode of action has been proposed for SMAX1 and SMXL2 after activation of the KAR pathway (Stanga et al., 2013; Soundappan et al., 2015; Stanga et al., 2016), but has still not been proven. The commonly used in research *rac*-GR24 is an equimolar racemic mixture of a strigol-like $GR24^{5DS}$ and its unnatural enantiomer $GR24^{ent\text{-}5DS}$; therefore it can activate both SL and KAR signaling (Scaffidi et al., 2014).

In addition to ubiquitination, other posttranslational modifications, such as phosphorylation, play a role in many plant hormonal pathways (Tang et al., 2008; Wang et al., 2013b; Zhang et al., 2013). Phosphorylation by kinases and dephosphorylation by phosphatases might influence the activity, localization, function, stability, and even the interaction profile of important signaling proteins. Reversible phosphorylation of plant proteins is observed mostly on serines (Ser) and threonines (Thr), and sometimes on tyrosine (Tyr) residues (Uhrig et al., 2013; Walton et al., 2015). The proteins of the family of the Ser/Thr-specific phosphoprotein phosphatases (PPPs) are one the most highly conserved among eukaryotes being responsible for approximately 80% of the protein phosphatase activity in the cells (Lillo et al., 2014). The 26 different catalytic PPPs C subunits that have been shown to be present in *Arabidopsis thaliana* are divided into different classes, depending on their sequence, structure, and mode of action (Figure 1) (Farkas et al., 2007; Moorhead et al., 2009).

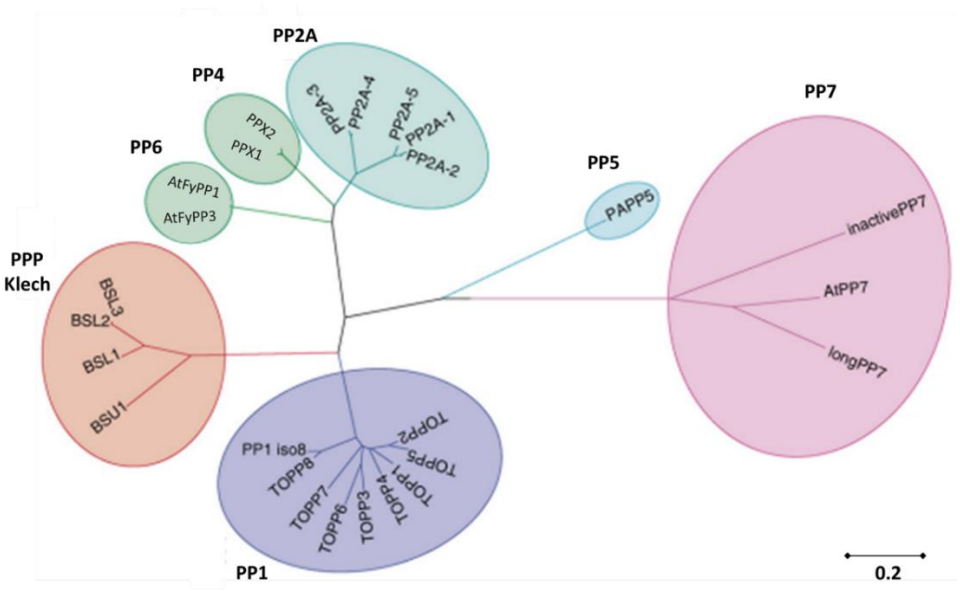

Figure 1. Family tree of *Arabidopsis thaliana* phosphoprotein phosphatase (PPP) catalytic C subunits. The bar represents 0.2 amino acid substitutions per site in the primary structure. Figure adapted from Farkas et al. (2007).

Previously, we have identified two members of the PP6 subfamily, phytochrome-associated serine (Ser)/threonine (Thr) protein phosphatase 1 (FyPP1) and its homolog FyPP3 as putative interactors of SMXL7 (Table 1; Chapter 4). Both FyPP1 and FyPP3 have high sequence similarity with the catalytic subunits of PP2A, therefore they are also referred as PP2A-like phosphatases. The catalytic C subunits PP2A and PP6 form trimeric and dimeric complexes with scaffolding A and regulatory B subunits that confer substrate specificity and regulate the phosphatase complex activity (Terol, 2002; Lillo et al., 2014). For instance, in *Arabidopsis*, there are five catalytic, three scaffolding, and 17 regulatory subunits of the PP2A subfamily, giving 255 possible combinations for the formation of heterotrimeric holoenzymes (Figure 2) (Lillo et al., 2014).

The PP6 in *Saccharomyces cerevisiae* (yeast), Suppressor of Initiation of Transcription 4 (SIT4), is known to form a dimer with regulatory SIT4-associated proteins (SAPs) (Stefansson and Brautigan, 2006). In *Arabidopsis*, a family of four SAP domain-like proteins (SAL1 to SAL4) has been identified as homologs of the B-type regulatory subunits of the *S. cerevisiae* PP6 (Luke et al., 1996; Stefansson and Brautigan, 2006; Morales-Johansson et al., 2009). The SAL1-SAL4 proteins share 45% to 72% sequence similarity and SAL1 has been shown to directly interact with FyPP1 (Dai et al., 2012). Interestingly, in the tandem affinity purification (TAP) experiments of SMXL7, we retrieved SAL4 (Chapter 4) as a putative prey, further supporting the hypothesis that the PP6 phosphatase complex associates with SMXL7.

Furthermore, in contrast to yeast, in which the PP6 complex consists of dimers, the PP6 of *Arabidopsis* might be composed of three subunits. Indeed, proteins characterized as the A-type scaffolding subunits

of the PP2A phosphatase (PP2AA), ROOTS CURL IN NAPHTHYLPHTHALAMIC ACID1 (RCN1) and PP2AA3, were also shown to form a PP6-type heterotrimeric holoenzyme *in vivo* together with FyPP1 and FyPP3 (FyPP1/3) and SAL1 (Dai et al., 2012). This PP6-type holoenzyme was found to interact directly with the auxin efflux carriers PIN-FORMED (PIN) to regulate their phosphorylation status, thus, influencing the auxin transport polarity in roots (Dai et al., 2012). Moreover, another role described for the FyPP1/3 phosphatase has been the control of the expansion pattern of leaf epidermal cells by influencing the PIN1 localization (Li et al., 2011b). Despite its role in the auxin signaling, this holoenzyme also negatively regulates the abscisic acid (ABA) pathway by direct interaction with and dephosphorylation of the transcription factor ABSCISIC ACID INSENSITIVE 5 (ABI5), leading to its degradation as a consequence promotion of seed germination and seedling development (Dai et al., 2013). Besides their involvement in plant hormone signaling, FyPP1 and FyPP3 might also regulate the flowering time in *Arabidopsis* by mediating the dephosphorylation of the phytochromes A and B (PhyA and PhyB) (Kim et al., 2002).

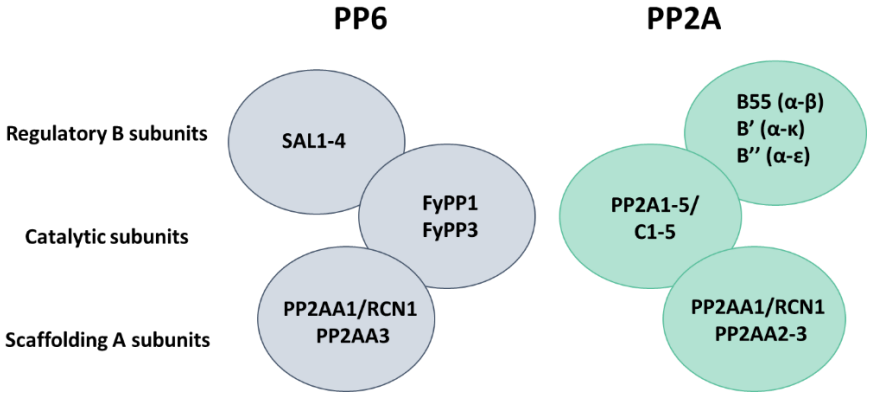

Figure 2. PP6 and PP2A regulatory B, catalytic C, and scaffolding A subunits in *Arabidopsis.*

The FyPP1, FyPP3, and SAL4 proteins were identified as putative interactors of SMXL7 by means of TAP (Chapter 4). Here, a possible link between the PP6-type holoenzyme and both SMXL7- and SMAX1-mediated signaling has was investigated. We provide biochemical evidence that FyPP1/3 might interact with SMXL7 and SMAX1 and further show that the mutations disrupting the function of the members of the PP6-type complex in *Arabidopsis* might affect both SMXL7- and SMAX1-related phenotypes.

RESULTS

Resolving interactions between SMXL proteins and PP6 complex components

FyPP1 and FyPP3 (FyPP1/3; AT1G50370/AT3G19980) were detected as putative interactors of SMXL7 in three out of four TAP experiments done in *Arabidopsis* cell cultures expressing *35S::GSrhino-SMXL7* (Table 1; Chapter 4) using qualitative analysis based on the subtraction of known background proteins (Van Leene et al., 2015). As the sequence of FyPP1 and FyPP3 differ on only three amino acid residues (Glu70Asp, His100Tyr, and Asn105Lys) (Dai et al., 2012), it was impossible to distinguish which of the two had been detected in the TAP-mass spectrometry (MS). Besides FyPP1/3, the SMXL7 TAP experiments also revealed SAL4 (AT3G45190) as a possible prey, which had been previously described as a regulatory B subunit of the PP6-type complex (Table 1) (Dai et al., 2012).

Table 1. Overview of the SMXL7 prey proteins purified by TAP

AGI	Protein	*GSrhino-SMXL7*
AT2G29970	SMXL7, SMAX1-LIKE 7	4
AT1G15750	TPL, TOPLESS	4
AT1G50370	**FyPP1/3, PHYTOCHROME-ASSOCIATED PROTEIN**	
AT3G19980	**PHOSPHATASE 1/3**	**3**
AT3G16830	TPR2,TOPLESS-related 2	3
AT5G27030	TPR3,TOPLESS-related 3	2
AT3G15880	TPR4, TOPLESS-related 4	2
AT2G28450	SINT1, SMXL7 INTERACTING PROTEIN 1	2
AT2G35900	SINT2, SMXL7 INTERACTING PROTEIN 2	1
AT3G45630	SINT3, SMXL7 INTERACTING PROTEIN 3	1
AT3G45190	**SAL4, SIT4 phosphatase-associated family protein**	**1**
AT2G05120	NUP133, Nucleoporin	1
AT1G80490	TPR1, TOPLESS-related 1	1

TAP experiments were done with *35S::GSrhino-SMXL7* as bait. Prey proteins were identified by means of peptide-based homology analysis of MS data. Background proteins were withdrawn based on the occurrence frequency of the copurified proteins in a large GS TAP data set (Van Leene et al., 2015). The number indicates the times the prey was identified in four experiments. AGI, Arabidopsis Genome Identifier.

Next, we investigated whether other subunits of the PP6 and PP2A complexes were present in the list of copurified proteins. To this end, the SMXL7 and ΔSMXL7 TAP data were searched with the MaxQuant software (Chapter 3). Not only FyPP1/3 and SAL4 could be identified among all copurified proteins, but also the scaffolding subunits RCN1 (AT1G25490) and PP2AA2 (AT3G25800) as well as the catalytic

subunits PP2A2 and PP2A3 (AT2G42500 and AT3G58500; Table 2). Although RCN1, PP2AA2 and PP2A2 are present on the list of TAP background proteins (Van Leene et al., 2015), we selected RCN1 for further study, because it had been previously reported to act as a scaffolding sub unit of the PP6-type holoenzyme (Dai et al., 2012).

Table 2. Identification of PPP subunits in SMXL7 and ΔSMXL7 TAP experiments

AGI	Protein	SMXL7 Mock				SMXL7 *rac*-GR24				ΔSMXL7 Mock				ΔSMXL7 *rac*-GR24			
		1	2	3	4	1	2	3	4	1	2	3	4	1	2	3	4
AT1G50370 AT3G19980	FyPP1 FyPP3	18.4	19.8	17.9	18.0	14.5	19.5	15.2	15.4	16.8	17.4	17.1	17.3	15.7	15.0	18.5	18.5
AT3G45190	SAL4	18.4	18.0	16.4	16.5	13.5	17.9	0.0	14.1	0.0	16.4	18.9	18.1	0.0	0.0	19.6	18.7
AT2G42500 AT3G58500	PP2A-3 PP2A-4	19.0	18.5	16.1	16.6	0.0	18.3	0.0	0.0	0.0	0.0	0.0	0.0	0.0	0.0	0.0	0.0
AT1G25490	RCN1	15.7	13.4	13.6	13.4	0.0	0.0	0.0	12.5	0.0	0.0	18.4	17.3	16.7	0.0	0.0	16.7
AT3G25800	PP2AA2	16.5	16.8	14.4	15.0	0.0	15.8	0.0	0.0	0.0	0.0	18.4	17.3	16.7	0.0	0.0	17.7

PPP subunits with their log2 intensity values detected in SMXL7 and ΔSMXL7 TAP experiments under mock and *rac*-GR24 treated conditions in four repeats using the MaxQuant software. No background proteins were subtracted.

Despite the convincing identification of FyPP1/3 as a putative prey of SMXL7 by means of TAP, the interaction between these proteins could not be validated in the first yeast two-hybrid (Y2H) screen with the full-length FyPP1 (Figure 3A). To exclude that the lack of interaction was due to technical problems, such as protein misfolding in yeast, we cloned the N-terminal part (FyPP-NT), consisting of the first 49 amino acids preceding the catalytic domain, which is identical for both FyPP1 and FyPP3, to repeat the Y2H analysis. FyPP-NT had been considered previously to be responsible for the interaction with SAL1, RCN1 (Dai et al., 2012), and ABI5 (Dai et al., 2013). Indeed, by using the Y2H LexA system, we could now detect the interaction between FyPP-NT fused to the GAL4-binding domain (BD) and SMXL7 connected to the GAL4 activation domain (AD) (Figure 3A). Then, we tested whether FyPP-NT is a specific interactor of SMXL7 or, in general, also associates with other components of the SL and KAR pathways. Interestingly, yeast cotransformed with FyPP-NT-AD and SMAX1-BD or D14-BD stained blue when spotted on inducible X-Gal-containing medium (Figure 3A,B), hinting at a possible interaction between these proteins, but not with MAX2 (Figure 3B). Moreover, no interaction was detected between SMXL7 or SMAX1 and SAL4 or RCN1 (Figure 3A). Eventually, a Y2H between the PP6 complex members confirmed the previously described interaction between FyPP-NT and RCN1 (Figure 3C). Lastly, the interaction between FyPP-NT and SAL4 or KAI2 could not be resolved by Y2H, because all three proteins show autoactivation when fused to BD (Figure 3B,C).

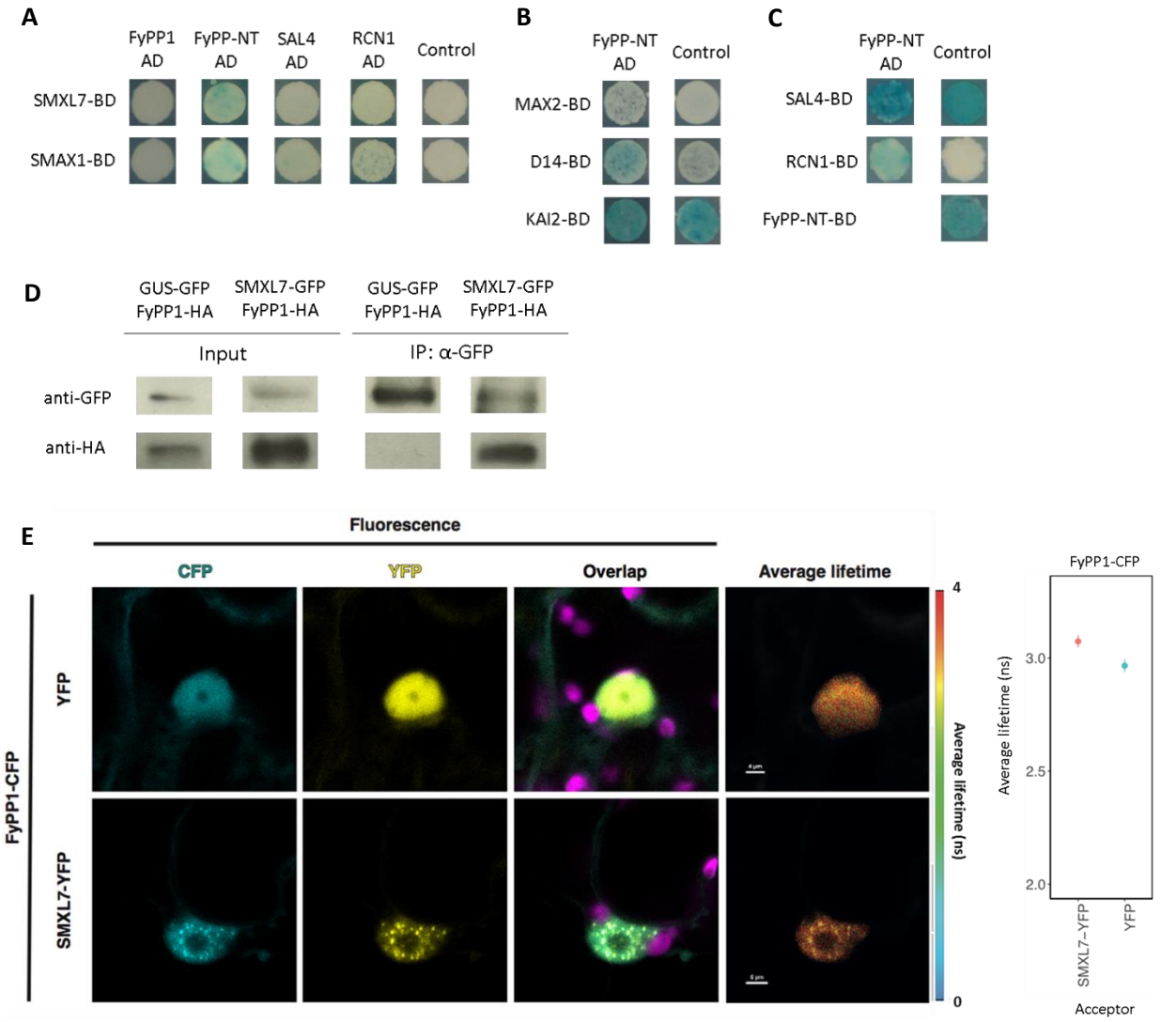

Figure 3. Validation of FyPP1 and SAL4 interactions. Y2H screen for the interaction between (A) FyPP1, FyPP-NT, SAL4, RCN1 with SMXL7/SMAX1, (B) FyPP-NT with MAX2, D14, and KAI2, (C) FyPP-NT with SAL4 and RCN1. (A-C) The EGY48 (p8opLacZ) yeast strain was cotransformed with the bait fused with GAL4-BD and prey fused with GAL4-AD or pB42AD for a negative control. Transformed yeasts were selected on SD Raf/GAL-Ura-Trp-His+X-Gal medium. (D) *In vivo* interaction between SMXL7-GFP and FyPP1-3HA revealed by co-IP assay. Protein extracts were prepared from *N. benthamiana* leaves transiently expressing *35S::SMXL7-GFP* or *35S:GUS-GFP* (control) and *35S::FyPP1-3HA*. Input means total protein lysate without immunoprecipitation. (E) Analysis of SMXL7-FyPP1 interaction by FRET-FLIM. *N. benthamiana* leaf epidermal cells were cotransformed with *35S::SMXL7-YFP* or *35S::YFP-NS* (control) and *35S::FyPP1-CFP*. Representative images in each row show the localization of single fusion proteins in the first and second panel, colocalization of the donor and acceptor in the third panel, and average CFP donor lifetime (indicating FRET) in the last panel. Color scheme for FLIM analysis indicates the CFP donor fluorescence lifetimes between 4 and 0 ns. The graphs represent the quantification of average CFP donor lifetime between 2 and 3.5ns. For each protein pair, data were acquired from 6-10 cells.

Next, we investigated the SMXL7-FyPP1 complex *in vivo* by means of coimmunoprecipitation (Co-IP) of SMXL7-green fluorescent protein (GFP) and (full-length) FyPP1-3HA transiently expressed in *Nicotiana benthamiana* leaves. As a result, FyPP1-3HA coprecipitated with SMXL7-GFP, whereas no association was discovered with the GUS-GFP fusion protein used as a negative control (Figure 3D), indicative that SMXL7 and FyPP1 belong to the same complex.

Finally, to further assess this interaction *in viv*o, we used Förster resonance energy transfer (FRET) with fluorescence lifetime imaging microscopy (FLIM). No FRET was observed between FyPP1 (full length) and SMXL7 (Figure 3E), when transiently coexpressed in *N. benthamiana* leaves. The 405nm laser was used to excite the cyan fluorescent protein (CFP)-fused donor in the presence of yellow fluorescent protein (YFP)-fused acceptor or nuclear localized YFP alone as a control. The mean CFP lifetimes were calculated and the decreased value in the presence of the acceptor indicates the occurrence of FRET. The average lifetime of the FyPP1-cyan fluorescent protein (CFP) donor measured in the nucleus was not reduced when cotransfected with the SMXL7-yellow fluorescent protein (YFP) acceptor, in comparison to a nuclear YFP without SMXL7 (*35S::YFP-NS*) (Figure 3E). Interestingly, although no FRET was detected, FyPP1-CFP and SMXL7-YFP localized into nuclear speckles (Figure 3E), which had been previously reported for the protein pairs SMXL7-D14 and SMXL7-TOPLESS-related protein 2 (TPR2) through FRET-FLIM and a transient bimolecular fluorescence complementation (BiFC) assay (Liang et al., 2016; Soundappan et al., 2015).

In summary, our results indicate an association between SMXL7 and FyPP1/3. The contradictory outcomes between Y2H and FRET-FLIM does not allow us to conclude whether the interaction is direct. Additionally, Y2H suggested that FyPP1/3 might also associate with SMAX1 and with the SL receptor D14.

Given the interaction between FyPP1 and SMXL7 or SMAX1, SMAX1 and SMXL7 could possibly be dephosphorylated by the PP6-type phosphatase complex. To test this hypothesis, we first verified whether SMXL7 and SMAX1 could be phosphorylated by searching the SMXL7 and SMAX1 TAP data set (Chapter 3 and 6) with the MaxQuant software for phosphorylated peptides. Four phosphopeptides of SMXL7 were discovered with the highest localization probability for the serine (S) residues S527, S577, S600/604, and S980/983 and two phosphopeptides of SMAX1 with serine residues 47 (S47) and 437 (S437) (Table 3). Thus, both SMAX1 and SMXL7 are phosphorylated, at least in *Arabidopsis* cell cultures. In addition, we searched the PhosPhat data base for already described phosphorylation sites for both proteins. As a result, two serine residues, S114 and S527 of SMXL7 we found as possibly phosphorylated, with the last one also revealed in our analysis (Table 3) and two of SMAX1, S862 and S670. Moreover, the phosphorylation site on S573 seems to be conserved between SMXL7 and D53 in rice.

Table 3. Putative phosphorylation sites identified in SMAX1 and SMXL7 sequences

Protein	AGI	Positions within proteins	Localization probability	Score for localization	Amino acid	Modified sequence
AT5G57710	SMAX1	436	0.633433	121.24	S	_ELAEIDSVS(ph)SPEVK_
		437	0.978891	97.214	S	_ELAEIDSVSS(ph)PEVK_
		47	0.998937	54.15	S	_NHGQTTPLHVAATLLAS(ph)PAGFLR_
AT2G29970	SMXL7	571	0.279011	70.145	S	_HTEDLS(ph)SSTTNSPLSFVTTDLGLGTIYASK_
		572	0.284941	67.728	S	_HTEDLSS(ph)STTNSPLSFVTTDLGLGTIYASK_
		573	0.262108	82.086	S	_HTEDLSSS(ph)TTNSPLSFVTTDLGLGTIYASK_
		577	0.867074	66.432	S	_HTEDLSSSTTNS(ph)PLSFVTTDLGLGTIYASK_
		580	0.769771	54.934	S	_HTEDLSSSTTNSPLS(ph)FVTTDLGLGTIYASK_
		980	0.497288	76.015	S	_LVAS(ph)RESPAEEETTGIQQFPAR_
		983	0.497288	76.015	S	_LVAS(ph)RESPAEEETTGIQQFPAR_
		527	0.985277	86.882	S	_MSLGS(ph)PTEK_
		600	0.612644	83.37	S	_NQEPS(ph)TPVSVER_
		604	0.579601	73.435	S	_NQEPSTPVS(ph)VER_

MS TAP data for SMAX1 and SMXL7 were analyzed with the MaxQuant software with a phosphorylation set as a variable modification.

The role of FyPP1/3 in SL and KAR pathways

To investigate the role of FyPP1 and FyPP3 in SMXL7- and SMAX1-mediated signaling, we isolated the T-DNA insertion mutants of *FyPP1* (*fypp1-1*) and *FyPP3* (*fypp3-1*) that had been described previously (Dai et al., 2012, 2013). The single mutants in both genes did not show significant phenotypic differences when compared to wild-type (WT) plants, probably due to functional redundancy between *FyPP1* and *FyPP3* (Dai et al., 2012). Therefore, we tried to generate *fypp1-1 fypp3-1* double mutants, which turned out to be lethal under our conditions. As the *fypp3-1* mutant retains a truncated form of *FyPP3* (Figure 4A), we isolated a second allele, *fypp3-2,* in the Columbia-0 (Col-0) accession carrying the T-DNA insertion in the seventh exon (Figure 4A). After confirmation by reverse transcription-polymerase chain reaction (RT-PCR) that the *FyPP3* transcript levels were reduced (Figure 4B), the *fypp1-1 fypp3-2* double mutant was generated. As the *fypp1-1 fypp3-2* homozygous plants were completely infertile, consistent with the previous observation for the *fypp1-1 fypp3-1* (Dai et al., 2012), we used the *fypp1-1 fypp3-2-/+* plants (*fypp1-1* is homozygous and *fypp3-2* is hemizygous) for the experiments. Finally, we also constructed *Arabidopsis* lines that stably expressed GFP-tagged FyPP1 under the control of the cauliflower mosaic virus (CaMV) 35S promoter. Two independent lines with moderate and low overexpression based on immunodetection of the FyPP1 protein levels were selected for further assays (Figure 4C).

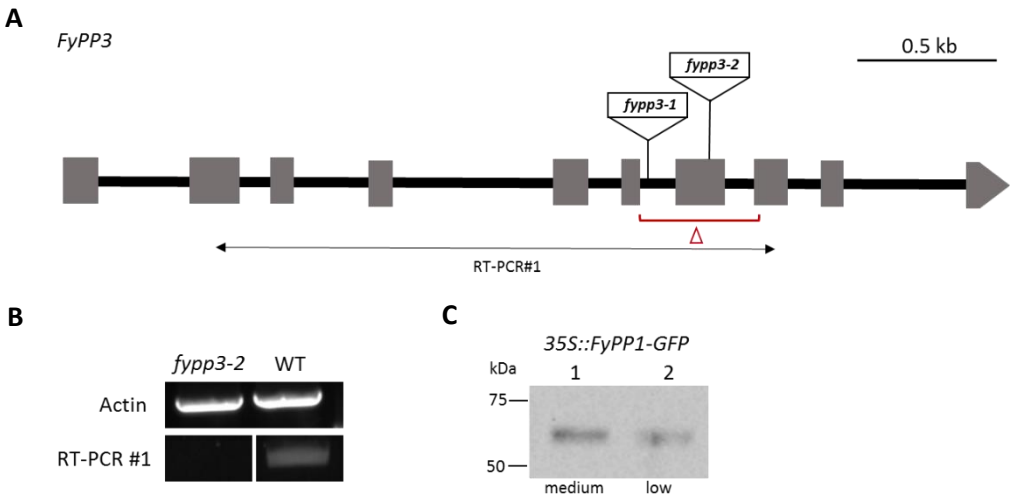

Figure 4. **Characterization of *FyPP3* T-DNA insertion and *FyPP1* overexpression lines.** (A) Schematic visualization of the *FyPP3* gene structure, T-DNA insertions in the corresponding mutants, and the primers used for RT-PCR. Grey boxes represent exons. The red bracket indicates the deletion (Δ) in the *fypp3-1* mutant due to the T-DNA insertion. (B) Transcript level of *FyPP3* in Col-0 and in the *fypp3-2* mutant. *ACTIN2* (*ACT2*; AT3G18780) primers were used as a standard. All primer sequences can be found in Supplemental Table 1. (C) FyPP1 protein expression level. FyPP1-GFP (62 kDa) was stably expressed in *Arabidopsis* seedlings under the control of the pCaMV35S promoter. Two independent lines were selected and the protein level was detected on immunoblots with anti-GFP antibody.

To study the involvement of FyPP1/3 in the SMXL7 pathway, we first investigated the lateral root density (LRD) phenotype. The SMXL6/7/8 subclade acts downstream of MAX2 to promote lateral root growth (Soundappan et al., 2015). Consistently, the *max2* mutant has an increased LRD, which is strongly suppressed in the *smxl678max2* quadruple mutant, while *smxl678* is characterized by decreased LRD (Kapulnik et al., 2011; Soundappan et al., 2015). In WT plants, addition of *rac*-GR24 reduces both the total number of emerged lateral roots and LRD in a MAX2-dependent manner (Ruyter-Spira et al., 2011). To examine whether *FyPP1/3* plays a role in SL signaling in the root, we tested the *fypp1-1 fypp3-2*-/+ population, consisting of *fypp1-1* homozygous plants and a mixture of homozygous (1/4) and hemizygous (2/4) *fypp3-2* and WT (1/4) plants, and the *35S::FyPP1-GFP2* overexpression line for the *rac*-GR24-induced lateral root response. To this end, the *fypp1-1 fypp3-2*-/+, *35S::FyPP1-GFP2*, and Col-0 plants were grown for 9 days in either mock (0.01% acetone) or treated conditions (1 µM *rac*-GR24). The number of emerged lateral roots was scored, the main root length was measured, and eventually the LRD was calculated. The *35S::FyPP1-GFP2* overexpression line had a significantly longer primary root length than that of Col-0 plants (Figure 5A; *P* value <0.001), consistent with published data (Dai et al., 2012) and confirming the functionality of the line. In agreement, a significantly shorter main root was measured for the *fypp1-1 fypp3-2*-/+ seedlings (Figure 5A; *P* value <0.001). Under mock

conditions, the LRD was significantly lower (*P* value <0.001) for the *fypp1-1 fypp3-2-*/+ seedlings than that for WT plants, whereas no difference was detected for the GFP-tagged *FyPP1* overexpression line. Analysis of the *rac*-GR24 treatment revealed that the response of *fypp1-1 fypp3-2-*/+ seedlings did not significantly differ from that of Col-0 (52%) while the sensitivity of plants expressing *35S::FyPP1-GFP2* was slightly lower than that of WT (Figure 5B, 47% and 57% LRD reduction, respectively; *P* value <0.05). In conclusion, *FyPP1/3* might be implicated in the SL-regulated LR development, as *fypp1-1 fypp3-2-*/+ plants had significantly lower LRD in mock, consistent with *smxl678* phenotype. In addition, less responsiveness towards *rac*-GR24 was observed in the *35S::FyPP1-GFP2* overexpression line. The effect could be masked in the *fypp1-1 fypp3-2-*/+ mutant, because it consists of a population of homozygous *fypp3-2*, hemizygous *fypp3-2*, and WT plants.

Besides its impact on the LRD, the *rac*-GR24 treatment decreases the hypocotyl elongation of seedlings grown under continuous red light (Nelson et al., 2011). In agreement, under mock conditions, the hypocotyl of *max2* mutants is longer than that of WT plants (Stirnberg et al., 2002; Shen et al., 2007). Another member of the SMXL family, SMAX1, was found to act downstream of MAX2 to regulate the hypocotyl elongation. Accordingly, *smax1* loss-of-function seedlings displayed a hypersensitive growth responses to light (Stanga et al., 2013). Considering a possible interaction between FyPP1/3 and SMAX1, we assessed whether PP6 might be involved in this SMAX1-related phenotype. To this end, *fypp1-1 fypp3-2-/+* mutants and both *35S::FyPP1-GFP* lines were grown in the presence and absence of 1 µM *rac*-GR24 under continuous red light, along with Col-0 plants and the *max2-1* mutant (Figure 5C, D). Under mock conditions, the hypocotyl was significantly longer in *max2-1* and *fypp1-1 fypp3-2-/+* mutants than that of WT (*P* value <0.001; Figure 5C). In agreement, both *35S::FyPP1-GFP* overexpression lines had a decreased hypocotyl length (*P* value <0.001; Figure 5D) when compared with Col-0 plants. However, all tested lines displayed a significant decrease in hypocotyl elongation in response to *rac*-GR24, except the *max2-1* seedlings, which, as expected, were insensitive to the treatment. Only one of the *35S::FyPP1-GFP* overexpression lines was slightly less responsive to *rac*-GR24, because the reduction in hypocotyl length was lower than that of WT plants (42% and 49% respectively; *P* value <0.05). Thus, we can conclude that *FyPP1/3* seems to be implicated in the regulation of the hypocotyl elongation under mock conditions, while the response to *rac*-GR24 is likely not affected.

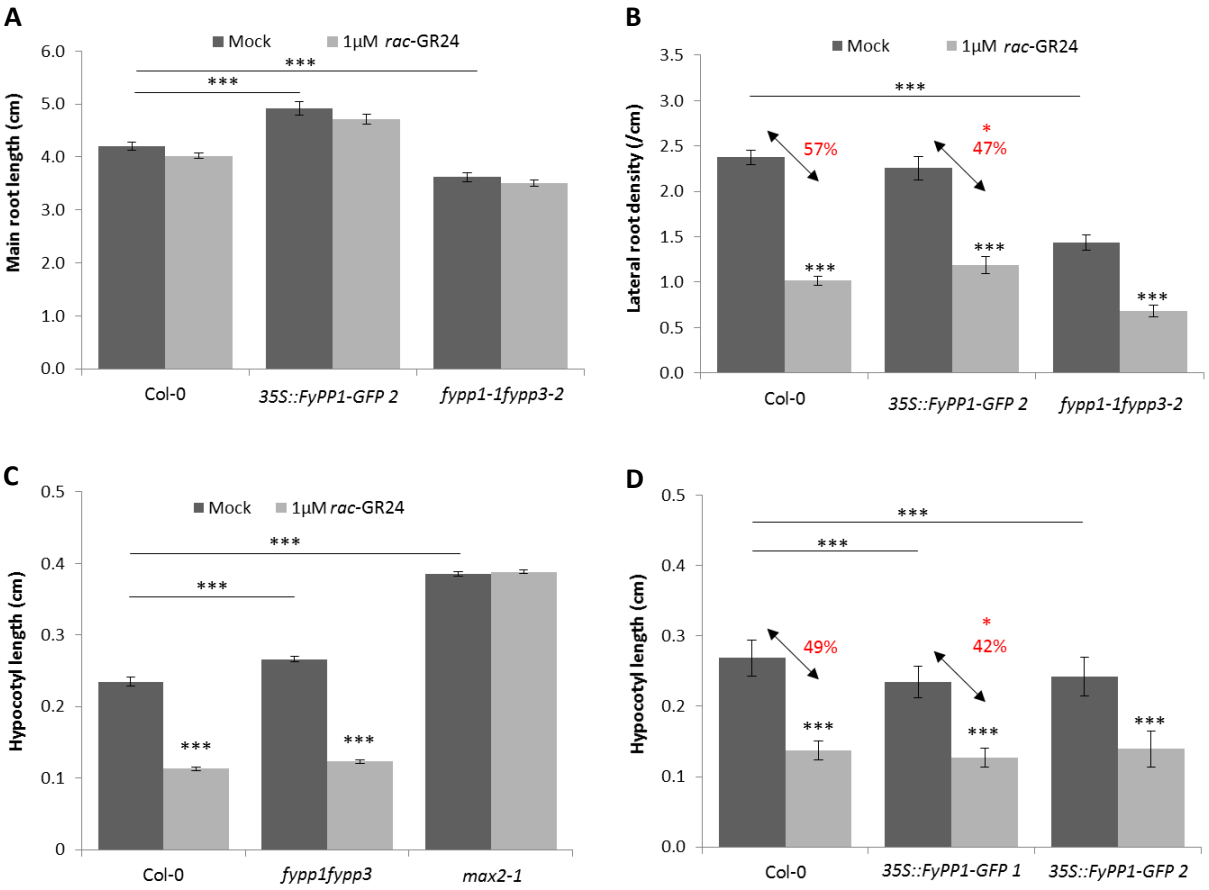

Figure 5. Lateral root density and hypocotyl assay for *FyPP1/3* mutant and overexpression lines. Main root length (A) and LRD (B) were analyzed in 9-day-old Col-0, *fypp1-1 fypp3-2-/+*, and *35S::FyPP1-GFP2* plants treated without (mock) or with 1 µM *rac*-GR24 (n>25). (C, D) Seeds of Col-0, *fypp1-1 fypp3-2-/+*, *35S::FyPP1-GFP1,* and *35S::FyPP1-GFP2* were sown on half-strength Murashige and Skoog (½MS) medium without sucrose, supplemented with 1 µM *rac*-GR24 or 0.01% acetone. After stratification, plates were exposed to white light for 3 h, followed by incubation in the dark for an additional 21 h, and ultimately to red light for 4 days (n=30). All the graphs represent means of three biological repeats ± SE. Asterisks indicate statistically significant differences between treatments, asterisks above the line- between genotypes and asterisks in red- in percentage reduction [*** *P* <0.001, * *P* <0.05; ANOVA-mixed model (A); Poisson regression model (B), and linear mixed model (C, D)].

Phenotypic characterization of a *sal4* mutant

The SAL4 protein is one of the B-type regulatory subunits of the PP6-type holoenzyme and it is expected to act in the same pathway as FyPP1/3 (Dai et al., 2012). To test whether *SAL4* plays a similar role in SL and KAR signaling, we first acquired two mutants carrying the T-DNA insertion in the first exon (*sal4-1*) and in the ninth exon (*sal4-2*, Figure 6A). The RT-PCR analysis verified the absence of transcripts in both *sal4* mutants when compared to the WT (Figure 6B).

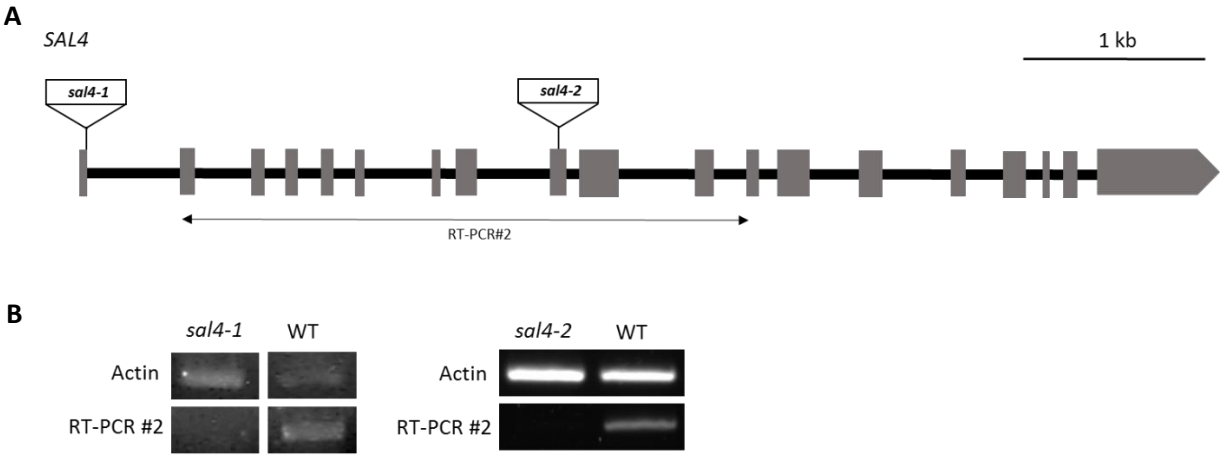

Figure 6. **Characterization of *sal4* T-DNA insertion mutants.** (A) Schematic visualization of *the SAL4* gene structure, T-DNA insertions, and the primer used for RT-PCR. Grey boxes represent exons. (B) Transcript level of *SAL4* in Col-0, *sal4-1,* and *sal4-2* mutants. *ACTIN2* (*ACT2*; AT3G18780) primers were used as a standard.

First, we examined the LRD phenotype in the same manner as described for the *FyPP1/3* mutant and overexpression lines. Under mock conditions, *sal4-1* seedlings were characterized by a significantly lower LRD (*P* value <0.001) than that of WT plants (Figure 7A). After treatment with *rac*-GR24, the decrease in LRD was significantly bigger for the *sal4-1* mutant (*P* value <0.01) than that in Col-0 (49% and 32%, respectively), indicating a higher sensitivity toward *rac*-GR24 in the root (Figure 7A).

In addition to the role in lateral root development in *Arabidopsis*, the SMXL6/7/8 proteins are also involved in the control of shoot branching (Soundappan et al., 2015; Wang et al., 2015). To further investigate the role of *SAL4* in this SL-related phenotype, we examined the number of rosette branches in the *sal4-1* mutant in comparison to Col-0 and *max2-1* plants. The average number of rosette branches in *sal4-1* plants was lower than that of Col-0 (*P* value <0.001), indicating that the SL signaling might be disturbed (Figure 7B). Consistent with previous data, the *max2-1* mutants had a significantly higher number of rosette branches than WT plants (Figure 7B) (Stirnberg et al., 2007).

Eventually, hypocotyl elongation was assessed in *sal4-1* and *sal4-2* plants grown under continuous red light to determine whether *SAL4* might be involved also in SMAX1-related phenotypes. As shown in Figure 7C, under mock conditions *max2-1* seedlings displayed significantly longer hypocotyls (*P* value <0.001) than Col-0. Only one of the *sal4* mutants displayed slightly increased hypocotyl (*P* value <0.01) in mock while the responses to *rac*-GR24 did not differ significantly between *sal4* mutants and Col-0 plants. To conclude, *SAL4* might be involved in SMXL7-related phenotypes, such as lateral root development and shoot branching, but its role in hypocotyl elongation is still unclear.

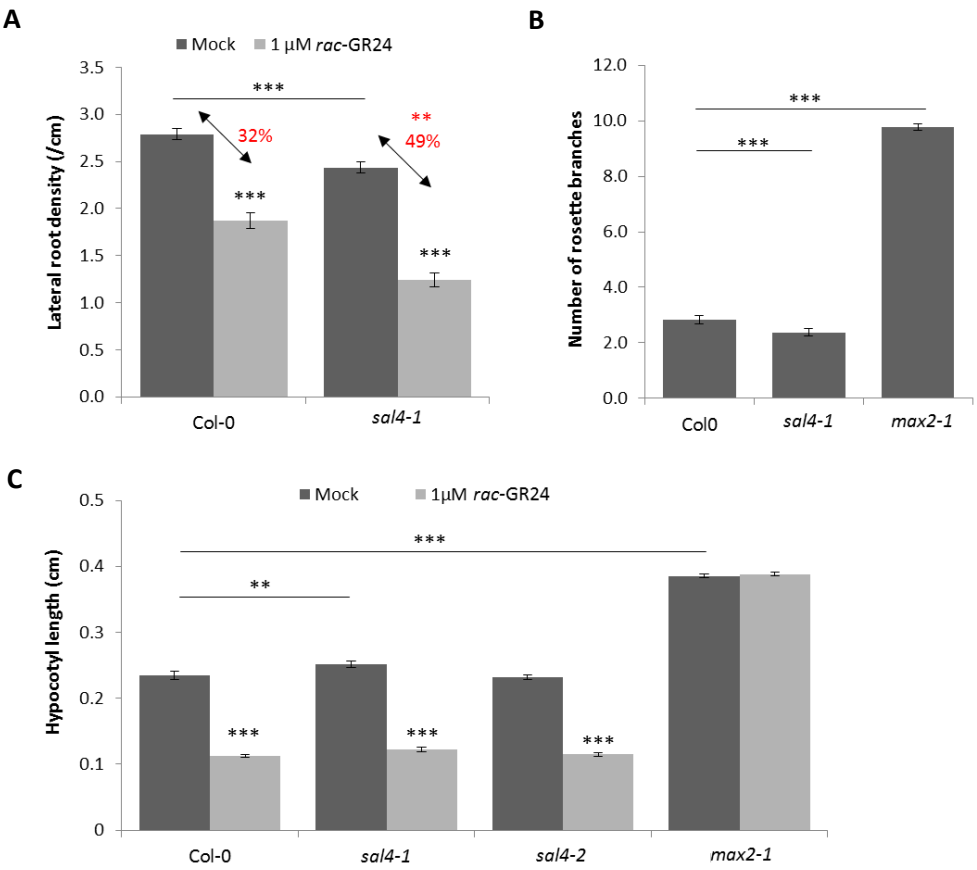

Figure 7. Characterization of *sal4* mutants. (A) LRD assay for Col-0 and the *sal4-1* mutant. LRD was analyzed in 9-day-old Col-0 and *sal4-1* plants treated without (mock) or with 1 µM *rac*-GR24 (n > 25). (B) Rosette branches of Col-0, *sal4-1,* and *max2-1* counted after 50 days of growth (n = 15). (C) Hypocotyl length of 4-day-old Col-0, *sal4-1, sal4-2,* and *max2-1* seedlings grown under continuous red light at 21°C (n = 25). Graphs represent means of three biological repeats ± SE. Asterisks indicate statistically significant differences between treatments, asterisks above the line- between genotypes and asterisks in red- in percentage reduction [*** *P* <0.001, ** *P* <0.01; Poisson regression model (A), Student's *t* test (B), linear mixed model (C)].

Phenotypic characterization of the *rcn1* mutant.

PP2AA1 or RCN1 is a known scaffolding subunit of PP2A phosphatases (Terol, 2002; Lillo et al., 2014), but it has been reported also to form a complex with FyPP1/3 (Dai et al., 2012). In the SMXL7 TAP analysis (Table 1), we did not identify RCN1 as a potential interactor of SMXL7. Nevertheless, while analyzing SMXL7 and ΔSMXL7 TAPs with the MaxQuant software, we could detect it several times among all copurified proteins (Table 2). To study its possible role in SMXL7- and SMAX1-related signaling, we first acquired a T-DNA insertion line that had been used previously in other studies (Blakeslee et al., 2007; Dai et al., 2012). Next, we analyzed the LRD, shoot branching, and hypocotyl elongation of this *rcn1* mutant, as done for the *SAL4* and *FyPP1/3* lines. The *rcn1* mutant was

characterized by an increased LRD under mock conditions (Figure 8A), consistent with the phenotype reported for *max2-1* plants (Kapulnik et al., 2011; Ruyter-Spira et al., 2011). When treated with *rac*-GR24, the LRD reduction was significantly lower than that for Col-0 seedlings (Figure 8A), indicating a lower sensitivity toward the treatment. Under both conditions, the response of the *rcn1* mutant was contrary to our previous observations for *fypp1 fypp3* and *sal4* plants. Furthermore, the number of rosette branches did not differ between the *rcn1* mutant and the WT (Figure 8B), indicating no involvement in the regulation of this phenotype. In contrast, a phenotype similar to that of *fypp1 fypp3* and *sal4-1* mutants, namely a slightly longer hypocotyl than that of Col-0 under mock conditions, was measured for *rcn1* seedlings grown under continuous red light (*P* value <0.01), but the response to the *rac*-GR24 treatment in this assay did not differ from that of the WT.

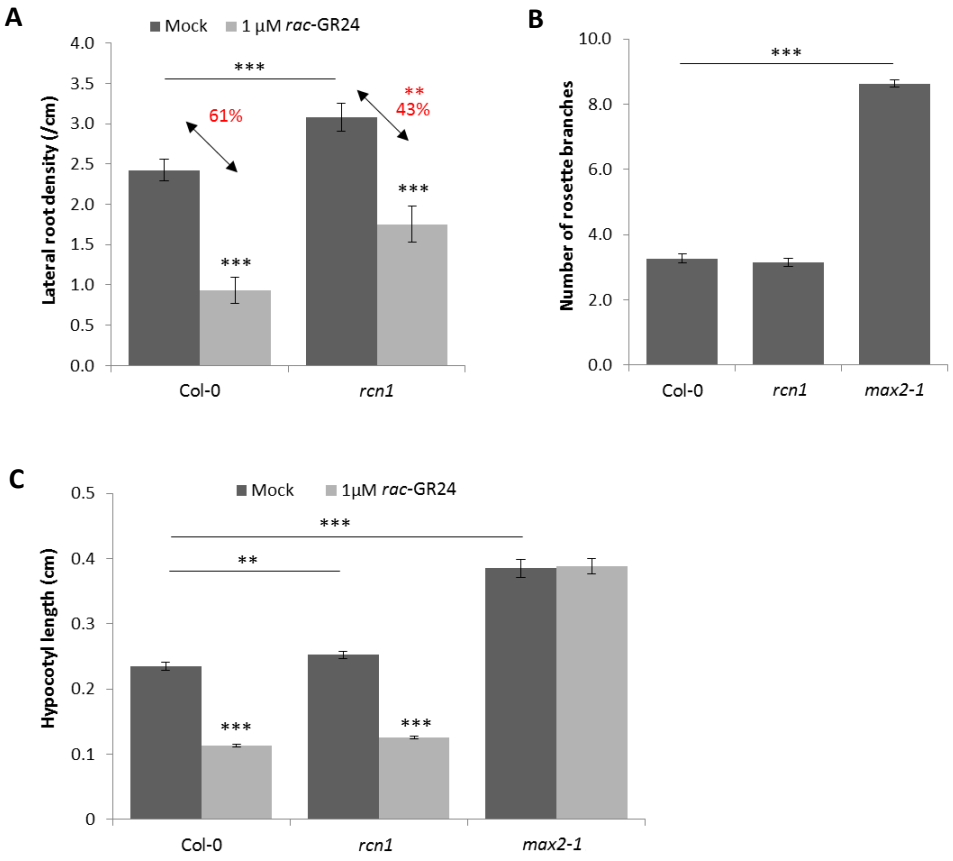

Figure 8. Characterization of the *rcn1* mutant. (A) LRD for Col-0 and *rcn1* mutant analyzed in 9-day-old plants treated without (mock) or with 1 µM *rac*-GR24 (n > 25). (B) Rosette branches of Col-0, *rcn1,* and *max2-1* counted after 50 days of growth (n = 15). (C) Hypocotyl lengths of 4-day-old Col-0, *rcn1,* and *max2-1* seedlings grown under continuous red light at 21°C (n = 25). Graphs represent means of three biological repeats ± SE. Asterisks indicate statistically significant differences between treatments, asterisks above the line- between genotypes and asterisks in red- in percentage reduction [*** *P* <0.001, ** *P* <0.01; Poisson regression model (A), Student's *t* test (B), linear mixed model (C)]

DISCUSSION

The process of protein phosphorylation by kinases and dephosphorylation by phosphates is one of the key mechanisms that regulates signal transduction in eukaryotic cells (Terol, 2002). Previously, the FyPP1/3 proteins have been found to control the light signaling and the auxin and ABA hormonal pathways (Dai et al., 2012, 2013; Zhu et al., 2017). Here, we present evidence that this PP6-type phosphatase might be implicated also in the regulation of the SL and/or KAR signaling.

TAP analysis in *Arabidopsis* cell cultures revealed FyPP1/3 as a potential prey of SMXL7 in three of the four executed repeats in mock. Whether these proteins interact directly is currently not clear. No association was observed in Y2H and FRET-FLIM assays between full-length proteins, whereas Y2H between SMXL7 and the N-terminal part of FyPP1/3 (FyPP-NT) yielded positive results, somehow in agreement with the previous demonstration that in Y2H FyPP-NT performs better than the full-length protein (Dai et al., 2012, 2013). The reason, although still unknown, might be due to some technical issues related to protein expression in a heterologous system. FRET-FLIM with FyPP-NT and SMXL7 would definitely give more insights and help to rule out whether such technical issues are at play. Interestingly, a possible interaction between FyPP-NT and D14 was also observed, suggesting that FyPP1/3 might form a complex with both D14 and SMXL7 or that it might be important for the D14-SMXL7 association. However, the interaction between D14 and FyPP1/3 should be further examined with *in vivo* methods, such Co-IP or FRET-FLIM.

Regardless of whether the SMXL7-FyPP1/3 interaction is direct, co-IP confirmed that they belong to the same complex, supporting a role for FyPP1/3 in SL responses. Still, to be of biological relevance, the proteins should be expressed in the same cellular compartments. FyPP1/3 proteins localize in the nucleus, the plasma membranes, and the cytoplasm (Dai et al., 2013). Hence, they show an overlapping localization pattern with SMXL7 that is expressed in the nucleus (Soundappan et al., 2015; Liang et al., 2016), but also in the cytoplasm (Chapter 4), implying that the interaction between SMXL7 and FyPP1/3 might indeed occur. Interestingly, the expression pattern of FyPP1 inside the nucleus changed from homogenous to speckled when the protein was coexpressed with SMXL7. Previously, the localization of SMXL7 to the nuclear speckles has been reported as well as the SMXL7-D14 and SMXL7-TPR2 association (Soundappan et al., 2015; Liang et al., 2016;). In general, nuclear speckles are frequently spotted near active transcription sites (Reddy et al., 2012). Thus, SMXL7 might possibly associate with active transcription sites and probably contribute to the gene expression repression (Liang et al., 2016). Recruitment of FyPP1/3 to the nuclear speckles when coexpressed with SMXL7 further suggests that this protein might be involved in SL signaling.

The PP6 holoenzyme comprises at least two subunits, a catalytic one, FyPP1/FyPP3, and a B-type regulatory one, belonging to family of SAL proteins in *Arabidopsis*. Remarkably, one of the regulatory subunits, SAL4, was also retrieved in the SMXL7 TAP analysis, hinting at a SMXL7 interaction not with a single protein phosphatase, but with the whole PP6 complex consisting of FyPP1/3 and SAL4. As no direct interaction between SMXL7 and SAL4 could be demonstrated by means of Y2H, SAL4 might possibly be copurified through the SMXL7-FyPP1/3 association. Although the direct interaction between FyPP1/3 and SAL1 was not validated by Y2H because of the autoactivation of both proteins, genetic evidence pointed toward an interaction between all four SAL proteins with FyPP1/3 to control root development (Dai et al., 2012). In the future, Co-IP would help to validate the presence of SAL4 in the complex with both SMXL7 and FyPP1.

To get insight into the role of PP6 in SL responses, we selected two SMXL6/7/8-related processes: lateral root development and shoot branching. Under mock conditions, the LRD of *fypp1-1 fypp3-2-/+* and *sal4-1* seedlings was lower than that of the WT, in agreement with the phenotype of the *smxl6,7,8* mutant and contrary to that of *max2-1* (Ruyter-Spira et al., 2011; Soundappan et al., 2015), hinting at FyPP1/3 and SAL4 as negative regulators of this SL-related phenotype. Accordingly, the *sal4-1* seedlings had an increased sensitivity to the SL analog, whereas plants overexpressing *FyPP1* were less sensitive. In the future, the *fypp1-1 fypp3-2-/+max2-1* and *sal4-1 max2-1* mutants should be tested to validate whether the observed phenotypes are related to SL effects. Additionally, the *sal4* mutant carries fewer branches than the WT, indicating that SAL4 might be also a negative regulator of shoot branching. However, this minor although significant effect might be as well due to the experimental conditions. Therefore, it remains to be determined whether the *sal4-2* and *FyPP1/3* mutants have the same phenotype and whether mutants affected in the PP6 complex can suppress the excessive branching of *max2-1* plants.

Now the question is of how the PP6 complex can be involved in the SL signaling. In a first model, we propose that the PP6 complex might control the phosphorylation status of the SMXL proteins or D14 and hence they are new PP6 substrates. Another possibility would be that the PP6 activity is regulated by the SMXL proteins or D14 and that, in this manner, SLs might influence the phosphorylation of PP6 targets. A PP6-type holoenzyme was reported to dephosphorylate PIN1 and PIN2 proteins in the root, thereby affecting the basal-to-apical membrane localization switch and, consequently, influencing the polar auxin transport (Dai et al., 2012). The interplay between SLs and the PIN1 localization has been clearly demonstrated in shoot branching (Ferguson and Beveridge, 2009; Hayward et al., 2009; Domagalska and Leyser, 2011; Shinohara et al., 2013), but also the influence of SLs on PIN protein expression has been evidenced in the root architecture regulation (Ruyter-Spira et al., 2011; Jiang et al., 2016). One of the models to explain the SL impact on shoot branching, the so-called canalization model, states that SLs affect bud outgrowth by reducing the polar auxin transport in the stem through the

removal of PIN1 from the cellular membrane (Domagalska and Leyser, 2011). Also, in the root, prolonged treatment with *rac*-GR24 reduced the expression levels of PIN1, PIN3, and PIN7 (Ruyter-Spira et al., 2011), whereas a short exposure did not affect the removal of PIN1 from the plasma membrane (Shinohara et al., 2013). In addition, the lateral root response to exogenous *rac*-GR24 is modulated by the interference with the polar auxin transport mostly through PIN1 (Jiang et al., 2016). Hence, it is possible that the altered sensitivity to *rac*-GR24 in lateral root development that we observed is caused by a PP6-dependent dephosphorylation of PIN proteins.

The KAR and SL pathways involve common and/or similar signaling components (reviewed in De Cuyper et al., 2017). Therefore, we verified whether the interaction with FyPP1/3 is unique for SMXL7 or whether it might also occur with its homolog, SMAX1. Indeed, by means of Y2H, we demonstrated the FyPP1/3 interaction with SMAX1, hinting at a possible role for the PP6 complex in the KAR pathway. However, further *in vivo* validation of this interaction through Co-IP or FRET-FLIM is required to confirm this preliminary observation. Nevertheless, the analysis of the mutants does not allow us to conclude that the PP6 complex is involved in the SMAX1-related phenotypes. Analysis of the *rac*-GR24 effect on the hypocotyl length revealed that all the tested FyPP1/3 and SAL4 mutants and transgenic lines responded in a WT-similar manner, with the exception of one overexpression line that displayed a slightly reduced, but significant, response to the treatment. However, under mock conditions, seedlings of *fypp1 fypp3-/+* and *sal4-1* exhibited longer hypocotyls than Col-0 when grown under continuous red light, consistent with the *max2-1* phenotype (Nelson et al., 2011). This observation suggests a positive role for PP6 in the SMAX1-related response, what is rather unexpected given its putative negative role in SMXL6/7/8-regulated phenotypes. It is also possible that the hypocotyl phenotype is not related to KAR effects. Besides its role in phytohormone signaling, FyPP1/3 has been shown to be involved in the phytochrome-mediated light pathway in relation to flowering time by direct dephosphorylation of phytochromes A and B (Kim et al., 2002). Hence, it will be important to examine whether this phenotype is the result of phytochrome dephosphorylation or a consequence of the activation of the MAX2-KAI2 signaling pathway, for instance by testing double mutants of the PP6-type subunits with *max2-1*. In addition to its involvement in hypocotyl growth, SMAX1 is also a negative regulator of the MAX2-KAI2-controlled seed germination (Stanga et al., 2013, 2016). FyPP1 and FyPP3 were also reported to negatively regulate seed germination through ABA signaling regulation (Dai et al., 2013). Therefore, it would be interesting to test whether FyPP1/3 and SAL4 could play a role in the *rac*-GR24 response in seeds.

In *Arabidopsis,* RCN1 was shown to be the third PP6 component that controls the PIN1 localization at the plasma membrane in the root (Dai et al., 2012). However, it can evenly regulate auxin responses by acting as a scaffolding subunit of PP2A (Blakeslee et al., 2007). Here, we could validate the interaction

between FyPP1 and RCN1 by means of Y2H, thus confirming previously described data (Dai et al., 2012). Whether RCN1 belongs to the SMXL7-FyPP1/3-SAL4 complex is still not clear. Firstly, in the TAP analysis, RCN1 was not identified as possible *bona fide* SMXL7 interactor, but it occurred in the list of copurified proteins and might be an unspecific binder. Secondly, the SL-related phenotypes of the *rcn1* mutant were not consistent with those of the *fypp1/3* and *sal4* mutants. Under control conditions, the *rcn1* seedlings displayed an increased LRD and a reduced sensitivity to *rac*-GR24, in contrast to the root phenotypes of the PP6 mutants. Additionally, the number of shoots between the *rcn1* and WT plants did not differ from that of Col-0. The involvement of RCN1 in more than one different PP enzyme complex might, of course, hamper the clear interpretation of the mutant phenotypes. Nevertheless, RCN1 might be part of PP6 to control the SMAX1-related responses, because in all tested mutants a similar phenotype was observed with regard to the hypocotyl elongation.

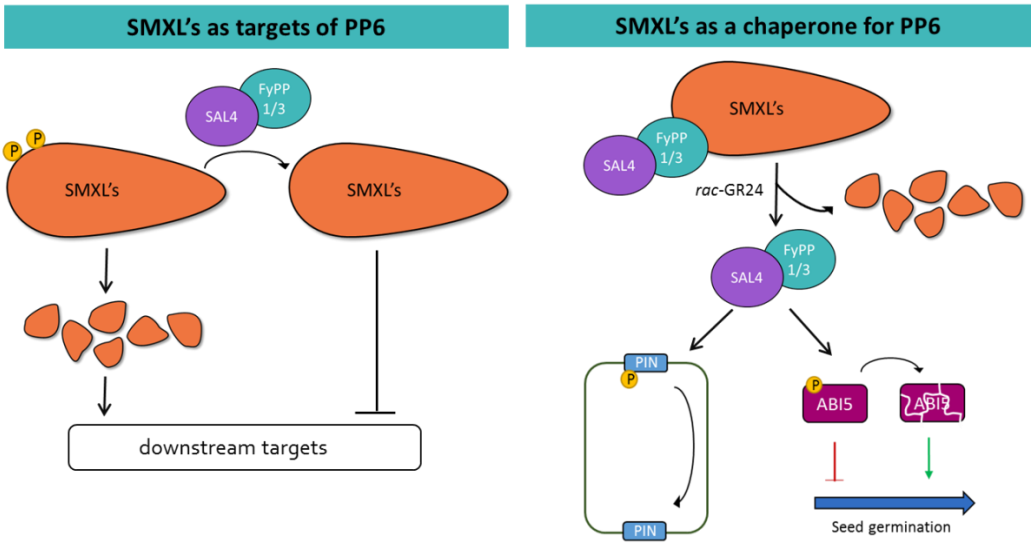

Figure 9. Two proposed models for the PP6 mode-of-action. PP6 dephosphorylates SMXL proteins, thereby influencing their stability/activity or SMXL proteins act as chaperones for the PP6 complex, which mediates the crosstalk between the SL signaling and other pathways.

To conclude, two possible, still to be elucidated, models could be proposed for the mode-of-action of the PP6-type holoenzyme (Figure 9). First, PP6 might directly influence the SL/KAR pathway by dephosphorylating the SMXL7/SMAX1 proteins and likewise stabilize the proteins by, for instance, inhibition of their ubiquitin-mediated degradation. Multisite phosphorylation of a protein has already been demonstrated to be necessary for its recognition by E3 ligase (Bao et al., 2010; Varedi et al., 2010; Yue et al., 2016). In the second model, we hypothesize that the PP6 complex might mediate the crosstalk between different response pathways. As the PP6 complex modulates auxin and ABA signaling (Dai et al., 2012, 2013), for instance, its effect on the LRD might be due to the interplay with auxin. In this scenario, SMXL7/SMAX1 would act as a chaperone protein or a kind of docking platform for the PP6

complex. After degradation of SMXL proteins upon a *rac*-GR24 treatment, the phosphatase complex might get released and become active for dephosphorylation of its target proteins.

Although the mode-of-action is still not known, biochemical and genetic evidence provided here indicate that FyPP1/3, SAL4, and RCN1 might regulate SMXL7- and/or SMAX1-related responses, further suggesting that, besides ubiquitination, protein phosphorylation might be an essential posttranslational modification in the SL and KAR pathways.

MATERIALS AND METHODS

Plant material and growth conditions

All mutant lines used in this study were in the Columbia-0 (Col-0) accession background. *fypp1-1* (SAIL_438_F11), *fypp3-1* (SAIL_851_C04), and *rcn1* (SALK_059903) mutants have been described previously (Dai et al., 2012). *fypp3-2* (SALK_150743), *sal4-1* (SALK_029221), and *sal4-2* (SAIL_337_G05) were purchased from the Salk Institute. The T-DNA insertions of *fypp3-2*, *sal4-1*, and *sal4-2* were confirmed by PCR; the homozygotes were identified by genotyping, the RNA was extracted from 5-day-old seedlings and further confirmed by RT-PCR expression analysis. Primers are listed in Supplemental Table 1. For overexpression, transgenic *Arabidopsis* seeds were generated by floral dip (Clough and Bent, 1998) with Col-0 as the background accession. Transgenic seeds were selected based antibiotic resistance. *Arabidopsis thaliana* (L.) Heynh. seeds were surface sterilized with consecutive treatments of 70% (v/v) ethanol with 0.05% (w/v) sodium dodecyl sulfate (SDS), washed with 95% (v/v) ethanol, sown on half-strength Murashige and Skoog (½MS) medium with 1% (w/v) sucrose (for root phenotyping) or without (for hypocotyl analysis). For stratification, plates were kept in the dark at 4°C for 2 days, whereafter they were transferred to a growth room with 21°C temperature and a 16-h light/8-h dark regime, unless mentioned otherwise.

Molecular cloning

All cloning was carried out by means of the Gateway® recombination (Thermo Fisher Scientific). Open Reading Frames (ORFs) were amplified from *Arabidopsis* cDNA with iProof™ High-Fidelity DNA Polymerase (Bio-Rad) and Gateway®-specific primers (Supplemental Table 1). The PCR products were cloned in pDONR221 with the BP Clonase® II enzyme mix (Invitrogen). The resulting entry vectors were used to clone the protein of interest into the destination vectors pGILDA and pB42AD (Y2H), pH7m24GW2 for C-terminal fusion with GFP/HA (Co-IP, overexpression), and pEarleyGate101 and pEarleyGate102 (FRET-FLIM) with the LR Clonase® II Plus enzyme mix (Invitrogen).

Western blot analysis

Total protein was extracted from 6-day-old seedlings and protein concentrations were determined by the Bradford assay (Bio-rad). For Western blotting, 60 µg of protein was used with rabbit anti-GFP monoclonal antibody (Invitrogen). The signal was captured through chemiluminescent substrates from the Western Lightning® Plus Enhanced Chemiluminescence kit (PerkinElmer) and X-ray films (Amersham Hyperfilm ECL; GE Healthcare). The Precision Plus Protein™ Dual Color Standards (Bio-Rad) was used as protein size marker.

Yeast two-hybrid

Y2H analysis was done as described (Cuellar et al., 2013) in two independent repeats. The polyethylene glycol (PEG)/lithium acetate method was used to cotransform the *Saccharomyces cerevisiae* EGY48 strain (Estojak et al., 1995) with the bait and prey. Transformants were selected on Synthetic Defined media containing galactose and raffinose (SD Gal/Raf) and lacking Ura, Trp, and His (Clontech). Three individual colonies were grown overnight in liquid cultures at 30°C and 10- and 100-fold dilutions were dropped on control media (SD Gal/Raf-Ura-Trp-His) and selective media containing additional X-Gal (Duchefa).

FRET-FLIM

FRET-FLIM analysis was done as described (Liang et al., 2016) with some modifications.

Co-IP assay

Proteins tagged with GFP and 3HA were transiently coexpressed by *A. tumefaciens*-mediated transformation in lower epidermal leaf cells as described previously (Boruc et al., 2010). Proteins were extracted from infiltrated leaf tissue 3 days after infiltration with the extraction buffer containing 150 mM Tris-HCl, pH 7.5, 150 mM NaCl, 10% (v/v) glycerol, 10 mM EDTA, 1 mM Na_2MoO_4, 1 mM NaF, 10 mM dithiothreitol, 0.5% (w/v) polyvinylpolypyrrolide, 1% (v/v) protease inhibitor cocktail (Sigma), and 1% (v/v) NP-40. According to the supplier's instruction, 25 µL of GFP-Trap® beads (ChromoTek GmbH) were incubated in 2 mL of total protein extract at 4°C for 3 h. The beads were washed three times with washing buffer [20 mM Tris-HCl, pH 7.5, 150 mM NaCl, 0.5% (v/v) NP-40] and then eluted with 40 µL of SDS-polyacrylamide gel electrophoresis sample buffer for immunoblot analysis. The precipitated proteins were detected by immunoblot analysis with a rabbit anti-GFP monoclonal antibody (Invitrogen) at a 1:2000 dilution or a mouse monoclonal anti-HA antibody (Sigma) at a 1:20000 dilution.

Physiological assays

To analyze the root phenotypes, seedlings were grown vertically for 9 days in a 16-h/8-h light/dark cycle at 21˚C. The lateral root primordia were counted under a light microscope (S4E, Leica Microsystems), whereafter the plates were scanned and the main root length was measured with the ImageJ software. For the hypocotyl elongation analysis, after stratification, seeds were exposed to white light for 3 h, transferred to darkness for 21 h, and then exposed to continuous red light for 4 days at 21˚C. After plates had been scanned, the hypocotyls were measured with the ImageJ 1.41 software. Rosette branches (shoots >1 cm) were counted in 50-day-old plants grown in soil under a standard 16-h/8-h light/dark cycle (22°C/18°C) in controlled-environment rooms with light provided by white fluorescent tubes.

SUPPLEMENTARY DATA

Supplemental Table 1. All primers used in this study.

ID		Sequence	Use
SMXL7	Fw	GGGGACAAGTTTGTACAAAAAAGCAGGCTCAATGCCGACACCAGTAACCACG	Cloning
SMXL7	Rev	GGGGACCACTTTGTACAAGAAAGCTGGGTATCAGATCACTTCGACTCTCG	Cloning
SMAX1	Fw	GGGGACAAGTTTGTACAAAAAAGCAGGCTCAATGAGAGCTGGTTTAAGTACG	Cloning
SMAX1	Rev	GGGGACCACTTTGTACAAGAAAGCTGGGTATCATACTGCCAAAGTAATAG	Cloning
FyPP1	Fw	GGGGACAAGTTTGTACAAAAAAGCAGGCTCAATGGATTTAGATCAATGG	Cloning
FyPP1	Rev	GGGGACCACTTTGTACAAGAAAGCTGGGTATCACAGGAAATAAGGAACAC	Cloning
FyPP-NT	Rev	GGGGACCACTTTGTACAAGAAAGCTGGGTATCAACCACAGACGGTGACAGGAC	Cloning
SAL4	Fw	GGGGACAAGTTTGTACAAAAAAGCAGGCTCAATGTTGGCCGCGACGCCTGCTC	Cloning
SAL4	Rev	GGGGACCACTTTGTACAAGAAAGCTGGGTATCAAGCAAGCTCTAACAAGCAGAC	Cloning
RCN1	Fw	GGGGACAAGTTTGTACAAAAAAGCAGGCTCAATGGCTATGGTAGATGAACCG	Cloning
RCN1	Rev	GGGGACCACTTTGTACAAGAAAGCTGGGTATCAGGATTGTGCTGCTGTGGAACC	Cloning
fypp3-2	Fw	GGATCAATGGATTTCCAAGGT	RT-PCR#1
fypp3-2	Rev	CAAGGCCTTTATCTTGGAACA	RT-PCR#1
sal4	Fw	CTGCTCTCTCTGCTGCTTCA	RT-PCR#2
sal4	Rev	ACTATCATCAGGGCTCTCCTTTC	RT-PCR#2

Chapter 6

Molecular insight into SMAX1 protein network in *Arabidopsis thaliana*

Sylwia Struk[1,2], Annick De Keyser[1,2], Robin Vanden Bossche[1,2], François-Didier Boyer[3], Geert Persiau[1,2], Dominique Eeckhout[1,2], Geert De Jaeger[1,2], Alain Goossens[1,2] and Sofie Goormachtig[1,2]

[1]Ghent University, Department of Plant Biotechnology and Bioinformatics, 9052 Ghent, Belgium,
[2]VIB, Center for Plant Systems Biology, 9052 Ghent, Belgium,
[3]Institut National de la Recherche Agronomique, Institut Jean-Pierre Bourgin, Versailles, France

S.S. was the main author of the manuscript and performed all experiments, except the molecular cloning partially performed by A.D.K., the acquisition of the TAP data prepared by G.P., D.E. and G.D.J. and transcriptional repression activity performed by R.V.B and A.G. F.D.B. kindly provided the synthetic strigolactone analog rac-GR24. S.G. supervised the project and contributed to the writing of the manuscript.

ABSTRACT

Smoke-derived karrikins and endogenously produced strigolactones control different aspects of plant development through a similar mechanism with MORE AXILLARY GROWTH2 (MAX2) as a common component and the closely related α/β hydrolases KARRIKIN INSENSITIVE 2 (KAI2) and DWARF 14 (D14) that perceive the respective signals. Based on genetic data, SUPPRESSOR OF MAX2 1 (SMAX1) was proposed as a downstream target of the KAI2-MAX2–mediated signaling. Here, we provide biochemical evidence for the KAI2-MAX2-SMAX1 complex formation. We show that SMAX1 is degraded in both cell cultures and *Arabidopsis thaliana* seedlings and that the mutation of certain amino acid motif in ΔSMAX1 causes its resistance to degradation. Additionally, we carried out tandem affinity purification (TAP) to elucidate the interaction network of SMAX1 and ΔSMAX1. By using different methods to analyze the TAP data, we point out candidate proteins that would be interesting to investigate in the future to establish how SMAX1 might control plant development.

INTRODUCTION

Karrikins (KARs) are a group of small butenolide compounds that are present in burning plant material (Flematti et al., 2004, 2011). To date, six KAR molecules have been detected in plant-derived smoke and approximately 50 analogs were chemically synthetized (Goddard-Borger et al., 2007; Sun et al., 2008; Flematti et al., 2009). The main role of KARs is the stimulation of germination in dormant seeds after wildfire in many smoke-responsive species (Nelson et al., 2012). Although KARs are not synthesized by plants, they elicit growth responses also in non-fire-following species. In *Arabidopsis thaliana,* KARs enhance seed germination and influence seedling photomorphogenesis (Nelson et al., 2009, 2010), whereas in several crop species they increase stress tolerance and seedling vigor (Jain et al., 2006; Kulkarni et al., 2006).

KARs share some structural similarities with strigolactones (SLs), carotenoid-derived phytohormones that play an additional role in the rhizosphere as a signaling cue for arbuscular mycorrhizal associations (Akiyama et al., 2005; Yoneyama et al., 2008) and germination of parasitic plants from the *Orobanchaceae* family (Yoneyama et al., 2010). Besides the structural resemblances, the KAR and SL pathways share a similar signaling mechanism. The F-box protein, MORE AXILLARY GROWTH 2 (MAX2), has a central function in mediating responses to both molecules (Nelson et al., 2011), whereas SLs and KARs are perceived through paralogous receptors, α/β-hydrolases DWARF14 (D14) and KARRIKIN-INSENSITIVE2 (KAI2), respectively (Hamiaux et al., 2012; Guo et al., 2013; Kagiyama et al., 2013; Nakamura et al., 2013; Zhao et al., 2013).

The D14 mode-of-action has been studied more thoroughly than that of KAI2. Upon binding and hydrolysis of SLs by D14, a conformational change is induced in the receptor, enabling an interaction with MAX2 and possibly also with downstream signaling partners, the SMAX1-LIKE (SMXL) 6, SMXL7, and SMXL8 proteins (Hamiaux et al., 2012; Zhao et al., 2015; Yao et al., 2016). A similar perception mechanism has been proposed for KAI2, although hydrolysis of KARs is not expected due to the chemical properties of the molecules (Guo et al., 2013; Zhao et al., 2013, 2015). Nonetheless, a conserved catalytic triad of Ser-His-Asp residues, which is essential for SL hydrolysis, has also been found to be necessary for KAI2 signal transduction (Hamiaux et al., 2012; Waters et al., 2014). Both D14 and KAI2 are highly specific in the chemical structures they perceive: D14 preferentially binds to SL in its natural configuration, such as 5-deoxystrigol (5DS) and is unresponsive to KARs, whereas the KAI2 pathway can be activated by KARs and SL analogs with an unnatural 2'S configuration, such as the 5DS enantiomer. The frequently used synthetic SL analog, *rac*-GR24, is a racemic mixture of two stereoisomers, 5DS and its enantiomer (ent-

5DS), that can effectively activate both the D14 and KAI2 pathways (Scaffidi et al., 2014). KAI2 might not only perceive KARs, but also an unknown endogenous molecule, referred as KAI2 ligand (KL), that is neither KAR nor SL (Conn and Nelson, 2016).

The most recently described downstream component of the KAR/KL pathway, SUPPRESSOR OF MAX2-1 (SMAX1), has been discovered by suppressor screening of the *max2* seed dormancy and long-hypocotyl phenotypes (Stanga et al., 2013). In *Arabidopsis*, seven genes are closely related to SMAX1, referred as SMAX1-LIKE (SMXL) that are subdivided into four phylogenetic subclades. Proteins from the subclade 1, SMAX1 and SMXL2 mediate KAR/KL responses (Stanga et al., 2013, 2016), whereas SMXL6, SMXL7, and SMXL8 proteins belong to subclade 4, the closest homologs of DWARF 53 (D53) in rice (*Oryza sativa*) and act in the SL pathway (Zhou et al., 2013; Soundappan et al., 2015). SMXL6, SMXL7, and SMXL8 (SMXL6/7/8) have been shown to function as SL-signaling repressors that are ubiquitinated and degraded upon treatment with *rac*-GR24 in a D14- and MAX2-dependent manner (Soundappan et al., 2015; Wang et al., 2015). A similar mechanism is proposed for SMAX1 upon activation of the KAI2 pathway, but biochemical evidence is still lacking. SMAX1 is a predicted target of MAX2 at early growth stages. The *smax1* loss-of-function mutant is characterized by low seed dormancy, reduced hypocotyl elongation, and enlarged cotyledons and is able to suppress the KAR-related phenotypes of *max2* (Stanga et al., 2013; Soundappan et al., 2015). Furthermore, some functional redundancy has been reported between SMAX1 and SMXL2 in hypocotyl growth regulation, but not in seed germination, leaf shape, or petiole orientation (Stanga et al., 2016). One of the proposed functions of SMXL proteins is transcription control. SMAX1, SMXL2, and SMXL6/7/8 were reported to have a C-terminal ETHYLENE RESPONSE FACTOR-associated amphiphilic repression (EAR) motif that facilitates their interactions with the transcriptional corepressors proteins, TOPLESS (TPL) and TOPLESS-RELATED (TPR) (Bennett and Leyser, 2014; Soundappan et al., 2015; Wang et al., 2015).

The current model of the KAI2-mediated signaling is based mainly on genetic data and similarity to the SL pathway. In *Arabidopsis*, the interaction between KAI2 and MAX2 has been detected by means of a yeast two-hybrid (Y2H) experiment (Toh et al., 2014), but the KAI2/MAX2/SMAX1/SMXL2 association as well as the KAR/*rac*-GR24-induced degradation of SMAX1 has not been evidenced yet. Here, we critically assess the proposed interactions through various biochemical studies. Additionally, by means of tandem affinity purification (TAP) with SMAX1 as bait, we identified various potential new interactors of SMAX1, opening venues to explain functioning of the KAI2 pathway.

RESULTS

SMAX1 interacts with components of the KAR/KL pathway

SMAX1 is a probable target of the Skp1-Cullin-F-box (SCF)-containing E3 ubiquitin ligase of MAX2 (SCF^{MAX2}) in response to KAI2-mediated signaling (Stanga et al., 2013; Soundappan et al., 2015). MAX2 localizes predominantly in the nucleus (Chapter 7; Stirnberg et al., 2007; Liang et al., 2016;) whereas KAI2 is expressed in both nucleus and cytoplasm (Chapter 8; Sun and Ni, 2011). To resolve the subcellular pattern of SMAX1, *Nicotiana benthamiana* (tobacco) leaves were transiently transformed with *proSMAX1::SMAX1-GFP* and examined under confocal microscopy. The GFP signal was exclusively detected in the nucleus (Figure 1A). Consistent with the transient expression data, the nuclear localization was also observed in roots of *Arabidopsis* stably transformed with *proSMAX1::SMAX1-GFP* (Figure 1B), although the GFP signal was very low. These data demonstrate that SMAX1 is located in the same compartment as other components of the KAR/KL pathway, MAX2, and KAI2.

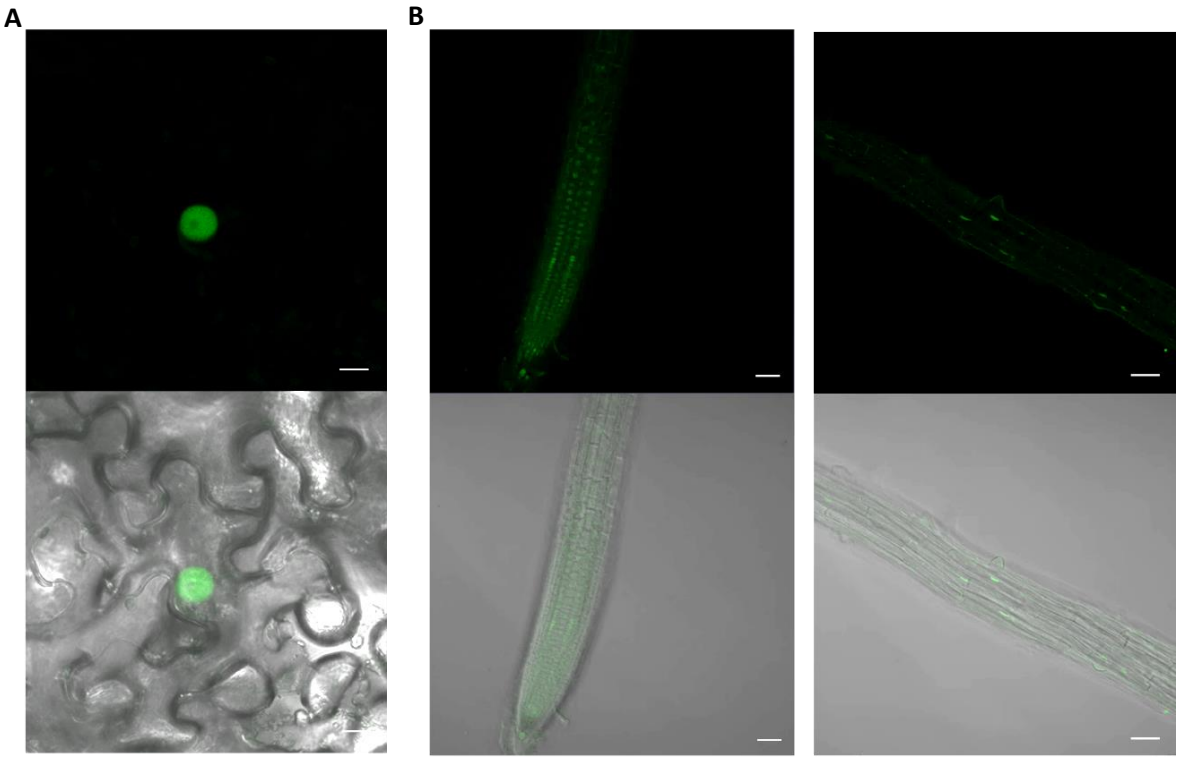

Figure 1. Subcellular localization of SMAX1. (A) SMAX1 protein localization analyzed by transient expression of *proSMAX1::SMAX1-GFP* in tobacco leaves. Scale bar, 10 µm. (B) Localization of SMAX1 in the root of 5-day-old *Arabidopsis* seedlings expressing *proSMAX1::SMAX1-GFP* analyzed by confocal microscopy. The distribution of the GFP signal is representative of several independent plant lines. Scale bar, 50 µm. Top panel GFP signal, bottom GFP merged with bright-field.

Related to SMAX1, SMXL6/7/8 proteins were shown to interact with the SL receptor D14 in a *rac*-GR24–dependent manner to activate downstream responses (Chapter 3; Wang et al., 2015; Jiang et al., 2016). A similar mode of action was expected for the KAR/KL receptor KAI2 and SMAX1. Here, we used the LexA-based Y2H system to validate the interactions between SMAX1 and its predicted partners, MAX2, KAI2, and TPL/TPR. To test the interaction with TPL/TPR, we used the N-terminal fragment of TPL (TPL-N), containing the LisH, CTLH, and TOP domains that had previously been described as crucial for binding to the EAR motif and mediating protein-protein interactions (Szemenyei et al., 2008; Pérez Cuéllar et al., 2013). In our analysis, yeast coexpressing SMAX1 fused to the GAL4-binding domain (BD) and KAI2 and TPL fused to the GAL4 activation domain (AD) colored blue when the colony was spotted on selective medium supplemented with 5-bromo-4-chloro-3-indolyl-β-D-galactopyranoside (X-gal), but no direct interaction with MAX2 was detected. Surprisingly, the addition of *rac*-GR24 to the selective medium had no influence on the tested interactions (Figure 2A), in contrast to the D14-SMXL7 association which occurs only in the presence of SL the analog (Chapter 3). Therefore, we carried out an additional validation of the KAI2-SMAX1 interaction with the Y2H GAL4 system that further confirmed previous results of the LexA-based Y2H method (Figure 2B). This time, however, slightly improved colony growth could be seen, when yeasts cotransformed with SMAX1-BD and KAI2-AD were spotted on the selective medium supplemented with 10 µM *rac*-GR24, suggesting that this interaction might be enhanced in the presence of the SL analog.

The interaction between SMAX1 and TPL raises the possibility that such complexes might regulate transcription in response to KAR/KL. Therefore, we used tobacco Bright Yellow 2 (BY-2) protoplasts to test whether SMAX1 has a potential repressor activity. To this end, SMAX1 was fused with the GAL4-binding domain (GAL4BD) under the control of the cauliflower mosaic virus (CaMV) 35S promoter and coexpressed with the firefly luciferase (fLUC) reporter gene containing the 35S promoter linked to the GAL4 upstream activation sequence. When compared with the control GUS-GAL4BD, the relative fLUC activity was significantly reduced when GAL4 was fused to SMAX1 (Figure 2C), indicating that SMAX1 can act as a transcriptional repressor, possibly due to association with TPL proteins, similarly as the SMXL6/7/8 proteins (Wang et al., 2015)

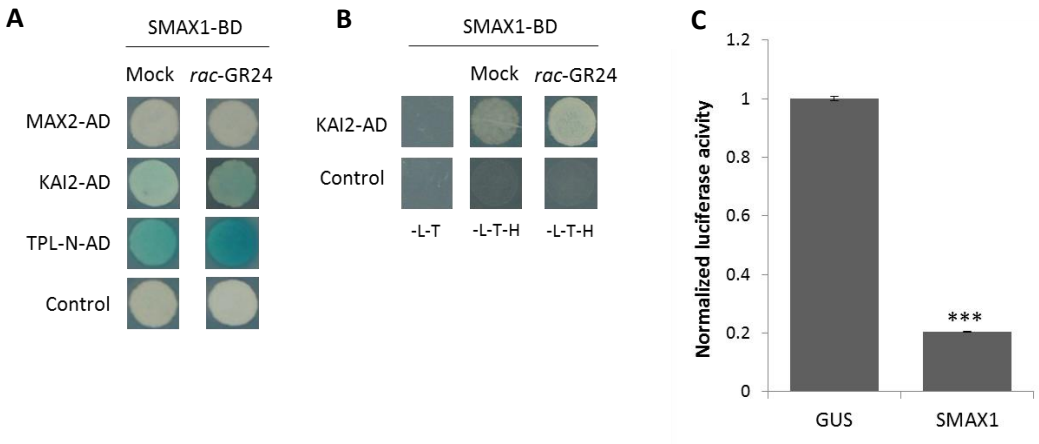

Figure 2. Analysis of SMAX1-interacting proteins and its repression activity. (A) The yeast (*Saccharomyces cerevisiae*) strain EGY48 (p8opLacZ) cotransformed with SMAX1-BD and MAX2, KAI2, or TPL fused with AD or pB42AD alone (control). Transformed yeasts were spotted on inducing medium containing Gal and Raf (SD Raf/Gal -U-T-H), supplemented with X-Gal. (B) Yeast cells cotransformed with SMAX1-BD and KAI2-AD or pGAD424gate alone (control) were grown on SD media lacking Leu and Trp (-L-T) as transformation control and on selective media lacking Leu, Trp and His (-L-T-H) to test protein interactions. (C) SMAX1 acting as a transcriptional repressor in transient expression assays. Transactivation assay in tobacco protoplasts transfected with a pUAS–fLUC reporter construct, effector construct SMAX1 or GUS (control) fused to GAL4BD, and a *35S:rLUC* normalization construct. Error bars represent ± SE of eight biological replicates. Asterisks represent significant differences (***, P <0.001, Student's *t* test).

Functional analysis of SMAX1-GS^{rhino} and ΔSMAX1-GS^{rhino} fusion proteins

For the identification of novel SMAX1-interacting partners, *Arabidopsis* cell cultures were transformed with N- and C-terminal fusions of SMAX1 and ΔSMAX1 with the GS^{rhino} tag driven by the *CaMV 35S* promoter. The ΔSMAX1 allele was generated based on the mutation found in the *d53* allele in rice that causes a protein resistance to *rac*-GR24–induced degradation (Figure 3A) (Jiang et al., 2013). After all the constructs had been found highly expressed in the cell cultures (Supplementary Figure 1), the responsiveness toward *rac*-GR24 was tested. To this end, cell cultures expressing *35S::GSrhino-SMAX1* and *35S::GSrhino-ΔSMAX1* were treated either with 1 µM *rac*-GR24 or 0.01% acetone (mock) at multiple time points. As shown in Figure 3B, starting from 30 min after treatment onward, the SMAX1 protein level decreased and protein recovery was observed 24 h after treatment, implying *rac*-GR24 induced degradation. As expected, the ΔSMAX1 protein level did not decrease upon treatment (Figure 3C), in

agreement with the observations for *d53* (Jiang et al., 2013) and ΔSMXL7 (Chapter 3; Soundappan et al., 2015), indicating the importance of this region for the SMAX1 function as well.

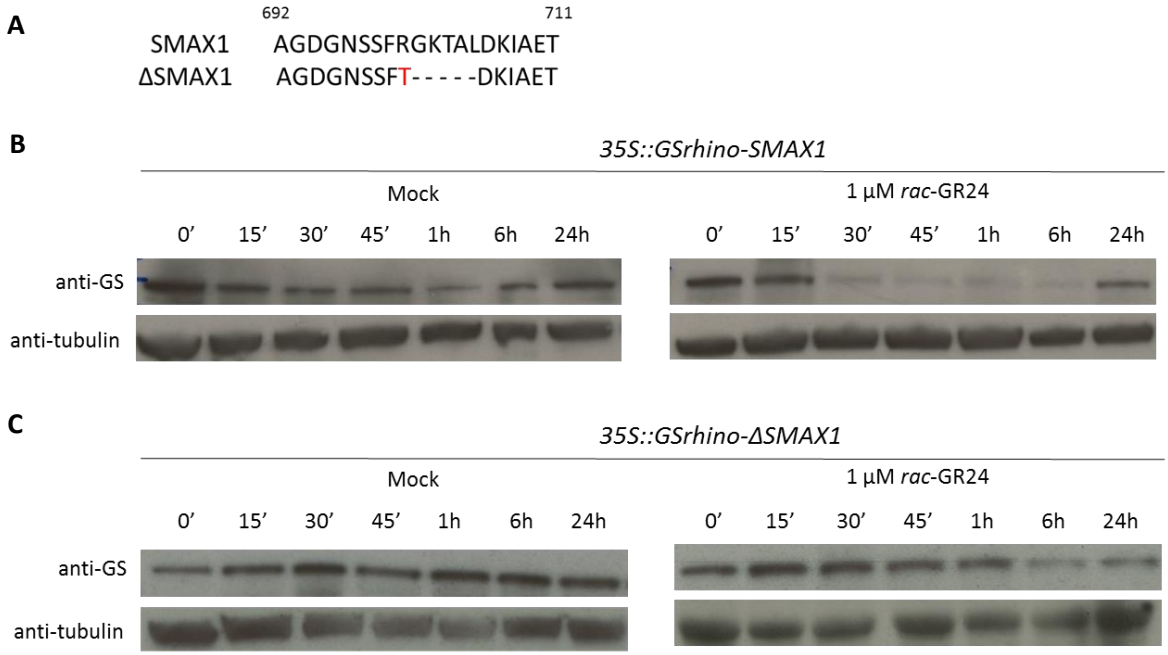

Figure 3. Degradation of SMAX1 in response to *rac*-GR24 in *Arabidopsis* cell cultures. (A) Protein alignment of the amino acid regions of SMAX1 and ΔSMAX1. The ΔSMAX1 protein carries a deletion of residues 671-675 (Gly-Lys-Thr-Ala-Leu) and an amino acid substitution at 670 (Arg to Thr). (B-C) Protein levels of SMAX1 in cell cultures transformed with *35S::GSrhino-SMAX1* (B) or *35S::GSrhino-ΔSMAX1* (C) at different time points after treatment without (acetone) or with 1 µM *rac*-GR24 (' min and h after treatment). Detection was done with anti-GS (top) and anti-tubulin (bottom) antibodies for loading control. The experiment was repeated twice with comparable results and one representative repeat is shown.

One of the potential problems with protein tagging might be the interference of a tag with the functionality of the bait. The best manner to test whether the bait is fully functional is by expressing the fusion protein in the corresponding mutant background and by analyzing the complementation of the mutant phenotype. Previously, the GFP-tagged SMXL7 expressed under the control of *35S* promoter has been found to restore only partially the number of shoot branches of the *smxl6 smxl7 smxl*8 *max2* (*s678max2*) mutant, whereas the same fusion driven by a native promoter fully complemented the *s678max2* mutant toward the expected *max2* phenotype (Liang et al., 2016). Hence, we generated the SMAX1-GS^{rhino} fusion driven by the native SMAX1 promoter (*proSMAX1::SMAX1-GSrhino*) and used this construct for the transformation into the *smax1* mutant background to further test its functionality *in*

planta. Western blot analysis allowed the selection of the line with the highest bait protein expression for mutant complementation analysis (plant 7; Supplementary Figure 1B). Currently, transgenic plants are being generated expressing *proSMAX1::GSrhino-SMAX1, proSMAX1::GSrhino-ΔSMAX1,* and *proSMAX1::ΔSMAX1-GSrhino* constructs in the *smax1* mutant background. Additionally, we also attempted to investigate the SMAX1-GSrhino and ΔSMAX1-GSrhino fusions under the control of *35S* promoter but expression of the bait protein could not be detected in any of the tested transgenic lines (data not shown).

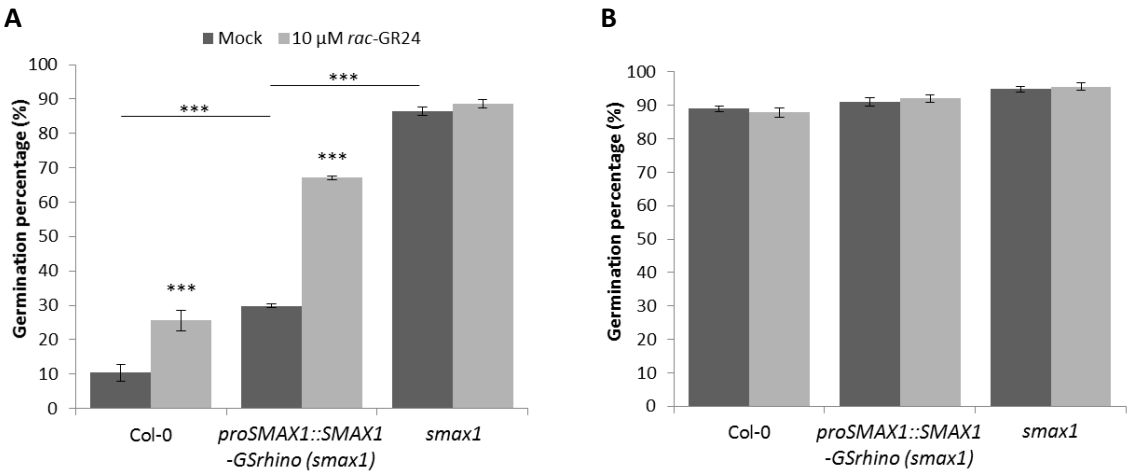

Figure 4. Partial complementation of the germination phenotype of *smax1* mutant by *proSMAX1::SMAX1-GSrhino* in suboptimal temperature conditions. Seeds were distributed in 96-well plates containing HEPES buffer with mock (acetonitrile) or 10 µM *rac*-GR24 and placed in the dark for 4 days at 24˚C (A) or in continuous light at 21˚C as a control (B). Asterisks indicate statistically significant differences between treatments and asterisks above the line- between genotypes (*** $P < 0.001$; logistic regression with the glimmix procedure). The experiments were repeated three times and the total mean of all biological repeats is presented. Data and error bars represent means ± SE.

The SMAX1 protein acts downstream of MAX2 and KAI2 to regulate the KAR/KL responses in *Arabidopsis,* such as seed germination under suboptimal conditions (Stanga et al., 2013; Soundappan et al., 2015). Consequently, the *kai2* and *max2* mutants exhibit an increased seed dormancy, whereas *smax1* is characterized by a very high germination frequency that cannot be inducted anymore by the addition of *rac*-GR24 (Nelson et al., 2011; Waters et al., 2012; Stanga et al., 2013). To examine whether the *proSMAX1::SMAX1-GSrhino* construct can complement the *smax1* phenotype, we compared the germination frequency of the Columbia-0 (Col-0) accession, *smax1,* and *proSMAX1::SMAX1-GSrhino*(*smax1*) transgenic lines in suboptimal temperature. Under mock conditions, the germination

frequency of *proSMAX1::SMAX1-GSrhino*(*smax1*) was significantly higher than that of Col-0, although not to the same extent as that of the *smax1* mutant (Figure 4A), hinting at a partial complementation. Nonetheless, the induction of germination did not differ significantly after addition of *rac*-GR24 between the *proSMAX1::SMAX1-GSrhino*(*smax1*) line and the wild type (146% and 125%, respectively), suggesting that the response to the SL analog was restored. As described above, the *smax1* mutant had a high germination frequency in both conditions without (mock) and with *rac*-GR24 treatment. In the control conditions (21°C, continous light) all tested lines displayed high germination frequency that was not induced by the treatment with *rac*-GR24 (Figure 4B).

Next, we investigated the response of *proSMAX1::SMAX1-GSrhino(smax1)* plants to *rac*-GR24. To this end, seedlings grown for 6 days in liquid half-strength Murashige and Skoog (½MS) medium were treated with mock (0.01% acetone) or with 1 µM *rac*-GR24 at six different time points. Similarly to the observations in cell cultures, the SMAX1 protein was degraded starting already 15 min after treatment, further confirming the functionality of the bait protein *in planta* (Figure 5).

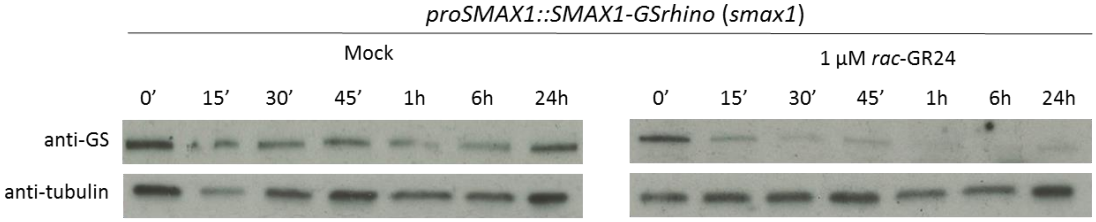

Figure 5. Degradation of SMAX1 in response to *rac*-GR24 in *Arabidopsis* seedlings. SMAX1 protein levels in *proSMAX1::SMAX1-GSrhino(smax1)* transgenic lines grown for 6 days in liquid ½MS medium. Samples were harvested at different time points upon either mock (0.01% acetone) or 1 µM *rac*-GR24 treatment (‘ min and h after treatment). Detection was done by immunoblotting with anti-GS (top) and anti-tubulin (bottom) antibodies for loading control. A representative picture of two repeats is shown.

Isolation of SMAX1 protein complexes in *Arabidopsis* cell cultures

To obtain a comprehensive view on the protein complexes to which SMAX1 belongs, TAP experiments were done in cell cultures expressing SMAX1 and ΔSMAX1, N- and C-terminally tagged with the GS^{rhino}. For each construct, two independent TAP experiments were carried out in each condition, without (mock) or with 1 µM *rac*-GR24 treatment. First, to distinguish *bona fide* interactors among all identified

proteins, we filtered out those that were present in a list of nonspecific and sticky binders based on the occurrence frequency of the copurified proteins in a few hundred TAP experiments with different baits done in *Arabidopsis* (Van Leene et al., 2015).

Table1. Overview of proteins identified by TAP with SMAX1 using qualitative analysis

AGI	Protein	*35::GSrhino-SMAX1*	
		Mock	*rac*-GR24
AT5G57710	SMAX1, SUPPRESSOR OF MAX2 1	2	2
AT5G11980	COG8, CONSERVED OLIGOMERIC GOLGI COMPLEX 8	2	1
AT2G26780	ARM repeat superfamily protein	2	1
AT5G51200	EMB3142, EMBRYO DEFECTIVE 3142	2	1
AT5G18620	CHR17, CHROMATIN REMODELING FACTOR17	2	1
AT4G02350	SEC15B, EXOCYST COMPLEX COMPONENT SEC15B	1	1
AT3G06400	CHR11, CHROMATIN-REMODELING PROTEIN 11	1	1
AT2G33470	GLTP1, GLYCOLIPID TRANSFER PROTEIN 1	1	1
AT4G27960	UBC9, UBIQUITIN-CONJUGATING ENZYME 9	1	1
AT3G08947	ARM repeat superfamily protein	1	-
AT2G36200	P-loop containing nucleoside triphosphate hydrolases superfamily protein	1	-
AT4G37460	SRFR1, SUPPRESSOR OF RPS4-RLD 1	1	-
AT4G01990	Tetratricopeptide repeat (TPR)-like superfamily protein	1	-
AT1G10940	ASK1, SNRK2-4, SNRK2.4, SRK2A | Protein kinase superfamily protein	1	-
AT1G26170	ARM repeat superfamily protein	1	-
AT2G31660	SAD2, URM9 | ARM repeat superfamily protein	1	-
AT1G16890	UBC36, UBC13B | ubiquitin-conjugating enzyme 36	1	-
AT1G47550	SEC3A, EXOCYST COMPLEX COMPONENT SEC3A	1	-
AT3G54470	Uridine 5' monophosphate synthase	1	-
AT2G20360	NAD(P)-binding Rossmann-fold superfamily protein	1	-
AT1G76850	SEC5A, EXOCYST COMPLEX COMPONENT SEC5	-	1
AT1G64230	UBC28, UBIQUITIN-CONJUGATING ENZYME 28	-	1
AT5G58410	HEAT/U-box domain-containing protein	-	1

Table 2. Overview of proteins identified by TAP with ΔSMAX1 using qualitative analysis

AGI	Protein	*35::GSrhino-ΔSMAX1*	
		Mock	*rac*-GR24
AT5G57710	SMAX1, SUPPRESSOR OF MAX2 1	2	2
AT5G12140	CYS1, CYSTATIN-1	2	2
AT1G15750	TPL, TOPLESS	2	2
AT5G27030	TPR3,TOPLESS-related 3	2	2

Proteins were identified with the peptide-based homology analysis of mass spectrometry data. Background proteins were withdrawn based on the occurrence frequency of copurified proteins in a large GS TAP data set (Van Leene et al., 2015). Numbers indicate the times the prey was identified in two experiments per column (mock/15 min *rac*-GR24) with *35S::GSrhino-SMAX1* (Table1) and *35S::GSrhino-ΔSMAX1* (Table 2). AGI, Arabidopsis Genome Initiative identifier. –, no prey identified in this experiment.

This qualitative manner of TAP data analysis allows the obtainment of a static view on the formed protein complexes. The resulting lists of identified proteins contained in total 23 putative SMAX1 (Table 1; Supplemental dataset 1) and three ΔSMAX1 (Table 2; Supplemental dataset 2) preys. All the proteins were copurified with the N-terminally tagged bait, but the C-terminal GS^{rhino} fusion did not yield any possible interactors. In none of the tested conditions, peptides of predicted SMAX1 interactors, MAX2, and KAI2, were detected. On the contrary, other partners, TPL and TPR3, were identified as preys of ΔSMAX1, but not of SMAX1. Interestingly, three members of the ubiquitin-conjugating enzyme (E2) family (UBC9/AT4G27960, UBC36/AT1G16890, and UBC28/AT1G64230) were associated with SMAX1, albeit in both conditions, indicating that a possible ubiquitination process occurred around the bait. In addition, among others, proteins were detected that are involved in many diverse processes, including exocytosis (SEC15B/AT4G02350, SEC3A/AT1G47550, SEC5A/AT1G76850), chromatin remodeling (CHR11/AT3G06400, CHR17/AT5G18620), nuclear transport (EMB3142/AT5G51200, SAD2/AT2G31660, ARM repeat superfamily protein/AT1G26170), protein ubiquitination (HEAT/U-box domain-containing protein/AT5G58410), and phosphorylation (ASK1/AT1G10940) (Table 1). Moreover, the TPL/TPR proteins and CYSTATIN1 (CYS1/AT5G12140) with endopeptidase inhibitor activity was found in all of the ΔSMAX1 TAP experiments.

Changes in the composition of the SMAX1 protein complex revealed by quantitative TAP

The previous approach to analyze TAP data allows the qualitative discovery of the interactors, but not a quantitative comparison between the samples. Hence, to examine the changes of the protein complexes formed around SMAX1 in the presence and absence of *rac*-GR24, we used a label free quantification (LFQ) algorithm integrated into the MaxQuant software (MaxLFQ) (Cox et al., 2014). After the mass spectrometry analysis of the TAP samples, the MaxQuant software was used to search spectra and MaxLFQ was applied to quantify the identified proteins between the tested conditions over the four replicates. To evaluate the reproducibility of the analysis, scatter plots were made that calculate the correlations of LFQ values between replicates. The Pearson correlation coefficients for all replicate pairs for SMAX1 ranged from 0.813 to 0.976 and for ΔSMAX1 from 0.859 to 0.976, demonstrating a good reproducibility, which is crucial for downstream analysis (Supplemental Figure 2).

Intensity based analysis

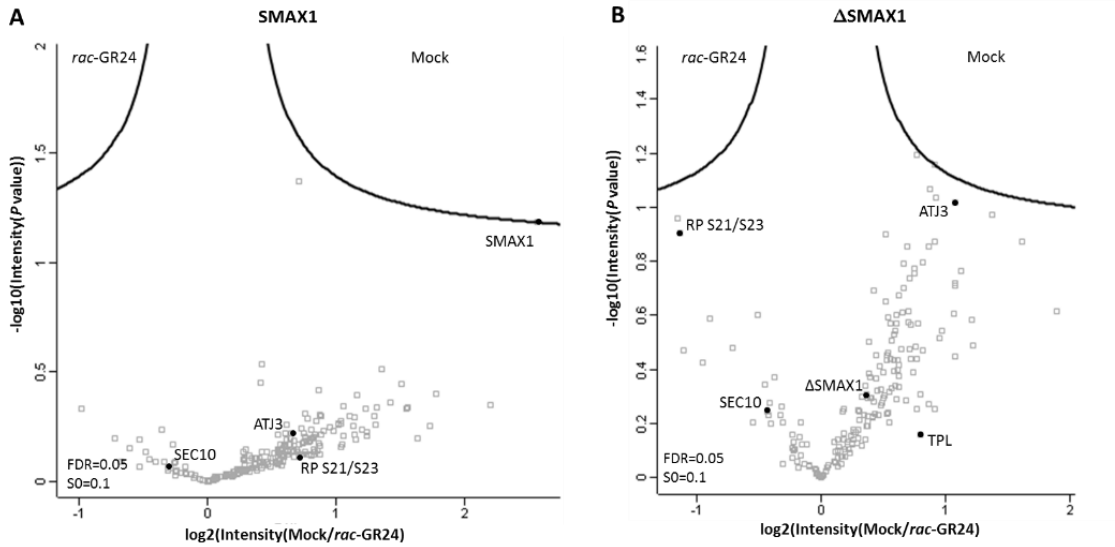

LFQ based analysis

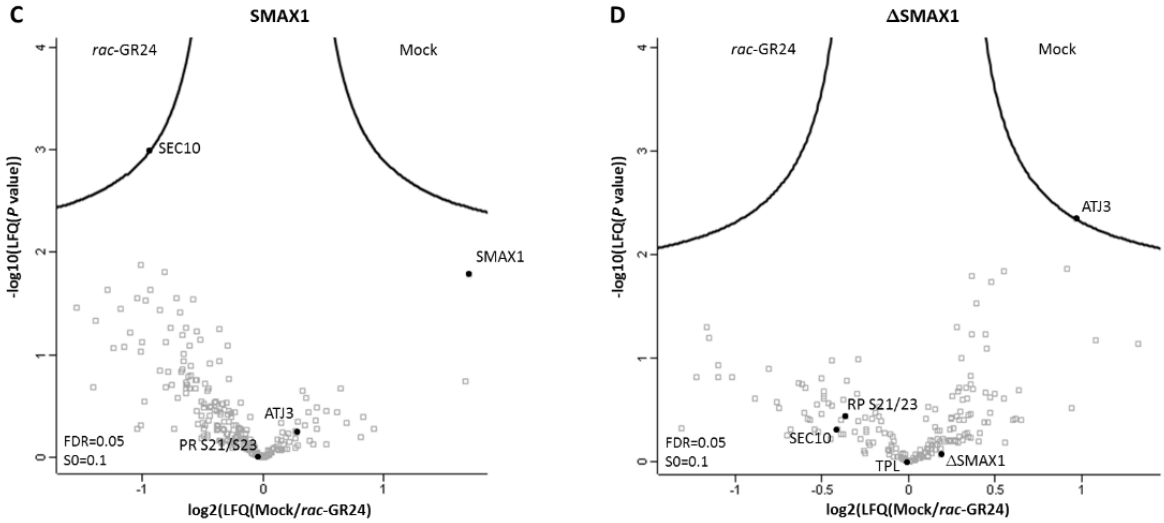

Normalization on the bait level

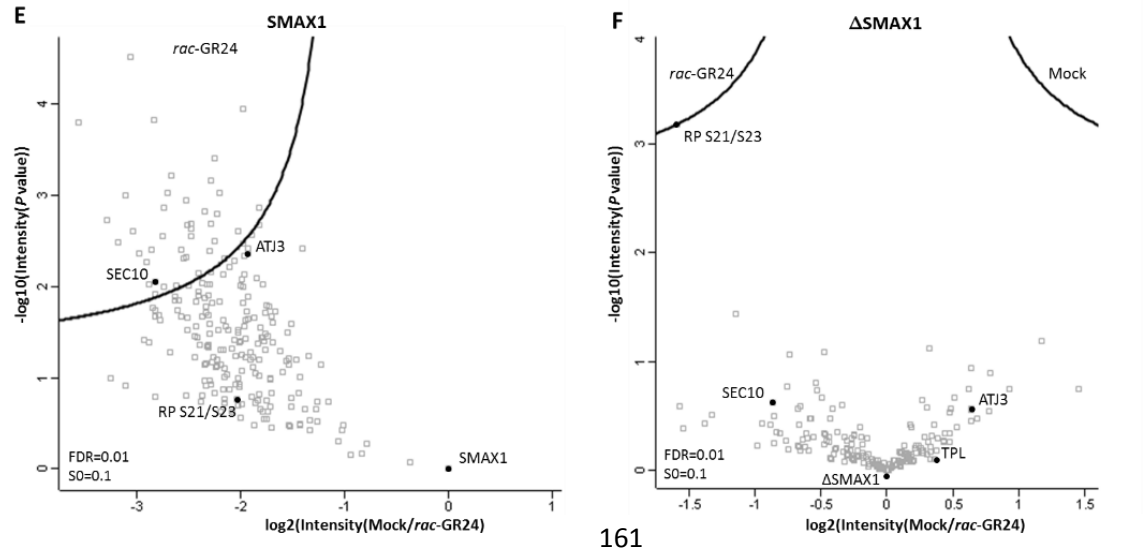

Figure 6. Dynamic changes of the SMAX1 and ΔSMAX1 protein complex composition. Volcano plots showing the distribution of all quantified proteins after filtering and statistical analysis, with their corresponding protein abundance ratios between two samples (mock/*rac*-GR24) over the *t* test *P* value (false discovery rate [FDR]=0.05, S0=0.1 [A-D]; FDR=0.01, S0=0.1 [E, F]). The cutoff curve indicates which hits are significantly more associated with SMAX1/ΔSMAX1 in mock (right) and after addition of *rac*-G24 (left). Analysis was based on intensity values (A, B, E, F) or on LFQ values (C, D). Protein distribution after normalization of the bait level (E, F).

Next, we used the Perseus software for statistical analysis to identify proteins interacting with SMAX1 and ΔSMAX1 only in one of the tested conditions. Firstly, in agreement with the previously described degradation of SMAX1, the abundance of the bait protein was clearly higher without treatment (mock) than after addition of *rac*-GR24 (Figure 6A,C), whereas the ΔSMAX1 level was stable under both conditions (Figure 6B,D). Hence, in the volcano plot based on not normalized intensity values, the SMAX1 protein was detected as significantly enriched in mock than after *rac*-GR24 treatment (Figure 6A), but it was not the case for ΔSMAX1. Also, in the volcano plot based on LFQ values, SMAX1 clearly separated from the other quantified proteins, although not crossing the significance line (Figure 6C).

A two-sided Student's *t* test applied on the LFQ intensity values resulted in the identification of one putative prey as significantly more associated with SMAX1 in the presence of *rac*-GR24, the exocyst complex component SEC10 (AT5G12370) (Figure 6C). Interestingly, this interaction was no longer differential in ΔSMAX1 TAPs (Figure 6D). On the contrary, DNAJ HOMOLOGUE 3 (ATJ3/AT3G44110) interacted significantly more with ΔSMAX1 in mock (Figure 6D), but copurified with SMAX1 in both conditions (Figure 6C). Thus, we can conclude that the mutation of the amino acid region in ΔSMAX1 affects not only the protein degradation, but also the composition of the protein complexes formed with the bait.

As degradation of the bait protein might hamper detection of some differential interactors, we implemented another normalization step, in which the intensity values of the bait were subtracted from those of the copurified proteins (Figure 6E,F). As this step greatly increased the number of preys identified as significantly more associated with SMAX1 in the presence of *rac*-GR24, a more stringent cutoff was used (FDR=0.01, S0=0.1). Even so, the total list of putative preys contained 57 proteins. Nevertheless, because background proteins were not subtracted, this list might still contain some false positives. Interestingly, except from SEC10, two other components of the exocyst complex, SEC15B and SEC8, were discovered as more associated with SMAX1 after *rac*-GR24 treatment (Supplemental Table

1), suggesting that the whole exocyst complex might be recruited to SMAX1 in the presence of the SL analog.

Concerning the known or predicted partners of SMAX1, TPL (AT1G15750) was identified as a putative interactor of ΔSMAX1, but not of SMAX1, in both tested conditions (Figure 6). Neither the KAI2 nor the SCF^{MAX2} complex components were detected among all proteins copurified with SMAX1 and ΔSMAX1.

DISCUSSION

The *smax1* loss-of-function has been reported to rescue the low seed germination and elongated hypocotyl of the *max2* mutant, but not to affect the SL-related phenotypes, such as the axillary shoot outgrowth (Stanga et al., 2013; Soundappan et al., 2015). Therefore, based on the genetic studies, SMAX1 has been proposed to function downstream of MAX2 and KAI2 to regulate responses to KAR and possibly KL (Stanga et al., 2013), but without biochemical evidence thus far.

Here, we used the Y2H method to obtain insights into the MAX2-KAI2-SMAX1 protein complex. We show that a direct interaction between SMAX1 and KAI2 occurs, in contrast to the D14-SMXL7 association, in the absence of *rac*-GR24. In SL signaling, binding and hydrolysis of *rac*-GR24 cause conformational changes in the D14 protein, subsequently allowing the interaction with MAX2 and possibly with the downstream targets, the SMXL6/7/8 proteins (Yao et al., 2016). Although KAR has been shown to bind to KAI2, a similar conformational change of the receptor has still not been observed (Guo et al., 2013). Hence, the interaction between KAI2 and SMAX1 might possibly occur independently of *rac*-GR24. The results of the Y2H GAL4 system suggested, however, that the formation of this complex might be improved by the addition of *rac*-GR24. Although validation by quantitative analysis is needed, for instance by using a β-galactosidase assay, it would be interesting to investigate whether the KAI2-SMAX1 interaction can be enhanced even more by the addition of KAR or $GR24^{ent\text{-}5DS}$.

A Förster resonance energy transfer (FRET) with fluorescence lifetime imaging microscopy (FLIM) study demonstrated the lack of direct interaction between MAX2 and SMXL7, suggesting that D14 might act as a bridge to facilitate the SMXL7-MAX2 association (Liang et al., 2016). Correspondingly, MAX2 has been reported previously to interact with KAI2 in the presence of *rac*-GR24 and KAR (Toh et al., 2014), whereas in our Y2H assay no MAX2-SMAX1 interaction had been found, possibly implying that KAI2 acts in a manner similar to that of D14 to connect these two proteins. As Y2H detects only direct interactions, another technique is advisable, such as yeast three-hybrid or co-immunoprecipitation (Co-IP) to investigate the MAX2-SMAX1 association.

In agreement with published data (Soundappan et al., 2015), we demonstrated the SMAX1 interaction with TPL by means of the Y2H assay, expanding the knowledge by showing that SMAX1 displays the similar repressor activity as SMXL6/7/8 (Wang et al., 2015). It remains to be determined, however, whether this transcriptional repression depends on the association with TPL/TPR proteins, as is the case for SMXL6/7/8 (Wang et al., 2015).

Further, we reveal for the first time that the SMAX1 protein is degraded in response to the *rac*-GR24 treatment both in *Arabidopsis* cell cultures and seedlings. We used a common SL analog *rac*-GR24 to mimic the KAR/KL responses, because it has been demonstrated to activate both D14- and KAI2-dependent signaling (Scaffidi et al., 2014). When compared to the complete SMXL7 degradation after addition of *rac*-GR24 (Chapter 3; Soundappan et al., 2015; Wang et al., 2015; Liang et al., 2016), the SMAX1 protein remained at a very low level over time. One possibility is that *rac*-GR24 is less active toward KAI2 than D14. Hence, the response to the specific enantiomer $GR24^{ent\text{-}5DS}$ or to KARs of the SMAX1 protein levels should be examined. In both rice and *Arabidopsis,* deletion of certain amino acids in D53 and SMXL6/7/8, respectively caused proteins to be resistant to *rac*-GR24–induced degradation (Jiang et al., 2013; Soundappan et al., 2015; Wang et al., 2015). Here, we provide evidence that this motif is also crucial for SMAX1 degradation and that the protein level did not decrease after addition of *rac*-GR24. Our results might point to a preserved role of this amino acid motif between SMAX1 and SMXL6/7/8.

To get more insights into the SMAX1 complex and discover novel components of the KAR/KL pathway, we carried out a TAP-MS analysis in cell cultures with two baits, SMAX1 and ΔSMAX1, in the absence (mock) and presence of the SL analog. The *rac*-GR24–induced degradation of SMAX1 in cell cultures revealed that the upstream signaling is active in this environment, whereas a partial complementation of the high seed germination phenotype of the *smax1* mutant indicated that the GS^{rhino} tag does not affect interactions with downstream pathway components. Three different approaches were used to analyze the TAP data. First, we filtered out from our list of copurified proteins those that were present in a list of nonspecific and sticky binders (Van Leene et al., 2015), revealing 23 putative preys of SMAX1 and three of ΔSMAX1. The second approach based on LFQ allowed the quantitative comparison between the samples to determine shifts in the protein complex stoichiometry in response to the treatment. As a result, we detected two proteins that interact with the bait in a *rac*-GR24–dependent manner: SEC10 that was significantly enriched in the SMAX1 TAPs in the presence of *rac*-GR24 and ATJ3 that was more associated with ΔSMAX1 in its absence (mock). Lastly, we introduced a normalization step based on the bait level that greatly increased the number of proteins significantly associated with SMAX1 after addition of *rac*-GR24, while only one outlier, the ribosomal protein S12/S23 family protein (AT5G02960) was found with ΔSMAX1 in the *rac*-GR24–treated condition. Nevertheless, the last analysis might contain some false positives, because the background proteins were not subtracted.

Notably, in none of our TAP-MS experiments we discovered either KAI2 or the core components of the SCF^{MAX2} complex. A possible explanation might be that transient or low-abundant interactions are missed because of the two-step purification process. From the known partners of SMAX1, the TPL/TPR proteins were identified only in the TAP experiments of ΔSMAX1. Our quantitative analysis of SMXL7 and ΔSMXL7 TAPs implied that the mutated protein version had a higher affinity toward TPL than the wild type (Chapter 3), possibly one of the reasons no TPL/TPR could be detected in the TAP experiments with SMAX1, but only with ΔSMAX1 as bait.

Regarding the novel SMAX1 interactors, a combination of the different methods to analyze the TAP data might reveal putative preys that would be interesting to investigate in the future. Our first candidates would be components of the exocyst complex, such as SEC10, because it interacts with SMAX1, but not with ΔSMAX1, in the presence of *rac*-GR24 only. In addition, three other members of this complex, SEC15B, SEC3A, and SEC5A have been discovered in our qualitative TAP analysis and two proteins, SEC15B and SEC8, after normalization on the bait level. The exocyst complex, involved in vesicle trafficking, participates in the cell morphogenesis of growing pollen tubes, root hairs, and etiolated hypocotyls (Cole et al., 2005; Wen et al., 2005; Hala et al., 2008), but also play a role in PIN1 and PIN2 recycling (Drdova et al., 2013) and cytokinesis (Fendrych et al., 2010). Considering the not overlapping localization pattern of SMAX1 (nucleus) and of the subunits of the exocyst complex (plasma membrane) (Chong et al., 2010; Fendrych et al., 2013), direct interactions are not expected. Probably, *rac*-GR24–induced degradation of SMAX1 might actively trigger exocytosis in the cell, but the exact function of this process in the *rac*-GR24 responses remains to be determined.

Another interesting candidate is ATJ3 that was identified as significantly more associated with ΔSMAX1 in mock conditions, whereas it was present in both conditions in the SMAX1 TAPs. ATJ3 was detected in all the ΔSMAX1 samples treated with *rac*-GR24, however the protein level was much lower than in mock, suggesting that this interaction is weakened in the presence of the SL analog. Degradation of SMAX1 might possibly obscure the dynamic association with ATJ3, because reduced bait protein level results in the decreased levels of all the proteins copurified with it. ATJ3 is a molecular chaperone of the HSP40 proteins that are ubiquitously expressed in various plant tissues (Shen et al., 2011). ATJ3 has been reported to interact physically with and repress the activity of the SHORT VEGETATIVE PHASE (SVP) transcriptional repressor involved in the control of floral meristems (Shen et al., 2011) and of the Salt Overly Sensitive2-Like Protein Kinase5 (PKS5) kinase regulating the plasma membrane H^+-ATPase (PM H^+-ATPase) action (Yang et al., 2010). Recent studies have also demonstrated that ATJ3 is implicated in seed

development, germination, and abiotic stress tolerance, possibly by regulating the *ABA-INSENSITIVE 3* (*ABI3*) gene expression (Salas-Muñoz et al., 2016). Thus, we can speculate that ATJ3 might be a linker integrating the KAR/KL and ABA pathways for seed germination, but first the SMAX1-ATJ3 interaction has to be validated.

In summary, we have provided the biochemical evidence for the previous genetic predictions of the interaction network between SMAX1 and the known core components of the KAR/KL pathway. In addition, we have shown that the TAP data can be analyzed in several ways to deliver information about both stable and dynamics interactions in the complex. We believe that our TAP data contain many interesting protein candidates that might help to further resolve the KAI2-mediated signaling.

MATERIALS AND METHODS

Molecular cloning

All cloning was carried out by Gateway® recombination (Thermo Fisher Scientific). For the construction of ΔSMAX1, the Arg (R) at the amino acid position 670 of pDONR207-SMAX1 was mutated into a Thr (T) and the next five amino acids (Gly-Lys-Thr-Ala-Leu) were deleted with the Spliced Overlap Extension PCR (SOE-PCR) (Higuchi et al., 1988). All primers are listed in Supplemental Table 2. TPL-N was previously described (Cuéllar Pérez et al., 2014).

Cell cultures transformation

Wild-type *Arabidopsis thaliana* (L.) Heynh. (Landsberg *erecta* [L*er*-0] cell suspension cultures (PSB-D) were transformed as described (Van Leene et al., 2007) through cocultivation with *Agrobacterium tumefaciens*. Cell cultures were maintained in 50 ml MSMO medium at 21°C with gentle agitation (130 rpm) in continuous dark and subsequently transferred to a light/dark (16 h/8 h) regime. Three weeks after transfer, protein expression was analyzed (see below). Cultures in which the bait protein was expressed were upscaled for TAP.

Western blot analysis

Proteins were extracted from cell cultures expressing *35S::GSrhino-SMAX1* and *35S::GSrhino-ΔSMAX1* 3 days after subculturing or from *proSMAX1::SMAX1-GSrhino* seedlings grown for 6 days in liquid half-strength Murashige and Skoog (½MS) medium with 1% (w/v) sucrose, treated with 1 µM *rac*-GR24 or acetone (mock). Cell material was harvested before and at six time points after treatment (15 min, 30 min, 45 min, 1 h, 6 h, and 24 h). Proteins were extracted with the TAP extraction buffer and concentrations were determined by the Bradford assay (Bio-Rad). Differences in protein levels were detected with Western blotting and GS tag-targeted peroxidase anti-peroxidase (PAP) antibodies (Sigma-Aldrich) and chemiluminescent substrates from the Western Lightning® Plus ECL kit (PerkinElmer). Anti-tubulin antibodies (Sigma-Aldrich) were used to determine equal loading. The Precision Plus Protein™ Dual Color Standards (Bio-Rad) was used as protein size marker.

Tandem-affinity purification

TAP was done as described (Van Leene et al., 2015) with some modifications. Cell culture material was harvested after 10 min of treatment with 1 µM *rac*-GR24 or 0.01% acetone. Protein interactors were identified by MS with an LTQ Orbitrap Velos mass spectrometer. In total, for each construct (N- and C-

terminally tagged SMAX1 and ΔSMAX1), two repeats were done in each condition. Proteins with at least two matched high-confident peptides were retained. Background proteins were filtered out based on the occurrence frequency of the copurified proteins in a large data set containing 543 TAP experiments with 115 different baits (Van Leene et al., 2015). For quantitative TAP analysis, MS spectra were searched with the MaxQuant software (version 1.4.1.2) (Cox and Mann, 2008) and relative, label-free proteins were quantified by means of the MaxLFQ algorithm. The MaxQuant output file was further analyzed with the Perseus software (version 1.5.3.2) as described in detail in Chapter 3. All the imputed missing values can be found in the Supplemental dataset 3. To normalize the bait level, the intensity of the SMXL7 was subtracted from the intensity value of each protein. A Student's *t* test was applied to determine the statistical outliers between the 'mock' and 'treatment' groups. The multiple hypothesis testing problem was corrected with a permutation based FDR (0.05 or 0.01) and the threshold value S0 was set at 0.1 by default or 0.5.

Yeast two-hybrid analysis

Y2H analysis was carried out as described (Cuellar et al., 2013) in two independent repeats. The *Saccharomyces cerevisiae* EGY48 strain (Estojak et al., 1995) was cotransformed with the bait and prey by the polyethylene glycol (PEG)/lithium acetate method. Transformants were selected on Synthetic Defined media containing galactose and raffinose (SD Gal/Raf) and lacking Ura, Trp, and His (Clontech). Three individual colonies were grown overnight in liquid cultures at 30°C and 10- and 100-fold dilutions were dropped on control media (SD Gal/Raf-Ura-Trp-His) and selective media with the addition of X-Gal (Duchefa).

Seed germination assay

Seeds were stored at least 6 weeks after harvest before their use for the assay. Seeds were distributed in 96-well plates containing 100 mM 4-(2-hydroxyethyl)-1-piperazineethanesulfonic acid (HEPES) buffer and Preservative for plant tissue cultures (Nalgene) with either 10 µM *rac*-GR24 or acetonitrile. Plates were incubated for 4 days at 24°C in the dark or in continuous light for a control. Germination was indicated by emergence of the radicle tip through the endosperm. The *max2-1* (Stirnberg et al., 2007) and *smax1-2* (Stanga et al., 2013) mutants have been described previously.

Subcellular localization analysis

The subcellular localization of SMAX1 was tested by transient expression of *proSMAX1::SMAX1-GFP* in *N. benthamiana* leaves by means of the *Agrobacterium*-mediated transformation or in 4-day-old *Arabidopsis* seedlings stably expressing *proSMAX1::SMAX1-GFP.* Fluorescence was detected with a Zeiss LSM5 Exiter confocal microscope.

Transient expression assay

Transient expression assays were done as described (Vanden Bossche et al., 2013). Protoplasts prepared from a Bright Yellow-2 tobacco cell culture were cotransfected with a reporter plasmid containing the firefly luciferase (fLUC) reporter gene driven by the LOX3 promoter (Pauwels et al., 2008), a normalization construct expressing Renilla luciferase (rLUC) under control of the 35S promoter (De Sutter et al., 2005), and an effector construct, SMAX1 under control of the 35S promoter. The p2GW7-GUS effector plasmid was used as a control. fLUC and rLUC activities were determined with the Dual-Luciferase reporter assay system (Promega). Variations in transfection efficiency and technical error were corrected by normalization of the fLUC by the rLUC activities. All transactivation assays were carried out in an automated experimental set-up with eight biological replicates for each effector combination.

SUPPLEMENTARY DATA

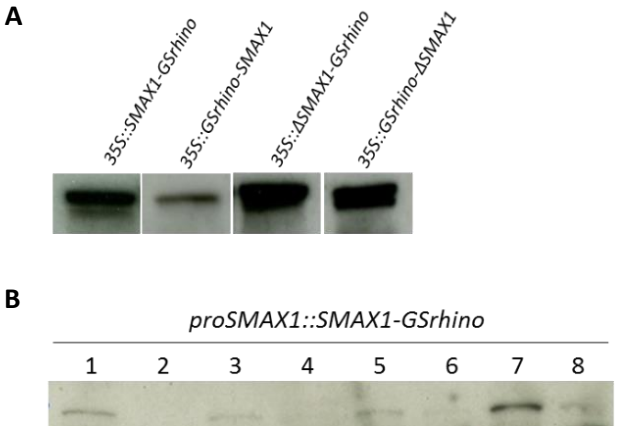

Supplemental Figure 1. Expression of GS^{rhino}-tagged SMAX1 in *Arabidopsis* cell cultures and young seedlings. (A) Protein levels of N- and C-terminally tagged SMAX1 and ΔSMAX1 in *Arabidopsis* cell cultures analyzed by means of immunoblotting. (B) Protein levels tested in eight independent transgenic lines transformed with *proSMAX1::SMAX1-GSrhino*. Detection was done with anti-GS antibodies. Molecular mass: 108.7 kDa for SMAX1; 21.9 kDa for GS^{rhino}.

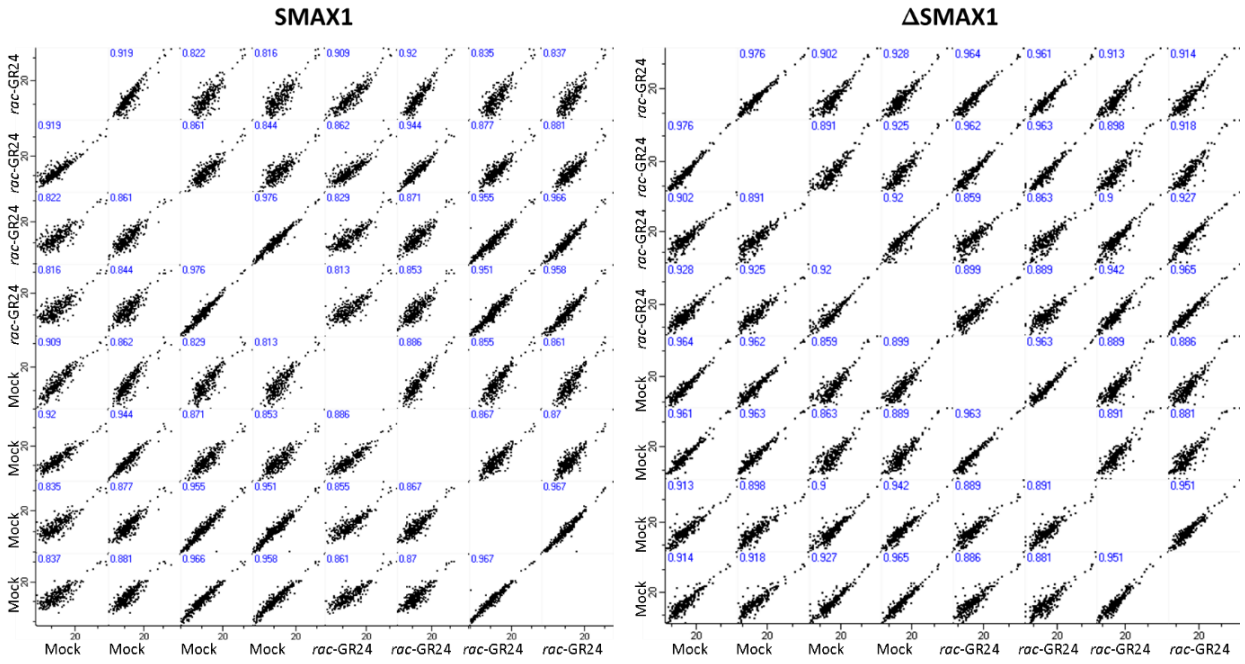

Supplemental Figure 2. Pearson correlation coefficients for SMAX1 and ΔSMAX1 N- and C-terminally tagged with the GS^{rhino} tag in samples treated without (mock) or with *rac*-GR24. The matrix of 56 correlation plots reveals high correlations between the LFQ intensities within the replicates; SMAX1 0.813-0.976, ΔSMAX1 0.859-0.976

Supplemental Table 1. Proteins found significantly more associated with SMAX1 upon *rac*-GR24 treatment after intensity-based normalization for the bait level.

AGI	Protein	-LOG(*P* value)	Fold change
AT2G01350	QPT, quinolinate phoshoribosyltransferase	4.521	3.060
AT3G18780	ACT2, actin 2	3.948	1.948
AT4G02350	SEC15B, Exocyst complex component 15B	3.827	2.838
AT5G58410	HEAT/U-box domain-containing protein	3.803	3.564
AT3G56130	Biotin/lipoyl attachment domain-containing protein	3.405	2.249
AT1G43170	RP1, ribosomal protein 1	3.220	2.671
AT4G09800 AT1G34030 AT1G22780	RPS18C, S18 ribosomal protein Ribosomal protein S13/S18 family PFL, Ribosomal protein S13/S18 family	3.161	2.288
AT1G02080	Transcription regulators	3.029	2.702
AT5G60670 AT3G53430 AT2G37190	Ribosomal protein L11 family protein	3.022	2.200
AT4G23540	ARM repeat superfamily protein	2.999	3.108
AT2G17670	Tetratricopeptide repeat (TPR)-like superfamily protein	2.945	2.530
AT1G23410 AT3G62250 AT2G47110 AT3G52590	Ribosomal protein S27a UBQ5,ubiquitin 5 UBQ6,ubiquitin 6 UBQ1,ubiquitin extension protein 1	2.866	2.746
AT3G53870 AT2G31610 AT5G35530	Ribosomal protein S3 family protein	2.863	1.824
AT5G26360	TCP-1/cpn60 chaperonin family protein	2.826	2.846
AT3G13470 AT1G55490 AT5G56500	TCP-1/cpn60 chaperonin family protein CPN60B,chaperonin 60 beta TCP-1/cpn60 chaperonin family protein	2.797	2.232
AT3G10380	SEC8, subunit of exocyst complex 8	2.722	3.295
AT5G24710	Transducin/WD40 repeat-like superfamily protein	2.694	2.287
AT4G33865 AT3G44010 AT3G43980	Ribosomal protein S14p/S29e family protein	2.694	2.475
AT3G23990 AT2G33210	HSP60, heat shock protein 60 Heat shock protein 60-2	2.671	2.510
AT3G04400 AT2G33370 AT1G04480	Ribosomal protein L14p/L23e family protein	2.637	2.476

AT5G25460 AT5G11420	DGR2, L-GALL RESPONSIVE GENE 2 DUF642, Protein of unknown function	2.608	3.033
AT5G07090 AT2G17360 AT5G58420	Ribosomal protein S4 (RPS4A) family protein	2.605	2.029
AT2G39260	Regulator of nonsense transcripts UPF2	2.555	2.749
AT3G22310	PMH1, Putative mitochondrial RNA helicase 1	2.547	2.478
AT2G37270	RPS5B, Ribosomal protein 5B	2.503	2.249
AT2G39725	LYR family of Fe/S cluster biogenesis protein	2.490	3.185
AT3G09810	IDH-VI, isocitrate dehydrogenase VI	2.404	2.863
AT2G20190	CLASP, CLIP-associated protein	2.399	2.568
AT5G16390	CAC1, Chloroplastic acetylcoenzyme A carboxylase 1	2.393	2.299
AT2G35630	MOR1, ARM repeat superfamily protein	2.367	2.978
AT5G55190 AT5G20010	RAN3, RAN GTPase 3 RAN-1,RAS-related nuclear protein-1	2.322	2.522
AT1G71270 AT1G71300	Vps52 / Sac2 family	2.313	2.554
AT3G50590	Transducin/WD40 repeat-like superfamily protein	2.305	2.155
AT2G46900	Basic helix-loop-helix, Nulp1-type	2.270	2.913
AT4G25630 AT5G52470	FIB2, Fibrillarin 2 FIB1, Fibrillarin 1	2.140	2.412
AT5G12370	SEC10, exocyst complex component 10	2.057	2.820
AT4G02030	Vps51/Vps67 family protein	2.022	2.887
AT5G66470	RNA binding, GTP binding	2.006	2.616
AT1G36180	ACC2, acetyl-CoA carboxylase 2	1.999	2.757
AT3G14990	Class I glutamine amidotransferase-like superfamily protein	1.920	2.822

Putative prey proteins found significantly more associated with SMAX1 in the presence than in the absence (mock) of *rac*-GR24 after normalization on the bait level. Student's *t* test analysis results from the Perseus software on a set of four independent TAP experiments on both mock and *rac*-GR24 treatment. FDR=0.01, S0=0.1

Supplemental Table 2. All primers used in this study.

ID		Sequence	Use
SMAX1	Fw	GGGGACAAGTTTGTACAAAAAAGCAGGCTCAATGAGAGCTGGTTTAAGTACG	Cloning
SMAX1	Rev	GGGGACCACTTTGTACAAGAAAGCTGGGTATCATACTGCCAAAGTAATAG	Cloning
ΔSMAX1	Fw	GGAGATGGAAATTCTAGTTTCACTGATAAGATTGCGGAAACTGTTAAG	Mutagenesis
ΔSMAX1	Rev	CTTAACAGTTTCCGCAATCTTATCAGTGAAACTAGAATTTCCATCTCC	Mutagenesis
proSMAX1	Fw	CGTTACCAAAAGGGGACATC	Cloning
proSMAX1	Rev	CATCGTTCTTCGTTTACTTCCA	Cloning
MAX2	Fw	GGGGACAAGTTTGTACAAAAAAGCAGGCTCAATGGCTTCCACTACTCTCTCC	Cloning
MAX2	Rev	GGGGACCACTTTGTACAAGAAAGCTGGGTATCAGTCAATGATGTTGCGGCTGTTC	Cloning
KAI2	Fw	GGGGACAAGTTTGTACAAAAAAGCAGGCTCCACCATGGGTGTGGTAGAAGAAGCTC	Cloning
KAI2	Rev	GGGGACCACTTTGTACAAGAAAGCTGGGTCTCACATAGCAATGTCATTACGAAT	Cloning

Supplemental dataset 1. Overview of all proteins identified in SMAX1 TAP experiments.

Supplemental dataset 2. Overview of all proteins identified in ΔSMAX1 TAP experiments.

Supplemental dataset 3. The list of all proteins copurified with SMAX1 and ΔSMAX1 with their corresponding LFQ and intensity values before and after imputation of missing values in mock and after addition of *rac*-GR24.

All Supplemental datasets are available via

https://www.dropbox.com/sh/u7uljams4eisy2l/AACnAnu7CYZj0xCh6uudjBlMa?dl=0

Chapter 7

Unraveling the MAX2 Network in *Arabidopsis thaliana*: Identification of the Protein Phosphatase PAPP5 as a Novel MAX2 Interactor

Sylwia Struk[1,2*], Carolien De Cuyper[1,2*], Lukas Braem[1,2,3,4], Anse Jacobs[1,2,3,4], Alan Walton[1,2,3,4], Annick De Keyser[1,2], Sara Coppin[1,2], Stephen Depuydt[1,2], Lam Dai Vu[1,2,3,4], Ive De Smet[1,2], François-Didier Boyer[5], Dominique Eeckhout[1,2], Geert Persiau[1,2], Kris Gevaert[3,4], Geert De Jaeger[1,2] and Sofie Goormachtig[1,2]

[1]Department of Plant Biotechnology and Bioinformatics, Ghent University, 9052 Ghent, Belgium,
[2]VIB, Center for Plant Systems Biology, VIB, 9052 Ghent, Belgium,
[3]Department of Biochemistry, Ghent University, 9000 Ghent, Belgium,
[4]VIB, Center for Medical Biotechnology, 9000 Ghent, Belgium
[5]Institut National de la Recherche Agronomique, Institut Jean-Pierre Bourgin, Versailles, France

Author contributions: C.D.C. and S.S. equally contributed to this work. C.D.C. performed all experiments, except MAX2 complementation assays, Y2H, BiFC, germination assay which were done by S.S., and the GFP-trapping experiments by S.S. and A.W., hypocotyl assay analyzed by A.J.. A.D.K., A.J., S.C., L.B., S.D., D.E. and G.P. helped with the acquisition of the data. L.D.V. and I.D.S. performed phosphopeptide enrichment experiment. F.D.B. kindly provided the synthetic strigolactone analog rac-GR24. S.G., K.G. and G.D.J. supervised the project and contributed to writing of the manuscript.

ABSTRACT

The F-box protein MORE AXILLARY GROWTH 2 (MAX2) is a central component in the signaling cascade of the plant hormone strigolactone as well as of the chemical compounds karrikins and, so far unknown karrikin metabolites that control seed germination. As proteins that function in the same signal transduction pathway often occur in large protein complexes, we aimed at resolving and discovering new players of the MAX2 protein network by tandem affinity purification (TAP). General SCF complex components and members of the COP9 signalosome, as well as 28 new MAX2 interactome proteins were copurified. Here, we report on the identification of a novel interactor of MAX2, PHYTOCHROME ASSOCIATED PROTEIN PHOSPHATASE 5 (PAPP5), a type 5 serine/threonine protein phosphatase. PAPP5 was characterized in detail in order to understand its role in the two different MAX2 mediated signaling pathways. Biochemical as well as genetic evidence has shown that PAPP5 plays a specific role in karrikin responses, i.e. being involved in MAX2 dependent seed germination but not in the strigolactone controlled processes such as shoot branching.

INTRODUCTION

F-box proteins represent one of the largest and most heterogeneous superfamilies in plants, modulating development, hormone signaling as well as defense pathways (Stefanowicz et al., 2015). All of them are characterized by an N-terminal conserved F-box motif and a C-terminal target-binding domain, which confers substrate specificity to the Skp1-Cullin-F-box (SCF) class of E3 ligases that ubiquitinate their substrates, typically to target them for proteolysis by the 26S proteasome (Vierstra, 2009; Xiao & Jang, 2000).

The F-box protein MORE AXILLARY GROWTH 2 (MAX2) is a central component in the signal transduction pathway of strigolactones as well as of smoke derived karrikins and other, so far unknown KARRIKIN INSENSITIVE 2 (KAI2) ligand (Nelson et al., 2011). Strigolactones are hormonal signals that affect multiple aspects of plant architecture, such as shoot branching, whereas karrikin/KAI2 ligand molecules activate seed germination and regulate early seedling development (Flematti et al., 2009; Al-Babili & Bouwmeester, 2015; Conn & Nelson, 2015). Apart from sharing MAX2, perception of both molecules involves an α/β hydrolase, with DWARF 14 (D14) shown to be necessary for strigolactone responses, whereas its paralog KAI2 required for karrikin induced effects in *Arabidopsis thaliana* (Arite et al., 2009; Hamiaux et al., 2012). As *kai2* mutants display developmental defects and karrikins enhance germination and seedling photomorphogenesis of non-smoke prone species too, KAI2 was proposed to perceive both smoke-derived karrikins signals as well as so far unknown, endogenous KAI2 ligand (Nelson et al., 2012; Conn & Nelson, 2015). Phenotypes observed in *max2* mutants can thus be strigolactone and/or karrikin/KAI2 ligand dependent. Indeed, *max2* mutant resembles combined phenotypes of *d14* and *kai2*, resulting from a loss of both D14 and KAI2 dependent signaling (Soundappan et al., 2015). Additionally, the synthetic and broadly used strigolactone analog *rac*-GR24 was shown to be an equimolar racemic mixture of a natural strigol-like molecule $GR24^{5DS}$ that activates the D14 dependent signal transduction, and its unnatural enantiomer $GR24^{ent\text{-}5DS}$ that initiates KAI2 specific signaling (Scaffidi et al., 2014). In this way, also *rac*-GR24 treatment provides information on the signaling cascades of both strigolactone and karrikin/KAI2 ligand molecules.

Upon perception, plants need to activate specific signaling cascades in order to trigger particular outcomes. A first level of discrimination is provided by the SUPPRESSOR OF MAX2 1 (SMAX1) LIKE (SMXL) proteins in *Arabidopsis* and their ortholog D53 in *Oryza sativa* (rice) (Jiang et al., 2013; Stanga et al., 2013; Zhou et al., 2013), which are known as negative regulators that are degraded in order to further activate downstream responses (Jiang et al., 2013; Stanga et al. 2013; Zhou et al., 2013). Different SMXL family members are targeted for degradation depending after strigolactone or karrikin/KAI2 ligand signaling (Stanga et al., 2013, 2016; Waters et al., 2014), i.e. members of subclade

1, SMAX1 and SMXL2, are involved in karrikin/KAI2 ligand pathway, whereas subclade 4 proteins, SMXL6, SMXL7 and SMXL8 mediate strigolactone signaling. Subclade 2 and 3 members, SMXL3, SMXL4 and SMXL5 function in strigolactone- and karrikin- independent phloem development (Wallner et al., 2017). D53 of rice was shown to group within the SMXL6, SMXL7 and SMXL8 phylogenetic clade (Soundappan et al., 2015). How SMXL/D53 proteins provide discrimination between both pathways is currently unknown because the downstream signaling cascade has not been revealed. Yet, a role in unfolding or remodeling protein complexes and/or a role as transcriptional repressors can be expected (Jiang et al., 2013; Stanga et al., 2013; Zhou et al., 2013; Soundappan et al., 2015; Wang et al., 2015; Liang et al., 2016).

Based on various biochemical and structural studies, it has been proposed that upon strigolactone perception D14 interacts with the SCF^{MAX2} complex and SMXL proteins, which are further targeted for ubiquitination (Jiang et al., 2013; Stanga et al., 2013; Zhou et al., 2013). Here, we aimed at identifying additional proteins belonging to MAX2 complexes using tandem affinity purification (TAP). TAP allows to get a general insight into all members of a protein complex in near physiological conditions (Puig et al., 2001). Thanks to this approach we have greatly expanded our knowledge of the MAX2 interactome. Moreover, we identified a novel interactor of MAX2, PHYTOCHROME ASSOCIATED PROTEIN PHOSPHATASE 5 (PAPP5), as being specifically involved in MAX2-KAI2 mediated pathway.

RESULTS

The MAX2 pathway is functional in *Arabidopsis* cell suspension cultures

Cell cultures were selected to perform the TAP experiments, because of the high protein yield and the possibility to perform trigger-based studies (Van Leene et al., 2015). We previously demonstrated that the early steps of both strigolactone and karrikin/KAI2 ligand signaling are active in the cell cultures because treatment with *rac*-GR24 induced the degradation of SMXL7 (Chapter 3) and SMAX1 (Chapter 6), respectively. Furthermore, when wild-type cell cultures were treated with *rac*-GR24 for various time points, the expression level of *BRC1* was rising over the course of the treatment, reaching a tenfold increase in 5 hours (Figure 1), indicating that downstream strigolactone signaling is active as well. The *BRC1* is not direct target of SMXL7 repression therefore, the increased *BRC1* expression is observed only after 5h while the degradation of SMXL7 starts after 15 min of treatment with *rac*-GR24 (Chapter 3). As above observations could not be made in mock treated conditions, this data demonstrates that in cell cultures, a fully operational MAX2 signaling cascade, guided by either the KAI2 and D14 receptor is present.

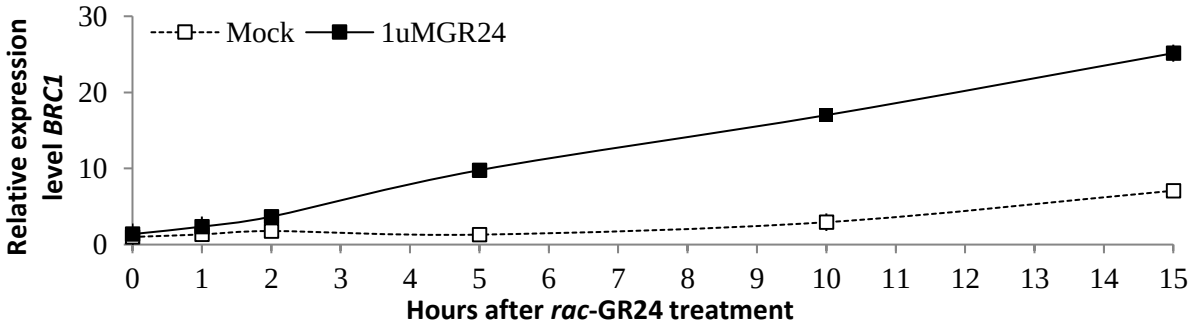

Figure 1. *Arabidopsis* cell suspension cultures are responsive to *rac*-GR24. The expression of the *BRC1* gene was assessed by qRT-PCR for its responsiveness to treatment with 1 µM *rac*-GR24 (solid line) compared to mock acetone treatment (dotted line). The experiment was repeated three times with comparable results and the total mean of all biological repeats is presented. Data and error bars represent means ± SE.

Tandem affinity purification of the MAX2 complex

The MAX2 protein complex in *Arabidopsis* cell cultures was resolved by means of TAP, as described by Van Leene et al., 2007. In brief, a translational fusion was made between the protein of interest, known as the bait, and a double affinity tag. Here, *Arabidopsis* cell suspension cultures were stably

transformed with the protein G/streptavidin-binding peptide (GS)-tagged bait protein under control of the 35S promoter, using *Agrobacterium tumefaciens*-mediated cocultivation (Van Leene et al., 2008). Only the N-terminal fusion construct *35S::GS-MAX2* was used in our analysis as preliminary TAP experiments using the C-terminal fusion construct *35S::MAX2-GS* did not yield any interactors. This N-tagged MAX2 protein was shown to be fully functional as it could complement both the shoot branching and lateral root density phenotype of *max2-1* mutants (Figure 2A,C). Additionally, the lateral root density of *max2-1* mutants, expressing the *35S::GS-MAX2* construct decreased upon *rac*-GR24 treatment, showing an equal sensitivity to Col-0 (Figure 2C).

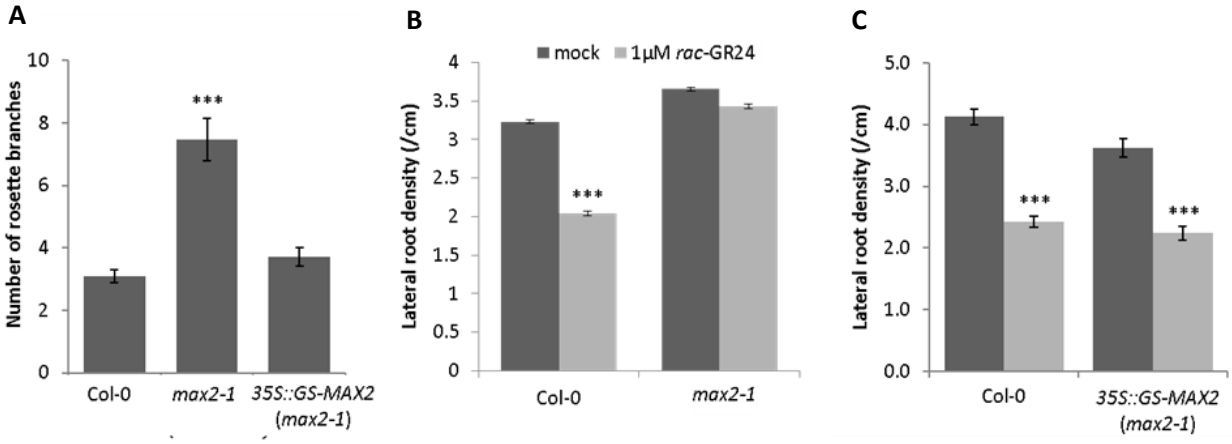

Figure 2. Shoot branching and lateral root density of *max2-1* overexpressing GS-MAX2. (A) Rosette branches of Col-0, *max2-1* and *35S::GS-MAX2* (*max2-1*) lines were counted after 50 days of growth (n = 18). (B-C) Lateral root density of Col-0, *max2-1* and *35S::GS-MAX2* (*max2-1*) lines was analyzed in 9-day-old plants (n = 45). Asterisks indicate statistical significant differences between genotypes (A) or treatments (B-C) (*** $P < 0.001$, Student's t test (A) Poisson regression model (B-C)). The experiments were repeated three times and the total mean of all biological repeats is presented. Data and error bars represent means ± SE.

To allow binding but not degradation of target proteins, we created a truncated MAX2 protein version, i.e. MAX2ΔFBOX, of which the first 60 amino acids were deleted to prevent the interaction with SKP1, and as a consequence with all other components of the SCF E3 ligase complex (Figure 3).

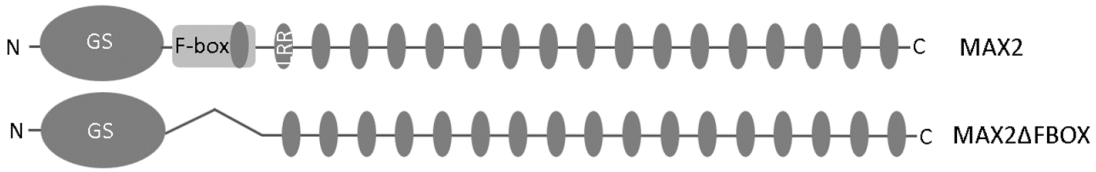

Figure 3. MAX2 baits used in TAP experiments. Schematic representation showing the wild-type (693 AA) and truncated (633 AA) versions of MAX2. GS = protein G, streptavidin-binding peptide tag, LRR = leucine-rich repeat.

The expression of the baits in cell cultures were checked by immunoblotting and high protein levels were detected for both constructs (Supplemental Figure 1). Because cell cultures were available that were grown in both long day conditions (PSB-L) as well as in continuous dark (PSB-D), to enlarge the possibility to obtain interesting interactors of MAX2, we executed the TAP analysis in both conditions. In addition, cell cultures were treated with either 1 µM *rac*-GR24 or 0.01% acetone (mock). We selected 5h treatment because the *BRC1* expression level increased at this time point in cell cultures treated with the strigolactone analog (Figure 1). Then cell material was harvested and the MAX2 protein complex was purified.

Table 1. Overview of prey proteins identified by TAP with MAX2 (A) and MAX2ΔFBOX (B) as bait.

A

AGI	Protein	PSB-L		PSB-D	
		Mock	*rac*-GR24	Mock	*rac*-GR24
AT4G34210.1	ASK11	1	1	0	0
AT4G34470.1	ASK12	0	0	0	1
AT3G60010.1	ASK13	2	2	2	1
AT5G42190.1	ASK2	2	2	2	2
AT1G20140.1	ASK4	2	2	2	2
AT5G14250.1	COP13	0	1	2	2
AT1G02090.1	COP15	0	0	1	1
AT5G42970.1	COP8	1	0	2	2
AT3G61140.1	CSN1	0	0	2	2
AT1G22920.1	CSN5A	0	1	2	2
AT5G56280.1	CSN6A	0	0	2	2
AT4G26430.1	CSN6B	0	0	1	1
AT4G02570.1	CUL1	2	2	2	2
AT4G39980.1	DHS1	0	0	1	0
AT3G59890.1	dihydrodipicolinate reductase	0	0	1	1
AT3G49250.1	DMS3	0	0	1	0
AT2G26990.1	FUS12	0	1	2	2
AT2G42620.1	MAX2	2	2	2	2
AT2G42810.1	**PAPP5**	**0**	**0**	**2**	**0**
AT3G06483.1	PDK	0	0	1	0
AT1G75950.1	SKP1	2	2	2	2
AT4G16340.1	SPK1	0	0	1	0
AT5G54550.1	unknown	0	0	2	2

B

AGI	Protein	PSB-L		PSB-D	
		Mock	*rac*-GR24	Mock	*rac*-GR24
AT5G36230.1	ARM repeat protein	0	0	0	1
AT1G60620.1	ATRPAC43	0	0	0	1
AT4G11260.1	ATSGT1B	1	0	1	2
AT3G10270.1	GYRB1	0	0	0	1
AT5G12030.1	HSP17.6	0	0	1	0
AT3G05780.1	LON3	0	0	0	1
AT2G42620.1	MAX2	2	2	2	2
AT5G35590.1	PAA1	0	0	0	1
AT2G42810.1	**PAPP5**	**0**	**0**	**2**	**2**
AT3G22480.1	PFD2	1	2	2	2
AT5G49510.1	PFD3	2	1	2	2
AT3G25230.1	ROF1	0	0	0	2
AT2G15430.1	RPB35.5A	0	0	1	2
AT4G28470.1	RPN1B	0	0	0	1
AT4G37460.1	SRFR1	0	0	0	1
AT5G25270.1	Ubiquitin-like protein	0	0	1	2

TAP experiments were performed in long-day (PSB-L) or continuous dark conditions (PSB-D), using cell cultures expressing *35S::GS-MAX2* (A) or *35S::GS-MAX2ΔFBOX* (B), treated mock or with 1 µM *rac*-GR24. Prey proteins were identified with peptide-based homology analysis of mass spectrometry data. Background proteins were withdrawn based on the frequency of occurrence of copurified proteins in a large GS TAP data set (Van Leene et al., 2015). The number indicates the times the prey was identified in 2 experiments with the bait protein. Abbreviations: AGI, Arabidopsis Genome Identifier; A detailed list can be found in Supplemental dataset 1.

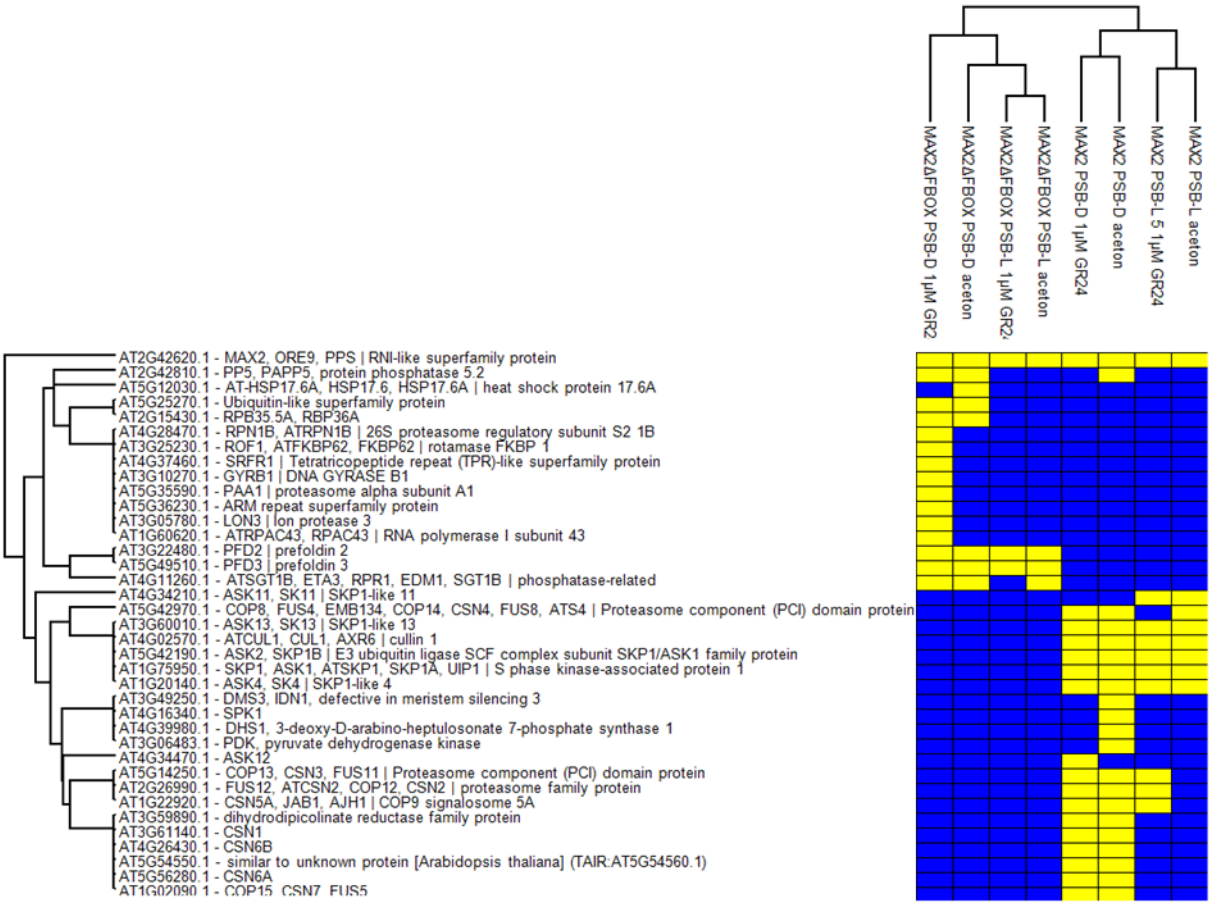

Figure 4. TAP of the MAX2 protein complex. Heatmap representing different members of the MAX2/MAX2ΔFBOX protein complex in different conditions. TAP experiments were performed in continuous dark (PSB-D) or in long-day (PSB-L) conditions. Cell cultures overexpressing the *35S::GS-MAX2* or the *35S::GS-MAX2ΔFBOX* constructs were treated mock or with 1µM *rac*-GR24 for 5 hours. Colors indicate presence (yellow) or absence (blue) of the protein.

In total, 37 proteins were identified as potential preys of MAX2 (Table 1, Supplemental dataset 1, and Figure 4). Proteins were retrieved with a role in seed germination (AT3G25230/ROF1 and AT4G11260/ ATSGT1B), cell cycle (AT3G10270/GYRB1), abiotic/biotic stress responses (AT3G25230/ROF1, AT3G05780/LON3, AT4G37460/SRFR1, AT4G11260/ATSGT1B, AT5G12030/HSP17.6, AT4G39980/DHS1), light signaling (AT2G42810/PAPP5), hormone signaling (AT3G25230/ROF1 and AT4G11260/ATSGT1B) or leaf and stomata development (AT2G15430/RBP36A). Two proteins with an unknown function were isolated as well (AT5G25270 and AT5G54550). Based on gene-ontology categories, using the PANTHER classification system, most MAX2 copurified proteins are involved in metabolic processes, such as protein modification, protein complex assembly, protein folding, proteolysis and translation. As the F-box protein MAX2 is known to be part of an E3 ligase, general SCF complex and proteasomal proteins (AT5G35590/PAA1, AT4G34210/ASK11, AT3G60010/ASK13,

AT4G02570/CUL1, AT1G20140/ASK4, AT1G75950/SKP1, AT4G34470/ASK12, AT5G42190/SKP1B) were indeed expected to be identified. Moreover, also seven out of the nine members of the CONSTITUTIVE PHOTOMORPHOGENIC 9 (COP9) signalosome (CSN) (Rozen et al., 2015) were copurified with MAX2 (AT3G61140/CSN1, AT2G26990/CSN2, AT5G14250/CSN3, AT5G42970/CSN4, AT1G22920/CSN5A, AT5G56280/CSN6A, AT4G26430/CSN6B, AT1G02090/CSN7). As SKP1 and CUL1 were not identified in the MAX2ΔFBOX complex, the deletion present in that construct indeed seemed to block the interaction with the SCF complex. No peptides could be detected of SMXL proteins, which are known targets of MAX2 for ubiquitination and 26S- proteasomal degradation (Stanga et al., 2013; Soundappan et al., 2015). Furthermore, in our experimental set-up, the MAX2-associated D14 and KAI2 proteins could also not be recovered (Kagiyama et al., 2013; Toh et al., 2014; Zhao et al., 2015).

Identification of the PAPP5 protein

We further focused on the interaction between MAX2 and the PHYTOCHROME-ASSOCIATED PROTEIN PHOSPHATASE (PAPP5). The *PROTEIN PHOSPHATASE 5* (*PP5*) gene in *Arabidopsis* and *Solanum lycopersicum* (tomato) was shown to be alternatively spliced, resulting in two protein isoforms that are differently localized in the cell (de la Fuente van Bentem et al., 2003). One of both transcripts is translated into a larger PP5 isoform as an additional exon that encodes for two putative transmembrane domains is present. Studies in tomato demonstrated that this larger isoform is an integral membrane protein which is targeted to the endoplasmic reticulum and nuclear envelope, whereas the smaller isoform is soluble and localized in the nucleus and cytoplasm (de la Fuente van Bentem et al., 2003). This last isoform is referred to as PAPP5 as it was shown to interact with phytochromes, thereby increasing their stability and activity (Ryu et al., 2005). Here, we have evidence that the last splice variant is present in our dataset, as a unique peptide of AT2G4281.1 could be identified, but not of AT2G4281.2 (Supplemental Figure 2, Supplemental dataset 1).

In order to interact, PAPP5 and MAX2 need to be present in the same cellular compartment, thus the localization pattern of both proteins was investigated and compared. Translational fusions of MAX2 and PAPP5 with GFP were transiently expressed in tobacco leaves. The N-terminal GFP fusion of MAX2, under control of its own promoter, was localized in the nucleus, which was in agreement with former observations (Shen et al., 2007; Liang et al., 2016) (Figure 5A). As the N-terminal GFP fusion of PAPP5 under control of its own promoter was unstable and did not result in a clear signal (data not shown), we analyzed this fusion protein under the control of the constitutive 35S promoter. PAPP5 localization was observed in both the nucleus and the cytoplasm, similar to what was described in previous publications (Chen et al., 1994; Ollendorff & Donoghue, 1997; Russell et al., 1999; Brown et al., 2000;

Borthwick et al., 2001; de la Fuente van Bentem et al., 2005; Ryu et al., 2005) (Figure 5A). In conclusion, MAX2 and PAPP5 share an overlapping localization pattern in the nucleus, where the interaction between both proteins might occur.

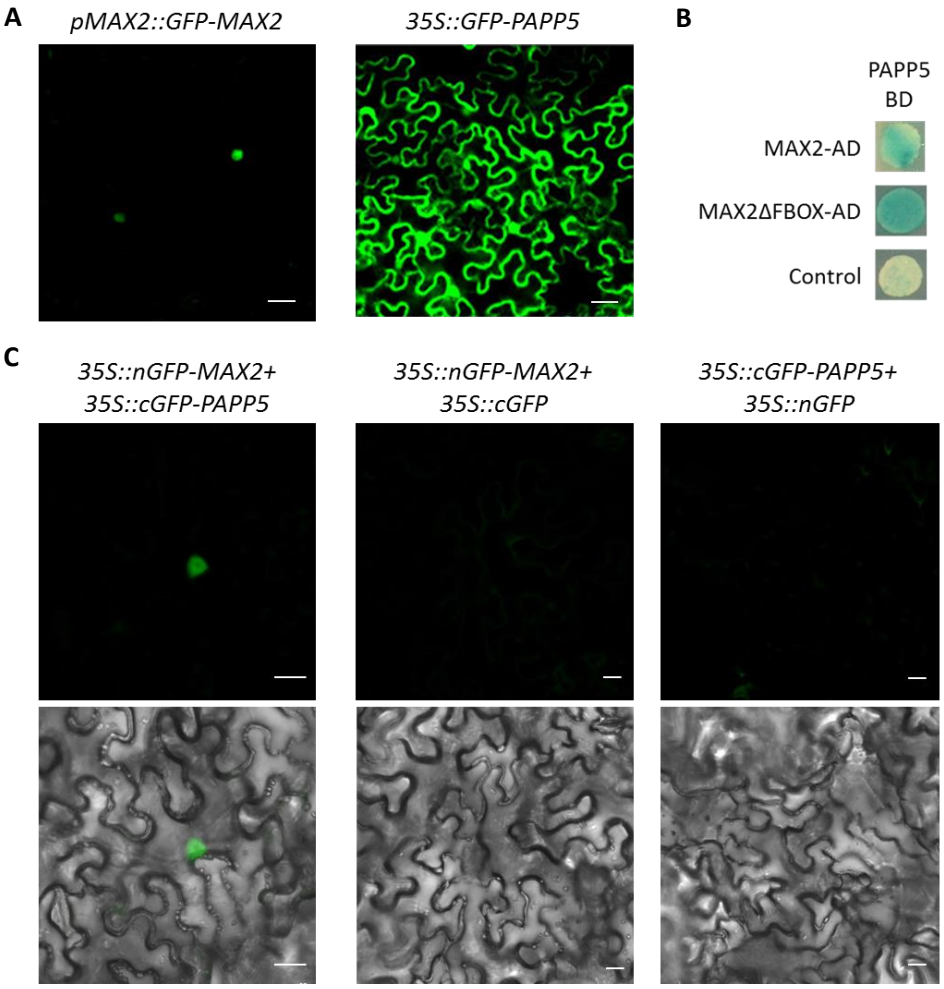

Figure 5. PAPP5 localization and interaction with MAX2/MAX2ΔFBOX. (A) Subcellular localization of MAX2 and PAPP5. *N. benthamiana* leaves were transiently transformed with *pMAX2::GFP:MAX2* (left) and *35S::GFP:PAPP5* (right). (B) Y2H screen of MAX2 and PAPP5 interaction. PAPP5 fused to GAL4-BD was tested for interaction with MAX2 and MAX2ΔFBOX fused to GAL4-AD or pB42AD for negative control. Yeasts transformed with both plasmids were selected on SD (Raf/Gal)-U-T-H medium supplemented with X-Gal. (C) BiFC analysis of MAX2 and PAPP5 interaction. Tobacco leaves were transiently transformed with *35S::nGFP-MAX2* and *35S::cGFP-PAPP5* fusion constructs. Each construct was coexpressed with corresponding GFP part (*35S::cGFP* or *35S::nGFP*) for a negative control. GFP signal only (top) or merged with bright-filed images (bottom) are shown. Scale 20 µm.

Next, we used a yeast two-hybrid assay to test whether MAX2 could interact directly with PAPP5. In our screen, yeast cotransformed with PAPP5 and MAX2 or MAX2ΔFBOX fused to the GAL4-BD or GAL4-AD domain, respectively, colored blue on the selective medium SD Raf/GAL U-T-H supplemented with X-Gal, indicating that interaction occurs between tested proteins (Figure 5B). We then set up a

Bimolecular Fluorescent Complementation (BiFC) assay in *N. benthamiana* leaves to detect where the MAX2-PAPP5 interaction takes place *in vivo* in the cell. To do so, fusion proteins were made with either the N-terminal (nGFP) or C-terminal (cGFP) fragment of GFP. Upon interaction between tested proteins these GFP-fragments can reassemble which results in fluorescence. To proof the association of MAX2 and PAPP5, different combinations of N- and C-terminal fusions with nGFP and cGFP were tested by transient coexpression in tobacco leaves. MAX2 and PAPP5 were shown to interact in the nucleus when combining the N-terminal nGFP fusion protein of MAX2 with the N-terminal cGFP fusion protein of PAPP5 (Figure 5C).

To confirm the interaction between MAX2 and PAPP5, and to better understand the potential role of PAPP5 in the MAX2 signaling pathway, a reciprocal TAP was performed using PAPP5 as a bait. *Arabidopsis* cell suspension cultures were transformed with the overexpression constructs *35S::GS-PAPP5* or *35S::PAPP5-GS*, and both protein purification and identification was done exactly the same way as for MAX2. As PAPP5 was only recovered as a MAX2 complex protein in the dark, reciprocal TAP experiments were performed using PSB-D cell suspension cultures, treated with 1 µM *rac*-GR24 or mock for 5 hours. However, no peptides of MAX2 could be identified. Experiments with the N-terminal tagged PAPP5 bait did not yield any preys, and only one putative PAPP5 interactor, AT3G58530/RNI-like superfamily protein, was detected using the C-terminal fusion protein (Table 2, Supplemental dataset 1).

Table 2. Prey proteins identified through TAP using PAPP5 as bait.

AGI	Protein	*35S::GS-PAPP5*		*35S::PAPP5-GS*	
		Mock	*rac*-GR24	Mock	*rac*-GR24
AT2G42810.1	PAPP5	2	2	2	2
AT3G58530.1	RNI-like superfamily protein	0	0	2	1

TAP experiments were performed in dark conditions, using GS-PAPP5 or PAPP5-GS as bait, mock or in presence of 1 µM *rac*-GR24. Prey proteins were identified using peptide-based homology analysis of MS data. Background proteins identified in control experiments were withdrawn. The number indicates the times the prey was identified in two experiments with each bait protein. Abbreviations: AGI, Arabidopsis Genome Identifier.

Post-translational modification such as phosphorylation can modulate protein function, localization or activity (Scott and Pawson, 2009). Given the interaction between the protein phosphatase, PAPP5 and MAX2, we tested whether MAX2 can be phosphorylated. To identify MAX2 phosphorylated residues we performed single-step affinity purification in seedlings expressing *35S::GS-MAX2* in *max2-1* mutant background followed by phospho-enrichment. After liquid chromatography-tandem mass spectrometry (LS-MS/MS) we identified two serine residues 116 (S116) and 453 (S453) as being phosphorylated with the highest probability score, giving strong evidence that MAX2 can be

phosphorylated in *Arabidopsis* seedling (Table 3). In addition, we searched the PhosPhat data base for already described phosphorylation sites of MAX2 and as a result one threonine residue, T251 was identified. Taken together, these results suggest that the direct interaction between PAPP5 and MAX2 might result in dephosphorylation of the MAX2 protein.

Table 3. List of identified phosphorylation sites of MAX2.

Protein	Amino acid	Positions within proteins	AGI	Localization probability	Score for localization	Phospho (STY) Probabilities
AT2G42620.1	S	114	MAX2	0.394693	93.011	S(0.395)PS(0.303)S(0.303)LELLLPQWPR
AT2G42620.1	S	117	MAX2	0.407374	65.563	S(0.185)PS(0.407)S(0.407)LELLLPQWPR
AT2G42620.1	S	453	MAX2	0.797717	42.64	VET(0.202)S(0.798)EADHEEEDDGYER
AT2G42620.1	T	452	MAX2	0.5	75.463	VET(0.5)S(0.5)EADHEEEDDGYER

Single-step affinity purification followed by phosphor-enrichment and subsequent mass spectrometry analysis revealed a putative phosphorylation sites on MAX protein. PEP: The posterior error probability (PEP) of the best identified modified peptide containing this site; Score: The Andromeda score of the best identified modified peptide containing this site; Score for localization: The Andromeda score of the MS/MS spectrum used for calculating the localization score for this site.

PAPP5 belongs to the KAI2 signaling complex

As MAX2 is a central player in both strigolactone and in karrikin/KAI2 ligand signaling, PAPP5 can play a general role in the signaling pathway of both or can be specifically involved in one of the two (Nelson et al., 2011). Apart from MAX2, both molecules are perceived by a specific α/β-hydrolase protein, respectively D14 and KAI2, to mediate diverse responses (Waters et al., 2012b). None of the receptors could be identified in our TAP experiments using the baits MAX2 or PAPP5. Moreover, TAP experiments with D14 and KAI2 as bait proteins did not reveal PAPP5 as a potential interactor. Only 2 potential preys of D14 were identified (LON3/AT3G05780.1, AK1/AT5G13280.1, Table 4, Supplemental dataset 1), while none for KAI2.

Table 4. Prey proteins identified through TAP using D14 as bait.

AGI	Protein	Mock	*rac*-GR24
AT3G03990.1	D14	2	2
AT3G05780.1	LON3	0	1
AT5G13280.1	AK-LYS1	0	1

TAP experiments were performed dark conditions, using GS-D14 as bait, mock or in presence of 1 µM *rac*-GR24. Prey proteins were identified using peptide-based homology analysis of MS data. Background proteins identified in control experiments were withdrawn. The number indicates the times the prey was identified in two experiments with each bait protein. Abbreviations: AGI, Arabidopsis Genome Identifier.

As weak, low-abundant or transient protein-protein interactions might be missed using TAP due to the two-step procedure, we used one-step affinity purification in combination with a label-free quantification (LFQ) analysis (Smaczniak et al., 2012) to resolve the D14- and KAI2- specific protein complexes. *Arabidopsis* cell cultures (PSB-L) expressing *35S::D14-GFP* and *35S::KAI2-GFP* were treated for 15 minutes with 1µM *rac*-GR24. Next, proteins were isolated in a single purification step and identified using LC-MS/MS. Afterward, spectra were searched with the MaxQuant software and MaxLFQ was used to quantify proteins identified with D14 and KAI2 over the four replicates (Cox et al., 2014). Subsequent statistical analysis allowed for the identification of prey proteins that were enriched with one of the tested baits, D14 or KAI2 (Supplemental Table 1). Interestingly, PAPP5 was found to be significantly more associated with KAI2 protein complexes, hinting at a role for PAPP5 in KAI2 rather than D14 signaling (Figure 6).

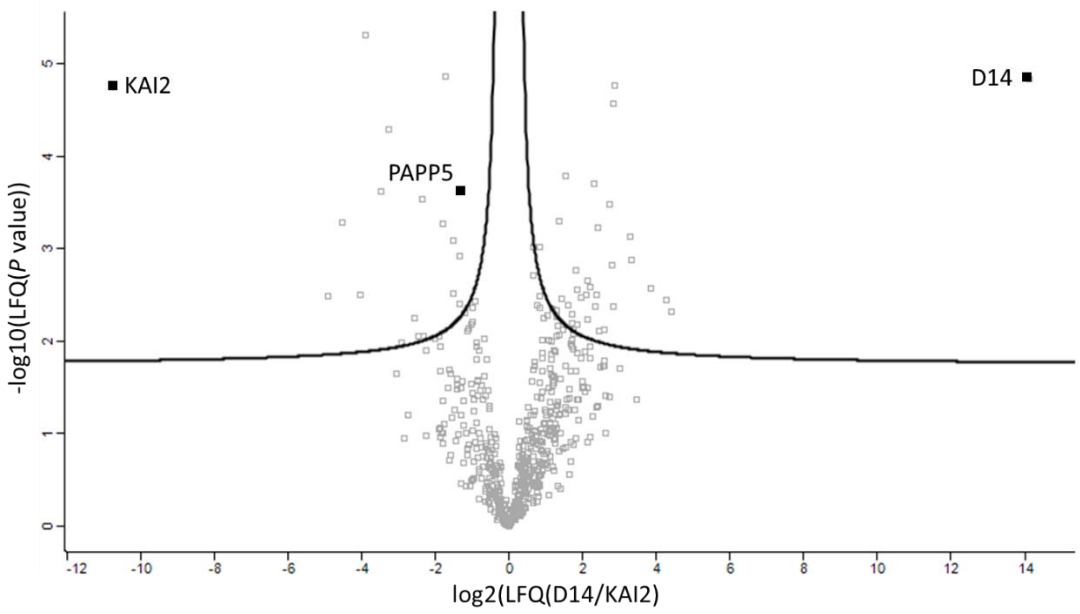

Figure 6. Differential protein complexes formed around D14 and KAI2 in cell cultures. Volcano plots showing the distribution of all quantified proteins after filtering and statistical analysis based on LFQ values, with their corresponding protein abundance ratios (KAI2/D14) over the *t* test *P* value (FDR=0.01, S0=0.1). The cutoff curve indicates which proteins are significantly more associated with D14 (right) and KAI2 (left).

We then asked whether PAPP5 could directly interact with KAI2 or D14. To test that, we carried out a Y2H assay in which we fused PAPP5 to GAL4-BD and both KAI2 and D14 to GAL4-AD. We found that neither KAI2 nor D14 cotransformed with PAPP5 in yeast cells could activate the expression of the reporter gene to allow for color reaction (Figure 7). This data indicates, that PAPP5 is a part of KAI2 complex, but not a direct KAI2 interactor.

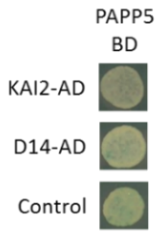

Figure 7. PAPP5 is not direct interactor of KAI2 and D14. Y2H screen of PAPP5 and KAI2/D14 interaction. PAPP5 fused to GAL4-BD was tested for interaction with KAI2 and D14 fused to GAL4-AD or pB42AD for negative control. Yeasts transformed with both plasmids were selected on SD (Raf/Gal)-U-T-H medium supplemented with X-Gal.

PAPP5 transcript and protein levels are not influenced by *rac*-GR24

Arabidopsis cell suspension cultures are responsive to *rac*-GR24, shown by the induction of the strigolactone responsive gene *BRC1* (Figure 1). By using qRT-PCR, changes in *PAPP5* expression levels were investigated but no differences could be detected in cell cultures that were treated mock or with 1 µM *rac*-GR24 for 1, 5, 10 or 15 hours (Figure 8A).

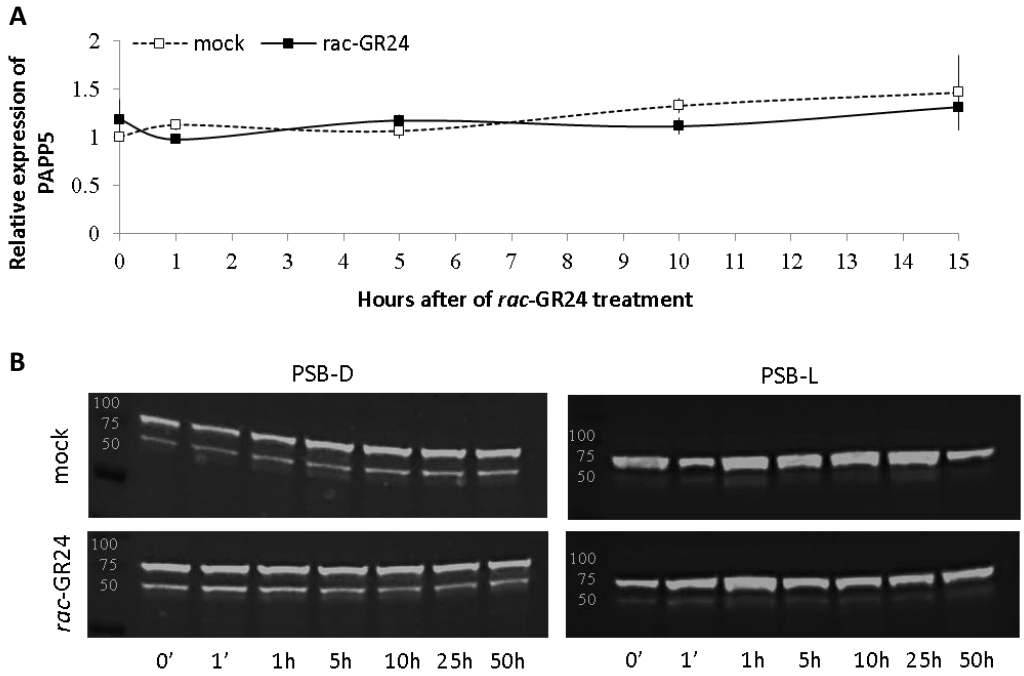

Figure 8. Impact of *rac*-GR24 on the transcript and protein level of PAPP5. (A) The expression of the *PAPP5* gene in cell cultures was assessed by qRT-PCR for its responsiveness to treatment with 1 µM *rac*-GR24 (solid line) and to mock (dotted line). The experiment was repeated three times with comparable results and the total mean of all biological repeats is presented. Data and error bars represent means ± SE. (B) PAPP5 protein levels upon treatment with *rac*-GR24. GS-PAPP5 protein levels in continuous dark grown (PSB-D) or long-day conditions (PSB-L) cell suspension cultures at different time points after mock treatment (top) or treatment with 1µM *rac*-GR24 (bottom). Detection was done using the peroxidase-antiperoxidase (PAP) antibody against the GS-tag. The experiment was repeated twice with comparable results and one representative repeat is shown.

In addition, the F-box protein MAX2 is expected to regulate ubiquitination and degradation of specific targets, such as SMXL proteins (Jiang et al., 2013; Wang et al., 2015; Zhou et al., 2013). To test whether PAPP5 might also be a substrate of SCF^{MAX2}, cell suspension cultures expressing *35S::GS-PAPP5* grown in continuous dark (PSB-D) or long-day conditions (PSB-L), were treated mock or with 1 µM *rac*-GR24 and samples were harvested before and at 6 different time points after treatment. Detection of PAPP5 was done by immunoblotting with anti-GS antibodies, but no differences in protein abundances could be observed (Figure 8B). Taken together, *rac*-GR24 does not seem to affect PAPP5 on the transcript or protein level in *Arabidopsis* cell cultures.

PAPP5 is not involved in shoot development

To further investigate the role of *PAPP5*, different phenotypes and responses towards *rac*-GR24 in the *papp5* mutant were assessed and compared to mutants defective in strigolactone and/or karrikin specific outcomes. Originally, strigolactones were discovered as plant hormones because of their big impact on shoot branching (Gomez-Roldan et al., 2008; Umehara et al., 2008). Upon flowering, *max2-1* and *d14-1* mutants are characterized by a bushy phenotype whereas *kai2-1* mutants have a similar shoot phenotype compared to wild-type Ler plants (Stirnberg et al., 2002; Waters et al., 2012b; Chevalier et al., 2014).

Here, we investigate the potential role of *PAPP5* in shoot branching by counting the number of rosette branches in the *papp5* mutant, compared to Col-0, *max2-1*, *d14-1* and *hyposensitive to light 3* (*htl3*), the *kai2* mutant allele in Col-0 background. The average number of rosette branches for *papp5* mutant, did not differ from the number of branches of Col-0 plants, indicating that strigolactone signaling is not disturbed (Figure 9). Though, *max2-1* and *d14-1* mutants had a significantly higher number of rosette branches compared to wild-type plants, which was in agreement with previous reports. In contrast to what is reported by Waters et al., 2012b, in our hands, a small decrease in the number of rosette branches was counted for *htl3* mutants, possibly explained by the different ecotype background (Ler versus Col-0).

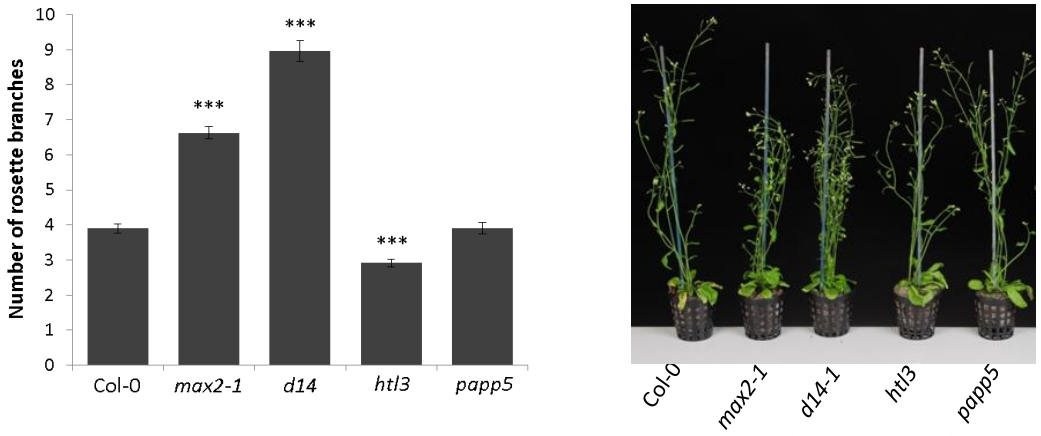

Figure 9. Shoot branching assay for *papp5* mutant. Rosette branches of Col-0, *max2-1*, *d14-1*, *htl3*, *papp5* mutants were counted after 50 days of growth (n = 18). Graphs represent means of three biological repeats ± SE. Asterisks indicate statistical significant differences (*** P < 0,001, Student's t test). On the picture one representative plant is shown.

PAPP5 regulates *rac*-GR24 responses in hypocotyl growth

In continuous red light, *max2-1* and *kai2-1* mutants have a longer hypocotyl compared to wild-type plants, whereas the hypocotyl length of *d14-1* mutants does not differ from Col-0 (Waters et al., 2012b). Additionally, *rac*-GR24 is known to decrease the hypocotyl length in these conditions in wild-type plants but not in *max2-1* or *kai2-1* mutants (Waters et al., 2012b). Col-0, *htl3* and *papp5* mutants, but not *max2-1*, displayed a shorter hypocotyl upon *rac*-GR24 treatment compared to mock conditions. Interestingly, similar to *max2-1* and *htl3*, a significantly longer hypocotyl was measured for the *papp5* mutant in mock hinting at a role for PAPP5 in hypocotyl growth (Figure 10A). The similarity in the elongated hypocotyl phenotype of *papp5*, *max2-1* and *htl*3 suggested that these genes might act in the same genetic pathway. Nevertheless, the hypocotyl length of *htl3papp5* double mutant was slightly but significantly longer than each of the single mutants when grown in mock conditions (Figure 10B). This additive effect suggests that KAI2 and PAPP5 might define two signaling pathways that are genetically separable.

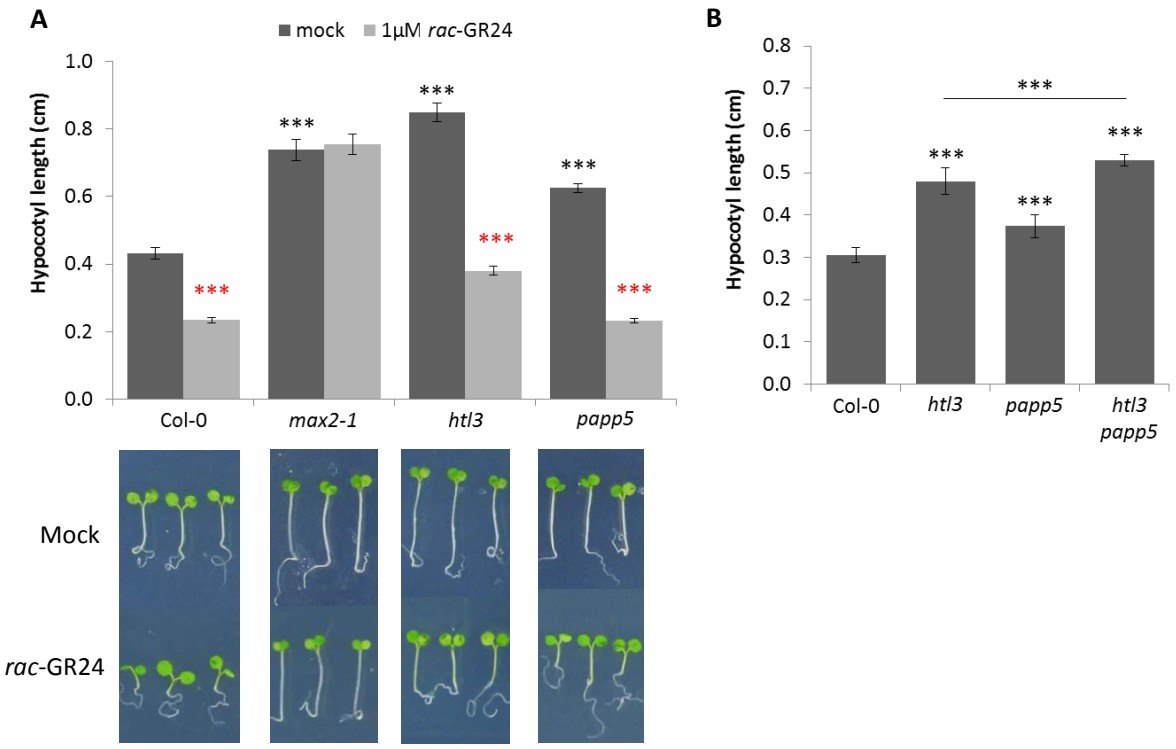

Figure 10. Hypocotyl assay for *papp5* mutant. Seeds were sown on ½ MS without sucrose, supplemented or not with 1 µM *rac*-GR24, incubated for 2 days at 4°C, exposed to light for 3 hours, followed by dark incubation for 21 hours before exposed to red light for 4 days. Graphs represent means of three biological repeats ± SE (n = 25). Black asterisks indicate statistical significant differences between genotypes and red asterisks between treatments [(*** $P < 0{,}001$, ANOVA-mixed model (A), Student's *t* test (B)]. On the picture three representative plants are shown (A).

Several transcriptional markers of karrikin and strigolactone response in seedlings have previously been reported, including *D14-LIKE2* (*DLK2*), *KAR-UP F-BOX1* (*KUF1*), *CHALCONE SYNTHASE* (*CHS*), *ELONGATED HYPOCOTYL 5* (*HY5*) and *SALT TOLERANCE HOMOLOG7* (*STH7*) (Nelson et al., 2010, 2011; Waters et al., 2012b; Walton et al., 2016). Considering the minor additive effect on the hypocotyl elongation in *htl3papp5* double mutant we investigated whether PAPP5 might mediate some responses to *rac*-GR24 in seedlings at the molecular level. To test that we assessed the accumulation of several marker transcripts, known to change in abundance in response to the strigolactone analog. For instance, transcript levels of *CHS*, *HY5* and *STH7* increase after treatment with *rac*-GR24 in MAX2-dependent manner (Nelson et al., 2011; Waters et al., 2012b; Walton et al., 2016). In our study, the *CHS* transcript responses to *rac*-GR24 in *papp5* and Col-0 seedlings were similar, however, the induction was lower in *papp5* mutants compared to wild-type (Figure 11). In addition, transcript level of *STH7* was not changed, while the level of *HY5* decreased in response to *rac*-GR24. Together, these data indicate that PAPP5 might be required for certain transcript responses to *rac*-GR24 in seedlings.

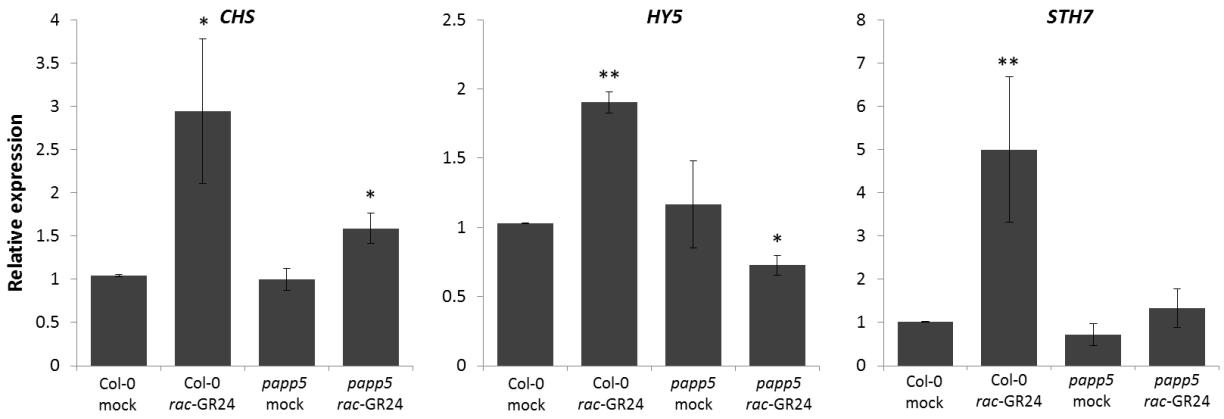

Figure 11. Expression of KAR/SL transcriptional markers in *papp5* seedlings. Transcripts detected by qRT-PCR using cDNA derived from seedlings grown for 4 days in the continuous red light on 1/2MS medium containing mock (0.01% acetone) or 1µM *rac*-GR24. Expression values are relative to the *ACTIN2* reference gene. Values represent mean (± SE) of three biological repeats. Significant difference between treatments was assessed by Student's *t* test (*, *P*< 0.05; **, *P*< 0.01).

PAPP5 is involved in *rac*-GR24 induced seed germination

Apart from inhibiting hypocotyl elongation, KAI2-pathway is best described to induce seed germination (Nelson et al., 2010; Waters et al., 2012b). In suboptimal temperature conditions, *Arabidopsis* Col-0 seeds respond to *rac*-GR24 by increasing the germination frequency, while *max2-1* and *htl3* mutants have a very low germination rate and are fully insensitive towards the treatment (Toh et al., 2008). As shown in Figure 12A, the germination frequency of both Col-0 and *papp5* mutant were increased to the same level after the addition of *rac*-GR24, which was not the case for *htl3* and *htl3papp5* lines. Additionally, the germination frequency in mock conditions was significantly lower for *papp5* compared to Col-0 (Figure 12A), suggesting that *PAPP5* might be a positive regulator of seed germination in the suboptimal temperature conditions. In the control conditions (21°C, continuous light) all tested lines displayed high germination frequency that was not induced by the treatment with *rac*-GR24 (Figure 12B).

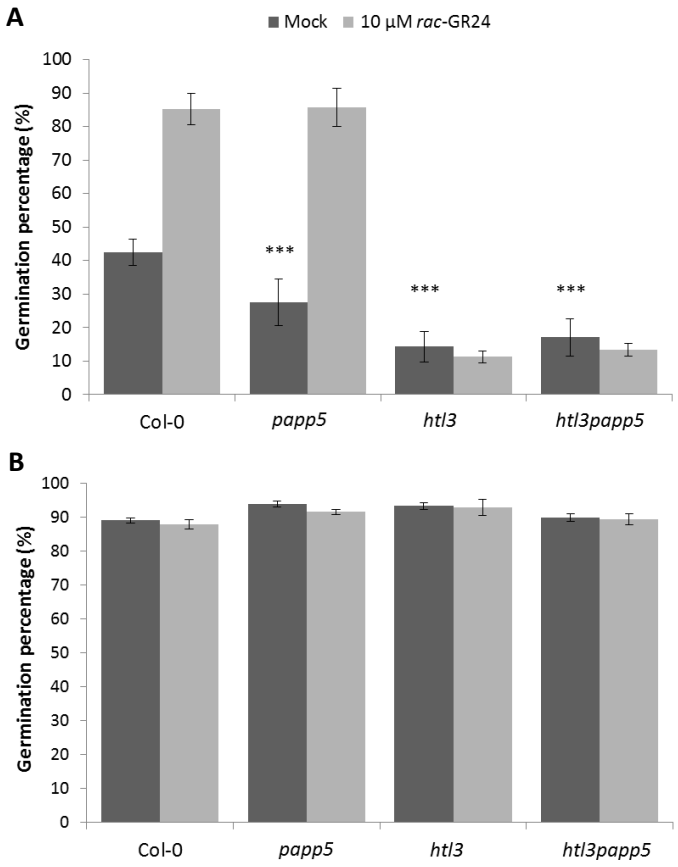

Figure 12. Seed germination assay of Col-0, *papp5, htl3* and *htl3papp5* mutants in suboptimal temperature conditions. Seeds were distributed in 96-well plate containing HEPES buffer with mock (acetonitrile) or 10 µM *rac*-GR24 and placed for 4 days at 24˚C in dark (A) or at 21˚C in the continuous light for the control (B). Asterisks indicate statistically significant differences between genotypes (*** $P < 0.001$, ** $P < 0.01$, logistic regression with the glimmix procedure). The experiments were repeated three times and the total mean of all biological repeats is presented.

DISCUSSION

In the last years, major breakthroughs have been made to unravel the signaling cascades of the structurally related strigolactone and karrikin molecules. Up to now, a very similar signaling mechanism was described, consisting of an α/β-fold hydrolase receptor, respectively D14 and KAI2, a common F-box protein MAX2 and downstream SMXL targets (Nelson et al., 2011; Soundappan et al., 2015; Stanga et al., 2013; Waters et al., 2012b). Still, many molecular players await their discovery and although SMXL proteins provide an important level of specificity, the quest for proteins that discriminate between strigolactone and karrikin/KAI2 ligand signaling is still going on.

Here, TAP was used in *Arabidopsis* cell cultures to further unravel the MAX2 interactome. In contrast to our experiments using D14 or KAI2 as baits, MAX2 TAP experiments were highly successful. Confirming the effectivity of the technique, SKP1 and CUL1, two known components of the MAX2 complex, were identified (Stirnberg et al., 2007; Zhao et al., 2014). Furthermore, different members of the COP9 signalosome as well as 28 novel MAX2 putative interacting proteins were detected. The high number of purified proteins might be a reflection of the pleiotropic role of MAX2 in diverse physiological processes. Because none of the CSN members was retrieved using the truncated MAXΔFBOX bait, we expect a regulatory role for the CSN, acting as a cullin deneddylase to maintain the SCF^{MAX2} activity. However, a role for the CSN in regulating phosphorylation and gene expression has also been described (Bech-Otschir et al., 2001; Huang et al., 2014). Here, we focus on the identification of PAPP5, while for a detailed characterization of the other interactors, we refer to future studies.

Some interactors of the F-box protein MAX2 are expected to be ubiquitinated and degraded, such as target proteins SMXL6,7,8 (Jiang et al., 2013; Wang et al., 2015; Zhou et al., 2013). We then tested whether PAPP5 might also be a substrate of SCF^{MAX2}. However, as PAPP5 protein levels were shown not to change after treatment with *rac*-GR24, neither in the dark nor in the light, we do not assume PAPP5 being a target of MAX2 for ubiquitination and degradation via the 26S proteasome. We rather expect that PAPP5 regulates the activity and/or stability of the MAX2 protein complex which affects downstream responses.

To understand the role of PAPP5 in the MAX2 signaling network, we performed a detailed analysis that combined biochemical studies, mutant phenotyping and qPCR analysis of SL/KAR markers. Copurification of PAPP5 with MAX2 in our TAP experiments was validated with both Y2H and BiFC, and proved a binary interaction between PAPP5 and MAX2ΔFBOX (Y2H) as well as MAX2 (Y2H, BiFC) in the nucleus. In addition, one-step affinity purifications identified PAPP5 as being significantly more associated with the KAI2 protein complex compared to D14 complex, but not directly interacting with

KAI2. Based on this data a role for PAPP5 as a unique member of the KAI2-MAX2-SMAX1 complex was hypothesized.

In agreement, we could not observe any difference in shoot branching phenotypes between *papp5* knockout mutants and wild-type plants, while seed germination and hypocotyl elongation, developmental programs in which KAI2 plays a prominent role, were affected. Indeed, likewise *htl3* and *max2-1*, *papp5* mutants exhibit longer hypocotyls than Col-0 when grown under red light. To test whether this phenotype is the result of an impaired MAX2-KAI2 signaling pathway, hypocotyl lengths were measured in *htl3papp5* double mutant. An additive effect of PAPP5 and KAI2 on hypocotyl growth was observed which suggests that both proteins might operate in separate pathways during hypocotyl elongation. Indeed, PAPP5 was previously described to influence phytochrome-mediated photoresponses (Ryu et al., 2005). As protein phosphatase, PAPP5 dephosphorylates biologically active P_{fr}-phytochrome A (PhyA), thereby increasing their ability to interact with the downstream signal transducer Nucleoside-diphosphate kinase 2 (NDPK2), and thus enhances the plant's response to light. As a consequence, a defect in hypocotyl growth might be the result of disturbed phytochrome-mediated signaling cascade. Nevertheless, the additive effect was rather small thus the influence of PAPP5 on the KAI2- controlled pathway cannot be excluded. In fact, PAPP5 might be required for a subset of transcriptional responses to *rac*-GR24 in seedlings. Under identical conditions to those used to examine hypocotyl length, transcript levels of several strigolactone and karrikin markers were not induced in the *papp5* mutant. Further on, when the germination frequency was tested in suboptimal temperature conditions, the *papp5* mutant showed lower germination in mock, similar to *htl3* phenotype, suggesting a possible involvement in KAI2-mediated signaling, while no additive effect was observed in *htl3papp5* double mutant. Taken together, our data show that PAPP5 is not involved in the MAX2-D14 regulated inhibition of shoot branching but might belong to the MAX2-KAI2 signaling complex, and influence seed germination in suboptimal conditions, hypocotyl elongation, and transcriptional responses in seedlings.

The exact mechanism by which PAPP5 can be involved seed germination and young seedling responses is not clear, however, we hypothesize that PAPP5 might affect the activity and/or stability of the KAI2-MAX2-SMAX1 complex. Indeed, PAPP5 is described as a versatile protein, that apart from being a phosphatase, can act as a chaperone as well (Park et al., 2011). Being a protein phosphatase, PAPP5 might dephosphorylate KAI2, MAX2 or SMAX1 proteins to activate the complex and facilitate the ubiquitination of SMAX1 proteins. MAX2 is the most convincing candidate for being a substrate of PAPP5, as direct interaction between the two proteins has been shown. Therefore, it is possible that phosphorylation of MAX2 makes the protein less active in the SMAX1 ubiquitination process, while dephosphorylation by PAPP5 could increase MAX2 activity. In agreement, *papp5* mutant displays

similar to *max2* phenotypes in seed germination, hypocotyl growth and transcriptional responses, because MAX2 protein cannot be dephosphorylated and therefore is less active in marking SMAX1 for degradation. It is thus likely, that the role of PAPP5 in MAX2-KAI2 signaling might be dephosphorylation of MAX2. If this is the case, a phosphorylation insensitive mutant version of MAX2 should exhibit a higher seed germination in suboptimal conditions, while the phenotype of the constitutively phosphorylated MAX2 should have a lower germination. To test this hypothesis, phosphorylation of MAX2 needs to be verified in *papp5* mutant background, where less phosphorylation is expected.

Another possibility is that MAX2, KAI2 or SMAX1 is recruited by PAPP5 to provide phosphatase specificity. Indeed, members of Ser/Thr-specific phosphoprotein phosphatases (PPP) family exhibit nonspecific phosphatase activity and specificity is provided by other interacting proteins (Shi, 2009). In human cells for example, binding of the molecular chaperones heat shock protein 90 (Hsp90) and Hsp70 to the TPR domain of PP5, activates its phosphatase activity and acts as a molecular bridge to enable dephosphorylation of specific substrates (Chen et al., 1996; Zeke et al., 2005; Connarn et al., 2014).

An alternative hypothesis is that PAPP5 might dephosphorylate SMAX1, influencing the phosphorylation-dependent ubiquitination that might be required for its degradation. The influence of phosphorylation on ubiquitination, and thus degradation of the modified protein, is a common theme in animal cell signaling and is also described in plants, however, to a much lesser extent (Lin et al., 2002; Welcker et al., 2004; Yada et al., 2004; Ju et al., 2007). By dephosphorylation of SMAX1, PAPP5 might control the availability of SMAX1 for degradation.

In conclusion, PAPP5 was identified as a novel MAX2 interactor, and genetic as well as biochemical analysis indicated that PAPP5 might act as a negative regulator of karrikin-controlled seed germination and hypocotyl elongation, probably by affecting the activity/stability of one or more members in the KAI2-MAX2-SMAX1 protein complex. We are convinced that many other interesting proteins might be hidden in our dataset, waiting for their discovery as key components in discriminating strigolactone and karrikin signaling. A detailed characterization of all members of the purified MAX2 complex will be of great value to further broaden our knowledge on the diverse MAX2 signaling networks.

MATERIALS AND METHODS

Plant material and growth conditions

Arabidopsis thaliana (ecotype Landsberg erecta) cell suspension cultures (PSB-D and PSB-L) were maintained as described previously (Van Leene et al., 2007). After 3 weeks of growth under continuous dark (PSB-D) or long-day (PSB-L), samples were treated with either 1 µM *rac*-GR24 or 0.01% acetone as a control. Seeds of *Arabidopsis thaliana* (L.) Heyhn. (accession Columbia-0) plants were surface sterilized with consecutive treatments of 70% (v/v) ethanol with 0.05% (w/v) sodium dodecyl sulfate (SDS), washed with 95% (v/v) ethanol, sown on half-strength Murashige and Skoog (1/2 MS) medium with 1% (w/v) sucrose (for root phenotyping) or without (for hypocotyl analysis), and stratified for 2 days at 4°C. The *max2-1* (Stirnberg et al., 2002), *htl3* allele (Toh et al., 2014) and *papp5* (Ryu et al., 2005) lines have been described previously.

Tandem-affinity purification

Cloning of transgenes encoding GS-tag fusions under control of the constitutive cauliflower tobacco mosaic virus 35S promoter and transformation of Arabidopsis cell suspension cultures (PSB-D and PSB-L) with direct selection in liquid medium were carried out as previously described (Van Leene et al., 2011). All primers used for cloning are listed in the Supplemental Table 2. TAP experiments were performed with 200 mg of total protein extract as input as described in Van Leene et al., 2015. Protein interactors were identified using an LTQ Orbitrap Velos mass spectrometer. Proteins with at least two matched high confident peptides were retained. Background proteins were filtered out based on frequency of occurrence of the copurified proteins in a large dataset containing 543 TAP experiments using 115 different baits (Van Leene et al., 2015).

Degradation of PAPP5

To determine whether PAPP5 protein levels are influenced by *rac*-GR24, cell cultures expressing N-terminally GS-tagged PAPP5 were treated with 1µM *rac*-GR24 or mock. Cell material was harvested before and at six time points after treatment. Further, proteins were extracted and concentrations were determined by the Bradford assay. Differences in protein levels were detected using western blotting with GS-tag targeted PAP (Peroxidase Anti-Peroxidase) antibodies and chemiluminescent substrates from the Western Lightning® Plus ECL kit (PerkinElmer). The Precision Plus Protein™ Dual Color Standards (Bio-Rad) was used as protein size marker.

Transient expression in *N. benthamiana*

WT *N. benthamiana* plants (4- to 5-week-old) were used for transient expression of constructs by *Agrobacterium tumefaciens*-mediated transformation of lower epidermal leaf cells as previously described (Boruc et al., 2010), using a modified infiltration buffer (10 mM $MgCl_2$, Merck; 10 mM MES pH 5.7, Duchefa; 100 µM Acetosyringone, Sigma-Aldrich) and addition of a P19 expressing *Agrobacterium* strain to boost protein expression (Voinnet et al., 2003). All *Agrobacterium* strains were grown for 2 days, diluted to OD 1 in infiltration buffer and incubated for 2-4 h at room temperature before mixing in a 1:1 ratio with other strains and injecting.

BiFC

35S::tag-ORF constructs using the N and C-terminal parts of GFP (nGFP and cGFP, respectively) were generated by double Gateway recombination using the pK7m24GW2 vector (Boruc et al., 2010). The constructs were coexpressed in *N. benthamiana* using *Agrobacterium* mediated transient transformation. Interactions were scored at 3 days after transformation by screening the lower epidermal cells for fluorescence using confocal microscopy.

Yeast transformation and yeast-two-hybrid

Expression clones for yeast two-hybrid were generated by LR Gateway recombination between respective Entry clones pGILDA or pB42AD. Y2H analysis was performed as described by Cuéllar et al., 2013, in two independent repeats. The polyethylene glycol (PEG)/lithium acetate method was used to cotransform *Saccharomyces cerevisiae* EGY48 strain (Estojak et al., 1995) with the bait and prey. Transformants were selected on Synthetic Defined media containing galactose and raffinose (SD Gal/Raf) and lacking Ura, Trp, and His (Clontech). Three individual colonies were grown overnight in liquid cultures at 30°C and 10- and 100-fold dilutions were dropped on control media (SD Gal/Raf-Ura-Trp-His) and selective media containing additionally X-Gal (Duchefa).

Phosphopeptide enrichment

Proteins were extracted from 6-day-old *Arabidopsis* seedlings expressing *35S::GS-MAX2* (*max2-1*) grown in liquid ½ MS medium. After single-step purification with IgG-Sepharose beads phospho-enrichment experiment was performed as described previously (Vu et al., 2017).

Affinity purification

D14 and KAI2 protein complexes were analyzed by the one-step affinity purification method (GFP-Trap) combined with label-free quantification (LFQ) analysis, as described (Smaczniak et al. 2012). The *Arabidopsis* cell cultures (PSB-L) overexpressing *35S::D14-GFP* and *35S::KAI2-GFP* constructs were treated for 15 min with 1µM *rac*-GR24. After harvesting, protein material was extracted and the GFP-Trap (Chromotek) was used to purify protein complexes following manufacturer's instructions. After LC-MS/MS, spectra were searched using the MaxQuant software and to identify and calculate MaxLFQ values for D14 and KAI2 interactors. A two-sided Student's *t* test was then performed in combination with a permutation-based correction for multiple hypothesis testing (FDR=0.01) and a threshold values established at S0=0.1.

Physiological assays

Rosette branches (shoots >1 cm) were counted in 50-day-old plants grown in soil under a standard 16-h/8-h light/dark cycle (22°C/18°C) in controlled environment rooms with light provided by white fluorescent tubes. To analyze root phenotype, seedlings were grown vertically for 9 days in the continuous light at 21˚C. The lateral root primordia were counted using a light microscope (S4E, Leica Microsystems). After that, the plates were scanned and the main root length was measured using ImageJ software and a digitizer tablet (Wancom). LRD was calculated by dividing the number of lateral roots by the corresponding primary root length. For the hypocotyl elongation analysis, after stratification seeds were exposed to white light for 3 hours, transferred to dark for 21 hours, and then exposed to continuous red light for 4 days. After scanning of the plates, the hypocotyls were measured using ImageJ 1.41 software. Thermoinduced seed dormancy assays were performed similarly to Toh et al. (2012). Seeds were used for the assay minimum at 6 weeks after harvesting. Seeds were distributed in 96-well plate containing 100 mM 4-(2-hydroxyethyl)-1-piperazineethanesulfonic acid (HEPES) buffer and Preservative for plant tissue cultures (Nalgene) with either 10 µM *rac*-GR24, or acetonitrile. Plates were incubated for 4 d at 24°C in dark or at 21°C in continuous light for the control. Germination was indicated by emergence of the radicle tip through the endosperm.

qRT-PCR

RNA was extracted with the RNeasy® Plant Mini Kit (Qiagen). 1µg RNA was used to make cDNA using the iScript™ cDNA Synthesis Kit and diluted to a finale volume of 500µl. The primers were designed with the primer design tool on Roche-applied-science (http://www.roche-applied-science.com). All primers (Supplemental Table 2) were diluted with water to a concentration of 5µM. All qRT-PCR experiments were performed in three technical repeats using 384-multiwell plates and detection by

SYBR® Green. Reaction mixes were composed by the Janus Robot with a final volume of 5µl and a 10% cDNA fraction using the SYBR® Green Master Mix (PerkinElmer). The Roche Lightcycler® 480 system (Roche Diagnostics) was used to execute all qRT-PCR reactions with following settings: 1x pre-incubation (95°C for 5 min), 45x amplification (95°C for 10 sec | 60°C for 10 sec | 72°C for 10 sec), 1x melting curve (95°C for 5 sec | 65°C->97°C for 1 min) and 1x cooling down (40°C for 10 sec). Ct-values and efficiency values were determined by the Lightcycler® 480 software and analyzed by the 2-ΔΔCt method (Livak & Schmittgen, 2001). The achieved expression data was normalized to the expression levels of *ACTIN2* (*ACT2*, AT3G18780).

SUPPLEMENTARY DATA

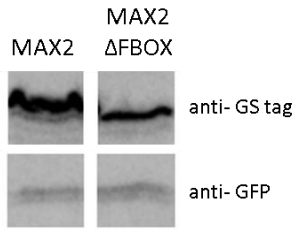

Supplemental Figure 1. Expression analysis of MAX2 baits. Protein levels of *35S::GS-MAX2* and *35S::GS-MAX2ΔFBOX* in *Arabidopsis* cell cultures were analyzed by means of immunoblotting. Total protein extract was loaded and detection was done using the peroxidase–antiperoxidase (PAP) antibody against the GS-tag after SDS-PAGE. Molecular weight of GS-tagged MAX2 is approximately 100 kDa. Anti-GFP antibodies were used as loading control (bottom), as GFP is present in the backbone of the vector.

AT2G42810.1

```
  1 METKNENSDV SRAEEFKSQA NEAFKGHKYS SAIDLYTKAI ELNSNNAVYW
 51 ANRAFAHTKL EEYGSAIQDA SKAIEVDSRY SKGYYRRGAA YLAMGKFKDA
101 LKDFQQVKRL SPNDPDATRK LKECEKAVMK LKFEEAISVP VSERRSVAES
151 IDFHTIEVEP QYSGARIEGE EVTLDFVKTM MEDFKNQKTL HKRYAYQIVL
201 QTRQILLALP SLVDISVPHG KHITVCGDVH GQFYDLLNIF ELNGLPSEEN
251 PYLFNGDFVD RGSFSVEIIL TLFAFKCMCP SSIYLARGNH ESKSMNKIYG
301 FEGEVRSKLS EKFVDLFAEV FCYLPLAHVI NGKVFVVHGG LFSVDGVKLS
351 DIRAIDRFCE PPEEGLMCEL LWSDPQPLPG RGPSKRGVGL SFGGDVTKRF
401 LQDNNLDLLV RSHEVKDEGY EVEHDGKLIT VFSAPNYCDQ MGNKGAFIRF
451 EAPDMKPNIV TFSAVPHPDV KPMAYANNFL RMFN
```

AT2G42810.2

```
  1 METKNENSDV SRAEEFKSQA NEAFKGHKYS SAIDLYTKAI ELNSNNAVYW
 51 ANRAFAHTKL EEYGSAIQDA SKAIEVDSRY SKGYYRRGAA YLAMGKFKDA
101 LKDFQQVKRL SPNDPDATRK LKECEKAVMK LKFEEAISVP VSERRSVAES
151 IDFHTIGNKP RSSSMPTKTA LAAVVAAVMV VAVRGFATTE ILMVLVSVVL
201 GTFWWGSFSG KVEPQYSGAR IEGEEVTLDF VKTMMEDFKN QKTLHKRYAY
251 QIVLQTRQIL LALPSLVDIS VPHGKHITVC GDVHGQFYDL LNIFELNGLP
301 SEENPYLFNG DFVDRGSFSV EIILTLFAFK CMCPSSIYLA RGNHESKSMN
351 KIYGFEGEVR SKLSEKFVDL FAEVFCYLPL AHVINGKVFV VHGGLFSVDG
401 VKLSDIRAID RFCEPPEEGL MCELLWSDPQ PLPGRGPSKR GVGLSFGGDV
451 TKRFLQDNNL DLLVRSHEVK DEGYEVEHDG KLITVFSAPN YCDQMGNKGA
501 FIRFEAPDMK PNIVTFSAVP HPDVKPMAYA NNFLRMFN
```

Supplemental Figure 2. *In silico* trypsin digest of both splice variants of PAPP5. The AT2G42810.1 unique peptide SVAESIDFHTIEVEPQYSGAR, indicated in blue, was present in the peptide pool of our TAP-dataset.

Supplemental Table 1. Overview of proteins associated with D14 and KAI2 in GFP trap experiment

D14 associated proteins	
AT1G04270.2	RPS15
AT1G04410.1	Lactate/malate dehydrogenase family protein
AT5G59970.1	Histone superfamily protein
AT1G12270.1	Hop1
AT1G79210.3	N-terminal nucleophile aminohydrolases (Ntn hydrolases) superfamily protein
AT1G17880.1	BTF3, ATBTF3
AT4G09800.1	RPS18C
AT1G47260.1	APFI, GAMMA CA2
AT5G54640.1	HTA1, RAT5, ATHTA1
AT1G52670.1	Single hybrid motif superfamily protein
AT1G53850.2	PAE1
AT1G56110.1	NOP56
AT5G37780.1	CAM1, TCH1, ACAM-1
AT1G72750.1	ATTIM23-2, TIM23-2
AT2G05990.2	MOD1, ENR1
AT2G06850.1	EXGT-A1, EXT, XTH4
AT2G17420.1	NTRA, ATNTRA, NTR2
AT2G20530.2	ATPHB6, PHB6
AT3G03990.1	**D14**
AT3G05060.1	NOP56-like pre RNA processing ribonucleoprotein
AT3G62830.2	UXS2, ATUXS2
AT4G12600.1	Ribosomal protein L7Ae/L30e/S12e/Gadd45 family protein
AT4G18100.1	Ribosomal protein L32e
AT4G37870.1	PCK1, PEPCK
AT5G07350.1	Tudor1, AtTudor1, TSN1
AT5G11520.1	ASP3, YLS4
AT5G11670.1	ATNADP-ME2, NADP-ME2
AT5G12140.1	ATCYS1, CYS1
AT5G25940.1	early nodulin-related
AT5G27120.1	NOP56-like pre RNA processing ribonucleoprotein
AT5G27760.1	Hypoxia-responsive family protein
AT5G41670.2	6-phosphogluconate dehydrogenase family protein
AT5G46430.2	Ribosomal protein L32e
AT5G55200.1	Co-chaperone GrpE family protein
AT5G63400.1	ADK1

KAI2 associated proteins	
AT1G02930.2	GSTF6
AT1G13440.1	GAPC-2, GAPC2
AT1G22300.2	GRF10, GF14 EPSILON
AT1G26630.1	FBR12, ATELF5A-2, ELF5A-2
AT1G44575.2	NPQ4, PSBS
AT1G67090.1	RBCS1A
AT1G72150.1	PATL1
AT2G35605.1	SWIB/MDM2 domain superfamily protein
AT2G42810.1	**PAPP5, PP5**
AT3G16640.1	TCTP
AT4G22710.1	CYP706A2
AT4G24190.2	SHD, AtHsp90.7, AtHsp90-7
AT4G31700.1	RPS6, RPS6A
AT4G37470.1	**KAI2**
AT5G10860.1	Cystathionine beta-synthase (CBS) family protein
AT5G16970.1	AT-AER, AER
AT5G56710.1	Ribosomal protein L31e family protein
AT5G61060.1	HDA05, HDA5, ATHDA5
ATCG00490.1	RBCL

Supplemental Table 2. All primers used in this study.

ID		Sequence	Use
BRC1	Fw	CTTCAGCAGCGGCGATGAG	qRT-PCR
BRC1	Rev	TTCCTCTTGTTTCGGTCGTGTTAG	qRT-PCR
MAX2	Fw	GGGGACAAGTTTGTACAAAAAAGCAGGCTCAATGGCTTCCACTACTCTCTCC	Cloning
MAX2	Rev	GGGGACCACTTTGTACAAGAAAGCTGGGTATCAGTCAATGATGTTGCGGCTGTTC	Cloning
D14	Fw	GGGGACAAGTTTGTACAAAAAAGCAGGCTCAATGAGTCAACACAACATCTTAG	Cloning
D14	Rev	GGGGACCACTTTGTACAAGAAAGCTGGGTATCACCGAGGAAGAGCTCGCCG	Cloning
KAI2	Fw	GGGGACAAGTTTGTACAAAAAAGCAGGCTCCACCATGGGTGTGGTAGAAGAAGCTC	Cloning
KAI2	Rev	GGGGACCACTTTGTACAAGAAAGCTGGGTCTCACATAGCAATGTCATTACGAAT	Cloning
MAX2ΔFBOX	Fw	GGGGACAAGTTTGTACAAAAAAGCAGGCTCAATGGCTCGTGGCAACGCTCGTGATC	Mutagenesis
PAPP5	Fw	GGGGACAAGTTTGTACAAAAAAGCAGGCTCAATGGAGACCAAGAATGAGAATTCTG	Cloning
PAPP5	Rev	GGGGACCACTTTGTACAAGAAAGCTGGGTATTAGTTGAACATCCTGAGAAAGTTG	Cloning
PAPP5	Fw	TGTCTCACTCCTCGTCAACCT	qRT-PCR
PAPP5	Rev	TTGTGGCTTCACCGGATAAT	qRT-PCR
CHS	Fw	GGCTATTGGCACTGCTAACCCTGAG	qRT-PCR
CHS	Rev	GTGAGGTTTCCGAATTGTCGACTTG	qRT-PCR
Hy5	Fw	ACATTTGGAGATCAAAGAAGGAA	qRT-PCR
Hy5	Rev	CGGAAGTTTCTTTTCCGACA	qRT-PCR
STH7	Fw	CATCTCCCGTTCTCTCTCACTTCT	qRT-PCR
STH7	Rev	CATTCTCTGCATAGTATTCCTCTGCT	qRT-PCR
ACT2	Fw	GGCTCCTCTTAACCCAAAGGC	qRT-PCR
ACT2	Rev	CACACCATCACCAGAATCCAGC	qRT-PCR

Supplemental dataset 1. Overview of all MAX2, MAX2ΔFBOX, D14 and PAPP5 TAP experiments. Available via https://www.dropbox.com/sh/uyd83n69jl5vi5q/AAAebr60IX4dXd0XTNudQowHa?dl=0

Chapter 8

Characterization of protein complexes involved in strigolactone and karrikin signaling by means of tandem affinity purification in *Arabidopsis thaliana* seedlings

Sylwia Struk[1,2], Carolien De Cuyper[1,2], Annick De Keyser[1,2], François-Didier Boyer[3], Geert Persiau[1,2], Geert De Jaeger[1,2] and Sofie Goormachtig[1,2]

[1]Ghent University, Department of Plant Biotechnology and Bioinformatics, 9052 Ghent, Belgium;
[2] VIB, Center for Plant Systems Biology, 9052 Ghent, Belgium;
[3]Institut National de la Recherche Agronomique, Institut Jean-Pierre Bourgin, Versailles, France

S.S. was the main author of the manuscript and performed all experiments, except obtaining transgenic plants for TAP that was done by C.D.C., the molecular cloning partially performed by A.D.K. and the acquisition of the TAP data prepared by G.P. and G.D.J. F.D.B. kindly provided the synthetic strigolactone analog rac-GR24. S.G. supervised the project and contributed to the writing of the manuscript.

ABSTRACT

Strigolactones and smoke-derived karrikins share not only structural similarities but also common components in their signaling cascades. The F-box protein MORE AXILLARY GROWTH 2 (MAX2) is a central player in both pathways, whereas the receptors are the closely related α/β-hydrolases DWARF14 (D14) and KARRIKIN-INSENSITIVE2 (KAI2). Although direct downstream targets have been identified, many questions remain regarding the regulation of these two pathways. Therefore, we aimed at resolving the protein complexes formed around MAX2, D14, and KAI2 by means of tandem affinity purification in *Arabidopsis thaliana* seedlings. Here, we report on the identification of a novel interactor of MAX2, CONSERVED IN CILIATED SPECIES AND IN THE LAND PLANTS 1 (CCP1) and provide genetic evidence for its role in MAX2-regulated hypocotyl elongation and seed germination. We also characterized the ALPHA-CRYSTALLIN DOMAIN 32.1 (ACD32.1) protein as a direct interactor of all known components of the strigolactone and karrikin signaling, but its exact role remains to be determined.

INTRODUCTION

Strigolactones (SLs) are carotenoid-derived phytohormones involved in many plant developmental aspects, including shoot branching, root growth, lateral root formation, root hair elongation, stem elongation, secondary growth, leaf expansion, and leaf senescence (Woo et al., 2001; Stirnberg et al., 2002; Snowden et al., 2005; Gomez-Roldan et al., 2008; Umehara et al., 2008; Arite et al., 2009; Kapulnik et al., 2011; Ruyter-Spira et al., 2011; Agusti et al., 2012). Besides their role as plant hormones, SLs also act as important rhizosphere signals by promoting associations with arbuscular mycorrhizal fungi (Akiyama et al., 2005, 2010) and by inducing germination of parasitic plants (Cook et al., 1966; Yoneyama et al., 2010). Under specific conditions, the germination of nonparasitic plants can also be induced by chemical compounds. For instance, by karrikins (KARs), active compounds found in smoke that trigger germination of many plant species after fire (Flematti et al., 2004). In non-fire-following species, including *Arabidopsis*, KAR induces seed germination and influence seedling photomorphogenesis, when grown under specific conditions that otherwise hamper germination (Nelson et al., 2009, 2010). Intense genetic analysis of these observations led to the hypothesis that plants might produce currently unknown endogenous KAI2 ligand (KL) that acts through the KAR pathway (Conn & Nelson, 2016).

In *Arabidopsis thaliana,* the SL and KAR/KL pathways share similar signaling cascades with a common role for the F-box protein MORE AXILLARY GROWTH 2 (MAX2) (Nelson et al., 2011). Typically for F-box proteins, MAX2 serves as the substrate selection subunit of the Skp1-Cullin-F-box (SCF)-containing E3 ubiquitin ligase, thus selecting target proteins for ubiquitination (Stirnberg et al., 2007; Zhao et al., 2014). MAX2 interacts with the SL receptor, the α/β-hydrolase DWARF14 (D14), and with its paralog, KARRIKIN-INSENSITIVE2 (KAI2) that perceives the KAR/KL (Hamiaux et al., 2012; Bythell-Douglas et al., 2013; Guo et al., 2013; Kagiyama et al., 2013; Nakamura et al., 2013; Zhao et al., 2013; Zhao et al., 2015). Once the signaling is activated, distinct members of the SUPPRESSOR OF MAX2-1 (SMAX1)-LIKE (SMXL) protein family are targeted by SCF^{MAX2} for ubiquitination and subsequent 26S proteasomal degradation to activate downstream components of both pathways. In *Arabidopsis,* SMAX1 and SMXL2 are the KAI2 signaling targets (Stanga, et al., 2013, 2016), whereas SMXL6, SMXL7, and SMXL8 (SMXL6/7/8) act downstream in the D14-controlled pathway (Soundappan et al., 2015; Wang et al., 2015). Hence, because of this interrelation, the *d14kai2* double mutant phenotype resembles that of *max2*, but the single receptor mutants reveal the effects of the specific pathway. For instance, D14 regulates SL-related phenotypes, such as shoot branching, and KAI2 controls seed germination, a KAR/KL-related phenotype. Some phenotypes, however, including leaf morphology or hypocotyl elongation, are influenced by both D14 and KAI2 (Waters et al., 2012). The synthetic SL analog *rac*-GR24, often used in research, is a racemic mixture of a strigol-like molecule $GR24^{5DS}$ and

its enantiomer GR24$^{ent\text{-}5DS}$ that activates preferentially the D14 and KAI2 pathways, respectively (Scaffidi et al., 2014).

Further downstream signaling has mostly been focused on the role of SLs in the control of shoot branching. Currently, two mechanisms are proposed, one dependent and another independent of transcription (Shinohara et al., 2013; Liang et al., 2016). Until now, in *Arabidopsis*, only one transcription factor, BRANCHED1 (BRC1), which is involved in the repression of axillary buds' outgrowth, has been suggested to be implicated in SL signaling (Aguilar-Martinez et al., 2007; Braun et al., 2012; Dun et al., 2012), although a recent study showed that SLs can also act independently of BRC1 (Seale et al., 2017). In addition, SMXL6/7/8 have a conserved ETHYLENE- RESPONSE FACTOR Amphiphilic Repression (EAR) motif, which is known to interact with the TOPLESS family proteins, hinting again at a transcriptional regulation (Jiang et al., 2013; Zhou et al., 2013). However, SMXL7 was found to control some aspects of shoot development in a partially EAR motif-independent manner, thus most probably nontranscriptionally (Liang et al., 2016). In the proposed transcription-independent mechanism, SLs inhibit shoot branching by triggering the removal of the PIN-FORMED 1 (PIN1) auxin efflux proteins from the plasma membrane of stem xylem parenchyma cells, thereby influencing the polar auxin transport (Bennett et al., 2006; Crawford et al., 2010; Shinohara et al., 2013). In the *smxl6smxl7smxl8max2* quadruple mutant, the *BRC1* expression is significantly upregulated and the PIN1 protein level is strongly downregulated in comparison to that in the *max2* single mutant, suggesting that both models might work in parallel to control the shoot architecture (Soundappan et al., 2015; Seale et al., 2017).

Additional elucidation of the MAX2 signaling pathway is of utmost importance to gain insight into the function and regulation of the SL- and KAR/KL-controlled protein complexes. Tandem Affinity Purification (TAP) followed by mass spectrometry (MS) analysis is a powerful method to identify interactors of a protein of interest (POI) (Van Leene et al., 2008, 2015). It is a suitable approach for the characterization of interaction networks, as exemplified by the cell cycle interactome (Van Leene et al., 2007) as well as for the identification of novel players in the signaling pathways (Pauwels et al., 2010, 2015). Here, we used TAP to study protein complexes formed around MAX2, D14, and KAI2 in young seedlings. Novel interactors have been identified and their role in the SL/KAR/KL signaling pathways will be discussed.

RESULTS

GS-tagged MAX2, KAI2, and D14 are functional *in planta*

To reveal the protein complexes involved in SL and KAR/KL signaling, constructs were generated in which the expression of GS-tagged MAX2, D14, and KAI2 was driven by the *35S* cauliflower mosaic virus promoter (pCaMV35S). These constructs were stably transformed in *Arabidopsis* Columbia-0 (Col-0) plants and in the corresponding mutant backgrounds *max2-1*, *d14*, and *hyposensitive to light 3* (*htl3*; the *kai2* mutant allele). For KAI2 and D14, both carboxy (C)- and amino (N)-terminal GS-tag fusions were made, whereas for MAX2 only the N-terminal fusion was used. To avoid artificially high final bait accumulation, but yet to obtain enough proteins for proper complex isolation, we selected transgenic lines with moderate bait expression levels. To this end, the bait protein levels were analyzed in the extract from 6-day-old seedlings by Western blot with anti-GS antibodies (Van Leene et al., 2015). As shown in Figure 1, various expression levels were obtained for the *35S::GS-MAX2* (Col-0) and *35S::GS-MAX2* (*max2-1*) lines. For further analysis, we chose lines #4 and #1, respectively. For D14 and KAI2, low levels of bait expression were found when expressed in the mutant backgrounds (Figure 1). As a result, lines *35S::GS-D14* #1, *35S::D14-GS* #4, *35S::GS-KAI2* #1 and *35S::KAI2-GS* #3 in the Col-0 background were selected for further analysis. For *35S::GS-D14*, no transgenic lines with detectable expression were obtained.

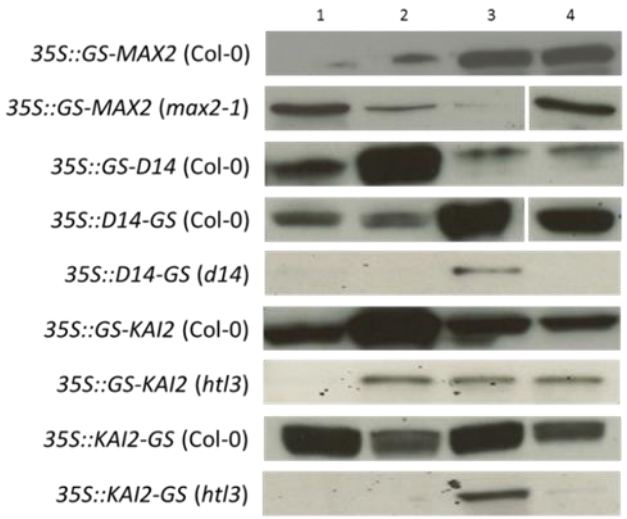

Figure 1. Protein expression analysis of *Arabidopsis* seedlings expressing GS-tagged MAX2, D14, and KAI2. Protein levels were tested in four independent transgenic lines for each N- and/or C-terminal GS tag fused with MAX2, D14, and KAI2. Detection was done with anti-GS antibodies. Molecular masses:.77.4 kDa for MAX2, 29.6 kDa for D14, 29.8 kDa for KAI1, and 21.9 kDa for the GS tag.

Next, we assessed the functionality of the bait proteins by analyzing SL-and KAR/KL-related phenotypes in the selected lines expressing GS-tagged MAX2, D14, and KAI2 in the corresponding mutant backgrounds. Shoot branching was tested as a phenotype controlled by MAX2 and D14 (Arite et al., 2009; Chevalier et al., 2014), whereas the hypocotyl length of red-light-grown seedlings was

selected as a KAI2-related phenotype (Waters et al., 2012). As already well described (Stirnberg et al., 2002, 2007; Chevalier et al., 2014), both *max2-1* and *d14* mutants are characterized by increased branching. Introduction of the *35S::GS-MAX2* into *max2-1* (line #1) reduced the number of shoot branches to that of Col-0, demonstrating that the fusion protein is functional in this transgenic line (Figure 2A). Expression of the *35S::GS-D14* construct in the *d14* background (line #3) resulted in a partial complementation of the mutant phenotype, because the number of rosette branches was intermediate between that of Col-0 and *d14* plants (Figure 2B). Lastly, the hypocotyl length was measured for *htl3* plants harboring *35S::GS-KAI2* and *35S::KAI2-GS* (line #2 and #3, respectively). The hypocotyls of *htl3* mutants were longer than those of Col-0 when grown under continuous red light (Waters et al., 2012). Both transgenic lines had shorter hypocotyls than the *htl3* mutant but were still significantly longer than those of Col-0 (Figure 2C), indicating that the constructs were partially complementing the mutant phenotype.

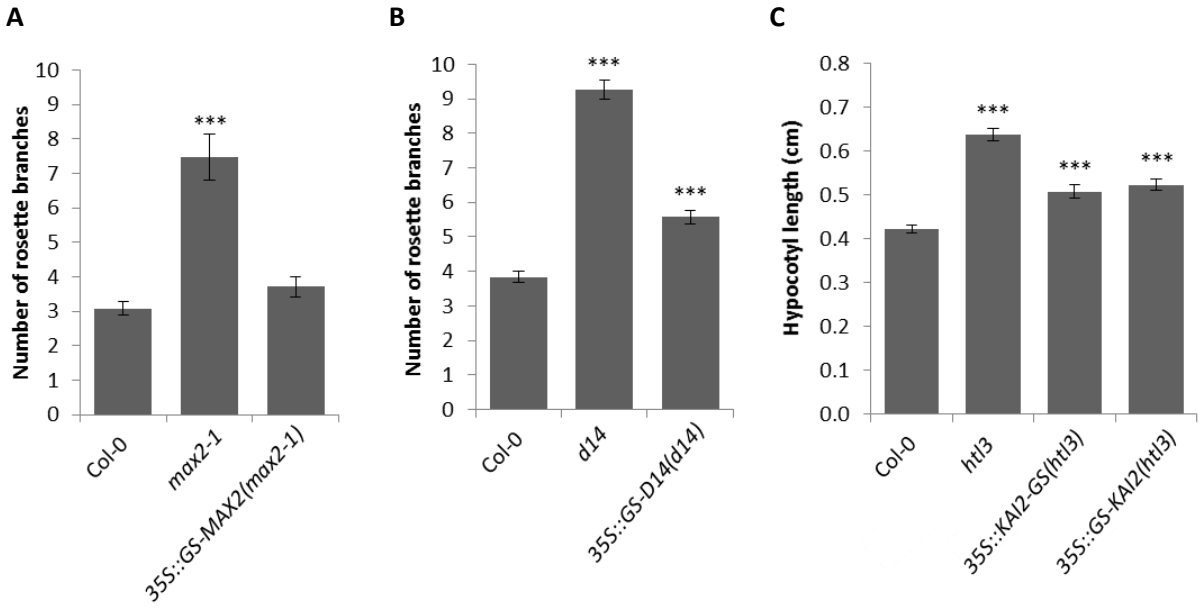

Figure 2. Shoot branching and hypocotyl elongation assay of GS-tagged MAX2, D14, and KAI2 overexpression lines. (A and B) Rosette branches of Col-0, *max2-1*, and *35S::GS-MAX2* (*max2-1*) (line #1) (A) and Col-0, *d14,* and *35S::GS-D14* (*d14*) (line #3) (B) counted after 50 days of growth (n>15). (C) Hypocotyl length of Col-0, *htl3*, *35S::KAI2-GS* (*htl3*) (line #3), and *35S::GS-KAI2* (*htl3*) (line #2) measured after exposure to red light for 4 days (n = 40). Asterisks indicate statistically significant differences between Col-0 and the mutants (*** $P < 0.001$, Student's *t* test). The experiments were repeated three times and the total mean of all biological repeats is presented. Data and error bars represent means ± SE.

Isolation of the MAX2 protein complex

To further assess the MAX2 interactome, we carried out three independent TAP experiments (Table 1, Supplemental dataset 1), two in the Col-0 background with the addition of 0.01% acetone (mock) or 1 µM *rac*-GR24 and one mock in *max2-1* seedlings. We selected 6h treatment based on the expression analysis *BRC1*, which was upregulated by the treatment with the SL analog at this time point (Chapter 7). In total, 11 proteins were copurified from which four were retrieved in more than one experiment. As expected, the known components of the SCF complex were identified, such as the ARABIDOPSIS SKP1 HOMOLOGUE 2 (ASK2; AT5G42190), CULLIN 1 (CUL1; AT4G02570), ARABIDOPSIS SKP1 HOMOLOGUE 1 (SKP1; AT1G75950), and RING-BOX 1 (RBX1; AT5G20570) (Table 1) (Stirnberg et al., 2007), further confirming functionality of the bait. Importantly, the SL receptor D14 was retrieved as well, albeit only once, when the bait was expressed in the mutant background. Additionally, six novel proteins were identified, from which only one in more than one experiment. Nevertheless, SMXL proteins, known MAX2 targets for ubiquitination and 26S proteasomal degradation (Stanga et al., 2013; Soundappan et al., 2015; Wang et al., 2015), could not be detected. Similarly, the MAX2-associated protein KAI2 was not retrieved in this analysis (Kagiyama et al., 2013; Toh et al., 2014).

Table 1. Overview of prey proteins identified by TAP with MAX2 as bait.

AGI	Protein	*35S::GS-MAX2*		*35S::GS-MAX2 (max2-1)*
		Mock	*rac*-GR24	Mock
AT2G42620	MAX2, MORE AXILLARY BRANCHES 2	1	1	1
AT5G42190	ASK2, ARABIDOPSIS SKP-LIKE 2	1	1	1
AT4G02570	CUL1, CULLIN 1	1	1	1
AT1G75950	SKP1, ARABIDOPSIS SKP1 HOMOLOGUE 1	1	1	1
AT3G16460	JAL34, JACALIN-RELATED LECTIN 34	-	1	1
AT5G20570	RBX1, RING-BOX 1	1	-	-
AT2G34560	CCP1,CONSERVED IN CILIATED SPECIES AND IN THE LAND PLANTS 1	1	-	-
AT1G54000	GLL22, GDSL LIPASE-LIKE PROTEIN 22	-	1	-
AT1G66280	BGLU22, Glycosyl hydrolase superfamily protein	-	1	-
AT3G20370	TRAF-like family protein	-	1	-
AT3G03990	D14, DWARF 14	-	-	1
AT3G14210	ESM1, EPITHIOSPECIFIER MODIFIER 1	-	-	1

TAP experiments were done on 6-day-old seedlings expressing *35S::GS-MAX2* treated with 0.01% acetone (mock) or with 1 µM *rac*-GR24. Prey proteins were identified with peptide-based homology analysis of MS data. Background proteins were withdrawn based on the occurrence frequency of copurified proteins in a large GS TAP data set (Van Leene et al., 2015). The number indicates whether prey was identified in one experiment per column. Abbreviations: AGI, Arabidopsis Genome Identifier; –, no prey identified in this experiment.

Localization to the same subcellular compartment is essential for the protein-protein interaction to occur. Therefore, for further analysis, we selected only those prey proteins that are predicted to localize in the nucleus, which is consistent with the MAX2 localization (Stirnberg et al., 2007; Liang et al., 2016). Transient overexpression of CONSERVED IN CILIATED SPECIES AND IN THE LAND PLANTS 1 (CCP1; AT2G34560), JACALIN-RELATED LECTIN 34 (JAL34; AT3G16460), and EPITHIOSPECIFIER MODIFIER 1 (ESM1; AT3G14210) in *Nicotiana benthamiana* leaves confirmed the nuclear localization of the selected proteins, although expression was also observed in the cytoplasm (Figure 3).

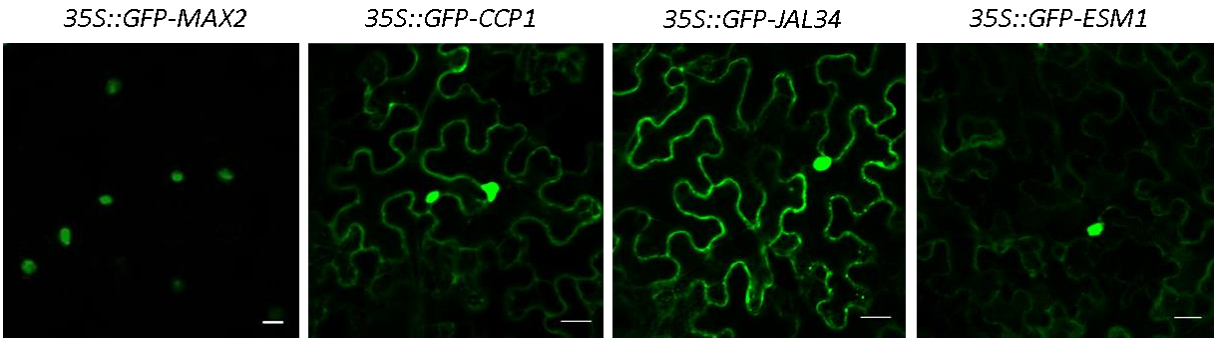

Figure 3. Subcellular localization of proteins used in this study. *N. benthamiana* leaves were transiently transformed with N-terminally green fluorescent protein (GFP)-tagged MAX2, CCP1, JAL34, and ESM1 and imaged by confocal microscopy. Scale bar 20 µm.

First, to validate the selected candidates, we used the LexA-based yeast two-hybrid (Y2H) assay, because it had previously been applied successfully to show the interaction between MAX2 and KAI2 proteins (Toh et al., 2014). In the screen, only yeasts cotransformed with the positive control MAX2 fused to the GAL4-binding domain (BD) and SKP1 fused to the GAL4 activation domain (AD) stained blue when spotted on selective medium lacking uracil, tryptophan, and histidine (SD-L-T-H) with the addition of 5-bromo-4-chloro-3-indolyl-β-D-galactopyranoside (X-gal) (Figure 4D). No other interaction could be visualized, indicating the lack of direct interaction between MAX2 and the selected preys in this system (Figure 4D).

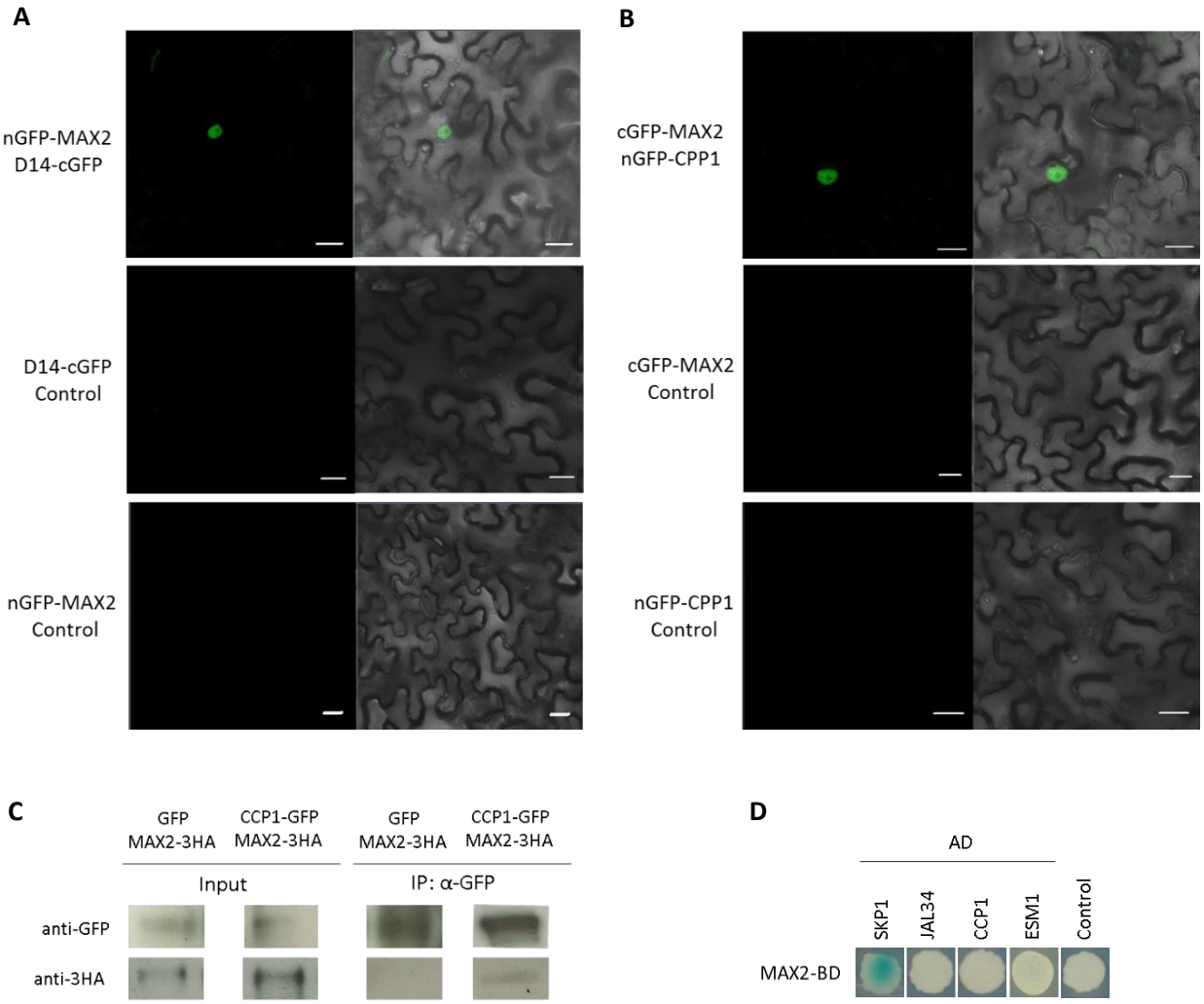

Figure 4. Validation studies of MAX2 interactions. *N. benthamiana* leaves were transiently transformed with *35S::nGFP-MAX2* and *35S::D14-cGFP* (A) or *35S::cGFP-MAX2* and *35S::nGFP-CPP1* (B). For the negative control, every construct was combined with the corresponding *35S::nGFP* or *35S::cGFP*. The GFP signal only (left) or merged with bright-field images (right) are shown. Scale bar 20 µm. (C) Interaction between CCP1-GFP and MAX2-3HA revealed by Co-IP. Protein extracts were prepared from *N. benthamiana* leaves transiently expressing CCP1-GFP and MAX2-3HA. Input means total protein lysate without immunoprecipitation. (D) Y2H screen of the selected MAX2 prey proteins. The EGY48 (p8opLacZ) strain of yeast (*Saccharomyces cerevisiae*) was cotransformed with MAX2 in pGILDA and prey proteins in pB42AD or pB42AD alone (control). Transformed yeasts were spotted on inducing medium containing galactose and raffinose supplemented with X-Gal. Yeast transformation done in two independent replicates gave consistent results.

We then assessed all the interactions by means of Bimolecular Fluorescence Complementation (BiFC) in which the proteins are fused with N-terminal or C-terminal fragments of GFP (nGFP and cGFP, respectively). As a positive control we used the well described MAX2-D14 association (Hamiaux et al., 2012; Zhao et al., 2015; Liang et al., 2016; Yao et al., 2016). As expected, when nGFP-MAX2 and D14-cGFP were transiently coexpressed in *N. benthamiana* leaves, a strong GFP signal was observed in

the nucleus (Figure 4A). Similarly, when cGFP-MAX2 and nGFP-CPP1 were coexpressed, the GFP signal was detected in the nucleus (Figure 4B). As a negative control, we coexpressed nGFP-MAX2, cGFP-MAX2, D14-cGFP, and nGFP-CPP1 together with the vector containing only the complementary GFP part. No fluorescence was detected for any of the tested combinations, indicating that the GFP could not be reconstituted without interaction between the tested proteins. No interaction was detected between MAX2 and JAL34 or ESM1 using BiFC (data not shown). Finally, we investigated the MAX2-CCP1 interaction by means of coimmunoprecipitation (Co-IP) of CCP1-GFP and MAX2-3HA transiently expressed in *N. benthamiana* leaves. As shown in Figure 4C, MAX2-3HA coprecipitated with CCP1-GFP *in vivo*, whereas no interaction was detected with the GFP protein alone that was used as a negative control (Figure 4C). Based on these data, we can conclude that the CCP1 protein is a part of a nucleus-localized MAX2 complex.

Toward the functional role of the MAX2-CCP1 interaction

CCP1 belongs to the p-loop–containing nucleoside triphosphate hydrolases protein superfamily and it is the closest homolog of KATANIN 1 (KTN1; AT1G80350), sharing 44% sequence identity (Figure 5). Both KTN1 and CCP1 contain AAA+ ATPase domain. Katanin is composed of two subunits, p60 with microtubule binding and severing activities, and the p80 regulatory subunit, targeting katanin to different subcellular localizations (Zhong, & Ye, 2007). KTN1 is the only p60 catalytic subunit identified thus far in *Arabidopsis*, whereas four orthologues of the regulatory p80 subunit have been reported (Wang et al., 2017a). KTN1 regulates the plant microtubule organization (Hartman et al., 1998; Stoppin-Mellet et al., 2007), also in response to phytohormones (Meier et al., 2001; Bouquin et al., 2003) and environmental stimuli (Nakamura et al., 2015).

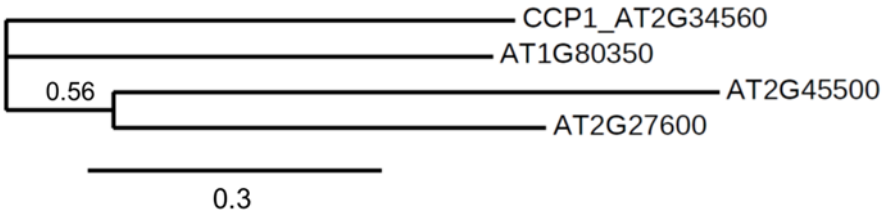

Figure 5. Phylogenetic analysis of CCP1. Maximum-likelihood tree by PhyML showing the relation of CCP1 with other ATP-binding proteins selected by a BLAST search with CCP1 against the *A. thaliana* genome. Values indicated at branch nodes represent bootstrap support derived from 100 bootstrap replicates. The scale bar corresponds to the number of amino acid substitutions per site.

To characterize the physiological function of the *CCP1* gene, we selected a SALK transfer DNA (T-DNA) insertion line, referred to as *ccp1.* The T-DNA of this line is inserted into the 5th exon of the gene (Figure 6A). To confirm that this T-DNA insertion line was a knockout, we tested the *CCP1* transcript level in the *ccp1* mutant by reverse transcription polymerase chain reaction (RT-PCR) with primers flanking the T-DNA insertion site (Figure 6A). No transcript was detected in the *ccp1* mutant, although the gene was expressed in Col-0 (Figure 6B), indicating that *ccp1* is a knockout and can be used to assess various SL-and KAR/KL-related phenotypes.

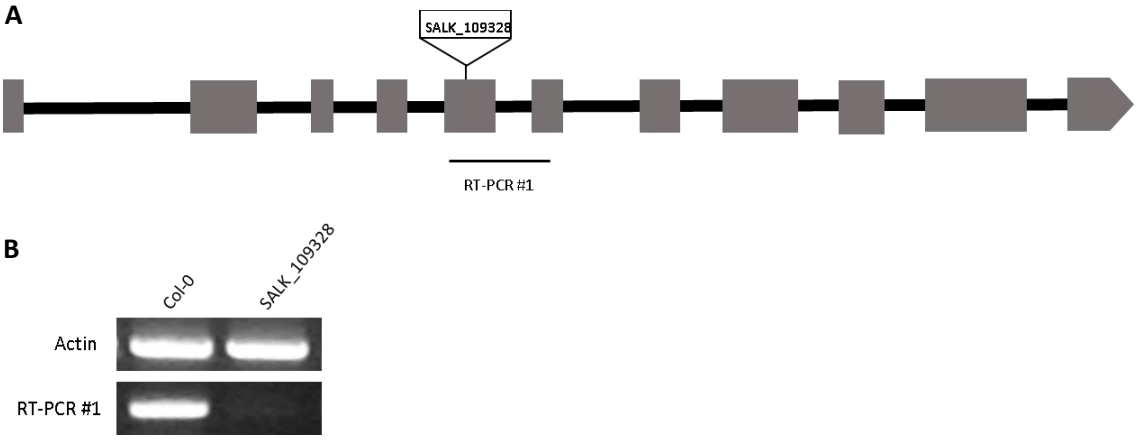

Figure 6. Characterization of *CCP1* T-DNA insertion mutant. (A) Schematic visualization of the *CCP1* gene structure, T-DNA insertion, and primers used for RT-PCR. Grey boxes represent exons. (B) Transcript level of *CCP1* in Col-0 and *ccp1* mutant. *ACTIN2* primers were used as a control. Primers are listed in the Supplemental Table 1.

The SL signaling mutants *max2-1* and *d14* are characterized by a bushy phenotype, whereas *kai2* has a number of shoot branches similar to that of Col-0 (Stirnberg et al., 2002; Chevalier et al., 2014; Waters et al., 2015). To examine the potential role of *CCP1* in shoot branching, we counted the total number of rosette branches in *ccp1*, Col-0, and *max2-1*. The average number of shoot branches for the *ccp1* mutant was similar to that of Col-0, but the *max2-1* mutant had a significantly higher number of rosette branches, confirming previous data (Figure 7A) (Stirnberg et al., 2002).

To test whether *CCP1* is involved in MAX2-mediated signaling in the root, *ccp1* and Col-0 plants were grown for 9 days under either mock (0.01% acetone) or treatment conditions (1 µM *rac*-GR24), the number of emerged lateral roots was counted, and subsequently, the lateral root density (LRD) was calculated. In mock-treated plants, the number of lateral roots and the LDR did not differ between Col-0 and *ccp1* mutant. Additionally, both Col-0 and *ccp1* seedlings grown on *rac*-GR24—containing medium displayed a significant (*P* value <0.001) decrease in the total number of emerged lateral

roots and a significant reduction (*P* value <0.001) in LRD, suggesting no involvement of *CCP1* in the root response to SLs (Figure 7B,C).

Next, we tested two KAR/KL-related phenotypes that are controlled by MAX2. Under continuous red light, the hypocotyl length of *max2* mutant is longer than that of Col-0 plants (Waters et al., 2012). Additionally, treatment with *rac*-GR24 is known to decrease the hypocotyl elongation of Col-0 seedlings grown under these conditions (Nelson et al., 2011), whereas the *max2* mutant remains insensitive. In our analysis, both Col-0 and *ccp1* seedlings were characterized by a reduced hypocotyl elongation when grown on *rac*-GR24–containing medium, but *max2-1* remained fully insensitive to this treatment (Figure 7D). Under mock conditions, the hypocotyl was longer in *max2-1* than that in Col-0, in agreement with previous observations (Nelson et al., 2011). Interestingly, an opposite phenotype, a significantly shorter hypocotyl, was observed for the *ccp1* mutant, hinting at a possible role in the hypocotyl elongation controlled by KAR/KL signaling.

In *Arabidopsis,* seed germination can be suppressed by suboptimal temperature conditions, called thermoinhibition. This induced seed dormancy can be overcome by addition of *rac*-GR24 (Toh et al., 2008). Under these conditions, *max2-1* seeds have a very low germination rate in mock and are insensitive to the exogenous *rac*-GR24 (Toh et al., 2012) (Figure 7E). As shown in Figure 7E, the germination frequency in mock conditions did not differ statistically between Col-0 and the *ccp1* mutant. Although *ccp1* seeds were responsive to the addition of *rac*-GR24, the germination induction was significantly lower than that of Col-0 (92% and 181%, respectively) (Figure 7E), suggesting that CCP1 might play a role in *rac*-GR24–induced seed germination. In the continuous light, germination frequency of tested mutants did not differ from that of Col-0 and no effect of *rac*-GR24 was observed (Figure 7F).

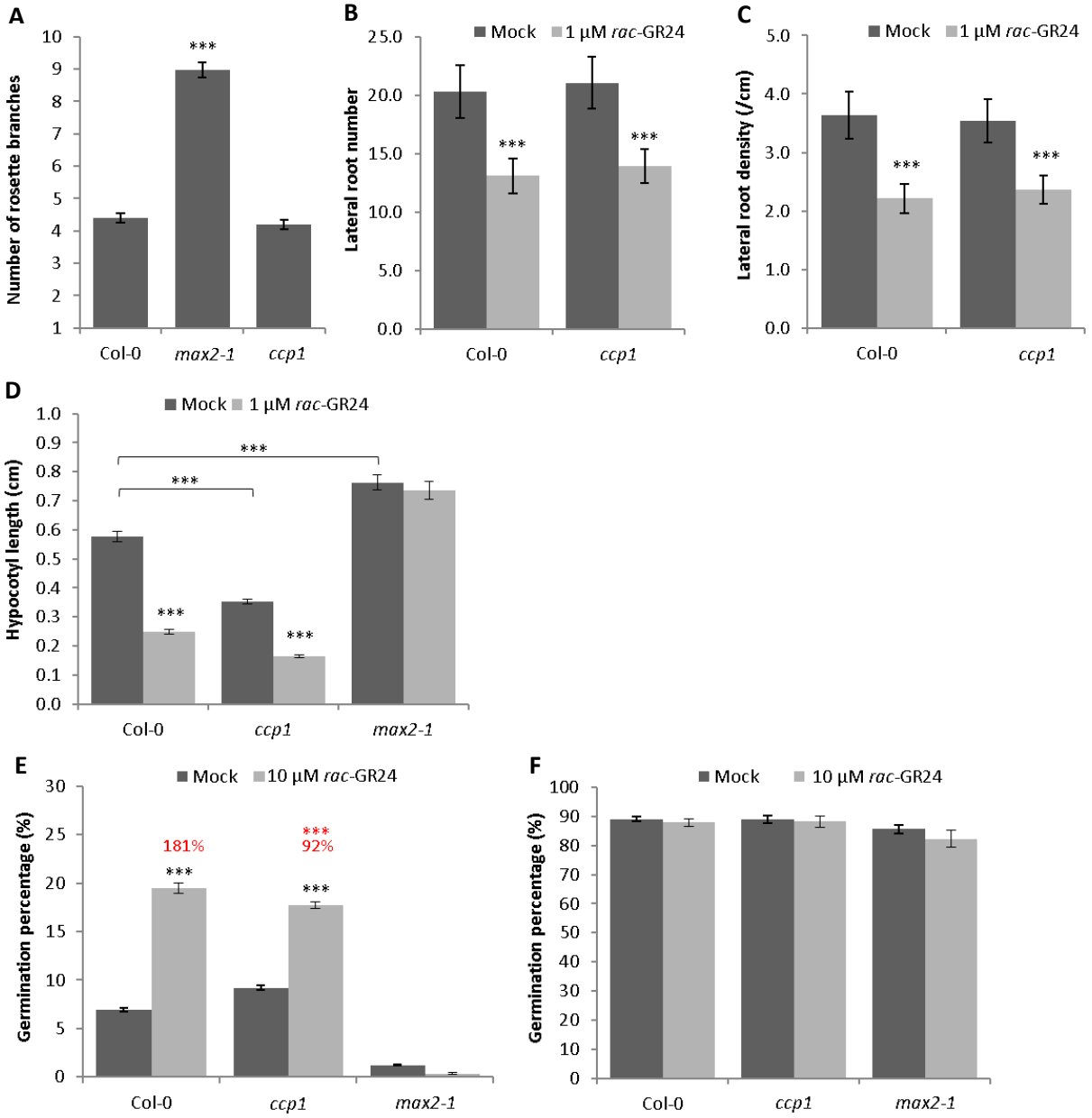

Figure 7. MAX2-related phenotypes of the *ccp1* mutant. (A) Shoot branching assay of Col-0, *max2-1,* and *ccp1* counted after 50 days of growth (n=18). Lateral root number (B) and LRD (C) of Col-0 and the *ccp1* analyzed in 9-day-old plants treated without or with 1 µM *rac*-GR24 (n = 30). (D) Hypocotyl length of 4-day-old Col-0, *ccp1,* and *max2-1* seedlings grown under continuous red light without or with 1 µM *rac*-GR24 (n = 40). (E) Germination assay for thermoinhibited seeds of Col-0, *ccp1,* and *max2-1.* Seeds were distributed in 96-well plates containing HEPES buffer without (0.1% acetonitrile) or 10 µM *rac*-GR24 and placed in the dark for 3 days at 24˚C (E) or in light at 21 ˚C for the control (F). Asterisks indicate statistically significant differences between treatments, asterisks above the lines- between genotypes and asterisks in red- in percentage increase (*** $P <$ 0.001, Student's *t* test (A), ANOVA mixed model (B), Poisson regression model (C), linear mixed model (D), and logistic regression with the glimmix procedure (E). The experiments were repeated three times and the total mean of all biological repeats is presented. Data and error bars represent means ± SE.

Novel components of the KAI2 protein complex

To detect components of protein complexes formed around D14 and KAI2, we carried out TAP experiments on 6-day-old seedlings treated with 0.01% acetone (mock) or with 1 µM *rac*-GR24. After MS analysis of the D14 TAPs, only the bait protein was retrieved (Supplemental dataset 2). No preys were identified, although D14 had been described previously to interact with MAX2 and SMXL6/7/8 (Hamiaux et al., 2012; Kagiyama et al., 2013; Nakamura et al., 2013; Soundappan et al., 2015; Wang et al., 2015). On the contrary, TAP experiments of KAI2 yielded in total six possible preys, from which three were retrieved in more than one experiment. Interestingly, D14 was identified twice in the mock-treated samples (Table 2, Supplemental dataset 3).

Table 2. Overview of prey proteins purified by TAP with KAI2 as bait protein.

AGI	Protein	*35S::GS-KAI2*		*35S::KAI2-GS*	
		Mock	*rac*-GR24	Mock	*rac*-GR24
AT4G37470	KAI2, KARRIKIN INSENSITIVE 2	1	1	1	1
AT1G06460	ACD32.1, ALPHA-CRYSTALLIN DOMAIN 31.2	1	1	-	1
AT4G13670	PTAC5, PLASTID TRANSCRIPTIONALLY ACTIVE 5	1	1	-	-
AT3G03990	D14, DWARF 14	1	-	1	-
AT4G34980	SLP2, SUBTILISIN-LIKE SERINE PROTEASE 2	-	1	-	-
AT4G33650	DRP3A, DYNAMIN-RELATED PROTEIN 3A	-	1	-	-
AT2G14120	DRP3B, DYNAMIN RELATED PROTEIN	-	1	-	-

TAP experiments were done on 6-day-old seedlings expressing *35S::GS-KAI2* and *35S:: KAI2-GS* treated without or with 1 µM *rac*-GR24. Prey proteins were identified with peptide-based homology analysis of MS data. Background proteins were withdrawn based on the occurrence frequency of copurified proteins in a large GS TAP data set (Van Leene et al., 2015). The number indicates whether a prey was identified in one experiment per column. Abbreviations: AGI, Arabidopsis Genome Identifier**.** –, no prey identified in this experiment.

All the preys that were retrieved at least in two TAP experiments were further analyzed. These were ALPHA-CRYSTALLIN DOMAIN 32.1 (ACD32.1; AT1G06460), PLASTID TRANSCRIPTIONALLY ACTIVE 5 (PTAC5; AT4G13670), and D14 (AT3G03990). First, the subcellular localization of the selected candidates was tested by transient overexpression in *N*. *benthamiana* leaves (Figure 8). Both KAI2 and D14 localized to the nucleus and cytoplasm. The subcellular localization of PTAC5 was previously reported in plastids, more specifically chloroplasts (Pfalz et al., 2006; Zhong et al., 2013). Here, we detected PTAC5 protein in the cytoplasm and other structures that might be indeed plastids. ACD32.1 was reported in *Arabidopsis* leaf and cell cultures peroxisome proteome (Reumann et al., 2007; Eubel et al., 2008) and in the *Arabidopsis* genome screen for proteins with putative peroxisome targeting signals (Reumann et al., 2004). Based on this knowledge we speculated that observed subcellular localization of ACD32.1 might be indeed in the peroxisomes, but in some cells also in the nucleus and cytoplasm (Figure 8).

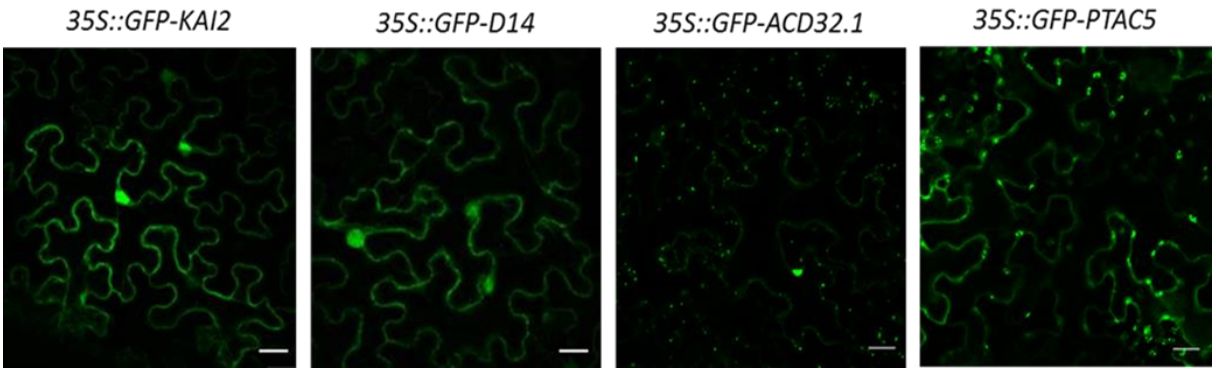

Figure 8. Subcellular localization and interaction studies of KAI2 preys. *N. benthamiana* leaves were transiently transformed with N-terminally GFP-tagged KAI2, D14, ACD32.1, and PTAC5 and imaged by confocal microscopy. Scale bar 20 µm.

First, we focused on the ACD32.1 protein, because it was present in almost all KAI2 TAP experiments. The STRING (Search Tool for the Retrieval of Interacting Genes/Proteins) analysis revealed SMAX1 as one of its predicted functional partners (Figure 9A). This protein-protein interaction data base contains the information related to both known and predicted interaction partners for a large number of organisms. Apart from physical interactions STRING describes also 'functional association', such as proteins that participate in the same metabolic pathway or cellular process. The association between ACD32.1 and SMAX1 was detected based on the gene coexpression and interaction of their orthologs in other organisms, gene neighborhood and text mining. Considering these data, we further tested the interaction between ACD32.1 and all proteins known to be part of both the SL and KAR/KL signaling pathways by means of the LexA-based Y2H. Indeed, ACD32.1 was able to interact directly with KAI2, MAX2, SMAX1, and SMXL7 both without and with the addition of *rac*-GR24 (Figure 9B). Interestingly, the interaction between ACD32.1 and D14 was faint and only visible after treatment with *rac*-GR24, similarly to what had been reported previously for the D14-SMXL6/7/8 association (Figure 9B) (Chapter 3; Soundappan et al., 2015; Wang et al., 2015; Liang et al., 2016). To conclude, ACD32.1 is an interesting candidate for further investigation of its biological role due to its interaction with all the known components of SL and KAR/KL pathways in *Arabidopsis*.

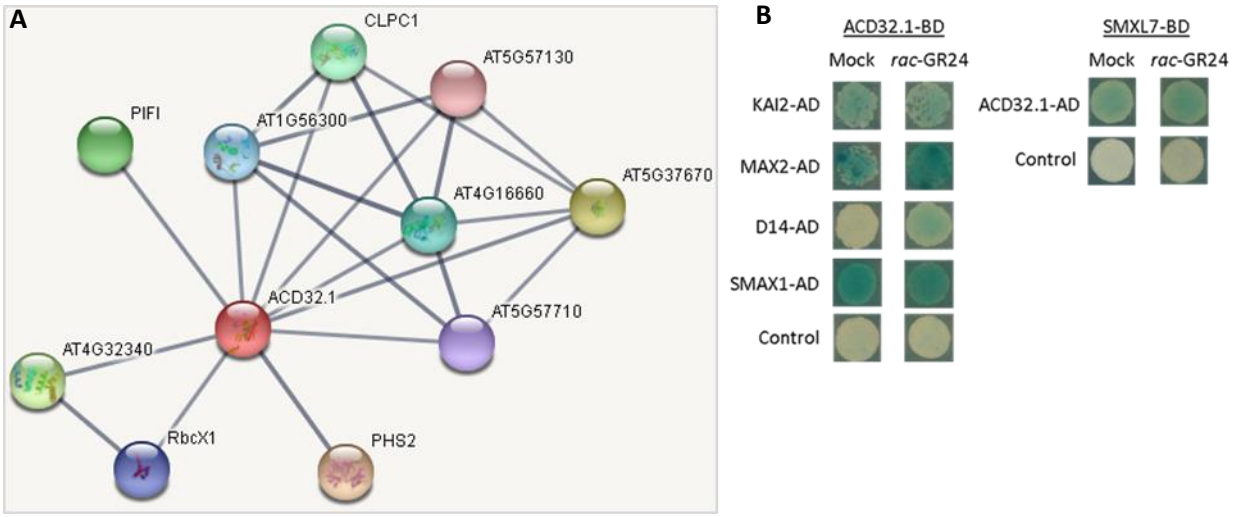

Figure 9. ACD32.1 interactions revealed by STRING and Y2H. (A) String network revealing connection between ACD32.1 and SMAX1 (AT5G57710). String analysis was performed to search for predicted functional partners of ACD32.1. Only high confidence interactions (score >0.700), indicating the estimated probability that a certain interaction is biologically meaningful, more specifically the likelihood of finding both proteins within the same KEGG (Kyoto Encyclopedia of Genes and Genomes) pathway, are shown. (B) Y2H study of ACD32.1 interactions. ACD32.1 fused to GAL4-BD was tested for its interaction with KAI2, MAX2, D14, and SMAX1 fused to GAL4-AD in the absence and in the presence of 10 µM *rac*-GR24, whereas SMXL7 fused with GAL4-BD was tested with ACD32.1-AD. For the negative control, proteins fused with GAL4-BD were tested with pB42AD. Yeasts transformed with both plasmids were selected on SD (Raf/Gal)-U-T-H medium supplemented with X-Gal. Out of three independent colonies, one representative is shown.

Next, we wished to unravel the striking KAI2-D14 association in TAP experiments. To this end, we used the LexA-based Y2H and BiFC for examination of the pairwise interaction and for *in vivo* validation, respectively. In the Y2H assay, yeast cotransformed KAI2-BD and D14-AD stained blue when spotted on the selective medium supplemented with X-Gal, but not when the KAI2-AD-D14-BD combination was used (Figure 10B). However, the blue color appeared as well in the negative control, in which yeasts were cotransformed with KAI2 fused to GAL4-BD and the pB42AD vector. This observation indicates that KAI2 is autoactive in Y2H assays and, hence, that it cannot be used to validate the D14-KAI2 interaction (Figure 10B). Further, to analyze the interaction by BiFC, eight different combinations for D14 and KAI2 with nGFP or cGFP fused N- or C-terminally were verified by coexpression in *N. benthamiana* leaves (Table 3). The GFP signal in the nucleus and cytoplasm was strong in half of these combinations (Figure 10A), but in the remaining half, no fluorescence was detected. As a negative control, each construct was cotransformed with the complementing GFP part, *35S::nGFP* or *35S::cGFP*. Fluorescence was discovered in the negative controls of nGFP-KAI2, cGFP-KAI2, and KAI2-cGFP, indicating that these constructs do not require the KAI2-D14 interaction

to reconstitute GFP. These data demonstrate that also by means of BiFC, the KAI2-D14 interaction cannot be validated.

Table 3. Overview of KAI2 and D14 constructs used in BIFC

	nGFP	cGFP	GFP signal		nGFP	cGFP	GFP signal
1	D14-nGFP	cGFP-KAI2	+	5	nGFP-D14	cGFP-KAI2	-
2	D14-nGFP	KAI2-cGFP	+	6	nGFP-D14	KAI2-cGFP	-
3	nGFP-KAI2	cGFP-D14	+	7	KAI2-nGFP	cGFP-D14	-
4	nGFP-KAI2	D14-cGFP	+	8	KAI2-nGFP	D14-cGFP	-

Different combinations of D14 and KAI2 N- and C-terminally fused with nGFP and/or cGFP used in the BiFC assay. +, GFP signal; -, no GFP signal.

Taken together, although the KAI2-D14 interaction was retrieved in half of the TAP experiments, further validation of its relevance cannot be obtained, either with Y2H, due to the high KAI2 autoactivation, or by BiFC analysis, because of the GFP protein self-reconstitution. Consequently, another assay, such as Co-IP, needs to be used to resolve the KAI2- D14 interaction.

Lastly, we investigated the association between KAI2 and PTAC5, which was identified in half of KAI2 TAP experiments. Nevertheless, this interaction could not be validated, either by Y2H or *in vivo* with BiFC analysis (data not shown), indicating that PTAC5 might be a false positive interactor.

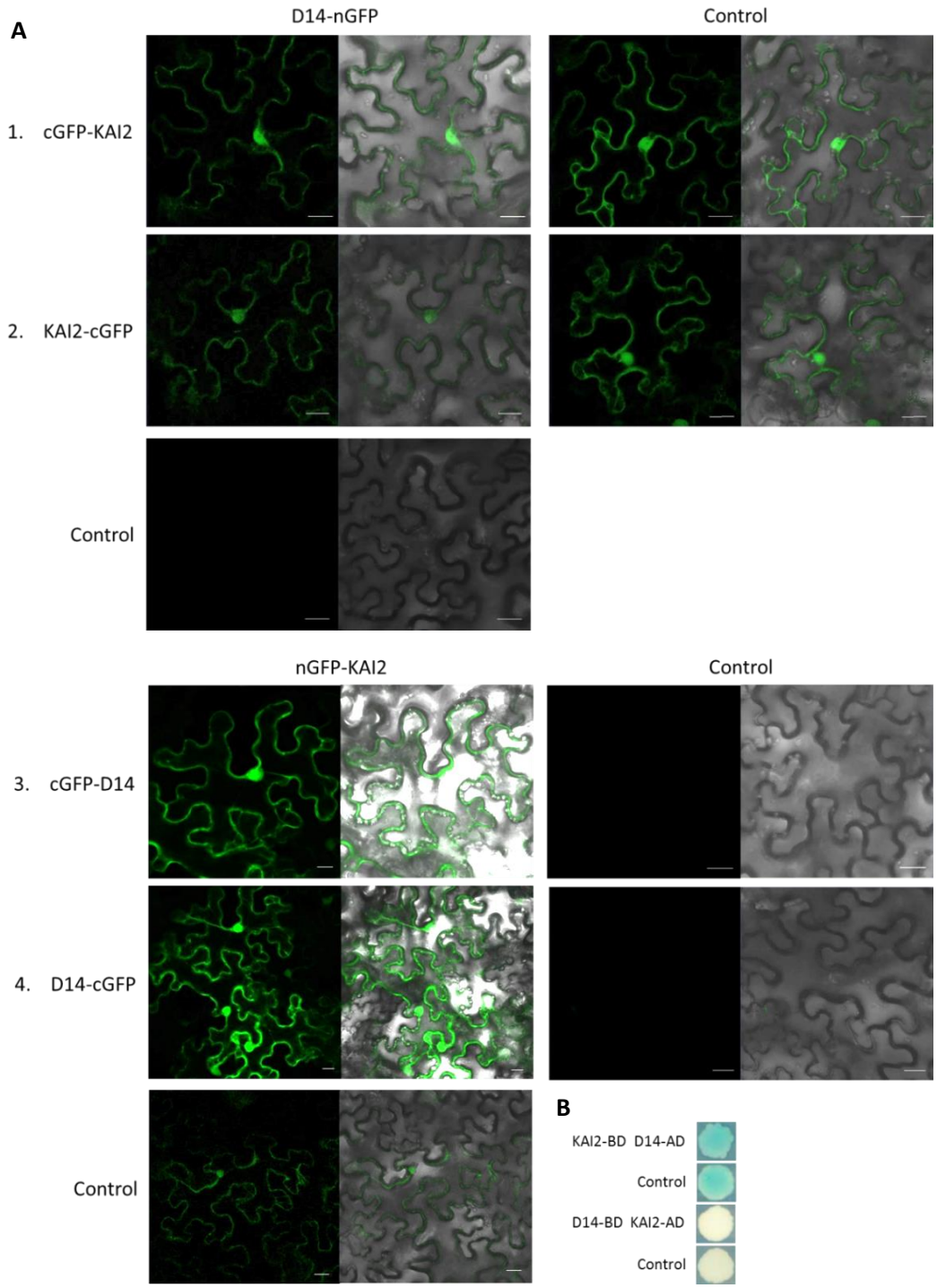

Figure 10. Validation of the KAI2-D14 interaction. (A) BiFC analysis of KAI2-D14 interaction in *N. benthamiana.* Leaves were transformed with eight different combinations of D14 and KAI2 N- and C-terminally fused with nGFP and/or cGFP. Only combinations yielding a GFP signal are shown. For the negative control, every construct was cotransformed with the corresponding GFP part, *35S::nGFP* or *35S::cGFP*. The GFP signal only (left) or merged with bright-field images (right). Scale bar 20 µm. (B) Y2H of KAI2 and D14 fused to GAL4-BD and GAL4-AD. For negative control, KAI2-BD and D14-BD were tested with pB42AD. Transformed EGY48 yeasts were spotted on inducing medium containing Gal and raffinose supplemented with X-Gal.

DISCUSSION

The MAX2 protein is a central component of the SL and KAR/KL pathways required for ubiquitination and degradation of target proteins (Nelson et al., 2011). In the past few years, there was a rapid progress in our understanding of the SL and KAR/KL signaling, including the discovery of the receptor proteins D14 and KAI2, respectively (Hamiaux et al., 2012; Bythell-Douglas et al., 2013; Guo et al., 2013; Kagiyama et al., 2013; Nakamura et al., 2013; Zhao et al., 2013; Zhao et al., 2015) and the SMXL family members as downstream targets (Soundappan et al., 2015; Wang et al., 2015; Stanga et al., 2016). Nevertheless, the interaction network of the core components still needs to be characterized to provide information about the pathway function and regulation. TAP is one of the most advanced methods that allows the isolation of protein complexes under near-physiological conditions, thus, providing an extensive view on the interaction networks (Van Leene et al., 2015).

Here, we used TAP in *Arabidopsis* seedlings as a unique approach to further unravel the MAX2, D14, and KAI2 interactome. TAP-MS analysis has been already successfully applied in *Arabidopsis* seedlings (Eloy et al., 2012; Vercruyssen et al., 2014) and has been demonstrated to have many advantages above cell cultures, especially for the elucidation of developmental pathways. For example, additional interactors of the ANGUSTIFOLIA3 protein have been found by using TAP *in planta* compared to TAP in cell cultures (Vercruyssen et al., 2014). Ideally, the bait protein is expressed under the control of the functional, endogenous promoter in the corresponding mutant background (Van Leene et al., 2015). In our analysis, we used the constitutive *35S* promoter to overexpress GS-tagged MAX2, D14, and KAI2. To test whether the tag does not interfere with the endogenous function, localization, or bait properties, complementation of mutant phenotypes was analyzed. We found that the N-terminally tagged MAX2 is fully functional, because it could restore the increased branching phenotype of the *max2-1* mutant to the wild-type level. On the contrary, when GS-tagged D14 and KAI2 were overexpressed in the corresponding mutant background, the tested phenotypes, shoot branching and hypocotyl length, respectively, were partially complemented. Plants expressing *35S::GS-D14* (*d14), 35S::GS-KAI2* (*htl3*), and *35S::KAI2-GS* (*htl3*) had an intermediate phenotypes between Col-0 and the corresponding mutant. A similar observation has been described for the SMXL7 protein. The *35S::SMXL7-yellow fluorescent protein (YFP)* construct transformed into the *smxl6 smxl7 smxl8 max2* background only partially restored the shoot branching of the mutant toward the expected *max2*-like branch number, whereas a similar fusion driven by the native SMXL7 promoter completely restored the branching phenotype. In addition, GFP-tagged D14 expressed under control of the native promoter could complement the increased branching phenotype of *d14-2/seto5* mutant (Chevalier et al. 2014). There are two possible explanations for the partial complementation of mutant phenotypes. Firstly, the functionality of the protein fusions can be

disturbed by the tag, such as incorrect protein folding. Secondly, a *35S* promoter activity different from the endogenous one can lead to missexpression or to too high accumulation of tagged proteins (Liang et al., 2016). Hence, it would be advisable to transform *d14* and *kai2* mutants with a similar fusion driven by the native D14 and KAI2 promoters and to check whether this fusion protein is able to completely restore the branching and hypocotyl phenotypes.

TAP experiments with MAX2 as bait successfully revealed well-known interactors of the F-box proteins, i.e., components of the SCF complex SKP1, ASK2, RBX1, and CUL1 (Stirnberg et al., 2007; Zhao et al., 2014). Furthermore, the interaction between MAX2 and D14 was detected. Although this interaction has been shown to be promoted by *rac*-GR24 addition (Hamiaux et al., 2012; Liang et al., 2016; Yao et al., 2016), it could be identified only once in a mock-treated sample. Thus, it is plausible that the endogenous SL levels in young *Arabidopsis* seedlings were sufficient to establish this MAX2-D14 interaction. Moreover, consistently with Förster resonance energy transfer-fluorescence-lifetime imaging microscopy (FRET-FLIM) data (Liang et al., 2016), our BiFC analysis corroborated that the MAX2-D14 interaction occurs in the nucleus. Besides the expected interactors, six novel prey proteins of MAX2 were identified, from which three were selected for further characterization based on the subcellular localization. Transient overexpression of JAL34, ESM1, and CCP1 in *N. benthamiana* leaves confirmed the predicted subcellular localization to the nucleus, corresponding with the MAX2 localization (Figure 3) (Stirnberg et al., 2007) and implying that the interactions between these proteins can occur.

To validate the interactions revealed by the TAP experiments, we needed a complementary method. Although Y2H is a quick and convenient technique to detect direct interactions, in our experiment, we could not confirm the interaction between MAX2 and any of the selected prey proteins. A possible explanation can be, that Y2H is done in a heterologous system, thus a negative result during Y2H does not indicate a negative interaction under native conditions (Kudla and Block 2016). Moreover, Y2H is used to detect direct interactions, but during TAP experiments the whole protein complexes are identified that do not necessarily interact directly with the bait. Therefore, we used BiFC and Co-IP in *N. benthamiana*, because both methods can provide more physiologically relevant context. Our *in planta* validation data confirmed that the association between MAX2 and CCP1 occurred in the nucleus. As Y2H results suggested that this interaction is not direct interaction, it is possible that other proteins might facilitate MAX2-CCP1 complex formation. Based on the phenotypic analysis, the components of KAR/KL pathway rather than SL are expected to have this role, for instance KAI2.

To understand the role of CCP1 in the MAX2 signaling, we carried out a detailed study of mutant phenotypes, including shoot branching, lateral root density, hypocotyl elongation, and seed germination analysis. The number of shoot branches in the *ccp1* mutant was similar to that in Col-0 and also the response to *rac*-GR24 in the roots was not altered. The only difference between the *ccp1* mutant and Col-0 were found in the MAX2- and KAI2-controlled phenotypes. When seedlings were grown for 4 days under continuous red light, the *ccp1* mutant had shorter hypocotyls, comparable to the *smax1* phenotype (Stanga et al. 2016) and opposite to the *max2-1* mutant. However, whether this effect is related to the MAX2 signaling should be determined by analysis of the *ccp1 smax1* and *ccp1 max2* double mutants. Furthermore, when the germination frequency was tested under suboptimal temperature conditions, the *ccp1* mutant was less responsive to the treatment with *rac*-GR24, suggesting again a possible involvement in the KAI2-mediated signaling.

CCP1 is related to KTN1, a microtubule-severing protein. The microtubule-severing process is one of the mechanisms that determines the spatiotemporal organization of microtubule arrays, which is essential for plant growth and development (Sedbrook & Kaloriti, 2008; Wasteneys & Ambrose, 2009). Mutants of KTN1 (*kat1*) exhibited decreased root, hypocotyl, stem, and leaf sizes as a result of a reduced cell expansion (Bichet et al., 2001; Burk et al., 2001). Thus, *CCP1* might plausibly play a comparable role in the cell expansion regulation in hypocotyl, with a reduced length in the mutant as a result. However, GFP-tagged CCP1 was localized to nucleus and cytoplasm when transiently expressed in tobacco leaf epidermis cells and no clear localization pattern at the microtubules was observed. Therefore, more in depth studies are required to confirm that CCP1 is a microtubule associated protein.

In addition, treatments with hormones, including auxin, gibberellin, brassinosteroids, ethylenes and abscisic acid have been shown to modify the cortical microtubule orientation (Baluska et al., 1993; Ishida & Katsumi, 1992; Zandomeni & Schopfer, 1993). *kat1* mutants exhibit altered cell growth-related responses to gibberellic acid and ethylene (Bouquin et al., 2003; Meier et al., 2001), hinting at a potential role of KTN1 in controlling the microtubule reorganization in response to hormones. Thus, we can hypothesize that CCP1 might be involved in the regulation of the microtubule orientation in response to *rac*-GR24. To prove this hypothesis, a GFP-tagged tubulin should be constitutively expressed in the *ccp1* mutant background or anti-tubulin antibodies should be used for whole-mount immunolabeling. The influence of SLs on actin, another cytoskeleton element, has already been described during root hair elongation in *Arabidopsis*, in which treatment with *rac*-GR24 alters the actin filament architecture and dynamics (Kumar et al., 2015). By affecting actin bundling, SLs have been proposed to influence the cellular trafficking and the PIN polar localization at the plasma membrane (Koltai, 2015).

A notable feature of the MAX2 TAP data is the detection of three prey proteins, JAL34, GLL22, and BGLU22 that might participate in the endoplasmic reticulum (ER) body-related defense system in *Arabidopsis.* ER bodies are ER-derived structures that are presumably involved in the metabolism of glycoside molecules producing repellents against pests and fungi. During homogenization of *Arabidopsis* roots, a β-glucosidase PYK10 might possibly form large protein aggregates that include other β-glucosidases (BGLU21 and BGLU22), the putative vacuolar protein GLL22, and cytosolic jacalin-related lectins (including JAL34). After cell damage, this complex is able to hydrolyze glucosides to produce toxic compounds (Nagano et al., 2008; Yamada et al., 2011). Considering that the JAL34-MAX2 interaction could not be validated either by BiFC or Y2H, we can speculate that the presence of the JAL34-BGLU22-GLL22 complex in the TAPs of MAX2 might be a false positive detection. Indeed, MAX2 could have associated with this protein aggregate after cell lysis, making this interaction physiologically irrelevant.

Partial functionality of bait proteins might affect interactors identified by means of TAP, possibly the reason why no preys for D14 were retrieved in any of the tested conditions. D14 is expected to interact with MAX2 and proteins from the SMXL6/7/8 clade. Perception of *rac*-GR24 by D14 has been shown to cause changes in the protein conformation, permitting a MAX2 and SMXL6/7/8 association (Hamiaux et al., 2012; Zhao et al., 2013, 2014; Zhou et al., 2013; Wang et al., 2015; Yao et al., 2016). Hence, another potential explanation is that D14 engages in the interactions with other proteins in a dynamic and transient manner that is challenging to detect by TAP, because this technique is more suitable for identification of stable interactions. In addition, SMXL proteins have been proven to be very difficult to detect, presumably due to their instability and rapid turnover, especially in the presence of *rac*-GR24 (Liang et al., 2016).

On the contrary, the KAI2 TAP yielded six interactors, among which ACD32.1 was found in three out of four repeats. The Y2H analysis confirmed that ACD32.1 is able to interact not only with KAI2, but also with other components of the SL and KAR/KL pathways. Interestingly, D14 associates with the ACD32.1 protein only in the presence of *rac*-GR24, likewise with the SMXL6/7/8 proteins (Soundappan et al., 2015; Wang et al., 2015; Liang et al., 2016). Transient expression analysis in *N. benthamiana* leaves demonstrated that ACD32.1 predominantly localizes to small cytoplasmic organelles, which are probably peroxisomes (Reumann et al., 2004, 2007; Eubel et al., 2008) but in some cells also to the nucleus and cytoplasm. To confirm the localization of ACD32.1 in the peroxisomes further colocalization studies are required with the peroxisomal marker such as peroxisomal targeting signal type 1, Ser-Lys-Leu, (SKL). Also, it remains to be determined where the interactions validated by Y2H occur by means of, for instance, BiFC or FRET. Previous reports showed that SL signaling takes place in the nucleus and a similar mechanism is predicted for the KAR/KL

signaling (Liang et al., 2016). Thus far, no information is available on the localization of the SL or KAR/KL pathway components to the peroxisomes; hence, the interaction with the ACD32.1 protein most probably occurs in the nucleus. The biological relevance of these interactions and the ACD32.1 function remains to be determined. ACD32.1 is an α-crystallin domain-containing protein with homology to small heat shock proteins at the C-terminal part (Chandler and Melzer, 2004). In *Arabidopsis,* the family of ACD proteins consists of 25 candidates (Scharf et al., 2001), but the knowledge about their role is limited. Some members have been suggested to be involved in the resistance to the tobacco etch virus in *Arabidopsis* (Whitham et al., 2000) and others in DNA binding (Nakano et al., 1997). Based on the homology to small heat shock proteins, ACD32.1 might function as a molecular chaperone. Also, proteins from the SMXL family share a weak similarity to HEAT SHOCK PROTEIN 101 (HSP101), a casein lytic proteinase (ClpB) chaperonin required for thermotolerance. Interestingly, the *ACD32.1* transcript level is negatively regulated by gibberellins and other flowering-promoting factors; therefore, this gene has been speculated to play a role in flowering repression (Chandler and Melzer, 2004).

Lastly, the interaction between two receptors, KAI2 and D14 could not be validated, either by Y2H or BiFC. The major pitfall of BiFC is the possibility of self-assembly of the GFP protein in the absence of tested protein-protein interactions with false positive fluorescence signals as a consequence (Kudla and Block, 2016). One of the reasons might be the too high concentrations of both GFP fragments in one cellular compartment, leading to reconstitution of the fluorescent protein. To distinguish the artifacts, we tested all the protein pairs yielding a fluorescent signal by coexpression with constructs containing only the complementing GFP part. In our experiment, all negative controls for the KAI2 protein resulted in a GFP signal, making it impossible to assess whether the KAI2-D14 interaction observed by BIFC is truly biologically relevant. Similarly, in the Y2H, KAI2 fused with the GAL4-binding domain showed a high autoactivation when cotransformed with the pB42AD empty vector for negative control. Under native conditions, the interaction between two proteins occurs only when certain conditions are fulfilled, e.g. the same subcellular localization, expression in the same tissue type or at the same developmental stage (Kudla and Block 2016). Regarding D14 and KAI2, both proteins have been found to localize in nucleus and cytoplasm (Figure 2) (Chevalier et al. 2014; Liang et al., 2016). Although they have distinct role in the SL or KAR/KL pathways, they are both involved in the *rac*-GR24–dependent inhibition of hypocotyl elongation (Scaffidi et al. 2014; Stanga et al. 2016) and the *rac*-GR24–induced LRD reduction (Cedrick Matthys, unpublished data).

To summarize, we showed that TAP is a suitable technique to identify interaction networks of POIs. The biochemical studies pointed out that the CCP1 protein might be a possible interactor of MAX2 and is seemingly involved in hypocotyl elongation and *rac*-GR24–induced seed germination. Other MAX2-related phenotypes, including surface measurements of cotyledons and leaf morphology

analysis, need to be tested as well as the phenotype of the *ccp1 max2* double mutant. It would be also worthwhile to examine the SL- and KAR/KL-related phenotypes in plants lacking the closely related CCP1, KTN1. In addition, ACD32.1 is another interesting candidate for further interaction studies and phenotypic analyses to resolve its involvement in the SL and KAR/KL signaling.

MATERIALS AND METHODS

Plant material and growth conditions

Seeds of *Arabidopsis thaliana* (L.) Heynh., accession Columbia-0 (Col-0) plants were surface sterilized by consecutive treatments of 70% (v/v) ethanol with 0.05% (w/v) sodium dodecyl sulfate (SDS), washed with 95% (v/v) ethanol, sown on half-strength Murashige and Skoog (½MS) medium with 1% (w/v) sucrose (for root phenotyping) or without (for hypocotyl analysis), and stratified for 2 days at 4°C. The *ccp1* mutant line used in this study is in the Col-0 background. The homozygous mutant line SALK_109328, carrying a T-DNA insertion in the 5th exon of the *CCP1* (AT2G34560) gene was selected by PCR genotyping. RT-PCR was used to assess the *CCP1* transcript level in the SALK_109328 mutant line with *ACTIN2* (*ACT2*, AT3G18780) as a control. The *max2-1*, *d14-1* and *htl3* mutants are in Col-0 background and have been described previously. The *max2-1 and htl3* mutants were isolated in the EMS screening; *max2-1* has an aspartate to asparagine amino acid change at position 581 (Stirnberg et al., 2002) while *htl3* has an in-frame, 15-bp deletion in the *HTL/KAI2* gene (Toh et al., 2014). The *d14-1* mutant was isolated from the Wisconsin DsLox T-DNA insertion collection (DsLoxHs137_07E) (Waters et al. 2012).

Molecular cloning

All cloning was carried out by means of Gateway® recombination (Thermo Fisher Scientific). Baits were amplified from *Arabidopsis* cDNA with iProof™ High-Fidelity DNA Polymerase (Bio-Rad) and Gateway®-specific primers (Supplemental Table 1). The PCR products were cloned in pDONR221 with the BP Clonase® II enzyme mix (Invitrogen). The resulting entry vectors were used to clone the POI into the destination vector pKNGS-rhino and pKCTAP for N- and C-terminal fusions, respectively (Van Leene et al., 2015), or in pK7m34GW for N-terminal GFP/nGFP/cGFP fusions or in pH7m24GW2 for C-terminal fusions with nGFP/cGFP, with the LR Clonase® II Plus enzyme mix (Invitrogen). All constructs were expressed under the control of the CaMV *35S* promoter.

Western blot analysis

Arabidopsis transgenic lines expressing the GS-tagged MAX2, D14, and KAI2 were grown in 20 mL of fresh liquid ½MS medium at 21°C by gentle agitation (90 rpm). After 6 days, the total protein extract was prepared by adding the TAP extraction buffer. Protein concentrations were determined by the Bradford assay (Bio-Rad). Equal amount of proteins, 60 µg for the bait expressed in Col-0 and *max2-1* background or 30 µg for the others was used for Western blotting with peroxidase-antiperoxidase (PAP) antibodies against the GS-rhino tag (Sigma-Aldrich). The signal was captured by means of chemiluminescent substrates from the Western Lightning® Plus Enhanced Chemiluminescence kit

(PerkinElmer) and X-ray films (Amersham Hyperfilm ECL; GE Healthcare). The Precision Plus Protein™ Dual Color Standards (Bio-Rad) was used as protein size marker.

Tandem affinity purification

Based on the protein expression data, TAP experiments were done for GS-tagged D14 and KAI2 expressed in the Col-0 background and for GS-tagged MAX2 in both the Col-0 and *max2-1* mutant background. TAPs were carried out as described (Van Leene et al., 2015), with some modifications. Based on this protocol 6-day-old seedlings were harvested after 6 h of treatment with 1 µM *rac*-GR24 or 0.01% acetone. TAP experiments were done with 50g of seedling which generates 400-600mg of total protein input. The obtained peptide mixture was analyzed by liquid chromatography-tandem MS (LC-MS/MS) with the LTQ Orbitrap Velos mass spectrometer (Thermo Fisher Scientific). Data were analyzed with the Mascot Distiller (version 2.4.1; MatrixScience). The Mascot Daemon interface was used to search the data with the Mascot search engine (version 2.4.1; MatrixScience) against the TAIRplus database. Proteins with at least two highly confident peptide matches were retained. Background proteins were filtered based on the occurrence frequency of the copurified proteins in a large data set containing 543 TAP experiments with 115 different baits (Van Leene et al, 2015).

Yeast two-hybrid

The Y2H analysis was done as described (Cuellar et al., 2013) in two independent repeats. The polyethylene glycol (PEG)/lithium acetate method was used to cotransform the *Saccharomyces cerevisiae* EGY48 yeast strain (Estojak et al., 1995) with the bait and prey. Transformants were selected on Synthetic Defined media containing galactose and raffinose (SD Gal/Raf) and lacking Ura, Trp, and His (Clontech). Three individual colonies were grown overnight in liquid cultures at 30°C and 10- and 100-fold dilutions were dropped on control media (SD Gal/Raf-Ura-Trp-His) and selective media containing additionally X-Gal (Duchefa). To test the influence of the SL analog on the interactions, 10 µM *rac*-GR24 or 0.01% acetone (control) was added to the medium.

Transient expression in *N. benthamiana* leaves

Wild-type *N. benthamiana* plants (4 to 5-week-old) were used as a transient protein expression system in the localization studies, BiFC, and Co-IP. Constructs were transiently expressed by *Agrobacterium tumefaciens*-mediated transformation of lower epidermal leaf cells as described previously (Boruc et al., 2010) with a modified buffer (10 mM $MgCl_2$, 10 mM MES, and 100 µM acetosyringone). For BiFC and localization analysis, lower epidermal cells were examined for fluorescence with confocal microscopy 3 days after infiltration. For Co-IP, infiltrated leaf tissue was harvested 3 days after infiltration and immediately frozen in liquid nitrogen.

Co-IP assay

The co-IP experiments from *N. benthamiana* leaves transiently coexpressing GFP- and 3HA-tagged proteins were carried out with GFP-Trap® beads (ChromoTek GmbH), according to the manufacturer's recommendations. The precipitated proteins were detected by immunoblot analysis with rabbit anti-GFP monoclonal antibody (Invitrogen) at a 1:2000 dilution or mouse monoclonal anti-HA antibody (Sigma-Aldrich) at a 1:2000 dilution.

Physiological assays

Rosette branches (shoots >1 cm) were counted in 50-day-old plants grown in soil under a standard 16-h/8-h light/dark cycle (22°C/18°C) in controlled-environment rooms with light provided by white fluorescent tubes. To analyze the root phenotype, seedlings were grown vertically for 9 days under continuous light at 21˚C. The lateral root primordia were counted under a light microscope (S4E, Leica Microsystems), whereafter the plates were scanned and the main root length was measured with the ImageJ software and a digitizer tablet (Wancom). LRD was calculated by dividing the number of lateral roots by the corresponding primary root length. For the hypocotyl elongation analysis, after stratification the seeds were exposed to white light for 3 h, transferred to darkness for 21 h, and then exposed to continuous red light for 4 days. After the plates had been scanned, the hypocotyls were measured with the ImageJ 1.41 software. Thermoinduced seed dormancy assays were carried out as described (Toh et al., 2012). Seeds were used for the assay at least 6 weeks after harvest. Seeds were distributed in 96-well plates containing 100 mM of 4-(2-hydroxyethyl)-1-piperazineethanesulfonic acid (HEPES) buffer and Preservative for plant tissue cultures (Nalgene) with either 10 µM *rac*-GR24, or 0.1% acetonitrile. Plates were incubated for 4 days at 24°C in the dark or at 21°C in the continuous light for the control. Germination was indicated by emergence of the radicle tip through the endosperm.

SUPPLEMENTARY DATA

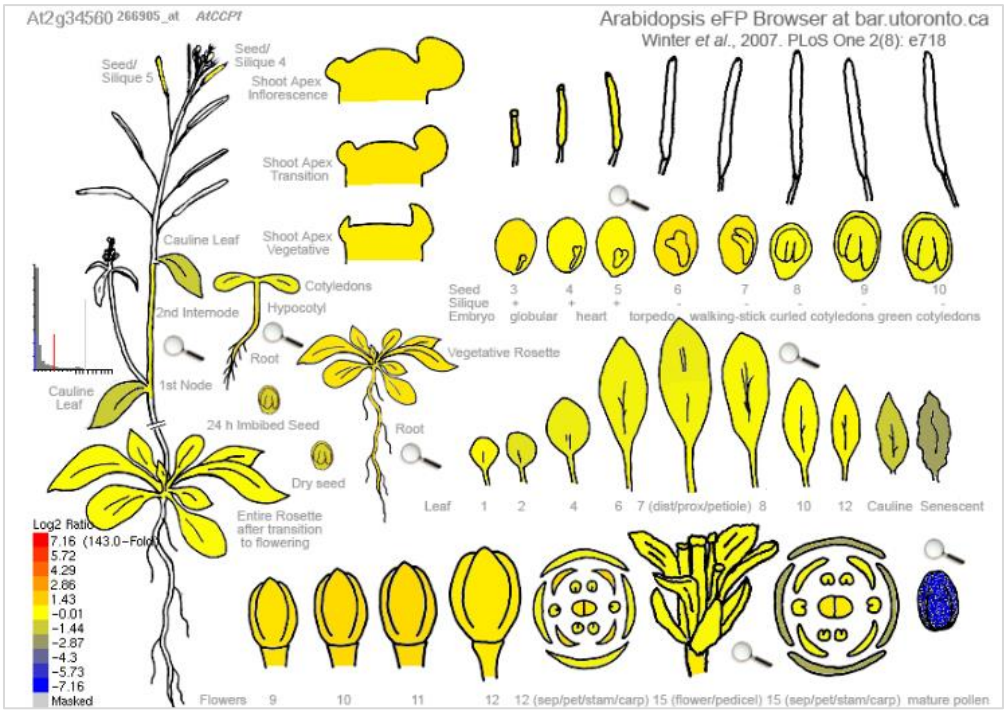

Supplemental Figure 1. The eFP visualization of the relative *CCP1* gene expression level during development in *Arabidopsis*. The color scheme represents the ratio of a tissue's expression level of *CCP1* to the median expression value calculated across all displayed samples for each probe set.

Supplemental Table 1. Primers used in this study.

ID		Sequence	Use
MAX2	Fw	GGGGACAAGTTTGTACAAAAAAGCAGGCTCAATGGCTTCCACTACTCTCTCC	Cloning
MAX2	Rev	GGGGACCACTTTGTACAAGAAAGCTGGGTATCAGTCAATGATGTTGCGGCTGTTC	Cloning
D14	Fw	GGGGACAAGTTTGTACAAAAAAGCAGGCTCAATGAGTCAACACAACATCTTAG	Cloning
D14	Rev	GGGGACCACTTTGTACAAGAAAGCTGGGTATCACCGAGGAAGAGCTCGCCG	Cloning
KAI2	Fw	GGGGACAAGTTTGTACAAAAAAGCAGGCTCCACCATGGGTGTGGTAGAAGAAGCTC	Cloning
KAI2	Rev	GGGGACCACTTTGTACAAGAAAGCTGGGTCTCACATAGCAATGTCATTACGAAT	Cloning
CCP1	Fw	GGGGACAAGTTTGTACAAAAAAGCAGGCTCAATGGCCACCGATGAGCCTTC	Cloning
CCP1	Rev	GGGGACCACTTTGTACAAGAAAGCTGGGTATTACTTGAGAATTTGGCTACC	Cloning
JAL34	Fw	GGGGACAAGTTTGTACAAAAAAGCAGGCTCAATGTCTTGGGACGATGGATC	Cloning
JAL34	Rev	GGGGACCACTTTGTACAAGAAAGCTGGGTATTATTTGGTTATTGGCGCG	Cloning
ESM1	Fw	GGGGACAAGTTTGTACAAAAAAGCAGGCTCAATGGCAGACAATTTGAATTTG	Cloning
ESM1	Rev	GGGGACCACTTTGTACAAGAAAGCTGGGTACTAATAATAGGCGGCGAGG	Cloning
ACD32.1	Fw	GGGGACAAGTTTGTACAAAAAAGCAGGCTCAATGGAGCATGAATCTATCACCGC	Cloning
ACD32.1	Rev	GGGGACCACTTTGTACAAGAAAGCTGGGTATCAAAGCTTTGGAATTACTATTCTCAG	Cloning
PTAC5	Fw	GGGGACAAGTTTGTACAAAAAAGCAGGCTCAATGGCTTCTTCTTCTCTACC	Cloning
PTAC5	Rev	GGGGACCACTTTGTACAAGAAAGCTGGGTATTATAAGTTTTTTTTGCCG	Cloning
ccp1	Fw	TGTCCCAAATCGAAGTCAAAC	Genotyping
ccp1	Rev	GGTACCAGGAGGACCAAAAAG	Genotyping
SALK LB1.3	-	ATTTTGCCGATTTCGGAAC	Genotyping
CCP1	Fw	ACCCCACGTACTTTAATGGTCT	RT-PCR#1

CCP1	Rev	TGGCTACCATAATCATCATTGAACT	RT-PCR#1
ACT2	Fw	GGCGATGAAGCTCAATCCAAA	RT-PCR
ACT2	Rev	GGTCACGACCAGCAAGATCAAG	RT-PCR

Supplemental dataset 1. Overview of all MAX2 TAP experiments. Available via https://www.dropbox.com/sh/nlx6ipio1e272ru/AABLITVuBiKbqaW3qf-_mHNua?dl=0

Supplemental dataset 2. Overview of all D14 TAP experiments. Available via https://www.dropbox.com/sh/nlx6ipio1e272ru/AABLITVuBiKbqaW3qf-_mHNua?dl=0

Supplemental dataset 3. Overview of all KAI2 TAP experiments. Available via https://www.dropbox.com/sh/nlx6ipio1e272ru/AABLITVuBiKbqaW3qf-_mHNua?dl=0

Discussion and perspectives

Phytohormones are signaling molecules produced at extremely low concentrations that orchestrate plant growth, development, and responses to changing environments. Although plant hormones are structurally not related and derived from different metabolic pathways, they share several common steps in their signaling cascades (Santner et al., 2009; Walton et al., 2015). Until now, a lot of research has been done to unravel the signaling mechanisms of most plant hormones, but our knowledge about one of the recently identified hormones, strigolactones, is still limited.

Strigolactone (hi)story

Strigolactones (SLs) were discovered more than five decades ago as germination stimulants for parasitic plants (Cook et al., 1966), but only years later their key role in the establishment of the symbiotic interaction with arbuscular mycorrhizal (AM) fungi was shown (Akiyama et al., 2005). Although they had been recognized for a long time, our understanding of the SL signal transduction pathway progressed extremely rapidly as soon as their role as plant hormones had been discovered (Gomez-Roldan et al., 2008; Umehara et al., 2008). Yet, only a few signaling components are known thus far, including the SL receptor DWARF14 (D14) that, after perception of the SL molecule, enables the interaction between the MORE AXILLARY BRANCHING2 (MAX2), which is part of the Skp-Cullin-F-box (SCF) complex, and the SUPPRESSOR OF MAX2 1 LIKE (SMXL) family of target proteins, resulting in their polyubiquitination and subsequent degradation (Soundappan et al., 2015; Wang et al., 2015; Yao et al., 2016). The SL signaling downstream of SMXL proteins is poorly understood, although their interaction with the transcriptional corepressors TOPLESS (TPL) and TOPLESS-RELATED (TPR) proteins has been reported (Chapter 3; Soundappan et al., 2015; Wang et al., 2015), as well as their indirect influence on the subcellular localization of the auxin efflux carrier PIN-FORMED 1 (PIN1) and on the levels of the BRANCHED 1 (BRC1) transcription factor (Aguilar-Martinez et al., 2007; Shinohara et al., 2013; Seale et al., 2017).

Karrikins (KARs), chemical compounds found in smoke (Flematti et al., 2013), make the hitherto simple SL story more tangled. SLs and KARs share similarities in chemical structures and in signaling components, such as the common MAX2 and KARRIKIN INSENSITIVE 2 (KAI2) or SMAX1/SMXL2 that

are the homologs of D14 and SMXL6/SMXL7/SMXL8 (SMXL6/7/8), respectively. KAI2 might also perceive unknown endogenous molecules, referred to as the KAI2-ligand (KL), that is neither KAR nor SL (Conn and Nelson, 2016). Both pathways regulate mostly different biological processes in plants but overlapping functions have been reported as well (Chapter 1). To add another complexity level, the commonly used SL analog, *rac*-GR24, is a racemic mixture of two stereoisomers that can activate both signaling pathways (Scaffidi et al., 2014).

To fully understand the SL action mechanism, all the players and their function need to be characterized. In this PhD, we aimed at expanding the knowledge on the protein-protein interaction network of the SL signaling in *Arabidopsis thaliana* by means of tandem affinity purification (TAP) with the known core components as baits. Furthermore, because the KAR and SL pathways cannot always be separated due to common signaling components and use of *rac*-GR24, we intended to obtain molecular insights into the KAR pathway as well.

Quantitative TAP to track changes in the SMXL7 protein complex composition

TAP coupled with mass spectrometry (MS) enables proteome-wide analysis for the identification of interactors of a protein of interest (bait). The great advantage of TAP-MS for the study of plant hormone signaling is its ability to detect indirect interactors, possibly leading to the characterization of larger protein complexes. This approach was used successfully to discover novel signaling components of many phytohormones, including auxin, abscisic acid, and jasmonate (Chapter 2; Pauwels et al., 2010; Fernandez-Calvo et al., 2011; Irigoyen et al., 2014; Karampelias et al., 2016). Typically, TAP-MS identifies static interactions and does not provide information about changes in protein complex composition in response to different stimuli (Van Leene et al., 2015). In Chapter 3, we implemented a label-free quantification (LFQ) (Cox et al., 2014) to the TAP-MS analysis of SMXL7 and ΔSMXL7 as a tool to detect differential interactors due to experimental contexts, in this case treatment with the SL analog. Quantitative TAP (qTAP) has been already successfully used to discover changes in protein complex compositions formed around ANGUSTIFOLIA3 in maize (*Zea mays*) (ZmAN3) that occur due to different developmental leaf stages (Nelissen et al., 2015). We show that qTAP can be used also to study differential interactions in plant hormone signaling.

Detection of previously reported *rac*-GR24-dependent interactions between SMXL7 and D14 has proven the effectiveness of the qTAP approach (Jiang et al., 2013; Zhou et al., 2013; Soundappan et al., 2015; Wang et al., 2015). As other differential interactors had not been identified, we speculated that bait degradation in response to the SL treatment might hinder the detection of some preys. Indeed, after introduction of a normalization step based on the intensity level of the bait protein itself, the number greatly increased of putative preys significantly associated with SMXL7 in the presence of

rac-GR24. Although the new list might contain false positives, we could detect CULLIN1 (CUL1), implying the presence of the SCF^{MAX2} complex in close proximity of SMXL7 or proteins related to the 26S proteasome, indicating that the proteasomal degradation pathway is activated in response to *rac*-GR24, albeit without MAX2 copurificaiton (Jiang et al., 2013; Zhou et al., 2013; Soundappan et al., 2015).

Despite the identification of known *rac*-GR24-induced interactions, we observed some discrepancies with currently proposed models of SL signaling. First, the TPR2 association with SMXL7 was significantly enhanced in mock treatments, contradicting the results of our own Y2H and the previously reported mammalian two-hybrid assay (Jiang et al., 2013). By contrast, addition of the SL analog had no influence on the interaction between ΔSMXL7 and TPR2. Second, D14 was not copurified with ΔSMXL7 under any of the tested conditions, although the *rac*-GR24-dependent D14-ΔSMXL7 interaction had been reported by Y2H, BiFC, pull-down, and FRET-fluorescence-lifetime imaging microscopy (FLIM) (Zhou et al., 2013; Jiang et al., 2013; Liang et al., 2016). The reason for this inconsistency might be the stoichiometric balance deviations between proteins in the complex. To date, in methods used to study the SL signaling, such as Y2H, BiFC, Co-IP, and FRET-FLIM, both tested proteins are overexpressed, whereas other potential complex components are absent or available at basal levels. In contrast, qTAP involves the overexpression of the bait only and enables the retention of stoichiometric relations with other members of the complex.

Based on the results of the SMXL7 and ΔSMXL7 qTAPs, we hypothesize that the *rac*-GR24 perception interrupts or weakens the SMXL7-TPL/TPR association, probably due to binding of (an)other protein(s) (Figure 1). Our candidate for this function is D14, because its interaction profile with SMXL7 is differing from that of TPR2. Subsequently, binding of D14 triggers ubiquitination and degradation of SMXL7 that activate downstream responses (Soundappan et al., 2015; Wang et al., 2015; Liang et al., 2016). In contrast, the affinity of ΔSMXL7 to TPL/TPR proteins seem to be stronger than that of the wild-type protein. As a result, the SL-bound D14 cannot disrupt the ΔSMXL7-TPL/TPR interaction and, consequently, activate the downstream signaling. This hypothesis needs to be further tested. For instance, cocrystallization studies of SMXL7 together with TPL/TPR or D14 could specify whether these proteins bind SMXL7 in the same domain, in which case sterical hindrance could dislocate TPL/TPR proteins upon SL perception by D14, or their affinities could be tested by binding studies with purified proteins in various combinations and conditions.

SINT proteins: SMXL interaction partners without phenotypic link?

Expansion of the SMXL7 interactome might help to characterize downstream signaling partners, but also to identify proteins that regulate its function, localization, or turn-over. As the qTAP of SMXL7 did

not reveal any novel interactors (Chapter 3), TAP data were analyzed in the qualitative manner, by subtracting known background proteins from the list of copurified preys (Van Leene et al., 2015). Although the D14 or MAX2 were not copurified, the interaction between SMXL7 and D14 was shown by means of qTAP (Chapter 3). The fact that MAX2 had not been identified in either the qTAP (Chapter 3) or the qualitative TAP analysis (Chapter 4) might be explained by a too transient interaction with SMXL7 to survive the multistep TAP protocol.

In Chapter 4, we characterized three prey proteins, referred as SMXL7 INTERACTING PROTEIN (SINT) 1, SINT2, and SINT3, for which the interaction with SMXL7 was validated by Y2H (SINT1, SINT2, and SINT3), BiFC (SINT 1), and FRET-FLIM (SINT1 and SINT2) (Table 1). Nevertheless, no plant phenotypic link has been observed yet that could biologically explain the involvement of SINT proteins in SL responses, or in the case of SINT3, also in KAR/KL responses. We tested only two of the most pronounced SMXL7-related phenotypes: shoot branching and lateral root density. As the SMXL6, SMXL7, and SMXL8 proteins function redundantly to control these phenotypes, single mutants do not differ from the wild-type plants. Moreover, although the lateral root density of density of the *smxl6 smxl7 smxl8* (*smxl678*) triple mutant is significantly lower than that of WT, the number of primary rosette branches did not differ. The most pronounced effect was the suppression of the SL-related phenotypes in *max2* by *smxl678* (Soundappan et al., 2015; Wang et al., 2015). This observation could indicate that even in the case of core pathway components the mutant phenotype is not always directly visible. Currently, we are looking in-depth into the role of SINT proteins by means of phenotypic assays on the overexpression lines and on multiple-order mutants between the *sint* and *smxl678max2* mutants. In addition, other MAX2-controlled phenotypes need to be tested, such as leaves senescence or stress responses, for which no role of SMXL proteins have been reported yet. SMXLs have been suggested to act as growth regulators whose activity is repressed after SL perception rather than acting simply to repress SL signaling. This hypothesis was based on the observation that the *smxl678* mutant do not entirely suppress *max2* phenotypes, but that the phenotypes are quantitatively opposite to the effect of *max2* (Soundappan et al., 2015). Thus, another explanation for the lack of SL-related phenotypes in the *sint* mutants might be that SINT1, SINT2 and SINT3 proteins act together with SMXL7 to regulate other, still unknown growth responses that might not be related to SLs.

As the three SINT proteins had not been studied in *Arabidopsis* yet, we used them as baits in a TAP analysis. Identification of interacting partners of an unknown protein can give a hint about the function of the protein under study, a principle better known as guilt-by-association. In none of the TAP experiments, SMXL7 could be detected as prey, possibly due to its intrinsic instability (Liang et al., 2016) and other proteins known to be involved in SL signaling were not copurified as well.

Nevertheless, the TAP experiments gave some ideas to direct future research on the SINT proteins. Firstly, one of the putative interactors of SINT1 is probably the transcription factor ANTHOCYANINLESS 2 (ANL2) that is crucial for anthocyanin accumulation and cutin biosynthesis (Kubo and Hayashi, 2011; Nadakuduti et al., 2012). Considering that MAX2 and KAI2 regulate drought stress by promoting cuticle development (Bu et al., 2014; Li et al., 2017), it would be interesting to test whether SINT1 might be indeed involved in these responses, for instance by analysis of the drought tolerance or cuticle thickness of *sint1* mutants. Secondly, although additional validation studies are needed, we provided some preliminary evidence by means of Y2H that SINT2 and SINT3 might form one complex. Based on the TAP experiments, both proteins seem to play a role in the processes related to the 26S proteasome, possibly hinting at the proteasomal degradation of SMXL7 (Chapter 4; Wang et al., 2015; Liang et al., 2016), therefore the SMXL7 protein stability should be verified in the *sint2* and *sint3* mutant backgrounds. Another explanation might be that SINT3, and consequently potentially interacting with it SINT2, are involved in the physical and functional integrity of the proteasome as has been already proposed for the SINT3 homolog in yeast, General Negative Regulator of Transcription Subunit 4 (NOT4). NOT4 was reported to contribute to the dynamic assembly and flexibility of the proteasome by association with the Ecm29 chaperone and several proteasome related subcomplexes (Panasenko et al., 2011). Thus, it is possible that the interaction between SMXL7 and SINT2 or SINT3 was detected because of the degradation of SMXL7 by 26S proteasome. If the mutations in *SINT3* and *SINT2* in *Arabidopsis* have only a minor effect of the proteasome stability, that is not affecting SMXL7 degradation, the SL-related phenotypes are indeed not expected in *sint2* and *sint3* mutants.

Besides the role in the proteasome integrity, the yeast SINT3 homolog, NOT4 is part of the Carbon Catabolite Repressed 4 (CCR4)–Negative on TATA-less (NOT) complex that regulates gene expression at all levels (Bai et al., 1999; Chen et al., 2001; Collart, 2016). Based on our biochemical results, we can hypothesize that SINT3 could play a role in both transcription-dependent and -independent responses to SLs. First, SINT3 was found to act as a transcriptional repressor and to probably interact with the corepressors TPL (Y2H) and SIN3-ASSOCIATED POLYPEPTIDE P18 (SAP18) (TAP) via the EAR motif present in the sequence. Furthermore, qTAP revealed that HISTONE DEACETYLATION COMPLEX 1 (HDC1) was significantly more associated with SINT3 without than after addition of *rac*-GR24. Thus, under mock conditions, SINT3 might repress transcription by recruiting chromatin-remodeling factors, such as HDC1 (Perrella et al., 2016), whereas *rac*-GR24 abolishes this process. SMXL7 can regulate some aspects of SL-related plant development independent of the EAR motif (Liang et al., 2016). SINT3 might possibly control these phenotypes because it has a repressive activity even after deletion of EAR peptide. To test this hypothesis, we will analyze the leaf morphology and branching angle in *sint3* mutant plants crossed with the *proSMXL7-SMXL7ΔEAR-Venus*(*s678max2-1*) line (Liang et al., 2016). In

addition to the transcriptional control, SINT3 might also be implicated in the PIN1 depletion from the plasma membrane in response to the SL analog (Seale et al., 2017). This assumption is based on the qTAP results, in which PIN1 was detected as significantly more associated with SINT3 in the presence than in the absence of *rac*-GR24. In the future, the PIN1-SINT3 interaction should be validated as well as the PIN1 trafficking in the *sint3* mutant after addition of the SL analog. Nonetheless, the lack of mutant phenotypes contradicts our hypothesis that SINT3 has an important position in the SL signaling. Considering that SINT3 is one of the three predicted *Arabidopsis* NOT4 homologs due to redundancy, the *sint3rbp1* double mutant and the *sint3rbp1rb2* triple mutant should be tested. Our Y2H assay indicated that SINT3 might be also be involved in KAR/KL signaling, but this proposition needs further investigation, including *in vivo* confirmation of the SINT1-SMAX1 interaction and analysis of the germination frequency of *sint3* and multiple-order mutants under suboptimal conditions.

Table 1. The overview of all the interactors under study in this thesis

			Validation methods							
Prey	Bait	TAP conditions	BiFC	Y2H	Co-IP	FRET-FLIM	Reciprocal TAP	Other possible interactors	Localization	Possible role in SL/KAR signaling
SINT1	SMXL7	cell cultures						---	nucleus cytoplasm	no effect
SINT2	SMXL7	cell cultures						SINT3	nucleus cytoplasm	no effect
SINT3	SMXL7	cell cultures						SMAX1 SINT2	nucleus cytoplasm	no effect
FyPP1	SMXL7	cell cultures	FyPP1 FL	FyPP-NT	FyPP1 FL	FyPP1 FL		SMAX1 D14 RCN1	nucleus cytoplasm PM	hypocotyl elongation lateral root density
SAL4	SMXL7	cell cultures						FyPP1/3 (?)	---	hypocotyl elongation lateral root density shoot branching
PAPP5	MAX2	cell cultures						KAI2	nucleus cytoplasm	seed germination
CCP1	MAX2	seedlings						---	nucleus cytoplasm	hypocotyl elongation seed germination
ACD32	KAI2	seedlings						MAX2 D14 SMXL7 SMAX1	nucleus cytoplasm peroxisomes(?)	---

Green- a positive result, red- a negative result, grey- not tested; FyPP1 FL- FyPP1 full length protein, FyPP-NT- FyPP1/3 N-terminal protein part; (?)- not certain; PM, plasma membrane

In Chapter 3, we introduced qTAP as a tool to identify differential interactors of a protein of interest in response to a trigger, namely addition of the hormone. In Chapter 4, we demonstrated that this method can be used also to study differences in the interaction profile of proteins with deletion or mutation in an important domain. As SINT3 is a predicted E3 ligase, deletion of the RING domain is expected to abolish the interaction with the ubiquitin-charged E2 ligase, but probably to preserve its

interaction with putative targets. The putative preys identified as statistically more associated with SINT3 or ΔRING-SINT3 with this method still need to be validated by another technique, such as Y2H, to confirm the effectiveness of the approach. Although still to be corroborated, two E2 ligases, UBC19 and UBC20, were detected in the SINT3 TAP experiments, whereas the interaction was abolished when the RING domain was deleted, indicating that both might act together with SINT3 as the ubiquitin donor. As the UBC19/20-SINT3 interaction was not detected in the Y2H screen for E2 ligases, another approach will have to be applied for validation.

The role of phosphorylation in SL and KAR/KL signaling

Besides ubiquitination, another common theme in plant hormone signaling is the reversible protein phosphorylation that is catalyzed by protein kinases and phosphatases. To date, information about the protein (de)phosphorylation contribution to the SL pathway is limited. One study in rice seedlings identified a set of eight proteins as differentially phosphorylated upon *rac*-GR24 treatment (Chen et al., 2014). Here, we expand this knowledge by the characterization two serine/threonine-specific phosphoprotein phosphatases (PPP) as potential interactors of SMXL proteins (Chapter 5) and of MAX2 (Chapter 7).

The qualitative TAP analysis revealed the PP6-type holoenzyme, consisting of the catalytic subunits Phytochrome-associated Ser/Thr protein phosphatase 1 (FyPP1), its homolog FyPP3 and the regulatory subunit SAP domain-like protein 4 (SAL4) as putative interactors of SMXL7 (Chapter 5). Although the use of different techniques could not resolve whether the FyPP1/3-SMXL7 interaction is direct, the formation of one complex was revealed by Co-IP (Table 1). Also, the interaction between D14 and the N-terminal part of the FyPP1/3 protein (FyPP-NT) was validated by Y2H, confirming its role in the SL signaling (Table 1). The Y2H assay implied no direct interaction between SAL4 and SMXL7, whereas the SAL4-FyPP1/3 association could not be validated due to technical limitations. Thus, additional experiments are necessary, such as Co-IP, FRET-FLIM, or BiFC to elucidate the association between SAL4 and both SMXL7 and FyPP1.

Interestingly, the expression pattern of FyPP1 inside the nucleus changed from homogenous toward speckled, when the protein was coexpressed together with SMXL7, even although no FRET between this pair was detected. Previously, SMXL7 had been reported to be localized to the nuclear speckles and also to be able to recruit its interacting partners, D14 and TPR2, to these structures (Soundappan et al., 2015; Liang et al., 2016). It indicates that FyPP1 might be an important player in the core SL signaling, because not all proteins interacting with SMXL7 are recruited to the speckles. In Chapter 4, FRET was detected between the SMXL7-SINT1 and SMXL7-SINT2 protein pairs throughout the nucleus,

but no speckles were observed. Accordingly, the phenotypic analysis revealed no SL-related phenotypes in the *sint1* and *sint2* mutants, but in the plants affected in *FyPP1/3*.

To get insight into the role of PP6 in the SL responses, we investigated two SMXL6/7/8-related phenotypes: lateral root development and shoot branching. Both FyPP1/3 and SAL4 seem to negatively regulate the lateral root density under mock conditions and also to alter the response toward *rac*-GR24 in the root (Figure 1). To confirm that these phenotypes are indeed related to SL effects, we have to analyze the *fypp1-1fypp3-2-/+max2-1* and *sal4-1max2-1* mutants. Consistently with the function as a negative regulator of the SL response in the root, the *sal4* mutant carries fewer branches than the wild type. Currently, we need to determine whether the *fypp1/3* mutants have the same phenotypes and whether mutants affected in the PP6 complex can suppress the excessive branching of the *max2-1* plants.

Two possible models could explain the involvement of the PP6 complex in the SL signaling. Firstly, the SMXL proteins or D14 might be targets of the PP6 complex for the control of their phosphorylation status. In the case of the SMXL proteins, phosphorylation might promote their ubiquitination and consequent degradation, whereas dephosphorylation by PP6 would stabilize them. The interplay between phosphorylation and ubiquitination is a common theme in mammalian cell signaling and has been described in plants as well, but to a lesser extent (Lin et al., 2002; Welcker et al., 2004; Yada et al., 2004; Ju et al., 2007; Yue et al., 2016). This hypothesis can be verified by checking the *rac*-GR24-dependent ubiquitination status of tagged SMXL proteins expressed in the *fypp1-1fypp3-2* and *sal4* mutant backgrounds and FyPP1 overexpression line, where respectively more and less ubiquitination is expected. Moreover, a western blot analysis with anti-phosphorylation antibodies would already give some indication about the possible modification of the phosphorylation status of SMXL proteins after treatment with *rac*-GR24.

In the second model, the PP6 activity is proposed to be regulated by the interaction with SMXL proteins or D14, so that SLs might influence the phosphorylation status of the PP6 targets, for instance, the PIN1 and PIN2 proteins (Dai et al., 2012). As the interplay of SLs and PIN proteins has been demonstrated both in roots and shoots (Ferguson & Beveridge, 2009; Domagalska & Leyser, 2011; Ruyter-Spira et al., 2011; Shinohara et al., 2013; Jiang et al., 2016), the observed phenotype might possibly be an effect of the PP6-dependent dephosphorylation of PIN proteins and of the altered polar auxin transport. In the shoot, it would be interesting to test whether the PIN1-GFP accumulation at the plasma membrane of xylem parenchyma cells is still altered in the *PP6* phosphatase mutants after *rac*-GR24 treatment (Bennett et al., 2006; Prusinkiewicz et al., 2009; Shinohara et al., 2013).

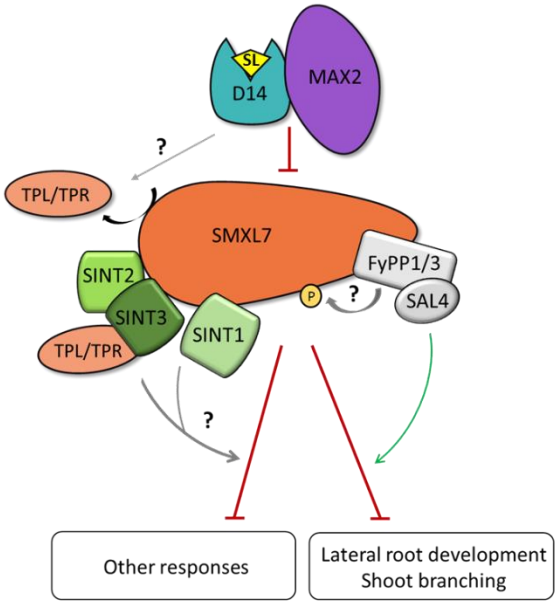

Figure 1. A proposed model explaining a possible role of the novel SMXL7 interacting proteins. In the presence of strigolactones, D14 and SCF^{MAX2} are recruited to SMXL7, whereas the TPL/TPR proteins dissociate from the complex. The SINT1, SINT2 and SINT3 proteins interact with SMXL7 and might be involved in still unknown responses. FyPP1/3 and SAL4 form a complex with SMXL7 and seem to negatively regulate the lateral root development and shoot branching. One of the proposed PP6 mode of action is dephosphorylation of SMXL7.

Besides the involvement of the PP6 holoenzyme in the SL pathway, the validation of the SMAX1- FyPP-NT interaction by Y2H hinted at its possible role in the KAR/KL signaling as well. However, the results of the hypocotyl elongation assay suggest a positive role for PP6 in this SMAX1-related response, which is opposed to the negative role demonstrated in the SMXL6/7/8-regulated phenotypes. Nevertheless, further *in vivo* confirmation, for instance by means of Co-IP or FRET-FLIM, is required to prove the interaction between FyPP1 and SMAX1. Scrutiny of other SMAX1-controlled phenotypes, such as seed germination, would shed also some light on the role of PP6 in the KAR/KL signaling (Stanga et al., 2013; Soundappan et al., 2015). It is also possible that the observed hypocotyl phenotype is not related to the KAR/KL effects. FyPP1/3 has been shown to dephosphorylate phytochromes A and B that regulate the phytochrome-mediated light pathway in relation to flowering time (Kim et al., 2002). Thus, to investigate whether the elongated hypocotyl of the *fypp1-1fypp3-2* and *sal4* mutants is the result of the dephosphorylation of the phytochromes or of the affected MAX2-KAI2 signaling, the double mutants of the PP6-type subunits with *max2-1* should be examined in the assay.

In Chapter 5, we also investigated whether the scaffolding subunit of the PP2A phosphatase complex ROOTS CURL IN NAPHTHYLPHTHALAMIC ACID1 (RCN1) might play a role in the SL and KAR/KL pathways, because it had been previously demonstrated to form a PP6-type holoenzyme together with FyPP1/3 and SAL1 (Dai et al., 2012). Although we could validate the interaction between RCN1 and FyPP-NT by means of Y2H, it is still unclear whether it belongs to the SMXL7-FyPP1/3-SAL4 complex. The impact on the lateral root density in the *rcn1* mutant was not consistent with that of the *fypp1/3* and *sal4* mutants. The *rcn1* seedlings displayed an increased lateral root density under control conditions and were less sensitive to *rac*-GR24, which is contradictory with the root phenotypes of the

PP6 mutants. Thus, it is plausible that in the case of the SL responses, RCN1 might form a complex with a PP2A-type phosphatase rather than with PP6. Indeed, in the TAP analysis, RCN1 was not identified as possible *bona fide* SMXL7 interactor, but occurred in the list of copurified proteins that also contains the two catalytic subunits PP2A-3 and PP2A-4 and the regulatory subunit PP2AA2. Thus, the PP2A phosphatase might possibly also be involved in the SL signaling, as can be quickly verified by the analysis of the *pp2a-3* and *pp2a-4* mutants. Another explanation could be that, by acting as a scaffolding subunit of PP2A, RCN1 can regulate the polar auxin transport (Blakeslee et al., 2007) and affect SL the responses in the root.

Another phosphatase, PAPP5, was identified in the MAX2 TAP experiments and seems to be a unique component in the MAX2-KAI2 signaling (Table 1) (Chapter 7). Indeed, in a one-step affinity purification PAPP5 was detected as significantly more associated with the KAI2 protein complex than with that of D14. In agreement, no shoot branching phenotype was observed for the *papp5* knockout mutants, whereas seed germination and young seedling responses, the KAI2-regulated developmental programs, were affected (Figure 2). The additive effect of the *papp5* and *kai2* mutations on hypocotyl elongation suggested that both proteins might act in distinct pathways. Indeed, the *papp5* phenotype might be a result of a disturbed phytochrome-mediated signaling cascade, because it had previously been shown to influence phytochrome-controlled photoresponses (Ryu et al., 2005). Nevertheless, the involvement of PAPP5 in the KAR/KL signaling cannot be completely excluded as the additive effect in *papp5htl3* double mutant was minor, although significant, and some transcriptional responses to *rac*-GR24 were affected in the *papp5* seedlings. In addition, under suboptimal temperature conditions, the *PAPP5* mutation affected the seed germination frequency, further hinting at a possible involvement in the KAI2-mediated signaling.

The exact mechanism by which PAPP5 can be implicated in young seedlings development and seed germination in suboptimal conditions is still unclear. Based on collected data, we hypothesize that PAPP5 might affect the activity and/or stability of the KAI2-MAX2-SMAX1 complex. The possibility that PAPP5 might be a target of MAX2 for ubiquitination and consequent degradation, similarly to SMXL6/7/8 (Soundappan et al., 2015; Wang et al., 2015; Liang et al., 2016) is rather unlikely, because the PAPP5 protein levels do not change upon treatment with *rac*-GR24. However, one ubiquitination site for PAPP5 had been identified in a proteome-wide ubiquitination site mapping experiment in *Arabidopsis* cell cultures (http://bioinformatics.psb.ugent.be/webtools/ubiquitin_viewer/) (Walton et al., 2016). Thus, MAX2 could probably still ubiquitinate PAPP5 for other purposes than proteasomal degradation, for instance for modification of its localization or interaction profile (Komander, 2009). This hypothesis can be verified in the future by a transient differential ubiquitination study.

As a protein phosphatase, PAPP5 might dephosphorylate KAI2, MAX2, or SMAX1 proteins to affect the KAI2-mediated signaling. MAX2 is the most convincing candidate as a PAPP5 substrate, because a direct interaction between the two proteins and phosphorylation sites on MAX2 have been shown. We can speculate that dephosphorylation by PAPP5 could increase MAX2 activity during the SMAX1 ubiquitination process. In agreement, because the MAX2 protein might be phosphorylated and, therefore, less active in marking SMAX1 for degradation, the seed germination of a *papp5* mutant was lower than that of Col-0. To test this hypothesis, we have, first of all, to verify the MAX2 phosphorylation in the *papp5* mutant background, in which less phosphorylation is expected than in the wild type. Alternatively, PAPP5 might dephosphorylate SMAX1, thereby influencing the phosphorylation-dependent ubiquitination to control in this manner the availability of SMAX1 for degradation. However, the interaction between PAPP5 and SMAX1 remains to be validated.

The data presented in Chapters 5 and 7 demonstrate that protein phosphorylation might be another key posttranslational modification in both the SL and KAR/KL pathways. We characterized three different phosphatases/PPP complexes that seem to have distinct functions and are promising study candidates for the future. Also, the analysis of the *Arabidopsis* phosphoproteome in response to the treatment with *rac*-GR24 or specific enantiomers would provide new insights into the regulation of the SL and KAR/KL signaling.

Is SMAX1 a copycat of SMXL7?

The SMAX1 mode of action in the KAR/KL pathway has been proposed based on genetic data and on the similarity to the signaling involving its homologs, SMLX6/7/8. In Chapter 6, we elaborate on the biochemical mode of action of the KAR/KL pathway. First, we show that SMAX1 interacts with KAI2 in the absence of *rac*-GR24, as opposed to the D14-SMAXL6/7/8 interaction (Chapter 3; Soundappan et al., 2015; Wang et al., 2015; Liang et al., 2016). Upon SL perception and hydrolysis, D14 undergoes a conformational change allowing the interaction with other pathway components (Yao et al., 2016), but it is still unknown whether a similar change can be induced in the KAI2 protein conformation (Waters et al., 2017). Although the KAR-to-KAI2 binding has been demonstrated, the hydrolysis of this molecule is not expected, because of its chemical structure (Guo et al., 2013) and might be the reason for the *rac*-GR24-independent formation of a KAI2-SMAX1 complex. The Y2H assay suggested that addition of the SL analog might improve this interaction, but application of more specific compounds for this pathway, such as KAR or $GR24^{ent\text{-}5DS}$, would be advisable to test this hypothesis. Also, the interaction between SMXL6 and D14 responds to *rac*-GR24 in a dose-dependent manner (Wang et al., 2015).

During the SL signaling, D14 acts as a bridge that facilitates the association between MAX2 and SMXL7 (Liang et al., 2016). KAI2 might function in a similar manner to connect MAX2 and SMAX1. This assumption is supported by the Y2H analysis that revealed an interaction between MAX2 and KAI2 that depended on *rac*-GR24 and KAR (Toh et al., 2014), whereas MAX2 and SMAX1 did not interact under any conditions (Chapter 6). We can hypothesize that if KAI2 undergoes a conformational change upon perception of *rac*-GR24 or KAR, it can influence the association with MAX2 only, whereas the SMAX1-binding site would not be affected, allowing the interaction even in the absence of the SL analog.

Surprisingly, in the SMAX1 TAP experiments, neither KAI2 nor MAX2 proteins were copurified. The reason might be that transient interactions are missed during the purification procedure. MAX2 was also not copurified in the SMXL7 TAP analysis, but CUL1 as well as 26S proteasome-related proteins were detected after normalization on the bait level with a higher association in the presence of *rac*-GR24 than under mock conditions (Chapter 3). This observation was not noticed when the same analysis was applied to the SMAX1 TAP (Chapter 6). Possibly, the used *rac*-GR24 in the experiments with both bait might be less active toward the KAR than the SL pathway. This hypothesis can be supported by immunoblotting that revealed a partial SMAX1 degradation in cell cultures in response to *rac*-GR24 (Chapter 6) in comparison to the complete SMXL7 degradation over time under the same conditions (Chapter 3). To test this assumption, the SMAX1 degradation should be examined in response to the specific enantiomer $GR24^{ent\text{-}5DS}$ or to KARs.

Deletion/mutation of a certain amino acid motif (RGKT) in SMXL6/7/8/D53 has been shown to hinder the protein degradation in response to *rac*-GR24 (Chapter 3, Jiang et al., 2013; Soundappan et al., 2015; Wang et al., 2015). In Chapter 6, we demonstrate that this motif is also crucial for the SMAX1 degradation in the presence of the SL analog, hinting at a preserved role of this amino acid sequence between SMAX1 and SMXL6/7/8. Based on the qTAP of SMXL7 and ΔSMXL7, we proposed a model in which the mutated protein is resistant to degradation because of its higher affinity toward TPL/TPR than its wild-type version, hence affecting the interaction with D14 or other components in the presence of *rac*-GR24 (Chapter 3). It is difficult to draw a similar conclusion based on the qTAP of SMAX1/ΔSMAX1. TPL/TPR proteins were detected only as preys of the mutated protein, but not of the full-length SMAX1, possibly implying that indeed ΔSMAX1 has an enhance affinity toward TPL/TPR. Nevertheless, KAI2 was not copurified in any of the TAP experiments with both SMAX1 and ΔSMAX1 as baits. Thus, still more experiments are required to uncover the mode of action of the KAI2-SMAX1-TPL/TPR complex.

Combination of different methods of TAP data analysis revealed putative preys of SMAX1 that would be interesting to study in the future. For instance, components of the exocyst complex, such as SEC10, SEC15B, SEC3A, SEC5A, and SEC8 were discovered with both qualitative and quantitative approaches. Another member of this complex, SEC5B, was copurified with SINT1, but none of the components was detected in the SMXL7 TAP (Chapters 3 and 4), possibly implying that the exocyst complex is involved in vesicle trafficking after activation of the KAR/KL pathway rather than the SL pathway. The establishment of symbiotic interactions between AM fungi and the root of the host plant requires extensive membrane dynamics that involves exocyst complexes (Genre et al., 2012). Symbiosis with AM is also one of the features attributed to the SL signaling (Akiyama et al., 2005, 2010). However, in rice, the KAI2 ortholog and not D14 was found to be essential for the initiation of symbiosis with AM, hinting at a role for the KAR/KL pathway (Gutjahr et al., 2015), but the involvement of SMXL proteins in this process has not been analyzed yet. As SMAX1 and subunits of the exocyst complex do not seem to have overlapping localization patterns, *rac*-GR24-induced SMAX1 degradation might probably trigger exocytosis in the cell that might then regulate the symbiosis with the AM fungi. Future studies are required to confirm the interaction between SMAX1 and members of exocyst complex, such as BiFC, Co-IP, or colocalization of both in the presence of *rac*-GR24. Also, root colonization by AM fungi in exocyst complex mutants in rice or petunia would help to verify our hypothesis.

Another interesting protein for further analysis is DNAJ HOMOLOGUE 3 (ATJ3) detected as significantly more associated with ΔSMAX1 under mock conditions, whereas in the SMAX1 TAP experiments, it was present under both conditions. One explanation might be that degradation of the bait obscures the dynamic association between the two proteins. ATJ3 was detected in all the ΔSMAX1 samples, but the protein level was much lower under *rac*-GR24-treated than under mock conditions, suggesting that this interaction is weakened in the presence of the SL analog. This interaction was not visible in the SMAX1 TAP, because the reduced level of the bait protein in the presence of the SL analog decreases the levels of all the proteins copurified with it. ATJ3 regulates the expression of the *ABSCISID ACID (ABA)-INSENSITIVE 3* (*ABI3*) gene, thereby influencing seed development, germination, and abiotic stress tolerance (Salas-Munoz et al., 2016). Therefore, ATJ3 might possibly be a linker between the KAR/KL and ABA pathways for seed germination. To prove this suggestion the validation of the SMAX1-ATJ3 interaction is required and analysis of *the rac*-GR24-induced seed germination in the *atj3* mutant.

In search for novel interaction partners of MAX2, KAI2, and D14

TAP can be carried out in different biological systems, such as *Arabidopsis* cell cultures or stably transformed plants. Cell cultures provide an easy and fast way to screen for interactions with the benefit of high protein yield and the possibility to execute trigger-based studies, whereas TAP in

Arabidopsis seedlings deliver data from a more developmentally relevant context (Dedecker et al., 2015; Van Leene et al., 2015). We used both systems to broaden the interaction network of the MAX2, D14, and KAI2 proteins (Chapter 7 and 8).

The TAP experiments with MAX2 as bait were highly successful in both cell cultures and seedlings, although more interacting partners were found in the former system (Chapter 7 and 8). Identification of well-known MAX2 complex components that are part of the SCF complex, ARABIDOPSIS SKP1 HOMOLOGUE 1 (SKP1), CULLIN 1 (CUL1), and RING-BOX 1 (RBX1) (Stirnberg et al., 2007) proved the strength of the TAP technique. Curiously, the SL receptor D14 was retrieved only once, when the MAX2 bait was expressed in the corresponding mutant background. In the recent SL signaling model, the *rac*-GR24 perception triggers a conformational change in the D14 receptor protein, allowing MAX2 binding (DWARF 3/D3 in rice [*Oryza sativa*]) (Yao et al., 2016). This finding is further supported by other validation methods in rice, petunia (*Petunia × hybrida*), and *Arabidopsis* (Hamiaux et al., 2012; Liang et al., 2016; Zhao et al., 2014; Zhao et al., 2015). We detected D14 as a MAX2 interactor only in the TAP done in the *max2* mutant background and without exogenous *rac*-GR24. One explanation might that the SL levels are higher in the *max2* mutant due to the upregulation of the SL biosynthesis genes *MAX3* and *MAX4* (Mashiguchi et al.2009) which would to trigger MAX2-D14 association. Moreover, the addition of SL also triggers degradation of D14 in the MAX2-dependent manner (Chevalier et al., 2014). The prolonged treatment with *rac*-GR24 thus possibly enhanced that process not allowing us to retrieve D14 as a prey of MAX2 under that condition.

Regarding novel interactors of MAX2, six proteins were identified *in planta* and 15 in cell cultures. No overlaps between the preys were found. As we did not study in detail all the interactions, it is difficult to evaluate which biological system is more suitable for the elucidation of the MAX2 signaling. In both cases, we could validate interactions with one of the novel identified preys, namely the PHYTOCHROME-ASSOCIATED PROTEIN PHOSPHATASE 5 (PAPP5), which has been discussed above, and the CONSERVED IN CILIATED SPECIES AND IN THE LAND PLANTS 1 (CCP1) (Table 1).

CCP1 seems to be an indirect MAX2 interactor playing a role in the MAX2-KAI2-related responses such as seed germination under suboptimal conditions and hypocotyl elongation (Figure 2) (Chapter 8). The opposite phenotypes of *ccp1* and *max2* mutants suggest that CCP1 might be a ubiquitination target of MAX2. This hypothesis, however, is contradicted by two observations. First, the response to *rac*-GR24 was not changed in the hypocotyl of the *ccp1* mutant. Second, the SMAX1 and SMXL2 proteins were reported as possibly the only targets of MAX2 required for the control of seed germination in suboptimal conditions and hypocotyl elongation in response to KAR/KL (Stanga et al., 2013, 2016). Nevertheless, CCP1 might still be a target of MAX2 but in response to other triggers than KAR/KL. The

MAX2 ortholog from *Physcomitrella patens* (*PpMAX2*) is probably involved in photomorphogenesis, while the response to KAR seems to be absent in moss. Moreover, *PpMAX2* is not able to complement the elongated hypocotyl phenotype of the *Arabidopsis max2* mutant, potentially because the downstream targets cannot be recognized (Lopez-Obando et al., 2018). Although we cannot rule out that KL exists in moss, the *CCP1* ortholog was detected in *Physcomitrella patens* (Hodges et.al., 2011), thus CCP1 might be a potential ancestral target of MAX2 regulating light-related responses. This will be investigated by the analysis of *ccp1max2-1* mutant, in which, in agreement with our hypothesis, the suppression *max2* phenotype is expected. Currently, we are also generating *ccp1smax1* double mutants to determine whether the observed phenotypes are due to affected KAR/KL signaling.

Moreover, CCP1 is a putative katanin, a microtubule-severing protein (Mcnally and Vale, 1993), related to KATANIN 1 (KTN1), which has been reported to regulate the plant microtubule organization in response to several phytohormones (Meier et al., 2001; Bouquin et al., 2003). Although additional experiments need to be performed to confirm the role of CCP1 as a katanin, for instance, by colocalization with tubulin or microtubule-binding proteins, we can speculate that CCP1 might promote a rapid reorganization of cellular microtubule arrays in response to *rac*-GR24. As proof, the *rac*-GR24 impact on microtubules should be tested in the wild types and in the *ccp1* mutant constitutively expressing GFP-tagged tubulin. Also, the response to compounds that are more specific for MAX2-KAI2 pathway, such as GR24$^{ent\text{-}5DS}$ or KAR, should to be tested as well.

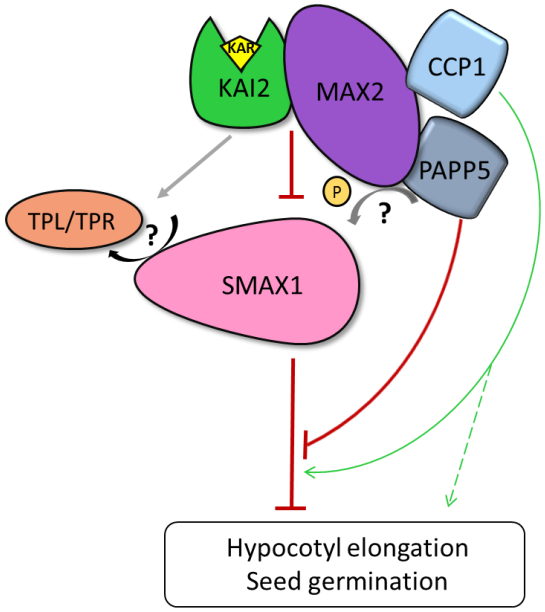

Figure 2. A proposed model explaining a possible role of the novel MAX2 interactors in the KAR/KL signaling. In the presence of KAR/KL, KAI2 and SCF^{MAX2} are recruited to SMAX1, whereas the TPL/TPR proteins might dissociate from the complex. PAPP5 interacts with MAX2 possibly leading to its dephosphorylation. As a result, PAPP5 might positively regulate the hypocotyl elongation and seed germination under suboptimal conditions. On the contrary, CCP1 seems to be a negative regulator of these phenotypes.

The TAP experiments of D14 and KAI2 yielded fewer preys when compared to that of MAX2, two or none interactors in cell cultures and none or six *in planta*, respectively. The observation that these

two baits could not fully complement the phenotypes of the corresponding mutants might explain why the TAP experiments of D14 and KAI2 were less effective. However, we cannot exclude that both proteins might engage in fewer or in transient interactions than MAX2. Nevertheless, some interesting observations were made when KAI2 was used as bait in *Arabidopsis* seedlings.

Firstly, we detected D14 as a putative prey of KAI2. A direct interaction between D14 and KAI2 is not expected, but they might possibly be copurified in one complex due to the binding to the same protein(s). The known interactor of both receptors, MAX2, does probably not play this role, because KAI2 and D14 share a well-conserved amino acid motif that is essential for the D14-MAX2 interaction (Waters et al., 2017; Yao et al., 2016), hinting at a similar mechanism for the KAI2-MAX2 binding. The D14-KAI2 association could not be validated with BiFC and Y2H, because of the limitations of these techniques. Additional methods, for instance Co-IP, should be used to test the relevance of this interaction. Although D14 and KAI2 play distinct roles in the SL or KAR/KL pathways, they localize to the same compartments (Chapter 8), have some overlapping expression patterns during plant development (Chapter 1), and are both involved in *ra*c-GR24-dependent hypocotyl elongation inhibition (Scaffidi et al., 2014; Stanga et al., 2016) and lateral root density reduction (Cedrick Matthys, unpublished data). Thus, although the interaction between KAI2 and D14 observed by TAP might indeed take place, it can be also an artifact without any physiological meaning.

Another intriguing protein found as a novel putative interactor of KAI2 in *Arabidopsis* seedlings is the ALPHA-CRYSTALLIN DOMAIN 32.1 (ACD32.1). The Y2H analysis revealed that ACD32.1 interacts directly not only with KAI2, but also with other components of the SL and KAR/KL pathways. Interestingly, the D14-ACD32.1 association depends on *rac*-GR24 (Table 1). Nevertheless, these preliminary results should be validated with additional techniques, such as BiFC or Förster resonance energy transfer (FRET). Based on its homology to small heat shock proteins, ACD32.1 might function as a molecular chaperone. As ACD32.1 had been demonstrated to interact with all the known components of the SL and KAR pathways, it might help or regulate the formation of the MAX2-KAI2-SMAX1 and MAX2-D14-SMXL7 complexes. In support for this hypothesis, the D14-ACD32.1 interaction depends on *rac*-GR24 just like the MAX2-D14-SMXL6/7/8 complex formation (Soundappan et al., 2015; Wang et al., 2015; Liang et al., 2016), whereas the KAI2-SMAX1 interaction occurs without *rac*-GR24 addition (Chapter 6), similarly to the KAI2 and SMAX1 association with the ACD32.1 protein. To verify these speculations, we could investigate the stability of SMXL proteins in response to the SL analog in the *acd32.1* mutant or check whether the interactions are affected in this mutant background by means of Co-IP. The biological relevance of the detected interactions and the function of the ACD32.1 protein remain to be determined by testing the *acd32.1* mutant phenotypes related to SL and KAR.

Eventually, the question arises as to why SMXL proteins had not been identified as preys in any of the TAP experiments with MAX2, D14, or KAI2 as baits. The simplest explanation might be that the prolonged treatment of *Arabidopsis* cell cultures and seedlings with *rac*-GR24 (5h and 6h, respectively) led to the degradation of SMXL proteins. We can speculate that to copurify SMXL proteins as preys of MAX2, D14, or KAI2, an experiment needs to be designed with a shorter treatment (10 min), preferentially with the GR24 enantiomers and in combination with quantitative data analysis (Chapter 3).

Final conclusions

In this thesis, we used TAP-MS to expand the interactome of the core components in the SL and KAR/KL pathways. However, we often did not find the expected interactors such as the known key players. One explanation might be that by the purification in cell cultures or seedlings we were not able to obtain the relevant context for certain interactions. Also, the small overlap between preys copurified in these two systems, for instance with MAX2 (Figure 3A), indicates that the interactions might vary depending on the used environment. Both KAR/KL and SL pathways play a role during very specific developmental stages in plants and these would be better for the interactome analysis. For instance, one step affinity purification (AP) allows for more tissue-specific studies due to the lower input requirement. Thus, it would be interesting to identify the KAI2 interactome in the imbibed seeds or red-light-grown seedlings and D14-controlled signaling, in the buds. In addition, *rac*-GR24 applied in our experiments activate both pathways and, in the future, the specific GR24 enantiomers should be applied instead.

We demonstrated that TAP data can be analyzed in both a qualitative and quantitative manner. The first one provides a static view on the interactors while the second one allows for the detection of proteins differentially interacting due to the experimental conditions. Consequently, little overlap was found between preys of SMXL7 and SMAX1 identified by using the two approaches (Figure 3B-C). In the qualitative TAP, relatively low number of interactors is obtained with a high signal-to noise ratio, that is often beneficial for downstream analyses (Van Leene et al., 2008). Moreover, it is a very reliable way of filtering data with a high confidence to detect *bone fide* interactors. Nevertheless, to generate a list of background proteins a lot of negative controls and purifications of unrelated baits in very similar experimental conditions are required. Moreover, any changes in the protocol might influence the protein identification in TAP-MS experiment. Conversely, quantitative TAP (LFQ) uses statistical analysis to detect proteins that are significantly enriched in one of the tested conditions, thus allows for identification of dynamic interactions. However, a high number of repeats is required and some of the identified preys might still be unspecific binders. As a consequence, both methods provide

complementary data, and ideally should be used in parallel to get a comprehensive view on the bait interactome.

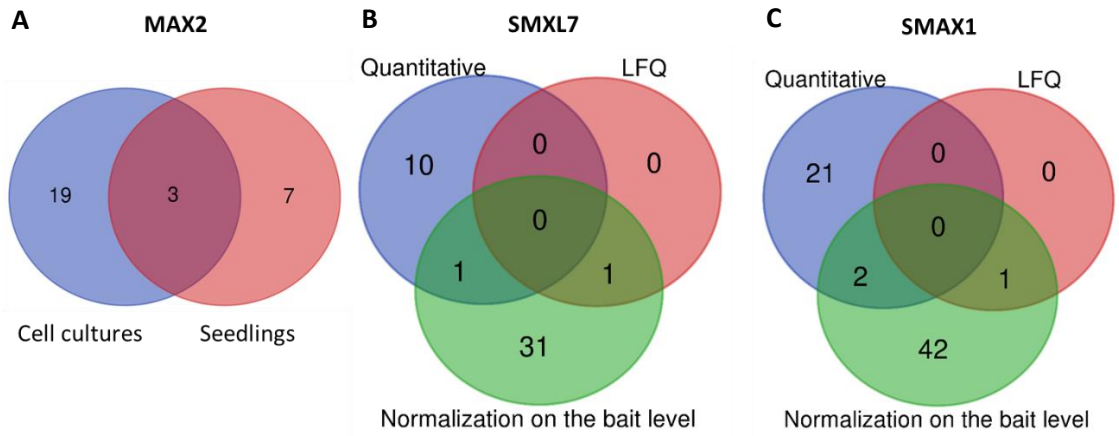

Figure 3. The comparison of the results between different TAP conditions and data analysis methods. Venn diagram showing (A) the overlap of MAX2 preys identified in *Arabidopsis* cell cultures vs seedlings and the overlap between preys identified with SMXL7 (B) or SMAX1 (C), using the qualitative and quantitative (LFQ and Normalization on the bait level) approaches to analyze TAP data

Many novel proteins were identified as potential interactors of the core components in the SL and KAR/KL pathways generating an extensive interactome network (Figure 4). Nevertheless, only few players were found to be associated with more than one prey and those might be worthwhile to investigate further in the future. For instance, besides TPL/TPR and FyPP1, four other preys, HEAT/U-box domain-containing protein (HEAT), SUPPRESSOR OF RPS4-RLD 1(SRFR1), ARM repeat superfamily protein (ARM) and Tetratricopeptide repeat (TPR)-like superfamily protein (TTP) were copurified with both SMXL7/ΔSMXL7 and SMAX1/ΔSMAX1 baits. Although the results discussed in this thesis are still too preliminary to firmly position one of the preys as a key signaling component, we propose few potential candidates that might help to broaden our understanding of the SL and KAR/KL pathways. The two novel preys of MAX2, CCP1 and PAPP5 are likely to be involved in KAR/KL-regulated seed germination and hypocotyl elongation albeit having opposite effects, while the PP6-type phosphatase complex copurified with SMXL7 might be a negative regulator of SL-controlled lateral root development and shoot branching. It is possible that other validated interactors of SMXL7 that could not be linked with the SL and/or KAR/KL responses, such as the SINT proteins, might not be involved in these signaling pathways, but rather have a function related to SMXL proteins only. Besides the preys studied in this thesis, many other interesting proteins might be hidden in this dataset (Figure 4) that might further expand our knowledge on the SL and KAR/KL signaling networks.

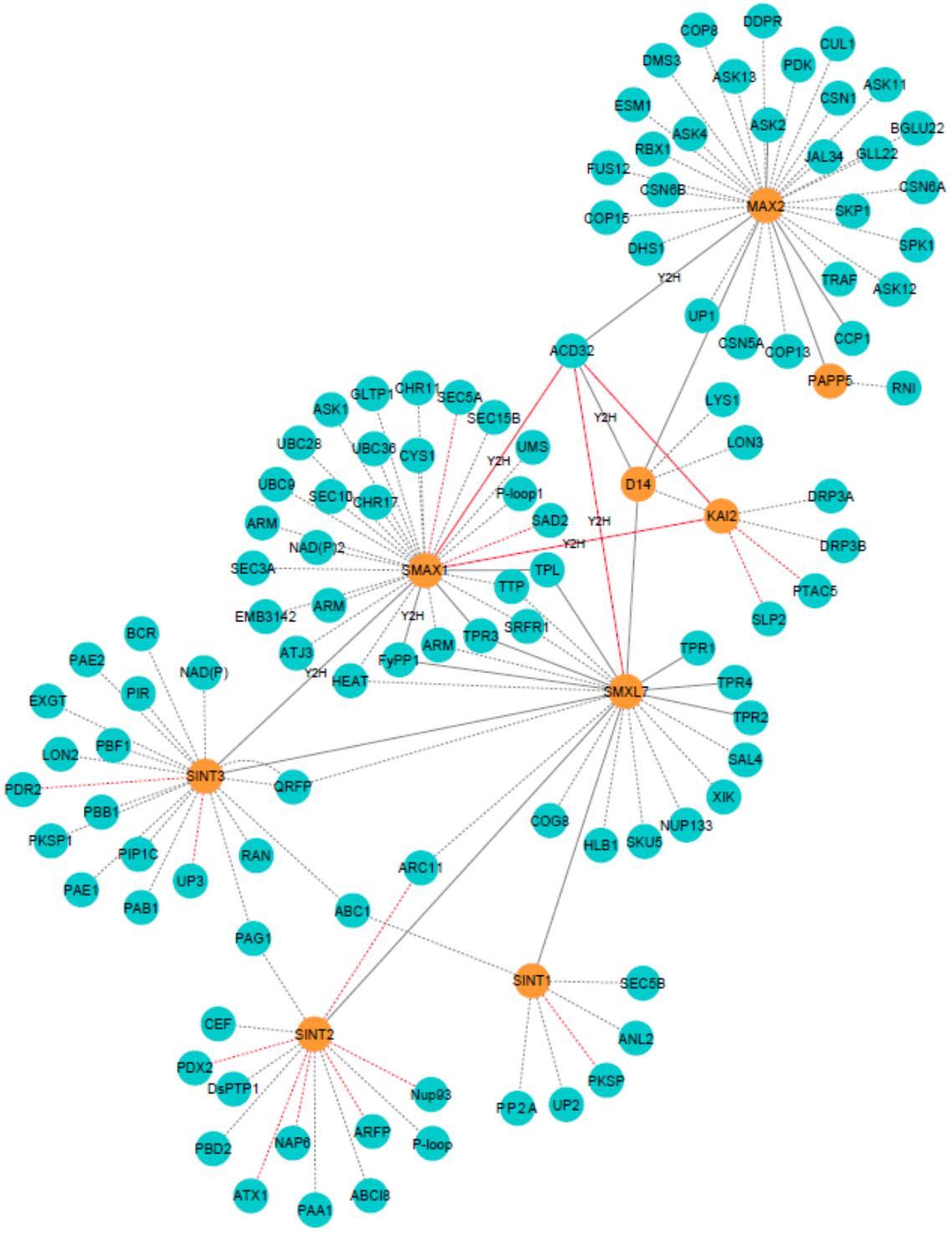

Figure 4. Visual representation of the network between all the baits used in this thesis and the preys identified with them. Network constructed using the Cytoscape software. The orange and blue nodes indicate the bait and prey proteins, respectively. Interactions identified only by means of TAP are represented by dotted connections (edges), while the interactions validated with at least one additional technique by a solid line. The red edges indicate coexpression between bait and prey based on the Cornet 2.0 tool (De Bodt et al., 2012). Y2H, the interaction only detected with this method.

References

Abe S., Sado A., Tanaka K., Kisugi T., Asami K., Ota S., …, Nomura T. (2014) Carlactone is converted to carlactonoic acid by MAX1 in *Arabidopsis* and its methyl ester can directly interact with AtD14 in vitro. *Proceedings of the National Academy of Sciences of the United States of America* 111, 18084-18089.

Aguilar-Martinez, J. A., Poza-Carrion, C., & Cubas, P. (2007). Arabidopsis BRANCHED1 acts as an integrator of branching signals within axillary buds. *Plant Cell* 19(2), 458-472.

Agusti J., Herold S., Schwarz M., Sanchez P., Ljung K., Dun E.A., ..., Greb T. (2011) Strigolactone signaling is required for auxin-dependent stimulation of secondary growth in plants. *Proceedings of the National Academy of Sciences of the United States of America* 108, 20242-20247 [Err. *Proceedings of the National Academy of Sciences of the United States of America* 109, 14277].

Akiyama K., Matsuzaki K.-i. & Hayashi H. (2005) Plant sesquiterpenes induce hyphal branching in arbuscular mycorrhizal fungi. *Nature* 435, 824-827.

Akiyama K., Ogasawara S., Ito S. & Hayashi H. (2010) Structural requirements of strigolactones for hyphal branching in AM fungi. *Plant and Cell Physiology* 51, 1104-1117.

Al-Babili, S., & Bouwmeester, H.J. (2015). Strigolactones, a Novel Carotenoid-Derived Plant Hormone. *Annual Review of Plant Biology* 66, 161-186.

Albert, T.K., Hanzawa, H., Legtenberg, Y.I., Ruwe, M.J. De, Heuvel, F. J. Van Den,…, Timmers, H.T.M. (2002). Identification of a ubiquitin-protein ligase subunit within the CCR4-NOT transcription repressor complex. *EMBO Journal* 21, 355–364.

Alberts B. (1998) The cell as a collection of protein (machines: preparing the next generation of molecular biologists. *Cell* 92, 291-294.

Alder A., Jamil M., Marzorati M., Bruno M., Vermathen M., Bigler P., ..., Al-Babili S. (2012) The path from β-carotene to carlactone a strigolactone-like plant hormone. *Science* 335, 1348-1351.

Armean I.M., Lilley K.S. & Trotter M.W.B. (2013) Popular computational methods to assess multiprotein complexes derived from label-free affinity purification and mass spectrometry (AP-MS) experiments. *Molecular and Cellular Proteomics* 12, 1-13.

Arite T., Iwata H., Ohshima K., Maekawa M., Nakajima M., Kojima M., Sakakibara H. & Kyozuka J. (2007) *DWARF10* an *RMS1/MAX4/DAD1* ortholog controls lateral bud outgrowth in rice. *Plant Journal* 51, 1019-1029.

Arite T., Umehara M., Ishikawa S., Hanada A., Maekawa M., Yamaguchi S. & Koyzuka J. (2009) *d14* a strigolactone-insensitive mutant of rice shows an accelerated outgrowth of tillers. *Plant and Cell Physiology* 50, 1416-1424.

Bai, Y., Salvadore, C., Chiang, Y. C., Collart, M. A., Liu, H. Y., & Denis, C. L. (1999). The CCR4 and CAF1 proteins of the CCR4-NOT complex are physically and functionally separated from NOT2, NOT4, and NOT5. *Molecular and Cellular Biology* 19(10), 6642-6651.

Baldrianová J., Černý M., Novák J., Jedelský P.L., Divíšková E. & Brzobohatý B. (2015) *Arabidopsis* proteome responses to the smoke-derived growth regulator karrikin. *Journal of Proteomics* 120, 7-20.

Baluska, F., Parker, J. S., & Barlow, P. W. (1993). A role for gibberellic-acid in orienting microtubules and regulating cell-growth polarity in the maize root cortex. *Planta, 191*(2), 149-157.

Bao, M. Z., Shock, T. R., & Madhani, H. D. (2010). Multisite phosphorylation of the Saccharomyces cerevisiae filamentous growth regulator Tec1 is required for its recognition by the E3 ubiquitin ligase adaptor Cdc4 and its subsequent destruction in vivo. *Eukaryotic Cell* 9(1), 31-36.

Bar D.Z., Atkatsh K., Tavarez U., Erdos M.R., Gruenbaum Y. & Collins F.S. (2018) Biotinylation by antibody recognition—a method for proximity labeling. *Nature Methods* in press (doi:10.1038/nmeth.4533).

Batelli G., Verslues P.E., Agius F., Qiu Q., Fujii H., Pan S., ..., Zhu J.-K. (2007) SOS2 promotes salt tolerance in part by interacting with the vacuolar H^+-ATPase and upregulating its transport activity. *Molecular and Cellular Biology* 27, 7781-7790.

Bech-Otschir, D., Kraft, R., Huang, X., Henklein, P., Kapelari, B., Pollmann, C., & Dubiel, W. (2001). COP9 signalosome-specific phosphorylation targets p53 to degradation by the ubiquitin system. *The EMBO Journal* 20, 1630-1639.

Bellati, J., Champeyroux, C., Hem, S., Rofidal, V., Krouk, G., Maurel, C., & Santoni, V. (2016). Novel aquaporin regulatory mechanisms revealed by interactomics. *Molecular & Cellular Proteomics* 15(11), 3473-3487.

Belles-Boix, E., Babiychuk, E., Montagu, M. V., Inze, D., & Kushnir, S. (2000). CEF, a SEC24 homologue of *Arabidopsis thaliana*, enhances the survival of yeast under oxidative stress conditions. *Journal of Experimental Botany* 51(351), 1761-1762.

Belmondo S., Marschall R., Tudzynski P., López Ráez J.A., Artuso E., Prandi C. & Lanfranco L. (2016) Identification of genes involved in fungal responses to strigolactones using mutants from fungal pathogens. *Current Genetics* , in press (doi: 101007/s00294-016-0626-y).

Bennett T., Sieberer T., Willett B., Booker J., Luschnig C. & Leyser O. (2006) The *Arabidopsis MAX* pathway controls shoot branching by regulating auxin transport. *Current Biology* 16, 553-563.

Bennett T. & Leyser O. (2014) Strigolactone signalling: standing on the shoulders of DWARFs. *Current Opinion in Plant Biology* 22, 7-13.

Bennett T., Liang Y., Seale M., Ward S., Müller D. & Leyser O. (2016) Strigolactone regulates shoot development through a core signalling pathway. *Biology Open* 5, 1806-1820.

Besbrugge, N., Van Leene, J., Eeckhout, D., Cannoot, B., Kulkarni, S. R., De Winne, N., . . . De Jaeger, G. (2018). GSyellow, a Swiss-Knife Tag for Functional Protein Analysis in Monocot and Dicot Plants. *Plant Physiology* (doi:10.1104/pp.18.00175)

Besserer A., Puech-Pagès V., Kiefer P., Gomez-Roldan V., Jauneau A., Roy S., ..., Séjalon-Delmas N. (2006) Strigolactones stimulate arbuscular mycorrhizal fungi by activating mitochondria. *PLoS Biology* 4, e226.

Besserer A., Bécard G., Jauneau A., Roux C. & Séjalon-Delmas N. (2008) GR24 a synthetic analog of strigolactones stimulates the mitosis and growth of the arbuscular mycorrhizal fungus *Gigaspora rosea* by boosting its energy metabolism. *Plant Physiology* 148, 402-413.

Beveridge C.A., Ross J.J. & Murfet I.C. (1996) Branching in pea. Action of genes *Rms3* and *Rms4*. *Plant Physiology* 110, 859-865.

Bhat R.A., Lahaye T. & Panstruga R. (2006) The visible touch: *in planta* visualization of protein-protein interactions by fluorophore-based methods. *Plant Methods* 2 12.

Bichet, A., Desnos, T., Turner, S., Grandjean, O., & Hofte, H. (2001). BOTERO1 is required for normal orientation of cortical microtubules and anisotropic cell expansion in *Arabidopsis*. *Plant Journal* 25(2), 137-148.

Biedrzycki, M. L., L, V., & Bais, H. P. (2011). The role of ABC transporters in kin recognition in *Arabidopsis thaliana*. *Plant Signal Behaviour* 6(8), 1154-1161.

Blakeslee J.J., Bandyopadhyay A., Lee O.R., Mravec J., Tipapiwatanakun B., Sauer M., ..., Murphy A.S. (2007) Interactions among PIN-FORMED and P-glycoprotein auxin transporters in *Arabidopsis*. *Plant Cell* 19, 131-147.

Blakeslee, J. J., Zhou, H. W., Heath, J. T., Skottke, K. R., Barrios, J. A., Liu, S. Y., & DeLong, A. (2008). Specificity of RCN1-mediated protein phosphatase 2A regulation in meristem organization and stress response in roots. *Plant Physiology* 146(2), 539-553.

Bogamuwa, S.P., and Jang, J.-C. (2014). Tandem CCCH zinc finger proteins in plant growth, development and stress response. *Plant Cell Physiology* 55, 1367–1375.

Booker J., Sieberer T., Wright W., Williamson L., Willett B., Stirnberg P., ..., Leyser O. (2005) *MAX1* encodes a cytochrome P450 family member that acts downstream of *MAX3/4* to produce a carotenoid-derived branch-inhibiting hormone. *Developmental Cell* 8, 443-449.

Booker, J., Auldridge, M., Wills, S., McCarty, D., Klee, H., and Leyser, O. (2004). MAX3/CCD7 is a carotenoid cleavage dioxygenase required for the synthesis of a novel plant signaling molecule. *Current Biology* 14, 1232-1238.

Borthwick, E.B., Zeke, T., Prescott, A.R., and Cohen, P.T.W. (2001). Nuclear localization of protein phosphatase 5 is dependent on the carboxy-terminal region. *FEBS Letters* 491, 279-284.

Boruc J., Van den Daele H., Hollunder J., Rombauts S., Mylle E., Hilson P., ..., Russinova E. (2010) Functional modules in the *Arabidopsis* core cell cycle binary protein-protein interaction network. *Plant Cell* 22 1264-1280.

Boruc, J., Mylle, E., Duda, M., De Clercq, R., Rombauts, S., Geelen, …, Russinova, E. (2010). Systematic localization of the Arabidopsis core cell cycle proteins reveals novel cell division complexes. *Plant Physiology* 152, 553-565.

Bouquin, T., Mattsson, O., Naested, H., Foster, R., & Mundy, J. (2003). The Arabidopsis lue1 mutant defines a katanin p60 ortholog involved in hormonal control of microtubule orientation during cell growth. *Journal of Cell Science 116*(5), 791-801.

Boute N., Jockers R. & Issad T. (2002) The use of resonance energy transfer in high-throughput screening: BRET versus FRET. *Trends in Pharmacological Sciences* 23, 351-354.

Boyer F.-D., de Saint Germain A., Pouvreau J.-B., Clavé G., Pillot J.-P., Roux A., ..., Rameau C. (2014) New strigolactone analogs as plant hormones with low activities in the rhizosphere. *Molecular Plant* 7, 675-690.

Bracha-Drori K., Shichrur K., Katz A., Oliva M., Angelovici R., ..., Ohad N. (2004) Detection of protein-protein interactions in plants using bimolecular fluorescence complementation. *Plant Journal* 40, 419-427.

Bradow J.M., Connick W.J. Jr. & Pepperman A.B. (1988) Comparison of the seed germination effects of synthetic analogs of strigol gibberellic acid cytokinins and other plant growth regulators. *Journal of Plant Growth Regulation* 7, 227-239.

Braun N., de Saint Germain A., Pillot J.-P., Boutet-Mercey S., Dalmais M., Antoniadi I., ..., Rameau C. (2012) The pea TCP transcription factor PsBRC1 acts downstream of strigolactones to control shoot branching. *Plant Physiology* 158, 225-238.

Brewer P.B., Yoneyama K., Filardo F., Meyers E., Scaffidi A., Frickey T., …, Beveridge C.A. (2016) *LATERAL BRANCHING OXIDOREDUCTASE* acts in the final stages of strigolactone biosynthesis in *Arabidopsis*. *Proceedings of the National Academy of Sciences of the United States of America* 113, 6301-6306.

Brown, L., Borthwick, E.B., & Cohen, P.T.W. (2000). Drosophila protein phosphatase 5 is encoded by a single gene that is most highly expressed during embryonic development. *Biochimica et Biophysica Acta (BBA) - Gene Structure and Expression* 1492, 470-476.

Bücherl C.A., van Esse G.W., Kruis A., Luchtenberg J., Westphal A.H., Aker J., ..., de Vries S.C. (2013) Visualization of BRI1 and BAK1(SERK3) membrane receptor heterooligomers during brassinosteroid signaling. *Plant Physiology* 162, 1911-1925.

Bücherl, C.A., Bader, A., Westphal, A.H., Laptenok, S.P., and Borst, J.W. (2014). FRET-FLIM applications in plant systems. *Protoplasma* 251, 383–394.

Brückner A., Polge C., Lentze N., Auerbach D. & Schlattner U. (2009) Yeast two-hybrid a powerful tool for systems biology. *International Journal of Molecular Science* 10, 2763-2788.

Bürckstümmer T., Bennett K.L., Preradovic A., Schütze G., Hantschel O., Superti-Furga G. & Bauch A. (2006) An efficient tandem affinity purification procedure for interaction proteomics in mammalian cells. *Nature Methods* 3, 1013-1019.

Bu Q., Lv T., Shen H., Luong P., Wang J., Wang Z., ..., Huq E. (2014) Regulation of drought tolerance by the F-box protein MAX2 in Arabidopsis. *Plant Physiology* 164, 424-439.

Buntru A., Trepte P., Klockmeier K., Schnoegl S. & Wanker E.E. (2016) Current approaches toward quantitative mapping of the interactome. *Frontiers in Genetics* 7, 74.

Burk, D. H., Liu, B., Zhong, R. Q., Morrison, W. H., & Ye, Z. H. (2001). A katanin-like protein regulates normal cell wall biosynthesis and cell elongation. *Plant Cell 13*(4), 807-827.

Burk, D. H., Zhong, R. Q., & Ye, Z. H. (2007). The katanin microtubule severing protein in plants. *Journal of Integrative Plant Biology* 49(8), 1174-1182.

Butler L.G. (1995) Chemical communication between the parasitic weed *Striga* and its crop host. A new dimension in allelochemistry. In *Allelopathy: Organisms Processes and Applications* ACS Symposium Series Vol. 582 pp. 158-168. American Chemical Society Washington D.C

Bythell-Douglas R., Waters M.T., Scaffidi A., Flematti G.R., Smith S.M. & Bond C.S. (2013) The structure of the karrikin-insensitive protein (KAI2) in *Arabidopsis thaliana*. *PLoS ONE* 8, e54758.

Carriba P., Navarro G., Ciruela F., Ferré S., Casadó V., Agnati L., ..., Franco R. (2008) Detection of heteromerization of more than two proteins by sequential BRET-FRET. *Nature Methods* 5, 727-733.

Causier, B., Ashworth, M., Guo, W., & Davies, B. (2012). The TOPLESS interactome: a framework for gene repression in Arabidopsis. *Plant Physiology 158*(1), 423-438.

Černý M., Novák J., Habánová H., Cerna H. & Brzobohatý B. (2016) Role of the proteome in phytohormonal signaling. *Biochimica et Biophysica Acta* 1864 1003-1015.

Chandler, J.W., and Melzer, S. (2004). An alpha-crystallin gene, ACD31.2 from Arabidopsis is negatively regulated by FPF1 overexpression, floral induction, gibberellins, and long days. *Journal of Experimental Botany* 55, 1433-1435.

Chang I.F., Curran A., Woolsey R., Quilici D., Cushman J.C., Mittler R., Harmon A. & Harper J.F. (2009) Proteomic profiling of tandem affinity purified 14-3-3 protein complexes in *Arabidopsis thaliana*. *Proteomics* 9, 2967-2985.

Charbonnier S., Gallego O. & Gavin A.-C. (2008) The social network of a cell: recent advances in interactome mapping. *Biotechnology Annual Review* 14, 1-28.

Cardazzo, B., Hamel, P., Sakamoto, W., Wintz, H., & Dujardin, G. (1998). Isolation of an *Arabidopsis thaliana* cDNA by complementation of a yeast abc1 deletion mutant deficient in complex III respiratory activity. *Gene, 221*(1), 117-125.

Champion, A., Picaud, A., & Henry, Y. (2004). Reassessing the MAP3K and MAP4K relationships. *Trends Plant Science* 9(3), 123-129.

Chen, M.X., McPartlin, A.E., Brown, L., Chen, Y.H., Barker, H.M. & Cohen, P.T. (1994). A novel human protein serine/threonine phosphatase, which possesses four tetratricopeptide repeat motifs and localizes to the nucleus. *The EMBO Journal* 13, 4278-4290.

Chen, M.-S., Silverstein, A.M., Pratt, W.B., and Chinkers, M. (1996). The tetratricopeptide repeat domain of protein phosphatase 5 mediates binding to glucocorticoid receptor heterocomplexes and acts as a dominant negative mutant. *Journal of Biological Chemistry* 271, 32315-32320.

Chen, J., Rappsilber, J., Chiang, Y. C., Russell, P., Mann, M., & Denis, C. L. (2001). Purification and characterization of the 1.0 MDa CCR4-NOT complex identifies two novel components of the complex. *Journal of Molecular Biology* 314(4), 683-694.

Chen S., Tao L., Zeng L., Vega-Sanchez M.E., Umemura K. & Wang G.-L. (2006) A highly efficient transient protoplast system for analyzing defence gene expression and protein–protein interactions in rice. *Molecular Plant Pathology* 7, 417-427.

Chen H., Zou Y., Shang Y., Lin H., Wang Y., Cai R., Tang X. & Zhou J.-M. (2008) Firefly luciferase complementation imaging assay for protein-protein interactions in plants. *Plant Physiology* 146, 368-376.

Chen, X., Chern, M., Canlas, P. E., Ruan, D., Jiang, C., & Ronald, P. C. (2010). An ATPase promotes autophosphorylation of the pattern recognition receptor XA21 and inhibits XA21-mediated immunity. *Proceedings of the National Academy of Sciences USA* 107(17), 8029-8034.

Chen, F., Jiang, L., Zheng, J., Huang, R., Wang, H., Hong, Z. & Huang, Y. (2014). Identification of differentially expressed proteins and phosphorylated proteins in rice seedlings in response to strigolactone treatment. *Plos One* 9, e93947.

Cheng M.-C., Kuo W.-C., Wang Y.-M., Chen H.-Y. & Lin T.-P. (2017) UBC18 mediates ERF1 degradation under light–dark cycles. *New Phytologist* 213, 1156-1167.

Chevalier F Nieminen K Sánchez-Ferrero J.C., Rodríguez M.L., Chagoyen M., Hardtke C.S. & Cubas P. (2014) Strigolactone promotes degradation of DWARF14 an α/β hydrolase essential for strigolactone signaling in *Arabidopsis*. *Plant Cell* 26, 1134-1150.

Chiwocha S.D.S., Dixon K.W., Flematti G.R., Ghisalberti E.L., Merritt D.J., ..., Stevens J.C. (2009) Karrikins: a new family of plant growth regulators in smoke. *Plant Science* 177, 252-256.

Chong, Y.T., Gidda, S.K., Sanford, C., Parkinson, J., Mullen, R.T. & Goring, D.R. (2010). Characterization of the *Arabidopsis thaliana* exocyst complex gene families by phylogenetic, expression profiling, and subcellular localization studies. *New Phytology* 185, 401-419.

Clark N.M., Hinde E., Winter C.M., Fisher A.P., Crosti G., Blilou I., ..., Sozzani R. (2016) Tracking transcription factor mobility and interaction in Arabidopsis roots with fluorescence correlation spectroscopy. *eLife* 5 e14770.

Clark N.M. & Sozzani R. (2017) Measuring protein movement oligomerization state and protein–protein interaction in *Arabidopsis* roots using scanning fluorescence correlation spectroscopy (scanning FCS). *Methods in Molecular Biology* 1610, 251-266.

Clegg R.M. (1995) Fluorescence resonance energy transfer. *Current Opinion in Biotechnology* 6, 103-110.

Clough, S.J., and Bent, A.F. (1998). Floral dip: a simplified method for Agrobacterium-mediated transformation of *Arabidopsis thaliana*. *Plant Journal* 16, 735-743.

Cole, R.A., Synek, L., Zarsky, V., and Fowler, J.E. (2005). SEC8, a subunit of the putative Arabidopsis exocyst complex, facilitates pollen germination and competitive pollen tube growth. *Plant Physiology* 138, 2005-2018.

Collart MA, 2016. The Ccr4-Not complex is a key regulator of eukaryotic gene expression. *Wiley Interdisciplinary Reviews: RNA* 7, 438-54.

Conn C.E., Bythell-Douglas R., Neumann D., Yoshida S., Whittington B., Westwood J.H., ..., Nelson D.C. (2015) Convergent evolution of strigolactone perception enabled host detection in parasitic plants. *Science* 349, 540-543.

Conn C.E. & Nelson D.C. (2016) Evidence that KARRIKIN-INSENSITIVE2 (KAI2) receptors may perceive an unknown signal that is not karrikin or strigolactone. *Frontiers in Plant Science* 6, 1219.

Connarn, J.N., Assimon, V.A., Reed, R.A., Tse, E., Southworth, D.R., Zuiderweg, E.R.P., …, & Sun, D. (2014). The Molecular Chaperone Hsp70 Activates Protein Phosphatase 5 (PP5) by Binding the Tetratricopeptide Repeat (TPR) Domain. *The Journal of Biological Chemistry* 289, 2908-2917.

Cook C.E., Whichard L.P., Turner B., Wall M.E. & Egley G.H. (1966) Germination of witchweed (*Striga lutea* Lour.): isolation and properties of a potent stimulant. *Science* 154, 1189-1190.

Cooper, J. W., Hu, Y., Beyyoudh, L., Yildiz Dasgan, H., Kunert, K., Beveridge, C. A., & Foyer, C. H. (2018). Strigolactones positively regulate chilling tolerance in pea and in Arabidopsis. *Plant Cell Environment.*

Couto D., Niebergall R., Liang X., Bücherl C.A., Sklenar J., Macho A.P., ..., Zipfel C. (2016) The *Arabidopsis* protein phosphatase PP2C38 negatively regulates the central immune kinase BIK1. *PLoS Pathogens* 12, e1005811.

Cox J. & Mann M. (2008) MaxQuant enables high peptide identification rates individualized p.p.b.-range mass accuracies and proteome-wide protein quantification. *Nature Biotechnology* 26, 1367-1372.

Cox J., Hein M.Y., Luber C.A., Paron I., Nagaraj N. & Mann M. (2014) Accurate proteome-wide label-free quantification by delayed normalization and maximal peptide ratio extraction termed MaxLFQ. *Molecular and Cellular Proteomics* 13, 2513-2526.

Crawford S., Shinohara N., Sieberer T., Williamson L., George G., Hepworth J., ..., Leyser O. (2010) Strigolactones enhance competition between shoot branches by dampening auxin transport. *Development* 137, 2905-2913.

Cristea I.M., Williams R., Chait B.T. & Rout M.P. (2005) Fluorescent proteins as proteomic probes. *Molecular and Cellular Proteomics* 4, 1933-1941.

Criqui, M.C., Criqui, M.C., Engler, J.D.A., Engler, J.D.A., Camasses, A., Camasses, A., Capron, A., Capron, A., Parmentier, Y., Parmentier, Y., et al. (2002). Molecular Characterization of Plant Ubiquitin- Conjugating Enzymes Belonging to the UbcP4/E2-C/UBCx/ UbcH10 Gene Family 1. *Plant Physiology* 130, 1230–1240.

Cuéllar Pérez A., Pauwels L., De Clercq R. & Goossens A. (2013) Yeast two-hybrid analysis of jasmonate signaling proteins. *Methods in Molecular Biology*. 1011 173-185.

Cuéllar Pérez A., Nagels Durand A., VandenBossche R., De Clercq R., Persiau G., Van Wees S.C.M., ..., Pauwels L. (2014) The non-JAZ TIFY protein TIFY8 from *Arabidopsis thaliana* is a transcriptional repressor. *PLoS ONE* 9, e84891.

Dai, M., Zhang, C., Kania, U., Chen, F., Xue, Q., McCray, T., Li, G., Qin, G., Wakeley, M., Terzaghi, W., et al. (2012). A PP6-type phosphatase holoenzyme directly regulates PIN phosphorylation and auxin efflux in Arabidopsis. *Plant Cell* 24, 2497-2514.

Dai, M., Xue, Q., McCray, T., Margavage, K., Chen, F., Lee, J.H., Nezames, C.D., Guo, L., Terzaghi, W., Wan, J., et al. (2013). The PP6 phosphatase regulates ABI5 phosphorylation and abscisic acid signaling in Arabidopsis. *Plant Cell* 25, 517-534.

Dale R. & Kato N. (2016) Truly quantitative analysis of the firefly luciferase complementation assay. *Current Plant Biology* 5, 57-64.

Davière J.-M. & Achard P. (2013) Gibberellin signaling in plants. *Development* 140, 1147-1151.

Daws M.I., Davies J., Pritchard H.W., Brown N.A.C. & Van Staden J. (2007) Butenolide from plant-derived smoke enhances germination and seedling growth of arable weed species. *Plant Growth Regulation* 51, 73-82.

Day R.N. & Schaufele F. (2005) Imaging molecular interactions in living cells. *Molecular Endocrinology* 19, 1675-1686.

De Bodt, S., Hollunder, J., Nelissen, H., Meulemeester, N., & Inze, D. (2012). CORNET 2.0: integrating plant coexpression, protein-protein interactions, regulatory interactions, gene associations and functional annotations. *New Phytologist* 195(3), 707-720.

De Cuyper C, Struk S, Braem L, Gevaert K, De Jaeger G, Goormachtig S, 2017. Strigolactones, karrikins and beyond. *Plant Cell Environment* 40, 1691-703.

de Folter S., Immink R.G.H., Kieffer M., Pařenicová L., Henz S.R., Weigel D., ..., Angenent G.C. (2005) Comprehensive interaction map of the Arabidopsis MADS box transcription factors. *Plant Cell* 17, 1424-1433.

de la Fuente van Bentem, S., Vossen, J.H., de Vries, K.J., van Wees, S., Tameling, W.I.L., Dekker, H.L., …, Cornelissen, B.J.C. (2005). Heat shock protein 90 and its co-chaperone protein phosphatase 5 interact with distinct regions of the tomato I-2 disease resistance protein. *The Plant Journal* 43, 284-298.

De Rybel B., Möller B., Yoshida S., Grabowicz Barbier de Reuille P., Boeren S., Smith R.S., …, Weijers D. (2013) A bHLH complex controls embryonic vascular tissue establishment and indeterminate growth in *Arabidopsis*. *Developmental Cell* 24, 426-437.

de Saint Germain A., Ligerot Y., Dun E.A., Pillot J.-P., Ross J.J., Beveridge C.A. & Rameau C. (2013) Strigolactones stimulate internode elongation independently of gibberellins. *Plant Physiology* 163, 1012-1025.

de Saint Germain A., Clavé G., Badet-Denisot M.-A., Pillot J.-P., Cornu D., Le Caer J.-P., ..., Boyer F.-D. (2016) An histidine covalent receptor and butenolide complex mediates strigolactone perception. *Nature Chemical Biology* 12, 787-794.

De Sutter, V., Vanderhaeghen, R., Tilleman, S., Lammertyn, F., Vanhoutte, I., Karimi, M., …, Hilson, P. (2005). Exploration of jasmonate signalling via automated and standardized transient expression assays in tobacco cells. *Plant Journal* 44, 1065–1076.

Deane C.M., Salwiński Ł., Xenarios I. & Eisenberg D. (2002) Protein interactions: two methods for assessment of the reliability of high throughput observations. *Molecular and Cellular Proteomics* 1, 349-356.

Dedecker M., Van Leene J. & De Jaeger G. (2015) Unravelling plant molecular machineries through affinity purification coupled to mass spectrometry. *Current Opinion in Plant Biology* 24, 1-9.

Delaux P.-M., Xie X., Timme R.E., Puech-Pages V., Dunand C., Lecompte E., ..., Séjalon-Delmas N. (2012) Origin of strigolactones in the green lineage. *New Phytologist* 195, 857-871.

Dharmasiri N., Dharmasiri S. & Estelle M. (2005) The F-box protein TIR1 is an auxin receptor. *Nature* 435, 441-445.

Ding X., Richter T., Chen M., Fujii H., Seo Y.S., Xie M., ..., Song W.-Y. (2009) A rice kinase-protein interaction map. *Plant Physiology*. 149 1478-1492.

Dixon A.S., Schwinn M.K., Hall M.P., Zimmerman K., Otto P., Lubben T.H., ..., Wood K.V. (2016) NanoLuc complementation reporter optimized for accurate measurement of protein interactions in cells. *ACS Chemical Biology* 11, 400-408.

Dixon K.W., Merritt D.J., Flematti G.R. & Ghisalberti E.L. (2009) Karrikinolide - a phytoreactive compound derived from smoke with applications in horticulture ecological restoration and agriculture. *Acta Horticulturae* 813, 155-170.

Domagalska, M.A., and Leyser, O. (2011). Signal integration in the control of shoot branching. *Nature Reviews Molecular Cell Biology* 12, 211-221.

Drdova, E.J., Synek, L., Pecenkova, T., Hala, M., Kulich, I., Fowler, J.E., Murphy, A.S., and Zarsky, V. (2013). The exocyst complex contributes to PIN auxin efflux carrier recycling and polar auxin transport in *Arabidopsis*. *Plant Journal* 73, 709-719.

Dun E.A., de Saint Germain A., Rameau C. & Beveridge C.A. (2012) Antagonistic action of strigolactone and cytokinin in bud outgrowth control. *Plant Physiology* 158, 487-498.

Ehlert A., Weltmeier F., Wang X., Mayer C.S., Smeekens S., Vicente-Carbajosa J. & Dröge-Laser W. (2006) Two-hybrid protein–protein interaction analysis in Arabidopsis protoplasts: establishment of a heterodimerization map of group C and group S bZIP transcription factors. *Plant Journal* 46, 890-900.

Eloy, N. B., Gonzalez, N., Van Leene, J., Maleux, K., Vanhaeren, H., De Milde, L., . . . Inze, D. (2012). SAMBA, a plant-specific anaphase-promoting complex/cyclosome regulator is involved in early development and A-type cyclin stabilization. *Proceedings of the National Academy of Sciences of the United States of America* 109(34), 13853-13858.

Estojak J., Brent R. & Golemis E.A. (1995) Correlation of two-hybrid affinity data with in vitro measurements. *Molecular and Cellular Biology* 15, 5820-5829.

Eubel, H., Meyer, E. H., Taylor, N. L., Bussell, J. D., O'Toole, N., Heazlewood, J. L., . . . Millar, A. H. (2008). Novel proteins, putative membrane transporters, and an integrated metabolic network are revealed by quantitative proteomic analysis of *Arabidopsis* cell culture peroxisomes. *Plant Physiology* 148(4), 1809-1829.

Eyckerman S., Titeca K., Van Quickelberghe E., Cloots E., Verhee A., Samyn N., ..., Tavernier J. (2016) Trapping mammalian protein complexes in viral particles. *Nature Communications* 7, 11416.

Farkas, I., Dombradi, V., Miskei, M., Szabados, L., & Koncz, C. (2007). Arabidopsis PPP family of serine/threonine phosphatases. *Trends in Plant Science* 12(4), 169-176.

Fendrych, M., Synek, L., Pecenkova, T., Toupalova, H., Cole, R., Drdova, E., …, Fowler, J.E.(2010). The Arabidopsis Exocyst Complex Is Involved in Cytokinesis and Cell Plate Maturation. *Plant Cell* 22, 3053-3065.

Fendrych, M., Synek, L., Pecenkova, T., Drdova, E.J., Sekeres, J., de Rycke, R, …, Zarsky, V. (2013). Visualization of the exocyst complex dynamics at the plasma membrane of Arabidopsis thaliana. *Molecular Biology of the Cell* 24, 510-520.

Ferguson, B. J., & Beveridge, C. A. (2009). Roles for Auxin, Cytokinin, and Strigolactone in Regulating Shoot Branching. *Plant Physiology* 149(4), 1929-1944.

Fernández-Calvo P., Chini A., Fernández-Barbero G., Chico J.-M., Gimenez-Ibanez S., Geerinck J., ..., Solano R. (2011) The *Arabidopsis* bHLH transcription factors MYC3 and MYC4 are targets of JAZ repressors and act additively with MYC2 in the activation of jasmonate responses. *Plant Cell* 23, 701-715.

Ferro E. & Trabalzini L. (2013) The yeast two-hybrid and related methods as powerful tools to study plant cell signalling. *Plant Molecular Biology* 83, 287-301.

Fields S. & Song O.-k. (1989) A novel genetic system to detect protein-protein interactions. *Nature* 340, 245-246.

Flematti G.R., Ghisalberti E.L., Dixon K.W. & Trengove R.D. (2004) A compound from smoke that promotes seed germination. *Science* 305, 977-977.

Flematti G.R., Goddard-Borger E.D., Merritt D.J., Ghisalberti E.L., Dixon K.W. & Trengove R.D. (2007) Preparation of 2*H*-furo[2.3-*c*]pyran-2-one derivatives and evaluation of their germination-promoting activity. *Journal of Agricultural and Food Chemistry* 55, 2189-2194.

Flematti G.R., Ghisalberti E.L., Dixon K.W. & Trengove R.D. (2009) Identification of alkyl substituted 2*H*-furo[2.3-*c*]pyran-2-ones as germination stimulants present in smoke. *Journal of Agricultural and Food Chemistry* 57, 9475-9480.

Flematti G.R., Scaffidi A., Goddard-Borger E.D., Heath C.H., Nelson D.C., Commander L.E., ..., Ghisalberti E.L. (2010) Structure−activity relationship of karrikin germination stimulants. *Journal of Agricultural and Food Chemistry* 58, 8612-8617.

Flematti G.R., Scaffidi A., Dixon K.W., Smith S.M. & Ghisalberti E.L. (2011) Production of the seed germination stimulant karrikinolide from combustion of simple carbohydrates. *Journal of Agricultural and Food Chemistry* 59, 1195-1198.

Flematti, G.R., Waters, M.T., Scaffidi, A., Merritt, D.J., Ghisalberti, E.L., Dixon, K.W., and Smith, S.M. (2013). Karrikin and Cyanohydrin Smoke Signals Provide Clues to New Endogenous Plant Signaling Compounds. *Molecular Plant* 6, 29-37.

Flematti G.R., Scaffidi A., Waters M.T. & Smith S.M. (2016) Stereospecificity in strigolactone biosynthesis and perception. *Planta* 243, 1361-1373.

Förster T. (2012) Energy migration and fluorescence. *Journal of Biomedical Optics* 17, 011002.

Fujikawa Y., Nakanishi T., Kawakami H., Yamasaki K., Sato M.H., Tsuji H., Matsuoka M. & Kato N. (2014) Split luciferase complementation assay to detect regulated protein-protein interactions in rice protoplasts in a large-scale format. *Rice* 7, 11.

Fukao Y. (2012) Protein-protein interactions in plants. *Plant Cell Physiology* 53, 617-625.

Gadeyne A., Sánchez-Rodríguez C., Vanneste S., Di Rubbo S., Zauber H., Vanneste K., ..., Van Damme D. (2014) The TPLATE adaptor complex drives clathrin-mediated endocytosis in plants. *Cell* 156, 691-704.

Galarneau A., Primeau M., Trudeau L.-E. & Michnick S.W. (2002) β-Lactamase protein fragment complementation assays as *in vivo* and *in vitro* sensors of protein–protein interactions. *Nature Biotechnology* 20, 619-622.

Galland, M., Huguet, R., Arc, E., Cueff, G., Job, D., and Rajjou, L. (2014). Dynamic proteomics emphasizes the importance of selective mRNA translation and protein turnover during *Arabidopsis* seed germination. *Molecular and Cellular Proteomics* 13, 252–268

Gavin A.-C., Maeda K. & Kühner S. (2011) Recent advances in charting protein–protein interaction: mass spectrometry-based approaches. *Current Opinion in Biotechnology* 22, 42-49.

Gehl C., Kaufholdt D., Hamisch D., Bikker R., Kudla J., Mendel R.R. & Hänsch R. (2011) Quantitative analysis of dynamic protein–protein interactions *in planta* by a floated-leaf luciferase complementation imaging (FLuCI) assay using binary Gateway vectors. *Plant Journal* 67, 542-553.

Genre, A., Ivanov, S., Fendrych, M., Faccio, A., Zarsky, V., Bisseling, T. & Bonfante, P. (2012). Multiple exocytotic markers accumulate at the sites of perifungal membrane biogenesis in Arbuscular Mycorrhizas. *Plant Cell Physiology* 53, 244-255.

Gfeller A., Liechti R. & Farmer E.E. (2010) *Arabidopsis* jasmonate signaling pathway. *Science Signaling* 3, cm4.

Ghebrehiwot H.M., Kulkarni M.G., Kirkman K.P. & Van Staden J. (2008) Smoke-water and a smoke-isolated butenolide improve germination and seedling vigour of *Eragrostis tef* (Zucc.) Trotter under high temperature and low osmotic potential. *Journal cf Agronomy and Crop Science* 194, 270-277.

Glatter, T., Schittenhelm, R. B., Rinner, O., Roguska, K., Wepf, A., Junger, M. A., . . . Gstaiger, M. (2011). Modularity and hormone sensitivity of the *Drosophila melanogaster* insulin receptor/target of rapamycin interaction proteome. *Molecular Systems Biology* 7, 547.

Goddard-Borger E.D., Ghisalberti E.L. & Stick R.V. (2007) Synthesis of the germination stimulant 3-methyl-2*H*-furo[2.3-c]pyran-2-one and analogous compounds from carbohydrates. *European Journal of Organic Chemistry* 2007, 3925-3934.

Gomez-Roldan V., Fermas S., Brewer P.B., Puech-Pagès V., Dun E.A., Pillot J.-P., …, Rochange S.F. (2008) Strigolactone inhibition of shoot branching. *Nature* 455, 189-194.

Gonzalez, N., Pauwels, L., Baekelandt, A., De Milde, L., Van Leene, J., Besbrugge, N., …, Inze, D. (2015). A Repressor Protein Complex Regulates Leaf Growth in Arabidopsis. *Plant Cell* 27, 2273-2287.

Goossens J., Swinnen G., Vanden Bossche R., Pauwels L. & Goossens A. (2015) Change of a conserved amino acid in the MYC2 and MYC3 transcription factors leads to release of JAZ repression and increased activity. *New Phytologist* 206, 1229-1237.

Goossens J., De Geyter N., Walton A., Eeckhout D., Mertens J., Pollier J., ..., Goossens A. (2016) Isolation of protein complexes from the model legume *Medicago truncatula* by tandem affinity purification in hairy root cultures. *Plant Journal* 88, 476-489.

Goto-Yamada, S., Mano, S., Nakamori, C., Kondo, M., Yamawaki, R., Kato, A., & Nishimura, M. (2014). Chaperone and protease functions of LON protease 2 modulate the peroxisomal transition and degradation with autophagy. *Plant and Cell Physiology* 55(3), 482-496.

Gruhler A., Schulze W.X., Matthiesen R., Mann M. & Jensen O.N. (2005) Stable isotope labeling of *Arabidopsis thaliana* cells and quantitative proteomics by mass spectrometry. *Molecular and Cellular Proteomics* 4, 1697-1709.

Gulshan, K., Thommandru, B., and Moye-Rowley, W.S. (2012). Proteolytic degradation of the Yap1 transcription factor is regulated by subcellular localization and the E3 ubiquitin ligase Not4. *Journal of Biological Chemistry* 287, 26796–26805.

Guo Y., Zheng Z., La Clair J.J., Chory J. & Noel J.P. (2013) Smoke-derived karrikin perception by the α/β-hydrolase KAI2 from *Arabidopsis*. *Proceedings of the National Academy of Sciences of the United States of America* 110, 8284-8289.

Gutjahr C., Gobbato E., Choi J., Riemann M., Johnston M.G., Summers W., ..., Paszkowski U. (2015) Rice perception of symbiotic arbuscular mycorrhizal fungi requires the karrikin receptor complex. *Science* 350, 1521-1524.

Ha C.V., Leyva-González M.A., Osakabe Y., Tran U.T., Nishimaya R., Watanabe Y., ..., Tran L.-S.P. (2014) Positive regulatory role of strigolactone in plant responses to drought and salt stress. *Proceedings of the National Academy of Sciences of the United States of America* 111, 851-856.

Hala, M., Cole, R., Synek, L., Drdova, E., Pecenkova, T., Nordheim, A., . . . Zarsky, V. (2008). An exocyst complex functions in plant cell growth in Arabidopsis and tobacco. *Plant Cell 20*(5), 1330-1345.

Hamiaux C., Drummond R.S.M., Janssen B.J., Ledger S.E., Cooney J.M., Newcomb R.D. & Snowden K.C. (2012) DAD2 is an α/β hydrolase likely to be involved in the perception of the plant branching hormone, strigolactone. *Current Biology* 22, 2032-2036.

Hartman, J. J., Mahr, J., McNally, K., Okawa, K., Iwamatsu, A., Thomas, S., . . . McNally, F. J. (1998). Katanin, a microtubule-severing protein, is a novel AAA ATPase that targets to the centrosome using a WD40-containing subunit. *Cell, 93*(2), 277-287.

Havugimana P.C., Hart G.T., Nepusz T., Yang H., Turinsky A.L., Li Z., ..., Emili A. (2012) A census of human soluble protein complexes. *Cell* 150, 1068-1081.

Heidari, B., Nemie-Feyissa, D., Kangasjarvi, S., & Lillo, C. (2013). Antagonistic Regulation of Flowering Time through Distinct Regulatory Subunits of Protein Phosphatase 2A. *Plos One, 8*(7).

Hein M.Y., Hubner N.C., Poser I., Cox J., Nagaraj N., Toyoda Y., ..., Mann M. (2015) A human interactome in three quantitative dimensions organized by stoichiometries and abundances. *Cell* 163, 712-723.

Higuchi R., Krummel B. & Saiki R.K. (1988) A general method of *in vitro* preparation and specific mutagenesis of DNA fragments: study of protein and DNA interactions. *Nucleic Acids Research* 16, 7351-7367.

Hink M.A., Shah K., Russinova E., de Vries S.C. & Visser A.J.W.G. (2008) Fluorescence fluctuation analysis of *Arabidopsis thaliana* somatic embryogenesis receptor-like kinase and brassinosteroid insensitive 1 receptor oligomerization. *Biophysical Journal* 94, 1052-1062.

Hodges, M. E., Wickstead, B., Gull, K., & Langdale, J. A. (2011). Conservation of ciliary proteins in plants with no cilia. *Bmc Plant Biology* 11.

Holtkotte X., Ponnu J., Ahmad M. & Hoecker U. (2017) The blue light-induced interaction of cryptochrome 1 with COP1 requires SPA proteins during *Arabidopsis* light signaling. *PLoS Genetics* 13, e1007044.

Holton, N., Nekrasov, V., Ronald, P. C., & Zipfel, C. (2015). The phylogenetically-related pattern recognition receptors EFR and XA21 recruit similar immune signaling components in monocots and dicots. *PLoS Pathogens* 11(1), e1004602.

Horstman A., Nougalli Tonaco I.A., Boutilier K. & Immink R.G.H. (2014) A cautionary note on the use of split-YFP/BiFC in plant protein-protein interaction studies. *International Journal of Molecular Science* 15, 9628-9643.

Hu, Q., He, Y., Wang, L., Liu, S., Meng, X., Liu, G., . . . Li, J. (2017a). DWARF14, a receptor covalently linked with the active form of strigolactones, undergoes strigolactone-dependent degradation in rice. *Frontiers in Plant Science* 8, 1935.

Hu, X. Y., Page, M. T., Sumida, A., Tanaka, A., Terry, M. J., & Tanaka, R. (2017b). The iron-sulfur cluster biosynthesis protein SUFB is required for chlorophyll synthesis, but not phytochrome signaling. *Plant Journal* 89(6), 1184-1194.

Huang, Y.-C., Lu, Y.-N., Wu, J.-T., Chien, C.-T., and Pi, H. (2014). The COP9 signalosome converts temporal hormone signaling to spatial restriction on neural competence. *PLoS Genetics* 10, e1004760.

Ito, S., Nozoye, T., Sasaki, E., Imai, M., Shiwa, Y., Shibata-Hatta, M., . . . Asami, T. (2015). Strigolactone regulates anthocyanin accumulation, acid phosphatases production and plant growth under low phosphate condition in *Arabidopsis. Plos One 10*(3), e0119724.

Ishida, K., & Katsumi, M. (1992). Effects of gibberellin and abscisic-acid on the cortical microtubule orientation in hypocotyl cells of light-grown Cucumber seedlings. *International Journal of Plant Sciences* 153(2), 155-163.

Irigoyen M.L., Iniesto E., Rodriguez L., Puga M.I., Yanagawa Y., Pick E., ..., Rubio V. (2014) Targeted degradation of abscisic acid receptors is mediated by the ubiquitin ligase substrate adaptor DDA1 in *Arabidopsis*. *Plant Cell* 26, 712-728.

Jain, N., Kulkarni, M.G., and van Staden, J. (2006). A butenolide, isolated from smoke, can overcome the detrimental effects of extreme temperatures during tomato seed germination. *Plant Growth Regulation* 49, 263-267.

Jamil M., Kanwal M., Aslam M.M., Khan S.U., Malook I., Tu J. & ur Rehman S. (2014) Effect of plant-derived smoke priming on physiological and biochemical characteristics of rice under salt stress condition. *Australian Journal of Crop Science* 8, 159-170.

Jefferson, R. A., Kavanagh, T. A., & Bevan, M. W. (1987). Gus Fusions - Beta-Glucuronidase as a Sensitive and Versatile Gene Fusion Marker in Higher-Plants. *Embo Journal* 6(13), 3901-3907.

Jia K.-P., Luo Q., He S.-B., Lu X.-D. & Yang H.-Q. (2014) Strigolactone-regulated hypocotyl elongation is dependent on cryptochrome and phytochrome signaling pathways in *Arabidopsis*. *Molecular Plant* 7, 528-540.

Jiang L., Liu X., Xiong G., Liu H., Chen F., Wang L., ..., Li J. (2013) DWARF 53 acts as a repressor of strigolactone signalling in rice. *Nature* 504, 401-405.

Jiang L., Matthys C., Marquez-Garcia B., De Cuyper C., Smet L., De Keyser A., ..., Goormachtig S. (2016) Strigolactones spatially influence lateral root development through the cytokinin signaling network. *Journal of Experimental Botany* 67, 379-389.

Johnson A.W., Gowada G., Hassanali A., Knox J., Monaco S., Razavi Z. & Rosebery G. (1981) The preparation of synthetic analogues of strigol. *Journal of the Chemical Society. Perkin Transactions 1* 1981, 1734-1743.

Johansson, M. J. O., & Bystrom, A. S. (2002). Dual function of the tRNA(m(5)U(54))methyltransferase in tRNA maturation. *RNA-a Publication of the RNA Society,* 8(3), 324-335.

Ju, D., Xu, H., Wang, X., and Xie, Y. (2007). Ubiquitin-mediated degradation of Rpn4 is controlled by a phosphorylation-dependent ubiquitylation signal. *Biochimica et Biophysica Acta (BBA) - Molecular Cell Research* 1773, 1672-1680.

Kagale, S., & Rozwadowski, K. (2011). EAR motif-mediated transcriptional repression in plants: an underlying mechanism for epigenetic regulation of gene expression. *Epigenetics* 6(2), 141-146.

Kagiyama M., Hirano Y., Mori T., Kim S.-Y., Kyozuka J., Seto Y., Yamaguchi S. & Hakoshima T. (2013) Structures of D14 and D14L in the strigolactone and karrikin signaling pathways. *Genes to Cells* 18, 147-160.

Kameoka H., Dun E.A., Lopez-Obando M., Brewer P.B., de Saint Germain A., Rameau C., Beveridge C.A. & Kyozuka J. (2016) Phloem transport of the receptor DWARF14 protein is required for full function of strigolactones. *Plant Physiology* 172, 1844-1852.

Kapulnik Y., Delaux P.-M., Resnick N., Mayzlish-Gati E., Wininger S., Bhattacharya C., ..., Koltai H. (2011) Strigolactones affect lateral root formation and root-hair elongation in *Arabidopsis*. *Planta* 233, 209-216.

Kapulnik, Y., and Koltai, H. (2014). Strigolactone involvement in root development, response to abiotic stress and interactions with the biotic soil environment. *Plant Physiology* 166, 1–29.

Karampelias M., Neyt P., De Groeve S., Aesaert S., Coussens G., Rolčik J., ..., Van Lijsebettens M. (2016) ROTUNDA3 function in plant development by phosphatase 2A-mediated regulation of auxin transporter recycling. *Proceedings of the National Academy of Sciences USA* 113, 2768-2773.

Kato N., Fujikawa Y., Fuselier T., Adamou-Dodo R., Nishitani A. & Sato M.H. (2010) Luminescence detection of SNARE-SNARE interaction in *Arabidopsis* protoplasts. *Plant Molecular Biology* 72, 433-444.

Keilhauer E.C., Hein M.Y. & Mann M. (2015) Accurate protein complex retrieval by affinity enrichment mass spectrometry (AE-MS) rather than affinity purification mass spectrometry (AP-MS). *Molecular and Cellular Proteomics* 14, 120-135.

Kepinski S. & Leyser O. (2005) The *Arabidopsis* F-box protein TIR1 is an auxin receptor. *Nature* 435, 446-451.

Kerppola T.K. (2008) Bimolecular fluorescence complementation (BiFC) analysis as a probe of protein interactions in living cells. *Annual Review of Biophysics* 37, 465-487.

Kim, D.H., Kang, J.G., Yang, S.S., Chung, K.S., Song, P.S., and Park, C.M. (2002). A phytochrome-associated protein phosphatase 2A modulates light signals in flowering time control in *Arabidopsis*. *Plant Cell* 14, 3043-3056.

Kim S.B., Suzuki H., Sato M. & Tao H. (2011) Superluminescent variants of marine luciferases for bioassays. *Analytical Chemistry* 83, 8732-8740 [Erratum *Analytical Chemistry* 84 4244].

Kim, S. H., Son, G. H., Bhattacharjee, S., Kim, H. J., Nam, J. C., Nguyen, P. D. T., . . . Gassmann, W. (2014). The Arabidopsis immune adaptor SRFR1 interacts with TCP transcription factors that redundantly contribute to effector-triggered immunity. *Plant Journal* 78(6), 978-989.

Kim D.I. & Roux K.J. (2016) Filling the void: proximity-based labeling of proteins in living cells. *Trendsin Cell Biology* 26, 804-817.

Kimura T., Hiraoka K., Kasahara N. & Logg C.R. (2010) Optimization of enzyme-substrate pairing for bioluminescence imaging of gene transfer using *Renilla* and *Gaussia* luciferases. *Journal of Gene Medicine* 12, 528-537.

Kohlen W., Charnikhova T., Liu Q., Bours R., Domagalska M.A., Beguerie S., ..., Ruyter-Spira C. (2011) Strigolactones are transported through the xylem and play a key role in shoot architectural response to phosphate deficiency in nonarbuscular mycorrhizal host Arabidopsis. *Plant Physiology* 155, 974-987.

Koltai H. (2011) Strigolactones are regulators of root development. *New Phytologist* 190, 545-549.

Koltai H. (2014) Implications of non-specific strigolactone signaling in the rhizosphere. *Plant Science* 225, 9-14.

Koltai, H. (2015). Cellular events of strigolactone signalling and their crosstalk with auxin in roots. *Journal of Experimental Botany* 66(16), 4855-4861.

Komander, D. (2009). The emerging complexity of protein ubiquitination. *Biochemical Society Transactions* 37, 937-953.

Konert, G., Trotta, A., Kouvonen, P., Rahikainen, M., Durian, G., Blokhina, O., . . . Kangasjarvi, S. (2015). Protein phosphatase 2A (PP2A) regulatory subunit B 'gamma interacts with cytoplasmic ACONITASE 3 and modulates the abundance of AOX1A and AOX1D in Arabidopsis thaliana. *New Phytologist* 205(3), 1250-1263.

Kraft, E., Stone, S. L., Ma, L., Su, N., Gao, Y., Lau, O. S., . . . Callis, J. (2005). Genome analysis and functional characterization of the E2 and RING-type E3 ligase ubiquitination enzymes of Arabidopsis. *Plant Physiology* 139(4), 1597-1611.

Kubo, H., Peeters, A. J., Aarts, M. G., Pereira, A., & Koornneef, M. (1999). ANTHOCYANINLESS2, a homeobox gene affecting anthocyanin distribution and root development in *Arabidopsis*. *Plant Cell* 11(7), 1217-1226.

Kubo, H., & Hayashi, K. (2011). Characterization of root cells of *anl2* mutant in *Arabidopsis thaliana*. *Plant Science* 180(5), 679-685.

Kudla J. & Bock R. (2016) Lighting the Way to protein-protein interactions: recommendations on best practices for bimolecular fluorescence complementation analyses. *Plant Cell* 28, 1002-1008.

Kulkarni, M.G., Sparg, S.G., Light, M.E., and van Staden, J. (2006). Stimulation of rice (*Oryza sativa* L.) seedling vigour by smoke-water and butenolide. *Journal of Agronomy and Crop Science 192*, 395-398.

Kumar, M., Pandya-Kumar, N., Dam, A., Haor, H., Mayzlish-Gati, E., Belausov, E., . . . Koltai, H. (2015). Arabidopsis response to low-phosphate conditions includes active changes in actin filaments and PIN2 polarization and is dependent on strigolactone signalling. *Journal of Experimental Botany* 66(5), 1499-1510.

Kwak, J.M., Moon, J.H., Murata, Y., Kuchitsu, K., Leonhardt, N., DeLong, A., and Schroeder, J.I. (2002). Disruption of a guard cell-expressed protein phosphatase 2A regulatory subunit, RCN1, confers abscisic acid insensitivity in *Arabidopsis. Plant Cell* 14, 2849-2861.

Kwaaitaal M., Schor M., Hink M.A., Visser A.J.W.G. & de Vries S.C. (2011) Fluorescence correlation spectroscopy and fluorescence recovery after photobleaching to study receptor kinase mobility *in planta*. *Methods in Molecular Biology* 779, 225-242.

Lackner D.H., Carré A., Guzzardo P.M., Banning C., Mangena R., Henley T., ..., Bürckstümmer T. (2015) A generic strategy for CRISPR-Cas9-mediated gene tagging. *Nature Communications* 6, 10237.

Lai, W. S., Carballo, E., Thorn, J. M., Kennington, E. A., & Blackshear, P. J. (2000). Interactions of CCCH zinc finger proteins with mRNA. Binding of tristetraprolin-related zinc finger proteins to Au-rich elements and destabilization of mRNA. *Journal of Biological Chemistry* 275(23), 17827-17837.

Lalonde S., Ehrhardt D.W., Loqué D., Chen J., Rhee S.Y. & Frommer W.B. (2008) Molecular and cellular approaches for the detection of protein–protein interactions: latest techniques and current limitations. *Plant Journal* 53, 610-635.

Langowski J. (2008) Protein–protein interactions determined by fluorescence correlation spectroscopy. *Methods in Cell Biology* 85, 471-484.

Laribee, R. N., Shibata, Y., Mersman, D. P., Collins, S. R., Kemmeren, P., Roguev, A., . . . Strahl, B. D. (2007). CCR4/NOT complex associates with the proteasome and regulates histone methylation. *Proceedings of the National Academy of Sciences of USA* 104(14), 5836-5841.

Larrieu A. & Vernoux T. (2015) Comparison of plant hormone signalling systems. *Essays in Biochemistry* 58, 165-181.

Lau S., Jürgens G. & De Smet I. (2008) The evolving complexity of the auxin pathway. *Plant Cell* 20, 1738-1746.

Lauressergues D., André O., Peng J., Wen J., Chen R., Ratet P., ..., Rochange S.F. (2014) Strigolactones contribute to shoot elongation and to the formation of leaf margin serrations in *Medicago truncatula* R108. *Journal of Experimental Botany* 66, 1237-1244.

Lechat M.-M., Pouvreau J.-B., Péron T., Gauthier M., Montiel G., Véronési C., ..., Delavault P. (2012) *PrCYP707A1* an ABA catabolic gene. is a key component of *Phelipanche ramosa* seed germination in response to the strigolactone analogue GR24. *Journal of Experimental Botany* 63, 5311-5322.

Lee C.-M., Adamchek C., Feke A., Nusinow D.A. & Gendron J.M. (2017) Mapping protein–protein interactions using affinity purification and mass spectrometry. *Methods in Molecular Biology* 1610, 231-249.

Lewandowska D., ten Have S., Hodge K., Tillemans V., Lamond A.I. & Brown J.W.S. (2013) Plant SILAC: stable-isotope labelling with amino acids of *Arabidopsis* seedlings for quantitative proteomics. *PLoS ONE* 8, e72207.

Leyser, O. (2018). Auxin signaling. *Plant Physiology* 176, 465-479.

Li C., Distelfeld A., Comis A. & Dubcovsky J. (2011a) Wheat flowering repressor VRN2 and promoter CO2 compete for interactions with NUCLEAR FACTOR-Y complexes. *Plant Journal* 67, 763-773.

Li, H., Lin, D., Dhonukshe, P., Nagawa, S., Chen, D., Friml, J., . . . Yang, Z. (2011b). Phosphorylation switch modulates the interdigitated pattern of PIN1 localization and cell expansion in Arabidopsis leaf epidermis. *Cell Research* 21(6), 970-978.

Li Y. (2011) The tandem affinity purification technology: an overview. *Biotechnology Letters* 33, 1487-1499.

Li W., Nguyen K.H., Watanabe Y., Yamaguchi S. & Tran L.-S.P. (2016a) *OaMAX2* of *Orobanche aegyptiaca* and *Arabidopsis AtMAX2* share conserved functions in both development and drought responses. *Biochemical and Biophysical Research Communications* 478, 521-526.

Li X., Xing J., Qiu Z., He Q. & Lin J. (2016b) Quantification of membrane protein dynamics and interactions in plant cells by fluorescence correlation spectroscopy. *Molecular Plant* 9, 1229-1239.

Li, W., Nguyen, K. H., Chu, H. D., Ha, C. V., Watanabe, Y., Osakabe, Y., . . . Tran, L. P. (2017a). The karrikin receptor KAI2 promotes drought resistance in *Arabidopsis thaliana*. *PLoS Genetics, 13*(11), e1007076.

Li, W., Lacey, R. F., Ye, Y., Lu, J., Yeh, K. C., Xiao, Y., . . . Zhao, Y. (2017b). Triplin, a small molecule, reveals copper ion transport in ethylene signaling from ATX1 to RAN1. *PLoS Genetic 13*(4), e1006703.

Liang J., Zhao L., Challis R. & Leyser O. (2010) Strigolactone regulation of shoot branching in chrysanthemum (*Dendranthema grandiflorum*). *Journal of Experimental Botany* 61, 3069-3078.

Liang Y., Ward S., Li P., Bennett T. & Leyser O. (2016) SMAX1-LIKE7 signals from the nucleus to regulate shoot development in Arabidopsis via partially EAR motif-independent mechanisms. *Plant Cell* 28, 1581-1601.

Lillo, C., Kataya, A. R., Heidari, B., Creighton, M. T., Nemie-Feyissa, D., Ginbot, Z., & Jonassen, E. M. (2014). Protein phosphatases PP2A, PP4 and PP6: mediators and regulators in development and responses to environmental cues. *Plant Cell Environment* 37(12), 2631-2648.

Lin, H.K., Wang, L., Hu, Y.C., Altuwaijri, S., and Chang, C. (2002). Phosphorylation-dependent ubiquitylation and degradation of androgen receptor by Akt require Mdm2 E3 ligase. *The EMBO Journal* 21, 4037-4048.

Lin H., Wang R., Qian Q., Yan M., Meng X., Fu Z., ..., Wang Y. (2009) DWARF27 an iron-containing protein required for the biosynthesis of strigolactones regulates rice tiller bud outgrowth. *Plant Cell* 21, 1512-1525.

Lin Q., Zhou Z., Luo W., Fang M., Li M. & Li H. (2017) Screening of proximal and interacting proteins in rice protoplasts by proximity-dependent biotinylation. *Frontiers in Plant Science* 8 749.

Ling J.-J., Li J., Zhu D. & Deng X.W. (2017) Noncanonical role of *Arabidopsis* COP1/SPA complex in repressing BIN2-mediated PIF3 phosphorylation and degradation in darkness. *Proceedings of the National Academy of Sciences USA* 114, 3539-3544.

Liu X., Wei W., Zhu W., Su L., Xiong Z., Zhou M., Zheng Y. & Zhou D.-X. (2017) Histone deacetylase AtSRT1 links metabolic flux and stress response in *Arabidopsis*. *Molecular Plant* 10, 1510-1522.

Liu J., He H., Vitali M., Visentin I., Charnikhova T., Haider I., ..., Cardinale F. (2015) Osmotic stress represses strigolactone biosynthesis in *Lotus japonicus* roots: exploring the interaction between strigolactones and ABA under abiotic stress. *Planta* 241, 1435-1451.

Liu Q., Zhang Y., Matusova R., Charnikhova T., Amini M., Jamil M., ..., Bouwmeester H.J. (2014) *Striga hermonthica MAX2* restores branching but not the Very Low Fluence Response in the *Arabidopsis thaliana max2* mutant. *New Phytologist* 202, 531-541.

Long Y., Stahl Y., Weidtkamp-Peters S., Postma M., Zhou W., Goedhart J., ..., Blilou I. (2017) *In vivo* FRET–FLIM reveals cell-type-specific protein interactions in *Arabidopsis* roots. *Nature* 548, 97-102.

Long R.L., Stevens J.C., Griffiths E.M., Adamek M., Gorecki M.J., Powles S.B. & Merritt D.J. (2011) Seeds of Brassicaceae weeds have an inherent or inducible response to the germination stimulant karrikinolide. *Annals of Botany* 108, 933-944.

Lopez-Obando, M., de Villiers, R., Hoffmann, B., Ma, L., de Saint Germain, A., Kossmann, J., . . . Bonhomme, S. (2018). *Physcomitrella patens* MAX2 characterization suggests an ancient role for this F-box protein in photomorphogenesis rather than strigolactone signalling. *New Phytologist*, doi:10.1111/nph.15214

López-Ráez, J. A., Shirasu, K., & Foo, E. (2017). Strigolactones in plant interactions with beneficial and detrimental organisms: The Yin and Yang. *Trends in Plant Science* 22(6), 527-537.

Luke, M. M., Della Seta, F., Di Como, C. J., Sugimoto, H., Kobayashi, R., & Arndt, K. T. (1996). The SAP, a new family of proteins, associate and function positively with the SIT4 phosphatase. *Molecular and Cellular Biology* 16(6), 2744-2755.

Luker K.E., Smith M.C.P., Luker G.D., Gammon S.T., Piwnica-Worms H. & Piwnica-Worms D. (2004) Kinetics of regulated protein–protein interactions revealed with firefly luciferase complementation imaging in cells and living animals. *Proceedings of the National Academy of Sciences USA* 101, 12288-12293.

Lumba S., Toh S., Handfield L.-F., Swan M., Liu R., Youn J.-Y., …, McCourt P. (2014) A mesoscale abscisic acid hormone interactome reveals a dynamic signaling landscape in *Arabidopsis*. *Developmental Cell* 29, 360-372.

Luo, L., Wang, H., Liu, X., Hu, J., Zhu, X., Pan, S., . . . Xu, G. (2018). Strigolactones affect the translocation of nitrogen in rice. *Plant Science 270*, 190-197.

Luo Q., Lian H.-L., He S.-B., Li L., Jia K.-P. & Yang H.-Q. (2014) COP1 and phyB physically interact with PIL1 to regulate its stability and photomorphogenic development in *Arabidopsis*. *Plant Cell* 26, 2441-2456.

Lv, S., Zhang, Y., Li, C., Liu, Z., Yang, N., Pan, L., . . . Wang, G. (2018). Strigolactone-triggered stomatal closure requires hydrogen peroxide synthesis and nitric oxide production in an abscisic acid-independent manner. *New Phytologist 217*(1), 290-304.

Lynch T.J., Erickson B.J., Miller D.R. & Finkelstein R.R. (2017) ABI5-binding proteins (AFPs) alter transcription of ABA-induced genes via a variety of interactions with chromatin modifiers. *Plant Molecular Biology* 93, 403-418.

Mabuchi, A., Soga, K., Wakabayashi, K., & Hoson, T. (2016). Phenotypic screening of Arabidopsis T-DNA insertion lines for cell wall mechanical properties revealed ANTHOCYANINLESS2, a cell wall-related gene. *Journal of Plant Physiology* 191, 29-35.

Macháň R. & Wohland T. (2014) Recent applications of fluorescence correlation spectroscopy in live systems. *FEBS Letters* 588, 3571-3584.

Mahfouz M.M., Kim S., Delauney A.J. & Verma D.P.S. (2006) *Arabidopsis* TARGET OF RAPAMYCIN interacts with RAPTOR which regulates the activity of S6 kinase in response to osmotic stress signals. *Plant Cell* 18, 477-490.

Malamy, J. E., & Benfey, P. N. (1997). Organization and cell differentiation in lateral roots of Arabidopsis thaliana. *Development* 124(1), 33-44.

Maloney V.J., Park J.-Y., Unda F. & Mansfield S.D. (2015) Sucrose phosphate synthase and sucrose phosphate phosphatase interact *in planta* and promote plant growth and biomass accumulation. *Journal of Experimental Botany* 66, 4383-4394.

Mangnus E.M. & Zwanenburg B. (1992) Tentative molecular mechanism for germination stimulation of *Striga* and *Orobanche* seeds by strigol and its synthetic analogues. *Journal of Agricultural and Food Chemistry* 40, 1066-1070.

Marzec M., Gruszka D., Tylec P. & Szarejko I. (2016) Identification and functional analysis of the *HvD14* gene involved in strigolactone signaling in *Hordeum vulgare*. *Physiologia Plantarum* 158, 341-355.

Martell J.D., Deerinck T.J., Sancak Y., Poulos T.L., Mootha V.K., Sosinsky G.E., Ellisman M.H. & Ting A.Y. (2012) Engineered ascorbate peroxidase as a genetically encoded reporter for electron microscopy. *Nature Biotechnology* 30, 1143-1148.

Martínez-Muñoz L., Barroso R., Dyrhaug S.Y., Navarro G., Lucas P., Soriano S.F., ..., Mellado M. (2014) CCR5/CD4/CXCR4 oligomerization prevents HIV-1 $gp120_{IIIB}$ binding to the cell surface. *Proceedings of the National Academy of Sciences USA* 111, E1960-E1969.

Maruta N., Trusov Y. & Botella J.R. (2016) Yeast three-hybrid system for the detection of protein-protein interactions. *Methods in Molecular Biology* 1363, 145-154.

Marzec M., Muszynska A. & Gruszka D. (2013) The role of strigolactones in nutrient-stress responses in plants. *International Journal of Molecular Sciences* 14, 9286-9304.

Mashiguchi, K., Sasaki, E., Shimada, Y., Nagae, M., Ueno, K., Nakano, T., . . . Asami, T. (2009). Feedback-regulation of strigolactone biosynthetic genes and strigolactone-regulated genes in *Arabidopsis*. *Bioscience, Biotechnology, and Biochemistry* 73(11), 2460-2465.

Matthys C., Walton A., Struk S., Stes E., Boyer F.-D., Gevaert K. & Goormachtig S. (2016) The Whats the Wheres and the Hows of strigolactone action in the roots. *Planta* 243, 1327-1337.

Matusova R., Rani K., Verstappen F.W.A., Franssen M.C.R., Beale M.H. & Bouwmeester H.J. (2005) The strigolactone germination stimulants of the plant-parasitic *Striga* and *Orobanche* spp. are derived from the carotenoid pathway. *Plant Physiology* 139, 920-934.

Mayzlish-Gati, E., LekKala, S. P., Resnick, N., Wininger, S., Bhattacharya, C., Lemcoff, J. H., . . . Koltai, H. (2010). Strigolactones are positive regulators of light-harvesting genes in tomato. *Journal of Experimental Botany* 61(11), 3129-3136.

Mcnally, F.J., and Vale, R.D. (1993). Identification of katanin, an atpase that severs and disassembles stable microtubules. *Cell* 75, 419-429.

Meekins, D. A., Guo, H. F., Husodo, S., Paasch, B. C., Bridges, T. M., Santelia, D., . . . Gentry, M. S. (2013). Structure of the Arabidopsis glucan phosphatase LIKE SEX FOUR2 reveals a unique mechanism for starch dephosphorylation. *Plant Cell* 25(6), 2302-2314.

Meier, C., Bouquin, T., Nielsen, M. E., Raventos, D., Mattsson, O., Rocher, A., . . . Mundy, J. (2001). Gibberellin response mutants identified by luciferase imaging. *Plant Journal 25*(5), 509-519.

Mersman, D. P., Du, H. N., Fingerman, I. M., South, P. F., & Briggs, S. D. (2009). Polyubiquitination of the demethylase Jhd2 controls histone methylation and gene expression. *Genes & Development* 23(8), 951-962.

Meyer K. & Selbach M. (2015) Quantitative affinity purification mass spectrometry: a versatile technology to study protein–protein interactions. *Frontiers in Genetics* 6, 237.

Miteva Y.V., Budayeva H.G. & Cristea I.M. (2013) Proteomics-based methods for discovery quantification and validation of protein–protein interactions. *Analytical Chemistry* 85, 749-768.

Möckli N. & Auerbach D. (2004) Quantitative β-galactosidase assay suitable for high-throughput applications in the yeast two-hybrid system. *BioTechniques* 36, 872-876.

Moorhead, G. B., De Wever, V., Templeton, G., & Kerk, D. (2009). Evolution of protein phosphatases in plants and animals. *Biochemical Journal* 417(2), 401-409.

Morell M., Ventura S. & Avilés F.X. (2009) Protein complementation assays: approaches for the in vivo analysis of protein interactions. *FEBS Letters* 583, 1684-1691.

Morffy N., Faure L. & Nelson D.C. (2016) Smoke and hormone mirrors: action and evolution of karrikin and strigolactone signaling. *Trends in Genetics* 32, 176-188.

Morsy M., Gouthu S., Orchard S., Thorneycroft D., Harper J.F., Mittler R. & Cushman J.C. (2008) Charting plant interactomes: possibilities and challenges. *Trends in Plant Science* 13, 183-191.

Mosbech A., Gibbs-Seymour I., Kagias K., Thorslund T., Beli P., Povlsen L., ..., Mailand N. (2012) DVC1 (C1orf124) is a DNA damage–targeting p97 adaptor that promotes ubiquitin-dependent responses to replication blocks. *Nature Structural and Molecular Biology* 19, 1084-1092.

Mravec J., Petrášek J., Li N., Boeren S., Karlova R., Kitakura S., Pařezová M., ..., Friml J. (2011) Cell plate restricted association of DRP1A and PIN proteins is required for cell polarity establishment in *Arabidopsis*. *Current Biology* 21, 1055-1060.

Mukhtar M.S., Carvunis A.-R., Dreze M., Epple P., Steinbrenner J., Moore J., ..., Dangl J.L. (2011) Independently evolved virulence effectors converge onto hubs in a plant immune system network. *Science* 333, 596-601.

Mulder, K. W., Inagaki, A., Cameroni, E., Mousson, F., Winkler, G. S., De Virgilio, C., . . . Timmers, H. T. (2007). Modulation of Ubc4p/Ubc5p-mediated stress responses by the RING-finger-dependent ubiquitin-protein ligase Not4p in *Saccharomyces cerevisiae*. *Genetics* 176(1), 181-192.

Nadakuduti, S. S., Pollard, M., Kosma, D. K., Allen, C., Ohlrogge, J. B., & Barry, C. S. (2012). Pleiotropic Phenotypes of the sticky peel Mutant Provide New Insight into the Role of CUTIN DEFICIENT2 in Epidermal Cell Function in Tomato. *Plant Physiology* 159(3), 945-960.

Nagano, A.J., Fukao, Y., Fujiwara, M., Nishimura, M., and Hara-Nishimura, I. (2008). Antagonistic jacalin-related lectins regulate the size of ER body-type beta-glucosidase complexes in Arabidopsis thaliana. *Plant Cell Physiology* 49, 969-980.

Nagels Durand, A., Moses, T., De Clercq, R., Goossens, A., and Pauwels, L. (2012). A MultiSite Gateway vector set for the functional analysis of genes in the model Saccharomyces cerevisiae. BMC Molecular Biology 13, 30.

Nagels Durand, A., Inigo, S., Ritter, A., Iniesto, E., De Clercq, R., Staes, A., . . . Goossens, A. (2016). The Arabidopsis Iron-Sulfur Protein GRXS17 is a Target of the Ubiquitin E3 Ligases RGLG3 and RGLG4. *Plant and Cell Physiology* 57(9), 1801-1813.

Nakano, T., Murakami, S., Shoji, T., Yoshida, S., Yamada, Y., and Sato, F. (1997). A novel protein with DNA binding activity from tobacco chloroplast nucleoids. *Plant Cell* 9, 1673-1682.

Nakamura H., Xue Y.-L., Miyakawa T., Hou F., Qin H.-M., Fukui K., ..., Asami T. (2013) Molecular mechanism of strigolactone perception by DWARF14. *Nature Communications* 4, 2613.

Nakamura, M. (2015). Microtubule nucleating and severing enzymes for modifying microtubule array organization and cell morphogenesis in response to environmental cues. *New Phytologist* 205(3), 1022-1027.

Navarro G., McCormick P.J., Mallol J., Lluís C., Franco R., Cortés A., ..., Ferré S. (2013) Detection of receptor heteromers involving dopamine receptors by the sequential BRET-FRET technology. *Methods in Molecular Biology* 964, 95-105.

Nelissen H., Eeckhout D., Demuynck K., Persiau G., Walton A., van Bel M., ..., De Jaeger G. (2015) Dynamic changes in ANGUSTIFOLIA3 complex composition reveal a growth regulatory mechanism in the maize leaf. *Plant Cell* 27, 1605-1619.

Nelson D.C., Riseborough J.-A., Flematti G.R., Stevens J., Ghisalberti E.L., Dixon K.W. & Smith S.M. (2009) Karrikins discovered in smoke trigger Arabidopsis seed germination by a mechanism requiring gibberellic acid synthesis and light. *Plant Physiology* 149, 863-873.

Nelson D.C., Flematti G.R., Riseborough J.-A., Ghisalberti E.L., Dixon K.W. & Smith S.M. (2010) Karrikins enhance light responses during germination and seedling development in *Arabidopsis thaliana*. *Proceedings of the National Academy of Sciences of USA* 107, 7095-7100.

Nelson, D.C., Scaffidi, A., Dun, E.A., Waters, M.T., Flematti, G.R., Dixon, K.W., …, Smith, S.M. (2011). F-box protein MAX2 has dual roles in karrikin and strigolactone signaling in *Arabidopsis thaliana*. *Proceedings of the National Academy of Sciences USA* 108, 8897-8902.

Nelson, D.C., Flematti, G.R., Ghisalberti, E.L., Dixon, K.W., and Smith, S.M. (2012). Regulation of Seed Germination and Seedling Growth by Chemical Signals from Burning Vegetation. *Annual Review in Plant Biology* 63, 107–130.

Nesvizhskii A.I. (2012) Computational and informatics strategies for identification of specific protein interaction partners in affinity purification mass spectrometry experiments. *Proteomics* 12, 1639-1655.

Nooren I.M.A. & Thornton J.M. (2003) Diversity of protein–protein interactions. *EMBO Journal* 22, 3486-3492.

Ollendorff, V., and Donoghue, D.J. (1997). The Serine/Threonine Phosphatase PP5 Interacts with CDC16 and CDC27, Two Tetratricopeptide Repeat-containing Subunits of the Anaphase-promoting Complex. *Journal of Biological Chemistry* 272, 32011-32018.

Ohta M., Matsui K., Hiratsu K., Shinshi H. & Ohme-Takagi M. (2001) Repression domains of class II ERF transcriptional repressors share an essential motif for active repression. *Plant Cell* 13, 1959-1968.

Pagliuca F.W., Collins M.O., Lichawska A., Zegerman P., Choudhary J.S. & Pines J. (2011) Quantitative proteomics reveals the basis for the biochemical specificity of the cell-cycle machinery. *Molecular Cell* 43, 406-417.

Panasenko, O., Landrieux, E., Feuermann, M., Finka, A., Paquet, N., & Collart, M. A. (2006). The yeast Ccr4-not complex controls ubiquitination of the nascent-associated polypeptide (NAC-EGD) complex. *Journal of Biological Chemistry* 281(42), 31389-31398.

Panasenko, O. O., David, F. P. A., & Collart, M. A. (2009). Ribosome Association and Stability of the Nascent Polypeptide-Associated Complex Is Dependent Upon Its Own Ubiquitination. *Genetics* 181(2), 447-460.

Panasenko, O. O., & Collart, M. A. (2011). Not4 E3 Ligase Contributes to Proteasome Assembly and Functional Integrity in Part through Ecm29. *Molecular and Cellular Biology*, 31(8), 1610-1623.

Pardo M. & Choudhary F.S. (2012) Assignment of protein interactions from affinity purification/mass spectrometry data. *Journal of Proteome Research* 11, 1462-1474.

Park, J.H., Lee, S.Y., Kim, W.Y., Jung, Y.J., Chae, H.B., Jung, H.S., Kang, C.H., Shin, M.R., Kim, S.Y., Su'udi, M., et al. (2011). Heat-induced chaperone activity of serine/threonine protein phosphatase 5 enhances thermotolerance in *Arabidopsis thaliana. New Phytologist* 191, 692-705.

Parker C.E., Mocanu V., Mocanu M., Dicheva N. & Warren M.R. (2010) Mass spectrometry for post-translational modifications. In *Neuroproteomics* (ed. O. Alzate) pp. 93-113. CRC Press/Taylor & Francis Boca Raton.

Pauwels, L., Morreel, K., De Witte, E., Lammertyn, F., Van Montagu, M., Boerjan, W., . . . Goossens, A. (2008). Mapping methyl jasmonate-mediated transcriptional reprogramming of metabolism and cell cycle progression in cultured Arabidopsis cells. *Proceedings of the National Academy of Sciences USA* 105(4), 1380-1385.

Pauwels L., Fernández Barbero G., Geerinck J., Tilleman S., Grunewald W., Cuéllar Pérez A., ..., Goossens A. (2010) NINJA connects the co-repressor TOPLESS to jasmonate signalling. *Nature* 464, 788-791.

Pauwels L., Ritter A., Goossens J., Nagels Durand A., Liu H., Gu Y., ..., Goossens A. (2015) The RING E3 ligase KEEP ON GOING modulates JASMONATE ZIM-DOMAIN12 stability. *Plant Physiology* 169, 1405-1417.

Peer W.A. (2013) From perception to attenuation: auxin signalling and responses. *Current Opinion in Plant Biology* 16, 561-568.

Pelletier J.N., Campbell-Valois F.-X. & Michnick S.W. (1998) Oligomerization domain-directed reassembly of active dihydrofolate reductase from rationally designed fragments. *Proceedings of the National Academy of Sciences USA* 95, 12141-12146.

Pesch M., Schultheiß I., Klopffleisch K., Uhrig J.F., Koegl M., Clemen C.S., ..., Hülskamp M. (2015) TRANSPARENT TESTA GLABRA1 and GLABRA1 compete for binding to GLABRA3 in Arabidopsis. *Plant Physiology* 168, 584-597.

Pérez Cuéllar, A., Pauwels, L., De Clercq, R., and Goossens, A. (2013). Yeast two-hybrid analysis of jasmonate signaling proteins. *Methods in Molecular Biol*ogy 1011, 173-185.

Perrella, G., Carr, C., Asensi-Fabado, M.A., Donald, N.A., Páldi, K., Hannah, M.A. & Amtmann, A. (2016). The Histone Deacetylase Complex 1 Protein of Arabidopsis Has the Capacity to Interact with Multiple Proteins Including Histone 3-Binding Proteins and Histone 1 Variants. *Plant Physiology* 171, 62–70.

Pfalz, J., Liere, K., Kandlbinder, A., Dietz, K. J., & Oelmuller, R. (2006). PTAC2,-6, and-12 are components of the transcriptionally active plastid chromosome that are required for plastid gene expression. *Plant Cell* 18(1), 176-197.

Pfleger K.D.G. & Eidne K.A. (2006) Illuminating insights into protein-protein interactions using bioluminescence resonance energy transfer (BRET) *Nature Methods* 3, 165-174.

Phee, B. K., Kim, J. I., Shin, D. H., Yoo, J., Park, K. J., Han, Y. J., . . . Hahn, T. R. (2008). A novel protein phosphatase indirectly regulates phytochrome-interacting factor 3 via phytochrome. *Biochemical Journal* 415(2), 247-255.

Piston D.W. & Kremers G.-J. (2007) Fluorescent protein FRET: the good the bad and the ugly. *Trends in Biochemical Sciences* 32, 407-414.

Prusinkiewicz, P., Crawford, S., Smith, R. S., Ljung, K., Bennett, T., Ongaro, V., & Leyser, O. (2009). Control of bud activation by an auxin transport switch. *Proceedings of the National Academy of Sciences USA 106*(41), 17431-17436.

Puig, O., Caspary, F., Rigaut, G., Rutz, B., Bouveret, E., Bragado-Nilsson, E., Wilm, M., and Séraphin, B. (2001). The Tandem Affinity Purification (TAP) Method: A General Procedure of Protein Complex Purification. *Methods* 24, 218-229.

Qu M., An B., Shen S., Zhang M., Shen X., Duan X., Balthasar J.P. & Qu J. (2017) Qualitative and quantitative characterization of protein biotherapeutics with liquid chromatography mass spectrometry. *Mass Spectrometry Reviews* 36, 734-754.

Rajjou, L., Belghazi, M., Huguet, R., Robin, C., Moreau, A., Job, C., and Job, D. (2006). Proteomic investigation of the effect of salicylic acid on *Arabidopsis* seed germination and establishment of early defense mechanisms. *Plant Physiology* 141, 910–923.

Ramírez-Sánchez O., Pérez-Rodríguez P., Delaye L. & Tiessen A. (2016) Plant proteins are smaller because they are encoded by fewer exons than animal proteins. *Genomics Proteomics Bioinformatics* 14, 357-370.

Ramisetty S.R. & Washburn M.P. (2011) Unraveling the dynamics of protein interactions with quantitative mass spectrometry. *Critical Review in Biochemistry and Molecular Biology* 46, 216-228.

Rasmussen A., Mason M.G., De Cuyper C., Brewer P.B., Herold S., Agusti J., ..., Beveridge C.A. (2012) Strigolactones suppress adventitious rooting in Arabidopsis and pea. *Plant Physiology* 158, 1976-1987.

Reddy, A. S., Day, I. S., Gohring, J., & Barta, A. (2012). Localization and dynamics of nuclear speckles in plants. *Plant Physiology* 158(1), 67-77.

Reumann, S., Babujee, L., Ma, C., Wienkoop, S., Siemsen, T., Antonicelli, G. E., . . . Jahn, O. (2007). Proteome analysis of Arabidopsis leaf peroxisomes reveals novel targeting peptides, metabolic pathways, and defense mechanisms. *Plant Cell* 19(10), 3170-3193.

Reumann, S., Ma, C., Lemke, S., & Babujee, L. (2004). AraPerox. A database of putative Arabidopsis proteins from plant peroxisomes. *Plant Physiology* 136(1), 2587-2608.

Rhee H.-W., Zou P., Udeshi N.D., Martell J.D., Mootha V.K., Carr S.A. & Ting A.Y. (2013) Proteomic mapping of mitochondria in living cells via spatially restricted enzymatic tagging. *Science* 339, 1328-1331.

Rodrigo-Peiris, T., Xu, X. M., Zhao, Q., Wang, H. J., & Meier, I. (2011). RanGAP is required for post-meiotic mitosis in female gametophyte development in *Arabidopsis thaliana*. *Journal of Experimental Botany* 62(8), 2705-2714.

Rohila, J. S., Chen, M., Cerny, R., & Fromm, M. E. (2004). Improved tandem affinity purification tag and methods for isolation of protein heterocomplexes from plants. *Plant Journal* 38(1), 172-181.

Rohila J.S., Chen M., Chen S., Chen J., Cerny R., Dardick C., (2006) Protein-protein interactions of tandem affinity purification-tagged protein kinases in rice. *Plant Journal* 46, 1-13.

Roux K.J., Kim D.I., Raida M. & Burke B. (2012) A promiscuous biotin ligase fusion protein identifies proximal and interacting proteins in mammalian cells. *Journal of Cell Biology* 196, 801-810.

Rozen, S., Füzesi-Levi, Maria G., Ben-Nissan, G., Mizrachi, L., Gabashvili, A., Levin, Y., Ben-Dor, S., Eisenstein, M., and Sharon, M. (2015). CSNAP Is a Stoichiometric Subunit of the COP9 Signalosome. *Cell Reports* 13, 585-598.

Russell, L.C., Whitt, S.R., Chen, M.-S., and Chinkers, M. (1999). Identification of Conserved Residues Required for the Binding of a Tetratricopeptide Repeat Domain to Heat Shock Protein 90. *Journal of Biological Chemistry* 274, 20060-20063.

Russinova E., Borst J.-W., Kwaaitaal M., Caño-Delgado A., Yin Y., Chory J. & de Vries S.C. (2004) Heterodimerization and endocytosis of Arabidopsis brassinosteroid receptors BRI1 and AtSERK3 (BAK1). *Plant Cell* 16, 3216-3229.

Ruyter-Spira C., Kohlen W., Charnikhova T., van Zeijl A., van Bezouwen L., de Ruijter N., ..., Bouwmeester H. (2011) Physiological effects of the synthetic strigolactone analog GR24 on root system architecture in Arabidopsis: another belowground role for strigolactones? *Plant Physiology* 155, 721-734.

Ryu, J.S., Kim, J.-I., Kunkel, T., Kim, B.C., Cho, D.S., Hong, S.H., …, Alonso, J.M. (2005). Phytochrome-Specific Type 5 Phosphatase Controls Light Signal Flux by Enhancing Phytochrome Stability and Affinity for a Signal Transducer. *Cell* 120, 395-406.

Salas-Muñoz, S., Rodríguez-Hernández, A.A., Ortega-Amaro, M.A., Salazar-Badillo, F.B. & Jiménez-Bremont, J.F. (2016). Arabidopsis AtDjA3 Null Mutant Shows Increased Sensitivity to Abscisic Acid, Salt, and Osmotic Stress in Germination and Post-germination Stages. *Frontiers in Plant Science* 7, 1–11.

Samodelov S.L., Beyer H.M., Guo X., Augustin M., Jia K.-P., Baz L., ..., Zurbriggen M.D. (2016) StrigoQuant: a genetically encoded biosensor for quantifying strigolactone activity and specificity. *Science Advances* 2, e1601266.

Sang D., Chen D., Liu G., Liang Y., Huang L., Meng X., ..., Wang Y. (2014) Strigolactones regulate rice tiller angle by attenuating shoot gravitropism through inhibiting auxin biosynthesis. *Proceedings of the National Academy of Sciences of the United States of America* 111, 11199-11204.

Santner, A., Calderon-Villalobos, L.I., and Estelle, M. (2009). Plant hormones are versatile chemical regulators of plant growth. *Nature Chemical Biology* 5, 301-307.

Satpathy S., Wagner S.A., Beli P., Gupta R., Kristiansen T.A., Malinova D., ..., Choudhary C. (2015) Systems-wide analysis of BCR signalosomes and downstream phosphorylation and ubiquitylation. *Molecular Systems Biology* 11, 810.

Sauer, M., Balla, J., Luschnig, C., Wisniewska, J., Reinohl, V., Friml, J., & Benkova, E. (2006). Canalization of auxin flow by Aux/IAA-ARF-dependent feedback regulation of PIN polarity. *Genes & Development* 20(20), 2902-2911.

Scaffidi, A., Waters, M.T., Bond, S.C., Dixon, K.W., Smith, S.M., Ghisalberti, E.L. & Flematti, G.R. (2012) Exploring the molecular mechanism of karrikins and strigolactones. *Bioorganic & Medicinal Chemistry Letters* 22, 3743-3746.

Scaffidi A., Waters M.T., Ghisalberti E.L., Dixon K.W., Flematti G.R. & Smith S.M. (2013) Carlactone-independent seedling morphogenesis in Arabidopsis. *Plant Journal* 76, 1-9.

Scaffidi A., Waters M.T., Sun Y.K., Skelton B.W., Dixon K.W., Ghisalberti E.L., Flematti G.R. & Smith S.M. (2014) Strigolactone hormones and their stereoisomers signal through two related receptor proteins to induce different physiological responses in Arabidopsis. *Plant Physiology* 165, 1221 1232.

Scharf, K.D., Siddique, M., and Vierling, E. (2001). The expanding family of Arabidopsis thaliana small heat stress proteins and a new family of proteins containing alpha-crystallin domains. *Cell Stress Chaperones* 6, 225-237.

Schoonheim P.J., Veiga H., da Costa Pereira D., Friso G., van Wijk K.J. & de Boer A.H. (2007) A comprehensive analysis of the 14-3-3 interactome in barley leaves using a complementary proteomics and two-hybrid approach. *Plant Physiology* 143, 670-683.

Schwille P., Meyer-Almes F.-J. & Rigler R. (1997) Dual-color fluorescence cross-correlation spectroscopy for multicomponent diffusional analysis in solution. *Biophysical Journal* 72, 1878-1886.

Scott J.D. & Pawson T. (2009) Cell signaling in space and time: where proteins come together and when they're apart. *Science* 326, 1220-1224.

Seale, M., Bennett, T., & Leyser, O. (2017). BRC1 expression regulates bud activation potential but is not necessary or sufficient for bud growth inhibition in Arabidopsis. *Development* 144(9), 1661-1673.

Sedbrook, J. C., & Kaloriti, D. (2008). Microtubules, MAPs and plant directional cell expansion. *Trends in Plant Science 13*(6), 303-310.

Seto Y., Sado A., Asami K., Hanada A., Umehara M., Akiyama K. & Yamaguchi S. (2014) Carlactone is an endogenous biosynthetic precursor for strigolactones *Proceedings of the National Academy of Sciences of USA* 111, 1640-1645.

Sheard L.B., Tan X., Mao H., Withers J., Ben-Nissan G., Hinds T.R., ..., Zheng N. (2010) Jasmonate perception by inositol-phosphate-potentiated COI1—JAZ co-receptor. *Nature* 468, 400-405.

Shen H., Luong P. & Huq E. (2007) The F-Box protein MAX2 functions as a positive regulator of photomorphogenesis in Arabidopsis. *Plant Physiology* 145, 1471-1483.

Shen, L., Kang, Y.G.G., Liu, L., and Yu, H. (2011). The J-Domain Protein J3 Mediates the Integration of Flowering Signals in Arabidopsis. *Plant Cell* 23, 499–514.

Shen H., Zhu L., Bu Q.-Y. & Huq E. (2012) MAX2 affects multiple hormones to promote photomorphogenesis. *Molecular Plant* 5, 750-762.

Shi, Y. (2009). Serine/Threonine Phosphatases: Mechanism through Structure. *Cell* 139, 468-484.

Shinohara N., Taylor C. & Leyser O. (2013) Strigolactone can promote or inhibit shoot branching by triggering rapid depletion of the auxin efflux protein PIN1 from the plasma membrane. *PLoS Biology* 11, e1001474.

Simons, J.L., Napoli, C.A., Janssen, B.J., Plummer, K.M. & Snowden, K.C. (2007) Analysis of the *DECREASED APICAL DOMINANCE* genes of petunia in the control of axillary branching. *Plant Physiology* 143, 697-706.

Smaczniak C., Immink R.G.H., Muiño J.M., Blanvillain R., Busscher M., Busscher-Lange J., ..., Kaufmann K. (2012a) Characterization of MADS-domain transcription factor complexes in *Arabidopsis* flower development. *Proceedings of the National Academy of Sciences USA* 109, 1560-1565.

Smaczniak C., Li N., Boeren S., America T., van Dongen W., Goerdayal S.S., de Vries S., Angenent G.C. & Kaufmann K. (2012) Proteomics-based identification of low-abundance signaling and regulatory protein complexes in native plant tissues. *Nature Protocols* 7, 2144-2158.

Smith S.M. & Waters M.T. (2012) Strigolactones: destruction-dependent perception? *Current Biology* 22, R924-R927.

Smith, S.M., and Li, J.Y. (2014). Signalling and responses to strigolactones and karrikins. *Current Opinion in Plant Biology* 21, 23-29.

Snowden K.C., Simkin A.J., Janssen B.J., Templeton K.R., Loucas H.M., Simons J.L., ..., Klee H.J. (2005) The *Decreased apical dominance1/Petunia hybrida CAROTENOID CLEAVAGE DIOXYGENASE8* gene affects branch production and plays a role in leaf senescence root growth and flower development. *Plant Cell* 17, 746-759.

Somssich M., Ma Q., Weidtkamp-Peters S., Stahl Y., Felekyan S., Bleckmann A., Seidel C.A.M. & Simon R. (2015) Real-time dynamics of peptide ligand-dependent receptor complex formation in planta. *Science Signaling* 8, ra76.

Song, X. G., Lu, Z. F., Yu, H., Shao, G. N., Xiong, J. S., Meng, X. B., . . . Li, J. Y. (2017). IPA1 functions as a downstream transcription factor repressed by D53 in strigolactone signaling in rice. *Cell Research 27*(9), 1128-1141.

Soós V., Sebestyén E., Juhász A., Pintér J., Light M.E., Van Staden J. & Balázs E. (2009). Stress-related genes define essential steps in the response of maize seedlings to smoke-water. *Functional and Integrative Genomics* 9, 231-242.

Sorefan K., Booker J., Haurogné K., Goussot M., Bainbridge K., Foo E., ..., Leyser O. (2003) *MAX4* and *RMS1* are orthologous dioxygenase-like genes that regulate shoot branching in *Arabidopsis* and pea. *Genes & Development* 17, 1469-1474.

Soundappan I., Bennett T., Morffy N., Liang Y., Stanga J.P., Abbas A., Leyser O. & Nelson D.C. (2015) SMAX1-LIKE/D53 family members enable distinct MAX2-dependent responses to strigolactones and karrikins in Arabidopsis. *Plant Cell* 27, 3143-3159.

Spallek T., Mutuku M. & Shirasu K. (2013) The genus *Striga*: a witch profile. *Molecular Plant Pathology* 14, 861-869.

Stagljar I., Korostensky C., Johnsson N. & te Heesen S. (1998) A genetic system based on split-ubiquitin for the analysis of interactions between membrane proteins *in vivo*. *Proceedings of the National Academy of Sciences USA* 95, 5187-5192.

Stahl Y., Grabowski S., Bleckmann A., Kühnemuth R., Weidtkamp-Peters S., Pinto K.G., ..., Simon R. (2013) Moderation of *Arabidopsis* root stemness by CLAVATA1 and ARABIDOPSIS CRINKLY4 receptor kinase complexes. *Current Biology* 23, 362-371.

Stanga J.P., Smith S.M., Briggs W.R. & Nelson D.C. (2013) *SUPPRESSOR OF MORE AXILLARY GROWTH2 1* controls seed germination and seedling development in Arabidopsis. *Plant Physiology* 163, 318-330.

Stanga J.P., Morffy N. & Nelson D.C. (2016) Functional redundancy in the control of seedling growth by the karrikin signaling pathway. *Planta* 243, 1397-1406.

Stefanowicz, K., Lannoo, N., and Van Damme, E.J.M. (2015). Plant F-box Proteins – Judges between Life and Death. *Critical Reviews in Plant Sciences* 34, 523-552.

Stefansson, B., & Brautigan, D. L. (2006). Protein phosphatase 6 subunit with conserved Sit4-associated protein domain targets IkappaBepsilon. *Journal of Biological Chemistry 281*(32), 22624-22634.

Stevens J.C., Merritt D.J., Flematti G.R., Ghisalberti E.L. & Dixon K.W. (2007) Seed germination of agricultural weeds is promoted by the butenolide 3-methyl-2*H*-furo[2.3-*c*]pyran-2-one under laboratory and field conditions. *Plant and Soil* 298, 113-124.

Stirnberg P., Furner I.J. & Leyser H.M.O. (2007) MAX2 participates in an SCF complex which acts locally at the node to suppress shoot branching. *Plant Journal* 50, 80-94.

Stirnberg P., van de Sande K. & Leyser H.M.O. (2002) *MAX1* and *MAX2* control shoot lateral branching in *Arabidopsis*. *Development* 129, 1131-1141.

Stoppin-Mellet, V., Gaillard, J., Timmers, T., Neumann, E., Conway, J., & Vantard, M. (2007). Arabidopsis katanin binds microtubules using a multimeric microtubule-binding domain. *Plant Physiology and Biochemistry 45*(12), 867-877.

Stryer L. (1978) Fluorescence energy-transfer as a spectroscopic ruler. *Annual Review of Biochemistry* 47, 819-846.

Subramanian C., Woo J., Cai X., Xu X., Servick S., Johnson C.H., Nebenführ A. & von Arnim A.G. (2006) A suite of tools and application notes for *in vivo* protein interaction assays using bioluminescence resonance energy transfer (BRET) *Plant Journal* 48, 138-152.

Sun K., Chen Y., Wagerle T., Linnstaedt D., Currie M., Chmura P., Song Y. & Xu M. (2008) Synthesis of butenolides as seed germination stimulants. *Tetrahedron Letters* 49, 2922-2925.

Sun X.-D. & Ni M. (2011) HYPOSENSITIVE TO LIGHT an alpha/beta fold protein. acts downstream of ELONGATED HYPOCOTYL 5 to regulate seedling de-etiolation. *Molecular Plant* 4, 116-126.

Sun Y., Rombola C., Jyothikumar V. & Periasamy A. (2013) Förster resonance energy transfer microscopy and spectroscopy for localizing protein–protein interactions in living cells. *Cytometry* 83A, 780-793.

Syafrizayanti Betzen C., Hoheisel J.D. & Kastelic D. (2014) Methods for analyzing and quantifying protein–protein interaction. *Expert Review in Proteomics* 11, 107-120.

Szemenyei H., Hannon M. & Long J.A. (2008) TOPLESS mediates auxin-dependent transcriptional repression during *Arabidopsis* embryogenesis. *Science* 319, 1384-1386.

Tamura K., Fukao Y., Iwamoto M., Haraguchi T. & Hara-Nishimura I. (2010) Identification and characterization of nuclear pore complex components in *Arabidopsis thaliana*. *Plant Cell* 22, 4084-4097.

Tang, Y. C., Akbulut, H., Maynard, J., Li, P. C., & Deisseroth, A. B. (2008). Vector Prime-Protein Boost Vaccine induces 20 Fold Decrease in the Levels of CD44(+)CD24(-/Low) Cancer Stem Cells in Epithelial Neoplasms. *Blood* 112(11), 1000-1000.

Tang W., Yuan M., Wang R., Yang Y., Wang C., Oses-Prieto J.A., ..., Wang Z.-Y. (2011) PP2A activates brassinosteroid-responsive gene expression and plant growth by dephosphorylating BZR1. *Nature Cell Biology* 13, 124-131.

Tang Y., Liu X., Liu X., Li Y., Wu K. & Hou X. (2017) *Arabidopsis* NF-YCs mediate the light-controlled hypocotyl elongation via modulating histone acetylation. *Molecular Plant* 10, 260-273.

Tardif G., Kane N.A., Adam H., Labrie L., Major G., Gulick P., Sarhan F. & Laliberté J.-F. (2007) Interaction network of proteins associated with abiotic stress response and development in wheat. *Plant Molecular Biology* 63, 703-718.

Tchekanda E., Sivanesan D. & Michnick S.W. (2014) An infrared reporter to detect spatiotemporal dynamics of protein-protein interactions. *Nature Methods* 11, 641-644.

Terol, J., Bargues, M., Carrasco, P., Perez-Alonso, M., & Paricio, N. (2002). Molecular characterization and evolution of the protein phosphatase 2A B' regulatory subunit family in plants. *Plant Physiology 129*(2), 808-822.

Thuring J.W.J.F., Nefkens G.H.L. & Zwanenburg B. (1997) Asymmetric synthesis of all stereoisomers of the strigol analogue GR24. Dependence of absolute configuration on stimulatory activity of *Striga hermonthica* and *Orobanche crenata* seed germination. *Journal of Agricultural and Food Chemistry* 45, 2278-2283.

Ticconi, C. A., Lucero, R. D., Sakhonwasee, S., Adamson, A. W., Creff, A., Nussaume, L., . . . Abel, S. (2009). ER-resident proteins PDR2 and LPR1 mediate the developmental response of root meristems to phosphate availability. *Proceedings of the National Academy of Sciences USA,* 106(33), 14174-14179.

Titeca K., Van Quickelberghe E., Samyn N., De Sutter D., Verhee A., Gevaert K., Tavernier J. & Eyckerman S. (2017) Analyzing trapped protein complexes by Virotrap and SFINX. *Nature Protocols* 12, 881-898.

Toh, S., Imamura, A., Watanabe, A., Nakabayashi, K., Okamoto, M., Jikumaru, Y., . . . Kawakami, N. (2008). High temperature-induced abscisic acid biosynthesis and its role in the inhibition of gibberellin action in Arabidopsis seeds. *Plant Physiology, 146*(3), 1368-1385.

Toh S., Kamiya Y., Kawakami N., Nambara E., McCourt P. & Tsuchiya Y. (2012) Thermoinhibition uncovers a role for strigolactones in Arabidopsis seed germination. *Plant and Cell Physiology* 53, 107-117.

Toh S., McCourt P. & Tsuchiya Y. (2012) *HY5* is involved in strigolactone-dependent seed germination in Arabidopsis. *Plant Signaling and Behavior* 7, 556-558.

Toh S., Holbrook-Smith D., Stokes M.E., Tsuchiya Y. & McCourt P. (2014) Detection of parasitic plant suicide germination compounds using a high-throughput *Arabidopsis* HTL/KAI2 strigolactone perception system. *Chemistry and Biology* 21, 988-998.

Toh S., Holbrook-Smith D., Stogios P.J., Onopriyenko O., Lumba S., Tsuchiya Y., Savchenko A. & McCourt P. (2015) Structure-function analysis identifies highly sensitive strigolactone receptors in *Striga*. *Science* 350, 203-207.

Tokunaga T., Hayashi H. & Akiyama K. (2015) Medicaol a strigolactone identified as a putative didehydro-orobanchol isomer from *Medicago truncatula*. *Phytochemistry* 111, 91-97.

Trigg S.A., Garza R.M., MacWilliams A., Nery J.R., Bartlett A., Castanon R., ..., Ecker J.R. (2017) CrY2H-seq: a massively multiplexed assay for deep-coverage interactome mapping. *Nature Methods* 14, 819-825.

Trotta, A., Wrzaczek, M., Scharte, J., Tikkanen, M., Konert, G., Rahikainen, M., . . . Kangasjarvi, S. (2011a). Regulatory subunit B'gamma of protein phosphatase 2A prevents unnecessary defense reactions under low light in Arabidopsis. *Plant Physiology* 156(3), 1464-1480.

Trotta, A., Konert, G., Rahikainen, M., Aro, E. M., & Kangasjarvi, S. (2011b). Knock-down of protein phosphatase 2A subunit B'gamma promotes phosphorylation of CALRETICULIN 1 in Arabidopsis thaliana. *Plant Signal Behaviour* 6(11), 1665-1668.

Tsuchiya Y., Vidaurre D., Toh S., Hanada A., Nambara E., Kamiya Y., Yamaguchi S. & McCourt P. (2010) A small-molecule screen identifies new functions for the plant hormone strigolactone. *Nature Chemical Biology* 6, 741-749.

Tsuchiya Y., Yoshimura M., Sato Y., Kuwata K., Toh S., Holbrook-Smith D., ..., Hagihara S. (2015) Probing strigolactone receptors in *Striga hermonthica* with fluorescence. *Science* 349, 864-868.

Tsuji H., Nakamura H., Taoka K.-i. & Shimamoto K. (2013) Functional diversification of FD transcription factors in rice components of florigen activation complexes. *Plant and Cell Physiology* 54, 385-397.

Tsuzuki S., Handa Y., Takeda N. & Kawaguchi M. (2016) Strigolactone-induced putative secreted protein 1 is required for the establishment of symbiosis by the arbuscular mycorrhizal fungus *Rhizophagus irregularis*. *Molecular Plant-Microbe Interactions* 29, 277-286.

Ueda H. & Kusaba M. (2015) Strigolactone regulates leaf senescence in concert with ethylene in Arabidopsis. *Plant Physiology* 169, 138-147.

Ueguchi-Tanaka M., Ashikari M., Nakajima M., Itoh H., Katoh E., Kobayashi M., ..., Matsuoka M. (2005) *GIBBERELLIN INSENSITIVE DWARF1* encodes a soluble receptor for gibberellin. *Nature* 437, 693-698.

Uhrig J.F. (2006) Protein interaction networks in plants. *Planta* 224, 771-781.

Uhrig, R. G., Labandera, A. M., & Moorhead, G. B. (2013). Arabidopsis PPP family of serine/threonine protein phosphatases: many targets but few engines. *Trends in Plant Science* 18(9), 505-513.

Ukleja, M., Valpuesta, J. M., Dziembowski, A., & Cuellar, J. (2016). Beyond the known functions of the CCR4-NOT complex in gene expression regulatory mechanisms: New structural insights to unravel CCR4-NOT mRNA processing machinery. *Bioessays* 38(10), 1048-1058.

Umehara M., Hanada A., Yoshida S., Akiyama K., Arite T., Takeda-Kamiya N., ..., Yamaguchi S. (2008) Inhibition of shoot branching by new terpenoid plant hormones. *Nature* 455, 195-200.

Umehara M., Cao M., Akiyama K., Akatsu T., Seto Y., Hanada A., ..., Yamaguchi S. (2015) Structural requirements of strigolactones for shoot branching inhibition in rice and Arabidopsis. *Plant and Cell Physiology* 56, 1059-1072.

Vanden Bossche, R., Demedts, B., Vanderhaeghen, R., & Goossens, A. (2013). Transient expression assays in tobacco protoplasts. *Methods in Molecular Biology 1011*, 227-239.

Van Leene J., Witters E., Inzé D. & De Jaeger G. (2008) Boosting tandem affinity purification of plant protein complexes. *Trends in Plant Science* 13 517-520.

Van Leene J., Stals H., Eeckhout D., Persiau G., Van De Slijke E., Van Isterdael G., ..., De Jaeger G. (2007) A tandem affinity purification-based technology platform to study the cell cycle interactome in *Arabidopsis thaliana*. *Molecular and Cellular Proteomics* 6, 1226-1238.

Van Leene, J., Hollunder, J., Eeckhout, D., Persiau, G., Van De Slijke, E., Stals, H., Van Isterdael, G., Verkest, A., Neirynck, S., Buffel, Y., et al. (2010). Targeted interactomics reveals a complex core cell cycle machinery in Arabidopsis thaliana. *Molecular Systems Biology* 6.

Van Leene J., Boruc J., De Jaeger G., Russinova E. & De Veylder L. (2011) A kaleidoscopic view of the *Arabidopsis* core cell cycle interactome. *Trends in Plant Science* 16, 141-150.

Van Leene J., Eeckhout D., Persiau G., Van De Slijke E., Geerinck J., Van Isterdael G., Witters E. & De Jaeger G. (2011) Isolation of transcription factor complexes form Arabidopsis cell suspension cultures by tandem affinity purification. *Methods in Molecular Biology* 754, 195-218.

Van Leene J., Eeckhout D., Cannoot B., De Winne N., Persiau G., Van De Slijke E., ..., De Jaeger G. (2015) An improved toolbox to unravel the plant cellular machinery by tandem affinity purification of *Arabidopsis* protein complexes. *Nature Protocols* 10, 169-187.

van Staden J., Jäger A.K., Light M.E. & Burger B.V. (2004) Isolation of the major germination cue from plant-derived smoke. *South African Journal of Botany* 70, 654-659.

Vanstraelen M. & Benková E. (2012) Hormonal interactions in the regulation of plant development. *Annual Review of Cell and Developmental Biology* 28, 463-487.

Varedi, K. S., Ventura, A. C., Merajver, S. D., & Lin, X. N. (2010). Multisite phosphorylation provides an effective and flexible mechanism for switch-like protein degradation. *Plos One 5*(12), e14029.

Vegh, A., Incze, N., Fabian, A., Huo, H., Bradford, K. J., Balazs, E., & Soos, V. (2017). Comprehensive Analysis of DWARF14-LIKE2 (DLK2) Reveals Its Functional Divergence from Strigolactone-Related Paralogs. *Frontiers in Plant Science* 8, 1641.

Vercruyssen, L., Verkest, A., Gonzalez, N., Heyndrickx, K. S., Eeckhout, D., Han, S. K., . . . Inze, D. (2014). ANGUSTIFOLIA3 Binds to SWI/SNF Chromatin Remodeling Complexes to Regulate Transcription during Arabidopsis Leaf Development. *Plant Cell 26*(1), 210-229.

Vernoux T., Brunoud G., Farcot E., Morin V., Van den Daele H., Legrand J., ..., Traas J. (2011) The auxin signalling network translates dynamic input into robust patterning at the shoot apex. *Molecular Systems Biology* 7, 508.

Verslues, P. E., Guo, Y., Dong, C. H., Ma, W., & Zhu, J. K. (2006). Mutation of SAD2, an importin beta-domain protein in Arabidopsis, alters abscisic acid sensitivity. *Plant Journal* 47(5), 776-787.

Vierstra R.D. (2009) The ubiquitin-26S proteasome system at the nexus of plant biology. *Nature Reviews Molecular Cell Biology* 10, 385-397.

Visentin I., Vitali M., Ferrero M., Zhang Y., Ruyter-Spira C., Novák O., ..., Cardinale F. (2016) Low levels of strigolactones in roots as a component of the systemic signal of drought stress in tomato. *New Phytologist* 212, 954-963.

Vizcaino, J.A., Csordas, A., Del-Toro, N., Dianes, J.A., Griss, J., Lavidas, I., Mayer, G., Perez-Riverol, Y., Reisinger, F., Ternent, T., et al. (2016). 2016 update of the PRIDE database and its related tools. *Nucleic Acids Research* 44, 11033.

Voinnet, O., Rivas, S., Mestre, P., and Baulcombe, D. (2003). Retracted: An enhanced transient expression system in plants based on suppression of gene silencing by the p19 protein of tomato bushy stunt virus. *The Plant Journal* 33, 949-956.

Vu, L.D., Verstraeten, I., Stes, E., Van Bel, M., Coppens, F., Gevaert, K., and De Smet, I. (2017). Proteome Profiling of Wheat Shoots from Different Cultivars. *Frontiers in Plant Science* 8, 332.

Wachsmuth M., Conrad C., Bulkescher J., Koch B., Mahen R., Isokane M., Pepperkok R. & Ellenberg J. (2015) High-throughput fluorescence correlation spectroscopy enables analysis of proteome dynamics in living cells. *Nature Biotechnology* 33, 384-389.

Wallner E.-S., López-Salmerón V. & Greb T. (2016) Strigolactone versus gibberellin signaling: reemerging concepts? *Planta* 243, 1339-1350.

Wallner E.-S., López-Salmerón V., Belevich I., Poschet G., Jung I., Grünwald K., Sevilem I., Jokitalo E., Hell R., Helariutta Y., Agustí J., Lebovka I., and Greb T. (2017) Strigolactone and karrikin-independent SMXL proteins are central regulators of phloem formation. *Current Biology*, in press.

Walter M., Chaban C., Schütze K., Batistic O., Weckermann K., Näke C., ..., Kudla J. (2004) Visualization of protein interactions in living plant cells using bimolecular fluorescence complementation. *Plant Journal* 40,428-438.

Walton A., Stes E., De Smet I., Goormachtig S. & Gevaert K. (2015) Plant hormone signalling through the eye of the mass spectrometer. *Proteomics* 15 1113-1126.

Walton A., Stes E., Goeminne G., Braem L., Vuylsteke M., Matthys C., ..., Goormachtig S. (2016a) The response of the root proteome to the synthetic strigolactone GR24 in *Arabidopsis*. *Molecular and Cellular Proteomics* 15, 2744-2755.

Walton, A., Stes, E., Cybulski, N., Van Bel, M., Inigo, S., Durand, A.N., Timmerman, E., Heyman, J., Pauwels, L., De Veylder, L., et al. (2016b). It's time for some "site"-seeing: novel tools to monitor the ubiquitin landscape in *Arabidopsis thaliana*. *Plant Cell* 28, 6-16.

Wang, D., Guo, Y., Wu, C., Yang, G., Li, Y., & Zheng, C. (2008). Genome-wide analysis of CCCH zinc finger family in Arabidopsis and rice. *BMC Genomics* 9, 44.

Wang C.M., Shang J.-X., Chen Q.-X., Oses-Prieto J.A., Bai M.-Y., Yang Y., ..., Sun Y. (2013a) Identification of BZR1-interacting proteins as potential components of the brassinosteroid signaling pathway in *Arabidopsis* through tandem affinity purification. *Molecularand Cellular Proteomics* 12, 3653-3665.

Wang, P., Xue, L., Batelli, G., Lee, S., Hou, Y. J., Van Oosten, M. J., . . . Zhu, J. K. (2013b). Quantitative phosphoproteomics identifies SnRK2 protein kinase substrates and reveals the effectors of abscisic acid action. *Proc Natl Acad Sci U S A 110*(27), 11205-11210.

Wang, Y., Sun, S., Zhu, W., Jia, K., Yang, H., and Wang, X. (2013c). Strigolactone/MAX2-Induced Degradation of Brassinosteroid Transcriptional Effector BES1 Regulates Shoot Branching. *Developmental Cell* 27, 681-688.

Wang J., Peng X., Peng W. & Wu F.-X. (2014) Dynamic protein interaction network construction and applications. *Proteomics* 14, 338-352.

Wang L., Wang B., Jiang L., Liu X., Li X., Lu Z., ..., Li J. (2015) Strigolactone signaling in Arabidopsis regulates shoot development by targeting D53-like SMXL repressor proteins for ubiquitination and degradation. *Plant Cell* 27, 3128-3142.

Wang R., Zhang Y., Kieffer M., Yu H., Kepinski S. & Estelle M. (2016) HSP90 regulates temperature dependent seedling growth in *Arabidopsis* by stabilizing the auxin co-receptor F-box protein TI R1. *Nature Communications* 7, 10269 [Erratum *Nature Communications* 7 11677].

Wang, C., Liu, W., Wang, G., Li, J., Dong, L., Han, L., . . . Kong, Z. (2017a). KTN80 confers precision to microtubule severing by specific targeting of katanin complexes in plant cells. *EMBO Journal* 36(23), 3435-3447.

Wang, Y., Pang, C., Li, X., Hu, Z., Lv, Z., Zheng, B., & Chen, P. (2017b). Identification of tRNA nucleoside modification genes critical for stress response and development in rice and Arabidopsis. *BMC Plant Biology 17*(1), 261.

Wasteneys, G. O., & Ambrose, J. C. (2009). Spatial organization of plant cortical microtubules: close encounters of the 2D kind. *Trends in Cell Biology* 19(2), 62-71.

Waters M.T., Brewer P.B., Bussell J.D., Smith S.M. & Beveridge C.A. (2012a) The Arabidopsis ortholog of rice DWARF27 acts upstream of MAX1 in the control of plant development by strigolactones. *Plant Physiology* 159, 1073-1085.

Waters M.T., Nelson D.C., Scaffidi A., Flematti G.R., Sun Y.K., Dixon K.W. & Smith S.M. (2012b) Specialisation within the DWARF14 protein family confers distinct responses to karrikins and strigolactones in *Arabidopsis*. *Development* 139, 1285-1295.

Waters M.T. & Smith S.M. (2013) KAI2- and MAX2-mediated responses to karrikins and strigolactones are largely independent of HY5 in Arabidopsis seedlings. *Molecular Plant* 6, 63-75.

Waters, M.T., Scaffidi, A., Sun, Y.K., Flematti, G.R., and Smith, S.M. (2014). The karrikin response system of Arabidopsis. *The Plant Journal* 79, 623-631.

Waters M.T., Scaffidi A., Flematti G. & Smith S.M. (2015a) Substrate-induced degradation of the α/β-fold hydrolase KARRIKIN INSENSITIVE2 requires a functional catalytic triad but is independent of MAX2. *Molecular Plant* 8, 814-817.

Waters M.T., Scaffidi A., Moulin S.L.Y., Sun Y.K., Flematti G.R. & Smith S.M. (2015b) A *Selaginella moellendorffii* ortholog of KARRIKIN INSENSITIVE2 functions in Arabidopsis development but cannot mediate responses to karrikins or strigolactones. *Plant Cell* 27, 1925-1944.

Waters, M. T., Gutjahr, C., Bennett, T., & Nelson, D. C. (2017). Strigolactone Signaling and Evolution. *Annual Review of Plant Biology* 68, 291-322.

Wehner N., Hartmann L., Ehlert A., Böttner S., Oñate-Sánchez L. & Dröge-Laser W. (2011) High-throughput protoplast transactivation (PTA) system for the analysis of Arabidopsis transcription factor function. *Plant Journal* 68, 560-569.

Wehr M.C., Laage R., Bolz U., Fischer T.M., Grünewald S., Scheek S., ..., Rossner M.J. (2006) Monitoring regulated protein-protein interactions using split TEV. *Nature Methods* 3, 985-993.

Wehry E.L. (1984) Review of *Principles of Fluorescence Spectroscopy* by J.R. Lakowicz. *American Scientist* 72, 395-396.

Wei C.-Q., Chien C.-W., Ai L.-F., Zhao J., Zhang Z., Li K.H., ..., Wang Z.-Y. (2016) The *Arabidopsis* B-box protein BZS1/BBX20 interacts with HY5 and mediates strigolactone regulation of photomorphogenesis. *Journal of Genetics and Genomics* 43, 555-563.

Welcker, M., Orian, A., Jin, J., Grim, J.A., Harper, J.W., Eisenman, R.N., and Clurman, B.E. (2004). The Fbw7 tumor suppressor regulates glycogen synthase kinase 3 phosphorylation-dependent c-Myc protein degradation. *Proceedings of the National Academy of Sciences of the USA* 101, 9085-9090.

Wen, T.J., Hochholdinger, F., Sauer, M., Bruce, W., and Schnable, P.S. (2005). The roothairless1 gene of maize encodes a homolog of sec3, which is involved in polar exocytosis. *Plant Physiology* 138, 1637-1643.

Wendrich J.R., Boeren S., Möller B.K., Weijers D. & De Rybel B. (2017) In vivo identification of plant protein complexes using IP-MS/MS. *Methods in Molecular Biology* 1497, 147-158.

Whitham, S.A., Anderberg, R.J., Chisholm, S.T., and Carrington, J.C. (2000). Arabidopsis RTM2 gene is necessary for specific restriction of tobacco etch virus and encodes an unusual small heat shock-like protein. *Plant Cell* 12, 569-582.

Winkler, G. S., Mulder, K. W., Bardwell, V. J., Kalkhoven, E., & Timmers, H. M. (2006). Human Ccr4-Not complex is a ligand-dependent repressor of nuclear receptor-mediated transcription. *Embo Journal* 25(13), 3089-3099.

Woo, H. R., Chung, K. M., Park, J. H., Oh, S. A., Ahn, T., Hong, S. H., . . . Nam, H. G. (2001). ORE9, an F-box protein that regulates leaf senescence in Arabidopsis. *Plant Cell 13*(8), 1779-1790.

Xiao, W., & Jang, J. (2000). F-box proteins in Arabidopsis. *Trends in Plant Science* 5(11), 454-457.

Xie D.-X., Feys B.F., James S., Nieto-Rostro M. & Turner J.G. (1998) *COI1*: an *Arabidopsis* gene required for jasmonate-regulated defense and fertility. *Science* 280, 1091-1094.

Xing S., Wallmeroth N., Berendzen K.W. & Grefen C. (2016) Techniques for the analysis of protein-protein interactions in vivo. *Plant Physiology* 171, 727-758.

Xu Y., Piston D.W. & Johnson C.H. (1999) A bioluminescence resonance energy transfer (BRET) system: application to interacting circadian clock proteins. *Proceedings of the National Academy of Sciences USA* 96, 151-156.

Xu X., Soutto M., Xie Q., Servick S., Subramanian C., von Arnim A.G. & Johnson C.H. (2007) Imaging protein interactions with bioluminescence resonance energy transfer (BRET) in plant and mammalian cells and tissues. *Proceedings of the National Academy of Sciences USA* 104, 10264-10269.

Xu Y., Miyakawa T., Nakamura H., Nakamura A., Imamura Y., Asami T. & Tanokura M. (2016) Structural basis of unique ligand specificity of KAI2-like protein from parasitic weed *Striga hermonthica*. *Scientific Reports* 6, 31386.

Yada, M., Hatakeyama, S., Kamura, T., Nishiyama, M., Tsunematsu, R., Imaki, H., Ishida, N., Okumura, F., Nakayama, K., and Nakayama, K.I. (2004). Phosphorylation-dependent degradation of c-Myc is mediated by the F-box protein Fbw7. *The EMBO Journal* 23, 2116-2125.

Yamada Y., Furusawa S., Nagasaka S., Shimomura K., Yamaguchi S. & Umehara M. (2014) Strigolactone signaling regulates rice leaf senescence in response to a phosphate deficiency. *Planta* 240, 399-408.

Yang J., Wagner S.A. & Beli P. (2015) Illuminating spatial and temporal organization of protein interaction networks by mass spectrometry-based proteomics. *Frontiers in Genetics* 6, 344.

Yao R., Ming Z., Yan L., Li S., Wang F., Ma S., ..., Xie D. (2016) DWARF14 is a non-canonical hormone receptor for strigolactone. *Nature* 536, 469-473.

Yao R., Wang F., Ming Z., Du X., Chen L., Wang Y., …, Xie D. (2017) ShHTL7 is a non-canonical receptor for strigolactones in root parasitic weeds. *Cell Research*, in press (doi: 10.1038/cr.2017.3)

Yamada, K., Hara-Nishimura, I., and Nishimura, M. (2011). Unique defense strategy by the endoplasmic reticulum body in plants. *Plant Cell Physiology* 52, 2039-2049

Yang, Y., Qin, Y., Xie, C., Zhao, F., Zhao, J., Liu, D., Chen, S., Fuglsang, A.T., Palmgren, M.G., Schumaker, K.S., et al. (2010). The Arabidopsis Chaperone J3 Regulates the Plasma Membrane H + -ATPase through Interaction with the PKS5 Kinase. *Plant Cell* 22, 1313–1332.

Yoneyama, K., Xie, X., Sekimoto, H., Takeuchi, Y., Ogasawara, S., Akiyama, K., Hayashi, H., and Yoneyama, K. (2008). Strigolactones, host recognition signals for root parasitic plants and arbuscular mycorrhizal fungi, from Fabaceae plants. *New Phytology* 179, 484-494.

Yoneyama K., Awad A.A., Xie X., Yoneyama K. & Takeuchi Y. (2010) Strigolactones as germination stimulants for root parasitic plants. *Plant and Cell Physiology* 51, 1095-1103.

Yoshida T., Fujita Y., Maruyama K., Mogami J., Todaka D., Shinozaki K. & Yamaguchi-Shinozaki K. (2015) Four *Arabidopsis* AREB/ABF transcription factors function predominantly in gene expression downstream of SnRK2 kinases in abscisic acid signalling in response to osmotic stress. *Plant Cell and Environment* 38, 35-49.

Yue, J., Qin, Q., Meng, S., Jing, H., Gou, X., Li, J., & Hou, S. (2016). TOPP4 Regulates the Stability of PHYTOCHROME INTERACTING FACTOR5 during Photomorphogenesis in Arabidopsis. *Plant Physiology* 170(3), 1381-1397.

Zandomeni, K., & Schopfer, P. (1993). Reorientation of microtubules at the outer epidermal wall of maize coleoptiles by phytochrome, blue-light photoreceptor, and auxin. *Protoplasma,* 173(3-4), 103-112.

Zeke, T., Morrice, N., Vázquez-Martin, C., and Cohen, Patricia T W. (2005). Human protein phosphatase 5 dissociates from heat-shock proteins and is proteolytically activated in response to arachidonic acid and the microtubule-depolymerizing drug nocodazole. *Biochemical Journal* 385, 45-56.

Zhang Y., van Dijk A.D.J., Scaffidi A., Flematti G.R., Hofmann M., Charnikhova T., …, Bouwmeester H.J. (2014) Rice cytochrome P450 MAX1 homologs catalyze distinct steps in strigolactone biosynthesis. *Nature Chemical Biology* 10, 1028-1033.

Zhang Y., Gao P. & Yuan J.S. (2010) Plant protein-protein interaction network and interactome. *Current Genomics* 11, 40-46.

Zhao J., Wang T., Wang M., Liu Y., Yuan S., Gao Y., ..., Li X. (2014) DWARF3 participates in an SCF complex and associates with DWARF14 to suppress rice shoot branching. *Plant and Cell Physiology* 55, 1096-1109.

Zhao L.H., Zhou X.E., Wu Z.-S., Yi W., Xu Y., Li S., ..., Xu H.E. (2013) Crystal structures of two phytohormone signal-transducing α/β hydrolases: karrikin-signaling KAI2 and strigolactone-signaling DWARF14. *Cell Research* 23, 436-439.

Zhao L.-H., Zhou X.E., Yi W., Wu Z., Liu Y., Kang Y., ..., Xu H.E. (2015) Destabilization of strigolactone receptor DWARF14 by binding of ligand and E3-ligase signaling effector DWARF3. *Cell Research* 25, 1219-1236.

Zhang, H., Zhou, H., Berke, L., Heck, A. J., Mohammed, S., Scheres, B., & Menke, F. L. (2013). Quantitative phosphoproteomics after auxin-stimulated lateral root induction identifies an SNX1 protein phosphorylation site required for growth. *Molecular & Cellular Proteomics* 12(5), 1158-1169.

Zhang, Y., Lv, S., & Wang, G. (2018). Strigolactones are common regulators in induction of stomatal closure in planta. *Plant Signal Behaviour*, e1444322.

Zheng K., Wang X., Weighill D.A., Guo H.-B., Xie M., Yang Y., ..., Chen J.-G. (2016) Characterization of *DWARF14* genes in *Populus*. *Scientific Reports* 6, 21593.

Zhong, L. L., Zhou, W., Wang, H. J., Ding, S. H., Lu, Q. T., Wen, X. G., . . . Lu, C. M. (2013). Chloroplast Small Heat Shock Protein HSP21 Interacts with Plastid Nucleoid Protein pTAC5 and Is Essential for Chloroplast Development in Arabidopsis under Heat Stress. *Plant Cell* 25(8), 2925-2943.

Zhou F., Lin Q., Zhu L., Ren Y., Zhou K., Shabek N., ..., Wan J. (2013) D14--SCF^{D3}-dependent degradation of D53 regulates strigolactone signalling. *Nature* 504, 406-410.

Zhu, T., Wu, Y., Yang, X., Chen, W., Gong, Q., & Liu, X. (2018). The Asparagine-Rich Protein NRP Facilitates the Degradation of the PP6-type Phosphatase FyPP3 to Promote ABA Response in Arabidopsis. *Molecular Plant* 11(2), 257-268.

Zwanenburg B. & Pospíšil T. (2013) Structure and activity of strigolactones: new plant hormones with a rich future. *Molecular Plant* 6, 38-62.

Sylwia Struk

E3-plein 73, 9050 Ledeberg
03-11-1988, Parczew (Poland)
0473 622 490
sylwiastruk@icloud.com
http://linkedin.com/in/sylwia-struk-32a5a6125

PROFESSIONAL EXPERIENCE

2017 **Junior researcher**

VIB-UGent Center for Plant Systems Biology, Belgium

PhD in Biochemistry and Biotechnology- to be defended in 2018

Proteomics approach to study strigolactone signaling

- Active participation in the international conferences
  - 1st and 2nd International Congress on Strigolactones
  - Plant Biology Europe Congress- Awarded with Poster Prize
  - Gordon Research Conferences- Plant Molecular Biology
- Guidance of three master students

2017 **Visiting scientist, 1 month**

The Sainsbury Laboratory at University of Cambridge, United Kingdom

- Plant phenotyping and protein-protein interaction studies using FRET-FLIM

2012 **Erasmus exchange internship, 3 months**

Ghent University, Belgium

- Heterologous protein expression of rice lectins in *Pichia pastoris*

SCIENTIFIC PUBLICATIONS

- Struk S, Dhonukshe P. (2014*) MAPs: cellular navigators for microtubule array orientations in Arabidopsis.* Plant Cell Reports 33(1):1-21
- Matthys C, Walton A, Struk S, Stes E, Boyer FD, Gevaert K, Goormachtig S. (2016) *The Whats, the Wheres and the Hows of strigolactone action in the roots.* Planta 1327-37
- De Cuyper C, Struk S, Braem L, Gevaert K, De Jaeger G, Goormachtig S. (2017) *Strigolactones, karrikins and beyond.* Plant Cell Environment 40(9):1691-1703
- Struk S, Braem L, Walton A, De Keyser A, Boyer FD, Persiau G, De Jaeger G, Gevaert K, Goormachtig S. *Quantitative TAP, an effective tool to investigate protein complex composition in plant hormone signaling: strigolatones in the spotlight.* Frontiers in Plants Science 9, 528

EDUCATION

2012 — **Master Biotechnology**
University of Life Sciences in Lublin, Poland
The identification of toxigenic fungi and mycotoxins in organic oats by using molecular methods

2012 — **Erasmus exchange, 1 semester**
Ghent University, Belgium

2011 — **Bachelor Biotechnology**
University of Life Sciences in Lublin, Poland

PERSONAL SKILLS AND COMPETENCES

Work skills and competences

Interactomics: AP-MS, Co-IP, BIFC, Y2H, FRET-FLIM
Plant genetics: Transformation, Genotyping, Phenotyping, Crossing
Molecular Biology: RNA/DNA extraction, molecular cloning, restriction digest, PCR/qRT-PCR, transient expression assay, bacterial and yeast transformation
Proteomics: Protein extraction, Western blot, mass spectrometry data analysis
Confocal Microscopy
Analyzing, presenting and communicating results

Personal skills

Team spirit	Eager to learn	Punctual
Good social skills	Self-motivated	Independent
Enthusiastic	Result-Oriented	Hard- working

Software

MS Office	●●●●●	CLC Main Workbench	●●●●●
ImageJ	●●●●○	Electronic Lab Notebook	●●●●○
Inkscape	●●●●○	MaxQuant	●●●●○
SAS	●●●○○	Perseus	●●●●○

Languages

Polish	●●●●●	English	●●●●○	Dutch	●●●●○

Interests

Squash — Baking — Board games